Design, Synthesis, and Optimization of CK1δ Inhibitors

Dissertation

zur Erlangung des Doktorgrades

der Mathematisch-Naturwissenschaftlichen Fakultät

der Christian-Albrechts-Universität zu Kiel

vorgelegt von

Jakob Zacharias Halekotte

aus Werl

Kiel 2016

Dekanin:	Prof. Dr. Natascha Oppelt
Erster Gutachter:	Prof. Dr. Christian Peifer
Zweiter Gutachter:	Prof. Dr. Bernd Clement
Tag der mündlichen Prüfung:	30. September 2016
Zum Druck genehmigt:	30. September 2016

Meiner Mutter

Abstract

The identification of protein kinase CK1 isoform δ as an important determinant in development and progression of severe pathogenic disorders such as Alzheimer's disease, amyotrophic lateral sclerosis, familial advanced sleep phase syndrome, and cancer has dramatically increased interest in small molecule inhibitors for both therapeutic approaches and basic research. Consequently, selective CK1δ inhibitors have been pursued with increasing interest over the past decade. However, the existence of further five evolutionary conserved human CK1 isoforms that possess similar, different, or even opposite physiological and pathophysiological implications renders the design of suitable candidates enormously complicated. Especially highly related CK1 isoforms δ and ε remain difficult to discriminate and have therefore often been reported as redundant, rather by means of missing evidence.

The present study reports on *in silico* design, synthesis, and biological evaluation of novel and optimized 4,5-diaryl-imidazoles as potent dual-specific ATP-competitive inhibitors of CK1 isoforms δ and ε as well as p38α mitogen-activated protein kinase. In fact, most promising candidate **191** is among the most effective CK1 inhibitors published to date with an IC_{50} value in the low single-digit nanomolar range and good selectivity in a panel of 321 protein kinases. Although its physicochemical properties require further optimization, acceptable efficacy in different human cancer cell lines has been observed. Consequently, **191** holds the potential to serve as an important biological tool for pharmacological evaluation of CK1-dependent activity such as in stem cell applications.

Apart from **191**, molecular modeling-aided approaches led to structurally divergent but highly potent inhibitors that have been designed in order to enhance specificity. Among the most promising candidates, **224** represented a creative-empirically generated molecule while **266** has been obtained by hybrid synthesis utilizing fragments from known compounds that exhibited suitable properties. Although significant impact on specificity has unfortunately not been examined, co-crystallization of **191**, **224**, and **266** with CK1δ and p38α revealed valuable structure-activity relationship insights that will surely prove beneficial for future attempts.

Kurzzusammenfassung

Die Identifikation der Protein Kinase CK1 Isoform δ als einer der bestimmenden Faktoren in Entwicklung und Progression schwerwiegender pathogener Störungen wie der Alzheimer-Erkrankung, der amyotrophen Lateralsklerose, des familiären vorverlagerten Schlafphasen Syndroms und Krebs hat die Kinase zu einem attraktiven Target sowohl für therapeutische Aspekte, als auch für Grundlagenforschung gemacht. Es ist daher kaum verwunderlich, dass die Bestrebungen hinsichtlich selektiver niedermolekularer CK1δ Inhibitoren innerhalb der vergangenen Dekade kontinuierlich zugenommen haben. Allerdings ist die Entwicklung derartiger Hemmstoffe durch die Existenz weiterer fünf evolutionär konservierter humaner CK1 Isoformen mit zum Teil ähnlicher, unterschiedlicher, oder sogar gegensätzlicher physiologischer und pathophysiologischer Bedeutung erheblich erschwert. Insbesondere die hochkonservierten Isoformen δ und ε sind bis heute durch kleine Moleküle nicht erfolgreich unterscheidbar und wurden daher in verschiedenen Zusammenhängen als redundant klassifiziert, ohne dass jedoch ausreichend Evidenz für diese Annahme geliefert werden konnte.

Die vorliegende Arbeit beschreibt das *in silico* basierte Design, die Synthese und die biologische Charakterisierung neuer und optimierter 4,5-Diaryl-imidazole als potente und dual-spezifische ATP-kompetitive Inhibitoren der CK1 Isoformen δ und ε sowie der p38α Mitogen-aktivierten Protein Kinase. Tatsächlich handelt es sich bei der vielversprechendsten Verbindung **191** um einen der potentesten CK1 Hemmstoffe die bis heute publiziert werden konnten. Der Inhibitor weist eine halbmaximale Hemmkonzentration im niedrigen einstelligen nanomolaren Bereich auf, zeigt gute Selektivität über 321 Protein Kinasen und ist biologisch aktiv in verschiedenen humanen Tumorzelllinien, obwohl seine physikochemischen Eigenschaften sicherlich noch weiterer Optimierung bedürfen. **191** besitzt somit das Potential als biologisches Tool in der fortschreitenden Untersuchung der pharmakologischen Bedeutung der CK1 entscheidend Beitrag zu leisten, gerade im Hinblick auf die zunehmende Anwendung Stammzell-basierter Testsysteme.

Abgesehen von **191** konnten mit Hilfe computergestützter Verfahren (Molecular Modelling) weitere strukturell unterschiedliche und hochpotente Inhibitoren mit dem Ziel einer Erhöhung der Spezifität entwickelt werden, von denen insbesondere zwei herausstachen: während **224** ein kreativ-empirisch designtes Molekül darstellt, wurde **266** durch Fragment-basierte Hybrid-Synthese dargestellt, wobei auf Teilstrukturen bekannter Verbindungen mit entsprechend gewünschten Eigenschaften zurückgegriffen wurde. Obgleich letztendlich keine signifikante Steigerung der Selektivität erzielt werden konnte, wurden durch Ko-Kristallisation von **191**, **224** und **266** mit der CK1δ und der p38α interessante Aspekte der Struktur-Wirkungsbeziehung aufgedeckt, die sich fraglos für zukünftige Bestrebungen als hilfreich erweisen werden.

Table of Contents

1 Introduction 1

1.1 Protein Phosphorylation and Protein Kinases 1

1.2 Protein Kinase CK1δ 3

1.2.1 CK1δ Kinase Domain Structure 5

1.2.2 Substrate Recognition and Substrates of CK1δ 9

1.2.3 Regulation of CK1δ Activity 13

1.2.4 Physiological and Pathophysiological Relevance of CK1δ 18

1.3 Kinase Inhibitors 24

1.3.1 Different Types of Small Molecule Kinase Inhibitors 26

1.3.2 Limitations and Challenges of Small Molecule Kinase Inhibitors 29

1.3.3 CK1δ Inhibitors 30

2 Aim of the Present Study 39

3 Molecular Modeling Strategies 40

3.1 *In Silico* Lead Structure Optimization 40

3.1.1 Influence of different Substituents in the Selectivity Pocket 47

3.1.2 Addressing the Phosphate- and Ribose-binding Regions 49

3.1.3 Alternatives for the Imidazole (Core Hopping) 53

3.1.4 Structural Water 56

3.1.5 Addressing the Solvent-exposed Hydrophobic Region II 58

4 Chemistry 71

4.1 Synthesis of Building Block 120 72

4.1.1 Procedure A 72

4.1.2 Procedure B 75

4.1.3 Synthesis of 2-unsubstituted 4,5-Diaryl-imidazole 76

4.2 Syntheses of Series 1: Pyridine-2-amines and -piperazines 78

4.2.1 S_NAr Reaction of 2-Fluoropyridines with Amines 78

4.2.2 S_N2 Reaction of Alkyl Halides with 2-Aminopyridines 80

4.3 Syntheses of Series 2: Amide Coupling 82
4.4 Syntheses of Series 3: Carbamide Derivatives 86
4.5 Syntheses of Series 4: Five-membered Heterocycles 88
4.5.1 Synthesis of 4-(dimethoxyphenyl)pyrrole-carboxamides 88
4.5.2 Synthesis of Thiazole-containing Side Chains 91
4.5.3 Synthesis of Imidazole-containing Side Chains 94
4.5.4 Synthesis of Triazole-containing Side Chains 96
4.6 Syntheses of Series 5: Propiolic Acid 97
4.7 Syntheses of Series 6: Hybrid Inhibitors 100
4.7.1 Synthesis of IWP-Hybrids 266 and 267 100
4.7.2 Synthesis of Imatinib-Hybrid 280 103
4.8 Sulfoxidation of Selected Compounds 104
4.9 Photochemical $_{\pi}6_{a}$-Electrocyclization of Diaryl-imidazoles 107
5 Results and Discussion 109
5.1 Characterization of Series 1 109
5.2 Characterization of Series 2 115
5.3 Characterization of Series 3 125
5.4 Characterization of Series 4 131
5.5 Characterization of Series 6 136
6 Conclusions 141
6.1 Design and Synthesis of Potent and Selective CK1δ Inhibitors 141
6.2 Structure-Activity Relationship of CK1δ Inhibitors 144
7 Experimental 150
7.1 Molecular Modeling 150
7.1.1 Software and Computational Resources 150
7.1.2 Protein Preparation 150
7.1.3 Ligand Preparation 152
7.1.4 Ligand Docking 152
7.2 Material and Methods 154

7.2.1 Reagents and Solvents ... 154
7.2.2 Methods and Instruments ... 154
7.3 Synthetic Procedures ... 159
7.3.1 Synthesis of Building Block 120 ... 159
7.3.2 Syntheses of Series 1: Pyridine-2-amines and -piperazines ... 175
7.3.3 Syntheses of Series 2: Amide Coupling ... 202
7.3.4 Syntheses of Series 3: Carbamide Derivatives ... 211
7.3.5 Syntheses of Series 4: Five-membered Heterocycles ... 222
7.3.6 Syntheses of Series 5: Propiolic Acid ... 253
7.3.7 Syntheses of Series 6: Hybrid Inhibitors ... 256
7.3.8 Sulfoxidation of Compounds: 4,5-Diaryl-2-(methylsulfinyl)-1*H*-imidazoles ... 269
7.3.9 Irradiation of *N*-Benzyl-4-(5-(4-fluorophenyl)-2-(methylthio)-1*H*-imidazol-4-yl)pyridin-2-amine ... 286
7.4 Biological Evaluation ... 287
7.4.1 Kinase Assays (IC_{50} determination) ... 287
7.4.2 Kinase Profiling ... 289
7.4.3 MTT Viability Assays ... 289
7.5 X-ray Crystallography ... 291
8 References ... 294
9 Appendix ... 315
List of Abbreviations ... 328
List of Figures ... 333
List of Tables ... 343
Erklärung zu § 8 Abs. 1 der Promotionsordnung ... 347
Danksagung ... 349
Curriculum Vitae ... 351

1 Introduction

1.1 Protein Phosphorylation and Protein Kinases

Reversible phosphorylation is one of the most important post-translational modifications of proteins and corresponds to the transfer of a phosphate group onto specific amino acid hydroxyl moieties by covalent attachment. Enzymes that catalyze phosphate transfer reactions are referred to as kinases and phosphatases. Protein kinases (PK) mediate γ-phosphate transfer from their cofactors adenosine or guanidine triphosphate (ATP, GTP) to serine and threonine (Ser/Thr-specific kinases) or tyrosine residues (Tyr-specific kinases). Several so-called dual-specific kinases have been reported to phosphorylate all three residues[1–4]. In contrast, cleavage of amino acid phosphate esters is catalyzed by protein phosphatases[1–4].

Phosphorylation of target proteins modifies protein function, stability, and localization either by induction of conformational rearrangement or activation and inactivation of protein interaction sites[4]. Consequently, reversible phosphorylation displays a crucial mechanism in most signal transduction cascades in eukaryotic cells, including e.g. metabolism, survival and apoptosis, transcription, proliferation, and differentiation[1,5]. Due to their physiological relevance, most PK act as members in highly regulated signaling networks of kinases and other effectors. Mutation and deregulation are closely related to numerous pathophysiological events and diseases such as tumorigenesis, inflammation, central nervous system (CNS) disorders, pain, cardiovascular diseases, and complications of diabetes and osteoporosis[6]. PK have therefore become one of the most intensively pursued targets in pharmacological research over the last decades[6,7].

518 PK are encoded in the human genome, nearly 2 % of all genes, which account for phosphorylation of at least 30 % of the human proteome[4,5]. According to sequence analysis, the human kinome is subdivided into seven distinct groups, though the focus of the current dissertation has been set to CK1 superfamily (**Figure 1**).

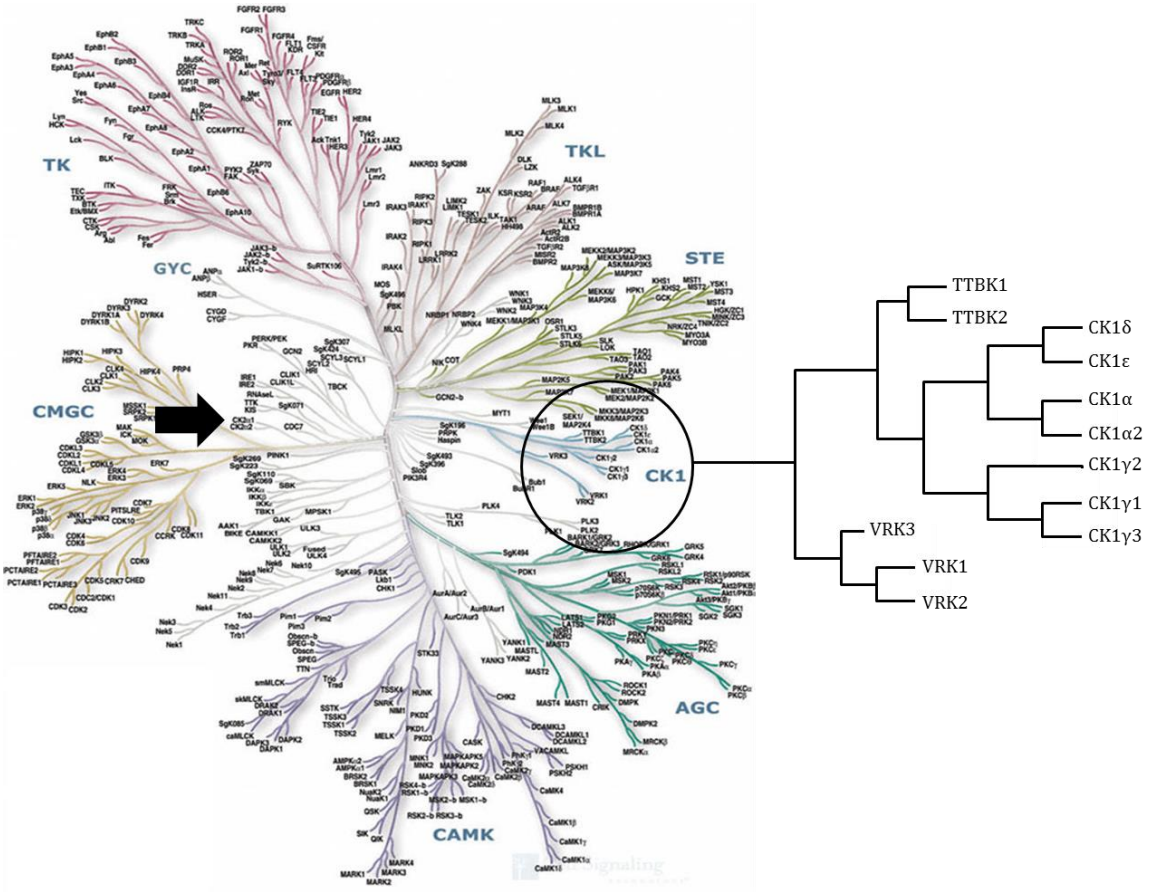

Figure 1 | The human kinome. Human kinases are subdivided into seven distinct groups: AGC = containing PKA, PKG, PKC families; CAMK = calcium/calmodulin-dependent protein kinase; CK1 = formerly known as casein kinase 1; CMGC = containing Cdk, MAPK, GSK3, CLK families; STE = homologs of yeast sterile 7, sterile 11, sterile 20 kinases; TK = tyrosine kinases; TKL = tyrosine kinase-like. Obviously, CK1 and CK2 (black arrow) family members are non-related. The phylogenetic tree is taken from MANNING *et al.*[5]. The dendrogram (right) is made in accordance to the same publication.

1.2 Protein Kinase CK1δ

In 1969 two distinct liver enzymes were amongst the first PK described in literature, referred to as casein kinases 1 and 2 with respect to their ability to phosphorylate casein *in vitro*. Several years later, in the early 1970s, the casein kinase "pseudo family" was supplemented by a third member, the Golgi casein kinase (G-CK) which is in fact the only one of these phosphorylating casein *in vivo*. Considering this confusing situation, it was decided in 1994 to rename the pseudo casein kinases in accordance to their acronyms to protein kinases CK1 and CK2[8]. It is further noteworthy that the enzymes formerly known as casein kinases represent phylogenetically non-related proteins which primarily share their ability to phosphorylate casein *in vitro*. While CK1 and CK2 represent distinct families, G-CK has recently been identified as a member of the atypical Fam20C (family with sequence similarity 20C) protein kinase family[5,8].

Since then, six distinct genes encoding human CK1 isoforms α, γ1, γ2, γ3, δ, and ε have been identified. These isoforms, together with their closest relatives tau tubulin kinases 1 (TTBK1) and 2 (TTBK2) and vaccinia-related kinases 1-3 (VRK1-3), represent one of the seven groups (CK1) of the human kinome (**Figure 1**). Another isoform from the bovine brain (CK1β) as well as diverse splice variants (transcription variants, TV) add to the diversity of this family[5,9–11].

The CK1 family members represent evolutionary highly conserved monomeric Ser/Thr-specific protein kinases with sequence homology referred to the catalytic domain of at least 51 % amongst CK1 isoforms and less than 21 % towards other members of the Ser/Thr kinase super-family[11]. Significant differences between CK1 isoforms are length and primary structure of the non-catalytic but regulatory carboxyl-terminal domains leading to molecular weights ranging from 37 kDa (CK1α) to 51 kDa (CK1γ3)[12]. The highest consensus within the CK1 family display isoforms δ and ε with more than 98 % sequence identity of their catalytic domains and at least 40 % of their C-termini[9,11,13].

CK1-mediated phosphorylation is generally second messenger independent and exclusively relies on ATP as a co-substrate[12]. Early studies also suggested CK1 isoforms to be dual-specific kinases, but it still remains undefined which isoforms are actually able to additionally phosphorylate tyrosine residues or whether they are able to do so at all[11,12].

In detail, two transcription variants (TV1, TV2) have been identified for the CK1 isoform δ gene *CSNK1D* that has been mapped to chromosome 17q25[14,15]. Although these variants include identical small N-terminal regions (eight amino acids) and kinase domains (286 amino acids), they

exclusively differ in the length of their C-termini, leading to transcripts of 415 (TV1) and 409 (TV2) amino acids with molecular weights of 47.2 kDa and 46.7 kDa, respectively (**Figure 2**)[9].

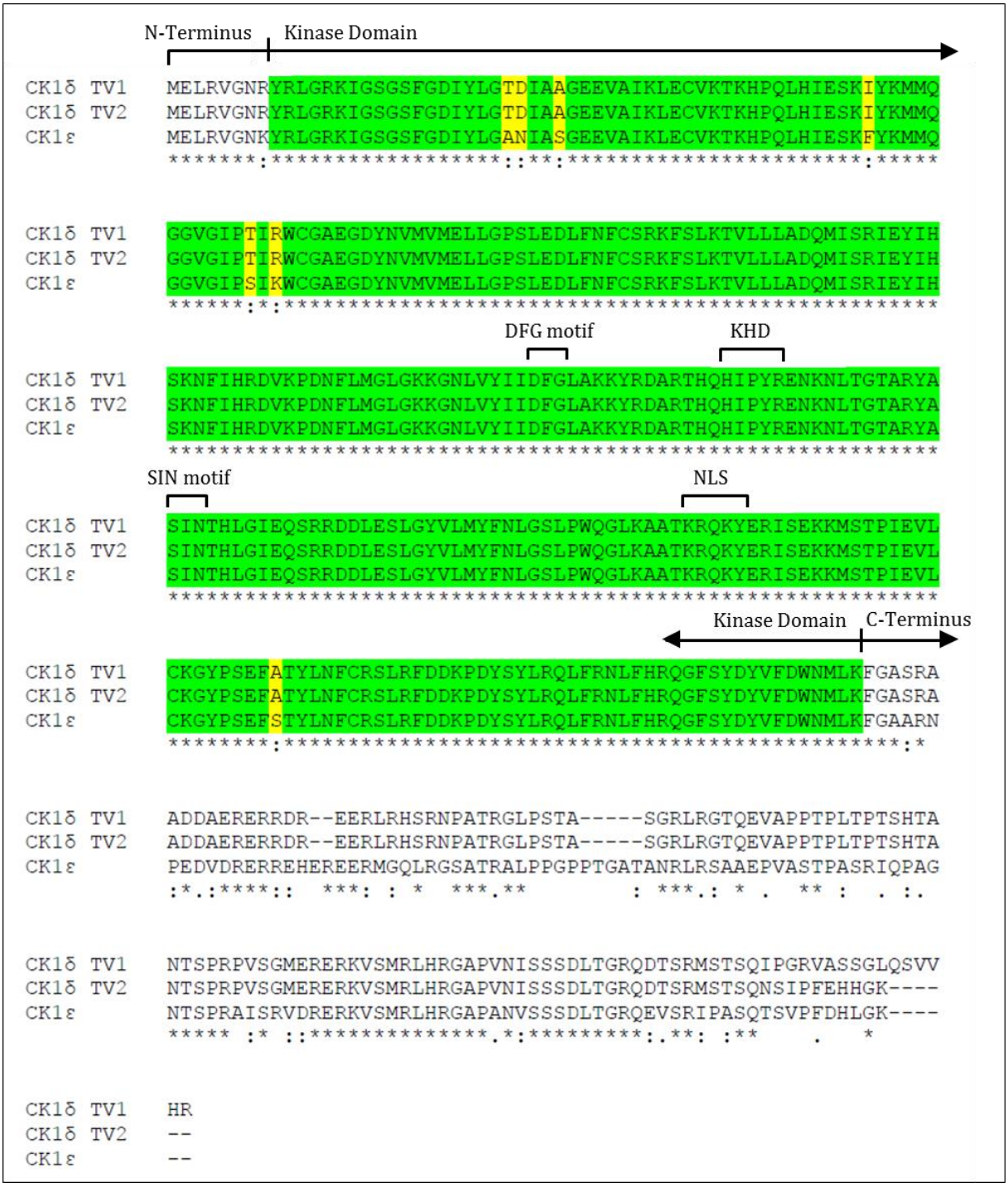

Figure 2 | Sequence alignment of human CK1δ transcription variants and CK1ε. The conserved N-terminal domain consists of amino acids 1-8, followed by the kinase domain (286 amino acids). Identical residues within the kinase domain are highlighted in green, different residues in yellow. The non-conserved C-terminal domains of CK1δ TV1/TV2 and CK1ε exhibit highly variable sequences. The alignment was generated by Clustal Omega[16] using transcript sequences for CK1δ TV1 (Gene Bank AAH03558.1), CK1δ TV2 (Gene Bank ABM64211.1), and CK1ε (Gene Bank ABM64212.1). For abbreviations DFG, KHD, SIN, NLS cp. **chapter 1.2**.

1.2.1 CK1δ Kinase Domain Structure

Crystal structures of CK1δ show the typical bilobal organization common to all protein kinases (**Figure 3**): the smaller N-terminal and the larger C-terminal domains (lobes) are connected by a linker loop, the so-called *hinge* region. This linker is included in a CK1-specific sequence motif[a] and contains the highly conserved Gly86 which is suggested to be crucial for domain flexibility. The nucleotide-binding site is positioned adjacent to the hinge within the cleft between both lobes[11,17,18].

The N-lobe primarily consists of five antiparallel β-sheets (β1ab, β2, β3, β4, and β5), one helical structure (αA) between strands three (β3) and four (β4), and the conserved glycine-rich P-loop, bridging strands one and two. The P-loop forms the ceiling of the ATP-binding region[18].

Four prominent antiparallel α-helices (αC, αE, αH, αI) set up the framework of the C-lobe, complemented by an approximately vertical helix (αF), three smaller helices (αB, αD, αG), four small β-sheets (β6-β9), and the T-loop (L-9D), L-EF, and L-HI. Two phosphate moiety-binding sites (W1, W2) have been identified within this lobe (**Figure 3**). Both sites are located easily accessible on the protein surface within hydrogen bonding distance to residues Arg178, Gly215, Lys224 (W1) and Arg157, Lys154 (W2), respectively[17,18].

The highly flexible loop L-EF adjacent to W1 contains a putative nuclear localization signal (NLS[b]) sequence at the junction to αF which is conserved in CK1 isoforms δ and ε. Another motif[c] within this loop is reportedly unique to the CK1 family[17,19]. Further optional phosphorylation sites are situated in close proximity to the regulatory T-loop. Especially Thr161 and Thr174 are likely targets for reversible phosphorylation as being exposed on the surface[17,18].

In CK1δ the T-loop is the equivalent of the so-called *activation-loop* (A-loop) in other protein kinases where it is located between the conserved DFG[d] and APE (Ala, Pro, Glu) motifs.[18] Interestingly, all CK1 family members lack the APE consensus sequence[19]. The appropriate triplet in CK1δ, though without equivalent functionality, is SIN[e] within a CK1-specific sequence motif ranging from the end of the T-loop over αD and into αE[17]. Conformational rearrangement of the T-loop regulates substrate access to the active site[2]. An additional important motif included in the T-loop is a conserved kinesin homology domain (KHD[f]) that is usually part of the head regions of microtubule motor proteins[18,20].

---

[a] Leu84, Leu85, Gly86, Pro87, Ser88, Leu89, Glu90, Asp91, Leu92, Phe93 (hinge motif)
[b] Thr220, Lys221, Arg222, Gln223, Lys224, Tyr225 (NLS)
[c] Ser210, Leu211, Pro212, Trp213, Gln214, Gly215, Leu216, Lys217, Ala218 (CK1 L-EF family motif)
[d] Asp194, Phe195, Gly151 (DFG)
[e] Ser181-Ile-Asn183 (SIN) within CK1-specific Thr184, His, Leu, Gly, Ile, Glu, Gln, Ser, Arg, Arg, Asp, Asp, Leu, Glu197
[f] His164, Ile165, Pro166, Tyr167, Arg168 (KHD)

Upon crystallization, homodimerization of CK1δ has been observed and a *dimerization domain* can be suggested including various amino acids of strands β1, β2, β3, and β7 as well as loops L-12 and L-78, helix αB, and the hinge (**chapter 1.2.3**, **Figure 8**). Whether homodimers are of any importance for *in vivo* settings still has to be investigated[9,17,21].

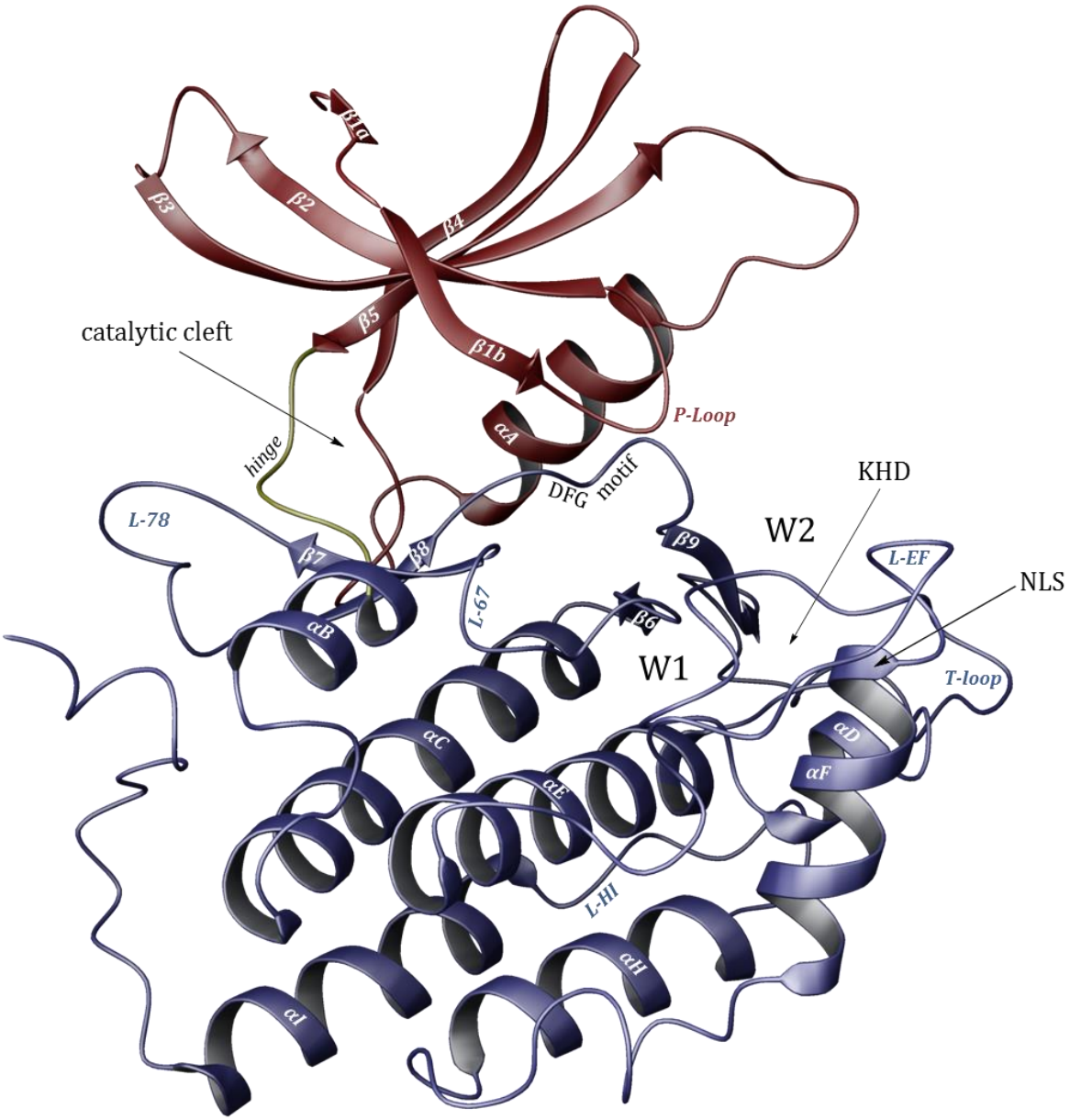

Figure 3 | Structural presentation of the CK1δ kinase domain. The N- (red) and C-terminal lobe (blue) are connected by the hinge region (yellow). The nucleotide binding site (not occupied) lies within the cleft between the domains. Indicated by arrows are the kinesin homology domain (KHD) and the nuclear localization signal (NLS). The significance of the DFG (Asp, Phe, Gly) motif for CK1δ has not been determined yet. The nomenclature is adapted from Xu *et al.*[18] and Longenecker *et al.*[17]. The figure refers to CK1δ crystallization by Huang *et al.* (PDB code 4HGT)[22].

In the absence of ATP CK1δ remains in a "closed conformation". Consequently, a slight rotation of the N-lobe is necessary to gain access to the catalytic cleft for nucleotide binding[17]**.** According to the pharmacophore model by TRAXLER and FURET the ATP-pocket of protein kinases ought to be subdivided into three distinct regions which mediate ATP-binding (**Figure 4**): first, the predominantly hydrophobic adenine-binding region (*AB*), supporting two hydrogen bonds (H-bonds) between hinge residues and the adenine moiety; second, the hydrophilic sugar pocket (*SP*) and third, the solvent-exposed and less conserved phosphate-binding region (*PB*). Adjacent to these, two non-conserved hydrophobic regions offer potential for the design of selective ATP-competitive inhibitors: the hydrophobic pocket I (*HPI*, *selectivity pocket*) and the solvent-exposed hydrophobic region II (*HRII*, *affinity pocket*). *HPI* is lined by the *gatekeeper* residue (Met82 in CK1δ) which allows or prohibits access to this cavity. Especially *HPI* is occupied by many potent kinase inhibitors[9,23]**.**

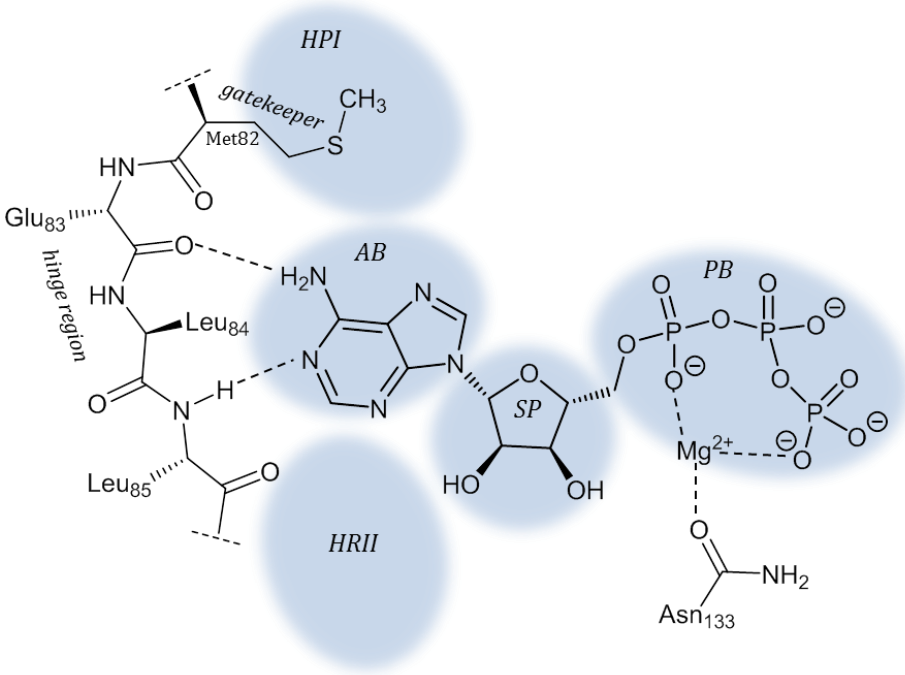

Figure 4 | ATP-binding mode in CK1δ. The representation is in accordance with crystallization results of CKi1 and magnesium-ATP complex (PDB code 1CSN) and the pharmacophore model by TRAXLER and FURET. For clarity, water molecules are left out[17,18,23].

Crystallization of yeast CK1-homolog CKi1 with ATP and magnesium by XU *et al*. revealed the exact nucleotide-binding mode for CK1 that is in line with the pharmacophore model[18]**.** In detail, two H-bonds are formed with hinge residues: Asp86 (Glu83 in CK1δ) accepts an H-bond donated by the adenine amino group while Leu88 (Leu85 in CK1δ) forms the second bond towards the adenine N1 atom. N7 interacts with CKi1 via water-mediated H-bonds with αA side chains of Glu55 (Glu52 in CK1δ) and Tyr59 (Glu56 in CK1δ, **Figure 5 A**). The ribose hydroxyl moieties form one direct bond towards L-67 Asp135 (Asp132 in CK1δ) and water-mediated contacts

towards L-5B Ser91 (Ser88 in CK1δ) and αB Asp94 (Asp 91 in CK1δ, **Figure 5 B**). P-loop residues Ser22, Gly24 (Ser19 and Gly21 in CK1δ), strand three (β3) Lys41 (Lys38 in CK1δ), and L-67 Lys133 (Lys130 in CK1δ) participate in stabilizing the ATP triphosphate moiety. One magnesium ion is complexed by the ATP α- and γ-phosphates and coordinated by L-67 Asn136 (Asn133 in CK1δ, **Figure 5 C**)[18].

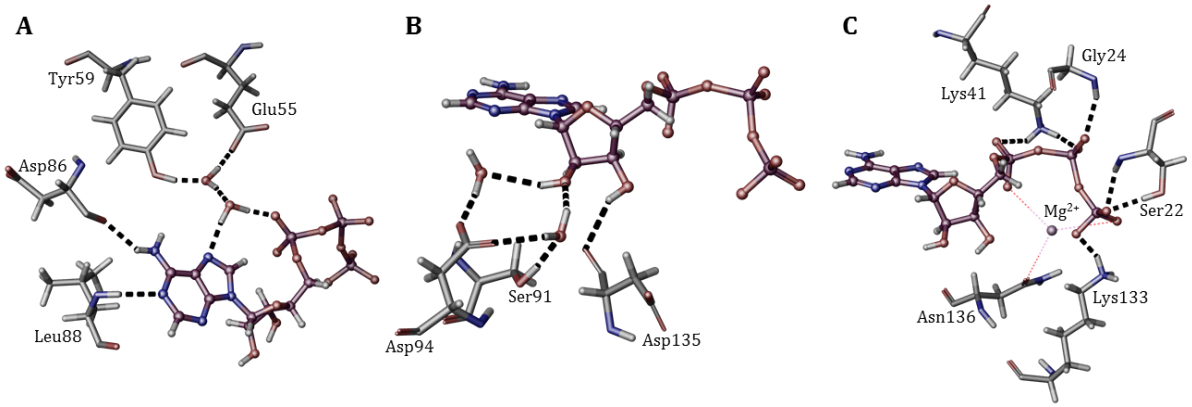

Figure 5 | Detailed ATP-binding mode in CKi1. Direct and water-mediated contacts between CKi1 and ATP adenine (A), ribose (B), and magnesium-phosphate moiety (C). Interactions were modeled according to XU *et al.* (PDP code 1CSN)[18].

1.2.2 Substrate Recognition and Substrates of CK1δ

Like all CK1 family members, CK1δ is a phosphate-directed Ser/Thr-specific protein kinase, preferentially catalyzing conversion of previously phosphorylated or acidic peptides. The canonical CK1 consensus sequence motif has been described as Ser(P)/Thr(P)-X-X-Ser/Thr with X being any amino acid and the phosphorylatable residue (Ser/Thr) located C-terminal of a phosphoserine Ser(P) or phosphothreonine Thr(P). The phosphorylated Ser(P)/Thr(P) can also be replaced by negatively charged acidic residues changing the motif to Asp_n/Glu_n-X-X-Ser/Thr with *n* ideally being three or four. Asp residues are thereby slightly more effective than Glu, but both are significantly less favored compared to phospho-primed substrates[19,24–27]. Apart from these, noncanonical consensus sequences have been identified e.g. in β-catenin in which the phosphorylatable Ser45 is implemented in a so-called SLS motif[g] followed downstream by acidic residues[28]. Furthermore, linking the sulfated lipids sulfatide and cholesterol-3-sulfate (SCS) to target proteins has been reported to affect CK1 isoform-specific phosphorylation: while sulfatide-mediated stimulation caused only a slight increase in phosphorylation of the potent Asp_n/Glu_n-X-X-Ser/Thr motif in myelin basic protein (MBP) by CK1δ, it highly excites CK1δ/γ-catalyzed phosphate transfer to Ras homolog family member A (RhoA). Therefore, phosphorylation of basic proteins may effectively be increased by SCS, as a consensus motif[h] for CK1α/δ/ε-mediated phosphorylation has been identified e.g. within SCS-binding proteins MBP and tau. Binding of SCS within this sequence, however, is suggested to be accomplished by the first three residues, presumably Lys, Gly, Arg[29]. Apart from this, substrate specificity of CK1 isoforms seems not to be achieved by preferring different target sequences[30].

The phosphate moiety-binding site W1 appears to be the major site for substrate organization with regard to the phosphate transfer. W1 was originally detected in crystallographic analysis as a sulfate- and tungstate-binding site, where the particular ion is coordinated via H-bonds by Arg178 (T-loop), Gly215 (L-EF) and Lys224 (αF)[17,18]. According to these observations molecular modeling brilliantly visualizes the preference of CK1 isoforms for previously phosphorylated substrates (**Figure 6**): the phosphate moiety of an *in silico* generated peptide[i], in accordance with the canonical consensus motif, is coordinated by the same residues as the sulfate/tungstate ion whereupon the phospho-acceptor hydroxyl group of the peptide target Ser is directed within H-bonding range of the ATP γ-phosphate. In dependency on the substrate, the highly flexible L-EF is able to adapt variable conformations and is likely to mediate different interactions.

[g] Ser45-Leu-Ser-$X_{2\text{-}5}$-Glu_n/Asp_n (SLS consensus motif)
[h] Lys/Arg-X-Lys/Arg-X-X-Ser/Thr (SCS-binding protein consensus motif)
[i] Ser(P), Ala, Ala, Ser (*in silico* peptide sequence)

Consequently, it has been designated as the *substrate-binding loop*[17,18]. Unprimed acidic substrates might act in a similar way as there are several basic residues within the T-loop (Arg178), L-EF (Lys217, Lys221, Arg222) and αF (Lys224) accessible for potential electrostatic interactions towards the acidic cluster of peptides[28].

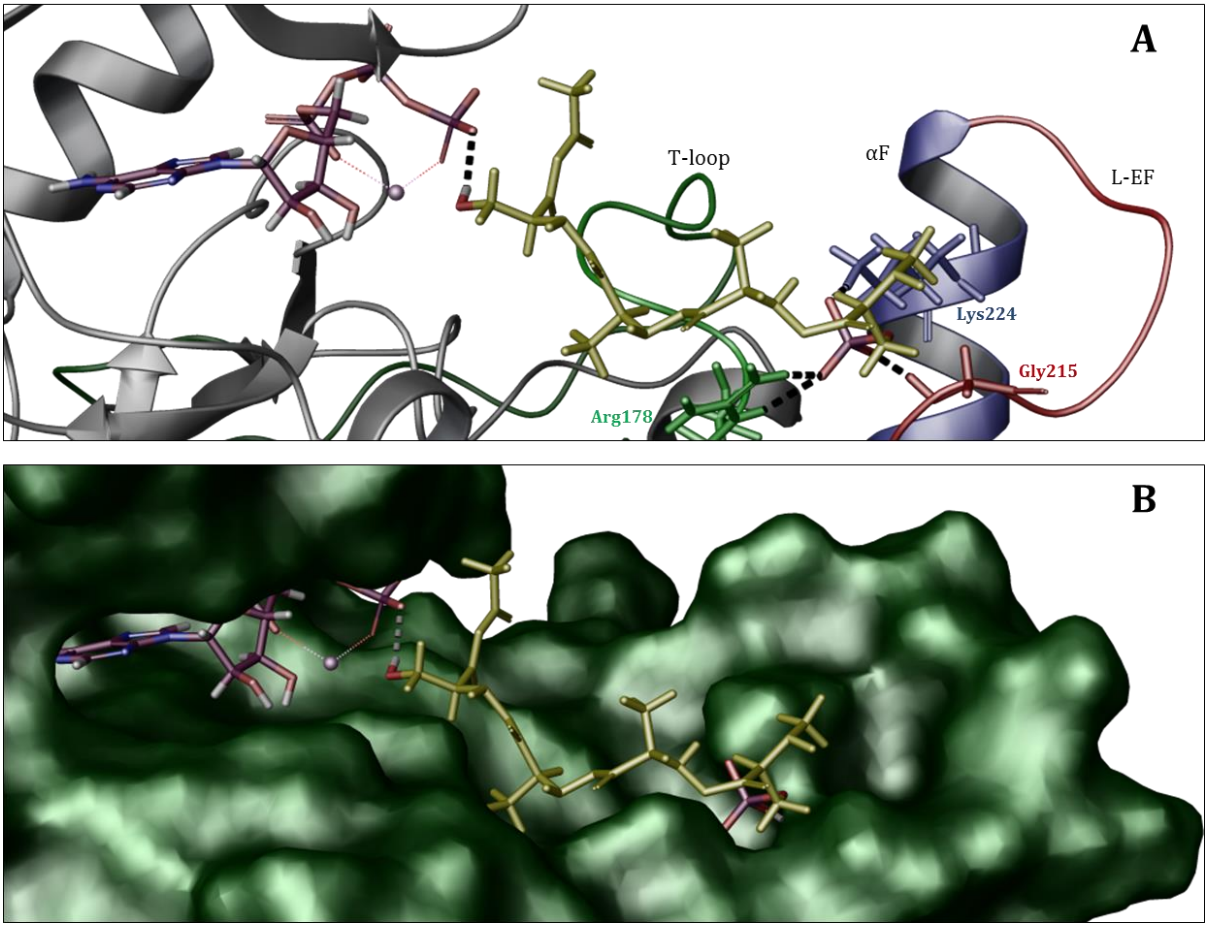

Figure 6 | Postulated substrate-binding mode at CK1δ phosphate-binding moiety W1. An *in silico* peptide (yellow) consisting of Ser(P)-Ala-Ala-Ser is coordinated by Arg178 (T-loop, green in A), Gly215 (L-EF, red in A) and Lys224 (αF, blue in A). The phosphorylatable Ser hydroxyl group is placed in H-bonding range towards ATP (maroon) γ-phosphate. A surface model (B) visualizes the close fitting of Mg^{2+}-ATP and substrate to the catalytic cleft of CK1δ. Modeling was performed based on MARIN *et al.*[28] (PDB code 1CSN[18], 4HGT[22]) utilizing Schrödinger software (**chapter 7.1**).

In addition to the phosphate-binding moiety W1 adjacent to the ATP-binding pocket several sites within the N- and C-terminal domain participate in substrate interaction[31]. CK1δ docking motifs have been identified in different proteins such as the Phe-X-X-X-Phe motif in nuclear factor of activated T-cells 1 (NFAT1) and period 2 (PER2) or the Ser-Gln-Ile-Pro motif in microtubule plus-end-binding protein 1 (EB1)[32,33]. As these motifs are not necessarily localized in proximity to the respective phosphorylation sites, it is suggested that their function refers to proper positioning and stabilization of kinase domain and substrate[34].

In the absence of docking motifs, the C-terminus has been observed to act in a similar manner: autophosphorylation and phosphorylation by other kinases within this region prevents substrate-binding as the C-terminal tail subsequently functions as a pseudo-substrate blocking access to the binding site[35].

Despite the fact that several substrates are *in vitro* targets of different CK1 family members, the isoforms possess strong *in vivo* substrate specificity. This specificity is presumably ascribed to non-conserved residues within the kinase domains as observed for the specific interaction between CK1δ/ε and PER[35] as well as isoform-specific phosphorylation of p53 by CK1 isoforms δ, ε, and α, but not CK1γ1-3[36].

In general, more than 150 substrates have been identified for CK1 family members to date. Although it is often difficult to assign distinct CK1 isoforms to particular substrates, more than 80 proteins have been ascribed to *in vitro* or *in vivo* phosphorylation by CK1δ in literature. An admittedly incomplete summarization of these proven CK1δ substrates is given in **Table 1**. In addition, it is likely that in cases of inhibition or knockdown several highly related isoforms like δ and ε are able to take over several substrates from each other in form of an *escape mechanism*.

Table 1 | Specified *in vitro* and *in vivo* CK1δ substrates of different species. The list is admittedly incomplete due to the fact that many CK1 substrates have not been assigned to distinct isoforms. The classification of substrates in this table is based on their major function and in association with **chapter 1.2.4**. Several substrates could appear in more than the assigned group.

Putative function	Substrates
Key regulatory stress-associated factors	p53[37], murine double minute 2 homolog (MDM2)[38], hypoxia-inducible factor 1α (HIF-1α)[39]
DNA-/RNA-associated proteins and transcription (factors)	Topoisomerase IIα (TOP2A)[40], DNA methyltransferase 1 (Dnmt1)[41], ubiquitin-like, with PHD and RING finger domains (UHRF1)[42], heterogeneous nuclear ribo-nucleoprotein A1 (hnRNP A1)[43], putative RNA helicase[43], forkhead box G1 (FoxG1)[44], nuclear factor of activated T-cells 1 (NFAT1)[31,32], yeast sterol regulatory element-binding protein homolog (Sre1N)[45], chromatin-associated protein swi6 (Swi6)[46]
Ribosome-associated proteins	Ribosomal proteins L4 (RPL4), L8 (RPL8), L13 (RPL13)[43], nucleolar protein 56 (Nop56)[43], LTV1[47,48], ENP1, Bystin (BYSL)[47], eukaryotic initiation factor 6 (eIF6), Tif6p[49]
Mitotic and meiotic control	Wee1[50], Rec8 meiotic recombination protein (Rec8)[51], endogenous meiotic inhibitor 2 (Emi2)[52]

Cytoskeleton- and scaffolding-associated functioning	α/β-tubulin[53], γ-tubulin[9,53,54], microtubule-associated proteins 1A (MAP1A)[31] and 4 (MAP4)[53], tau[29,53,55], end-binding 1 (EB1)[33], stathmin[53], Ran-binding protein microtubule-organization center (RanBPM)[56], Ras homolog family members A and B (RhoA, RhoB)[29,57], keratin 17[43], connexin-43 (Cx43)[58], desmoglein 2[43], annexin II/lipocortin II[43], Sid4[59], protein kinase C-potentiated myosin phosphatase inhibitor of 17 kDa (CPI-17)[60]
Vesicular trafficking and Golgi-associated functioning	Snapin[61], protein kinase D2 (PKD2)[62], ADP-ribosylation factor GTPase-activating protein (ARF GAP1)[63]
Neurodegeneration-associated proteins	β-secretase (BACE1)[64], presenilin-2 (PS-2)[65], cyclin-dependent kinase 5 (Cdk5)[66], α-synuclein[67], parkin[68], myelin basic protein (MBP)[29], cyclic AMP response element-binding protein (CREB)[69], TAR DNA-binding protein of 43 kDa (TDP-43)[70]
Circadian rhythm-associated functioning	Period 1-3 (PER1-3)[71–74], brain and muscle Arnt-like protein 1 (BMAL1)[9,75], cryptochromes 1 (CRY1) and 2 (CRY2)[9,75], proliferator-activated receptor γ co-activator 1α (PGC-1α)[76], frequency (FRQ)[77], white collar-1 (WC-1)[78]
Cancer development-associated functioning	Bid[9,79], β-catenin[80], axin[15], dishevelled (Dvl)[15], adenomatous polyposis coli (APC)[81], dapper1a (Dpr1a)[82], full-length cubitus interruptus (Ci-155)[83], yes-associated protein (YAP)[84], sprouty2 (SPRY2)[85], fat[86], neural precursor cell expressed developmentally down-regulated protein 4 (NEDD4)[87], metastasis suppressor 1 (MTSS1)[88], nucleoside diphosphate kinase A (nm23-H1)[89], deoxycytidine kinase (dCK)[90]
Viral proteins	Simian virus 40 large T-antigen (SV40 T-Ag)[91], human herpes virus (HHV) E3 ubiquitin ligase (ICP0)[92], human cytomegalovirus phosphoprotein (ppUL44)[93]
Various receptor- and second messenger-related proteins	Estrogen receptor α (ERα)[94], amplified in breast cancer 1 (AIB1)[94], adiponectin[95], transmembrane tumor necrosis factor α (mTNFα)[96], dopamine- and cAMP-regulated neuronal phosphoprotein (DARPP-32)[97,98]

1.2.3 Regulation of CK1δ Activity

Given its ubiquitous expression and the large number of substrates, a tight regulation of constitutively active and second messenger independent CK1δ seems mandatory, even though CK1 family members were thought for many years to be lacking any regulatory mechanisms[99]. Of course, upstream protein kinases and phosphatases are indirectly regulating CK1δ-mediated phosphorylation of certain substrates by adding or removing phosphate moieties and hence creating or eliminating consensus phosphorylation motifs. Cyclic AMP-dependent protein kinase A (PKA) has e.g. been reported to prime substrates for subsequent phosphorylation by CK1δ[78]. Besides this indirect regulation, direct mechanisms have been identified to affect CK1δ activity: regulation of *CK1δ* expression, subcellular localization, protein-protein interactions, and post-translational modification.

Regulation of *CK1δ* Expression

CK1δ appears ubiquitously expressed, but expression levels vary in adjustment to its respective physiological function in different tissues, organs, and cell types[100]. Consequently, expression levels rely to some extend on cellular circumstances and can be adapted in stress response, e.g. upon stimulation by viral transformation[101] or DNA-damaging effectors like topoisomerase inhibitors etoposide and camptothecin or γ-irradiation[37,53]. Appropriate observations exhibited increased levels of *CK1δ* mRNA and protein as reaction to induction of p53 *in vivo*[37]. Gastrin[62], adiponectin[95], and presumably insulin[102] have been linked to elevated *CK1δ* expression levels as well.

Subcellular Localization and Protein-Protein Interactions

At protein level CK1δ is distributed between nucleus and cytoplasm and it is even covalently attached or stably associated to (plasma) membranes, cytoskeleton proteins, receptors, and diverse nuclear and cytosolic factors[11,100]. This spatial sequestration appears both permanent and temporary: permanent, as mammalian CK1δ is predominantly cytosolic, especially enriched at the Golgi apparatus and the endoplasmic reticulum (ER); and temporary, as it colocalizes with the centrosome in interphase and spindle poles in mitosis[103]. While nucleocytoplasmic shuttling is often explained by the NLS, gastrin has also been reported to enhance nuclear accumulation of CK1δ, potentially by activating the cholecystokinin 2 receptor (CCK2R)[62]. The majority of spatial and temporal subcellular organization, however, is reportedly achieved by scaffold proteins that

mediate sequestration and anchorage of CK1δ to organelles and membranes or assembly of functional complexes (**Figure 7**)[9,104]. Anchorage of CK1δ to organelles and membranes is e.g. mediated by the A-kinase anchoring protein 450 (AKAP450) which recruits CK1δ and CK1ε in an isoform-specific manner and tethers them to centrosome and Golgi apparatus without affecting substrate interaction[105]. Although AKAP450 is necessary for Golgi targeting of both isoforms and localization of isoform ε at the centrosome, the latter does not apply to isoform δ. CK1δ possesses a centrosomal localization signal (CLS) comprising several residues between positions 278 and 364 within its C-terminus[106]. DEAD-box RNA-helicase 3 (DDX3) is recruited to CK1δ/ε upon Wnt-activation and stimulates phosphorylation of dishevelled (Dvl) by acting as an allosteric activator of CK1[107]. Other scaffold proteins like EB1 direct proper positioning of complexes[33] or isoform-specifically inhibit CK1δ activity such as dysbindin paralog CK1-binding protein (CK1BP) in human brain[108]. In other cases complex formation is required for translocation to the nucleus (**Figure 7**)[13].

Although scaffolding proteins interact with CK1δ and CK1ε kinase domains, as shown by the use of C-terminal truncation mutants, and although they are often phosphorylated during the process (e.g. DDX3, EB1, CK1BP, CRY, PER), they are not necessarily CK1 substrates (e.g. AKAP450)[33,105,108]. Consequently, scaffold proteins represent important regulatory mechanisms by dynamically recruiting (and sometimes inhibiting) specific isoforms upon need and selectively creating and channeling access to certain substrates. In addition, they provide another level of regulation as they are tightly regulated themselves[104,105].

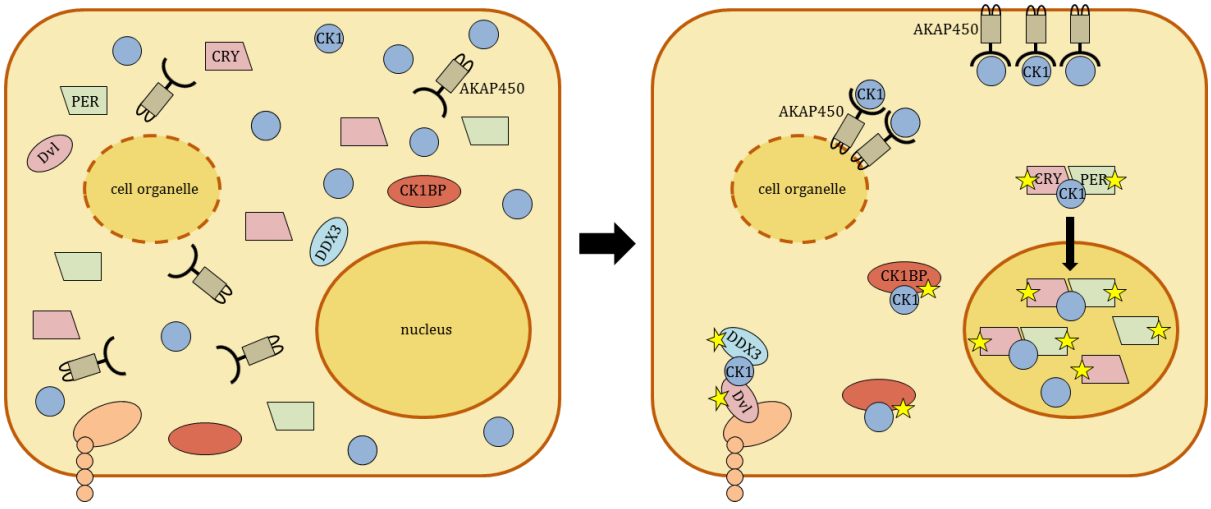

Figure 7 | Scaffold protein-mediated subcellular spatial organization. AKAP450 anchors CK1δ/ε to membranes and organelles, DDX3 binds CK1δ/ε and promotes Dvl phosphorylation, CRY-PER-CK1δ/ε complexes translocate to the nucleus, CK1BP binds and inhibits CK1δ. Phosphorylation is represented by yellow stars. The figure is adapted from Good *et al.*[104].

Additionally, crystallographic studies of CK1δ revealed the formation of homodimers which is suggested to provide another negative regulatory mechanism *in vivo* as intermolecular interaction of the dimerization domains accounts for exclusion of ATP from the catalytic cleft (**Figure 8**)[21].

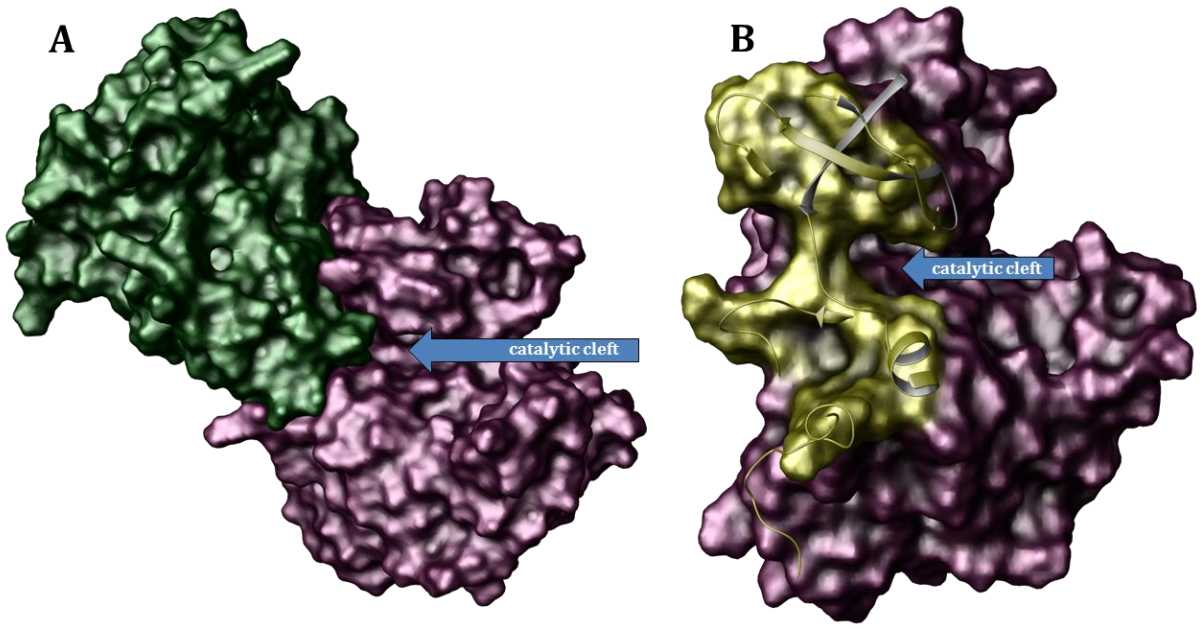

Figure 8 | Homodimerization of CK1δ. Monomers 1 (purple) and 2 (green) form dimers via interaction of their dimerization domains (A). The dimerization domain (yellow) includes various amino acid residues of strands β1, β2, β3, and β7 as well as loops L-12 and L-78, helix αB, and the hinge region (B, PDB code 4HGT[22]).

Post-translational Modification

Reversible phosphorylation represents the major mechanism in post-translational modification of CK1δ, either by intramolecular autophosphorylation or phosphorylation by other protein kinases. Studies using CK1δ truncation mutants identified six potential autophosphorylation sites within an inhibitory C-terminal domain (**Figure 9 B**), although not all of them seem to influence kinase activity. Autophosphorylation of Ser318, Thr323, Thr329, Ser331, and Thr337, but not Ser328 generates sequence motifs summarized as Ser(P)/Thr(P)-X-X-Y that might act as pseudosubstrates and inhibit kinase activity, with Y being any amino acid except Ser/Thr[109].

Besides autophosphorylation, cAMP-dependent protein kinase (PKA), protein kinase C α (PKCα), checkpoint kinase 1 (Chk1), cyclin E-activated cyclin-dependent kinase 2 (Cdk2/E), and p35-activated cyclin-dependent kinase 5 (Cdk5/p35), as well as protein kinase B (Akt) and CDC-like kinase 2 (CLK2) have been identified to participate in regulatory phosphorylation within the

C-terminal region of CK1δ[110–113]. Site-directed phosphorylation by all of these kinases led to decreased CK1δ kinase activity. Among these, PKA has to be considered as the main cellular kinase targeting predominantly Ser370 *in vitro* and *in vivo*[110]. Colocalization of PKA and CK1δ is achieved by AKAP450-mediated anchorage to the centrosome (**Figure 9 C**)[110]. Interestingly, Ser370 which has not been defined as an autophosphorylation site is also a target for PKCα, Chk1, Akt, and CLK2. PKCα and Chk1, however, additionally phosphorylate residues which certainly do represent autophosphorylation sites[110–112]. Dephosphorylation by various Ser/Thr-specific protein phosphatases and cleavage of the C-terminus are mechanisms to overcome inhibitory phosphorylation within the C-terminal region. While multiple phosphatases are believed to be capable of activating CK1δ, only the catalytic subunit of protein phosphatase 1 ($PP1_C$) has been characterized in this context[109]. $PP1_C$ has also been outlined as an AKAP substrate, though not AKAP450, suggesting a colocalization of CK1δ, $PP1_C$, and PKA (**Figure 9 C**)[114]. Interestingly, inhibitor-2 of $PP1_C$ is phosphorylated by CK1, CK2, and glycogen synthase kinase 3 (GSK-3) leading to activation of $PP1_C$, even though the exact CK1 isoform has not been defined (**Figure 9 A**)[115].

Although not a proper post-translational modification, heparin has been reported to activate only full length CK1δ *in vitro*, presumably by interaction with the partially positively charged C-terminus which was prohibited by preincubation of CK1δ with $PP1_C$ or C-terminal truncation. Heparin is unlikely to represent a physiological regulator of CK1δ, but interaction of regulatory compounds with the C-terminus imitating dephosphorylation can be deemed possible (**Figure 9 A**)[19,116].

Apart from phosphorylation events, CK1δ levels are controlled by the anaphase-promoting complex/cyclosome (APC/C^{Cdh1}) during cell cycle exit in the developing cerebellum. APC/C activator protein cadherin 1 (Cdh1) isoform-specifically targets CK1δ for ubiquitination by the ubiquitin E3-ligase complex APC/C and subsequent degradation (**Figure 9 A**)[117].

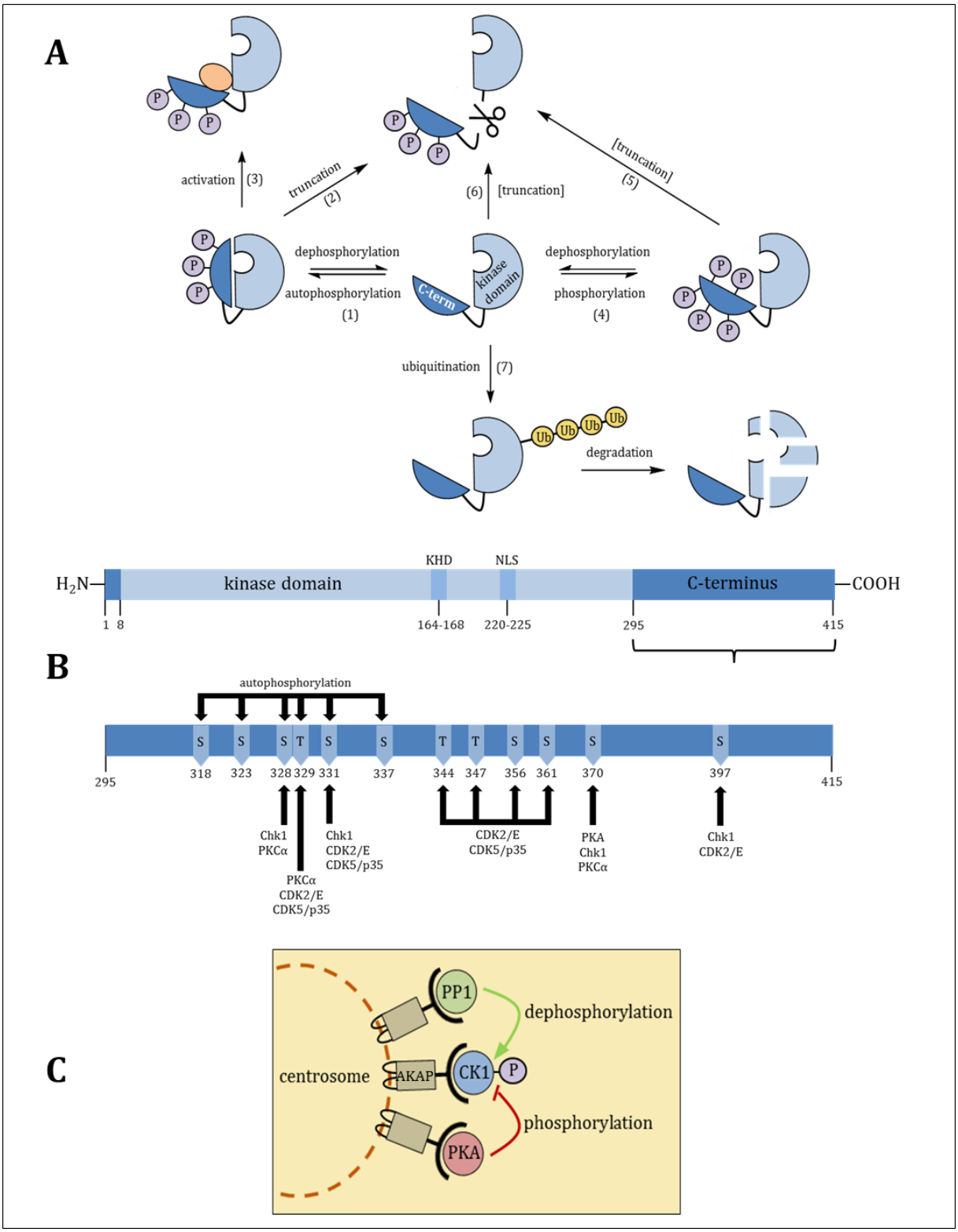

Figure 9 | Post-translational regulation of CK1δ. Mechanisms of post-translational regulation (A): inactivation by C-terminal autophosphorylation (1) or phosphorylation by other kinases (4) and subsequent activation by phosphatases (1, 4 *vice versa*), C-term truncation (2, 5) or interaction with activator molecules (3). Truncation is also imaginable without previous phosphorylation (6). CK1δ is marked for degradation by ubiquitination (7). Brackets indicate insufficient evidence. Phosphorylation sites within the CK1δ TV1 C-terminal domain (B, adapted from KNIPPSCHILD *et al.*[9]). Colocalization of CK1δ, PKA, and PP1C is mediated by AKAPs (C)[109–117].

1.2.4 Physiological and Pathophysiological Relevance of CK1δ

CK1δ-mediated regulatory activity is associated with numerous physiological and pathophysiological processes. Many of these represent responding to situations of cellular stress: in *Saccharomyces cerevisiae* yeast CK1δ homologue Hrr25 is directly involved in DNA repair mechanisms[11–13] and human CK1δ is upregulated through its connection to p53 in an autoregulatory feedback loop[9,37]. Upon DNA damage-activated p53 binds to a p53 response element within *CSNK1D* and initiates transcription. Tumor suppressor p53 is phosphorylated by CK1δ (and CK1ε) at several sites in order to preserve genomic integrity by inducing either cell cycle arrest or apoptosis. CK1δ/ε-mediated phosphorylation at Ser15 and Thr18 stabilizes and activates p53 by diminishing interaction with its inhibitory counterpart mouse double minute 2 homolog (MDM2). Interestingly, MDM2 is targeted by CK1δ as well and phosphorylation can either lead to enhanced binding of MDM2 to p53 with subsequent degradation of p53 in unstressed cells or prepare MDM2 for ubiquitination and proteolysis[9,38]. CK1δ is also suggested to negatively regulate p53 by forming complexes with MDM2 under non-stress conditions[118]. Under hypoxic conditions activation of p53 is initiated by transcriptional activator hypoxia-inducible factor 1α (HIF-1α) which promotes cell survival under these circumstances and is negatively regulated by CK1δ[9,12]. In addition, CK1δ influences cellular processes such as DNA transcription and methylation[40–42,70], translation (ribosomal assembly and biogenesis)[43,47–49], mitosis and meiosis[50–52], and signal transduction[94–96]. CK1δ-mediated regulation and disorder in cytoskeleton-associated processes, circadian rhythm, and development of cancer are discussed in detail below. CK1δ further phosphorylates various viral proteins, thereby playing a role in parasites infection[91–93]. Pathogenic phosphorylation of TAR DNA-binding protein of 43 kDa (TDP-43) has been associated with upregulated CK1δ activity in amyotrophic lateral sclerosis (ALS)[119]. Naturally, complete coverage of physiological or pathophysiological CK1δ-mediated processes is not given and research continuously increases the understanding of the roles of CK1δ in health and disease.

Cytoskeleton-associated Functions and Alzheimer's Disease

Protein kinase CK1δ activity has repeatedly been highlighted to be essential for accurate cell cycle progression, cytokinesis, and vesicular trafficking[53,54,120]. In interphase cells CK1δ associates with membrane structures of the trans Golgi network (TGN) where it presumably holds regulatory tasks in the budding of clathrin-coated vesicles. Furthermore, a general role in vesicular trafficking has been suggested: CK1δ interacts with and phosphorylates the soluble SNARE[j]-associated protein snapin[53,61]. Supporting observations proved yeast CK1δ homologue

[j] *N*-ethylmaleimide-sensitive fusion protein attachment protein receptor (SNARE)

Hrr25 involvement in vesicle budding from the endoplasmic reticulum[121]. Besides TGN membranes CK1δ localizes with microtubules and centrosomes suggesting participation in microtubule-mediated transport processes, as CK1δ kinase domain is known to contain a KHD[20,53]. During mitosis CK1δ shows enhanced affinity for tubulins in response to genotoxic stress exposure. It is therefore increasingly recruited to mitotic spindles and centrosomes, likely in the meaning of a mitotic checkpoint signal to assure ordered rearrangement of the microtubule network and chromosome segragation[53,54]. Phosphorylation of α- and β-tubulins by CK1δ directly modulates microtubule dynamics, while CK1δ-mediated phosphorylation of microtubule-associated proteins 1A (MAP1A)[31], 4 (MAP4)[53], γ-tubulin[9,53,54], and tau[29,53,55], as well as stathmin and the Ran-binding protein in the microtubule organization center (RanBPM)[56], influences microtubule assembly, disassembly, and stability[53]. Consequently, inhibition of CK1δ leads to p53-dependent cell cycle arrest or apoptosis, depending on the cell line in question[54,120]. Retardation of cytokinesis also occurs upon CK1δ-mediated phosphorylation and subsequent ubiquitination and degradation of Sid4[59].

Centrosomal functions of CK1δ include neurite outgrowth and ciliogenesis. While neuritogenesis requires Wnt3a-dependent and centrosomal CK1δ-mediated Dvl phosphorylation[106], formation of primary cilia presumably comprises regulation of microtubule networks and ciliary distribution of effector proteins. In addition, ciliogenesis also relies on AKAP450-mediated microtubule nucleation at the Golgi, Golgi organization, and vesicular trafficking. Therefore, direct interaction of CK1δ and the anchoring protein has been reported to be crucial for coordination of AKAP450-dependent Golgi positioning[122]. In contrast, CK1δ might also play a role in Wnt5a-induced primary cilia disassembly by contributing to Dvl2 phosphorylation, although its participation remains somewhat uncertain and CK1ε has been shown to be the predominant centrosomal kinase in this case[123].

During T-cell activation CK1δ manages centrosome translocation to the immunological synapse by increasing microtubule growth speed and stabilization via binding and phosphorylation of EB1[33]. By the way, EB1 has also been found to serve in ciliogenesis, though direct association with CK1δ has not been reported in this context[124].

Apart from physiological events, microtubule-associated phosphorylation by CK1δ is closely connected with neurodegenerative disorders and especially with the pathogenesis of Alzheimer's disease (AD). AD is characterized by the appearance of neurofibrillary tangles of accumulated tau protein and senile neuritic plaques, eventually causing neurons to die. CK1δ is upregulated more than 30-fold in AD brain, leading to pathological hyperphosphorylation of tau and subsequent microtubule destabilization and tau fibrillization[55,125,126]. Furthermore, CK1δ acts as a priming kinase for GSK-3β-mediated tau phosphorylation and activates cyclin-

dependent kinase 5 (Cdk5), another kinase participating in phosphorylation of tau[66,127]. Sequential cleavage of the amyloid-β precursor protein (βAPP) by proteases β-secretase and presenilin-dependent γ-secretase yields the neurotoxic peptide amyloid-β that is the main component of senile plaques. Both proteases are to a certain degree CK1δ-regulated as β-secretase and presenilin-2 represent known targets[64,65]. Amyloid-β in turn has been reported to stimulate CK1 activity, suggesting a vicious circle that might explain the progressive character of the disease[128].

Besides its AD participation CK1δ phosphorylates α-synuclein and parkin, both key determinants in the pathogenesis of Parkinson's disease[67,68].

CK1δ in Circadian Rhythm and its Connection to FASPS

Numerous physiological processes are subject to time of day-dependent regulation. Besides external effectors such as light, temperature, and food biochemical activity within every cell is regulated by an autonomous circadian clock. This intracellular timer consists of transcriptional activators and repressors that reciprocally regulate their own expression in an oscillating system[129]: heterodimers of brain and muscle ARNT-like protein (BMAL1) or neuronal PAS domain protein 2 (NPAS2) and CLOCK initiate transcription of *Period* (*PER1-3*), *Cryptochrome* (*CRY1/2*), and *REV-ERBα* genes. Furthermore, cytoplasmic PER levels are controlled by reversible CK1δ/ε-mediated phosphorylation, followed by degradation. Proteasomal digestion is avoided by the formation of CRY-PER complexes that bind CK1δ/ε and translocate to the nucleus where they repress transcription of BMAL1-CLOCK target genes[9,129,130].

About 10 % of all genes are under control of this circadian autoregulatory feedback loop. Among them are of course regulators of the cell cycle such as *Wee1*, encoding a tyrosine kinase that inhibits mitotic entry and is degraded in the course of CK1δ-mediated phosphorylation[50,129]. PGC-1α is activated upon nutritional signals and coordinates circadian metabolic processes by cross-activation of circadian (*BMAL1*, *REV-ERBα*) and metabolic gene expression[76,131]. CK1δ-mediated phosphorylation represses transcriptional activity of PGC-1α and initiates its degradation[76]. Additionally, circadian proteins are important regulators responding to oxidative stress. BMAL1, for instance, is a regulator of p53-induced cell cycle arrest upon DNA-damage and PER proteins possess tumor suppressor capacity[9,132–135].

CK1 isoforms δ and ε are central effectors in the regulation of circadian proteins. Stability and subcellular localization of PER proteins are regulated by the interplay of reversible phosphorylation and dephosphorylation by CK1δ/ε and PP1, leading to alteration of the length of circadian cycles[73,136]. Interestingly, even though CK1δ and CK1ε have often been considered

redundant in this context, CK1δ might possess a predominant position because absence of CK1δ - but not CK1ε - has been reported to significantly lengthen circadian periods in mice[74]. This observation is supported by investigations from zebrafish that prove CK1δ to be crucial for circadian timing, whereas CK1ε is only of minor importance[137]. Another modulator of period length that is differently affected by CK1δ and CK1ε is enhancer box (E-box) repressor prohibitin 2 (PHB2). Although the exact mechanism remains uncertain, knockdown of *CK1δ* decreases *PHB2* mRNA and conversely, knockdown of *CK1ε* has been reported to increase PHB2 protein level[138]. BMAL1, CRY1, and CRY2 are phosphorylated by CK1δ and CK1ε in a redundant manner. But while BMAL1, PER1, and PER2 are subject to direct phosphorylation, CRY proteins and PER3 are dependent on PER1 or PER2 acting as scaffold proteins. Consequently, PER-CRY complexes bind CK1δ/ε and translocate CRY-mediated to the nucleus[75,139].

Taken together, it is not surprising that alterations such as mutation and misregulation within this network are closely associated with sleeping disorders and even tumorigenesis, as well as cardiovascular and metabolic disorders[76,129]. The most prominent among sleeping disorders is probably familial advanced sleep phase syndrome (FASPS) which is characterized by early evening onset of sleep, early morning awakening, and a shortened circadian period. FASPS is caused by mutation either within the CK1-binding domain of human *PER2* or the catalytic domain of *CSNK1δ* (T44A mutation), the latter expressing proteins with decreased catalytic activity[140]. In addition, circadian rhythm disruptions are generally connected to bipolar subjects and have been discussed as starting point for pharmacological intervention in this context[141].

CK1δ-associated Functions in the Development of Cancer

Tumorigenesis is generally related to pathological changes due to mutation or misregulation in various signaling pathways with the result of independently proliferating and often highly resistant cancer cells. Especially participation of CK1δ in pathways referring to cell proliferation, genomic integrity, and the regulation of key modulator proteins in stress situations such as p53, MDM2, and β-catenin support the oncogenic importance of this protein kinase. Consequently, mutation of either CK1δ itself or phosphorylation sites of CK1δ-targeted substrates contributes to cancerogenesis. For instance, a gain-of-function mutation within the autoregulatory C-terminal domain of CK1δ (R324H), though without affecting autophosphorylation, has been identified in an adenomatous colorectal polyp[142]. Furthermore, different mutations affecting ATP-binding affinity in different tumor entities lead to either elevated or reduced catalytic activity with variable influence on tumor growth and oncogenic potential[143,144]. CK1δ mutations identified in various tumors are summarized in **Table 2**.

Table 2 | CK1δ mutants in different tumor entities. The structural domain comprising the point mutation(s) is given in parentheses. P66T, R69K refers to a double mutant.

Mutation	Consequence	Tumor entity
R324H (autoregulatory C-term)	Gain of function	Adenomatous colorectal polyp[142]
T67S (ATP-bind. domain)	Increased catalytic activity	Colorectal cancer[143]
I68N (ATP-bind. domain)	Decreased catalytic activity	Colorectal cancer[143]
P66T, R69K (ATP-bind. domain)	Decreased catalytic activity	Colorectal cancer[143]
S97C (ATP-bind. domain)	Decreased ATP-bind. affinity	Breast cancer, ductal carcinoma[144]

Alterations in the expression of *CK1δ* have been described for various human tumors (**Table 3**) whereas the effect of up- or downregulation strongly depends on the tissue-based cellular background and tumor entity. Interestingly, while decreased expression of *CK1δ* is associated with prolonged survival of patients with colorectal cancer, the same applies to elevated expression levels in several forms of breast cancer, leukemia, and glioma[145,146]. In many cases it is worth mentioning that it remains unknown whether the alteration in *CK1δ* levels represent cause or consequence of oncogenic events[145].

Table 3 | CK1δ misregulation in different tumor entities. Increase and/or decrease primarily refer to *CK1δ* mRNA, although this is predominantly in accordance with up-/downregulation on protein level. In cases of *altered expression* the reference did not specify levels compared to healthy tissue. *Reduced immunostaining* has not been specified as well.

Misregulation	Tumor entity
Increased expression	Chorioncarcinomas[120]
Increased expression	High-grade pancreatic ductal adenocarcinomas[147]
Decreased expression	Lymphoid neoplasms[148]
Increased expression	Breast tumors[149]
Altered expression	Colorectal cancer[146]
Reduced immunostaining	Ductal carcinomas *in situ*, invasive breast carcinomas[13]
Increased expression	Tumors of bladder, brain, kidney, lung, melanoma, ovarian, pancreatic, prostate, and hematopoietic system[145]

In addition to p53-related participation in apoptotic pathways CK1δ-mediated phosphorylation of Bid prevents cleavage by caspase 8 and therefore inhibits Fas-mediated apoptosis[79]. The anti-apoptotic potential is of particular importance because resistance to apoptosis is crucial for various human tumors. Consequently, inhibition of CK1δ/ε has been reported to reduce pancreatic tumor growth effectively and to enhance the amount of dead cancer cells by re-sensitization for

Fas-induced apoptosis[147]. Besides, this provides evidence that CK1δ/ε are jointly responsible for aberrant proliferation[147]. The Wingless/Int-1 (Wnt) and β-catenin, Hedgehog (Hh), and Hippo signaling pathways are further CK1δ-dependent cascades contributing to tissue development, growth, and homeostasis. Mutations in regulatory mediators as well as aberrant activation of these pathways are frequently associated with the development of various human cancers[9,150].

In Wnt/β-catenin signaling CK1 isoforms synergistically perform positive and negative regulatory functions. Without pathway activation cytoplasmic β-catenin is regulated by β-catenin destruction complexes consisting of Axin, adenomatous polyposis coli (APC), GSK-3β, and CK1 isoforms α, δ, and ε. Axin acts as a scaffold and directly binds the components of the complex. CK1δ and GSK-3β, presumably supported by CK1ε, phosphorylate APC in order to increase binding affinity of APC towards β-catenin and thus promote β-catenin recruitment to the complex. Bound β-catenin is phosphorylated by CK1α, thereby primed for GSK-3β-mediated phosphorylation and subsequent ubiquitination (β-Trcp E3 ligase) and proteasomal degradation. Upon pathway stimulation, binding of Wnt ligand to transmembrane receptors Frizzled and low-density lipoprotein receptor-related protein 5 or 6 (LRP5/6) is followed by binding of dishevelled (Dvl) to Frizzled and consecutive phosphorylation (CK1γ1) and activation of LRP5/6. Subsequent recruitment of the destruction complex implies inhibition of GSK-3β. Axin and Dvl phosphorylation by CK1δ/ε, catalyzed by Wnt-activated DDX3, promotes GSK-3β inhibition and induces conformational changes and destruction complex dissociation. Finally, β-catenin degradation is prevented, and accumulated β-catenin translocates to the nucleus where it binds T-cell factor/lymphoid enhancer factor (TCF/LEF) and initiates transcription of target genes. Additionally, CK1δ-mediated phosphorylation of dapper 1a (Dpr1a) disrupts the inhibitory interaction of Dpr1a and Dvl and therefore activates Wnt signaling[9,15,151].

The role of CK1δ in both Hh and Hippo signaling is of negative regulatory nature: consecutive phosphorylation of full-length cubitus interruptus (Ci-155), the *Drosophila melanogaster* homolog of human glioma-associated oncogene transcription factors 2 and 3, by CK1δ and GSK-3 triggers proteolysis and inhibits Hh target gene transcription. In the Hippo pathway, phosphorylation of transcriptional co-activator Yes-associated protein (YAP) by large tumor suppressor kinase (LATS) primes for CK1δ-mediated phosphorylation and subsequent ubiquitination (β-Trcp E3 ligase) and degradation. So in this case, too, target gene transcription is prohibited[9].

Finally, the involvement of CK1δ-dependent phosphorylation in regulation of tumor suppressors sprouty 2 (SPRY2)[85] and Fat (*Drosophila melanogaster* homolog of human FAT)[86], as well as metastasis suppressors MTSS1 (metastasis suppressor 1)[88] and nucleoside diphosphate kinase A (nm23-H1)[89], confirms the oncogenic potential of CK1δ and underlines the protein kinase as an interesting drug target for cancer treatment.

1.3 Kinase Inhibitors

The eminent position of phosphorylation events in cellular signaling and the high prevalence of kinase-associated mutation and dysregulation in development and progression of serious diseases have already made protein kinases the most pursued drug targets in pharmaceutical research of the twenty-first century[7]. Since kinase research has predominantly been concentrated on cancer treatment, now inflammation, central nervous system disorders, and cardiovascular or diabetic complications are getting into the center of attention as well[7,152]. Currently, more than 20 small molecule kinase inhibitors (smKI) in clinical trials and plenty more potential modulators at the preclinical stage are tested for these indications[152].

Back in the early 1980s, isoquinoline sulfonamide derivatives were characterized as the first generation of smKI that blocked kinase activity in an ATP-competitive manner. Pharmaceutical research virtually kicked off with the identification of *Streptomyces staurosporeus*-isolated bisindolyl maleimide staurosporine as the first nanomolar, but still highly non-selective kinase inhibitor in 1986[153].Although non-selective and of relatively low potency, fasudil hydrochloride progressed to clinical trials for the treatment of cerebral vasospasm and became the first approved (Japan) smKI in 1995[153]. Discouragement soon took possession of research communities as selective inhibition of protein kinases was regarded impossible due to the highly conserved ATP-binding site. Fortunately this was proved wrong in 1991 when *Streptomyces hygroscopius* agent rapamycin was shown to selectively prevent activity of mammalian target of rapamycin (mTOR)[7,153,154].

The breakthrough of smKI in clinical use came 2001 with the FDA-approval of imatinib (Gleevec®). ATP-competitive tyrosine-kinase inhibitor imatinib effectively inhibits Bcr-Abl (breakpoint cluster region-Abelson tyrosine kinase) fusion protein and represented a milestone in targeted cancer therapy[7]. In the course of this achievement additional eight kinase inhibitors entered clinical use until 2009 and the remarkable number of further 19 smKI has been established in therapy since 2011. Intense efforts have afforded more than one million publications, 5000 crystal structures, and multiple inhibition assays targeting more than four-fifth of the human kinome, leading to the FDA-approval of 28 low-molecular kinase inhibitors and three rapalogs to date (status January 2016, **Table 4**)[7,152].

Table 4 | FDA-approved small molecule kinase inhibitors as of January 2016. FDA-approval refers only to the first date of authorization. More than three targets for a single inhibitor are referred to as *multiple*. Ser/Thr kinase (1), tyrosine kinase (2), lipid kinase (3) smKI, rapalogs (4)[6,7,152,155–158]. For explanation of types I to V cp. **chapter 1.3.1**. Abbreviations: INN, international nonproprietary name; ALL, acute lymphoblastic leukemia; AMD, age-related macula degeneration; B-Raf^{V600}, B-Raf V600 mutant; CLL, chronic lymphocytic leukemia; CML, chronic myelogenous leukemia; CRC, colorectal cancer; FL, follicular lymphoma; GIST, gastrointestinal stromal tumors; HCC, hepatocellular cancer; IPF, idiopathic pulmonary fibrosis; MCL, mantle cell lymphoma; MTC, medullary thyroid cancer; NSCL, non-small cell lung carcinoma; PC, pancreatic cancer; RCC, renal cell carcinoma; SEGA, subependymal giant cell astrocytoma; SLL, small lymphocytic leukemia; STS, soft-tissue sarcoma; TC, thyroid carcinoma; TP, transplantation.

	INN	Trade name	Type	Targets	Indications	FDA approval
1	Dabrafenib	Tafinlar®	I	B-Raf^{V600}	melanoma	2013
	Palbociclib	Ibrane®	I	Cdk	breast cancer	2015
	Trametinib	Mekinist®	III	MEK	melanoma	2013
	Vemurafenib	Zelboraf®	I	B-Raf^{V600}	melanoma	2011
2	Afatinib	Gilotrif®	V	EGFR, Her2	NSCLC	2013
	Axitinib	Inlyta®	I	multiple	RCC	2012
	Bosutinib	Bosulif®	I	Bcr-Abl, Src	CML	2012
	Cabozantinib	Cometriq®	II	multiple	MTC	2012
	Ceritinib	Zykadia®	I	ALK	NSCLC	2014
	Crizotinib	Xalkori®	I	ALK, ROS1, MET	NSCLC	2011
	Dasatinib	Sprycel®	I	multiple	CML, ALL	2006
	Erlotinib	Tarceva®	I	EGFR	NSCLC, PC	2004
	Gefitinib	Iressa®	I	EGFR	NSCLC	2003
	Ibrutinib	Imbruvica®	V	BTK	MCL, CLL	2013
	Imatinib	Gleevec®	II	multiple	CML, GIST, ALL	2001
	Lapatinib	Tykerb®	I, II	EGFR, Her2	breast cancer	2007
	Lenvatinib	Lenvima®	I, II	multiple	TC	2015
	Nilotinib	Tasigna®	II	multiple	CML	2007
	Nintedanib	Ofev®	II	VEGFR, PDGFR, FGFR	IPF	2014
	Pazopanib	Votrient®	I	multiple	RCC, STS	2009
	Ponatinib	Iclusig®	II	multiple	CML, ALL	2012
	Regorafenib	Stivarga®	II	multiple	CRC, GIST	2012
	Ruxolitinib	Jakafi®	I	JAK	myelofibrosis	2011
	Sorafenib	Nexavar®	II	multiple	RCC, HCC, TC	2005
	Sunitinib	Sutent®	I	multiple	RCC, GIST	2006

2	Tofacitinib	Xeljanz®	I	JAK	rheumatoid arthritis	2012
	Vandetanib	Caprelsa®	I	multiple	MTC	2011
3	Idelalisib	Zydelig®	II	PI3K	CLL, FL, SLL	2014
4	Everolimus	Zortress®	IV	mTOR	TP, SEGA, RCC	2009
	Sirolimus	Rapamune®	IV	mTOR	TP, AMD	1999
	Temsirolimus	Torisel®	IV	mTOR	RCC	2007

1.3.1 Different Types of Small Molecule Kinase Inhibitors

Most kinase inhibitors, including 23 of the currently approved 28 compounds, are inhibitors of tyrosine kinases. Further four of them are inhibitors of Ser/Thr-specific kinases and idelalisib (Zydelig®) is the only one targeting a lipid kinase[7,152]. Considering binding mechanisms and structural features, smKI are subdivided into six subgroups: ATP-competitive inhibitors (Types I, II, I ½), allosteric inhibitors (Type III, IV), and covalent inhibitors (Type V)[156,159]. Several substances possess characteristics of more than one of these binding modes[7].

Type I inhibitors displace ATP from the active state of PK whereas the activation-loop resides in the so-called DFG-in conformation. Type I pharmacophores usually consist of heterocyclic systems occupying the adenine-binding region and form H-bonds with hinge residues. As this region is highly conserved within the kinome, additional side chains occupy the less conserved hydrophobic regions I and II, adjacent to the ATP-binding site[156]. Especially the non-conserved gatekeeper residue which regulates access to hydrophobic pocket I is a central determinant for the development of selective kinase inhibitors[154].

Type II inhibitors stabilize the inactive conformation of kinases. Emanating from the active state (DFG-in) the Asp residue of the DFG motif is rotated by 180° (DFG-out) and the active site is blocked for ATP[154]. Type II inhibition has therefore been called *indirectly ATP-competitive*[159]. Rearrangement of the activation-loop towards the inactive state permits access to another hydrophobic pocket (*deep pocket*) which is less conserved and provides additional prospects for kinase-specific inhibition[156].

Type II inhibitors have commonly been assumed to have an intrinsic selectivity advantage over type I binders, though binding mode analysis were unable to provide evidence for this thesis[158]. It has further been observed that, while many kinases are sensitive to type II inhibition, others appear to be incapable of adapting the inactive DFG-out conformation. In general, DFG-in/out rearrangement is especially common for tyrosine kinases[158]. Significant differences between

inhibitor binding modes I and II are based on their binding kinetics: while rapid association and dissociation is common for type I, type II exhibits slow binding kinetics and prolonged residence time[157]. In addition to type I and II binders, several inhibitors have been identified to induce conformations that are intermediate between active and inactive state[158].

Type I ½ inhibitors are recently identified intermediates of types I and II. They occupy domains between hydrophobic pocket I and deep pocket and thereby interrupt the *hydrophobic spine* (*regulatory spine*) which is essential for kinase activity[159,160]. The hydrophobic spine is a highly conserved regulatory motif which consists of four not contiguous amino acid residues that originate from different parts of the kinase. One of these residues is the conserved DFG phenylalanine (**Figure 10**). Type I ½ inhibitors are suggested to bind both DFG-in and DFG-out conformation[159].

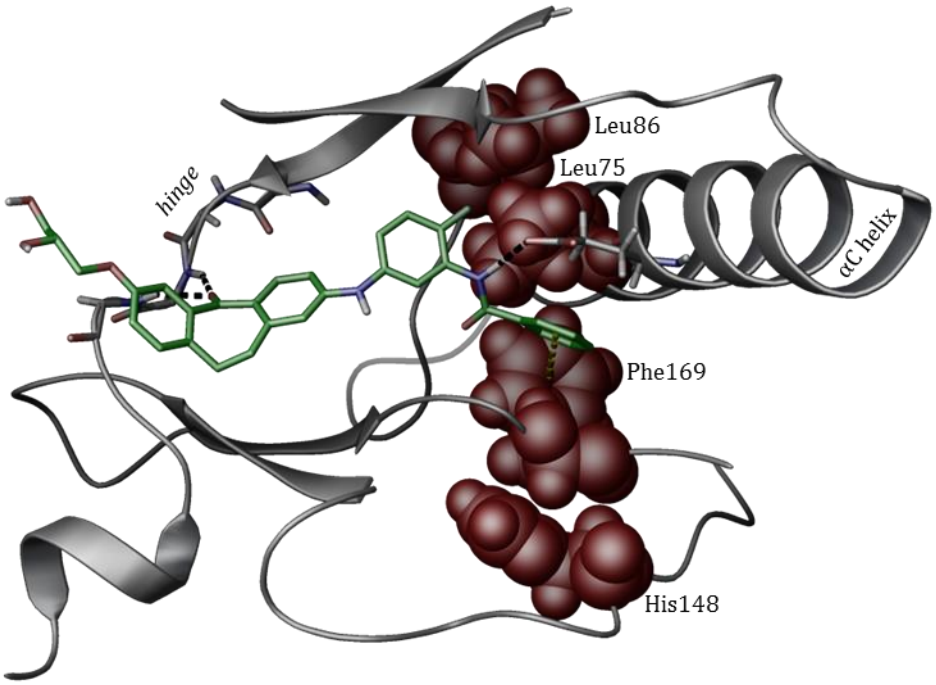

Figure 10 | Interruption of the hydrophobic spine by type I ½ inhibitors on the example of dibenzosuberone derivative 1 in p38α mitogen-activated protein kinase. Binding of the inhibitor (green) interrupts the hydrophobic spine (red). H-bonds (black dashed lines) are formed towards hinge and αC-helix. Hydrophobic interaction (yellow dashed line) accommodates DFG Phe169. Dibenzosuberone derivative **1** refers to (*S*)-*N*-(5-((7-(2,3-dihydroxypropoxy)-5-oxo-10,11-dihydro-5*H*-dibenzo[*a*,*d*][7]annulen-2-yl)amino)-2-fluorophenyl)benzamide (**1**) by FISCHER *et al*. The figure was modeled in accordance to the same publication (PDB code 3UVQ)[161].

Although the majority of reported smKI inhibit target kinases in an ATP-competitive, often type I-dependent manner, and although several highly selective probes have been achieved, the evolutionary conservation of the ATP-binding site favors off-target effects[7]. ATP-competitive

inhibitors also require particular high affinity and good bioavailability to compete with nucleotides *in vivo* (2-10 mM)[153,159]. Intense efforts are therefore invested in the development of ATP non-competitive approaches:

Allosteric inhibitors bind outside the ATP-binding site and induce conformational changes that negatively modulate kinase activity. The allosteric site can either be adjacent to (Type III) or remote from the ATP-binding pocket (Type IV)[7]. These binding sites are often unique to single kinases and type III and IV binders thereby tend to the highest degrees of selectivity known for smKI so far[156]. Especially the substrate-binding site is assumed to exhibit enormous potential as an allosteric site[153,154]. At the moment, trametinib (Mekinist®) is the only type III inhibitor in the market and, except of rapamycin derivatives, not a single type IV binder has been approved to date[154].

Covalent inhibitors (Type V) irreversibly bind to the active site of target kinases. Electrophilic moieties of the inhibitor react with nucleophilic cysteine residues in a MICHAEL addition and are therefore covalently attached to the ATP-binding pocket[7,156]. This type of inhibition is suggested to achieve increased specificity and potency, but concerns have been raised about possible toxicity[7,156]. With afatinib (Gilotrif®, **2 Figure 11**) and ibrutinib (Imbruvica®) two covalent inhibitors have already entered clinical use in 2013[7,152].

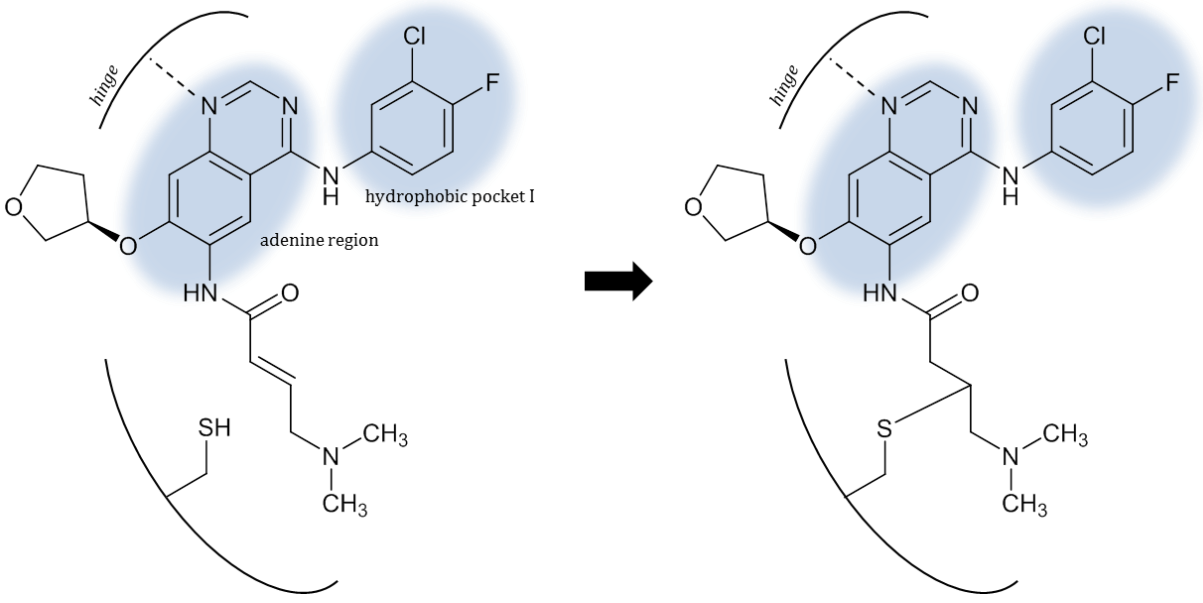

Figure 11 | Binding mode of irreversible type V inhibitor afatinib. Afatinib (**2**) displays a type I binding mode: the quinazoline core occupies the adenine-binding region and forms an H-bond towards a hinge residue. The halogen-substituted phenyl moiety extends into *HPI*. But unlike type I inhibition, the enone moiety reacts with a nucleophilic cysteine residue in a MICHAEL addition and covalently attaches the ligand to the active site of epidermal growth factor receptor (EGFR)[7].

1.3.2 Limitations and Challenges of Small Molecule Kinase Inhibitors

Despite tremendous achievements in kinase-concerning drug discovery over the past years, several challenges and limitations remain to be solved. The majority of current smKI were identified by high throughput screening or based on previously approved therapeutics using fragment-based approaches such as analogue synthesis, isosteric replacement, or compound hybridization. Consequently, many smKI possess structural similarity and concentrate on a small subset of the human kinome. Among the currently available kinase inhibitors all but two have been developed for cancer treatment[7,156]. In fact, only 10-15 % of the human kinome are covered by approved inhibitors[155]. Given the fact that most of the approved smKI are type I, accompanied by several type II and I ½, and only one type III, but not a single type IV binder, suitable assay and model systems are required to identify allosteric sites and inactive conformations[2,154]. Even in the case of type I inhibition, high throughput screening-based approaches are becoming less effective, due to the restricted availability of scaffolds from compound libraries. Innovative structures and screening methods will soon become urgently needed[7].

Therapeutic application is often limited by rapidly evolving resistances and severe side effects[7]. Point mutations within the Bcr-Abl kinase domain, for instance, make cancer cells resistant to imatinib treatment[7]. Especially mutation of the gatekeeper residue is a common event in drug resistance mechanisms[7,154]. Apart from second line kinase inhibitors which inhibit already resistant PK, irreversible type V inhibitors are assumed beneficial in this context. Multitarget kinase inhibitors that block multiple signaling cascades and combined application of different smKI are also suggested to prevent resistance development as tumors are known to dynamically adapt to the disturbance by single (target) inhibitors[6,7,162]. Additionally, tumors represent heterogeneous masses consisting of different cancer cell populations that can be traced back to different aberrant signaling pathways. Thus, specific inhibition might not be capable of effectively stemming tumor growth and even select for drug resistant cells[6,163]. On the contrary, ZHANG *et al.* have postulated that "it is forbiddingly dangerous to welcome promiscuous compounds […] without a rational strategy to control their specificity and therapeutic index"[164].

In summarization, the above emphasizes the increasing importance of personalized medicine and genetic profiling[6]. Controlling the balance between selectivity and beneficial effects of promiscuous drugs seems inevitable for reasonable clinical use of small molecule kinase inhibitors[164,165]. Furthermore, unexpected toxicity and poor solubility or bioavailability often abrogate therapeutic use during preclinical and clinical stages[156,162].

1.3.3 CK1δ Inhibitors

The involvement of CK1δ in the pathogenesis of severe disorders such as Alzheimer's disease, amyotrophic lateral sclerosis, FASPS, and cancer has dramatically increased interest in small molecule inhibitors for therapeutic application[9,119,166]. Unfortunately, the design of suitable compounds proves highly complicated due to the existence of several CK1 isoforms that possess similar, different, or even opposite physiological and pathophysiological implications[166]. Especially the highly conserved CK1 isoforms δ and ε remain difficult to discriminate and have therefore often been reported as redundant, rather by means of missing evidence. Consequently, only a relatively small subset of CK1δ inhibitors has been reported so far and not a single representative reached clinical stages[166]. Most of these small molecules, if not all of them, represent ATP-competitive type I inhibitors[9], although it has to be noted that it remains unknown whether the kinase is even able to adopt an inactive DFG-out conformation. Regrettably, the comparison of these compounds proves difficult because their half maximal inhibitory concentrations (IC_{50}) have been determined at different ATP concentrations and, in some cases, have not been assigned to distinct isoforms. Allosteric inhibitors (type III) have not been reported so far and covalent inhibition seems unlikely due to the absence of addressable cysteine residues in the active site of CK1δ. Nevertheless, several of the published small molecule inhibitors display high potency and good CK1-specificity. A selection of the most promising or interesting molecules has been classified in this work due to mainly structural and developmental aspects into first generation inhibitors, pyridinyl-imidazoles and-isoxazoles, benzimidazoles and -thiazoles, purines and pyrazolo-pyrimidines or –pyridines, and amino-anthraquinones.

First Generation CK1δ Inhibitors

Isoquinoline sulfonamide derivative CKI-7 (**3**) became the first ever reported CK1 inhibitor in 1989, although non-selective and unable to discriminate between CK1 isoforms or to cross cell membranes[167,168]. The first compound exhibiting selectivity among isoforms followed in 2000. IC261 (**4**) inhibited CK1 isoform δ and ε with increased potency (IC_{50} = 1 μM) compared to isoform α (IC_{50} = 10 μM). Interestingly, IC261 shows slight deviation from the type I inhibition concept as it stabilizes the kinase in a state midway between apo and cofactor-bound structure[166,169]. The cell-permeable indoline compound proved valuable in several pharmacological studies despite the fact that IC261 itself is a potent inhibitor of tubulin polymerization[166,170]. During the following decade, naturally derived compounds have been identified by high throughput screening. *Thujopsis dolabrata* (-)-matairenisol (**5**) and anticancer

alkaloid lamellarin 3 (**6**), isolated from marine invertebrates, inhibit CK1 isoforms in a presumably ATP-competitive manner, but with low selectivity concerning the complete kinome[171,172].

Table 5 | First generation CK1δ inhibitors[167–169,171–173].

#	Structure	IC_{50} (μM)	ATP (μM)
3	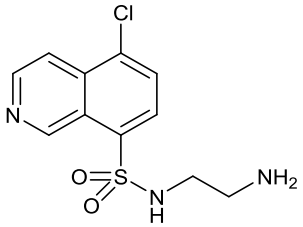	6 (CK1)[173]	100
4	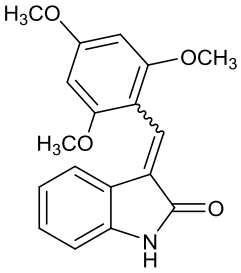	1.0 (CK1δ/ε)[169] 2.5 (CK1δ/ε)[173]	10 100
5	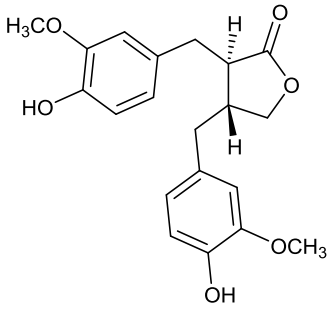	10 (CK1)[171]	10
6	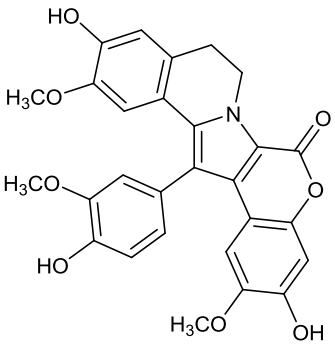	0.41 (CK1δ/ε)[172]	15

Pyridinyl-imidazoles and -isoxazoles (*Teardropbinder*)

The 4,5-diaryl-imidazole core of these compounds originally derives from inhibitors of p38 mitogen-activated protein kinases (MAPK) which have been referred to as "teardropbinders" due to their three-dimensional structure[159]. Selectivity over p38 MAPK isoforms is therefore a common problem for these substances. For instance, p38 MAPK inhibitor SB-202190 (**7**) non-specifically blocks CK1δ with moderate potency (IC_{50} = 0.6 μM) and most likely without significant isoform-selectivity[174]. In 2004 D4476 (**8**) was identified to prevent CK1 activity nearly an order of magnitude more potent (IC_{50} = 0.3 μM) than IC261 in a rather CK1-specific manner *in vitro*. In a panel of 30 additional kinases only p38α and phosphoinositide-dependent kinase 1 (PDK1) were inhibited, but although it is suggested to favor CK1δ/ε, discrimination among isoforms has not been reported[173]. Potent and rather CK1-selective inhibition was achieved with the development of pan-CK1δ/ε inhibitor PF-670462 (**9**) by Pfizer Global Research and Development (CK1δ IC_{50} = 0.013 μM, CK1ε IC_{50} = 0.080 μM, **Figure 12 A**). Besides CK1δ/ε it was active against several kinases including p38, GSK3β, PKA, and PKC[175]. *In vivo* studies revealed beneficial use in the treatment of bipolar disorder, addictive behavior, and aberrant circadian behavior[9]. Promising compounds have also been reported in 2009 by PEIFER *et al*.: 3,4-diaryl-isoxazole **10** proved a potent dual inhibitor for CK1δ and p38α MAPK (CK1δ IC_{50} = 0.047 μM, p38α IC_{50} = 2.52 μM). Interestingly, changing the scaffold towards 4,5-diaryl-imidazole **11** significantly increased potency and generated limited isoform-selectivity for CK1δ over CK1ε (CK1δ IC_{50} = 0.005 μM, CK1ε IC_{50} = 0.073 μM, p38α IC_{50} = 0.019 μM). Oxidation of the thioether afforded sulfoxide **12** with even enhanced isoform-selectivity (CK1δ IC_{50} = 0.011 μM, CK1ε IC_{50} = 0.447 μM, p38α IC_{50} = 0.041 μM). Due to the acrylamide moiety, which could potentially function as a MICHAEL acceptor, covalent binding might be suggested, but is unlikely as neither CK1δ nor CK1ε possess suitable cysteine residues, and consequently, ATP-competitive inhibition has been demonstrated[176]. Unfortunately, the same moiety accounts for reduced stability and thereby limited usability *in vivo*[148,176].

Table 6 | Pyridinyl-imidazole and -isoxazole CK1δ inhibitors[173–176].

#	Structure	IC_{50} (μM)	ATP (μM)
7	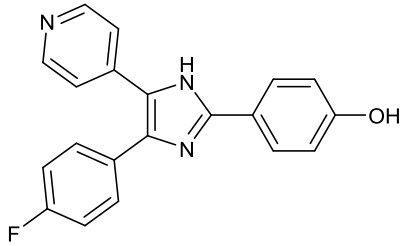	0.6 (CK1δ)[174]	50

8	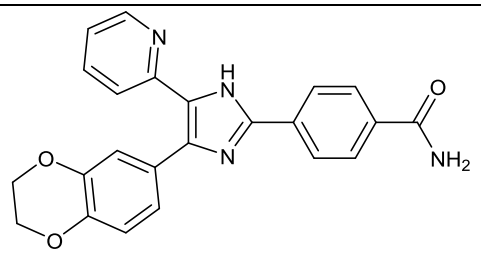	0.3 (CK1δ)[173]	100
9	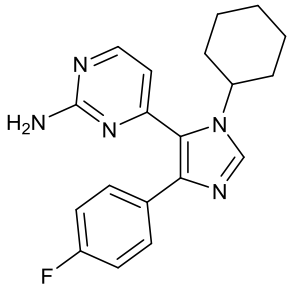	0.013 (CK1δ)[175] 0.080 (CK1ε)[175]	10
10	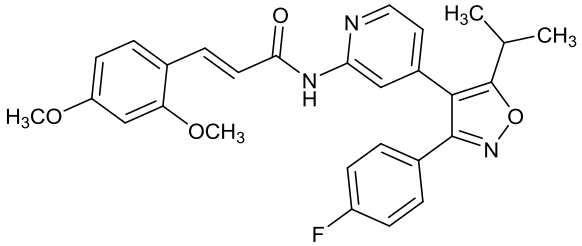	0.47 (CK1δ)[176] 2.52 (p38α)[176]	100
11	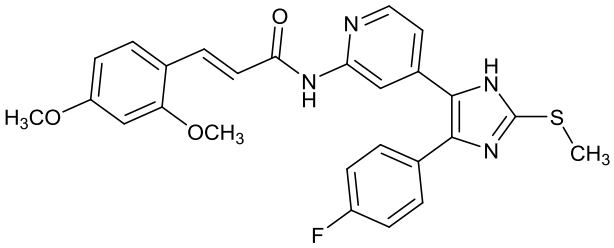	0.005 (CK1δ)[176] 0.073 (CK1ε)[176] 0.019 (p38α)[176]	100
12	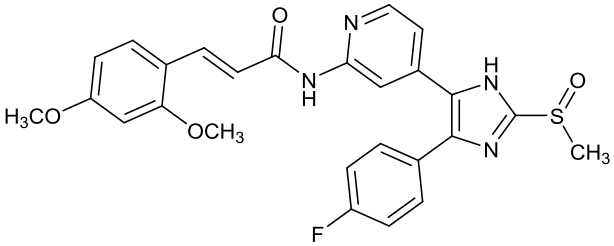	0.011 (CK1δ)[176] 0.447 (CK1ε)[176] 0.041 (p38α)[176]	100

Benzimidazoles and Benzothiazoles (*Linearbinder*)

In contrast to teardrop-like structures, benzimidazole and benzothiazole derivatives exhibit linear pharmacophores (*linearbinder*)[159]. Already in 1990 halogenobenzimidazole nucleoside

5,6-dibromo-1-(*β*-D-ribofuranosyl)benzimidazole (**13**) was shown to be slightly active on non-related CK1 and CK2[177], followed by the more potent but still highly unselective 4,5,6,7-tetrabromo-2-mercaptobenzimidazole (**14**) in 2003[178] and the first substituted benzothiazole (TG003, **15**) in 2004[179,180]. Several years later the first benzimidazole-based linearbinders had been developed as highly potent and selective CK1δ inhibitors *in vitro*. The most promising **16** even exhibited increased affinity towards isoform δ compared to ε (CK1δ IC_{50} = 0.040 µM, CK1ε IC_{50} = 0.199 µM, **Figure 12 B**). Selectivity profiling over 442 kinases revealed additional inhibition of only CK1α, CDC-like kinases 1 (CLK1) and 4 (CLK4), dual specificity tyrosine-phosphorylation-regulated kinase 1A (DYRK1A) and 1B (DYRK1B), and phosphatidylinositol 5-phosphate 4-kinase type-2γ (PIP5K2C)[181]. Further optimization led to closely related and even more potent benzimidazole **17** with increased isoform-specificity (CK1δ IC_{50} = 0.02 µM, CK1ε IC_{50} = 0.21 µM), favorable physiochemical properties, and excellent selectivity: in a panel of 442 protein kinases additional inhibitory activity was limited to CK1α and wild-type and mutant forms of Fms-like tyrosine kinase 3 (FLT-3)[182]. Interestingly, parallel development of benzimidazole **18** by another research group and subsequent optimization towards pyrrolopyridinone **19** and derivatives achieved highly potent and selective inhibitors for CK1γ which were only slightly active on the δ isoform. Consequently, the binding mode of this pyrrolopyridinone does not exhibit the typical linearbinder-character in CK1δ crystal structures[22,183].

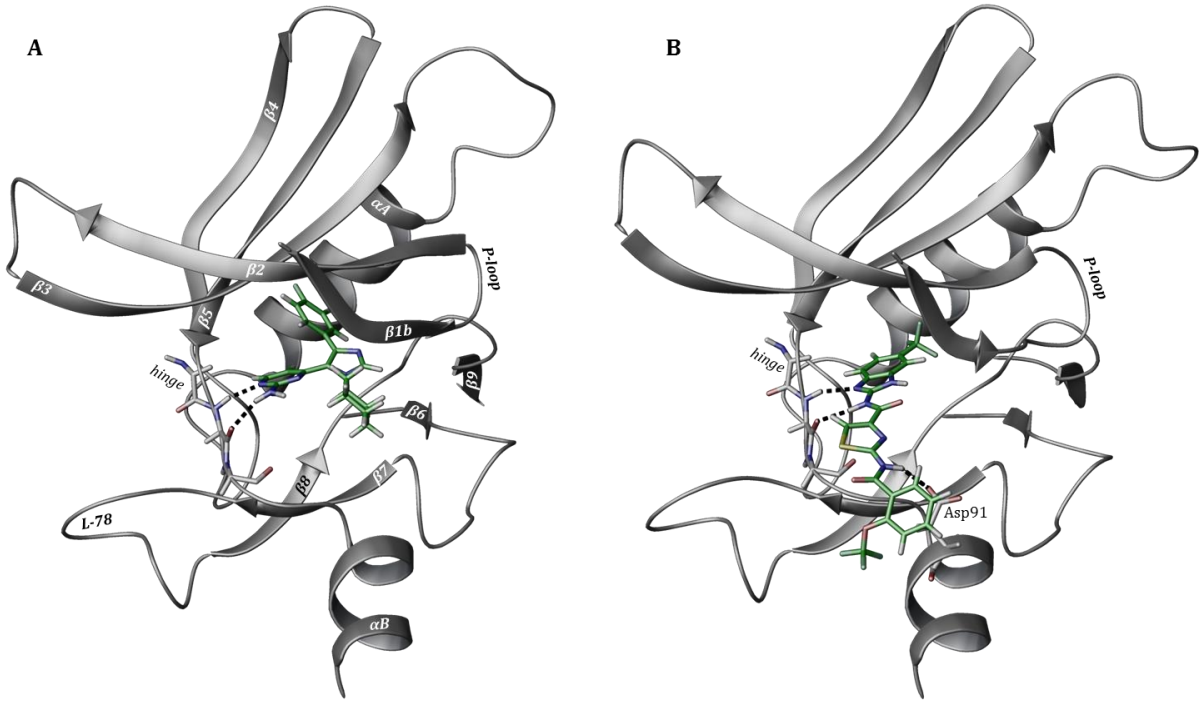

Figure 12 | Crystal structures of inhibitors 9 and 16 in CK1δ. Comparison of teardropbinder **9** (A, PDB code 3UZP)[184] and linearbinder **16** (B, PDB code 4TWC)[181] in CK1δ.

In addition, synthesis of compounds including benzothiazole cores instead of benzimidazoles has produced a batch of potent and cell permeable inhibitors for CK1δ (**20**, IC_{50} = 0.01 μM), although IC_{50} values of CK1ε inhibition are missing and selectivity profiles seem less favorable. Several kinases from a panel of 290 kinases were also inhibited including CK1 isoforms α, γ2, and ε, CLK1 and CLK4, DYRK1A and DYRK1B, FLT1, myosin light chain kinase 3 (MCLK3), and platelet-derived growth factor receptor (PDGFR)[119].

Table 7 | Benzimidazole and benzothiazole CK1δ inhibitors[22,119,177–183]. Abbreviation: n.d., not defined.

#	Structure	IC_{50} (μM)	ATP (μM)
13	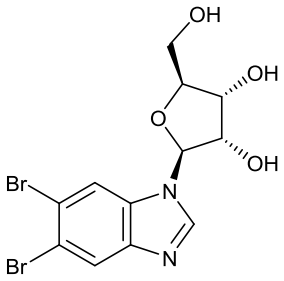	n.d.[177]	n.d.
14	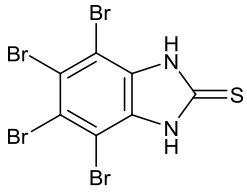	2.2 (CK1)[178]	20
15	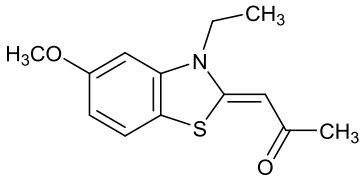	0.4 (CK1δ)[180] 0.55 (CK1ε)[180]	n.d.
16	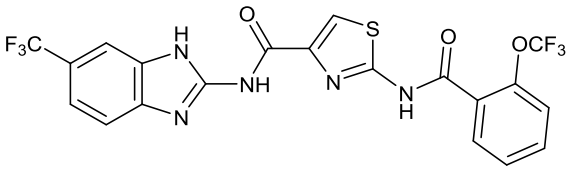	0.040 (CK1δ)[181] 0.199 (CK1ε)[181]	10
17	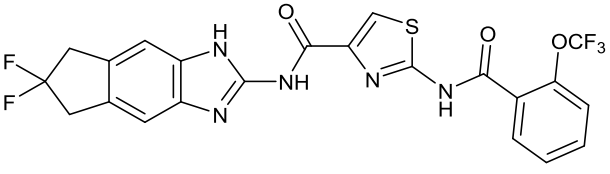	0.02 (CK1δ)[182] 0.21 (CK1ε)[182]	10

18	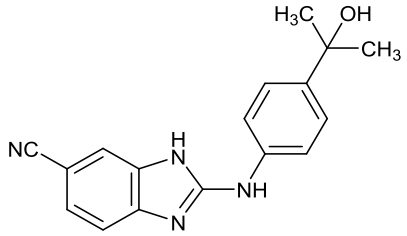	0.018 (CK1γ)[183] 2.32 (CK1δ)[183] 9.18 (CK1α)[183]	n.d.
19	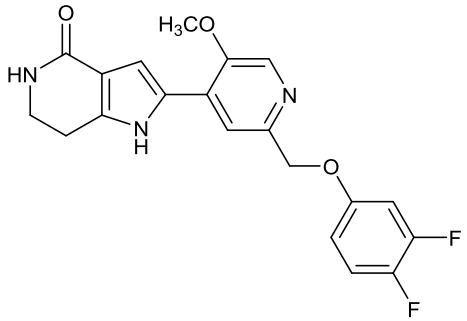	0.005 (CK1γ)[22] 0.040 (CK1δ)[22] 0.251 (CK1α)[22]	32 8 11
20	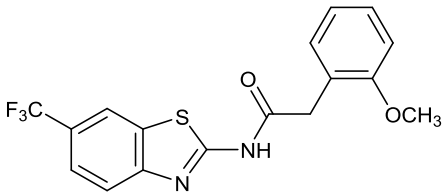	0.01 (CK1δ)[119]	10

Purines and Pyrazolo-pyrimidines or -pyridines

In 2008 roscovitine derivative (R)-DRF053 (**21**) was shown to be a potent dual inhibitor of CK1 (IC_{50} = 0.014 μM) and Cdk family kinases (Cdk1/cyclin B IC_{50} = 0.220 μM, Cdk5/p25 IC_{50} = 0.080 μM) *in vitro*, but without discrimination of isoforms[185]. Five years later structurally similar trisubstituted purine compound SR-2890 (**22**) and its derivatives were reported to exhibit excellent potency (CK1δ IC_{50} = 0.004 μM), striking activity in human cancer cell lines, and acceptable selectivity, hitting six off-targets out of 442 kinases. Among them there were CK1ε and FLT3 wild-type and mutant kinases[186].

The first pyrazolo-pyrimidine-based CK1 inhibitor PF-4800567 (**23**) has been published in 2009 by Pfizer Global Research and Development. PF-4800567 is a highly potent and selective inhibitor for CK1 isoform ε (CK1ε IC_{50} = 0.032 μM) with less activity on isoform δ (CK1δ IC_{50} = 0.711 μM). In a panel of 50 additional kinases only EGFR showed significant inhibition and *in vivo* studies revealed alteration of the circadian clock period[175]. In 2012 a novel pyrazolo-pyrimidine lead structure **24** for CK1-specific inhibition[187] was postulated, although in need of further optimization. This was followed in 2013 by the discovery of pyrazolo-pyridine

MRT00033659 (**25**) as a dual, though neither potent nor selective, inhibitor of CK1δ (IC_{50} = 0.8935 μM) and Chk1[188].

Table 8 | Purine and pyrazolo-pyrimidine or –pyridine CK1δ inhibitors[185-188].

#	Structure	IC_{50} (μM)	ATP (μM)
21	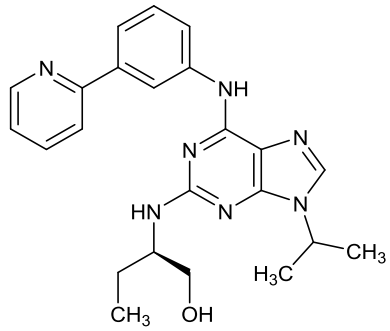	0.014 (CK1)[185] 0.220 (Cdk1/B)[185] 0.080 (Cdk5/p25)[185]	15
22	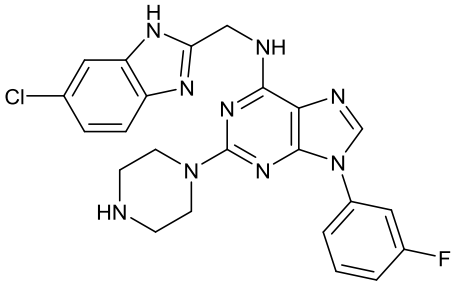	0.004 (CK1δ)[186]	10
23	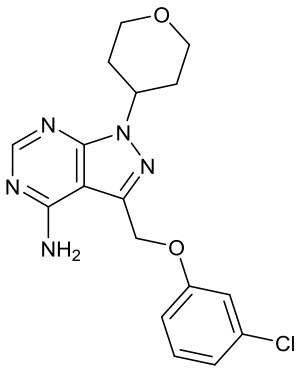	0.711 (CK1δ)[175] 0.032 (CK1ε)[175]	10
24	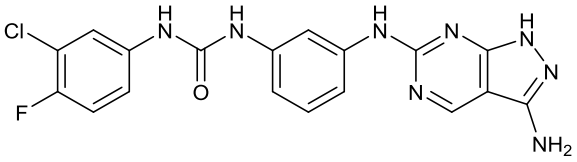	0.078 (CK1)[187]	n.d.
25	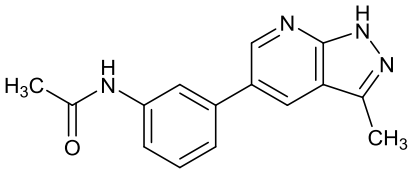	0.8935 (CK1δ)[188]	20

Amino-anthraquinones

Structure-based virtual screening by Cozza *et al*. in 2008 identified 5,8-diaminoanthraquinone (**26**) from a group of known CK2 inhibitors to be active against CK1δ as well. Although of weak potency and rather unselective it provides a completely novel lead structure for structure-based drug design regarding inhibition of CK1δ[189].

Table 9 | Amino-anthraquinone CK1δ inhibitor 26[189].

#	Structure	IC_{50} (μM)	ATP (μM)
26	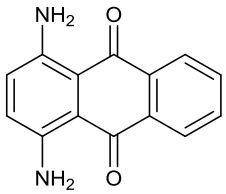	0.3 (CK1δ)[189]	n.d.

2 Aim of the Present Study

The importance of protein kinase CK1 in development and progression of serious diseases has dramatically increased interest in isoform-specific inhibition as discussed in **chapters 1.2.4** and **1.3.3**. In this context, especially highly conserved CK1 isoforms δ and ε are suggested to possess enormous potential. Although several δ and ε subgroup-specific inhibitors have been reported so far, actually only very few of them display at least tendencies for isoform-selective activity. Consequently, structure-activity relationship (SAR) data is rare and suitable mechanisms for the rational design of δ and ε discriminating probes with high selectivity are still to be developed.

Starting point of this dissertation was the previously by PEIFER *et al*. designed diaryl-imidazole inhibitor **12**[176]. Its excellent potency in the low nanomolar range and its tendency for isoform δ-specific inhibition marked it as a lead structure for further investigation. Unfortunately, direct usage of **12** was prohibited by instability based on a MICHAEL acceptor present in the molecule.

The inevitable optimization procedure followed a well-established workflow for structure-based drug development in medicinal chemistry: *in silico* lead structure optimization was followed by hit synthesis and biological evaluation. The objectives were therefore summarized as:

(1) Design and synthesis of chemically stable, potent, specific, and ideally isoform-selective (≥ 100-fold) CK1δ inhibitors starting from **12**

(2) Establishment of SAR by successive comparison of *in silico* and *in vitro* generated results and identification of selectivity-determinants for CK1δ-specific inhibition

(3) Verification of modeling results (proof of concept) by co-crystallization of potent and stable compounds in CK1δ and structurally related kinases (CK1ε, p38α)

3 Molecular Modeling Strategies

Molecular modeling[k] provides a powerful tool for structure-based drug design in medicinal chemistry. More than 100,000 three-dimensional protein structures have been solved to date that allow tightly focused studies of structure-activity relationships (SAR). Therefore, the integration of experimental *in vitro* or *in vivo* methods with *in silico* generated results is well-established in protein research[190,191]. Despite the immense benefit we have to accept that molecular modeling is also a highly limited technique. The multitude of essential parameters such as enthalpic and entropic effects, flexibility, and hydration states of proteins and ligands, as well as the cooperative interplay of hydrophilic and hydrophobic interactions, require an extensive knowledge of the medicinal chemist that often goes beyond software-mediated calculation[191,192]. Every *in silico* generated model requires reasonable questioning and a definite awareness of the difference between model and reality, as summarized by BISSANTZ *et al*.:

"Finally, as the level of confidence in structure-based design has increased, it is important to emphasize that any modeled binding mode remains a model until it is experimentally validated."[191]

3.1 *In Silico* Lead Structure Optimization

Starting point for the *in silico* optimization of lead structure **12** was the definition of its central pharmacophore. Therefore, the binding mode of **12** was postulated based on molecular modeling (**Figure 13**), receiving nearly identical results as published by PEIFER *et al*.[176]. Two H-bonds are formed between hinge residue Leu85 and the 2-aminopyridine moiety (hinge-binder). Core catalytic residues Lys38 and Asp149[144,184] coordinate a structural water molecule[l] within the catalytic cleft which donates an H-bond towards an imidazole nitrogen of **12**. The gatekeeper residue Met82 is rotated by 180° towards Pro66 (cp. **Figure 15**)[144,184] relative to the CK1δ apo structure (PDB code 3UYS) and permits access to the selectivity pocket (*HPI*) which is occupied by the 4-fluorophenyl moiety. Pro66 is of essential importance for selectivity as only few kinases possess equivalent residues that allow the observed gatekeeper rotation[144]. The cinnamic acid side chain of **12** extends into the solvent-exposed hydrophobic region (*HRII*). In addition, lead **12** includes one chiral center at the oxidized sulfur atom at the imidazole 2-position. Consequently, both enantiomers have been considered, but docking analysis did not reveal any significant differences. In literature the racemate is reported with one exception[193].

[k] For detailed information on modeling performance and computational software cp. experimental **chapter 7.1**
[l] Ideally coordinated water molecule within the active site, please refer **chapter 3.1.4**

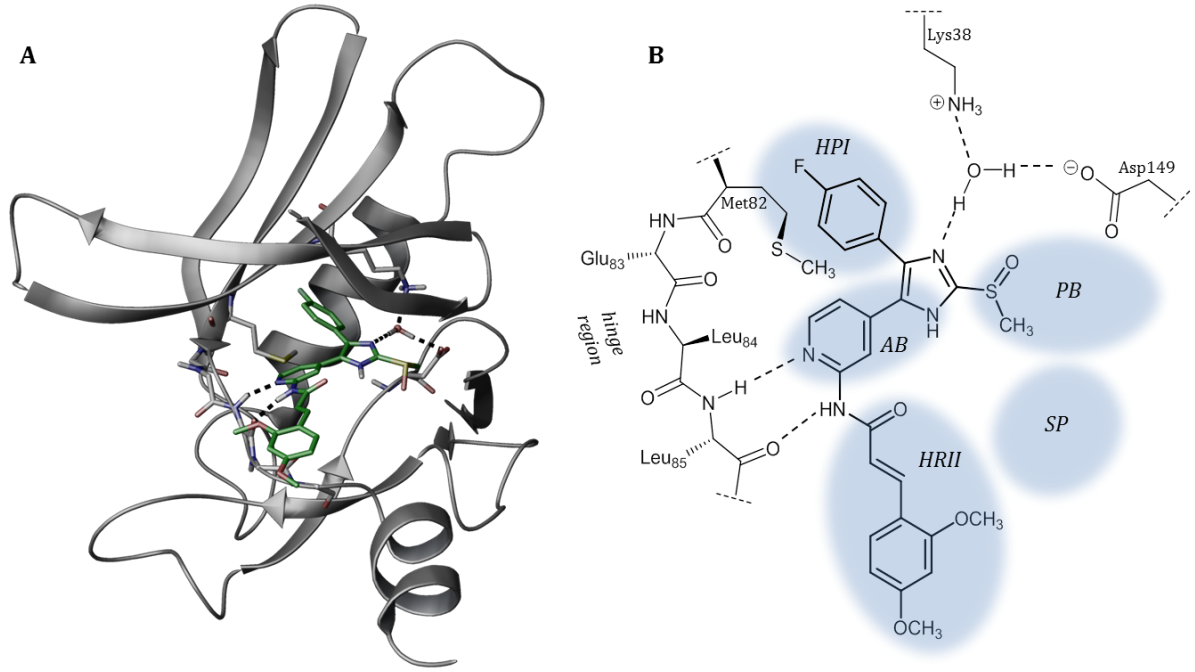

Figure 13 | Postulated binding mode of lead structure 12 in CK1δ. The 2D interaction diagram (B) was generated in accordance to the modeling results (A, PDB code 3UZP).

The assumed binding mode of **12** was compared to published binding modes of structurally similar inhibitors that had been crystallized with CK1δ or related kinases (**Table 10**). Among them there were pan-CK1δ/ε inhibitors PF-670462 (**9**)[184] and PF-5006739 (**27**)[194], several CK1δ-targeting 3,4-diaryl-pyrazoles (**28**-**31**)[165] as well as seven p38α MAPK inhibitors: pyridinyl-imidazoles SB203580 (**32**) and SB220025 (**33**), pyrimidinyl-imidazoles SB216995 (**34**) and SB218655 (**35**)[195], and pyridinyl-pyrazolon **36**[196].

Table 10 | Schematic binding modes of related diaryl-heterocyclic inhibitors crystallized with CK1δ or p38α. H-bonds formed between inhibitor and hinge residues are indicated by arrows[165,194–196].

#	Structure	Protein kinase	PDB code
9	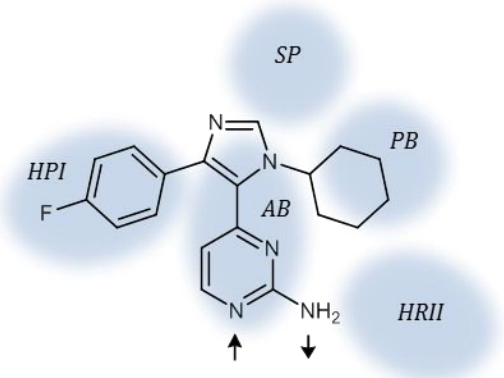	CK1δ	3UYS, 3UZP[184]

27	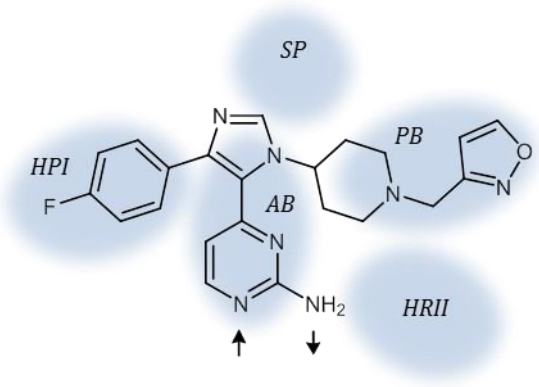	CK1δ	4TN6[194]
28	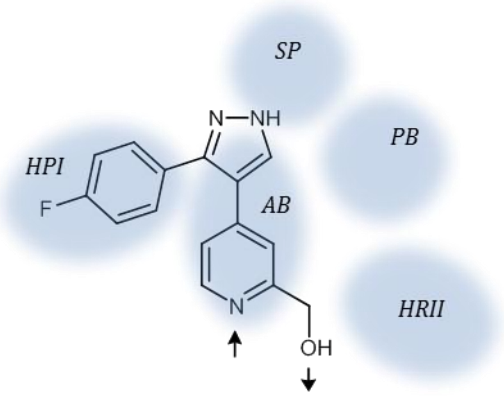	CK1δ	4KBC[165]
29	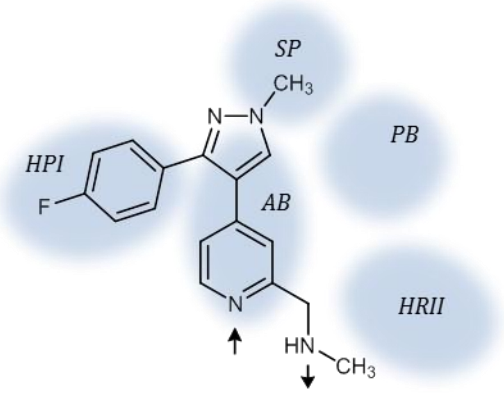	CK1δ	4KB8[165]
30	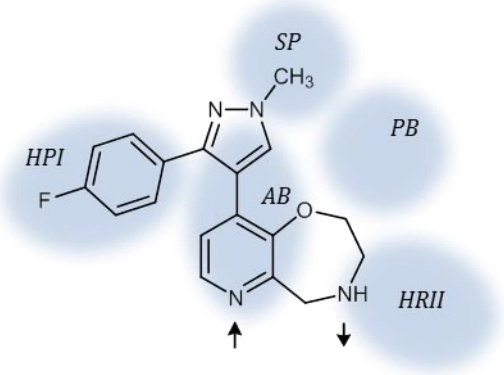	CK1δ	4KBA[165]

31	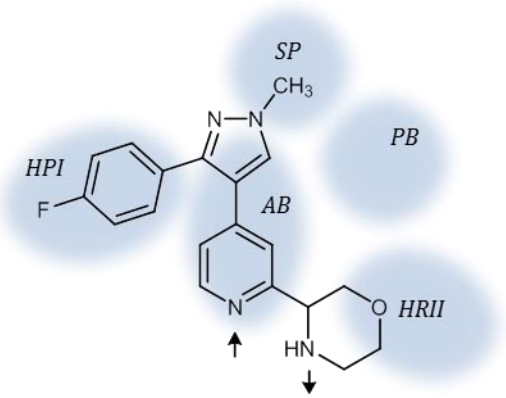	CK1δ	4KBK[165]
32	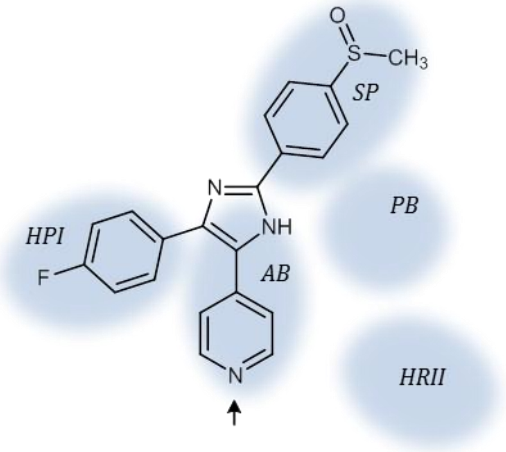	p38α	1A9U[195]
33	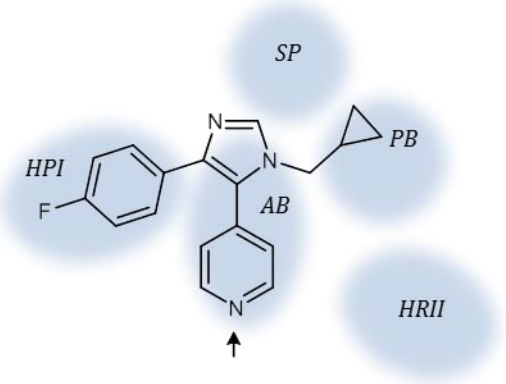	p38α	1BL6[195]

34	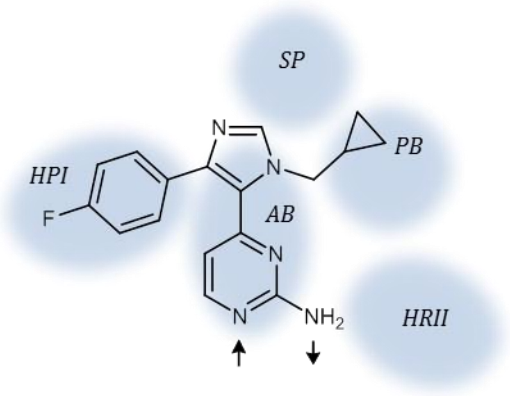	p38α	1BMK[195]
35	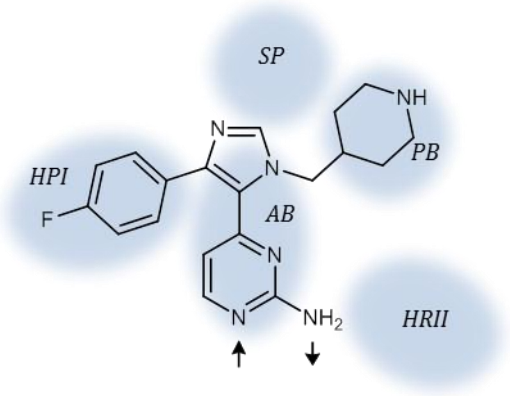	p38α	1BL7[195]
36	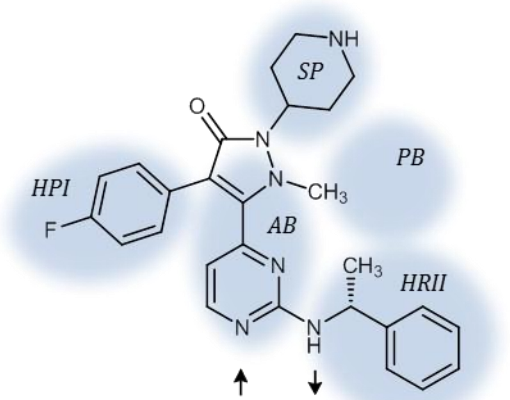	p38α	1YWR[196]

Evaluation of these crystallographic studies revealed crucial structural requirements for optimal inhibition of CK1δ and p38α. Consequently, characterization of core interactions led to the definition of a central pharmacophore for *in silico* optimization (**Figure 14**): the 4-fluorophenyl moiety is shared by every considered inhibitor and has been reported ideal for occupation of *HPI* concerning selectivity over most other kinases. A vicinal pyridin-4-yl or pyrimidin-4-yl moiety accepts an H-bond from the hinge region and is a main determinant for potency[165,184,195–201]. An amino group in 2-position of this heterocycle has also proved beneficial: the positive mesomeric

effect (+M) increases the electron density at the pyridine ring and thereby the acceptor strength of the ring nitrogen. The amino moiety itself forms a second H-bond towards the hinge region[184,191,195–197,201]. Both the fluorophenyl and the pyridine moiety are connected by five-membered heterocycles bearing an unsubstituted nitrogen atom for H-bonding[184,194,195,197,198,200,201]. It seems that five-membered rings are the optimal choice in this position as they dictate an ideal angle for the positioning of the aryl moieties within the ATP-pocket. Further influence on binding kinetics can be exerted by targeting the remaining less conserved domains of the active site. Several studies have already examined the consequences of different substituents at the five-membered heterocycle addressing the CK1δ and p38α sugar- and phosphate-binding regions. Although the importance for activity and selectivity remains uncertain, these sites represent the major positions for modifying physicochemical properties[165,176,184,194,194,197–204]. Albeit less understood, targeting the solvent-exposed and rather vast hydrophobic front region of the catalytic cleft (*HRII*) is reportedly beneficial in gaining both potency and specificity and will be the main topic of this dissertation[176,195–197,200,201]. Addressing *HRII* by hydrophobic substituents replaces the suboptimal hydration (hydrophobic effect) and might be suggested to account for large gains in binding free energy (ΔG). In addition, sterically demanding groups shield the hydrophobic surface and the deeper cavities of the ATP-binding pocket from surrounding water.

It is further noteworthy that the initial toxicity problem of pyridinyl-imidazoles regarding cytochrome P450 (CYP450) inhibition has been shown to be positively influenced by different substitution pattern at the imidazole and the pyridine ring[197].

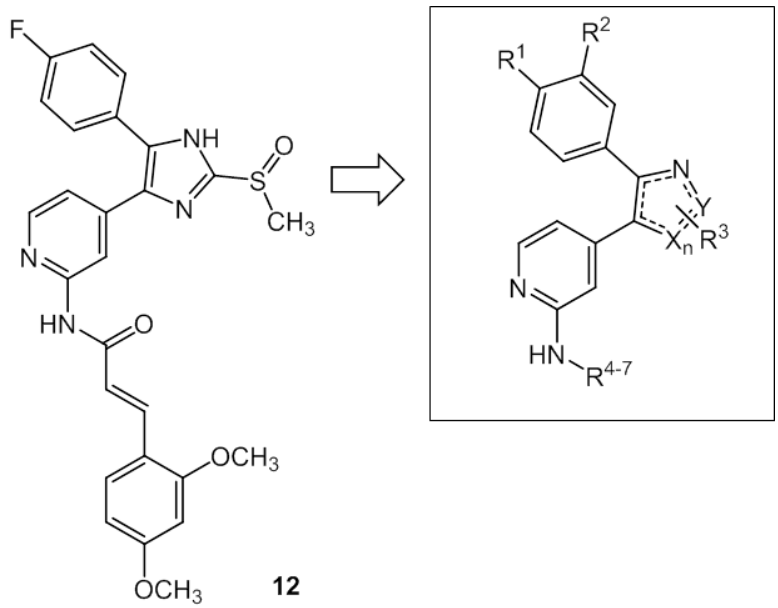

Figure 14 | Central pharmacophore for *in silico* lead structure optimization. The central pharmacophore has been defined with X and Y being carbon, nitrogen, oxygen, or sulfur (n = 0-3).

Subsequent molecular modeling studies were performed to predict the influence of consecutive variation of the defined moieties and to identify promising candidates for synthesis and biological evaluation. The main focus has consequently been put on possible gains of potency and selectivity for CK1δ, mediated by different side chains at positions R^4 to R^7 addressing the hydrophobic region II and thereby diminishing interactions towards CK1ε and p38α.

In general, docking algorithms imply two mating operations: first, the prediction of possible binding modes for the ligand in question; and second, the calculation (scoring) of the binding free energy (ΔG)[192]. As relying on ΔG is certainly the most appropriate technique in practice[191], *in silico* modeling results were compared based on their predicted Glide scores which approximately reflect ΔG. It has further to be kept in mind that credibility of molecular modeling decreases with increasing flexibility of the protein structure in question. Especially modeling studies regarding the highly flexible and solvent-exposed hydrophobic region II require *in vitro* and ideally crystallographic proof of concept.

In CK1δ excellent results were easily afforded by the fast Glide Docking procedure. Unfortunately, molecular docking of **12** in CK1ε and p38α is not suitable to explain its activity in these kinases: rational docking modes have only been received by the computational costly and time-consuming Induced Fit Docking (IFD), though without appropriate scoring. Regarding the limited available computational resources, the Induced Fit Docking protocol is generally inaccessible for compound screening[205]. Even Glide Docking approaches based on IFD-mediated protein preparation did not yield suitable scoring for CK1ε and p38α. Screening of these kinases was therefore not purposeful in the context of this dissertation.

3.1.1 Influence of different Substituents in the Selectivity Pocket

The fluorinated aryl moiety is a main determinant for selectivity regarding a large subset of other kinases. Consequently, the addressed hydrophobic back pocket (*HPI*) present in both CK1 and p38 has often been termed the "selectivity pocket". In CK1 isoforms δ and ε the pocket mainly consists of residues Met80, Val81, and Met82, while in p38 it is Thr, Val, and Leu, respectively. Despite these differences in primary sequence, hydrophobic environment and size of the sites are quite similar[165,197]. The main difference, however, is located at the entrance of the pocket. In p38 MAPK the relatively small gatekeeper residue Thr readily provides access to *HPI*, while in CK1δ/ε 180° rotation of the larger gatekeeper Met82 is required. Subsequently, the 4-fluorophenyl moiety penetrates deeply into the cavity forming strong hydrophobic interactions with residues Met80 and Met82 (**Figure 15**)[184].

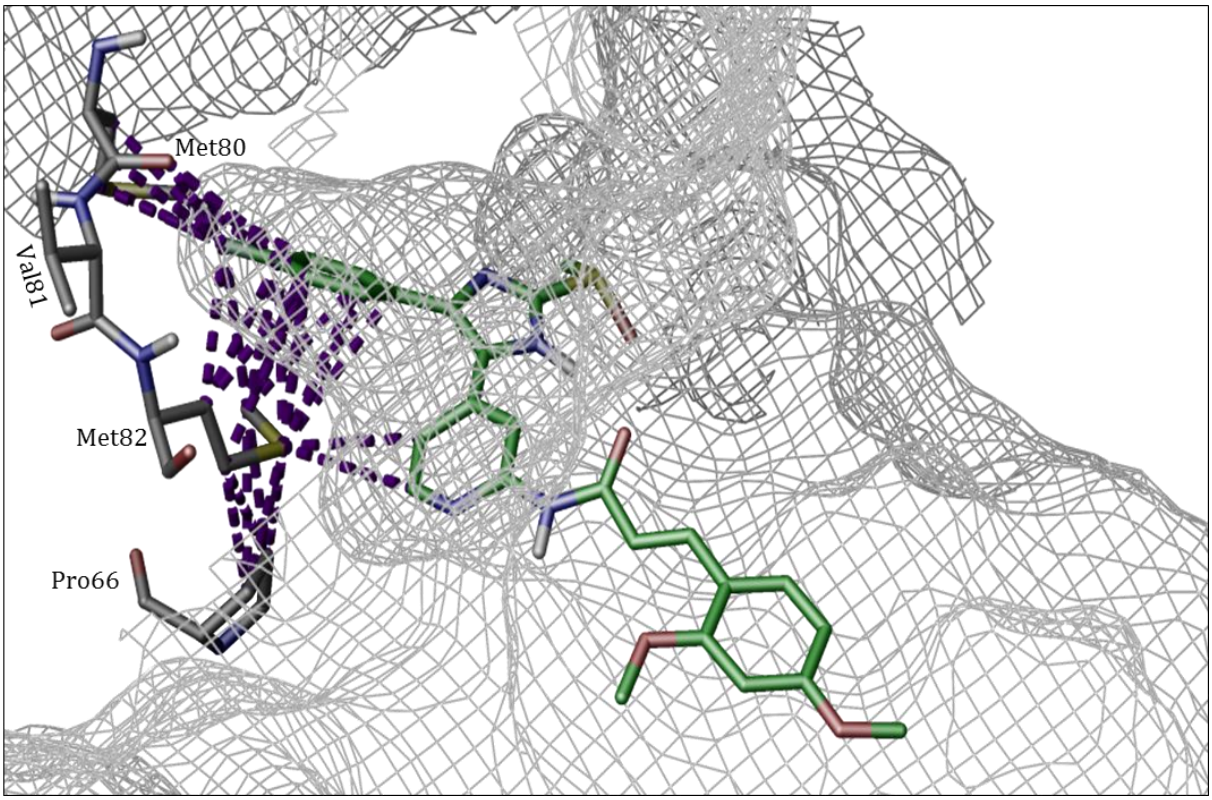

Figure 15 | Positioning of the 4-fluorophenyl moiety of 12 within the selectivity pocket of CK1δ. The halogenated aryl moiety penetrates deeply into the pocket forming hydrophobic interactions (violet) with Met80 and Met82. Met82 is rotated towards Pro66 (PDB code 3UZP)[184].

Although several studies have already reported the optimal fitting of the 4-fluorophenyl moiety within the selectivity pocket, this has only been experimentally evaluated for p38α[197,206]. On account of this, modeling studies have been performed to investigate the influence of different *para* and *meta* substituents for R^1 (**Figure 15**) in CK1δ. Hydrophobic substituents were selected

in accordance to experimental results published for p38α considering the observations of CRAIG[207].

The *in silico* results revealed the assumed behavior based on the experimental data of p38α (**Table 11**). Different small substituents (H, F, Cl, CH_3) are tolerated in *para*- and *meta*-position but without any significant gain in ΔG. Optimal binding within hydrophobic cavities has empirically been defined upon 55 % occupation of the pockets volume by the ligand[191] which is approximately achieved only with this set of substituents. Except for the tolyl group, *para*-substitution seems to be slightly favored. Sterically more demanding groups or larger halogen substituents (Br, I, *meta*-CF_3, OCH_3) are also accepted, preferentially in *meta*-position, but affect the overall positioning of the ligand in the active site: a weaker penetration depth of the aryl moiety leads to weakening or disruption of several hydrophobic and hydrophilic interactions by alteration of donor-acceptor distances and decreased inhibition potency has to be suggested. Bulky functionalities (isopropyl, cyclohexyl, *para*-CF_3) are not tolerated and did not provide rational binding modes of these derivatives.

Table 11 | *In silico* influence of different substituents for R¹ and R² in CK1δ. Lead structure **12** is deposited in grey.

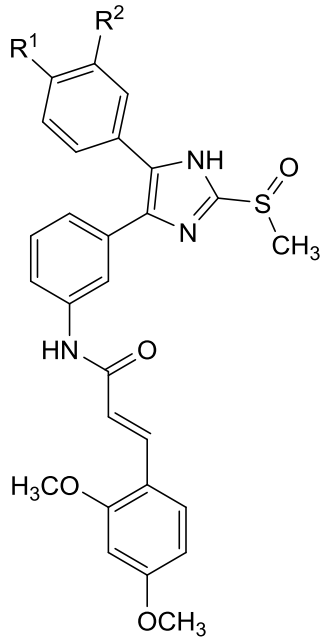

#	R¹	R²	Glide score
37	CH_3	H	-14.0
38	F	F	-14.0
39	CH_3	H	-13.8
40	Cl	H	-13.8
12	F	H	-13.7
41	H	H	-13.7
42	H	F	-13.5
43	I	I	-13.2
44	H	Cl	-13.0
45	Br	H	-12.6
46	I	H	-12.6
47	H	OCH_3	-12.1
48	H	Br	-12.0
49	H	CF_3	-11.6
50	OCH_3	H	-11.2

3.1.2 Addressing the Phosphate- and Ribose-binding Regions

Substitution of the imidazole core in order to target the phosphate- and ribose-binding domains of CK1δ and p38α has already been studied intensely by several groups[176,194,197–204]. Herein, the main benefit in p38 MAPK inhibition is the modification of physicochemical properties[197] while few CK1δ inhibitors additionally exhibited slightly enhanced selectivity over other kinases, though not CK1ε[204]. Especially the 2-thioether functionality has been highlighted by several publications for its high potency and its ability to effectively reduce CYP inhibition[176,197,203]. The sulfanyl group is further predestined to act as a linker for moieties that address the hydrophilic domains of the active site[202]. Bulky residues at the sulfanyl, however, can be assumed to decrease activity[197]. Interestingly, synthetic easily accessible sulfoxides such as **12** which are expected as the main metabolites have been postulated to increase CK1 isoform-selectivity (**Table 6**)[176,200]. Substitution at the 1- and 3-position of the imidazole has also been examined for p38α and less intensely for CK1δ inhibitors. The nitrogen atom directed towards the back side of the pocket participates in H-bonding and does not tolerate substitution[197]. In contrast, the nitrogen positioned towards the solvent-exposed entrance of the cleft has repeatedly been screened carrying different predominantly hydrophilic moieties. Unfortunately, the effect of this substitution remains less clear and has been discussed controversely[176,194,197,198,200–202,204]. Albeit a beneficial gain of selectivity for CK1δ is generally conceivable, moieties in this position can be suggested to cause steric hindrance within the inhibitor if bulky side chains are existent in 2-position of the pyridine[198]. *In silico* optimization studies have therefore been limited to the 2-position of the imidazole in this dissertation.

The aim was to evaluate the benefit of hydrophilic substituents that might be linked to the exocyclic sulfur atom at the imidazole 2-position of **12**, thereby replacing the methyl group. Flexible aliphatic *n*-alcoholic moieties with increasing length were screened in a first attempt. In a second step, chiral centers were introduced into these substituents and additional hydroxyl groups were added to address specific amino acids for H-bonding. The use of chiral residues in this context was expected to influence selectivity *in vitro* and *in vivo* due to the less-conserved character of the addressed domains. In order to promote the introduction of chirality even further, moiety screening included several chiral iminosaccharides from a compound list provided by the Ferrier Research Institute (Victoria University of Wellington, New Zealand). These molecules were connected (*in silico*) to the imidazole 2-position via a nitrogen instead of a sulfur linker as this seemed the most promising method for potential synthetic approaches. Synthetic realization of this concept, however, has been the topic of the master thesis of SCHMIDT

in 2015 who functionalized diaryl-oxazoles with iminosaccharides (**Figure 16**)[208]. A selection of top hits from several *in silico* screenings is given in **Table 12**.

Table 12 | *In silico* screening top hits with different hydrophilic moieties for R³ in CK1δ.

	#	R³	Glide score
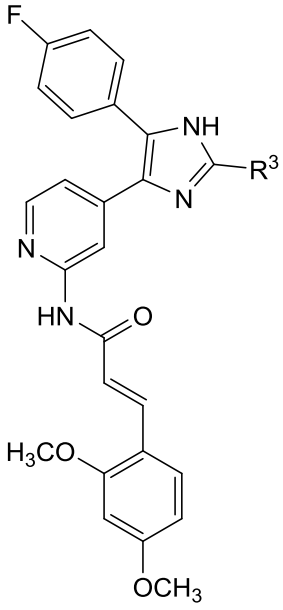	**51**	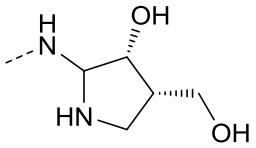	-16.5
	52	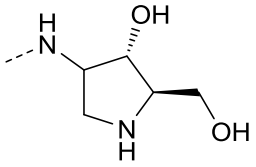	-16.5
	53	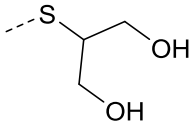	-15.9
	54	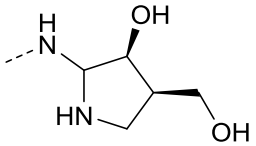	-15.4
	55	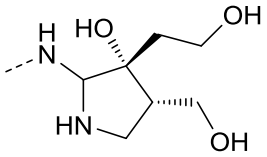	-15.4
	56	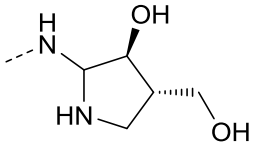	-15.2
	57	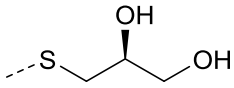	-15.2
	58	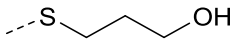	-15.1
	59	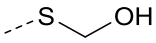	-15.1
	60	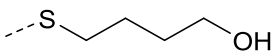	-14.8
	61	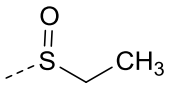	-14.1
	12	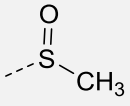	-13.7
	62	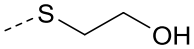	-13.5

Modeling exhibits the expected excellent results with high gains in ΔG. Hydroxyl groups of primary aliphatic alcohol substituents interact either with residue Asp132 or Ser17. Additional hydroxyl and amine groups of polyvalent alcohols and iminosaccharides also permit H-bonds with residues Ile15, Asp91, and Asn133. It is noteworthy that these residues have predominantly been suggested to participate in substrate recognition and ATP-binding. Nevertheless, the enhanced calculated Glide scores could be misleading as additional H-bond donors do not necessarily increase ΔG. In fact, the formation of additive H-bonds requires replacement of potentially coordinated water molecules from the addressed regions (cp. **chapter 3.1.4**). Regrettably, this is not completely represented in docking and might overcompensate the enthalpic gains. The calculated binding mode of top hit **51** in CK1δ is exemplified in **Figure 16**.

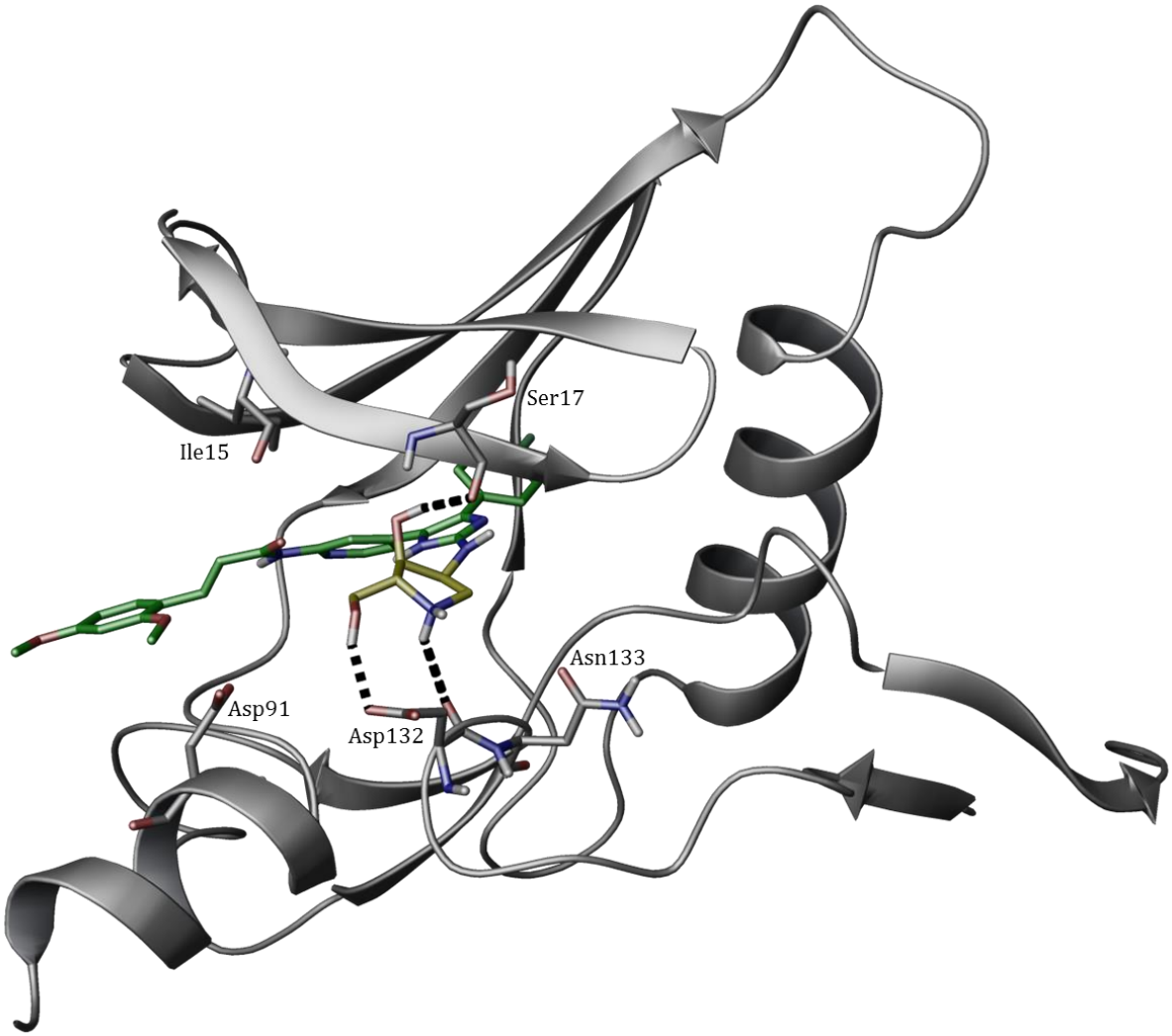

Figure 16 | Postulated binding mode of 51 in CK1δ. Hydroxyl moieties of the iminosaccharide (yellow) form H-bonds with residues Ser17 and Asp132. Interactions between other parts of the ligand and the kinase are not shown (PDB code 3UZP).

Despite these results, the enormous gain in ΔG does not seem to account for *in vitro* studies as suggested from initial evaluation by SCHMIDT[208]. Only compound **64** out of three iminosaccharide-substituted ligands **64**-**66** exhibited a significant but rather weak increase in activity compared to the unsubstituted analog **63** in kinase assays (**Figure 17**). Further biological data concerning inhibition of CK1 isoforms δ, ε, and α did not reveal any significant isoform-specificity. In cell assays a complete lack of activity was observed[208]. According to the results of SCHMIDT, unfavorable hydration of ligand (and protein) is most likely to compensate the potential gain in ΔG upon H-bond formation by high desolvation penalties. The complete loss of inhibitory activity in cells might be due to inability of plasma membrane penetration or rapid intracellular metabolization. In this context it has to be noted that hydroxyl moieties provide additional sites for derivatization and inactivation of compounds *in vitro* and *in vivo*[197].

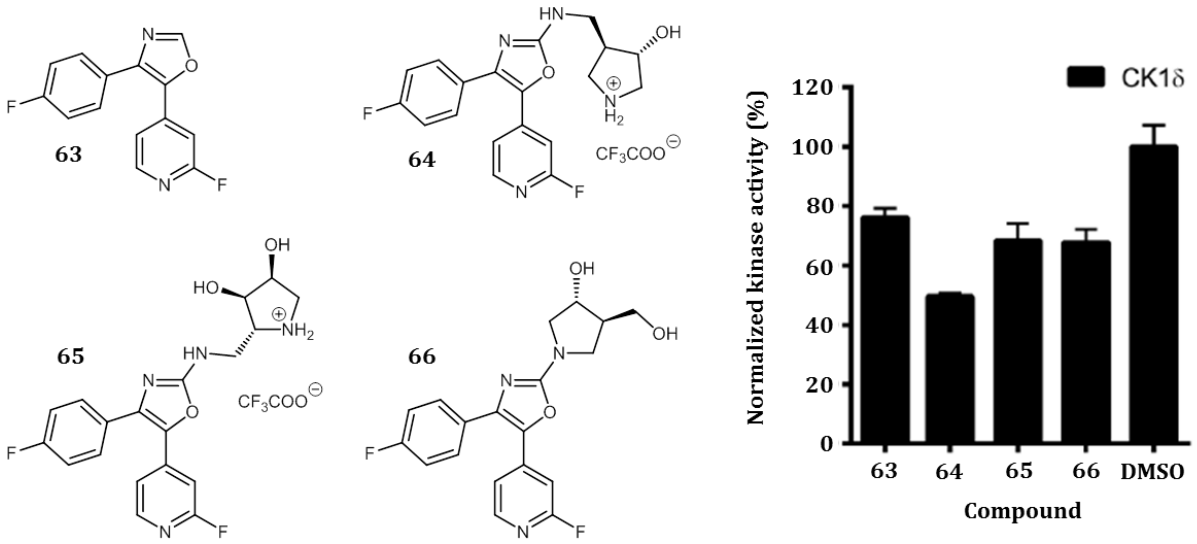

Figure 17 | *In vitro* biological evaluation of diaryl-oxazoles by SCHMIDT. Iminosaccharide-substituted compounds **64**, **65**, **66** derived from unsubstituted compound **63** (left). Residual activity of CK1δ at 10 μM inhibitor is shown in relation to control (DMSO). Each bar shows the mean value of n = 3 experiments ± standard deviation (right, modified from SCHMIDT[208]).

Even though no increase in potency and selectivity might be achieved, hydrophilic substituents have in general been used to beneficially modify physicochemical properties such as solubility and oral bioavailability, but this was not the focus of the present dissertation. The weak overall activity of these compounds is most likely provoked by the fluorine substituent at *ortho*-position of the pyridine. The strong negative inductive effect could weaken the pyridine H-bond acceptor which is the main determinant for potency of this inhibitor class.

3.1.3 Alternatives for the Imidazole (Core Hopping)

Although the majority of teardrop-like CK1δ inhibitors published to date consist of variably substituted diaryl-imidazoles, alternatives have been reported. Among them were the less potent oxazoles[208] and isoxazoles[176], but also several highly active pyrazoles[165]. An *in silico* core hopping has been performed to identify promising alternatives in order to improve potency and selectivity regarding CK1δ. Imidazoles are further less favorable regarding potential CYP inhibition[197].

The substitution pattern of the lead structure was retained while the core imidazole was consecutively replaced by heterocyclic scaffolds from the Glide fragment library (Schrödinger®, cp. **chapter 7.1.3** and **Table 13**). It is therefore not surprising that predominantly five-membered heterocycles were received, although without significant gains in ΔG compared to the lead structure. Strikingly, an H-bond acceptor positioned towards the structural water is conserved among the top hits and its absence consequently leads to reduced predicted affinity (i.e. less negative scores). Apart from this, prediction is less simple as multiple parameters determine the quality of H-bond acceptation in an additive but non-linear fashion. In general, aromatic nitrogen acceptors are slightly favored to aromatic oxygens and electron-donating effectors (positive mesomeric and inductive effects) increase acceptor strength while electron-withdrawing (negative mesomeric and inductive effects) ones lead to weakened H-bonds[191,199].

Consequently, pyrazole scaffold **67** shows slightly improved values (i.e. more negative scores) for ΔG when compared to lead **12**, presumably caused by the electronic effect of the vicinal nitrogens. In contrast, isoxazole **68** which accepts the H-bond via the nitrogen atom exhibits reduced predicted affinity values, suggesting weakened H-bonding due to the vicinal negative inductive effect. Interestingly, oxazole **69** and imidazole **12** depict nearly equivalent values. On the other hand, even oxygen H-bond acceptors such as furan **70** unexpectedly show ΔG values similar to imidazole and their acceptor strength seems to be further increased through additional ring nitrogens (oxazole **71**, isoxazole **72**). A selection of suitable five-membered heterocyclic scaffolds from *in silico* screenings is given in **Table 13**.

Furthermore, the fitting of four- and six-membered heterocycles has also been investigated. While pyridine derivative **73** is well tolerated with scores similar to lead structure **12**, four-membered azete **74** exhibits a significant loss in ΔG. This effect is most likely due to the angles between the vicinal aryl moieties and the core heterocycle (**Figure 18**). Five- and six-membered aromatic scaffolds generally dictate similar angles, though in dependency of substitution and the existence of heteroatoms. The slight decrease of the pyridine scaffold might be caused by less penetration depth into the selectivity pocket (**Figure 18**). In contrast, four-membered aromatic

systems generate taller angles, forcing the vicinal aryl moieties further apart and leading to suboptimal fitting (cp. **Figure 18**). The postulated binding mode of the azete (*in silico*) derivative e.g. shows only a single H-bond towards the hinge instead of the initial bidentate binding.

Table 13 | *In silico* core hopping results for the imidazole of lead 12 in CK1δ. H-bond acceptors are indicated by arrows.

	#	C	Glide score
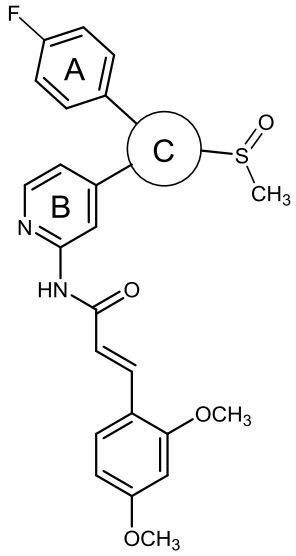	**67**	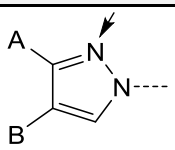	-14.2
	71	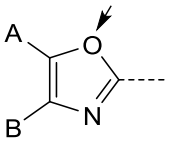	-14.1
	69	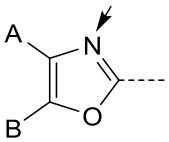	-13.9
	12	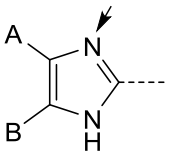	-13.7
	72	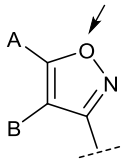	-13.7
	70	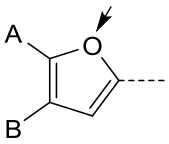	-13.6
	73	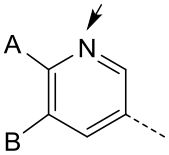	-13.5
	68	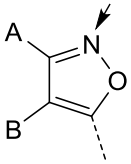	-13.3
	74	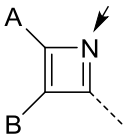	-12.0

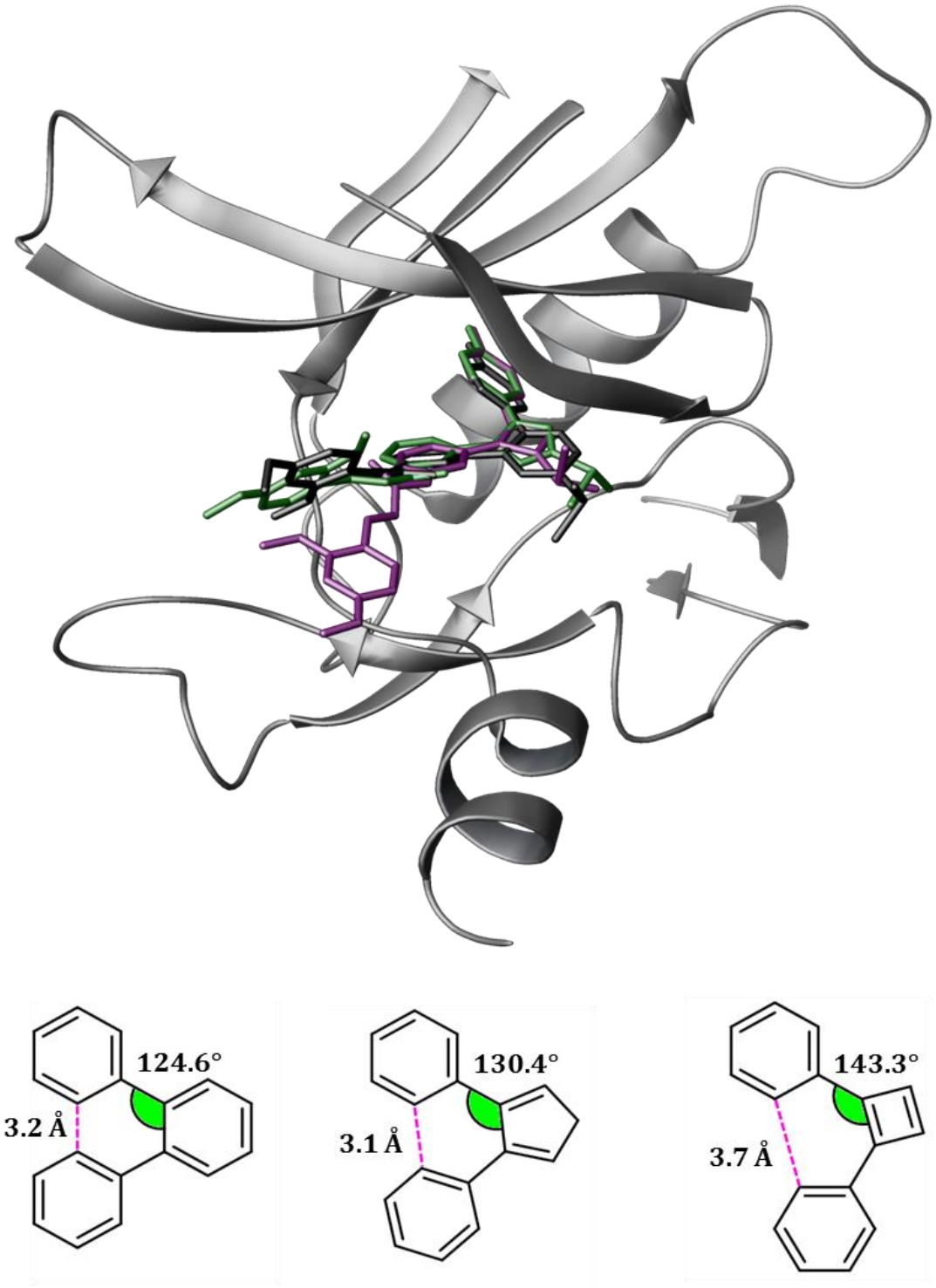

Figure 18 | Postulated binding modes of 12, 73, and 74 in CK1δ. Smaller aromatic systems dictate increased angles leading to less optimal fitting of the azete scaffold **74** (violet) compared to imidazole **12** (green) and pyridine **73** (black) scaffolds. The indicated distances refer to the 3D structure and thus the angle of torsion. All data refer to energetically minimized structures.

Taken together, the *in silico* core hopping suggests no significant increase in potency for CK1δ by the use of alternatives for the lead imidazole. Nevertheless, the replacement would surely be tolerated regarding pharmacological or physicochemical (or synthetic) reasons.

3.1.4 Structural Water

In the apo state of kinases when neither inhibitor nor cofactor is bound, the active site is flooded with water. Consequently, every binding event requires water displacement and should therefore be entropically favorable. Although binding sites are characterized by highly disordered water that is readily replaceable in practice, several water molecules are buried more deeply and interact with the protein environment through multiple H-bonds. Some of these can even be considered part of the binding site and a displacement has to be assumed as energetically disfavorable. These water molecules are ideally coordinated by not less than three H-bonds with protein side chains and are referred to as *structural water*. Replacement of non-ideally coordinated water might be possible and depends on the local geometry[191].

In human CK1δ one specific water molecule is conserved over all crystal structures[m] published in the Protein Data Bank (PDB). Although not ideally coordinated, it is deeply buried in the phosphate-binding region within H-bonding distance to Lys38 and Asp149. Another bond is formed towards ATP-competitive ligands whenever possible. In order to evaluate the possibility of replacement, several substituents at the 4-fluorophenyl moiety and the imidazole core were screened *in silico*. The best hits from this screening are depicted in **Table 14** and **Figure 19**. In derivative **75**, a hydroxymethyl substituent in 2-position of the 4-fluorophenyl moiety exhibits significant gain in ΔG. Interestingly, the hydroxyl group interacts neither with Lys38 nor with Asp149. Instead, an H-bond is accepted from Tyr56 (**Figure 19 B**). Displacement of the water molecule might also be achieved by substituents at the imidazole nitrogen. A hydroxyethyl moiety in **76** only interacts with Lys38 (**Figure 19 C**) while a chiral hydroxycyclopropyl moiety in **77** adopts the exact H-bonds from the water molecule (**Figure 19 D**). Both structures show energy values equivalent to the lead compound. The missing gain in ΔG as compared to the 4-fluoro-2-(hydroxymethyl)phenyl moiety is most likely due to steric hindrance within the ligand.

Table 14 | Screening hits for the replacement of the structural water. Glide scores are given beyond **75**, **76**, **77**, and lead **12**. R = (*E*)-4-(2-(3-(2,4-dimethoxyphenyl)acrylamido)pyridin-4-yl.

12	75	76	77
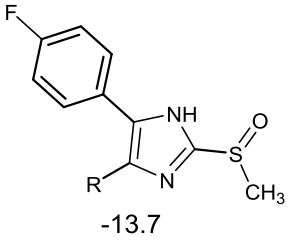	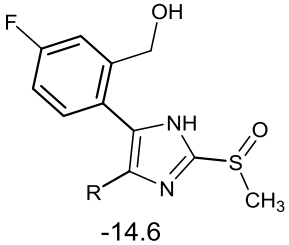	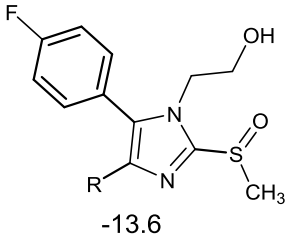	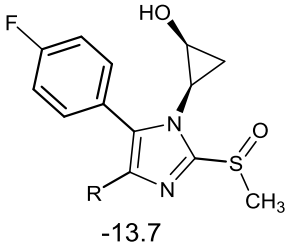
-13.7	-14.6	-13.6	-13.7

[m] Human CK1δ PDB codes: 3UYS, 3UYT, 3UZP, 4TW9, 4TN6, 4TWC, 4KB8, 4KBA, 4KBC, 4KBK, 4HGT, 4HNF

These results assume that replacement of the conserved water molecule within the CK1δ active site might be possible, although the *in vitro* and *in vivo* benefit has to be determined experimentally. Even if no gain in potency can be achieved, this approach might prove valuable in gaining selectivity. An equivalent water molecule cannot be detected in CK1ε crystal structures[n] and the analogue position in the p38α active site is occupied by residue Lys53.

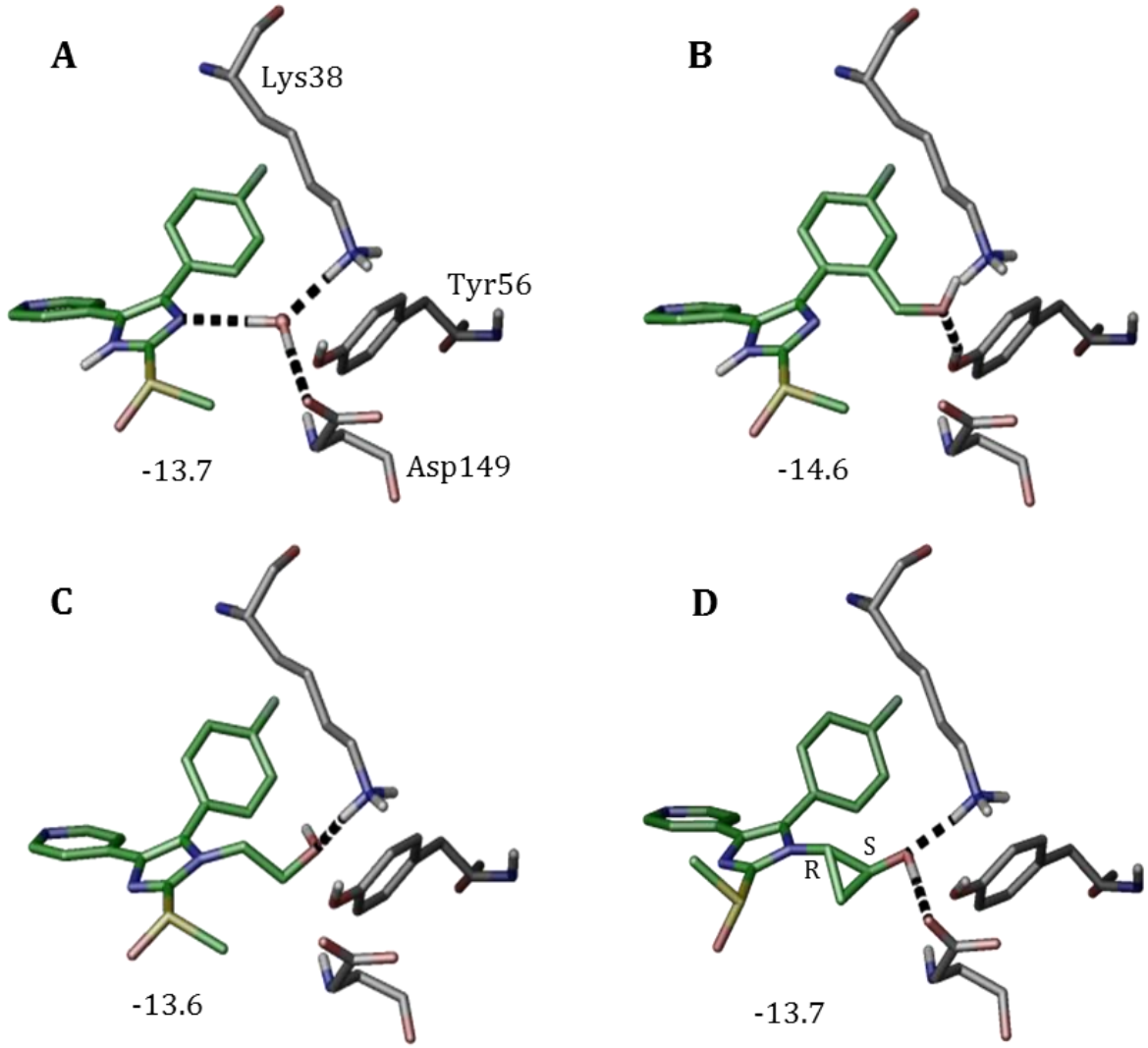

Figure 19 | Replacement of a conserved water molecule in CK1δ. One conserved water molecule in the CK1δ active site interacts with Lys38, Asp149, and the ligand **12** (A). It might be replaceable by a hydroxymethyl group in 2-position of the 4-fluorophenyl moiety in **75** (B) and a hydroxyethyl group in **76** (C) or a chiral hydroxycyclopropyl group in **77** (D) at the imidazole nitrogen. The (*E*)-3-(2,4-dimethoxyphenyl)acrylamide side chains (cp. lead structure **12**) in 2-position of the pyridine are not displayed. Glide scores are given beyond the structures.

[n] Human CK1ε PDB codes: 4HNI, 4HOK

3.1.5 Addressing the Solvent-exposed Hydrophobic Region II

The evolutionary less-conserved and solvent-exposed *HRII* does not participate in cofactor-binding and has therefore been associated with gains in both potency and selectivity regarding ATP-competitive small molecule kinase inhibitors[197]. Presumably hydrophobic residues form a lipophilic groove in the front region of the catalytic cleft, restricted by an agglomeration of acid and hydrophilic residues at the rim. Although CK1 isoforms δ and ε share the same residues[o] in this region, they slightly differ in their three-dimensional organization. The correspondent domain in p38α MAPK is formed by different residues[p] leading to significant distinction in its geometry (**Figure 20**).

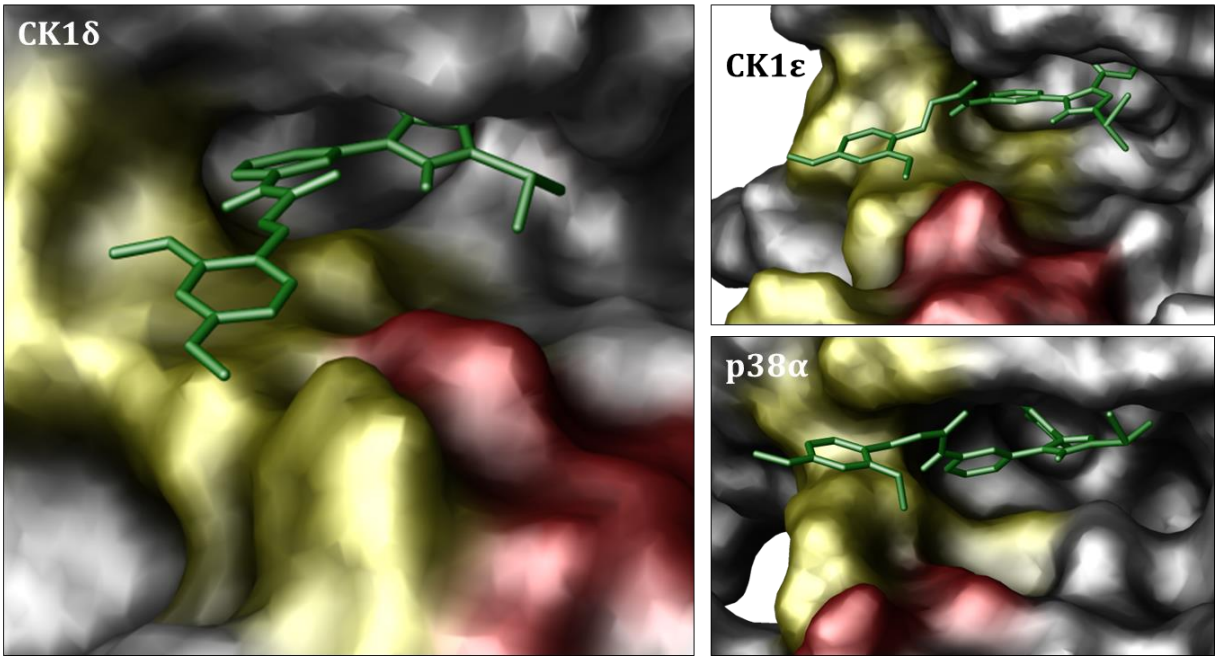

Figure 20 | Positioning of 12 in the hydrophobic region II of CK1δ, CK1ε, and p38α. The lipophilic groove (yellow) is restricted by acid and hydrophilic residues at the rim of the region (red). Modeling refers to PDB codes 3UZP, 4HNI, and 1BMK.

CK1δ and CK1ε provide spacious and mainly planar hydrophobic front regions. Especially isoform δ allows optimal fitting with high flexibility. Consequently, the displayed binding mode of lead structure **12** in CK1δ shows an entirely planar conformation of the (*E*)-3-(2,4-dimethoxyphenyl)-*N*-(pyridin-2-yl)acrylamide moiety. In CK1ε and p38α torsion about two dihedrals along the acrylamid chain leads to either syn- or anticlinal conformation. Energetically, these conformers can be assumed slightly less favored, thereby providing a possible explanation for the rather weak preference for CK1δ over the other two kinases.

[o] Human CK1δ/ε *HRII* residues: Ile15, Leu25, Leu84, Leu85, Gly86, Pro87, Ser88, Leu92, Phe95, Leu135, Leu138
[p] Human p38α *HRII* residues: Val30, Ala40, Leu108, Met109, Gly110, Ala111, Leu167

In p38α the hydrophobic region II is significantly less spacious and shows an overall non-planar folding. The overhang of the larger N-terminus generates a relatively flat channel which is occupied by the dimethoxyphenyl moiety and confines rotational flexibility (**Figure 20**). In addition, the hinge is "dislocated forwards" (**Figure 21**) enforcing the above mentioned rotation of the side chain. In contrast, protein structure alignment of CK1δ and CK1ε depicts only minimal shifts in the hinge region which do not seem suitable to justify the torsion within the acrylamide moiety. Furthermore, an accommodation of the 2,4-dimethoxyphenyl moiety by the flexible L-78 loop has been reported for CK1δ[176] (and therefore presumably CK1ε) whereas the equivalent loop in p38α is significantly smaller and differently orientated.

The (*E*)-conformation of the acrylamide, however, is conserved in all three binding modes (**Figure 21**). This is not surprising as the (*Z*)-conformer is associated with losses in ΔG in any of these kinases and has to be assumed less bioactive.

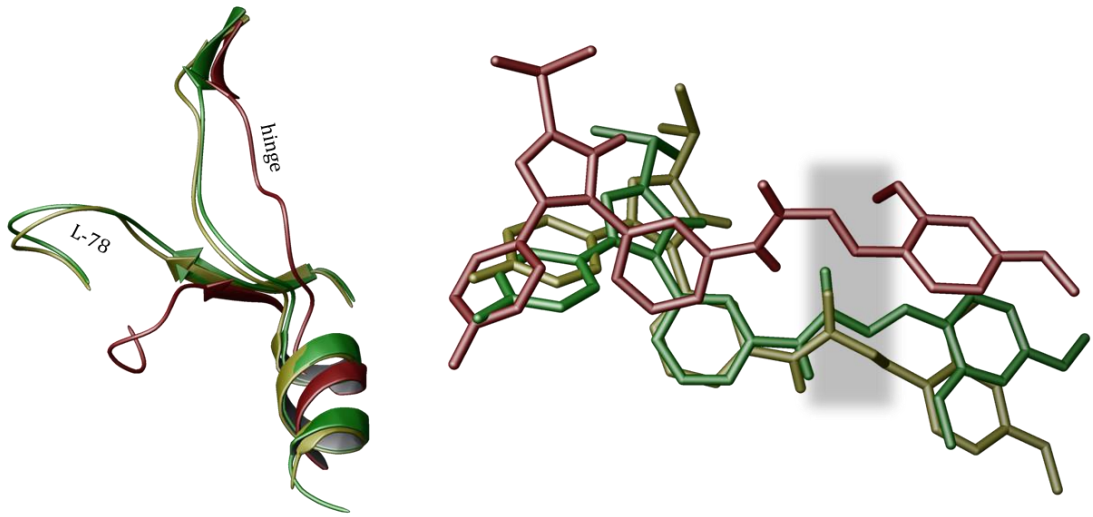

Figure 21 | Protein structure alignment of CK1δ, CK1ε, and p38α. The hinge of p38α (red) is displaced in relation to CK1δ (green) and CK1ε (yellow, left). Different conformation of ligands (**12**) taken from the protein structure alignment (right), though the (*E*)-conformation (grey box) is preserved. Modeling refers to PDB codes 3UZP, 4HNI, and 1BMK.

Taken together, the solvent-exposed front region seems potentially suited for the improvement of both potency and selectivity regarding CK1δ. Lipophilic side chains most likely enhance affinity through multiple VAN DER WAALS interactions. Methoxyphenyl moieties might be ideal in this context as they can additionally interact with adjacent water molecules and thereby shield the hydrophobic region from the surrounding polar environment[200]. As this is the main issue of the present dissertation, multiple *in silico* studies have been performed to evaluate suitable candidate compounds for subsequent synthetic realization. These were subdivided into six distinct series regarding the type of substituent at the *ortho*-pyridine position of 4-(5-(4-fluorophenyl)-2-(methylsulfinyl)-1*H*-imidazol-4-yl)pyridin-2-amine (**78**, **Figure 22**).

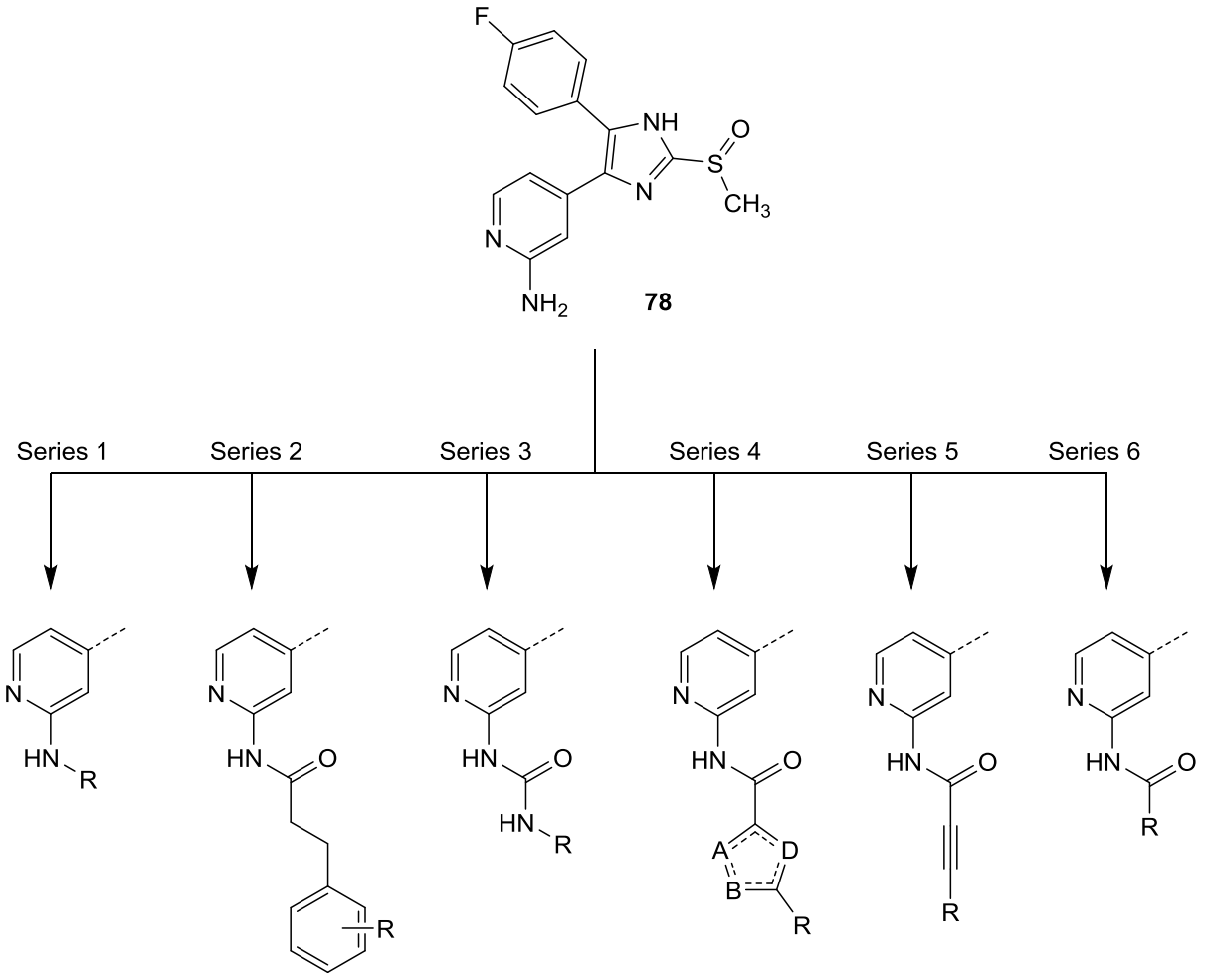

Figure 22 | Schematic representation of series 1 to 6 deriving from 78. Residues (R) are defined in the following chapters.

Primary and Secondary Amino Substituents (Series 1)

The predicted planar conformation of the lead structure side chain is enabled by the sp^2 hybridization of the acrylamide carbon atoms. Therefore, the carbonyl functionality and the π-bond were abolished from the structure to gain complete sp^3 hybridization within the linker, leading to significantly enhanced flexibility for derivative **79** (**Figure 23**). In addition, increased chemical and oxidative stability were expected as the MICHAEL acceptor has been regarded responsible for instability of lead structure **12**. In general, enhanced rotational freedom is associated with the confinement of translational and rotational degrees of freedom and thereby negatively influences the entropic contribution to the energetic binding profile of inhibitors[209]. Increased flexibility can also be assumed to initiate a loss of selectivity as flexible moieties and flexible kinase residues easily adapt to each other[159]. It has further been suggested that deletion of the carbonyl group is accompanied by decreased activity as the negative inductive effect of the carbonyl polarizes the N-H-bond of **12** whereas the positive inductive effect of an alkyl chain

might weaken the H-bond donor. The carbonyl group might further be beneficial for positioning the N-H in the correct angle.

As expected, modeling results for **79** exhibit high degrees of flexibility within hydrophobic region II, whereas the conformation of the diaryl-imidazole scaffold is highly conserved in all rational *in silico* binding modes (**Figure 23**). Consequently, additional off-target effects have to be assumed as the folding of the solvent-exposed front region is less determining for specificity in the case of highly flexible side chains. Modeling also indicates reduced potency of **79** for CK1δ in relation to **12**. These screening results were anticipated and will have to be evaluated *in vitro*.

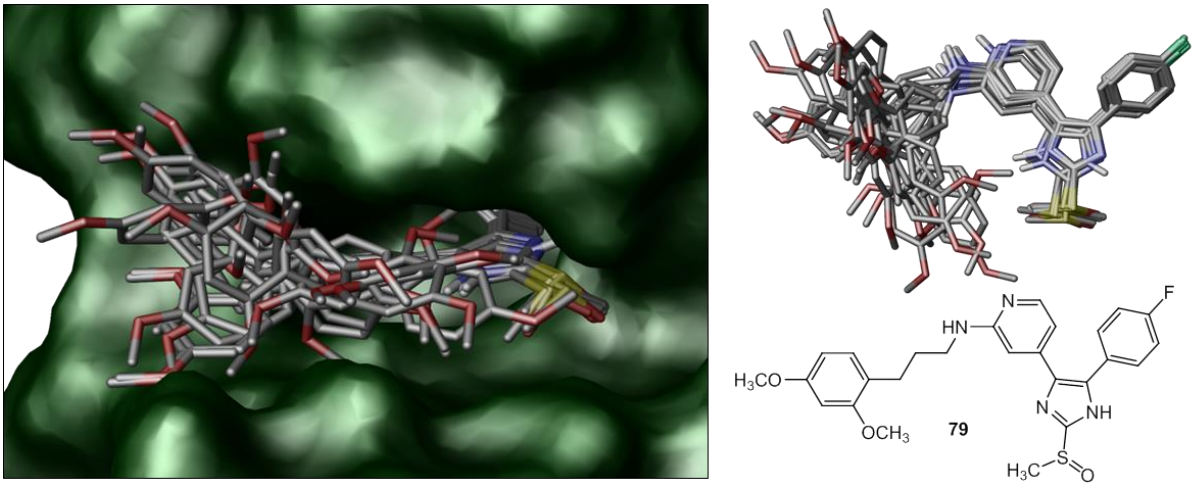

Figure 23 | Postulated binding modes of 79 in CK1δ. Alignment of several possible binding modes illustrates the high flexibility of the *N*-3-(2,4-dimethoxyphenyl)propyl side chain within the hydrophobic region II (left). In contrast, the diaryl-imidazole scaffold is highly conserved in all binding modes (right). Modeling refers to PDB code 3UZP.

Although removing both the carbonyl group (sp^2) and the π-bond (sp^2) of **12** is most likely to afford overall less potent and selective inhibitors it is thought to represent an important proof of concept. Furthermore, the length of the linker side chain and the influence of different di- and trimethoxy substitution pattern at the final phenyl moiety should be investigated. It has to be noted that in all series the focus has been put on different methoxyphenyl moieties as explained previously (**chapter 3.1.5**)[200]. Mono-methoxy substitution has not been considered as it has been reported to be most favorable for p38α inhibition, whereas di- and trimethoxy substituents impair fitting in this kinase[200]. The linker was thereby varied from zero to three carbon atoms.

Unfortunately, no preferences have been observed *in silico* regarding substitution or linker length. Multiple combinations show similar scoring without revealing any distinct trends, which is most likely due to the planar and spacious folding of this CK1δ region. The overall scoring is, as expected, significantly increased (i.e. loss of ΔG) as compared to lead structure **12** (**Table 15**).

Short or non-existent linker chains combined with unfavorable substitution in the *ortho*-positions cause intramolecular steric hindrance and are least favored.

Another approach was to investigate if additional H-bonds might be formed with hydrophilic side chains at the rim of the hydrophobic region (**Figure 20**, red surface). Therefore the terminal aryl moiety was exchanged for a dimethylamino group which might be positively charged under physiological conditions. In fact, an H-Bond towards Asp91 can be observed *in silico* with cyclic and aliphatic linkers containing three or four carbon atoms in a row (**Figure 24**), though without any significant improvement in ΔG as compared to more lipophilic moieties. This H-bond should therefore be considered rather weak. The influence of this interaction *in vitro*, however, has to be examined experimentally.

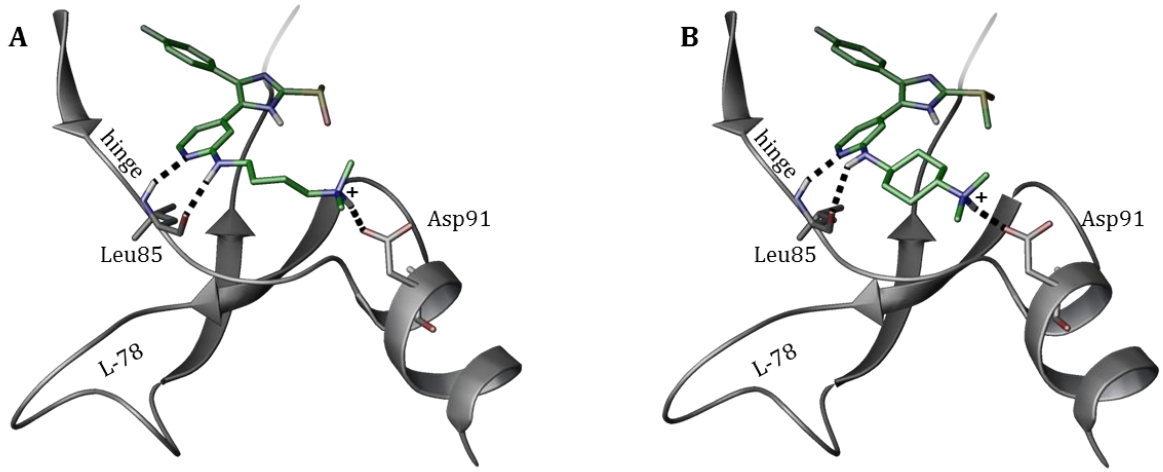

Figure 24 | *In silico* binding mode of 80 and 81 addressing Asp91. Positively charged dimethylamino side chains linked to the 2-aminopyridine through aliphatic (A) or cyclic (B) linkers (cp. **Table 15**). Asp91 is positioned at the rim of CK1δ hydrophobic region II (PDB code 3UZP).

Besides primary amines several less flexible secondary amines were screened, expecting strong losses in activity as they prevent formation of the second H-bond with the hinge. Alternatives for the final dimethoxyphenyl moiety have also been computationally examined. An overview over several *in silico* screened compounds is given in **Table 15**. For clarity, only those which have been selected for syntheses from these screenings have been included (cp. syntheses **chapter 4.2**). Apart from the mentioned intentions they have been selected upon commercial availability or synthetic feasibility.

Table 15 | *In silico* screened compounds of series 1 that have been selected for syntheses. Series 1 refers to primary and secondary amine substituents. As these compounds exhibit considerable losses in ΔG anyway, they are sorted by structure instead of Glide score.

	#	R^4 / R^5	Glide score
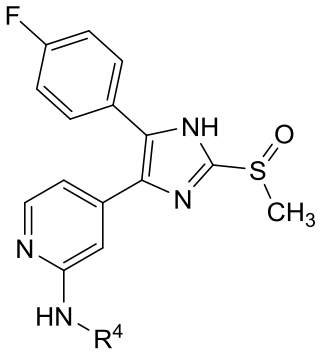	**82**	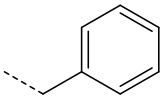	-11.8
	83	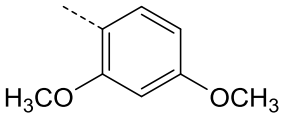	-10.9
	84	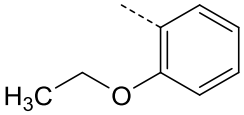	-11.2
	85	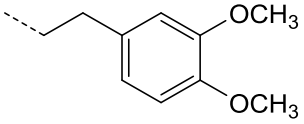	-12.0
	86	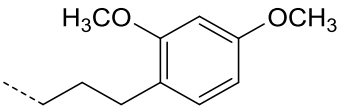	-11.7
	87	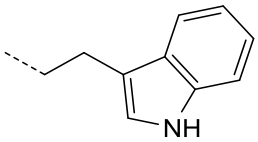	-12.7
	88	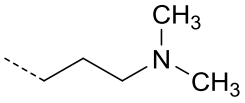	-11.6
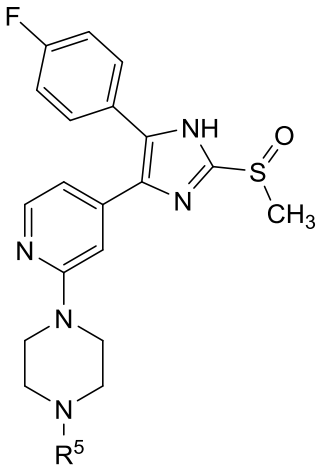	**89**	H	-8.4
	90	CH_3	-8.4
	91	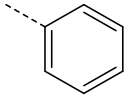	-10.7

Propionic Acid Substituents (Series 2)

The second series was mainly motivated by two distinct intentions: first, to provide evidence for the importance of acyl moieties at the 2-aminopyridine position regarding potency for CK1δ. The hypothesis was that the carbonyl function might strengthen the adjacent H-bond donor and support positioning of the N-H group in the correct angle (cp. series 1). Second, to avoid an α,β-unsaturated carbonyl moiety (MICHAEL acceptor) such as in **12** that is considered responsible for specificity and instability, but not for potency. Propionic acid (sp^3) instead of cinnamic acid (sp^2) side chains were assumed to account for highly active and chemically stable inhibitors. If so, these compounds might further be used for crystallographic evaluation in CK1δ, CK1ε, and p38α as a decrease in selectivity has to be suggested in the absence of the π-bond. The carbonyl group only partially restricts flexibility compared to the first series. Previous studies also highlighted the influence of acyl moieties in the exact position for metabolic stability[200].

As discussed for series 1, different substitution pattern for double and triple methoxy-substituted 3-phenylpropionic acid moieties were screened *in silico* (**Table 16**). Modeling suggests trimethoxy substitution to be slightly favored over dimethoxy derivatives - with the exception of the 3,4-dimethoxy pattern which exhibits superior gains in ΔG. Interestingly, derivative **102**, lacking the π-bond of the lead structure, shows identical scoring compared to **12**. Although losses in selectivity are most likely, all compounds can be considered highly potent regarding the *in silico* results. Synthetic realization, however, concentrated on commercially available 3-phenylpropionic acids from this series (cp. syntheses **chapter 4.3**) in order to generate highly stable and active inhibitors as biological tools for further *in vitro* evaluation.

Table 16 | *In silico* screened compounds of series 2. Series 2 refers to di- and trimethoxy-substituted 3-phenylpropionic acid side chains at the 2-aminopyridine.

	#	R^6	Glide score
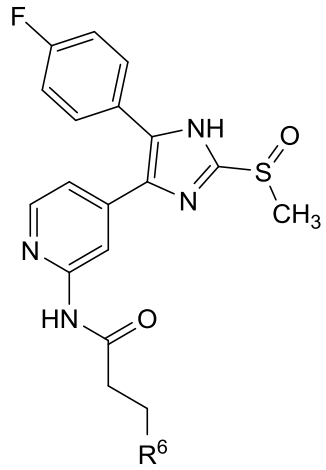	**92**	2,3,6-Trimethoxyphenyl	-14.6
	93	3,4-Dimethoxyphenyl	-14.6
	94	2,3,4-Trimethoxyphenyl	-14.5
	95	3,4,5-Trimethoxyphenyl	-14.4
	96	2,3,5-Trimethoxyphenyl	-14.3
	97	2,4,5-Trimethoxyphenyl	-14.3
	98	2,4,6-Trimethoxyphenyl	-14.3
	99	2,3-Dimethoxyphenyl	-14.1
	100	2,6-Dimethoxyphenyl	-13.9
	101	3,5-Dimethoxyphenyl	-13.8
	102	2,4-Dimethoxyphenyl	-13.7
	103	2,5-Dimethoxyphenyl	-13.6

Carbamide Substituents (Series 3)

The slightly different position of the hinge region in CK1 isoforms δ and ε on the one hand and p38α on the other has been taken into account in the third series. The idea was to generate additional rigidity in this domain to gain selectivity for CK1δ (and presumably CK1ε) over other kinases, especially p38α. Substitution with isocyanates at the 2-aminopyridine affords carbamide derivatives. These carbamides might be able to form a third H-bond towards hinge residue Leu85 and restrict rotational freedom of the side chain by waiving sp^3 hybridized carbon atoms.

The idea of an additional H-bond towards the hinge has been confirmed by molecular modeling. Docking studies with stereotype carbamide compound **104** (**Figure 25**) exhibit an excellent gain in ΔG (Glide score = -17.2), presumably caused by the intended tridentate hinge-binder. It has to be noted, though, that carbamides are known to possess unfavorable physicochemical properties, especially regarding solubility. Thereby the *in silico* observed advantages might be (over) compensated *in vitro* which has to be evaluated experimentally. In fact, several approved small molecule kinase inhibitors such as sorafenib, regorafenib, and lenvatinib possess carbamide functionalities[7]. Differently substituted 3-phenylcarbamides were synthesized (cp. syntheses **chapter 4.4**) and biologically tested. The selection of isocyanates was carried out based on commercial availability.

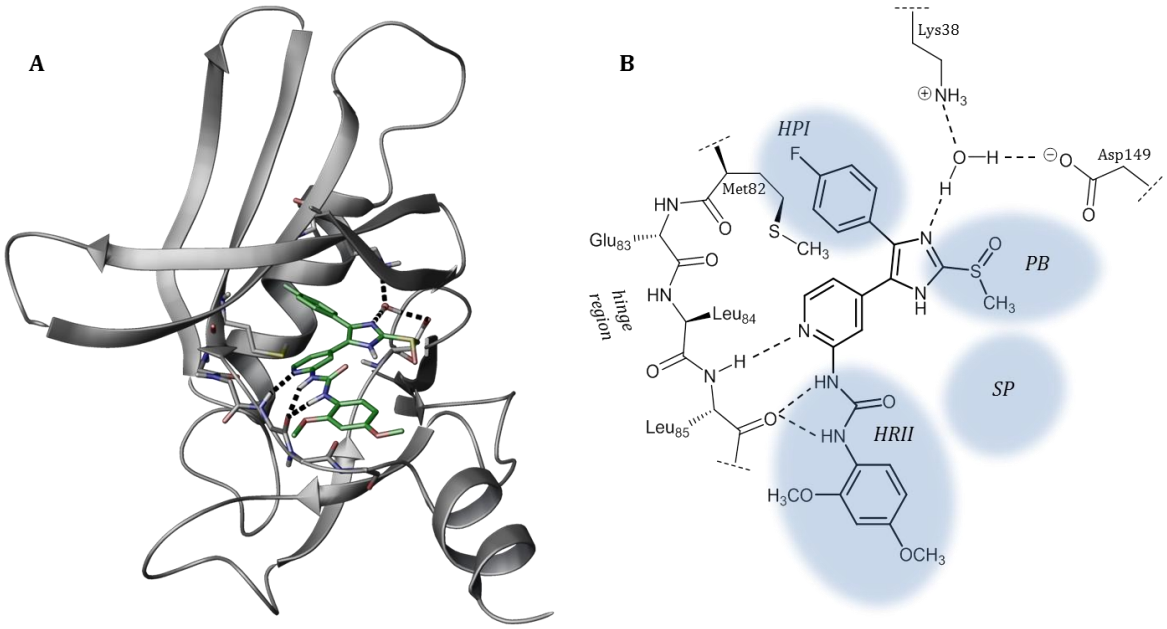

Figure 25 | Postulated binding mode of carbamide derivative 104 in CK1δ. The 2D interaction diagram (B) was formulated in accordance to the modeling results (A, PDB code 3UZP).

Conservation of the (*E*)-configured π-Bond (Series 4 and 5)

The suspected advantages and disadvantages of the (*E*)-configured π-bond of lead **12** have already been discussed: increased isoform-selectivity over CK1ε but also chemical instability (MICHAEL acceptor potential) and the existence of a less bioactive (*Z*)-isomer. In addition, the reactivity of the α,β-unsaturated carbonyl compound is enhanced through the vicinal phenyl moiety. Consequently, the idea was to minimize MICHAEL acceptor reactivity while conserving an (*E*)-like geometry either by using five-membered heterocycles (series 4) or alkyne moieties (series 5). The additional rigidification caused by altered hybridization, sp^2 in heterocyclic systems and *sp* in alkynes, was also assumed to positively affect selectivity over different kinases as this is a well-established mechanism in this context[159]. In addition, an entropy-driven contribution to the binding free energy can be assumed as rigidification of ligands is associated with beneficial modification of degrees of freedom upon binding to the active site[209]. Especially heterocyclic scaffolds (series 4) have been considered beneficial (**Table 17**): first, aromatic systems including an N-H group in β-position of the carbonyl function might enable a third H-bond towards hinge Leu85 as discussed for carbamide derivatives (cp. series 3); second, additional contribution to kinase specificity was suggested as bulky substituents at the 2-aminopyridine have been reported to decrease inhibitory activity for p38α[198]. Although less bulky, the linear geometry of alkynes (*sp* hybridization) was supposed to have an analogue effect due to the slightly different position of the hinge in p38α (cp. **chapter 3.1.5**).

Molecular modeling studies using 4–(2,4-dimethoxyphenyl)-1*H*-pyrrol-2-carboxylic acid (stereotype series 4 compound **105**) and 3-(2,4-dimethoxyphenyl)propiolic acid (stereotype series 5 compound **106**) as side chains at the 2-aminopyridine of **78** confirmed this hypothesis, although fitting of **105** and **106** in p38α still has to be assumed (**Figure 26**).

Subsequently, several five-membered heterocycles were screened *in silico* for their binding in CK1δ in order to identify suitable candidates for syntheses (**Table 17**). These studies indicate the fourth series to be more effective than the fifth. Heteroaromatic scaffolds containing an N-H group show the highest gain in ΔG (Glide scores ≤ -16.6) as they are suggested to act as tridentate hinge-binders. Among the remaining heterocyclic systems the calculated activity explicitly depends on the included heteroatoms in accordance to the HASB concept. In general, nitrogen accounts for higher gains in ΔG than sulfur, while oxygen is least active (cp. **109**-**112**, **Table 17**). The preference for additional aromatic moieties over alkyne side chains is most likely due to multiple VAN DER WAALS interactions and entropic (hydrophobic) effects within the hydrophobic region II. The scoring of the alkyne derivative **106** (Glide score = -13.7) matches that of lead structure **12** (Glide score = -13.7).

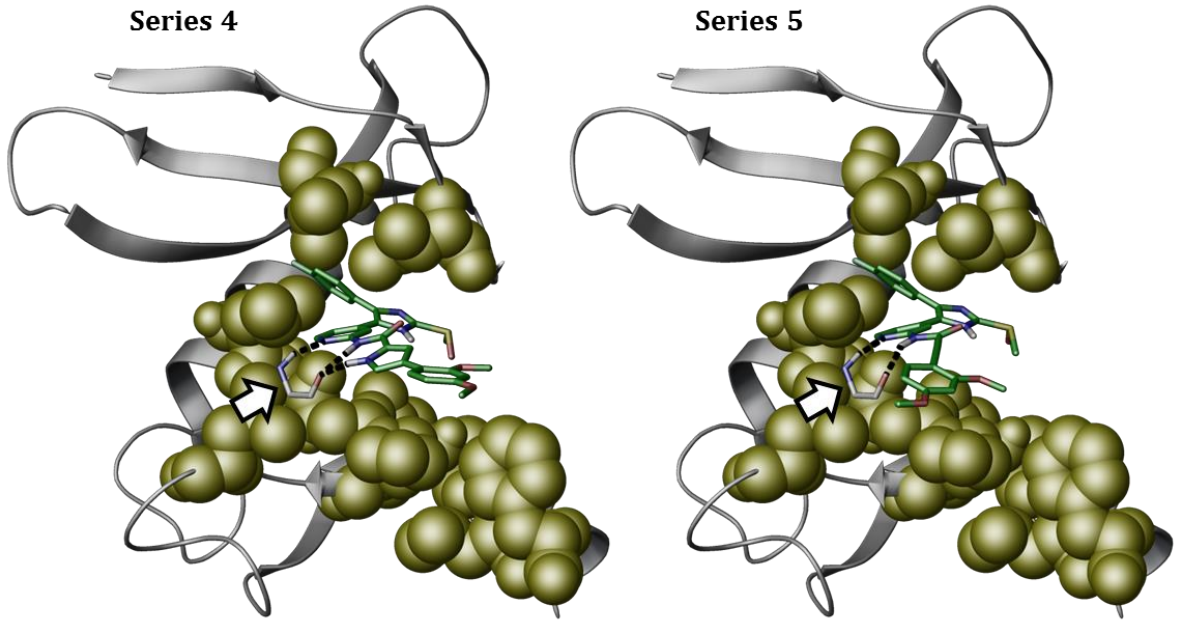

Figure 26 | Postulated binding modes of 105 and 106 in CK1δ. Three H-bonds are formed between compound **105** (series 4) and hinge Leu85 (arrow) while compound **106** (series 5) represents a bidentate hinge-binder. *HRII* residues are indicated with their VAN DER WAALS radii by yellow spheres (PDB code 3UZP).

In summary, both series represent interesting approaches that can be assumed to beneficially affect selectivity for CK1δ over other kinases. Especially the heteroaromatic side chains (series 4) might further provide enhanced potency, though this has to be evaluated *in vitro*.

Table 17 | *In silico* screened compounds of series 4 and 5. These series refer to acyl side chains that were designed to mimic the (*E*)-configured π-bond of the lead structure bearing either five-membered heterocycles (series 4) or an alkyne moiety (series 5). R = 2,4-dimethoxyphenyl.

		R^7	Glide score
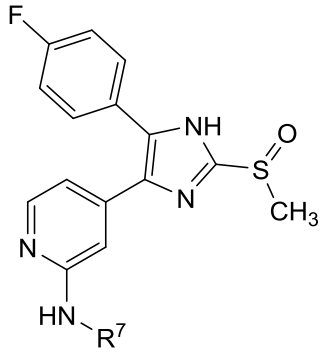	**107**	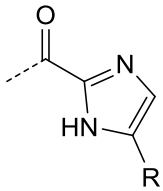	-16.8
	105	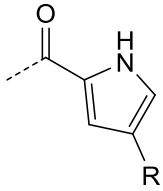	-16.7
	108	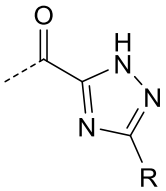	-16.6
	109	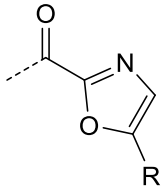	-14.6
	110	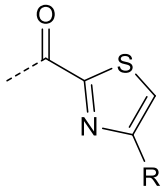	-14.6
	111	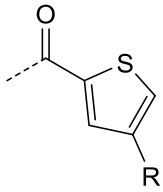	-14.3
	112	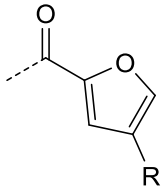	-14.1
	106	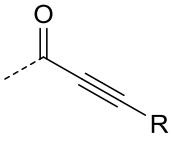	-13.7

Hybrid Inhibitors (Series 6)

Another approach was to adapt side chains from known kinase inhibitors with suitable properties and to attach them to 2-aminopyridinyl-imidazole **78**. Recent studies identified a class of nanomolar Porcupine (Porcn) inhibitors to be moderate inhibitors of CK1 isoform δ without showing inhibitory activity on the ε isoform and p38α at an inhibitor concentration of 1.0 μM (unpublished data by KUHL and KNIPPSCHILD). Porcn is a membrane-associated *O*-acyltransferase family member that catalyzes Wnt palmitoylation and thereby initiates Wnt activity. The compounds have therefore been initially designated as inhibitors of Wnt production (IWP)[210].

Molecular docking studies postulated a binding mode for these IWP with the dihydrothieno[3,2-*d*]pyrimidin-4-one side chain interacting with the hydrophobic region II of CK1δ. This binding mode is in accordance with the hypothesis of *HRII* being a main determinant for selectivity. The idea was to examine whether this effect can be grafted onto diaryl-imidazole inhibitors by hybridization. Although *in silico* evaluation of the generated hybrid inhibitors (**115**, **116**) deriving from IWP-2 (**113**) and IWP-4 (**114**, **Figure 28Figure 27**)[210] exhibited slight losses in ΔG compared to lead structure **12**, the *in vitro* effect on kinase specificity is worth to be investigated experimentally.

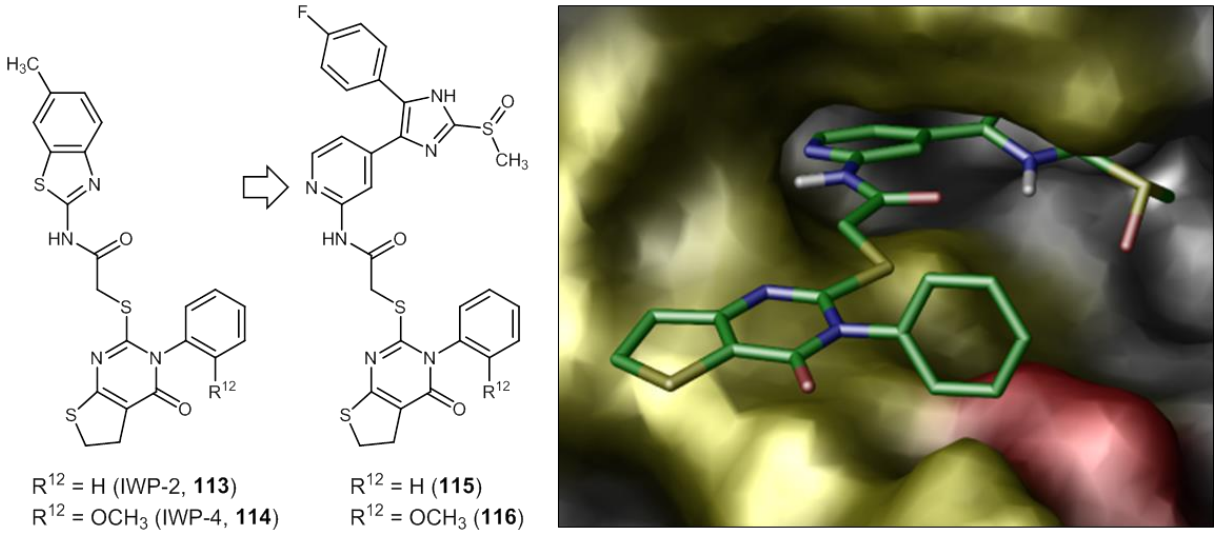

Figure 27 | Hybrid inhibitors 115 and 116 deriving from Porcn inhibitors 113 and 114. The postulated binding mode of **115** in CK1δ is depicted (right) (PDB code 3UZP).

The second class of hybrids concentrated on the 4-((4-methylpiperazin-1-yl)methyl)benzamide moiety of multiple tyrosine kinase inhibitor imatinib (**117**, **Figure 28**)[7,211]. The aromatic feature of the side chain was assumed to form multiple VAN DER WAALS interactions with the hydrophobic region II while the 4-methylpiperazine which will be positively charged under physiological conditions might donate an H-bond towards Asp91 (cp. series 1). Interestingly,

modeling suggested significant enthalpic gains (Glide score = -14.7) for hybrid inhibitor **118**, though no additional H-bond formation could be observed *in silico*. Regarding the development of imatinib itself, the moiety was introduced to enhance water solubility as well as oral bioavailability[211].

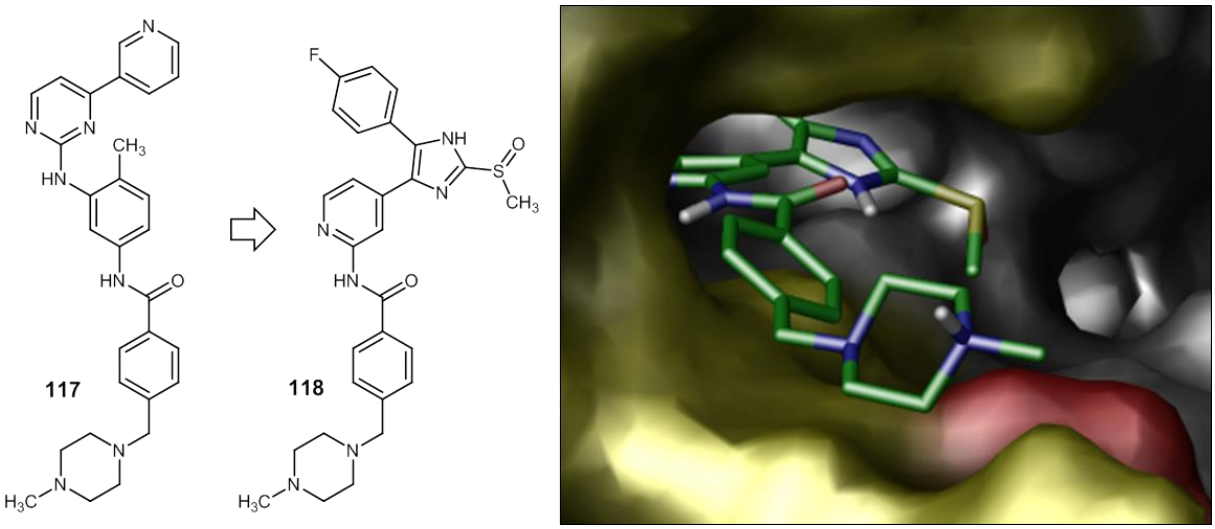

Figure 28 | Hybrid inhibitor 118 deriving from imatinib. The postulated binding mode in CK1δ is depicted (right) (PDB code 3UZP).

4 Chemistry

In order to synthesize differently amino-substituted 2-aminopyridinyl-imidazoles for SAR studies, a straightforward four-step synthesis towards 2-fluoro-4-(5-(4-fluorophenyl)-2-(methylthio)-1*H*-imidazole-4-yl)pyridine (**119**) has been established (**Figure 29**). Nucleophilic aromatic substitution (S_NAr) afforded alkyl amino-substituted diaryl-imidazoles (series 1), or the unsubstituted 2-aminopyridine derivative (**120**, building block). Coupling of **120** with activated carboxylic acids and isocyanates provided the respective amides (series 2, 4-6) and carbamides (series 3). Subsequent sulfoxidation towards sulfoxides was performed with several selected compounds. Both sulfides and sulfoxides have been biologically evaluated.

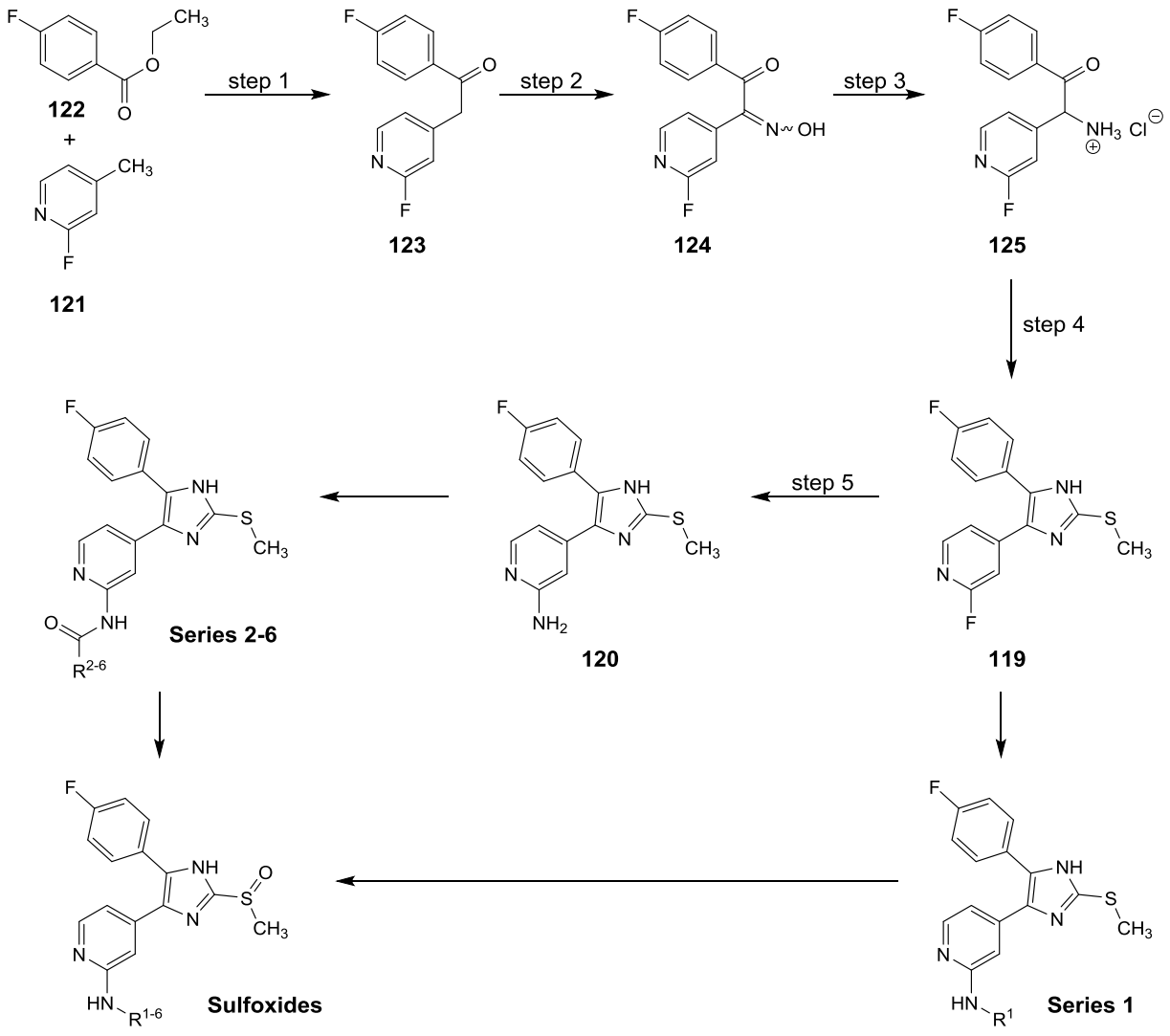

Figure 29 | Synthetic route towards inhibitors of series 1-6. Syntheses are given as an overview and will be discussed in detail in the following chapters (**4.1** to **4.8**).

4.1 Synthesis of Building Block 120

The syntheses of key intermediate **119** and building block **120** have already been described in literature and were mainly adapted from THOMPSON *et al.*[212] and LAUFER *et al.*[203]. In general, the five-step synthetic route depicted in **Figure 29** has been followed (procedure A). An alternative procedure has been performed starting from 2-amino-4-methylpyridine (**126**, procedure B) as nucleophilic aromatic substitution (S_NAr) towards **120** is critical and requires harsh reaction conditions (step 5, **Figure 29**). Low overall yields of this alternative protocol, however, led to acquisition of a high pressure reactor to cope with S_NAr of **119** as large quantities of building block **120** were required.

4.1.1 Procedure A

Ethanone **123** is easily accessible by the protocol of THOMPSON *et al.*[203,212] from 2-fluoro-4-methylpyridine (**121**) and ethyl 4-fluorobenzoate (**122**) in a CLAISEN-similar condensation. The CH-acidic methyl group in *ortho*-position to the picoline nitrogen is readily deprotonated by strong bases. Mesomeric stabilization involving the ring nitrogen is mandatory for reasonable progression of this step. The respective carbanion attacks the benzoate carbonyl group and replaces the ethanolate in a nucleophilic S_N2t substitution. The reaction was performed at temperatures between 0 °C and 25 °C (room temperature, rt) using sodium bis(trimethylsilyl)amide (NaHMDS) in anhydrous tetrahydrofuran (THF) under protective gas atmosphere (nitrogen) to afford **123** in quantitative yields.

The equivalent 2-bromo-4-methylpyridine (**127**) was reacted analogously, though the appropriate ethanone **128** was obtained in significantly reduced yields (**Figure 30**).

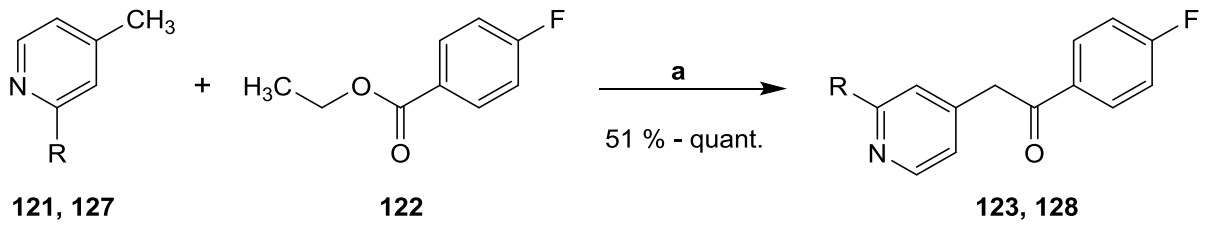

Figure 30 | Synthesis of ethanone derivatives 123 and 128. **121**, **123**: R = F; **127**, **128**: R = Br. **a**) NaHMDS, anhyd. THF, 2 h 0 °C then 1 h rt. Yield: quant. (**123**), 51 % (**128**).

The respective α-oximinoketones **124** and **129** were synthesized through nitrosation from the ethanones by exposure to nitrous acid at room temperature in excellent yields (**Figure 31**)[203]. ^{1}H NMR data indicated predominant formation of the favored regioisomer of at least 95 %.

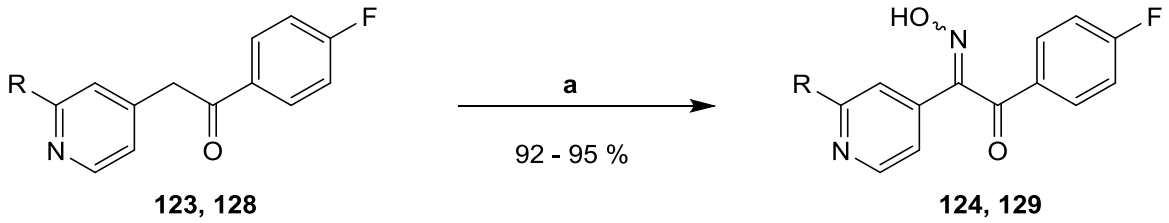

123, 128 **124, 129**

Figure 31 | Synthesis of α-oximinoketones 124 and 129. **123**, **124**: R = F; **128**, **129**: R = Br. **a**) Glacial acetic acid, $NaNO_2$, 1h 0 °C then 3.5 h rt. Yield: 95 % (**124**), 92 % (**129**).

Reduction of hydroxime **124** by catalytic hydrogenation using palladium on activated charcoal (Pd/C) afforded α-ketoamine **125**[203]. Acidic conditions were required for this synthesis to prevent reduction towards the amino alcohol. As 2-halogenopyridines are reportedly sensitive to primary alcohols regarding acid-catalyzed S_NAr reactions, the sterically more demanding 2-propanol was saturated with hydrogen chloride gas and used as solvent. Formation of the respective 2-isopropanoxy pyridine, however, would require heating under reflux[213]. The desired 2-aminoethanone hydrogen chloride was prepared under atmospheric pressure of hydrogen gas and intense stirring in good yields.

Despite using even more gentle reaction conditions as compared to literature[203], 2-bromopyridinyl α-ketoamine has not been maintained. Instead, hydrogenolytic cleavage afforded *ortho*-unsubstituted pyridine **130** (**Figure 32**).

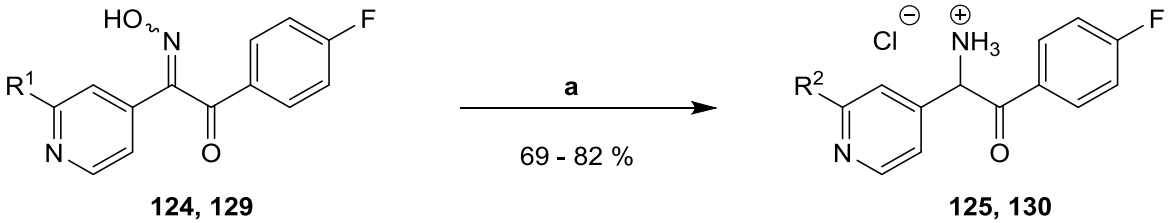

124, 129 **125, 130**

Figure 32 | Reduction of hydroximes 124, 128 towards α-aminoketones 125, 130. **124**, **125**: R^1 = R^2 = F; **129**, **130**: R^1 = Br, R^2 = H. **a**) H_2, Pd/C, 1 atm, HCl-saturated 2-propanol, 12 h rt. Yield: 82 % (**125**), 69 % (**130**).

Cyclization of α-ketoamine **125** using methyl thiocyanate in anhydrous *N*,*N*-dimethylformamide (DMF) gave key intermediate 2-methylthio-4,5-diaryl imidazole **119** in one step following a protocol based on an advanced MARCKWALD synthesis by ASINGER[203,214]. Conveniently, progress of the reaction was tracked visually: the initially light orange mixture turned an intensive bright orange upon heating to reflux under nitrogen. Completion of the reaction was indicated by

fading of the color. ^{1}H NMR spectroscopy indicated formation only of the favored imidazole tautomer (i.e. at least 95 %) which was obtained in good yields (**Figure 33**).

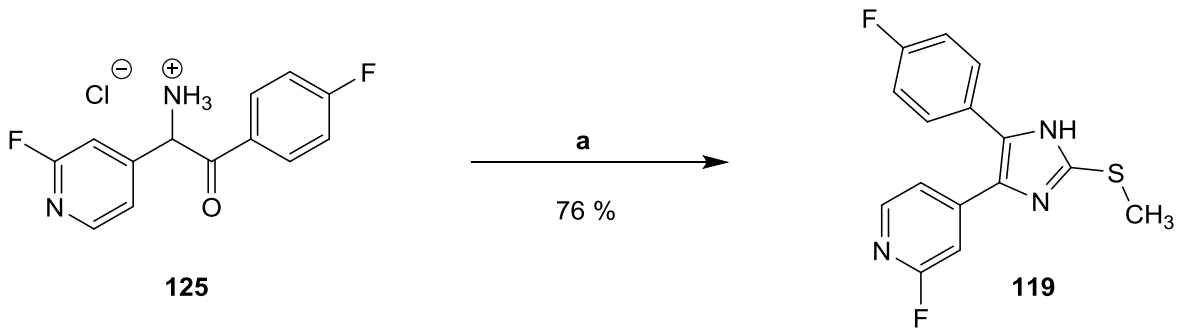

Figure 33 | Ring closure of α-ketoamine 125 towards key intermediate 119. **a**) Methyl thiocyanate, DMF, 45 min reflux then 45 min rt.

In a final step, building block **120** was accessible through a TSCHITSCHIBABIN reaction in concentrated ammonia at 180 °C under pressure (**Figure 34**)[193]. The electron deficient pyridine moiety is activated for S_NAr in *ortho*-position by the positive mesomeric effect of the ring nitrogen. The strong electronegative character of the fluorine atom in this exact position further enhances reactivity. Consequently, the respective amide attacks the pyridine C2 and substitutes the fluorine in an addition-elimination mechanism.

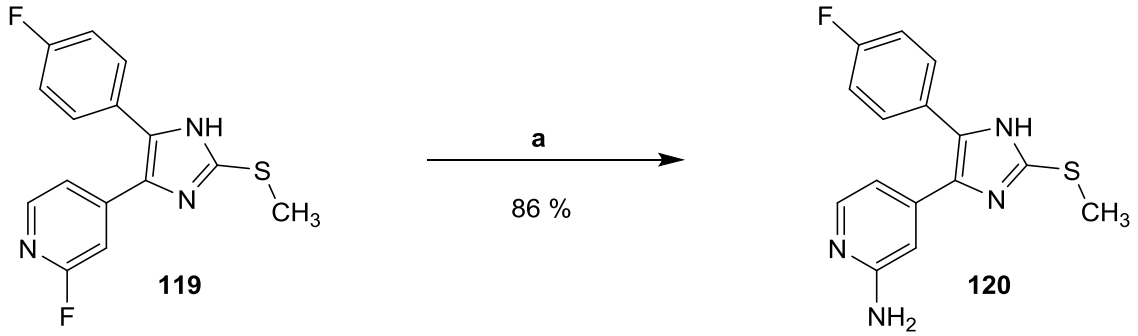

Figure 34 | Synthesis of building block 120 by S_NAr. **a**) Conc. aq. NH_3, 20-30 bar, 18 h 180 °C.

Interestingly, literature protocols typically involved copper(I) iodide-mediated catalysis[193] which led in our hands to partial cleavage of the thioether: although the by-product has not been isolated, mass spectrometry analysis indicated formation of the imidazole-2-thione. In fact, catalysis is not required under these conditions and abandoning copper(I) iodide from the reaction even enhanced yields in relation to literature.

An alternative method reported by PEIFER *et al.*[176] for an analogous 3,4-diaryl-isoxazole has been approached as well. The procedure involved the reaction of 2-fluoropyridine derivatives with sodium azide to afford the appropriate tetrazoles and subsequent reduction towards 2-aminopyridines. This technique, however, could not be adapted for the imidazole-containing

compound **119** and several approaches gave only unconverted starting material (**Figure 35**). This is interesting as the reaction proceeds well with analogous scaffolds including isoxazoles[176] or thiazoles[215] in place of the imidazole. It is most likely that the electron-donating effect of the imidazole reduces activation of the pyridine and thereby prevents formation of the MEISENHEIMER-like complex by S_NAr.

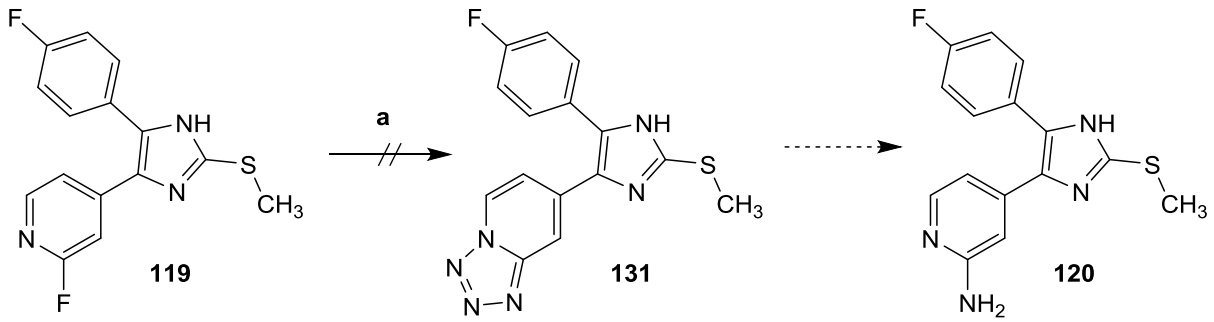

Figure 35 | Alternative potential procedure for the preparation of 120 from 119 via tetrazolo derivative 131. **a**) NaN_3, DMSO, 3 h 140 °C.

4.1.2 Procedure B

Procedure B was performed to investigate whether building block **120** could be synthesized starting from 2-amino-4-methylpyridine (**126**). Protection of **126** was performed using di-*tert*-butyl dicarbonate (Boc_2O) in *tert*-butanol affording carbamate **132**[202]. The Boc-protecting group has been selected because it is stable under basic conditions and readily cleaved upon treatment with acid which is beneficial for the following steps. Introduction of a second Boc group to **13** was achieved through STEGLICH-like esterification in THF adding 4-(dimethylamino)pyridine (4-DMAP) as a nucleophilic catalyst leading to compound **133**[216]. Interestingly, when **126** and Boc anhydride were reacted in THF, quantitative conversion towards 1,3-bis(4-methylpyridin-2-yl)carbamide (**134**) has been observed. The respective ethanone **135** was afforded from **133** following THOMPSON'S protocol as described for procedure A[203,212] in dramatically reduced yields. One of the Boc groups was cleaved in the process. It was further possible to synthesize **135** directly from mono-protected **132**, though with an increasing number of non-identified by-products and only when the reaction temperature was lowered to -78 °C. Nitrosation[203] gave α-oximinoketone **136** in approximately quantitative rates with less than 5 % of the non-preferred regioisomer (^1H NMR). Subsequent reduction[203] produced α-aminoketone **137** as a mixture of 2-aminopyrdinyl hydrogen chloride and the respective carbamate (mass spectrometry only). Finally, **120** was obtained by ring closure based on ASINGER (**Figure 36**)[203,214].

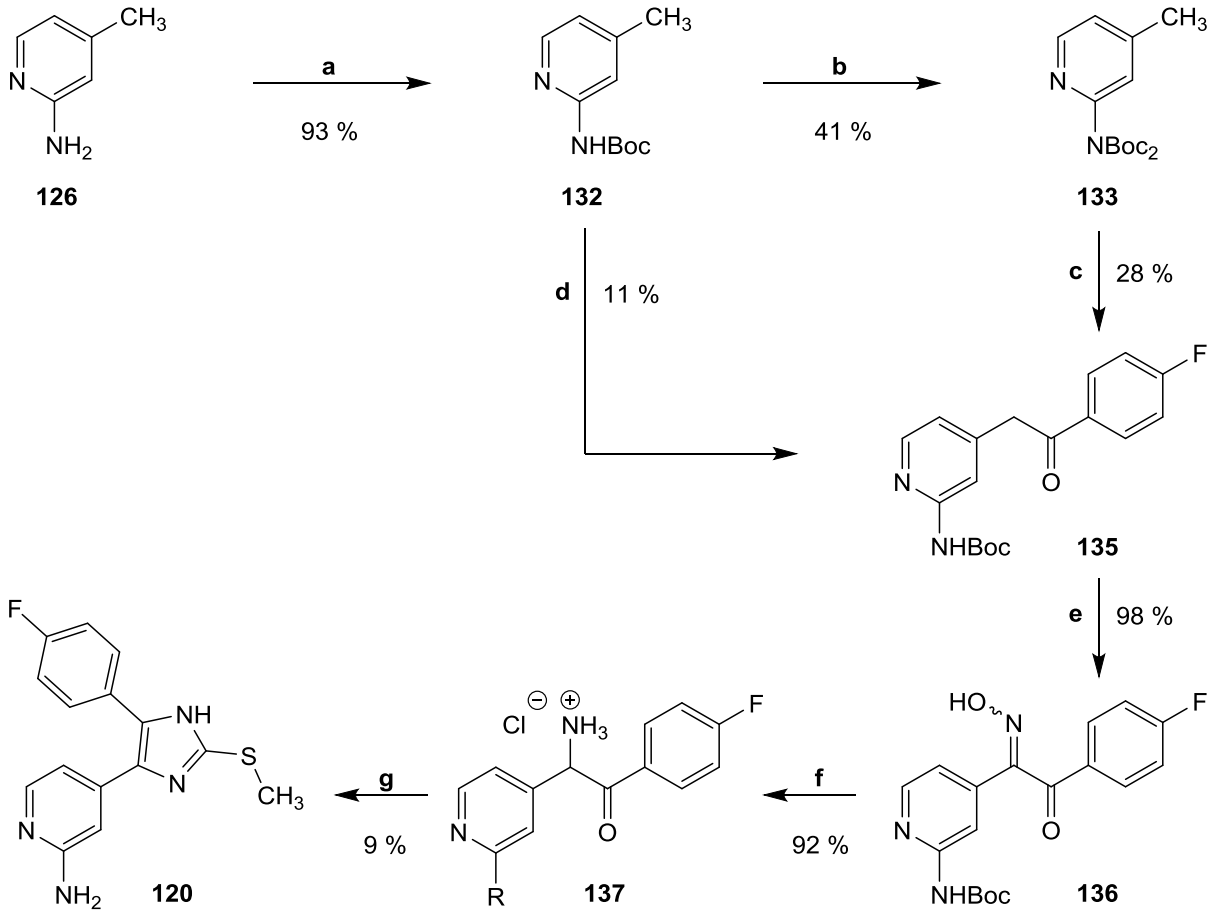

Figure 36 | Synthetic procedure B towards building block 120. **137**: R = $NH_3^+Cl^-$, NHBoc. **a**) Boc_2O, *tert*-butanol, 12 h rt. **b**) Boc_2O, 4-DMAP, THF, 24 h rt. **c**) **122**, NaHMDS, THF, 2 h 0 °C then 1 h rt. **d**) NaHMDS, **122**, 1 h -78 °C to rt then 2 h rt. **e**) Glacial acetic acid, $NaNO_2$, 1h 0 °C then 3.5 h rt. **f**) H_2, Pd/C, 1 atm, HCl-saturated 2-propanol, 12 h rt. **g**) Methyl thiocyanate, DMF, 45 min reflux then 45 min rt.

4.1.3 Synthesis of 2-unsubstituted 4,5-Diaryl-imidazole

In order to enable possible functionalization at the imidazole 2-position by nucleophilic substituents, a synthetic pathway towards 2-unsubstituted diaryl-imidazoles has been established (**Figure 37**). Oxidation of 1-(4-fluorophenyl)-2-(2-fluoropyridin-4-yl)ethan-1-one (**123**) was achieved in accordance to THAHER *et al.*[217,218] by selenium dioxide and gave 1,2-diketone **138**. Ring closure, however, was performed following a different protocol to avoid the use of formaldehyde. In fact, an elegant microwave-assisted method has been published by BRATULESCU[219]: the 1,2-diketone was reacted with ammonium acetate and methenamine (hexamethylenetetramine) as an *in situ* source of formaldehyde in the absence of solvent. Instead, a catalytic amount of glacial acetic acid was added to generate a thick paste-like medium. In this medium the polar solvent absorbs microwave radiation and creates catalytic

centers (hot spots) which initiate rapid cyclization and provide 4,5-disubstitued imidazole **139** in good yields.

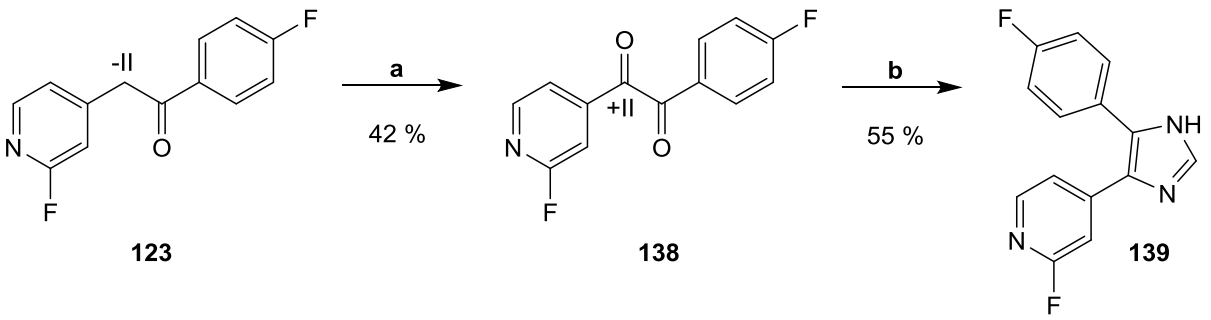

Figure 37 | Synthesis of 2-unsubstituted 4,5-diary-imidazole 139. **a**) SeO_2, glacial acetic acid, 1.5 h 95 °C. **b**) CH_3COONH_4, methenamine, glacial acetic acid (cat.), 4 min 117 °C (microwave).

It has to be noted that this synthetic approach has not been followed any further as the analog functionalization in 4,5-diaryl-oxazole and –thiazole inhibitors of CK1δ has become content to the master thesis of SCHMIDT[208] and SCHEHR[215], as well as SCHEHR'S dissertation (current labor).

4.2 Syntheses of Series 1: Pyridine-2-amines and -piperazines

In general, two different synthetic routes have been established to synthesize 4-(5-(4-fluorophenyl)-2-(methylthio)-1*H*-imidazol-4-yl)pyridin-2-amines. First, different aromatic and aliphatic primary and secondary amino substituents have been introduced at the pyridine 2-position of **119** by S_NAr (**chapter 4.2.1**). And second, by reacting aliphatic alkyl halides with 2-aminopyridines in an S_N2 mechanism (**chapter 4.2.2**):

4.2.1 S_NAr Reaction of 2-Fluoropyridines with Amines

The activation of 2-fluoropyridine **119** for S_NAr reactions has already been discussed (**4.1.1**). Different aromatic and aliphatic primary amines and piperazines are well-tolerated as nitrogen nucleophiles in this position following the procedure by LAUFER *et al*. (**Figure 38**)[197,203]. The nucleophilic substitutions could be performed in the absence of solvent (*green chemistry*). Instead, 2-fluoropyridine derivative **119** was dissolved or suspended in an excess of the respective amine and heated to 160 °C in a glass screw cap. These syntheses were performed by KUHL during her bachelor thesis[220] in 2013. In general, primary amines gave better yields than the applied piperazines. The appropriate amines and piperazines applied as starting material are summarized in **Table 18**.

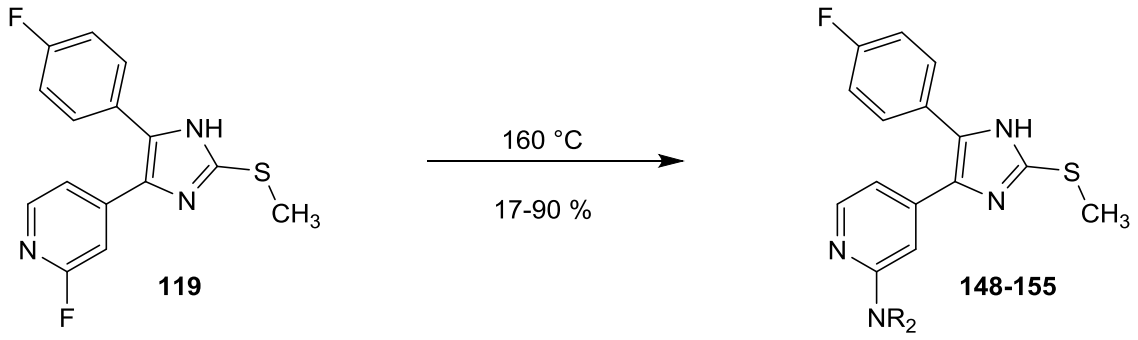

Figure 38 | Synthesis of pyridin-2-amine derivatives. Moieties (R) are given in **Table 18**.

Table 18 | Amines applied for S_NAr reaction towards pyrdin-2-amines. (Series 1).

Amine or Piperazine		# Product	Yield (%)
140	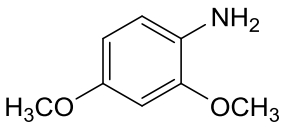	**148**	54
141	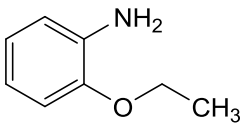	**149**	52
142	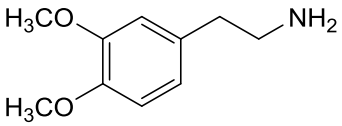	**150**	90
143	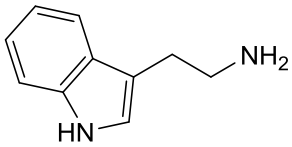	**151**	73
144	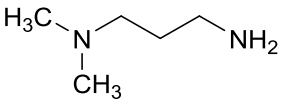	**152**	35
145	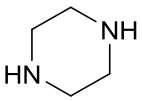	**153**	17
146	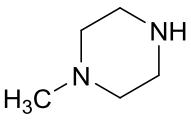	**154**	23
147	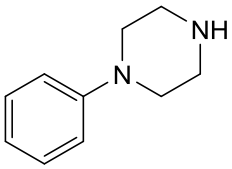	**155**	50

4.2.2 S_N2 Reaction of Alkyl Halides with 2-Aminopyridines

The idea was to incorporate primary alkyl halides such as 1-(3-bromopropyl)-2,4-dimethoxy-benzene (**156**) and 2-aminopyridines in an S_N2 reaction to provide the appropriate *N*-alkylpyridine-2-amines. As **156** was commercially not available it has been prepared from 2,4-dimethoxycinnamic acid (**157**) in three steps:

Reduction of 2,4-dimethoxycinnamic acid (**157**) towards the appropriate propionic acid **158** and alcohol **159**, respectively, was generally based on a procedure by LAL *et al.*[221], though the first step was adapted for microwave (**Figure 39**): 3-(2,4-dimethoxyphenyl)propionic acid (**158**) was obtained in a Pd/C-catalyzed reaction of **157** with cyclohexene acting as the reduction equivalent. The propionic acid was subsequently treated with lithium aluminum hydride under protecting gas atmosphere to give 3-(2,4-dimethoxyphenyl)propan-1-ol (**159**). Both reductive steps showed almost quantitative conversion.

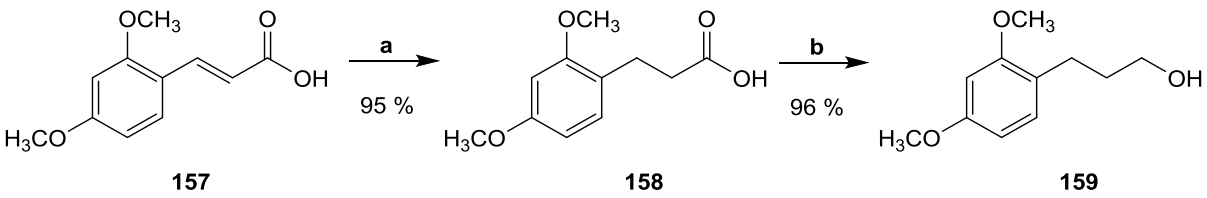

Figure 39 | Reduction of 2,4-dimethoxycinnamic acid (157). **a**) Pd/C, cyclohexene, methanol, 3 min (microwave). **b**) $LiAlH_4$, THF, 1 h rt.

Subsequent transformation of primary alcohol **159** into the desired alkyl bromide **156** was achieved by APPEL reaction with triphenylphosphine (PPh_3) and *N*-bromosuccinimide (NBS) instead of the usually applied carbon tetrabromide (**Figure 40**)[222].

Figure 40 | Conversion of primary alcohol 159 into alkyl bromide 156 by APPEL reaction. **a**) NBS, PPh_3, dichloromethane (DCM), 2 h rt.

In the following approaches, benzyl bromide has been used as an analog of **156** to determine suitable reaction conditions. The aim was to react the alkyl bromides in an S_N2 mechanism with building block **120** or Boc-protected building block **160**. Yields, however, were unsatisfying and an unacceptable amount of by-products was observed, among them e.g. a dibenzyl derivative (mass spectrometry data). As the 2-aminopyridine moiety of the building block is a poor

nucleophile in general and the protecting group of **160** has not been cleaved, substitution at the imidazole 1-nitrogen can be assumed, though the products have not been isolated. Hence, benzylation of Boc-protected 2-amino-4-methylpyridine (**132**) was tested: in the absence of the imidazole heterocycle, the S_N2t reaction readily afforded the benzyl carbamate **161** in good yields and high purity. Subsequently, *de-novo* synthesis starting from **161** gave the desired *N*-benzyl-4-(4-(4-fluorophenyl)-2-(methylthio)-1*H*-imidazol-5-yl)pyridin-2-amine (**162**). The procedure involved the already discussed steps of CLAISEN-like condensation towards the respective ethanone **163**, nitrosation, reduction, and cyclization (cp. **chapter 4.1**)[203,214] in excellent overall yields. Analogue synthesis applying 1-(3-bromopropyl)-2,4-dimethoxybenzene (**156**) afforded primary amine **164**[q].

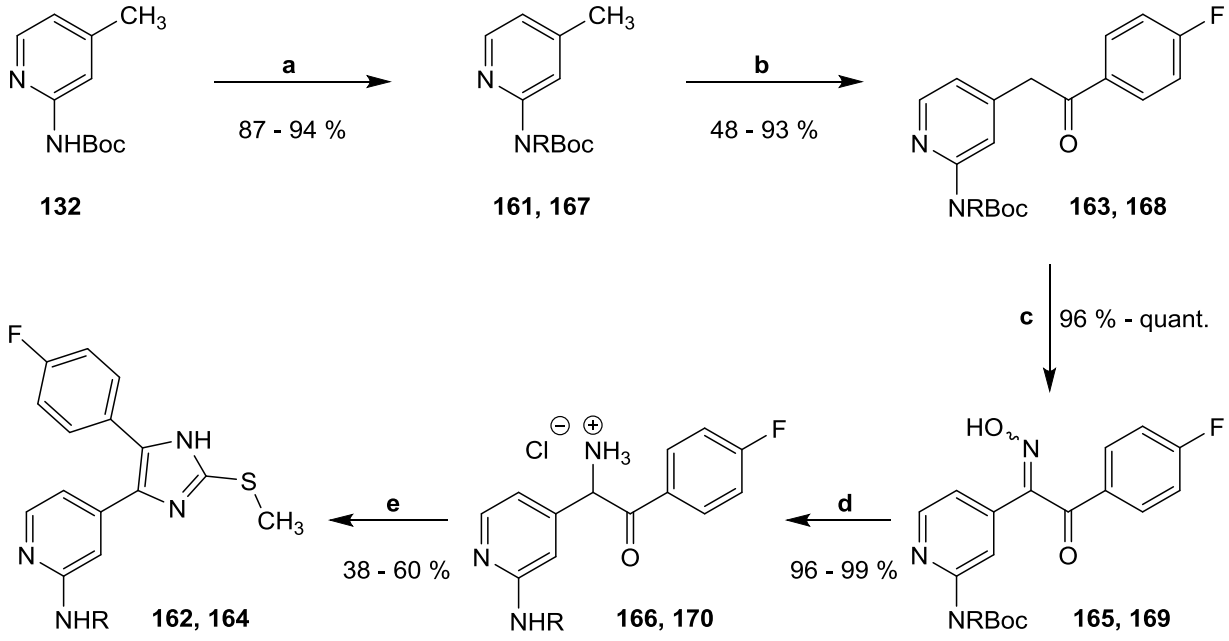

Figure 41 | *De-novo* synthesis of *N*-alkylated 4,5-diaryl-imidazoles. **161-163**, **165**, **166**: R = benzyl; **164**, **167-170**: R = 3-(2,4-dimethoxyphenyl)propyl. **a**) NaH, benzyl bromide or **156**, DMF, 20 min 0 °C then 2 h 0 °C to rt. Yield: 87 % (**161**), 94 % (**167**). **b**) **122**, NaHMDS, THF, 2 h 0 °C then 1 h rt. Yield: 93 % (**163**), 48 % (**168**). **c**) Glacial acetic acid, $NaNO_2$, 1h 0 °C then 3.5 h rt. Yield: 96 % (**165**), quant. (**169**). **d**) H_2, Pd/C, 1 atm, HCl-saturated 2-propanol, 12 h rt. Yield: 96 % (**166**), 99 % (**170**). **e**) Methyl thiocyanate, DMF, 45 min reflux then 45 min rt. Yield: 60 % (**162**), 38 % (**164**).

It is further noteworthy that **167** can also be synthesized from 3-(2,4-dimethoxyphenyl)-*N*-(4-methylpyridin-2-yl)propanamide (**171**) by $LiAH_4$-mediated reduction of the carbonyl affording **172** and subsequent Boc-protection. In order to provide **171**, propionic acid **158** was activated by (benzotriazol-1-yloxy)tripyrrolidinophosphonium hexafluorophosphate (PyBOP) and reacted with 2-amino-4-methylpyridine (**126**) in an amide coupling (for mechanism cp. **chapter 4.3**).

[q] **164** = *N*-(3-(2,4-dimethoxyphenyl)propyl)-4-(5-(4-fluorophenyl)-2-(methylthio)-1*H*-imidazol-4-yl)pyridin-2-amine

4.3 Syntheses of Series 2: Amide Coupling

Differently substituted 3-phenylpropionic acids were to be reacted with building block **120** in amide couplings. In order to determine the ideal coupling reagent, 2-amino-4-methylpyridine (**126**) as an analog of **120** was coupled with commercially available 3-(2,5-dimethoxy-phenyl)propionic acid (**173**) using either CDI[r], PyBOP, HATU[s], DCC[t], EDCI[u] plus 1-hydroxybenzotriazole (HOBt), or T3P[v] plus HOBt (**Table 19**). Equivalent reaction conditions were chosen if possible and the actual coupling was performed in all approaches for 12 h at 110 °C. The elevated temperature is necessary as 2-aminopyridine derivatives represent poor nucleophiles and more gentle conditions led to significantly decreased yields.

Table 19 | Determination of different amide coupling reagents.

Coupling reagent	Yield (%)	Product
CDI	72	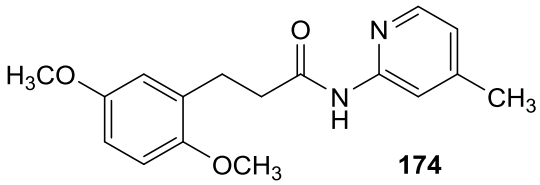 **174**
PyBOP	78	
HATU	75	
DCC	n.d.*	
EDCI, HOBt	55	
T3P, HOBt	0	

***** The overall yield was ~84 % but the pure product could not be isolated due to a single by-product.

Comparable yields and good purity were obtained by the use of CDI, PyBOP, and HATU while EDCI/HOBt gave lower amounts of the desired product. DCC exhibited formation of a single by-product which prevented isolation of pure **174**. No conversion of starting material has been observed upon use of the T3P/HOBt system.

Amide synthesis using CDI (**175**) is a standard procedure[223] which does not necessarily need an additional base as imidazole is generated *in situ* (**Figure 42**): in a first step the propionic acid (**173**) is deprotonated by one of the imidazole moieties. Nucleophilic attack of the carboxylate at the CDI carbonyl is followed by rapid formation of an acyl carboxy-imidazole and an imidazole which react together to afford the activated acylimidazole. The activated species and amine **126** are subsequently converted into the desired amide **174** in a S_N reaction. In practice, the acylimidazole step was reacted for at least 1 h before the amine was added.

[r] CDI = *N*,*N*'-carbonyldiimidazole
[s] HATU = 1-(bis(dimethylamino)methylene)-1*H*-1,2,3-triazolo[4,5-*b*]pyridinium-3-oxid hexafluorophosphate
[t] DCC = *N*,*N*'-dicyclohexylcarbodiimide
[u] EDCI = 1-ethyl-3-(3-dimethylaminoproyl)carbodiimide
[v] T3P = 1-propylphosphonic acid cyclic anhydride

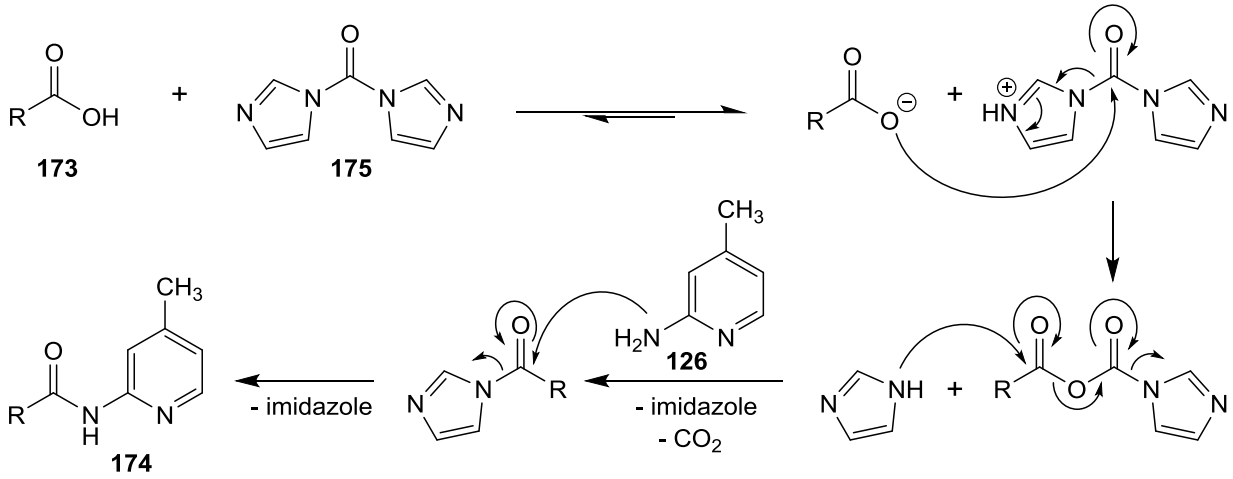

Figure 42 | Mechanism of CDI-mediated amide coupling. R = 3-(2,5-dimethoxyphenyl)propyl.

Coupling reagents based on phosphonium or aminium/uronium salts of 1*H*-benzotriazoles HOAt[w] (**176**) and HOBt (**177**) operate by similar mechanisms. HATU (**178**, **Figure 43**) has initially been reported as the HOAt uronium salt (*O*-isomer), though X-ray analysis identified the less reactive aminium form (*N*-isomer) to be the favored isomer. Activation is initiated by formation of oxy-7-azabenzotriazole (OAt) active esters (**179**) which react with the amine component. In general these active esters are known to repress racemization. Unfortunately, direct reaction of the amine with the coupling reagent itself leads to stable guanidinium derivatives in a side-reaction[223,224]. Phosphonium salt reagents such as PyBOP (**180**, **Figure 43**) act analogously through the respective oxybenzotriazole (OBt) active esters (**181**) without formation of the disadvantageous by-product. Active ester **181** has exemplarily been isolated and analyzed. Both HOAt and HOBt derivatives require deprotonation of the carboxylic acid by an alternative base in a first step which is usually realized by addition of HÜNIG'S base (*N*,*N*-diisopropylethylamine, DIPEA). The reactions are driven by formation of thermodynamically stable phosphine oxide (**182**) and tetramethylcarbamide (**183**), respectively (**Figure 44**). PyBOP[223–225] has been developed as the non-toxic alternative of its precursor BOP[x].

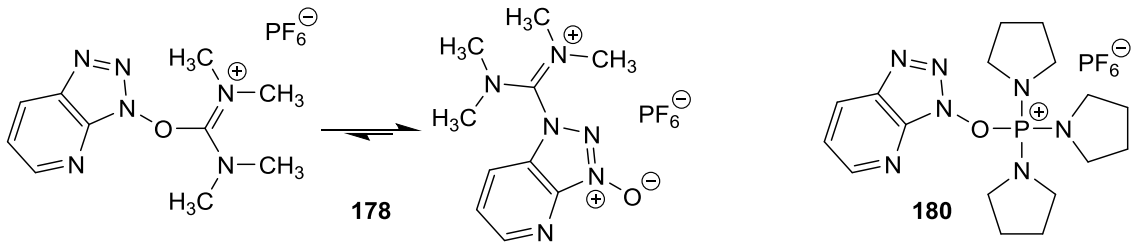

Figure 43 | Coupling reagents HATU (178) and PyBOP (180). At least for HATU, *O*- and *N*-isomers have been reported.

[w] HOAt = 1-hydroxy-7-azabenzotriazole
[x] BOP = (benzotriazol-1-yloxy)tris(dimethylamino)phosphonium hexafluorophosphate

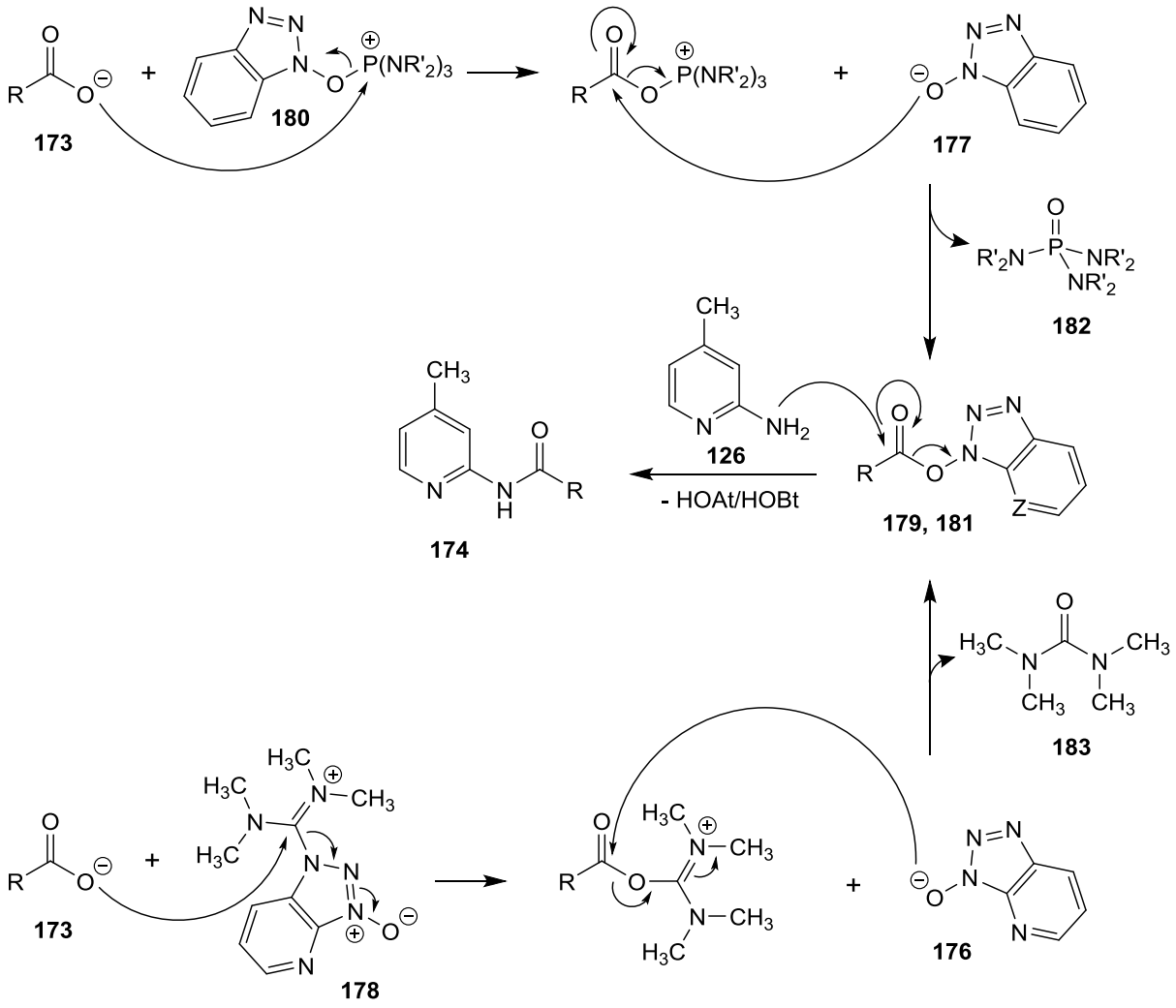

Figure 44 | Mechanism of HATU- and PyBOP-mediated amide coupling. R = 3-(2,5-dimethoxyphenyl)propyl; NR'$_2$ = pyrrolidin-1-yl. **179**: Z = N; **181** Z = C.

DCC (**184**)-mediated STEGLICH-amidation also provided the desired product in similar amounts. In general, carbodiimides were the first coupling reagents described in literature, though they have lost much of their importance in peptide coupling due to the number of possible by-products. In order to reduce side-reactions, the addition of HOBt has proved beneficial by initially converting the intermediate *O*-acylcarbamide **185** into the active ester **181**. An alternative base is not necessary as DCC itself deprotonates the carboxylic acid. In the case of STEGLICH-esterification the reaction depends on 4-DMAP-mediated catalysis[224,226]. Regarding the current amidation, application of the catalyst did not reveal any effect on yield, but has been associated with the reduction of by-products. Nevertheless, the product has not been obtained purely: the compellent carbamide by-product **186** which has been indicated by mass spectrometry could not be separated from amide **174** (**Figure 45**).

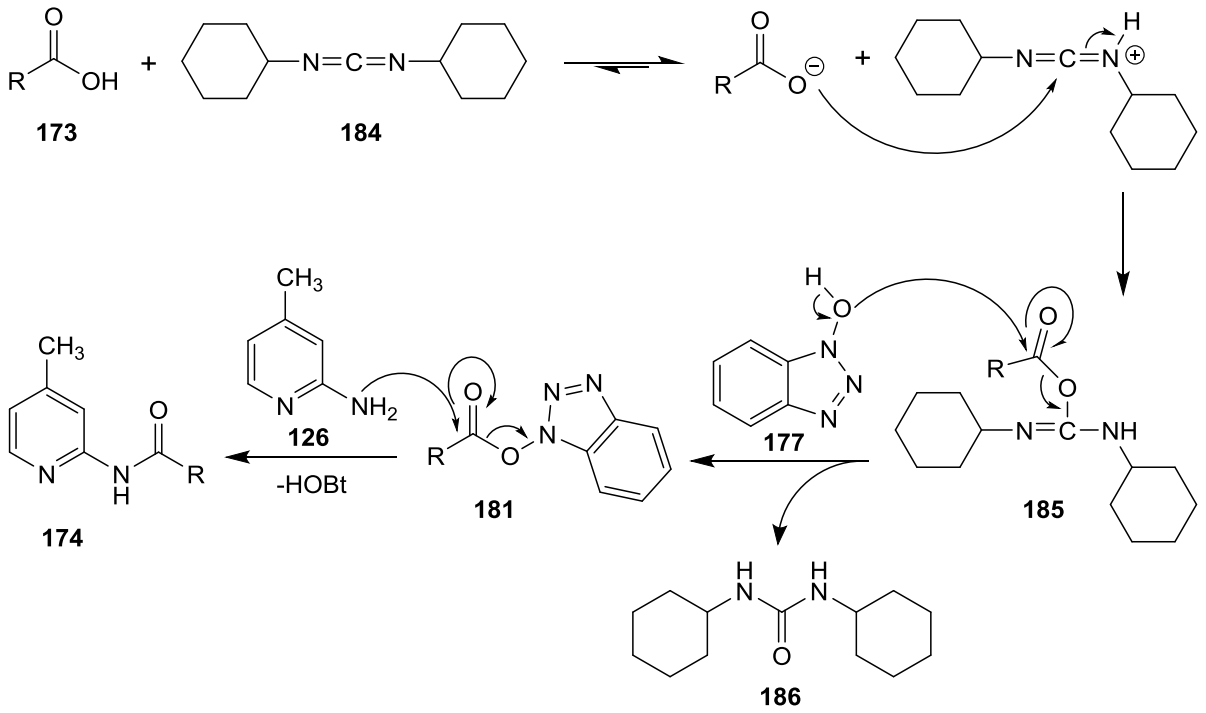

Figure 45 | Mechanism of DCC-mediated amide coupling. R = 3-(2,5-dimethoxyphenyl)propyl.

In contrast to reactions mediated by DCC, carbodiimide reagent EDCI generates carbamide by-products which can readily be separated from the product. The decreased yield in this work, however, led to the refusal of both DCC and EDCI for further amidations. Consequently, amide coupling reactions have been performed using CDI or PyBOP for their easy handling, high yields, good purity, and cost-effectiveness.

In accordance, 3-(2,4-dimethoxyphenyl)- (**158**), 3-(2,5-dimethoxyphenyl)- (**173**), 3-(2,3-dimethoxyphenyl)- (**187**), 3-(3,4-dimethoxyphenyl)- (**188**), and 3-(3,4,5-trimethoxyphenyl)-propionic acid (**189**) have been coupled CDI-mediated with building block **120** to obtain the respective amides **190-194** (**Figure 46**). The decreased yields in relation to the appropriate dummy reaction presumably depend on the more demanding purification.

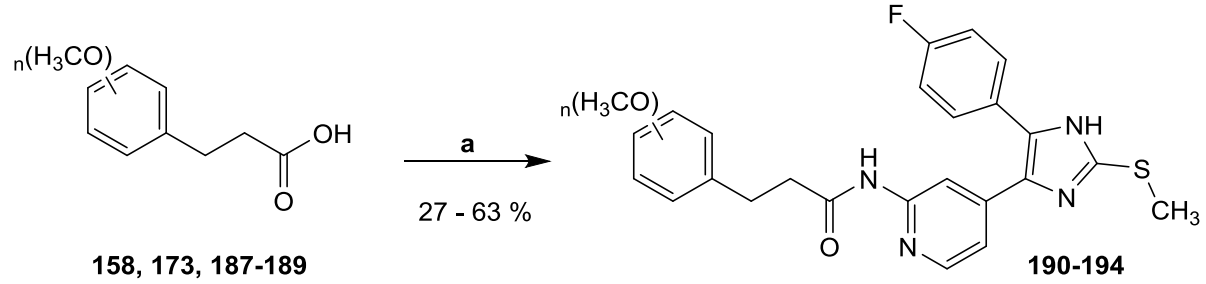

Figure 46 | Amide coupling of 3-(di-/tri-methoxyphenyl)propionic acids and 120. **158**, **190**: 2,4-dimethoxyphenyl; **173**, **191**: 2,5-dimethoxyphenyl; **187**, **192**: 2,3-dimethoxyphenyl; **188**, **193**: 3,4-dimethoxyphenyl; **189**, **194**: 3,4,5-trimethoxyphenyl. **a**) CDI, 120 °C, DMF, rt then 12 h 110 °C. Yield: 27 % (**190**), 39 % (**191**), 63 % (**192**), 57 % (**193**), 49 % (**194**).

4.4 Syntheses of Series 3: Carbamide Derivatives

Heterocumulenes such as isocyanates represent chemically highly active molecules which readily react with different nucleophiles. Accordingly, isocyanates **195**-**203** (**Table 20**) have been converted with building block **120** into the respective carbamides **204**-**212** in a WÖHLER-like synthesis[227]. Addition of HÜNIG'S base led to increased yields. Mechanistically, the nucleophilic attack of the amine at the *sp*-hybridized isocyanate carbon atom leading to formation of the trigonal-planar (sp^2) transitional state depicts the rate-determining step (**Figure 47**)[228]. Unfortunately, the resulting carbamide derivatives were hardly soluble in most standard solvents and purification was tedious. **207** and **211** have therefore not been isolated in adequate purity.

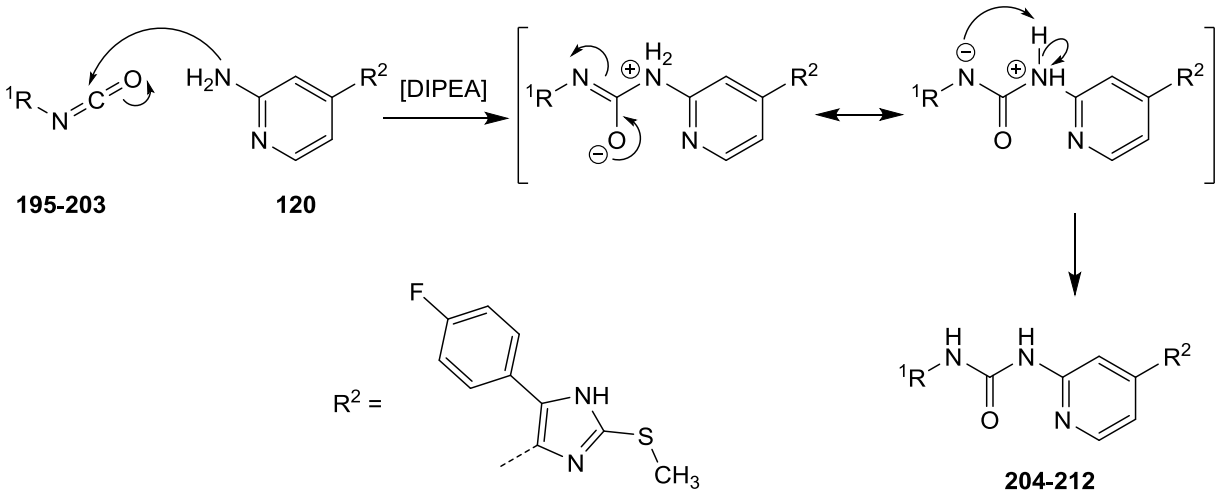

Figure 47 | Mechanism of carbamide derivative synthesis. For isocyanate R^1 cp. **Table 20**.

Beside amines, isocyanates react with different nucleophiles as characterized for **195**: in the presence of water the isocyanate is converted into the respective carbamic acid **213** which is instable and decomposes into carbon dioxide and the appropriate amine **214**. The amine further reacts with another isocyanate molecule to the dimer carbamide **215** (**Figure 48**) that can be isolated.

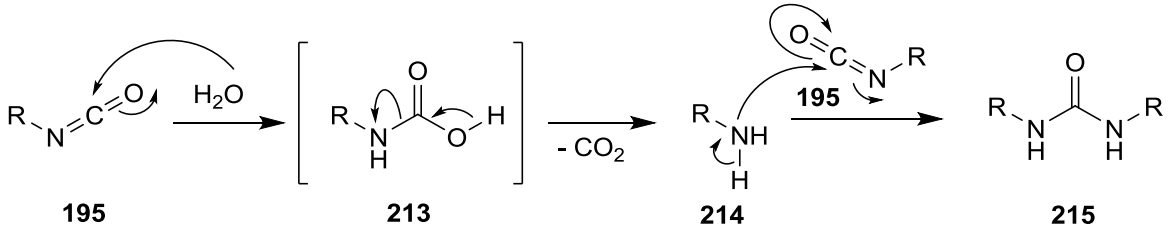

Figure 48 | Formation of dimer carbamide by-product 215 from isocyanate 195 in the presence of water. R = 2,4-dimethoxyphenyl.

The reactions have therefore been performed in anhydrous DMF under protective gas atmosphere. Addition of molecular sieve to the reaction mixture has also proved beneficial[229].

Table 20 | Isocyanates applied for synthesis of carbamide derivatives. (Series 3).

Isocyanate		# Product	Yield (%)
195	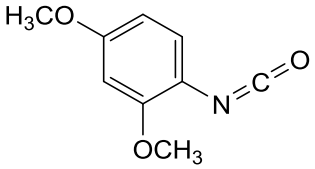	**204**	21
196	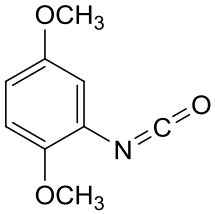	**205**	15
197	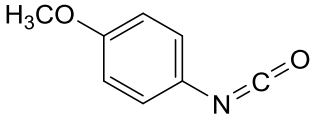	**206**	26
198	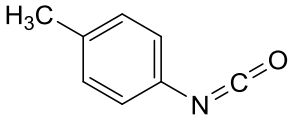	**207**	n.d.*
199	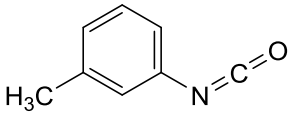	**208**	28
200	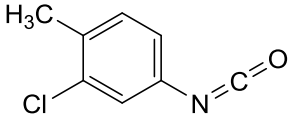	**209**	34
201	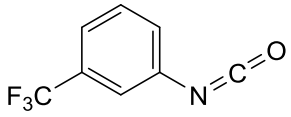	**210**	26
202	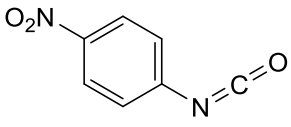	**211**	n.d.*
203	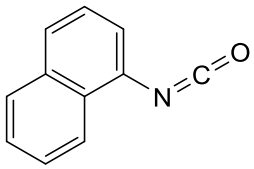	**212**	41

***** Product has been identified by mass spectrometry, but has not been isolated in adequate purity.

4.5 Syntheses of Series 4: Five-membered Heterocycles

As discussed in **chapter 3.1.5** several side chains conserving the originally present (*E*)-configuration within different five-membered heterocycles (**Figure 49**) should be coupled in the pyridine *ortho*-position of building block **120**. None of these heterocyclic acids were commercially available and therefore a selection ought to be prepared in parallel synthesis. Among them were pyrroles, thiazoles, imidazoles, and triazoles.

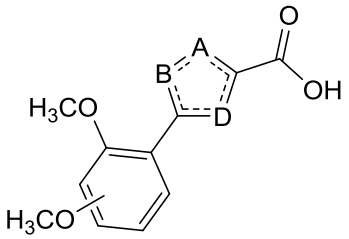

Figure 49 | Schematic representation of acid side chains of series 4. A, B, D refer to carbon, nitrogen, or sulfur.

4.5.1 Synthesis of 4-(dimethoxyphenyl)pyrrole-carboxamides

Synthesis of 4-(2,4-dimethoxyphenyl)pyrrol-2-carboxylic acid (**216**) has been realized in three steps starting from ethyl 4-bromo-1*H*-pyrrole-2-carboxylate (**217**, **Figure 50**)[230]. First, the pyrrole nitrogen was protected using Boc anhydride. The obtained carbamate (**218**) was subsequently converted in a SUZUKI cross-coupling using organoboronic acid to afford ethyl 4-(2,4-dimethoxyphenyl)-1*H*-pyrrole-2-carboxylate (**219**). Simple ester hydrolysis in diluted alkali gave pyrrolic acid **216**. Finally, the respective carboxamide **220** was obtained by amide coupling of **216** and building block **120**. Reaction conditions for successful amide couplings were first evaluated in a dummy synthesis of *N*-(4-methylpyridin-2-yl)-1*H*-pyrrol-2-carboxamide (**221**) using 1*H*-pyrrole-2-carboxylic acid and 2-amino-4-methylpyridine (**126**).

Unfortunately, **220** was subject to slow oxidation under atmospheric conditions maybe towards a pyrrole *N*-oxide (not isolated) as alkylation of the pyrrole nitrogen with methyl iodide or benzyl bromide forestalled this side reaction. The alkyl groups have also been introduced successfully on the step of carboxylate **219** and acid **216**, though with decreasing yields. *N*-Methylated 4-(2,5-dimethoxyphenyl)pyrrolic acid (**222**) and the appropriate carboxamide **223** have been synthesized in accordance to this procedure. Active ester **224** of 3-(2,4-dimethoxy)-1-methyl-1*H*-pyrrole-2-carboxylic acid (**225**) has been isolated and analyzed exemplarily.

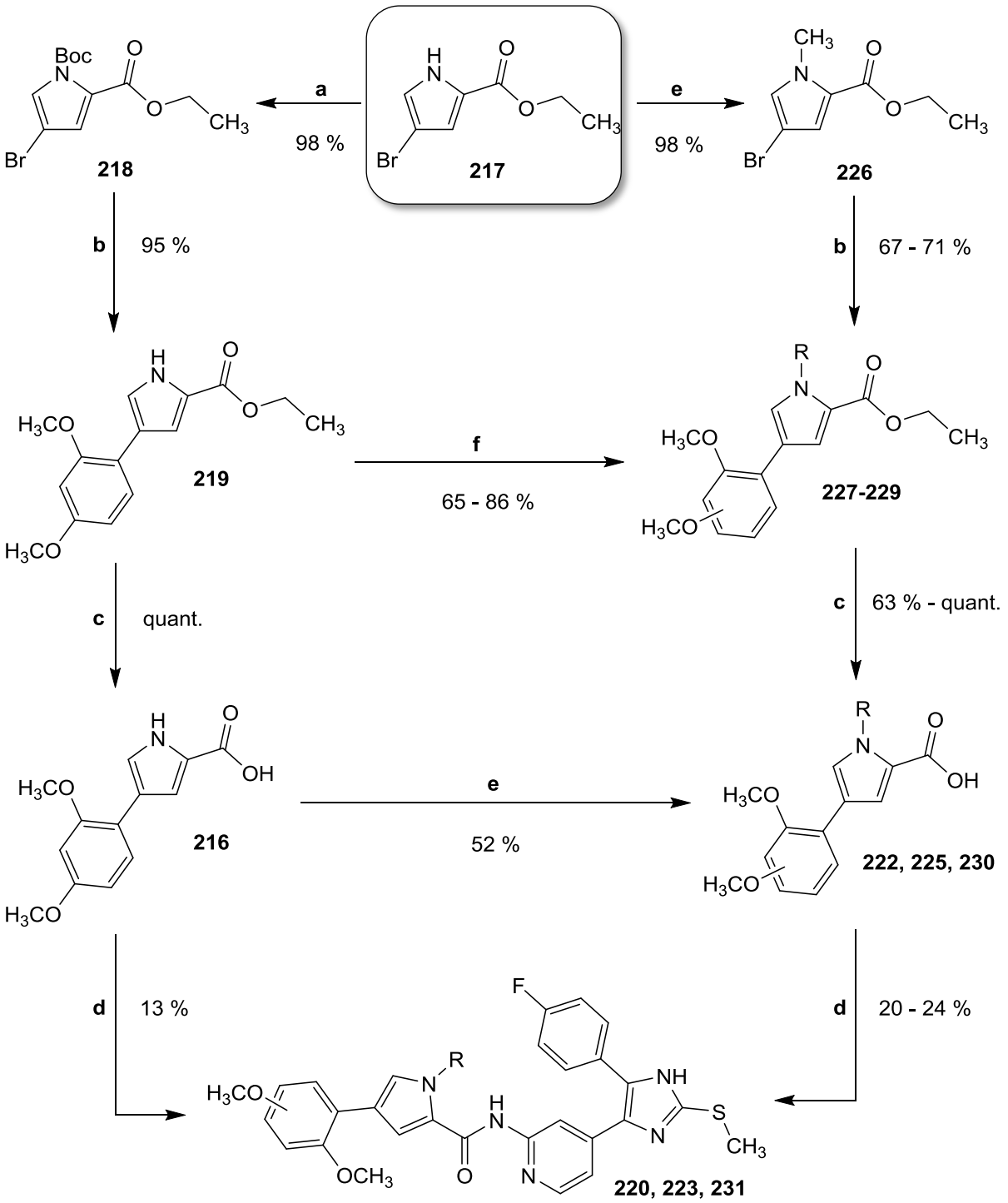

Figure 50 | Synthesis of carboxamides 220, 223, 231 of Series 4. **220**: R = H, 2,4 dimethoxyphenyl; **227**, **225**, **231**: R = CH_3, 2,4-dimethoxyphenyl; **228**, **230**: R = Bn, 2,4 dimethoxyphenyl; **223**, **224**, **230**: R = CH_3, 2,5-dimethoxyphenyl. **a**) Boc_2O, 4-DMAP, ACN, 1 h rt. **b**) 2,4-dimethoxyphenyl boronic acid, $Pd(PPh_3)_4$, aq. Na_2CO_3, DMF, 4 h reflux then 12 h rt. Yield: 67 % (**227**), 71 % (**229**). **c**) aq. NaOH, THF/methanol, 5 h 50 °C then 12 h rt. Yield: 63 % (**230**), quant. (**222**), quant. (**225**) **d**) PyBOP, DIPEA, DMF, 30 min rt, then **120**, 12 h 110 °C. Yield: 13 % (**220**), 20 % (**223**), 24 % (**231**). **e**) NaH, DMF, 20 min 0 °C, then CH_3I, 15 min 0 °C then 2.5 h rt. Yield: 52 % (**225**). **f**) NaH, DMF, 20 min 0 °C, then CH_3I or BnBr, 15 min 0 °C then 2.5 h rt. Yield: 65 % (**228**), 86 % (**227**).

With respect to the rather low yields, efforts were undertaken to enhance nucleophilicity of the 2-aminopyridine moiety by deprotonation of the amino group. Therefore, amine **120** has been stirred with sodium hydride in DMF at room temperature before active ester **224** was added. Interestingly, by analyzing the product ^{1}H NMR data suggested the side chain to be mainly attached to the imidazole nitrogen assuming this to be the predominant position for deprotonation. It has to be mentioned, though, that the respective NMR data suffered from poor resolution and did not allow complete analysis. Nevertheless, the imidazole and amide NH are herein only slightly visible whereas they normally produce clear and distinct signals.

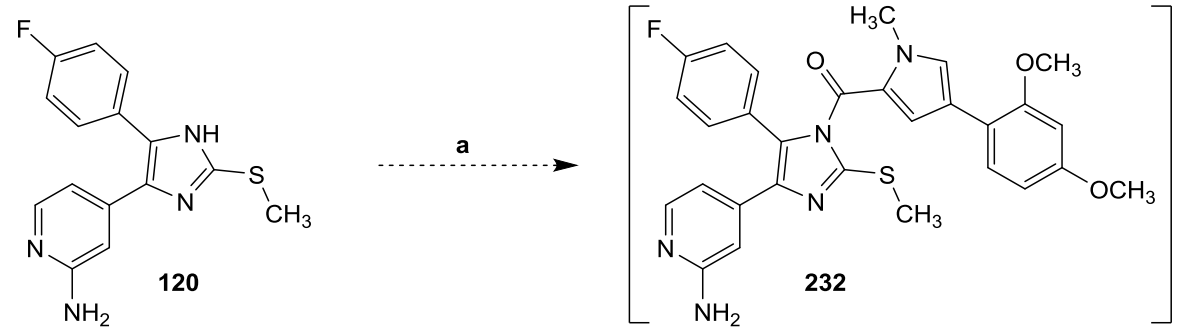

Figure 51 | Reaction of building block 120 and active ester 224 in the presence of base. **a**) NaH, DMF, 30 min rt, then **224**, 72 h rt.

Based on these observations we decided an intermediate protection of the imidazole: **120** was to be deprotonated at the imidazole NH at -78 °C by one equivalent of *n*-butyllithium (^{n}BuLi) and temporarily protected as the collaborating carbamic acid **233**. Therefore, carbon dioxide was bubbled through the reaction mixture at -40 °C. Subsequently, careful addition of *tert*-butyllithium (^{t}BuLi) at -78 °C in order to deprotonate the amino group was followed by addition of active ester **224**. The reaction was allowed to reach room temp. over a period of approx. 12 h. Unfortunately, this approach also failed and the starting material was regained unconverted.

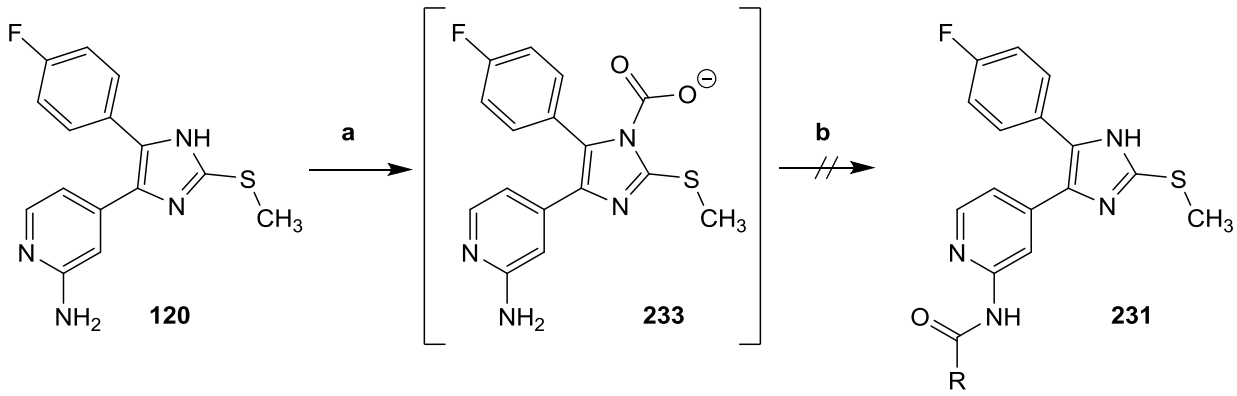

Figure 52 | Aimed reaction procedure towards 231 via intermediate protection of the imidazole nitrogen. R = 4-(2,4-dimethoxyphenyl)-1-methyl-1*H*-pyrrole-2-yl. **a**) ^{n}BuLi, THF, 35 min -78 °C, then CO_2, 1.5 h -40 °C. **b**) ^{t}BuLi, 30 min -78 °C, then **224**, -78 °C to rt over 12 h, 12 h rt.

4.5.2 Synthesis of Thiazole-containing Side Chains

Synthesis of 4-(2,4-dimethoxyphenyl)thiazole-2-carboxylic acid (**234**) has been performed in three steps: first, bromination of 2,4-dimethoxycetophenone (**235**) in ω-position or FRIEDEL-CRAFTS acylation of 1,3-dimethoxybenzene (**236**); second, cyclization of the appropriate 2,4-dimethoxyphenacyl halides **237** and **238** in accordance to HANTZSCH thiazole synthesis; and third, ester hydrolysis of thiazole-2-carboxylate **239**.

4.5.2.1 ω-Bromination of Acetophenones

The acid-catalyzed ω-halogenation of acetophenone is a standard procedure[231]: enolization is followed by electrophilic attack of the bromine molecule at the nucleophilic enole carbon. An acidic milieu is inevitable as basic catalysis is known to provide triple ω-halogenated derivatives. Although the reaction worked satisfactory for the conversion of acetophenone (**240**) into phenacyl bromide (**241**), it failed when 2,4-dimethoxyacetophenone (**235**) was applied as starting material. As expected, the positive mesomeric effect of the methoxy groups activates the aromatic compound for electrophilic substitution in the *ortho*- and *para*-positions. Consequently, 3-bromo-2,4-dimethoxyphenacyl bromide (**242**) was obtained instead (**Figure 53**).

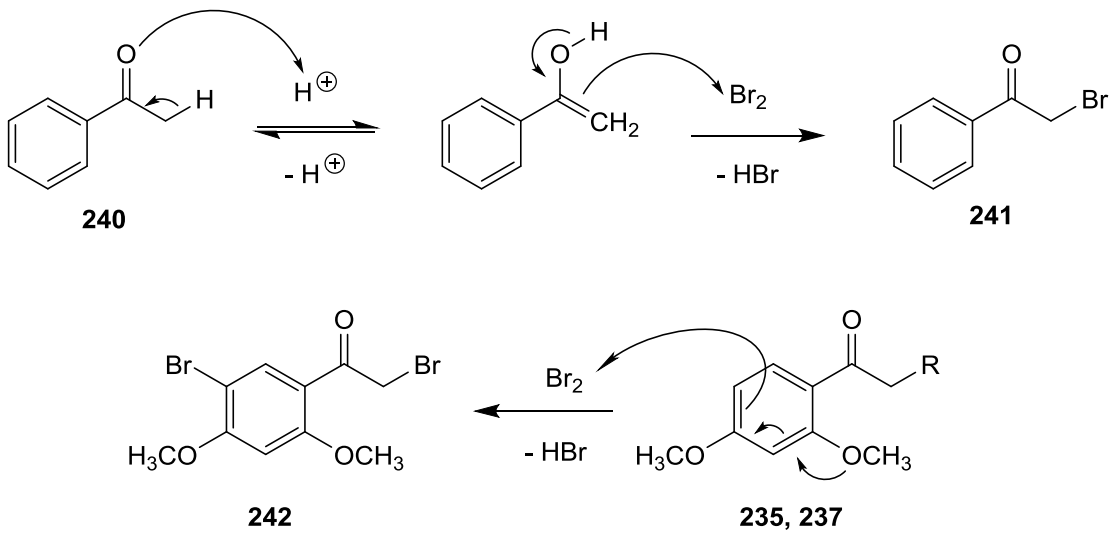

Figure 53 | Acid-catalyzed ω-bromination of acetophenones with bromine. **235**: R = H; **237**: R = Br.

This problem was handled following the protocol by KING *et al.*[232]: copper(II) bromide selectively brominates the ω-position of activated acetophenones in ethyl acetate. In fact, nearly quantitative conversion was obtained upon addition of two equivalents of $CuBr_2$. The appropriate mechanism is most likely characterized by a radical reaction involving simultaneous one-electron transfers within the copper-bound enolate complex whereas copper(II) is reduced to copper(I) (**Figure 54**)[233].

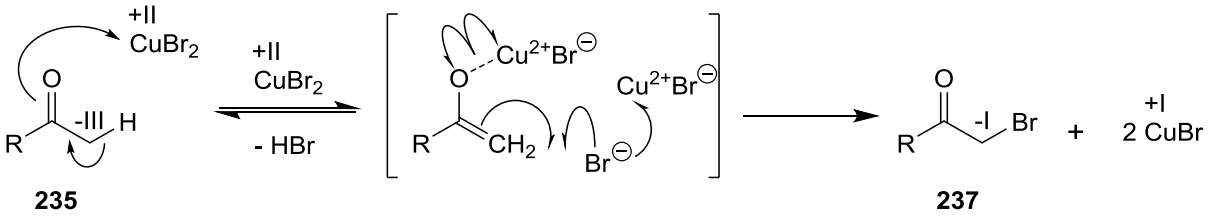

Figure 54 | Selective radical ω-bromination of 2,4-dimethoxyacetophenone with Copper(II) bromide. R = 2,4-dimethoxyphenyl.

4.5.2.2 FRIEDEL-CRAFTS Acylation of 1,3-Dimethoxybenzene

The S_EAr reaction was performed in accordance to standard literature[231] using 1,3-dimethoxybenzene (**236**) and chloroacetyl chloride (**243**). Addition of a LEWIS acid catalyst is inevitable for the formation of acylium ions which attack the aromatic compound in an electrophilic manner. The procedure readily afforded 2,4-dimethoxyphenacyl chloride (**238**) in equivalent yields as reported in literature (**Figure 55**).

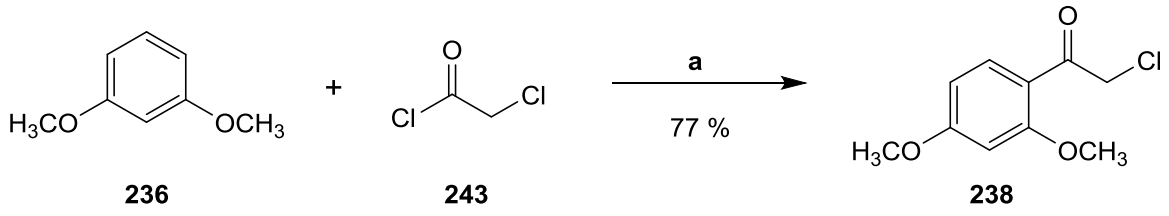

Figure 55 | FRIEDEL-CRAFTS acylation of 1,3-dimethoxybenzene. **a**) $AlCl_3$, 3 h 0 °C.

4.5.2.3 Cyclization of Phenacyl Halides by HANTZSCH Synthesis

The cyclization of phenacyl halides **237** and **238** was achieved with thioamide **244** by HANTZSCH thiazole synthesis following a protocol for microwave radiation[234]. Mechanistically, the reaction comprises two steps in accordance to the HSAB concept[235]: substitution of the halogen atom by the thiol tautomer of **244** in an addition-elimination (S_N2t) mechanism and formation of an imine by intramolecular *exo-trig* cyclization (**Figure 56**). In accordance to the BALDWIN rules[235] it is most likely that these two steps do not occur in a definite order: initial formation of the imine might be followed by intramolecular *exo-tet* cyclization as well. The mechanism provides rapid access to thiazole derivative **239** in good yields and purity.

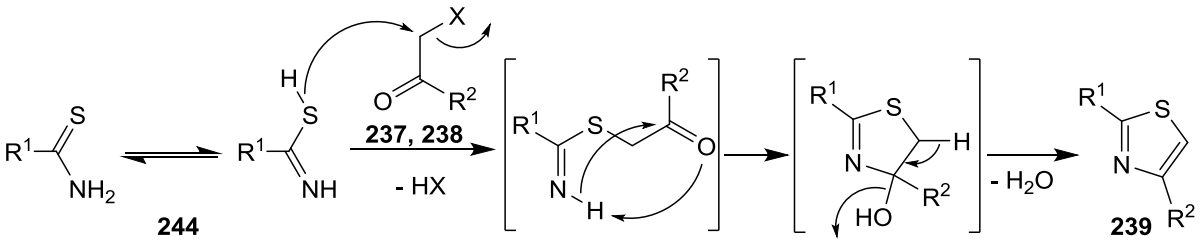

Figure 56 | Cyclization mechanism of phenacyl halides and thioamide 244 by HANTZSCH synthesis. R^1 = ethyl carboxylate; R^2 = 2,4-dimethoxyphenyl; X = Br, Cl.

4.5.2.4 Ester Hydrolysis of Ethyl Thiazole-2-carboxylate 239

Several systematic approaches have been tried out for ester hydrolysis of **239** in diluted alkali to gain carboxylic acid **234**. These involved different solvents and bases, temperatures, and variation of reaction time. Unfortunately, formation of the carboxylic acid has in all cases been followed by rapid and quantitative decarboxylation towards 4-(2,4-dimethoxyphenyl)thiazole (**245**). The desired product has therefore only been obtained as an unstable intermediate which could not be isolated.

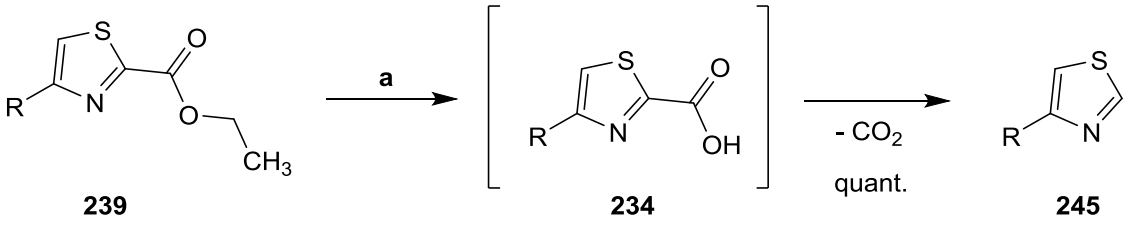

Figure 57 | Ester hydrolysis and subsequent decarboxylation of ethyl thiazole-2-carboxylate 239. R = 2,4-dimethoxyphenyl. **a**) Aq. NaOH, THF/methanol, 48 h rt.

4.5.3 Synthesis of Imidazole-containing Side Chains

Preparation of ethyl 4-(2,4-dimethoxyphenyl)-1*H*-imidazole-2-carboxylate (**246**) was achieved from α-ketoamine **247**. Cyclization of **247** with thioamide **244** was followed by ester hydrolysis in order to obtain carboxylic acid **248**.

4.5.3.1 Synthesis of α-Ketoamine 247

2-Amino-1-(2,4-dimethoxyphenyl)ethan-1-one (**247**) was readily synthesized by two different procedures. In order to prevent intermolecular dimerization of the α-ketoamine it was synthesized as the more stable hydrogen chloride.

Based on the protocol by SUZUKI *et al.*[229,236] activation of 2,4-dimethoxybenzoic acid (**249**) by use of CDI and subsequent conversion of the reactive species with strong bases and methyl isocyanate gave oxazole **250** in moderate yields. Decarboxylation of the methyl carboxylate with release of carbon dioxide and methanol, and cleavage of the oxazole scaffold under harsh reaction conditions gave the appropriate phenacyl ammonium chloride **247**. The reaction conditions include a strong acidic milieu and reflux temperature (**Figure 58**).

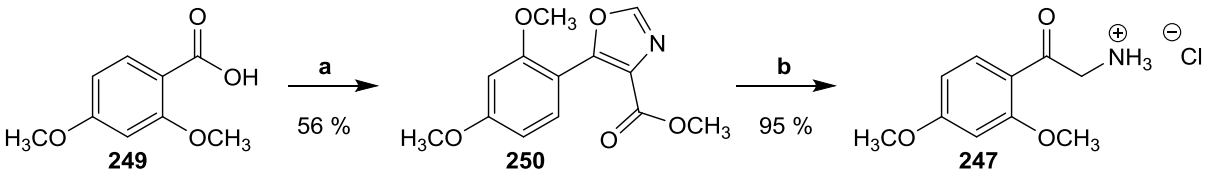

Figure 58 | Synthesis of α-ketoamine 247 in two steps via an oxazole intermediate. **a**) CDI, methyl isocyanate, NaHMDS, THF, 12 h rt. **b**) Conc. HCl/methanol (1:1), 4 h reflux.

Due to the only moderate yields of oxazole **250** another synthetic procedure towards the α-ketoamine was established: 2,4-dimethoxyphenacyl bromide (**237**) was transformed quantitatively into the appropriate α-ketoamine **247** hydrogen chloride via DELÉPINE reaction[237]. The reaction implies acid-based hydrolysis of quaternary hexamethylenetetramine salt **251** to afford primary amines (**Figure 59**). The intermediate has not been isolated.

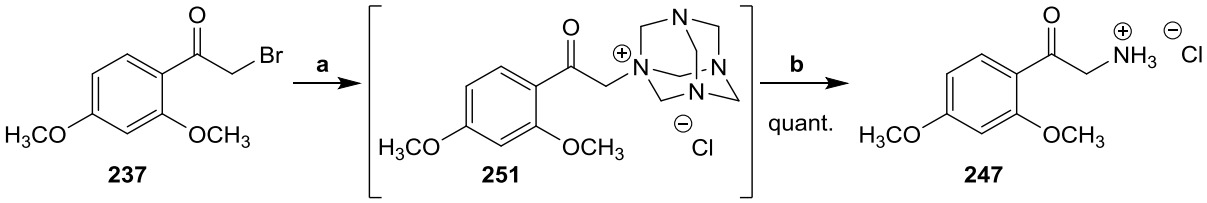

Figure 59 | DELÉPINE synthesis of α-ketoamine 247. **a**) Methenamine, chloroform, 4 h rt. **b**) Conc. HCl/methanol, 3 h reflux.

4.5.3.2 Cyclization of Phenacyl Ammonium Chloride 247

The cyclization step of α-ketoamine **247** towards ethyl imidazole-2-carboxylate **246** was again performed with thioamide **244**[238]. In contrast to the discussed thiazole synthesis by HANTZSCH (**chapter 4.5.2.3**), the thiol group herein acts as a leaving group instead of a nucleophile. The product **246** was obtained in moderate yields upon heating to reflux in an acetate-buffered system. A HANTZSCH-similar reaction mechanism can be assumed involving two S_N2t reactions, one of them an *exo-trig* cyclization towards a 4,5-dihydro-1*H*-imidazole (**Figure 60**). Consequently, methylation of the sulfur atom with MEERWEIN'S salt trimethyloxonium tetrafluoroborate[239] (**252**) increased yields from 35 % to 78 % and reduced the number of by-products: alkylation prevented the tautomeric equilibrium and led to enhanced nucleophilicity of the nitrogen and an improved leaving group. Thereby, the thiazole group acts first as a nucleophile attacking a methyl group of the alkylation reagent followed by its function as a leaving group during the ring formation step. The methylated intermediate **253** has not been isolated.

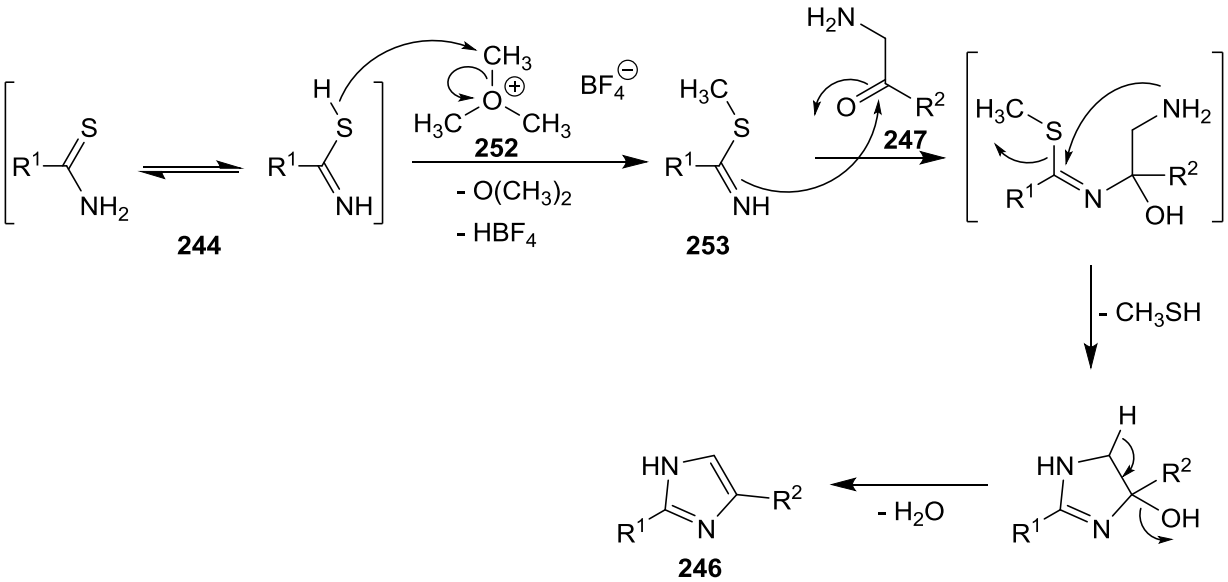

Figure 60 | Cyclization mechanism of α-ketoamine 247 with thioamide 244. R^1 = ethyl carboxylate; R^2 = 2,4-dimethoxyphenyl.

4.5.3.3 Ester Hydrolysis of Ethyl Imidazole-2-carboxylate 246

Regrettably, all approaches to prepare carboxylic acid **248** by hydrolysis of ethyl ester **246** exhibited the same problem as discussed for the respective thiazole-2-carboxylic acid **234** (**Figure 61**): rapid decarboxylation towards the 2-unsubstitued imidazole derivative **254**. Although the decarboxylation did not seem to occur quantitatively as observed in the case of the thiazole derivative, it was in this case neither possible to isolate the desired product **248** nor the by-product **254**.

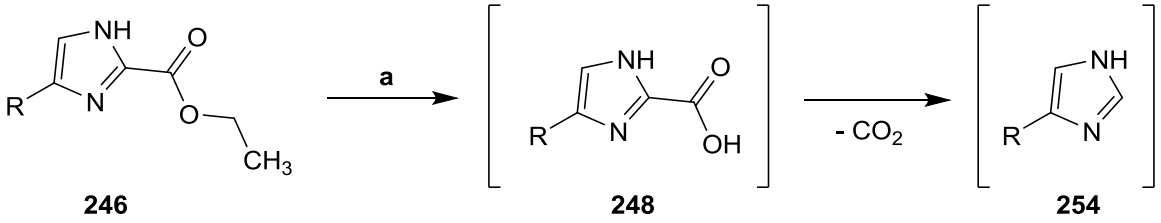

Figure 61 | Ester hydrolysis and subsequent decarboxylation of ethyl imidazole-2-carboxylate 246. R = 2,4-dimethoxyphenyl. **a**) Aq. NaOH, THF/methanol, 48 h rt.

4.5.4 Synthesis of Triazole-containing Side Chains

The idea was to synthesize ethyl 3-(2,4-dimethoxyphenyl)-1*H*-1,2,4-triazole-5-carboxylate (**255**) in an analog approach by cyclization of 2,4-dimethoxybenzohydrazide (**256**) and thioamide **244**. Hydrazide **256** was prepared from 2,4-dimethoxybenzoic acid (**249**) and hydrazine hydrate via the methyl carboxylate in quantitative yields (**Figure 62**)[240].

Cyclization[241] of the hydrazide and thioamide **244**, however, could not be performed satisfactory. Although the desired triazole has been identified in the reaction mixture by mass spectrometry, conversion was minimal and isolation of a pure product failed completely. Regarding these data, the main product might be the decarboxylated triazole, though this could not be isolated either. Based on the observations from thiazole- and imidazole-2-carboxylates regarding decarboxylation, this approach has not been pursued any further.

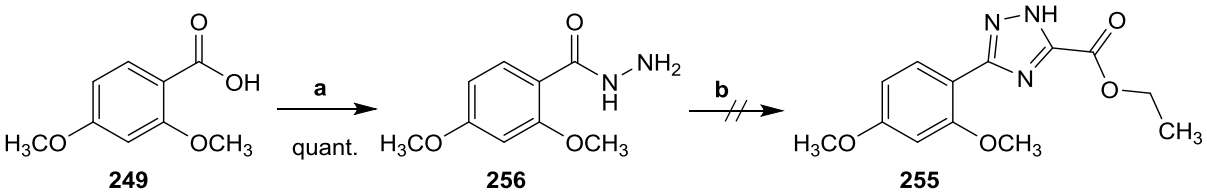

Figure 62 | Synthesis of 2,4-dimethoxybenzohydrzide 256. **a**) Conc. H_2SO_4, methanol, 4 h reflux, then N_2H_4, 30 min rt to reflux. **b**) **244**, optional $[(CH_3)_2O]BF_4$, optional DMF or NMP, h 180 °C.

4.6 Syntheses of Series 5: Propiolic Acid

Synthesis of 3-(2,4-dimethoxyphenyl)propiolic acid (**257**) was realized in three steps[242]: preparation of the appropriate methyl propiolate **258** in two steps by the COREY-FUCHS procedure was followed by ester hydrolysis.

4.6.1.1 COREY-FUCHS Synthesis of Methyl Propiolate 258

The first step of the COREY-FUCHS reaction is a WITTIG-like one-carbon homologation of 2,4-dimethoxybenzaldehyde (**259**) towards the respective 1,1-dibromoalkene **260** in acceptable yields (41 %)[242]. The reactive ylide species is generated *in situ* from tetrabromomethane (**261**) and triphenylphosphine (**262**, **Figure 63**). Subsequently, the ylide carbanion approaches the appropriate 2,4-dimethoxybenzaldehyde (**151**) carbonyl group in a nucleophilic attack generating a four-membered oxaphosphetane intermediate by [2+2]-cycloaddition. The immense affinity of phosphor and oxygen, however, accounts for instability of the oxaphosphetane which irreversibly decomposes into **260** and triphenylphosphine oxide[228,235].

In the second step, treatment with ^{n}BuLi at -78 °C initially initiates a bromine/lithium exchange at the sterically more hindered position. The α-lithiated bromoalkene anionotropically [1,2]-rearranges via the carbenoid by selective movement of the aryl moiety to the alkyne α-position in accordance to the FRITSCH-BUTTENBERG-WIECHELL rearrangement. The appropriate alkyne is promptly deprotonated by another equivalent of ^{n}BuLi. Subsequent addition of methyl chloroformate (**263**) led to propiolate **258** in good yields (87 %) through S_N2t reaction of lithium acetylide and the electrophile[228].

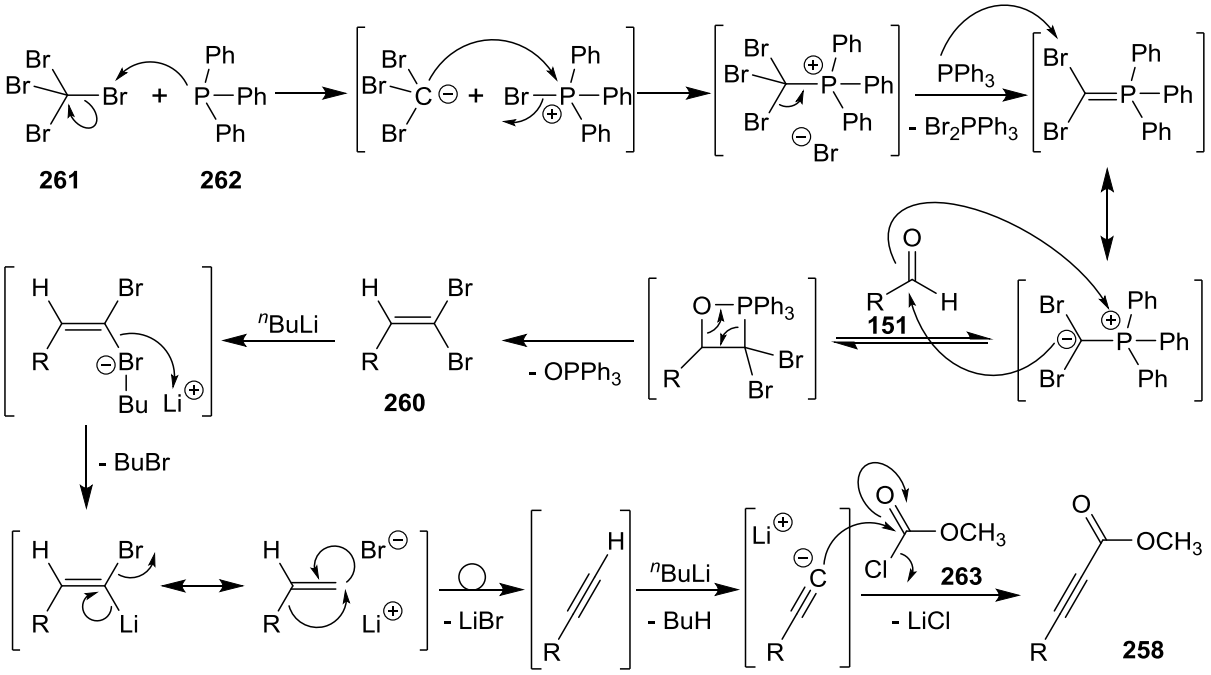

Figure 63 | Reaction mechanism of the COREY-FUCHS synthesis of methyl propiolate 258. R = 2,4-dimethoxyphenyl.

4.6.1.2 Ester Hydrolysis of Methyl Propiolate 258

Hydrolysis of methyl propiolate **258** was achieved under mild reaction conditions using lithium hydroxide at room temperature. Lithium hydroxide is a mild base which has been reported to allow safe hydrolysis of less stable compounds[243] and has therefore been chosen to afford **257**.

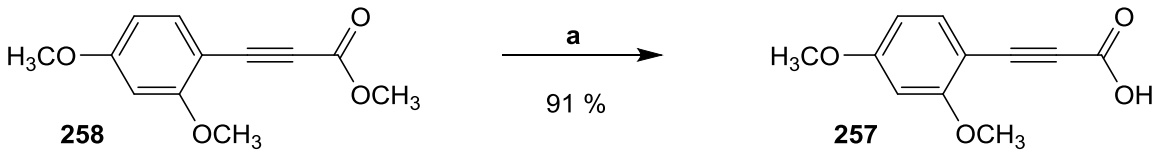

Figure 64 | Ester hydrolysis of methyl propiolate 258. a) $LiOH \cdot H_2O$, THF/methanol/water (4:1:1), 12 h rt.

4.6.1.3 Coupling of Propiolic Acid 257 and Building Block 120

The coupling of 2,4-dimethoxyphenylpropiolic acid (**257**) and building block **120** has been approached through different procedures regarding reaction temperature and coupling reagents. As the propiolic acid was assumed to be less stable, the reaction was first performed with DCC under 4-DMAP-catalysis at -20 °C and room temperature. QIAN *at al.* had reported to use this protocol for the coupling of phenylpropiolic acid and aniline[226]. The 2-aminopyridine

nucleophile of building block **120**, however, is less reactive as pyridine represents an electron deficient aromatic scaffold which did not react under these conditions. Further approaches have been performed using PyBOP, CDI, HATU, and the activated propioloyl chloride at consecutively elevated temperatures. The appropriate propioloyl chloride has been prepared from **257** and oxalyl chloride in dichloromethane (DCM) with catalytic amounts of DMF. Conversion to the desired carboxamide **264** has been observed between 80 °C and 110 °C by mass spectrometry from the reaction mixture. Unfortunately, formation of **264** has always been accompanied by a multitude of by-products and was indicated by a shift of color towards intense red. It has not been evaluated, though, whether the color indicates successful conversion or degradation. The product could not be isolated.

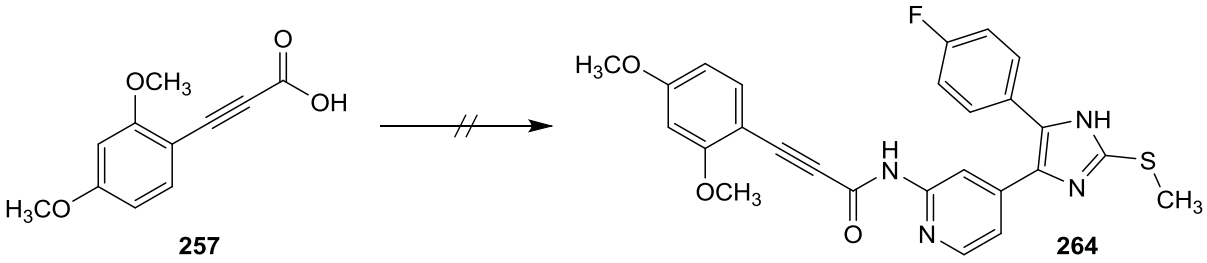

Figure 65 | Coupling of propiolic acid 257 and building block 120 failed in different approaches. At least purification could not be performed successfully.

The consequent idea was to react building block **120** with phosgene (or better its less critical analogs diphosgene and triphosgene, respectively) in order to synthesize the appropriate carbamic chloride **265**. This might be converted with 1,1-dibromoalkene **260** to the desired carboxamide **264**. The reaction, however, has not been performed to date.

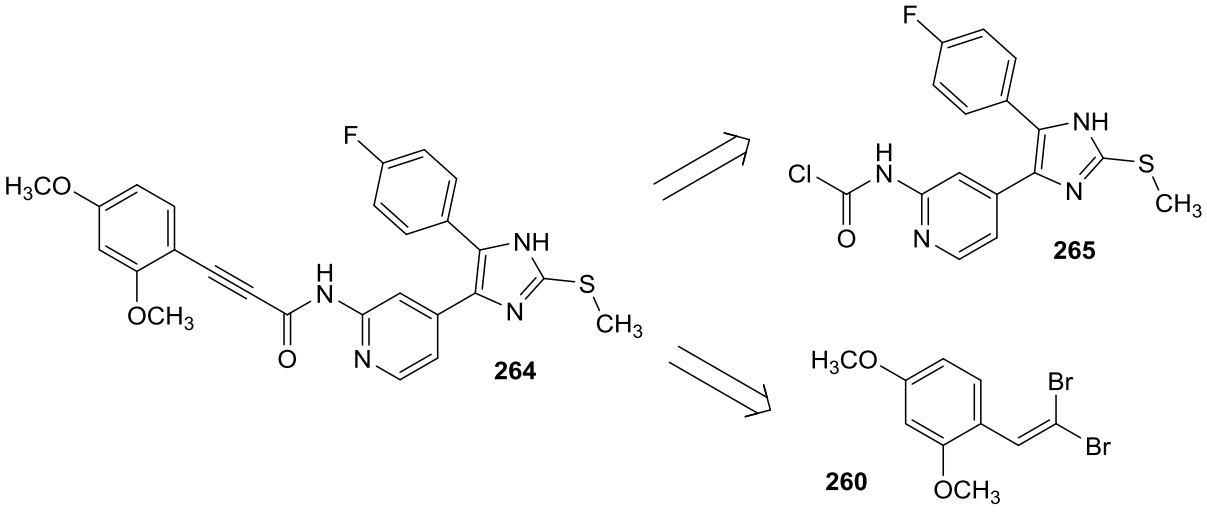

Figure 66 | Retrosynthetic contemplation of propiolic carboxamide 264.

4.7 Syntheses of Series 6: Hybrid Inhibitors

As discussed in **chapter 3.1.5**, side chains were adapted from reported Porcn inhibitors IWP-2 (**113**) and IWP-4 (**114**), as well as from approved Bcr-Abl inhibitor imatinib (**117**). The imatinib-hybrid, however, has not been received. All side chains were synthesized in accordance to literature procedures[210,244].

4.7.1 Synthesis of IWP-Hybrids 266 and 267

Preparation of the dihydrothieno[3,2-*d*]pyrimidin-4-one side chains has been performed in two steps following the protocol by BARALDI *et al.*[210,245] from acrylonitrile (**268**) and methyl thioglycolate (**269**, **Figure 67**): the MICHAEL adduct **270** reacts in the presence of 1,8-diazabicyclo-[5.4.0]undec-7-ene (DBU) in methanol through intramolecular *exo-dig* THORPE-ZIEGLER-like cyclization to afford methyl 3-amino-4,5-dihydrothiophene-2-carboxylate (**271**) in moderate yields (45 %).

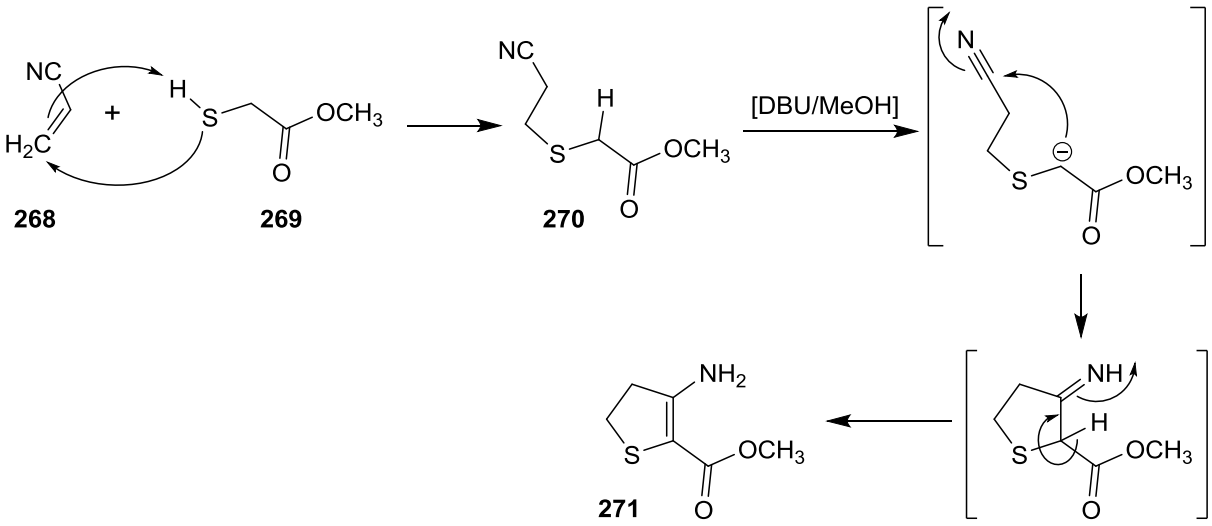

Figure 67 | Reaction mechanism of consecutive MICHAEL-like addition and THORPE-ZIEGLER-like cyclization to afford 271.

Thienopyrimidines **272** and **273** were obtained by ring closure of enamino ester **271** and phenyl isothiocyanates **274** and **275** via thiocarbamide intermediates and intramolecular *exo-trig* cyclization (**Figure 68**)[210,245]. Although thin layer chromatography (TLC) and high performance liquid chromatography (HPLC) control showed high turnover of starting material

into the desired products, purification was tedious and caused rather low yields of 28 % (**272**) and 14 % (**273**), respectively.

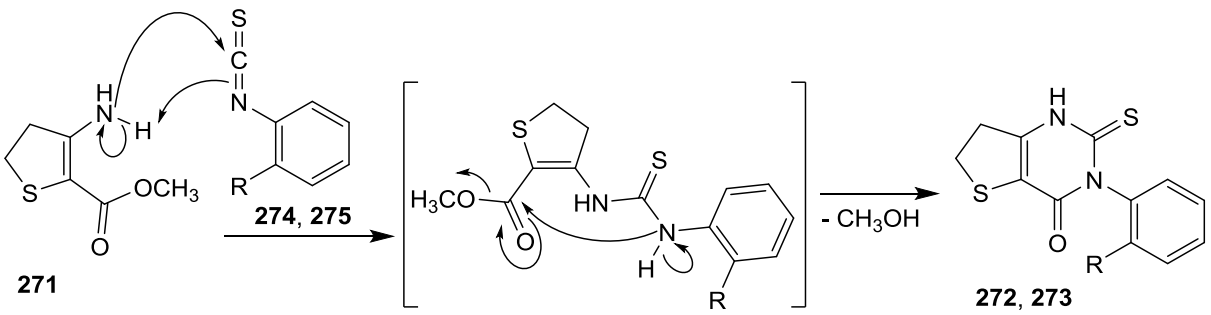

Figure 68 | Cyclization mechanism of 271 and phenyl isothiocyanates towards thienopyrimidines. **274**, **272**: R = H; **275**, **273**: R = OCH_3.

These side chains were attached to building block **120** via a 2-chloroacetyl chloride linker (**Figure 69**)[210]. An evaluation of suitable reaction conditions was performed starting from 2-amino-4-methylpyridine (**126**): S_N2t reaction with the linker gave 2-chloro-*N*-(4-methylpyridin-2-yl)acetamide (**276**) which was coupled with aniline in a first attempt, and with thienopyrimidine **272** in a second to give **277**[y] and **278**[z], respectively (**Figure 69**).

[y] **277** = *N*-(-methylpyridin-2-yl)-2-(phenylamino)acetamide
[z] **278** = *N*-(4-methylpyridin-2-yl)-2-((4-oxo-3-phenyl-3,4,6,7-tetrahydrothieno[3,2-*d*]pyrimidin-2-yl)thio)acetamide

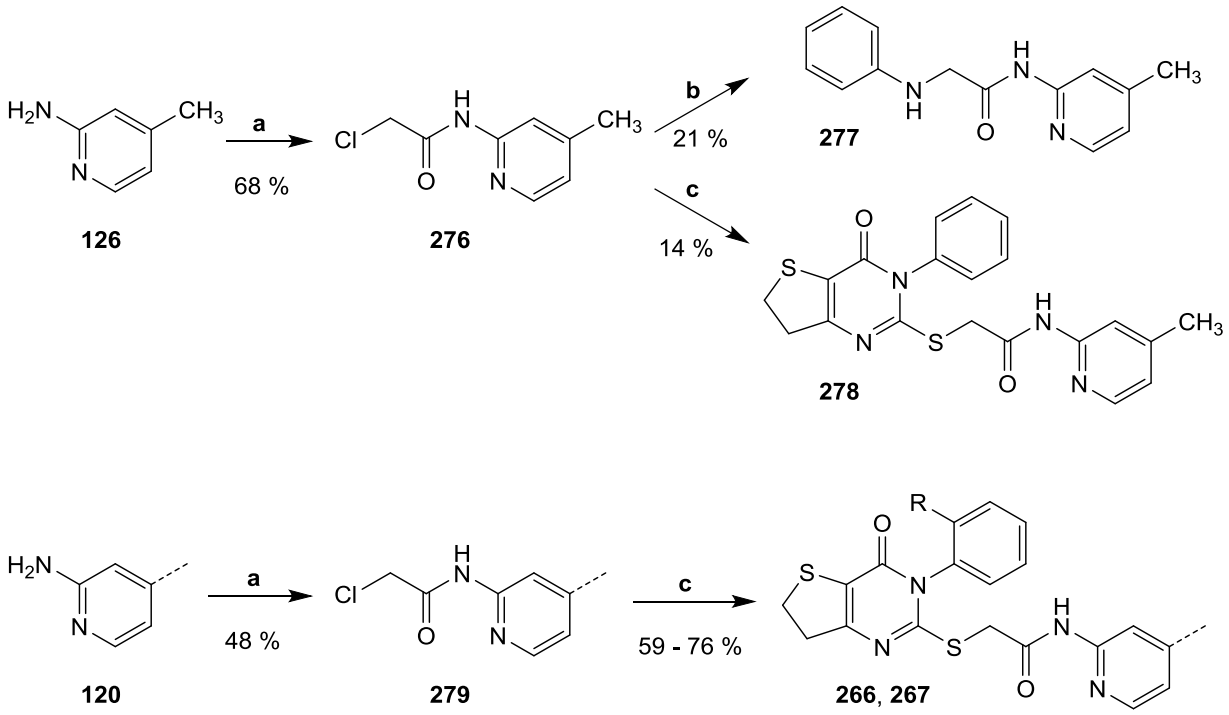

Figure 69 | Synthesis of hybrid inhibitors 266, 267. **266**: R = H; **267**: R = OCH_3. **a**) Chloroacetyl chloride, Et_3N, DCM, 12 h rt. **b**) Aniline, Et_3N, DMF, 2 h 80 °C. **c**) **272** or **273**, Et_3N, DMF, 2 h 80 °C. Yield: 59 % (**266**), 76 % (**267**).

4.7.2 Synthesis of Imatinib-Hybrid 280

4-((Methylpiperazin-1-yl)methyl) benzoic acid (**281**) was synthesized from 4-(bromomethyl)benzoic acid (**282**) and *N*-methylpiperazine following the procedure by MACDONALD *et al.*[244]. Thereby, formation of the by-product 1,4-bis(4-carboxybenzyl)-1-methylpiperazin-1-ium chloride (**283**) has been observed, but could largely be oppressed by adding the piperazine component in one portion (**Figure 71**).

Unfortunately, amide coupling approaches of **281** and building block **120** initially failed. Besides the moderate nucleophilicity of the 2-amino-pyridine moiety of **120**, the ampholytic character of **281** has to be regarded responsible: in solution the equilibrium is shifted by an intramolecular protonation towards the carboxylate (**Figure 70**) with reduced carbonyl reactivity which is rather insensitive for activation and amide coupling.

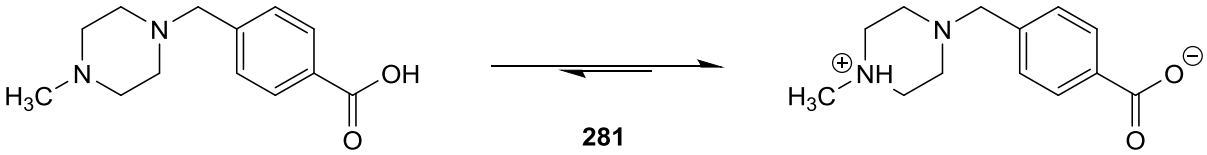

Figure 70 | Ampholytic character of 281 in pH neutral solution.

Even adaptation of the reaction for microwave synthesis in accordance to the protocol by JOHANNES[229] did not initiate product formation. Finally, HATU-mediated conversion into the desired amide has been observed by mass spectrometry from the reaction mixture upon an exchange of solvent from DMF towards NMP, though in rather low percentage (approx. 11 %, HPLC). Regrettably, the product could not be isolated and **280** has not been obtained purely.

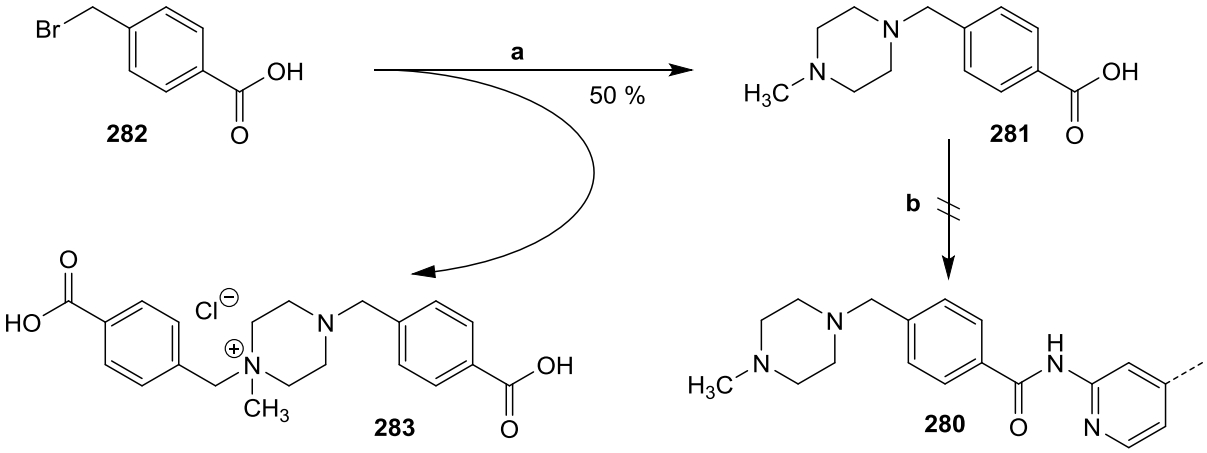

Figure 71 | Synthesis of hybrid inhibitor 280. **a**) *N*-Methylpiperazine, *n*-butanol, 2 h rt. **283** has been isolated as a by-product. **b**) **120**, HATU, DIPEA, NMP, 30 min rt then 30 min 90 °C (100 W). **280** has not been isolated purely.

4.8 Sulfoxidation of Selected Compounds

Sulfoxides are most likely to represent the main metabolites (cp. **chapter 3.1.2**). Therefore, oxidation of several sulfide compounds has been performed in accordance to PEIFER *et al*. using Oxone® (potassium peroxymonosulfate[aa], **284**) as the oxidant[176]. Oxidation by Oxone® combines a catalyst-free and environmental friendly (*green*) procedure with synthetic advantages such as high yield and purity, high sensitivity, and easy handling[246,247]. Although the inclination towards overoxidation is less pronounced than for other reagents, the reaction conditions need to be accurately controlled: Oxone® also oxidizes sulfides to the respective sulfones consuming two equivalents of oxidant (**Figure 72**), though the reaction can be quenched on the sulfoxide level. Consequently, strict monitoring of the reaction progress is inevitable. Nevertheless, the sulfone is obtained as a by-product in low percentage.

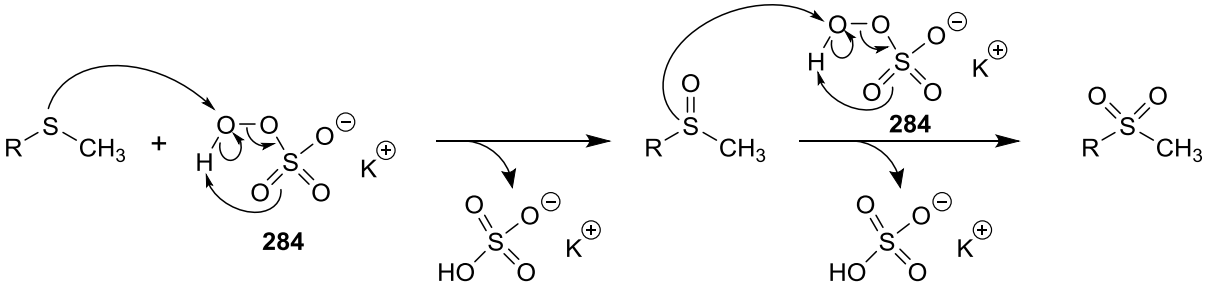

Figure 72 | Postulated reaction mechanism of sulfide oxidation using Oxone®.

Several selected compounds from different series have been oxidized following the mentioned protocol with Oxone® in a mixture of THF and water at 0 °C and room temperature. The reaction time typically ranged from 30 min to 2 h, dependent on the amount of sulfide. Hybrid inhibitors (series 6) have not been included as oxidation of the thienopyrimidine sulfur atom has to be expected. The selected compounds, products, and appropriate yields are given in **Table 21**. Low yields are rather due to critical purification than uncomplete conversion.

[aa] Oxone® = triple salt ($2\ KHSO_5 \cdot KHSO_4 \cdot K_2SO_4$)[246]

Table 21 | Sulfoxidation of selected compounds. R = 4-fluorophenyl. Products are assigned to the appropriate series 1, 2, 3, and 4. Test compound **160** does not belong to any series. Start. = starting material.

	# Start.	# Product	Product structure	Yield (%)
	160	**285**	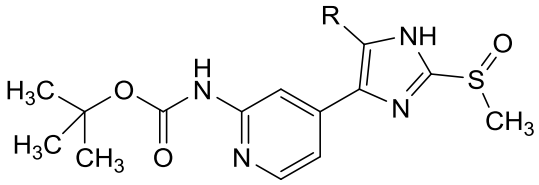	75
	162	**82**	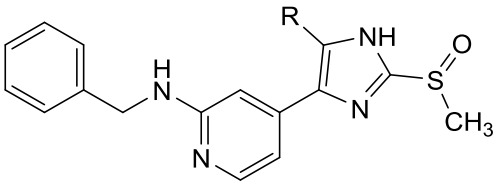	47
1	**149**	**84**	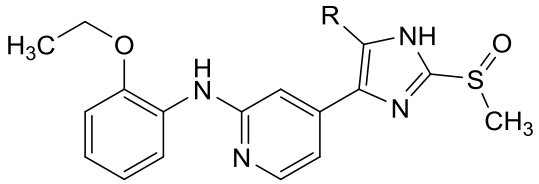	82
	150	**85**	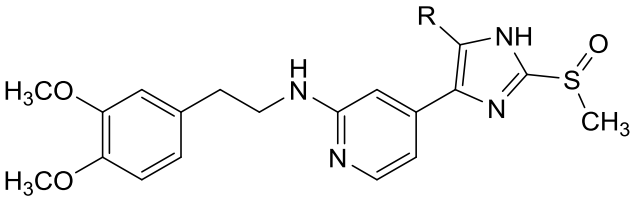	39
	190	**102**	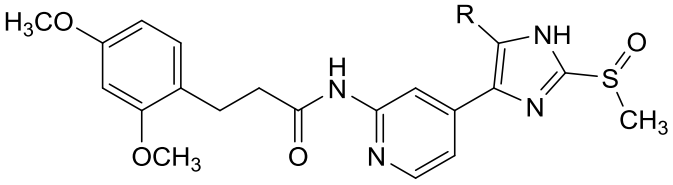	93
2				
	191	**103**	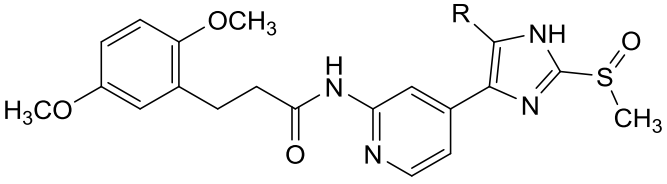	26

	204	**104**	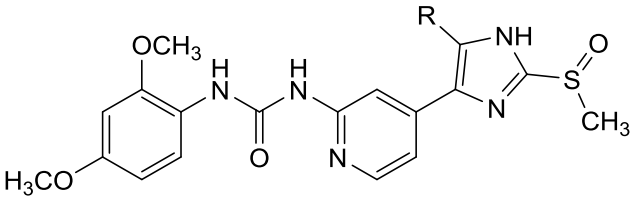	22
	206	**286**	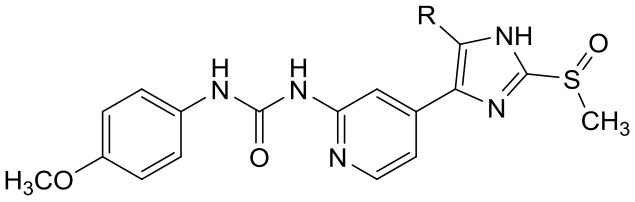	61
	208	**287**	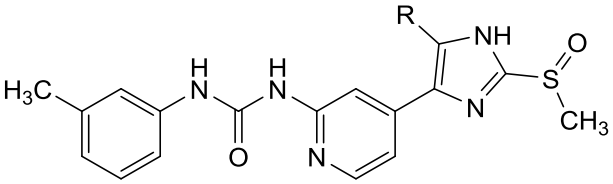	72
3				
	209	**288**	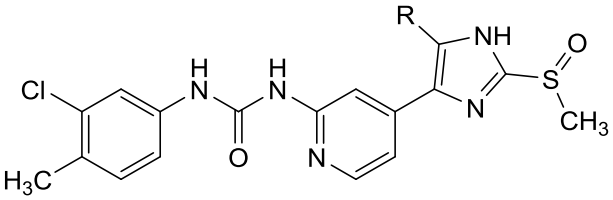	75
	210	**289**	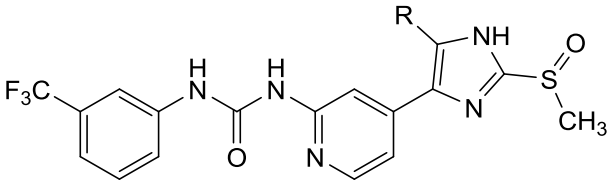	73
	212	**290**	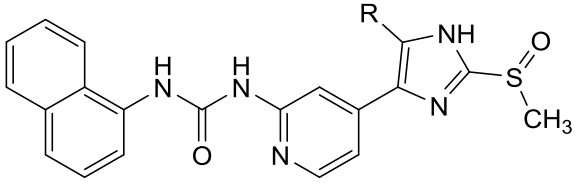	70
4	**231**	**291**	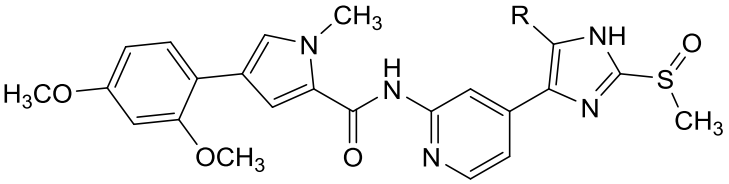	88

4.9 Photochemical $_{\pi}6_a$-Electrocyclization of Diaryl-imidazoles

The caging concept of active compounds using photo-cleavable protecting groups is well-established in our working group. Consequently, the potential suitability of 4,5-diaryl-imidazoles was evaluated by ultraviolet (UV) irradiation of **162** in THF with a wavelength of 365 nm (**Figure 73**). Thereby it has been found that the concept is not applicable for this class of inhibitors: interestingly, **162** underwent a $_{\pi}6_a$-electrocyclization reaction towards the appropriate tetracyclic planar system **292**. In fact, conversion was higher than 24 %, but purification significantly lowered yields. Similar reactions have been reported for structurally related compounds leading to Janus kinase (JAK) inhibitors[212], though **292** has not been biologically tested.

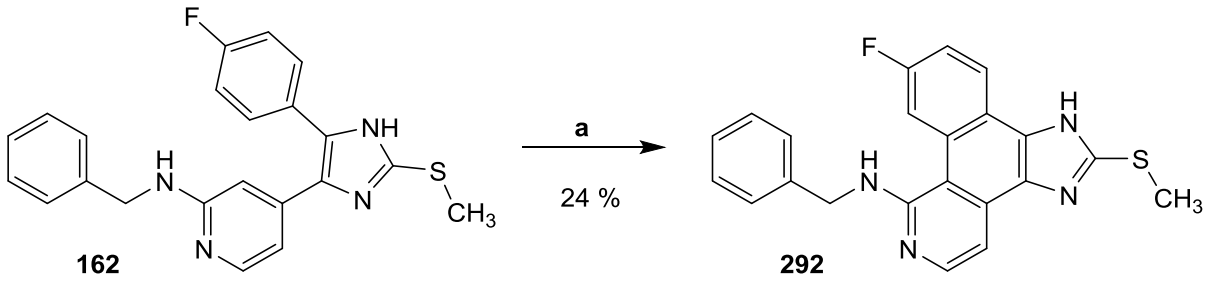

Figure 73 | Photochemical $_{\pi}6_a$-electrocyclization of 162. a) THF, 2 min 365 nm (5.4 W).

Mechanistically, the $_{\pi}6_a$-electrocyclization follows the orbital-symmetry-based WOODWARD-HOFFMANN rules for pericyclic reactions (**Figure 74**)[235]. The conjugated system involved in the photochemical cyclization comprises six π-electrons ($_{\pi}6$). In accordance to the rules the reaction is permitted as the sum of the participating ($4q$ + 2)-components is uneven. By antarafacial ($_a$) rotation of the *terminal* orbitals about 90° a new molecule orbital and thereby the respective σ-bond is formed.

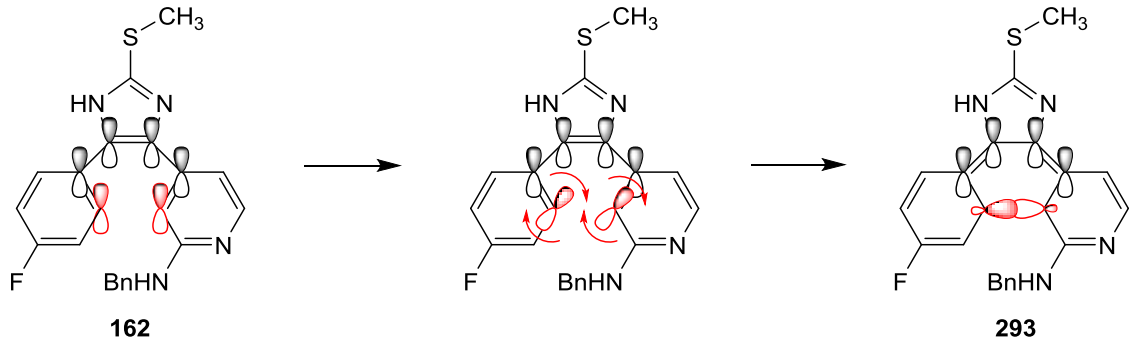

Figure 74 | WOODWARD-HOFFMANN-based photochemical $_{\pi}6_a$-electrocyclization mechanism of 162.

The photochemically-induced conrotatory reaction (antarafacial rotation) inevitably affords the *trans*-product with respect to the hydrogens in question (**Figure 75**). In the presence of atmospheric oxygen or other oxidants, however, the dihydro-intermediate **293** oxidatively strives for an aromatic system leading to **292**. Intermediate **293** has not been isolated.

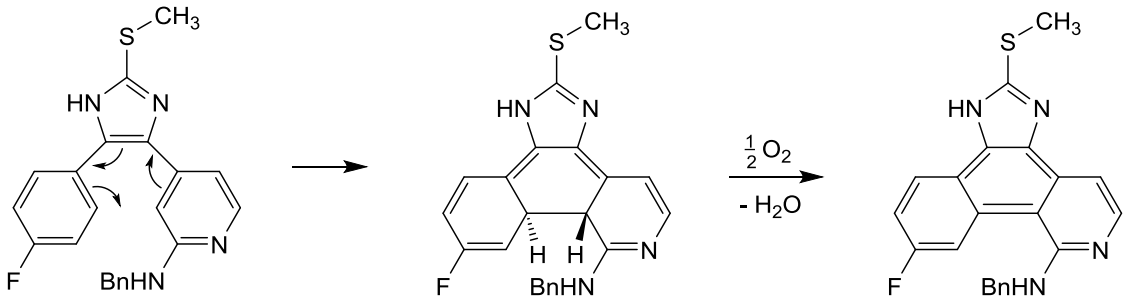

162 **293** **292**

Figure 75 | Reaction mechanism of $\pi 6_a$-electrocyclization towards 292. Dihydro-intermediate **293** is initially oxidized in the presence of atmospheric oxygen.

5 Results and Discussion

The identification of CK1δ as an important determinant in the progression of various severe diseases has made it an attractive target for both therapeutic approaches and ongoing research[9,119,166]. Consequently, isoform-specific CK1 inhibitors are pursued with increasing interest. In the scope of this dissertation, 38 newly designed and synthesized CK1δ inhibitors arranged in five series (1, 2, 3, 4, 6) have been implemented in biological characterization. All compounds are based on lead structure **12** and its non-sulfoxidized derivative **11**, originally deriving from p38α MAPK inhibitors, and were classified as ATP-competitive type I binders[176]. Biological evaluation has been performed in collaboration with the group of PROF. DR. UWE KNIPPSCHILD (Department of General and Visceral Surgery, Ulm University Hospital, Germany) by MARC KRÜGER[248] and CHIARA IANES[249], or results were acquired commercially from ProQinase GmbH (Freiburg, Germany). The newly synthesized small molecule inhibitors were initially screened in kinase assays on CK1δ and CK1ε, complemented by screenings against CK1α, CK1γ3, and p38α for several compounds. Their activity in cell culture has been evaluated using different human cancer cell lines. The most promising compound **191** has additionally been screened over a panel of 321 protein kinases by ProQinase GmbH in order to identify potential off-targets. It has further been co-crystallized by the group of PROF. DR. DANIEL RAUH (Institute of Chemical Biology, Dortmund University of Technology, Germany) with p38α which should be considered the main off-target of the current teardrop-like inhibitor class. Moreover, crystallization of **224** and **266** in CK1δ and CK1ε has also been performed by the group of PROF. DR. ULRICH BAUMANN (Department for Chemistry, University of Cologne, Germany).

5.1 Characterization of Series 1

Kinase Assays

The compounds of series 1 are lacking the carbonyl group and the π-bond of **11** and **12** leading to complete sp^2 hybridization of the side chain linker atoms. Structurally, these molecules resemble early ATP-competitive p38α MAPK inhibitors developed by LAUFER *et al.*[197,202,213]. In order to investigate their biological activity they were assayed at 10 μM in the presence of 100 μM ATP against CK1 isoforms δ, ε, α, and γ3 as well as p38α. The measurement thereby referred to the normalized residual phosphorylation activity of the respective kinase using GST-p53 fragment (aa 1-64), α-casein, or GST-CK1δ fragment (aa 305-375) as substrates[248,249]. The results of these initial screens are shown in **Figure 76**.

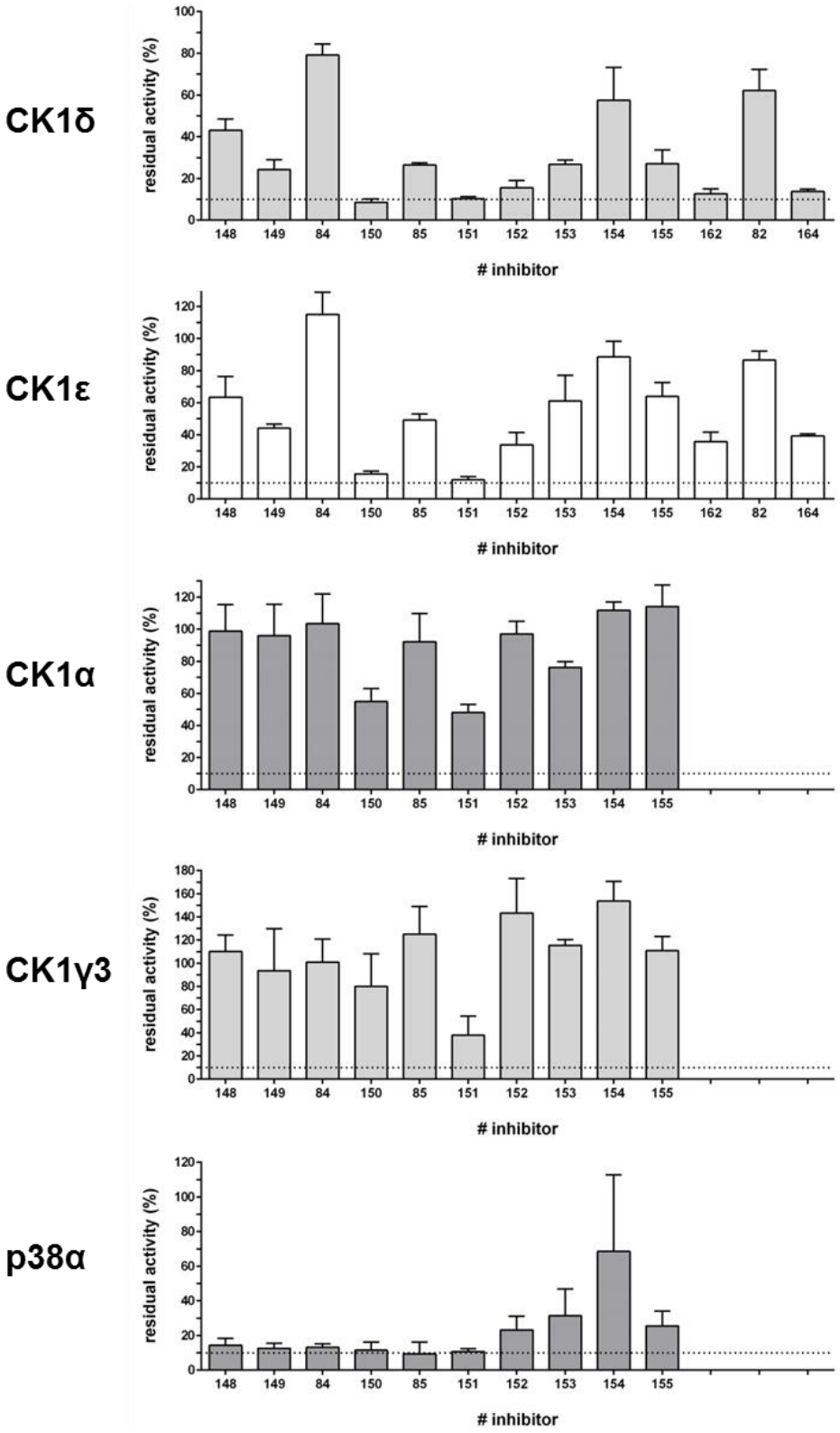

Figure 76 | Inhibition of CK1 isoform and p38α kinase activity by inhibitors of series 1 at a concentration of 10 μM. Compounds **148-155**, **84**, **85** have been biologically evaluated in kinase assays against CK1δ, CK1ε, CK1α, CK1γ3, and p38α. Compounds **162**, **82**, **164** have only been tested against CK1δ and CK1ε. GST-p53 fragment (aa 1-64) (CK1δ, ε, α), α-casein (CK1γ3), or GST-CK1δ fragment (aa 305-375) (p38α) have been used as substrate. The inhibitors were screened in triplicate measurement in the presence of 100 μM ATP. Residual activities were normalized to DMSO. Error bars indicate the standard error of the mean (SEM)[248,249].

As expected, the initial screenings identified compounds of series 1 as dual-specific inhibitors of CK1δ and p38α. Although CK1 isoforms α and γ3 were only slightly affected, the inhibitors did not significantly discriminate between CK1δ and CK1ε. At an assay concentration of 10 μM the most efficient inhibition of CK1δ has been observed for compound **150**, reducing the residual kinase activity of CK1δ and CK1ε to approximately 9 % and 16 %, respectively, followed by compounds **151** (10 % and 12 %), **162** (13 % and 36 %), and **164** (14 % and 39 %). Among all compounds of series 1, **162** and **164** also exhibited the strongest isoform-preferring potential as inhibition of CK1ε was approximately threefold less pronounced in comparison to CK1δ. Consequently, half maximal inhibitory concentration (IC_{50}) values have been determined for **150**, **151**, and **164** in order to validate their isoform-specificity (**Figure 77**). Compound **162** has not been considered as it had already been characterized by LAUFER *et al*. as a p38α inhibitor with moderate potency (IC_{50} = 139 nM)[197].

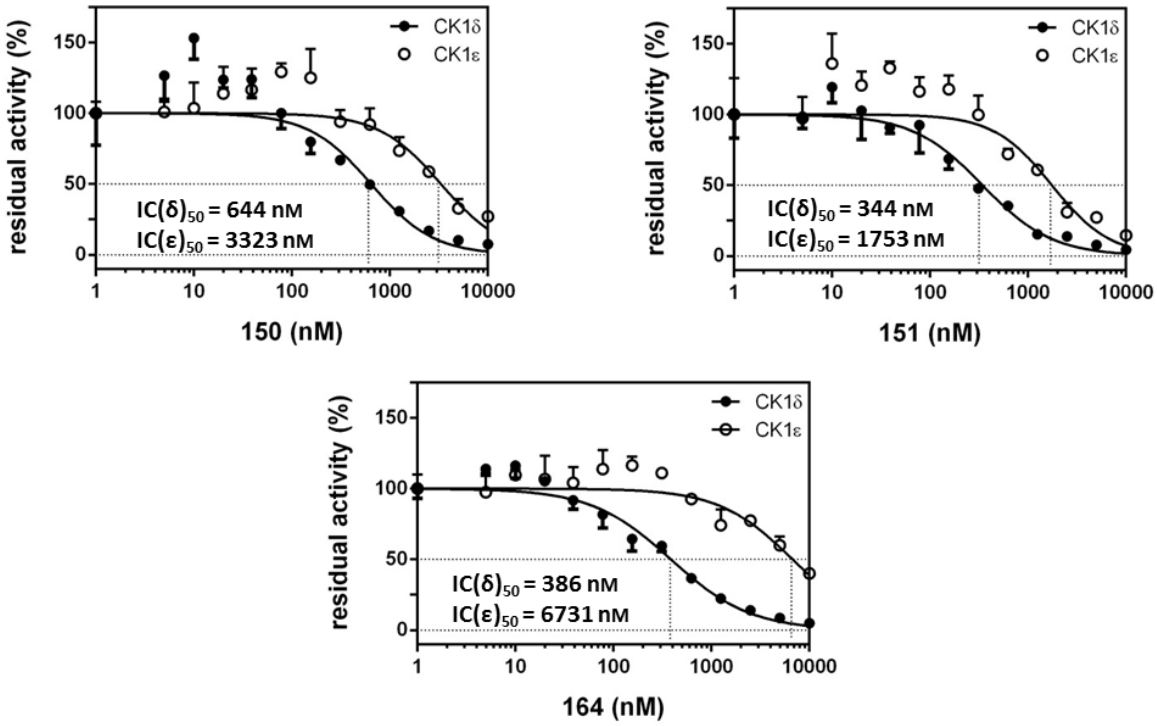

Figure 77 | IC_{50} determination of series 1 compounds 150, 151, and 164. IC_{50} values have been determined using CK1δ or CK1ε and α-casein as substrate. Error bars indicate the SEM[248,249].

IC_{50} determination of these compounds exhibited both moderate potency and isoform-specificity regarding CK1δ and CK1ε. While **150**, **151**, and **164** showed half maximal inhibition of CK1δ at 644 nM, 344 nM, and 386 nM, respectively, CK1ε activity was approximately five-fold less effective inhibited by **150** (IC_{50} = 3323 nM) and **151** (IC_{50} = 1753 nM), and even 17-fold by **164** (IC_{50} = 6731 nM), highlighting especially the latter for further optimization. With respect to their

IC_{50} values **151** and **164** are comparable with the well-known inhibitor D4476 (**8**, CK1δ IC_{50} = 0.3 μM)[173].

Although molecular modeling-based affinity prediction within *HRII* of CK1δ is rather error-prone due to the flexibility of the domain, **150**, **151**, and **164** were among the best hits from computational screenings with nearly equivalent scoring (cp. **Table 22**). Modeling even predicted **151** to be the most potent inhibitor of series 1, though the order of **150** and **164** has been inverted. Nevertheless, these results provide a first proof of concept for the applicability of the computational model as *in silico* and *in vitro* approaches generated comparable results.

Table 22 | IC_{50} values and Glide scores of compounds 150, 151, and 164[248,249].

#	Structure	Glide Score (CK1δ)	IC_{50} (nM)
150	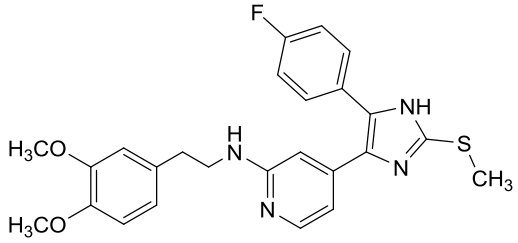	-14.2	644 (CK1δ) 3323 (CK1ε) n.d. (p38α)
151	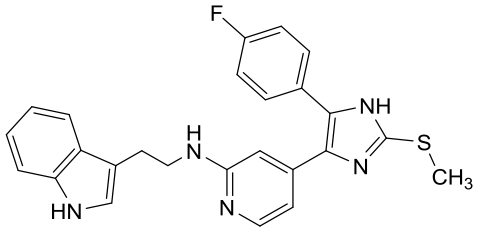	-14.7	344 (CK1δ) 1753 (CK1ε) n.d. (p38α)
164	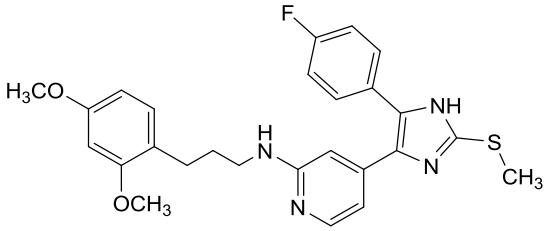	-13.7	386 (CK1δ) 6731 (CK1ε) n.d. (p38α)

Structurally, these results point towards side chains including aryl moieties, presumably methoxy-substituted phenyls, which are attached to the pyridine-2-amine of **120** by an *n*-ethyl or *n*-propyl linker. Interestingly, compound **164** which is the most promising inhibitor of series 1 regarding its isoform-preferring potential, represents the "sp^3 derivative" of non-oxidized lead structure **11** considering the carbon atoms of the side chain linker. Consequently, this structural element can be assumed to be an important determinant for isoform-specificity. Sulfoxidation of compounds **149**, **150**, and **162** leading to **84**, **85**, and **82** significantly reduced efficacy for CK1δ while the effect on CK1ε seemed to be less pronounced. However, the efficacy for p38α has apparently not been affected by sulfoxidation (cp. **Figure 76**).

Cellular Assays

Intending to provide evidence for beneficial physicochemical parameters, the efficacy of several compounds has been evaluated in cellular assays using different human cancer cell lines. The increasing molecular weight and the often lipophilic character of kinase inhibitors is readily accompanied by a loss of cell permeability and solubility, leading to poor efficacy in cellular systems.

In order to determine their effect on cell viability compounds of series 1 have been implemented in colorimetric 3-(4,5-dimethylthiazol-2-yl)-2,5-diphenyltetrazolium bromide (MTT) assays at a concentration of 20 µM, 10 µM (**162**, **82**), or 25 µM (**164**) using the CK1-dependent human colorectal adenocarcinoma epithelial cell line HT-29[248,249].

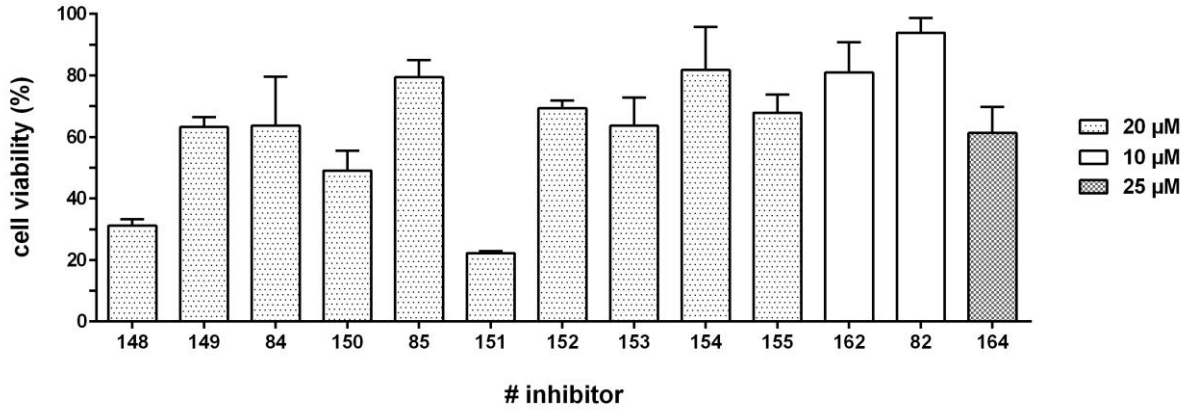

Figure 78 | Cell viability of HT-29 cells after treatment with series 1 compounds at concentrations of 10 µM, 20 µM, or 25 µM. The inhibitors were screened in triplicate measurement. Cell viability was normalized to mock. Error bars indicate the SEM[248,249].

The initial screens indicated compounds **151** and **148** to be the most promising candidates of series 1 in HT-29 cells. At 20 µM they significantly reduced viability to approximately 22 % and 31 %, respectively. **164**, however, has also been observed to be active in cells, though not potent, leading to cell viability of approximately 61 % at 25 µM. In general, the overall efficacy of the tested compounds in the cellular system was rather low but significant with the exception of compound **82** that did not seem to affect cell viability at 10 µM. The results of these screens are shown in **Figure 78**.

In addition, the half maximal effective concentration (EC_{50}) has been determined for **151** to validate the inhibitory effect on HT-29 cells (**Figure 79**)[248]. The inhibitor exhibited an EC_{50} value in the high single-digit micromolar range (EC_{50} = 9.3 µM) revealing the necessity of further optimization in order to enhance cell penetration and to gain applicability as a biological tool.

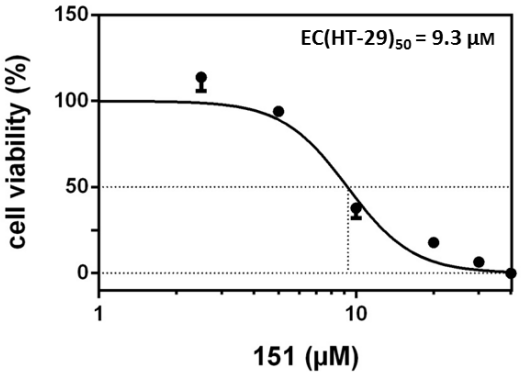

Figure 79 | EC_{50} determination of compound 151 in HT-29 cells. Error bars indicate the SEM[248].

5.2 Characterization of Series 2

Kinase Assays: IC_{50} Determination

Series 2 compounds were conceptually derived from lead structure **12** and its non-sulfoxidized derivative **11** by deletion of the potentially reactive π-bond (MICHAEL acceptor). Furthermore, **190** and derivatives (series 2) were hypothetically obtained by introduction of a carbonyl function at the α-methylene group of secondary amine **164**. Consequently, the design of series 2 should be considered an optimization of series 1 compounds. In addition, structure-activity relationship data were gained by consecutively varying the methoxy substitution pattern of the terminal phenyl moiety. Their biological activity has been evaluated in kinase assays against CK1δ and CK1ε at 10 μM in the presence of 10 μM ATP. **190**, **191**, and **103** have additionally been assayed against CK1α. The assays have been performed using α-casein as substrate[248,249].

The compounds exhibited excellent inhibition of CK1δ reducing the residual activity below 5 % in all cases (**Figure 80**). In addition, all compounds effectively inhibited CK1ε, although less potently. Especially sulfoxidation of **191** leading to **103** seemed to increase isoform-specificity regarding CK1δ and CK1ε. Interestingly, sulfoxide **103** also exhibited enhanced potency for CK1α compared to non-oxidized **191**. Both **190** and **191** were significantly less active against CK1α.

In order to validate their inhibitory potential of CK1 isoforms δ and ε IC_{50} values have been determined for all compounds (**Figure 81**). The assayed inhibitors of series 2 exhibited IC_{50} values in the low nanomolar range for CK1δ indicating high affinity and potency with the most promising compound being **191** (CK1δ IC_{50} = 4 nM, CK1ε IC_{50} = 25 nM). Regarding inhibition of CK1ε, isoform-specificity was rather low as **192** possessed the highest isoform-discriminating effect with IC_{50} values of 20 nM (CK1δ) and 233 nM (CK1ε), respectively. Unfortunately, the promising discrimination by **103** observed in the initial screens could not be confirmed.

As **191** was the most active compound IC_{50} values have commercially been obtained for CK1δ and p38α from ProQinase GmbH revealing a ten-fold preference for CK1δ (CK1δ IC_{50} = 1 nM, p38α IC_{50} = 10 nM). The IC_{50} value for CK1δ, however, is an extrapolated result as it was outside the concentration range, though it was at least < 3 nM in their assays. These results also identified the limits of the present computational model as the *in silico* generated Glide scores did not adequately correlate with the biological data. Apparently, the utilized molecular modeling approaches were not suitable to predict the influence of sulfoxidation and varying

methoxy substitution patterns in *HRII*. The *in vitro* determined IC_{50} values and *in silico* received Glide scores are summarized in **Table 23**.

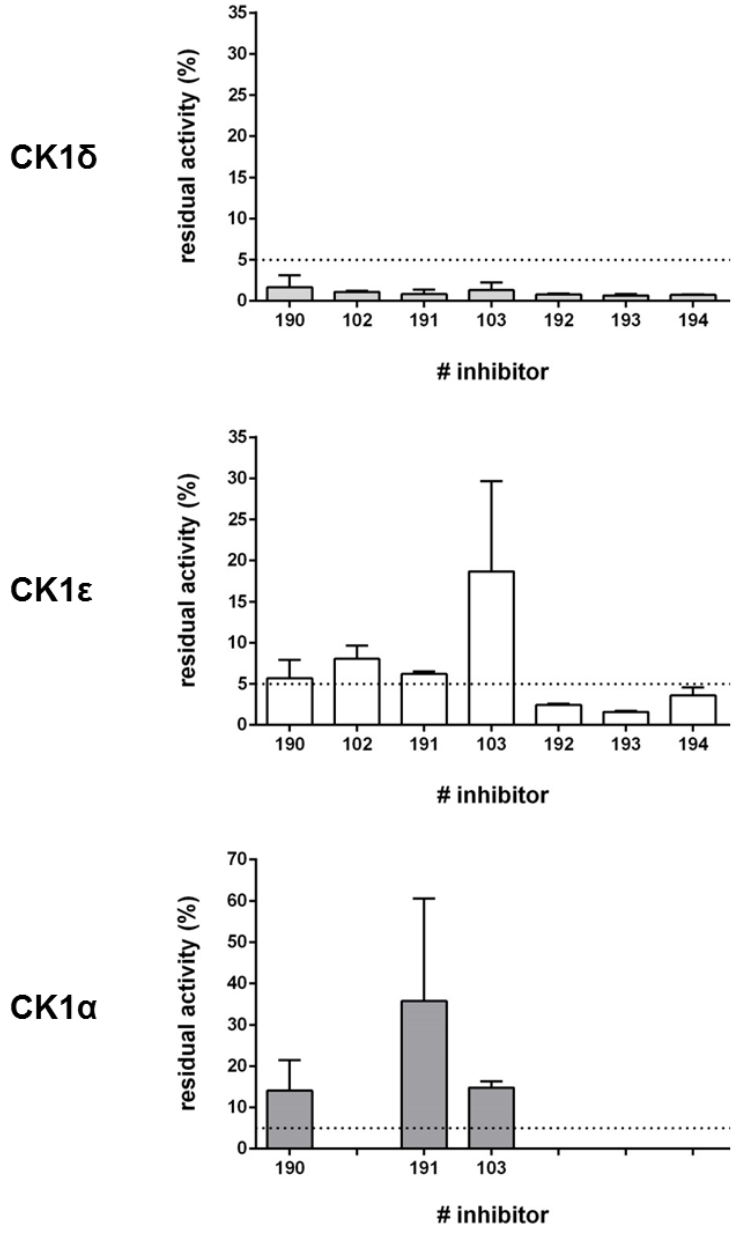

Figure 80 | Inhibition of CK1 isoform kinase activity by inhibitors of series 2 at a concentration of 10 µM. Compounds **190-194**, **102**, **103** have been biologically evaluated in kinase assays against CK1δ and CK1ε. Compounds **190**, **191**, **103** have additionally been tested against CK1α. α-Casein has been used as substrate. The inhibitors were screened in triplicate measurement in the presence of 10 µM ATP. Residual activities were normalized to DMSO. Error bars indicate SEM[248,249].

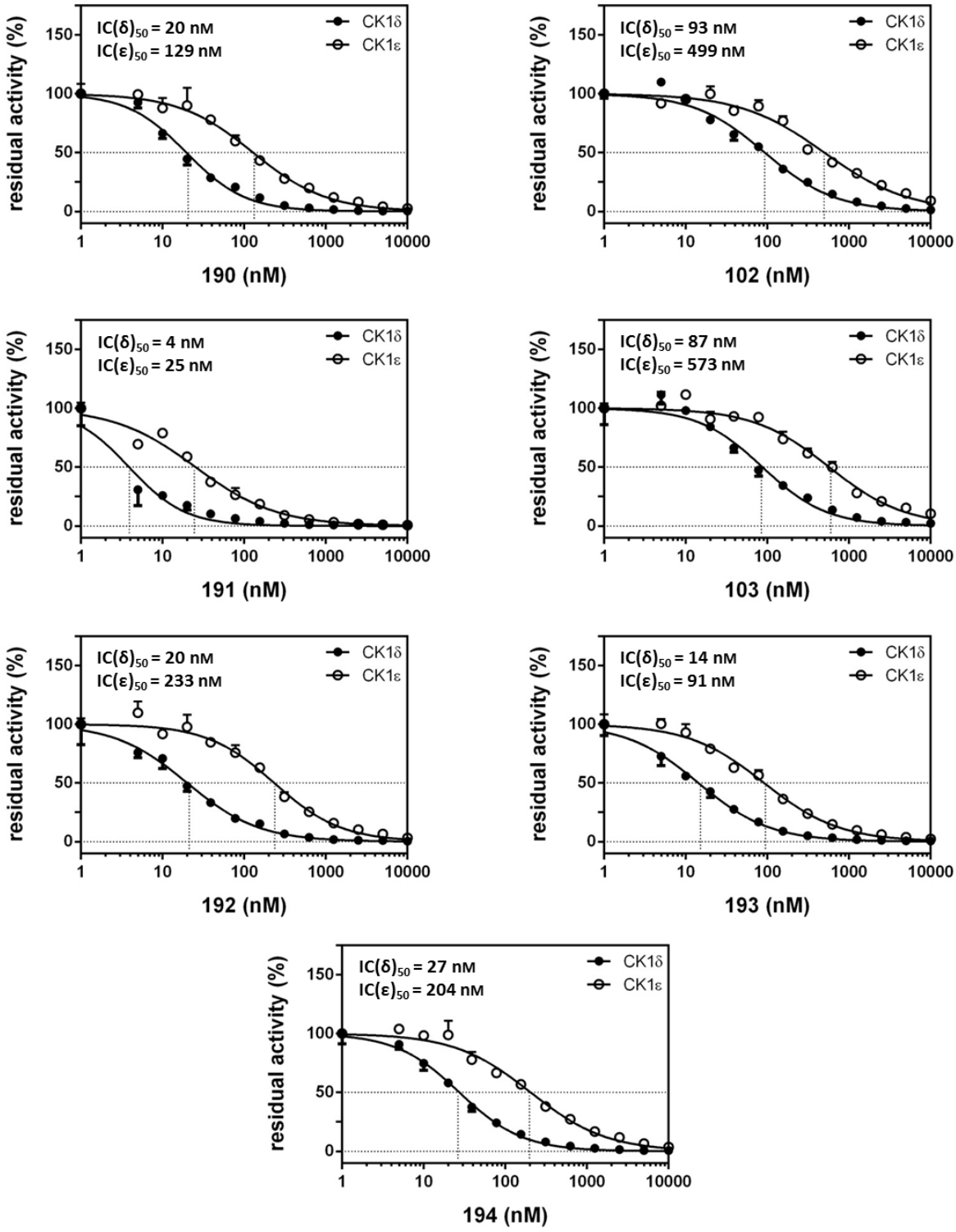

Figure 81 | IC_{50} determination of series 2 compounds 190-194, 102, and 103. IC_{50} values have been determined using CK1δ or CK1ε and α-casein as substrate. Error bars indicate the SEM[248,249].

Table 23 | IC_{50} values and Glide scores of series 2 compounds[248,249].

#	Structure	Glide Score (CK1δ)	IC_{50} (nM)
190	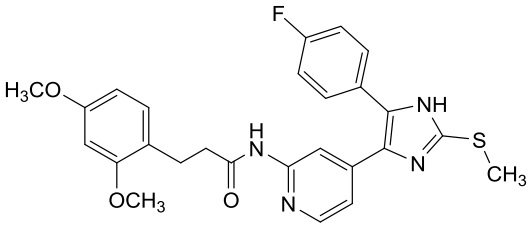	-13.8	20 (CK1δ) 129 (CK1ε) n.d. (p38α)
102	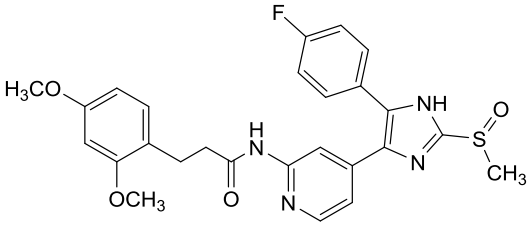	-14.7	93 (CK1δ) 499 (CK1ε) n.d. (p38α)
191	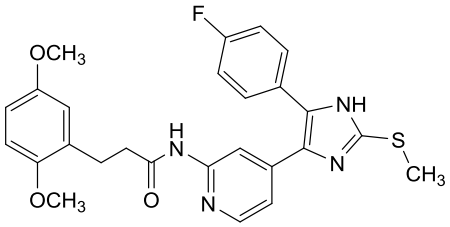	-13.6	4 (CK1δ) 25 (CK1ε) < 3 (CK1δ)[PQ] 10 (p38α)[PQ]
103	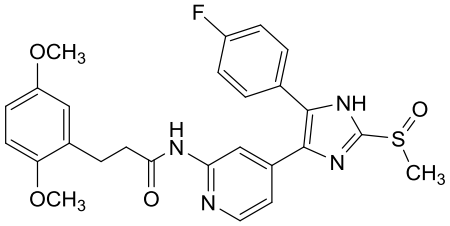	-14.2	87 (CK1δ) 573 (CK1ε) n.d. (p38α)
192	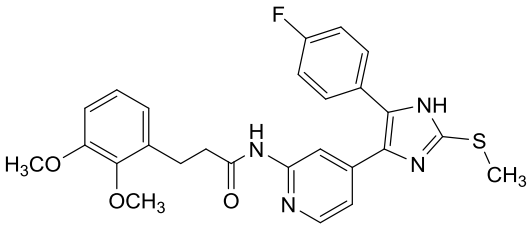	-13.7	20 (CK1δ) 233 (CK1ε) n.d. (p38α)
193	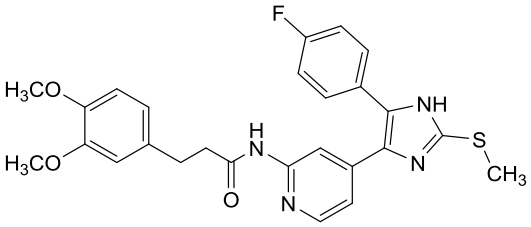	-14.3	14 (CK1δ) 91 (CK1ε) n.d. (p38α)
194	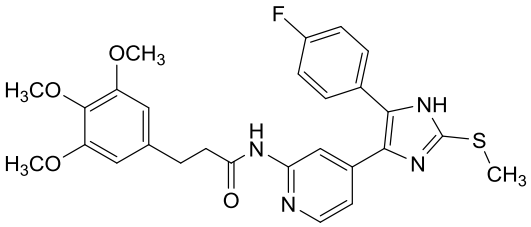	-13.6	27 (CK1δ) 204 (CK1ε) n.d. (p38α)

[PQ] IC_{50} value has been determined by ProQinase GmbH.

Regarding SAR methoxyphenyl-substituted propionic acid side chains proved beneficial in order to gain potency. Thereby, differently dimethoxyphenyl-substituted derivatives exhibited similar IC_{50} values in the low double-digit nanomolar range with the exception of 2,5-dimethoxyphenyl-possessing **191** which showed significantly enhanced activity. In principle, dimethoxyphenyl substitution was slightly favored over one appropriate trimethoxy substitution pattern (**194**). All compounds of series 2 represented potent inhibitors of CK1δ, though only slightly discriminating the ε isoform. **191** reaches the inhibitory potential of lead compound **12** (CK1δ IC_{50} = 11 nM, CK1ε IC_{50} = 447 nM) and its non-oxidized derivative **11** (CK1δ IC_{50} = 5 nM, CK1ε IC_{50} = 73 nM)[176] and is therefore among the most potent CK1δ inhibitors published to date. As expected, removal of the potential MICHAEL acceptor of **12** led to chemical stability of the inhibitors. Introduction of the carbonyl group starting from compounds **150** (CK1δ IC_{50} = 644 nM, CK1ε IC_{50} = 3323 nM) and **164** (CK1δ IC_{50} = 386 nM, CK1ε IC_{50} = 6731 nM) towards **193** (CK1δ IC_{50} = 14 nM, CK1ε IC_{50} = 91 nM) and **190** (CK1δ IC_{50} = 20 nM, CK1ε IC_{50} = 129 nM) led to increased potency for CK1δ by 157- and 20-fold, respectively. CK1ε was inhibited 37- and 52-fold more potently. Considering this enormous increase of potency upon introduction of the carbonyl function as well as the reported benefit on metabolic stability[200], the appropriate amide group should be considered mandatory for further approaches. Interestingly, sulfoxidation of **190** and **191** which favored CK1δ by approximately seven- and six-fold did not significantly affect isoform-specificity (**102:** five-fold, **103:** seven-fold). This was unexpected as oxidation of **11** (fifteen-fold) towards lead **12** strongly increased the CK1δ-preference to approximately 41-fold indicating the π-bond of **12** to be a potential determinant for selectivity but not potency.

Kinase Assays: Selectivity Profiling

In order to investigate **191** regarding kinase selectivity the inhibitor has been screened over a panel of 320 wild-type protein kinases and B-Raf V600E by ProQinase GmbH. The assays revealed good specificity for CK1δ hitting only five additional kinases (residual kinase activity ≤ 50 %) apart from CK1 isoforms δ, ε, and α at a concentration of 100 nM (**Figure 82**). Among them was unsurprisingly p38α, but also highly related c-Jun N-terminal kinases 2 and 3 (JNK2, JNK3), lymphocyte-specific protein tyrosine kinase (LCK), and Receptor-interacting serine/threonine-protein kinase 2 (RIPK2). Potent inhibition with residual activities below 20 %, however, has only been observed for CK1δ (residual activity = 3 %) and CK1ε (residual activity = 7 %). JNK3 (residual activity = 37 %) and RIPK2 (residual activity = 45 %) were inhibited less potently while CK1α (residual activity = 26 %), p38α (residual activity = 22 %), JNK2 (residual activity = 21 %), and LCK (residual activity = 26 %) exhibited reduced residual kinase activities between 20 % and 30 %. The inhibited enzymes were predominantly Ser/Thr-

specific kinases deriving from three distinct superfamilies (CK1, CMGC, TKL) with the exception of LCK (TK) which selectively phosphorylates tyrosine residues. Fortunately, CK1γ3 showed only weak inhibition (residual activity = 73 %) while isoforms γ1 (residual activity = 100 %) and γ2 (residual activity = 91 %) nearly remained unaffected. Residual kinase activities of the complete screening are given in **Supplementary Table 1**. Regarding the determined IC_{50} value of 4 nM, **191** represents a highly specific inhibitor of CK1δ and CK1ε with an overall selectivity (residual activity < 50 %) score of 0.027.

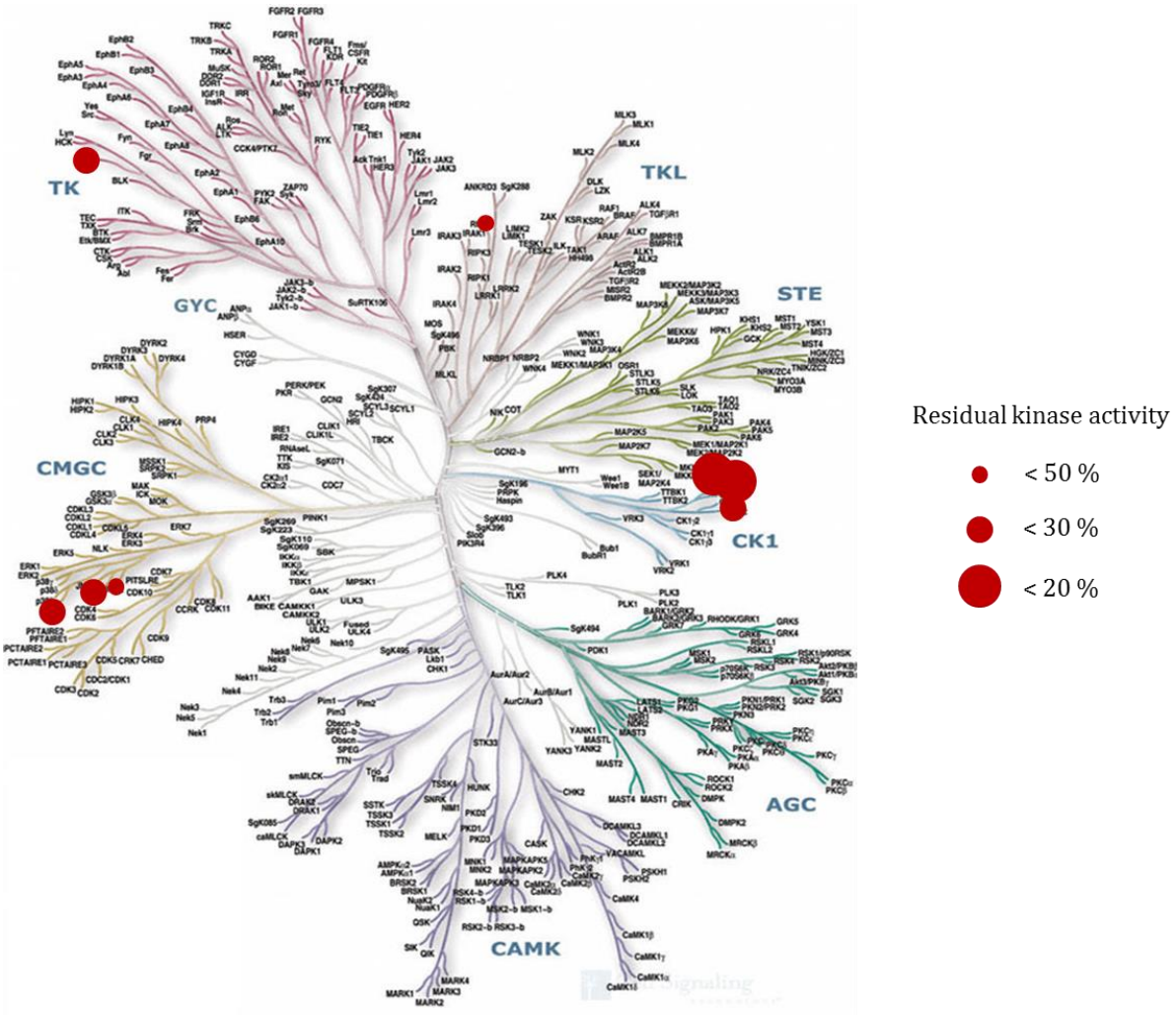

Figure 82 | Schematic representation of the selectivity profile of 191 at a concentration of 100 nM. The inhibitor has been screened over a panel of 320 wild-type protein kinases and B-Raf V600E by ProQinase GmbH. The phylogenetic tree is taken from MANNING *et al.*[5].

Cellular Assays

The efficacy of series 2 inhibitors in cellular assays was initially evaluated at 10 µM using the CK1-dependent human pancreatic adenocarcinoma cell lines Colo357 and Panc89 (**Figure 83**)[248,249].

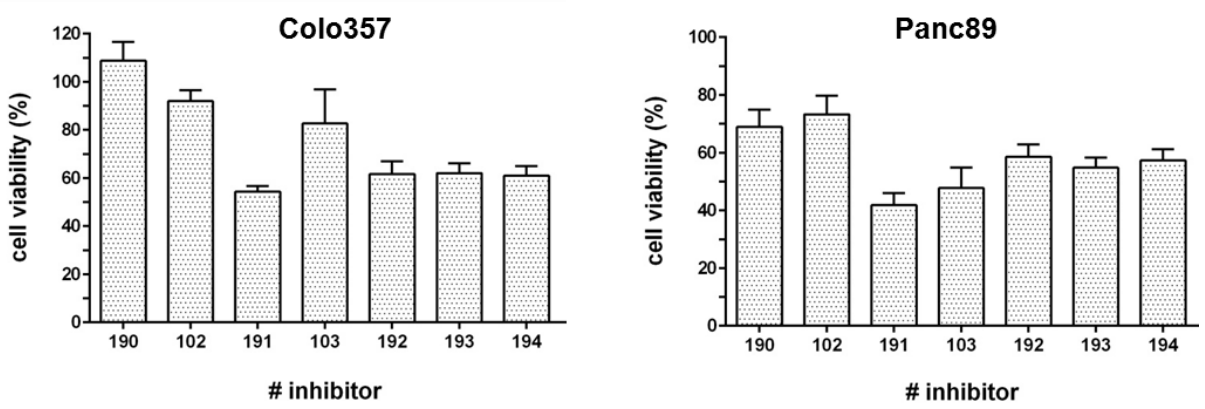

Figure 83 | Cell viability of Colo357 and Panc89 cells after treatment with series 2 compounds at a concentration of 10 µM. The inhibitors were screened in triplicate measurement. Cell viability was normalized to mock. Error bars indicate the SEM[248,249].

The assays identified **191**, **192**, **193**, and **194** as rather potent inhibitors of cell viability in both cell lines, while **190** as well as sulfoxides **102** and **103** did not reveal significant efficacy in Colo357 cells. In Panc89 cells, however, weak but significant inhibition by **190** and **102** was observed while the effect mediated by **103** was comparable to **191**-**194** indicating cell line- or tumor entity-dependent inhibition. Furthermore, the 2,4-dimethoxyphenyl substitution pattern of **190** and **102** seems to negatively influence cellular efficacy. In order to further examine this effect, **190** was screened over the tumor cell lines Colo357, Panc-1, and MiaPaca-2 at 15 µM[249]. The results of these screens are shown in **Figure 84**.

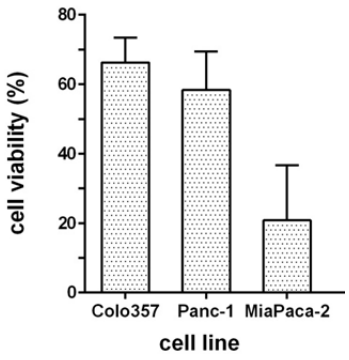

Figure 84 | Cell viability of Colo357, Panc-1, and MiaPaca-2 cells after treatment with 190 at a concentration of 15 µM. The inhibitor was screened in quadruplicate measurement. Cell viability was normalized to mock. Error bars indicate the SEM[248,249].

Interestingly, cell viability was reduced to similar extents in Colo357 and Panc-1 cells while the MiaPaca-2 cell line showed enhanced sensitivity for the inhibitor.

As **191** was the most promising probe of series 2 its efficacy has been validated by EC_{50} determination in CK1-dependent Colo357 and Panc89 cells (**Figure 85**). MTT assays revealed EC_{50} values in the low single-digit micromolar range (Colo357 EC_{50} = 3.5 µM, Panc89 EC_{50} = 1.5 µM) indicating significant improvement in efficacy starting from series 1. The different EC_{50} values also promote the thesis of cell line specific inhibition.

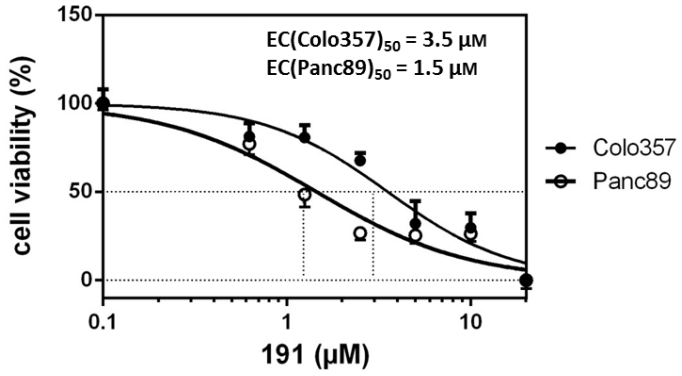

Figure 85 | EC_{50} determination of compound 191 in Colo357 and Panc89 cells. Error bars indicate the SEM[248].

X-ray Crystallography

The biological evaluation identified chemically stable compound **191** as a potent and specific inhibitor of CK1δ, CK1ε, and p38α. Consequently, the exact binding mode in these kinases ought to be examined by X-ray crystallography in cooperation with PROF. DR. DANIEL RAUH and PROF. DR. ULRICH BAUMANN. Unfortunately, co-crystallization of **191** with CK1δ and CK1ε has not been successful to date. Nevertheless, the binding pose in p38α has been revealed (**Figure 86**).

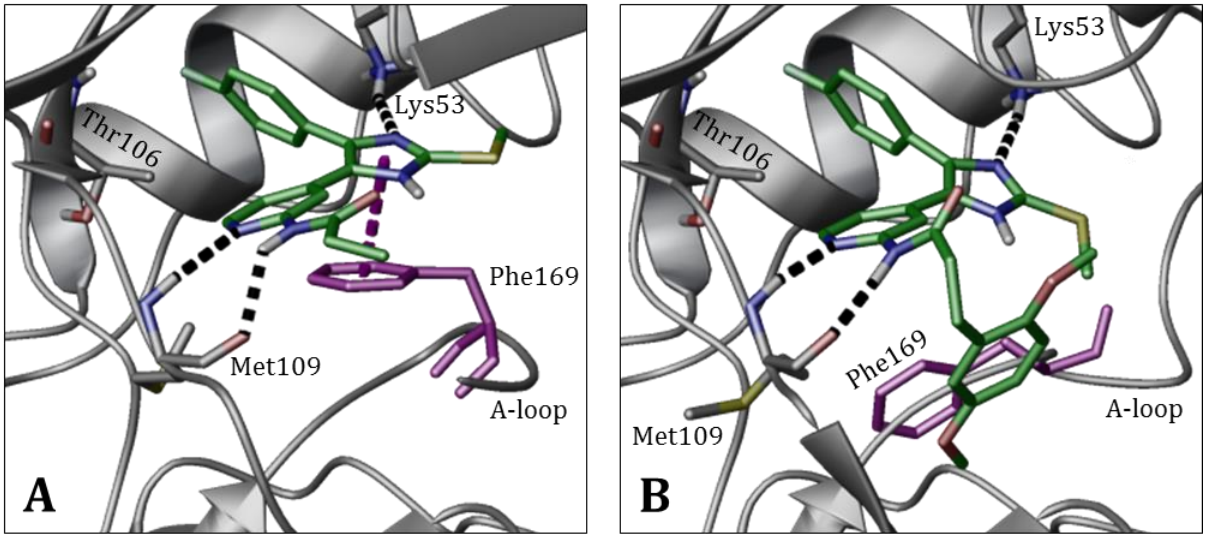

Figure 86 | Binding mode of 191 in p38α MAPK. Binding mode revealed by X-ray crystallography (A) in comparison to the *in silico* model (B). The DFG Phe169 occupies different conformations: DFG-out (A), DFG-in (B). The propionic acid side chain has not been completely resolved by X-ray analysis (A). Modeling (B) refers to PDB code 1BMK[195]. π-π-stacking is indicated by a violet dashed line. X-ray analysis has been performed by the group of PROF. DR. DANIEL RAUH.

X-ray crystallographic analysis and molecular modeling revealed highly similar binding poses for **191** in p38α MAPK. The 4-fluorophenyl moiety penetrates into *HPI* lined by the gatekeeper Thr106. The 2-aminopyridine acts as a bidentate hinge-binder forming two H-bonds with Met109. Lys53 donates another H-bond accepted by the imidazole nitrogen of **191**. The propionic acid side chain is situated in *HRII* which is significantly less spacious compared to CK1δ and CK1ε. Therefore, the side chain has not completely been resolved by X-ray analysis indicating high flexibility of the moiety in this domain. The major difference between *in silico* model and crystallographic data referred to the conformation of the DFG motif at the junction of the activation-loop (A-loop). Molecular modeling of p38α has been performed based on a crystal structure including the structurally similar teardrop-like inhibitor **34** (PDB code 1BMK)[195]. Binding of **34** to p38α obviously retained the DFG-in conformation of the kinase (type I inhibition). Co-crystallization of p38α and **191**, however, revealed that the inhibitor initiates

rotation of the Phe169 residue out of its hydrophobic deep pocket (DFG-out). The DFG-out-like conformation is stabilized by π-π-stacking interaction between Phe169 and the imidazole ring of **191** gaining additional binding affinity. Consequently, the obtained DFG-out-like crystal structure has been aligned to a published DFG-out conformation of p38α (**Figure 87**).

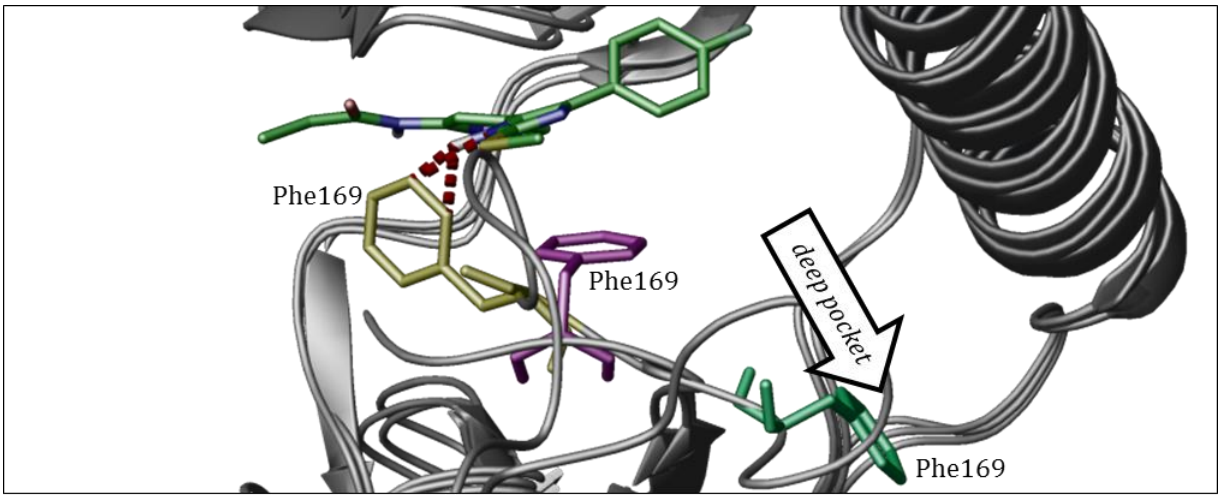

Figure 87 | Protein alignment of the obtained crystal structure of 191 in p38α with published DFG-in and DFG-out conformations of the kinase. Rotation of Phe169 from the active DFG-in (turquoise, PDB code 1BMK)[195] towards the DFG-out conformation (yellow, PDB code 1WBT)[250] permits access to the deep pocket. The obtained crystal structure (violet) exhibits a conformation halfway between DFG-in and DFG-out. Fitting of **191** (green) into the DFG-out state of the kinase might be forestalled by steric clashes (bad contacts, red dashed lines).

The alignment revealed that **191** actually stabilizes a conformation halfway between active DFG-in and inactive DFG-out state of the kinase (DFG-half-out). Rotation of Phe169, however, seemed sufficient in order to permit access to the deep pocket, although this cavity is not addressed by the inhibitor. X-ray analysis thereby provided strong evidence that **191** might rather be a type I ½-like inhibitor of p38α, whereas it is in fact likely that the ligand is able to bind both DFG-in and DFG-half-out conformation. Regarding the DFG-out state steric clashes between inhibitor and Phe169 can be assumed to forestall fitting. The shift between active and inactive conformation could further explain the non-correlating results from p38α-based Glide scoring and *in vitro* obtained data.

5.3 Characterization of Series 3

Kinase Assays

The crystallographic data gained by co-crystallization of **191** and p38α supported the thesis assuming beneficial effects on selectivity by rigidification side chains addressing *HRII*. Consequently, the *sp*²-hybridized planar carbamide linker of series 3 compounds was suggested to forestall adjustment to the restricted *HRII* of p38α while the equivalent domain in CK1δ is more spacious and planar. The carbamide group might further enable a third H-bond towards hinge residue Leu85 (CK1δ) leading to strengthened ligand-receptor binding. It has to be noted, though, that the effect of additional H-bonds is often not reliably predictable and requires *in vitro* evaluation[191]. Therefore, compounds **204**-**206**, **208**-**210**, **212**, **104**, and **286**-**290** have been screened at 10 µM against CK1δ and CK1ε in the presence of 10 µM ATP. **204**, **104**, **206**, **286**, **209**, **210**, and **212** have additionally been tested against CK1α (**Figure 88**)[248,249].

The initial screenings showed effective reduction of CK1δ residual kinase activity only slightly less potent than compounds of series 2. In addition, especially **104** but also **204**, **209**, and **210** exhibited promising isoform-specificity over CK1ε. CK1α was overall less potently inhibited.

Subsequent IC_{50} determination has been performed to validate the effect of promising compounds **204**, **104**, **205**, **206, 209**, and **210** on CK1 isoforms δ and ε (**Figure 89**)[248,249]. IC_{50} values stretching across the low double-digit to the low triple-digit nanomolar range identified the appropriate carbamides as rather potent or moderate inhibitors that slightly prefer CK1 isoform δ. Interestingly, dimethoxyphenyl-substituted carbamides **204** (CK1δ IC_{50} = 19 nM, CK1ε IC_{50} = 227 nM) and **205** (CK1δ IC_{50} = 31 nM, CK1ε IC_{50} = 186 nM) represented the most promising derivatives of series 3 indicating again the dimethoxy substitution pattern to be positively suited to fit in *HRII* of CK1δ. In addition, **204** exhibited the strongest isoform-specificity by twelve-fold among this series. As observed before, sulfoxidation significantly reduced potency without positive gains in selectivity in most cases. In fact, only **289** (CK1δ IC_{50} = 88 nM, CK1ε IC_{50} = 623 nM) showed enhanced properties compared to its non-oxidized derivative **210** (CK1δ IC_{50} = 169 nM, CK1ε IC_{50} = 498 nM) while conversion of **204** towards the appropriate sulfoxide **104** (CK1δ IC_{50} = 153 nM, CK1ε IC_{50} = 910 nM) was accompanied by losses of both potency and specificity. The naphthyl-substituted carbamide **290** (CK1δ IC_{50} = 48 nM, CK1ε IC_{50} = 182 nM) displayed another promising scaffold that was rather potent despite sulfoxidation. Unfortunately, an IC_{50} value for its non-oxidized derivative **212** has not been determined.

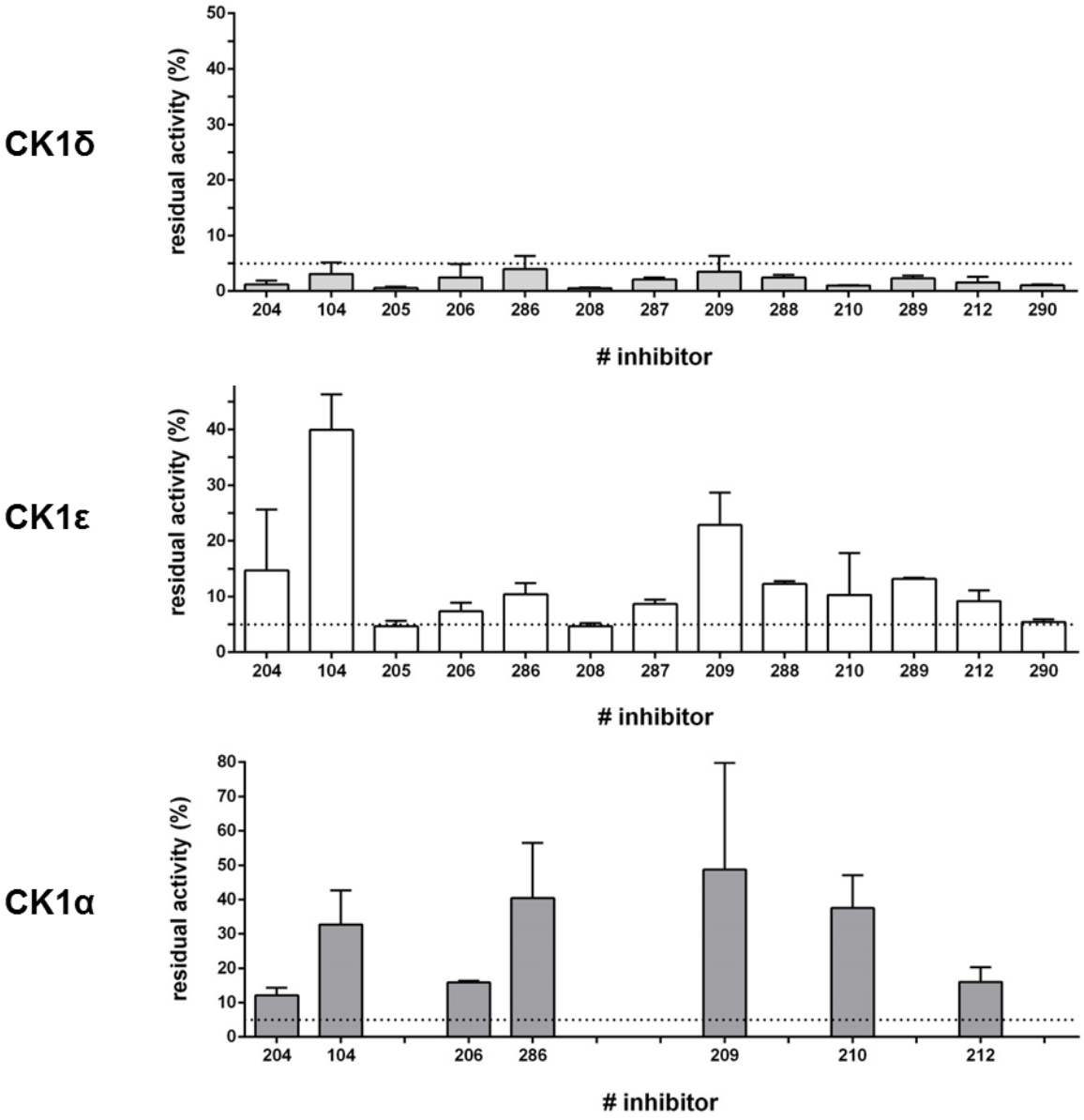

Figure 88 | Inhibition of CK1 isoform kinase activity by inhibitors of series 3 at a concentration of 10 µM. Compounds **204-206**, **208-210**, **212**, **104**, and **286-290** have been biologically evaluated in kinase assays against CK1δ and CK1ε. Compounds **204**, **104**, **206**, **286**, **209**, **210**, and **212** have additionally been tested against CK1α. α-Casein has been used as substrate. The inhibitors were screened in triplicate measurement in the presence of 10 µM ATP. Residual activities were normalized to DMSO. Error bars indicate the SEM[248,249].

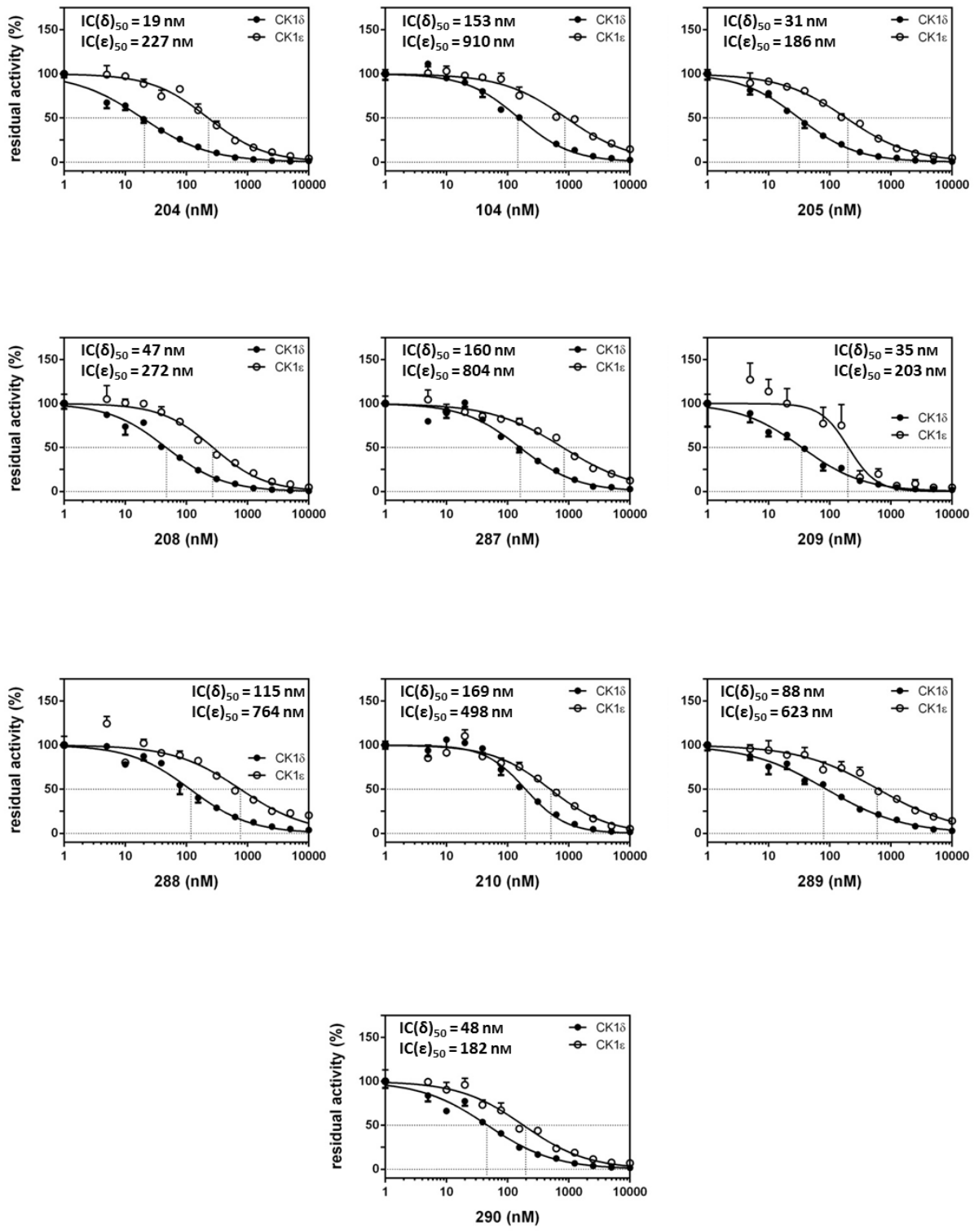

Figure 89 | IC_{50} determination of series 3 compounds 204, 205, 208-210, 104, and 287-290. IC_{50} values have been determined using CK1δ or CK1ε and α-casein as substrate. Error bars indicate the SEM[248,249].

The enormous predicted affinities indicated by Glide scores ranging from -17.1 for compound **104** to -12.5 for compound **208** (**Table 24**), however, have not been confirmed as **191** (Glide score = -13.6) was still the most effective inhibitor characterized so far. It might be possible, though, that physicochemical parameters such as limited solubility of the carbamides restrained their theoretical potency. Regarding the effect of rigidification on inhibition of p38α, **204** has been submitted to ProQinase GmbH for further IC_{50} determination. The assays showed values in the low double-digit nanomolar range for CK1δ (IC_{50} = 10 nM) and p38α (IC_{50} = 28 nM) assuming carbamides to be inept to initiate selectivity in this context. Nevertheless, especially **204** proved promising in order to discriminate CK1 isoforms and might therefore be worth optimizing.

Table 24 | IC_{50} values and Glide scores of series 3 compounds[248,249].

#	Structure	Glide Score (CK1δ)	IC_{50} (nM)
204	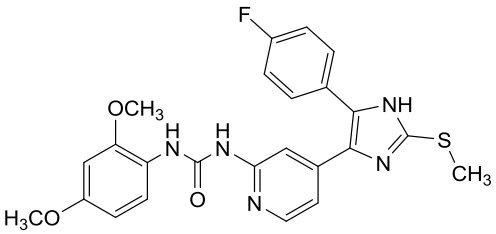	-16.6	19 (CK1δ) 227 (CK1ε) 10 (CK1δ)^{PQ} 28 (p38α)^{PQ}
104	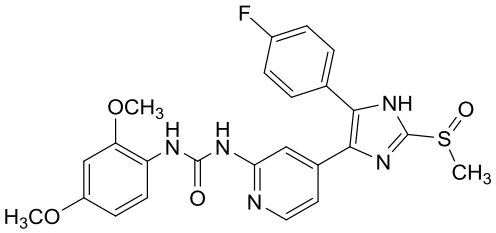	-17.1	153 (CK1δ) 910 (CK1ε) n.d. (p38α)
205	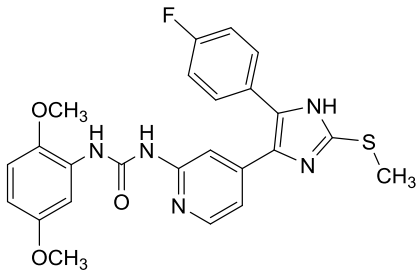	-17.0	31 (CK1δ) 186 (CK1ε) n.d. (p38α)
208	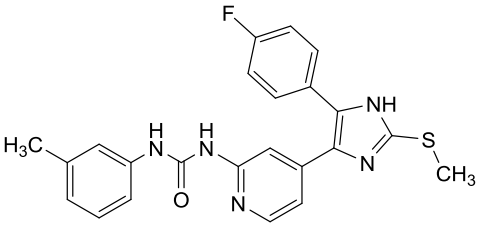	-12.5	47 (CK1δ) 272 (CK1ε) n.d. (p38α)
287	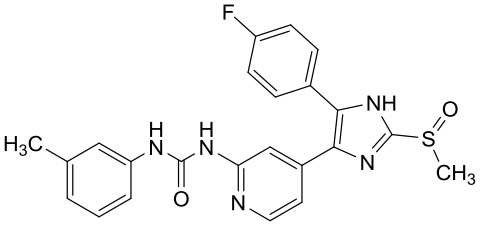	-15.8	160 (CK1δ) 804 (CK1ε) n.d. (p38α)

209	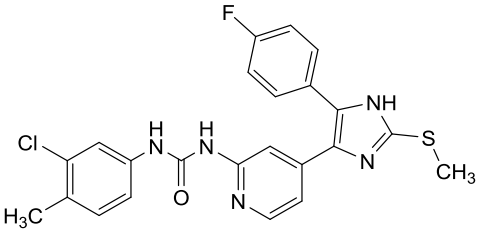	-15.7	35 (CK1δ) 203 (CK1ε) n.d. (p38α)
288	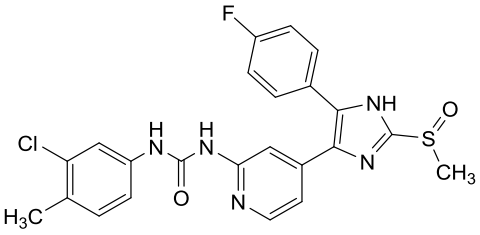	-15.7	115 (CK1δ) 764 (CK1ε) n.d. (p38α)
210	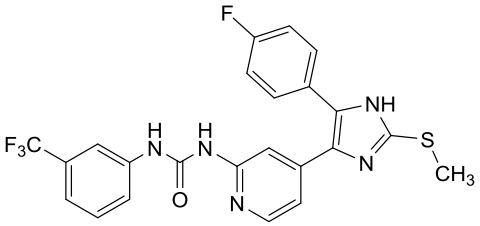	-14.8	169 (CK1δ) 498 (CK1ε) n.d. (p38α)
289	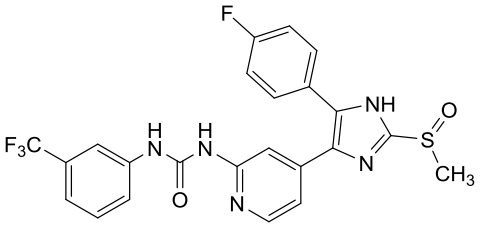	-14.3	88 (CK1δ) 623 (CK1ε) n.d. (p38α)
290	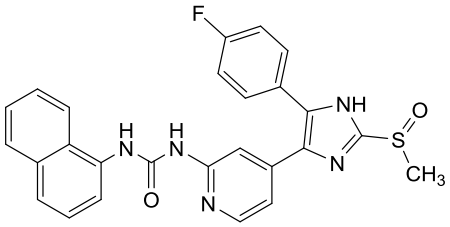	-15.6	48 (CK1δ) 182 (CK1ε) n.d. (p38α)

[PQ] IC_{50} value has been determined by ProQinase GmbH.

Cellular Assays

The inhibitors of series 3 were screened in cellular assays at a concentration of 10 µM using the discussed human pancreatic adenocarcinoma cell lines Colo357 and Panc89 in order to evaluate their cellular efficacy (**Figure 90**)[248,249].

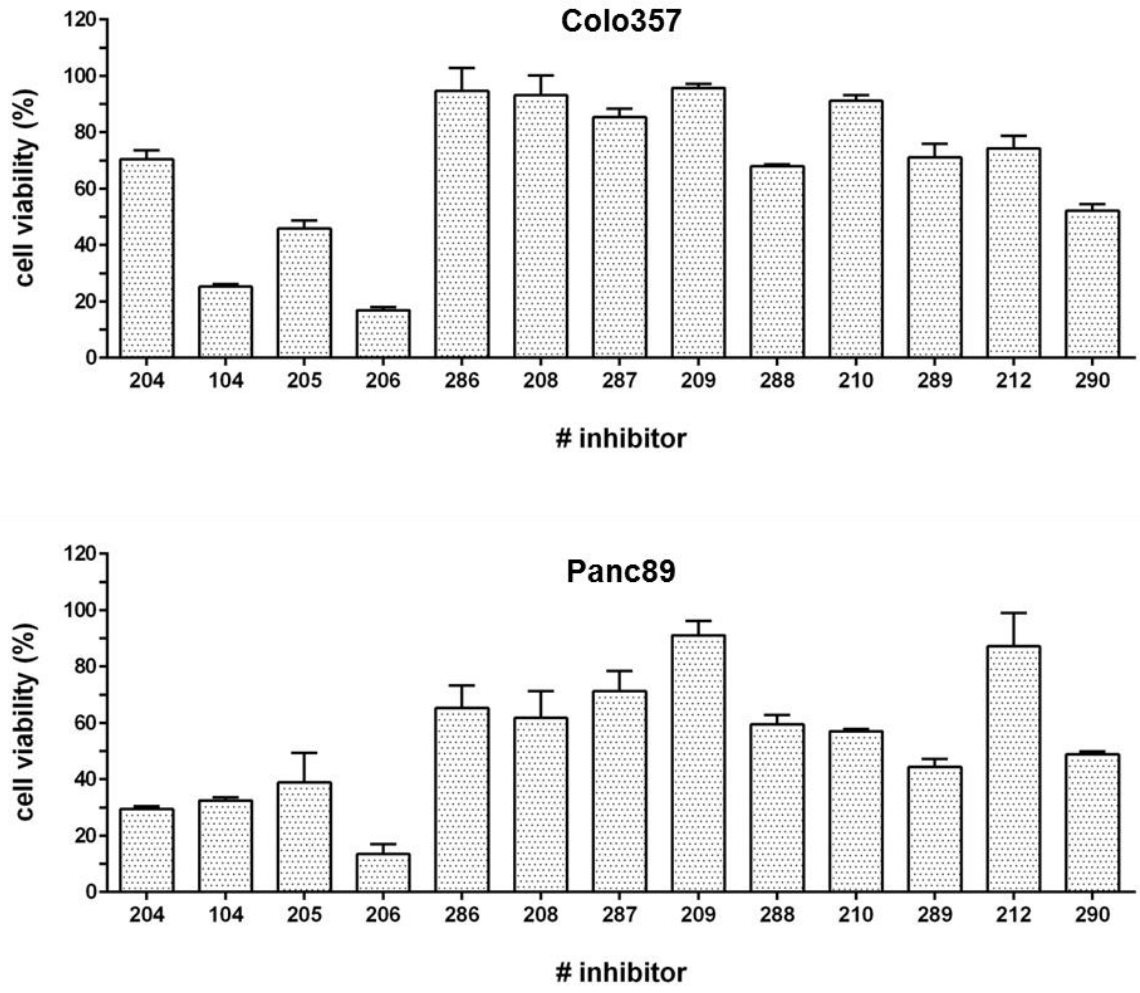

Figure 90 | Cell viability of Colo357 and Panc89 cells after treatment with series 3 compounds at a concentration of 10 µM. The inhibitors were screened in triplicate or quadruplicate measurement. Cell viability was normalized to mock. Error bars indicate the SEM[248,249].

The majority of series 3 derivatives reduced cell viability rather weakly, indicating poor cell penetration which is presumably due to their unfavorable physicochemical properties such as solubility. Nevertheless, especially compounds **206** and **104**, followed by **205** and **204**, exhibited promising effects as they reduced metabolic activity at best (**206**) below 20 % in both cell lines. Fortunately, these results excellently fit with the previous findings as all four of them represent methoxyphenyl-substituted carbamides. In general, Panc89 cells seemed more sensitive to treatment with small molecule kinase inhibitors than Colo357 cells.

5.4 Characterization of Series 4

Kinase Assays

The intention of series 4 compounds was to enhance selectivity by rigidification of side chains and conservation the (*E*)-configured π-bond of lead structure **12** within 4-(dimethoxyphenyl)-substituted pyrroles. Especially p38α was assumed to be less potently inhibited by compounds **232**, **291**, and **224** as bulky side chains have been reported to negatively affect fitting into the p38α ATP-pocket[198]. The inclusion of the discussed π-bond of **12** in heterocyclic scaffolds was further meant to reduce reactivity of the potential MICHAEL acceptor while conserving the bond itself as well as the resulting sp^2 hybridization. Chemical stability, however, has not been gained unless the pyrrole nitrogen was methylated (cp. **chapter 4.5.1**). Unfortunately, *N*-alkylation forestalled the idea of a tridentate hinge-binder. Consequently, molecular modeling estimated addition of the methyl group by a predicted loss of binding free energy: while the Glide score of non-methylated **105**, for instance, is -16.7 it is modified for methylated **291** leading to -13.6. The modeled poses of **105** and **291** in CK1δ are shown in **Figure 91**.

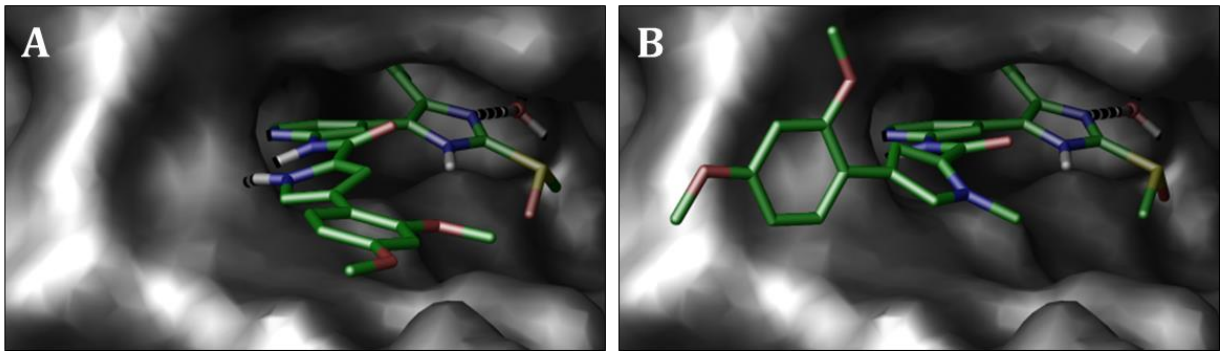

Figure 91 | Postulated binding modes of 105 (A) and 291 (B) in CK1δ. (PDB code 3UZP).

According to molecular modeling methylation of the pyrrole nitrogen of **105** leading to **291** forces the heterocycle to rotate by approximately 180°, thereby affecting the overall orientation within *HRII*. Consequently, **291** does only represent a bidentate hinge-binder. Although enthalpic losses can theoretically be assumed in relation to non-methylated **105**, they might not necessarily be translated into decreased *in vitro* efficacy as previous results indicated the entropic effect to be the determining factor regarding affinity for *HRII*. Considering the calculated Glide scores which are in the range of series 2 compounds, potent inhibition can still be suggested. Therefore, derivatives **232**, **291**, and **224** have been assayed at 10 μM against CK1δ and CK1ε in order to evaluate their biological activity (**Figure 92**)[249].

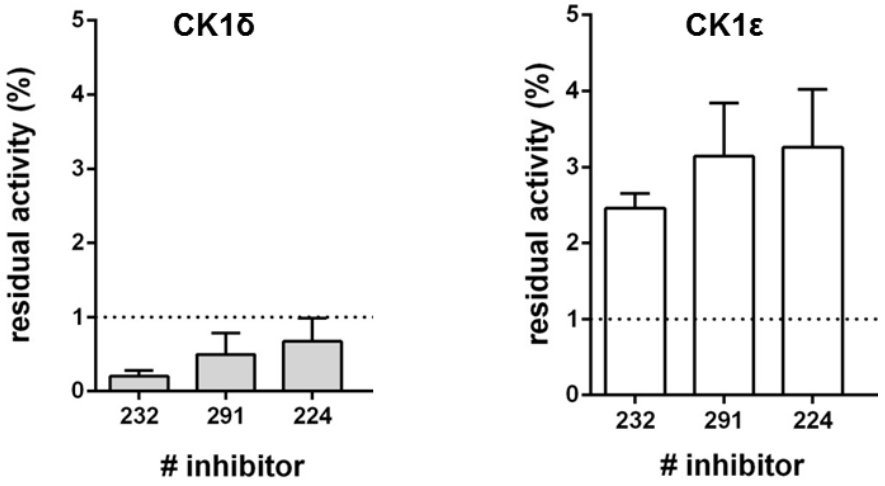

Figure 92 | Inhibition of CK1 isoform kinase activity by inhibitors of series 4 at a concentration of 10 µM. Compounds **232, 291,** and **224** have been biologically evaluated in kinase assays against CK1δ and CK1ε. α-Casein has been used as substrate. The inhibitors were screened in triplicate measurement in the presence of 10 µM ATP. Residual activities were normalized to DMSO. Error bars indicate the SEM[249].

In fact, the initial screens identified **232**, **291**, and **224** as potent inhibitors that reduced residual CK1δ activity below 1 % at a concentration of 10 µM, though without significant discrimination of CK1ε. Subsequently, IC_{50} values have been determined to validate the observed effects (**Figure 93**)[249].

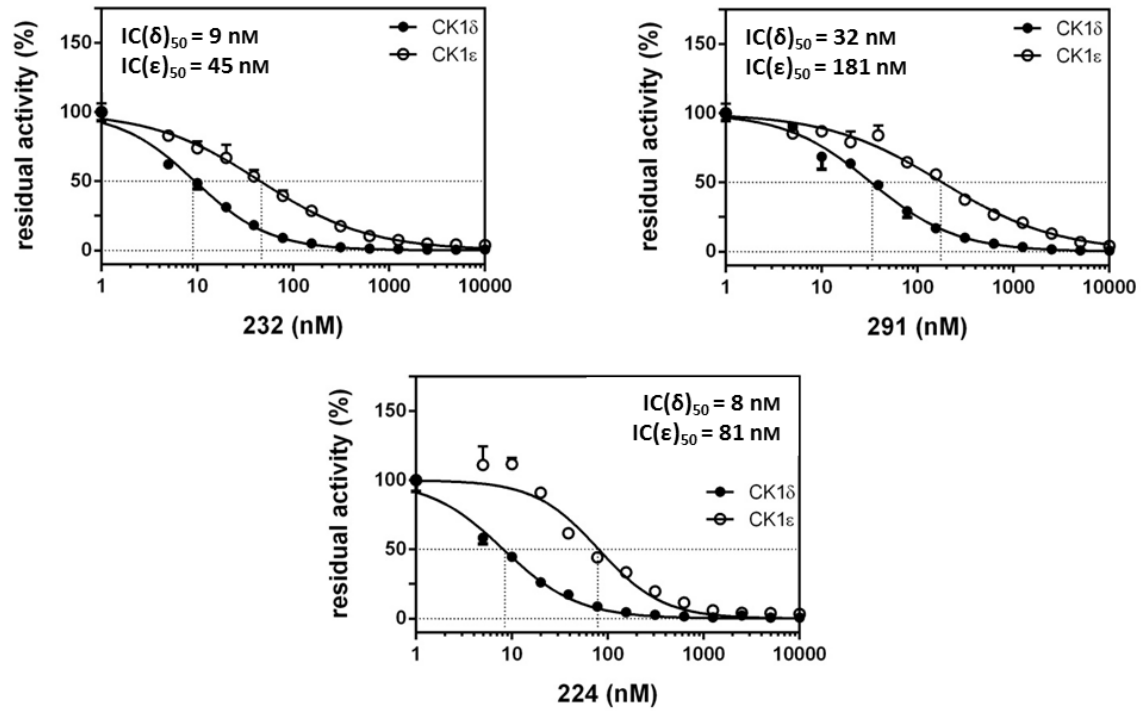

Figure 93 | IC_{50} determination of series 4 compounds 232, 291, and 224. IC_{50} values have been determined using CK1δ or CK1ε and α-casein as substrate. Error bars indicate the SEM[249].

Fortunately, IC_{50} determination confirmed the assumption of series 4 derivatives being rather potent inhibitors of CK1δ comparable to series 2. **232** (CK1δ IC_{50} = 9 nM, CK1ε IC_{50} = 45 nM) and **224** (CK1δ IC_{50} = 8 nM, CK1ε IC_{50} = 81 nM) exhibited IC_{50} values in the single-digit nanomolar range while sulfoxidation of **232** seemed to reduce potency by three- to four-fold leading to still highly effective **224** (CK1δ IC_{50} = 32 nM, CK1ε IC_{50} = 181 nM). Significant discrimination of CK1 isoforms δ and ε, however, has not been observed as **224** was the most specific inhibitor in this context favoring CK1δ by approximately ten-fold. In order to further validate specificity CK1δ and p38α IC_{50} values have been determined for **224** by ProQinase GmbH. Regrettably, the expected positive gains in specificity have been disproved as **224** exhibited potent dual-specific inhibition. The assays showed half maximally reduced CK1δ activity after treatment with < 3 nM inhibitor, corresponding to an extrapolated IC_{50} value of 1 nM, which is only by approximately three- to ten-fold more effective than the determined inhibition of p38α (IC_{50} = 10 nM). IC_{50} values are summarized in **Table 25**.

Table 25 | IC_{50} values and Glide scores of series 4 compounds[249].

#	Structure	Glide Score (CK1δ)	IC_{50} (nM)
232	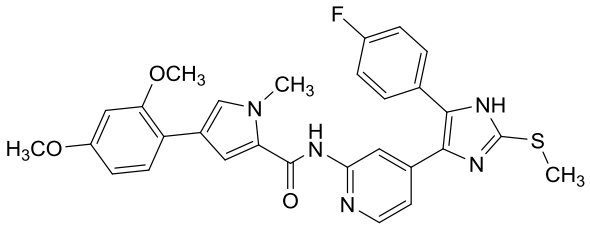	-14.4	9 (CK1δ) 45 (CK1ε) n.d. (p38α)
291	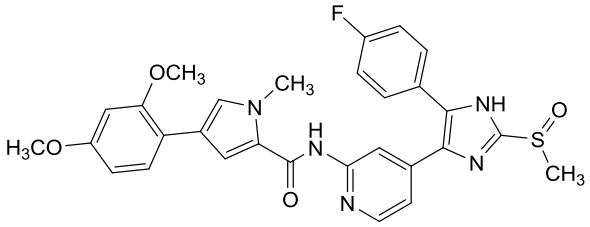	-13.6	32 (CK1δ) 181 (CK1ε) n.d. (p38α)
224	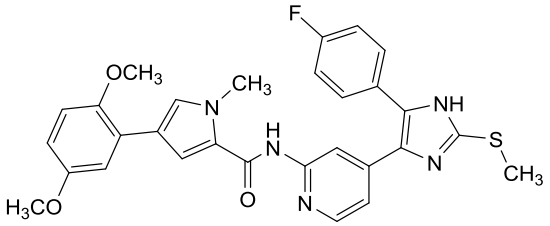	-14.2	8 (CK1δ) 81 (CK1ε) < 3 (CK1δ)[PQ] 10 (p38α)[PQ]

[PQ] IC_{50} value has been determined by ProQinase GmbH.

Structurally, the 4-(2,5-dimethoxyphenyl)-substituted pyrrole **224** seems to be slightly favored over the 2,4-dimethoxyphenyl substitution pattern of **232** in the context of specificity, although both CK1ε and p38α have also been potently inhibited. Sulfoxidation accounted for a loss of potency without significantly increased specificity. Nevertheless, sulfoxide **291** still represented

a highly potent inhibitor of CK1δ. Considering the overall high affinity which is in the range of series 2 derivatives, molecular modeling-based prediction has insofar been confirmed.

Cellular Assays

In order to evaluate efficacy on the cellular level **232**, **291**, and **224** have been applied to MTT assays in a concentration of 15 μM using the different human cancer cell lines Colo357, Panc-1, and MiaPaca-2 (**Figure 94**)[249]. Interestingly, Colo357 cells repeatedly exhibited enhanced resistance to treatment with small molecule CK1δ inhibitors while Panc-1 and MiaPaca-2 cells were significantly more sensitive. The overall efficacy was rather low but definite with the strongest effect in MiaPaca-2 cells, reducing cell viability to approximately 50 %. In general, the inhibitors did not reveal any structural preferences leading to similar inhibition of metabolic activity of Panc-1 and MiaPaca-2 cell lines. In Colo357 cells, however, **224** seemed slightly favored over **291** while **232** did not seem to express any effect at all. Considering the limited cellular efficacy despite IC_{50} values in the low nanomolar range it is most likely that the high molecular weight and the lipophilic character of these inhibitors accounted for poor solubility in cell medium and poor cell penetration.

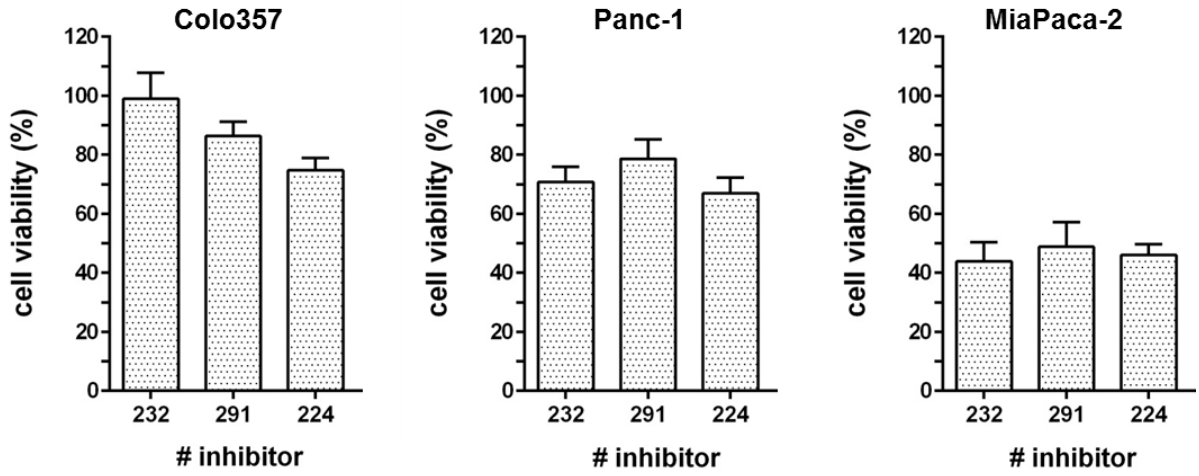

Figure 94 | Cell viability of Colo357, Panc-1, and MiaPaca-2 cells after treatment with series 4 compounds at a concentration of 15 μM. The inhibitors were screened in triplicate or quadruplicate measurement. Cell viability was normalized to mock. Error bars indicate the SEM[249].

X-ray Crystallography

In order to validate the predicted binding mode crystal structures of CK1δ in complex with **224** have been achieved by the group of PROF. DR. ULRICH BAUMANN (**Figure 95**).

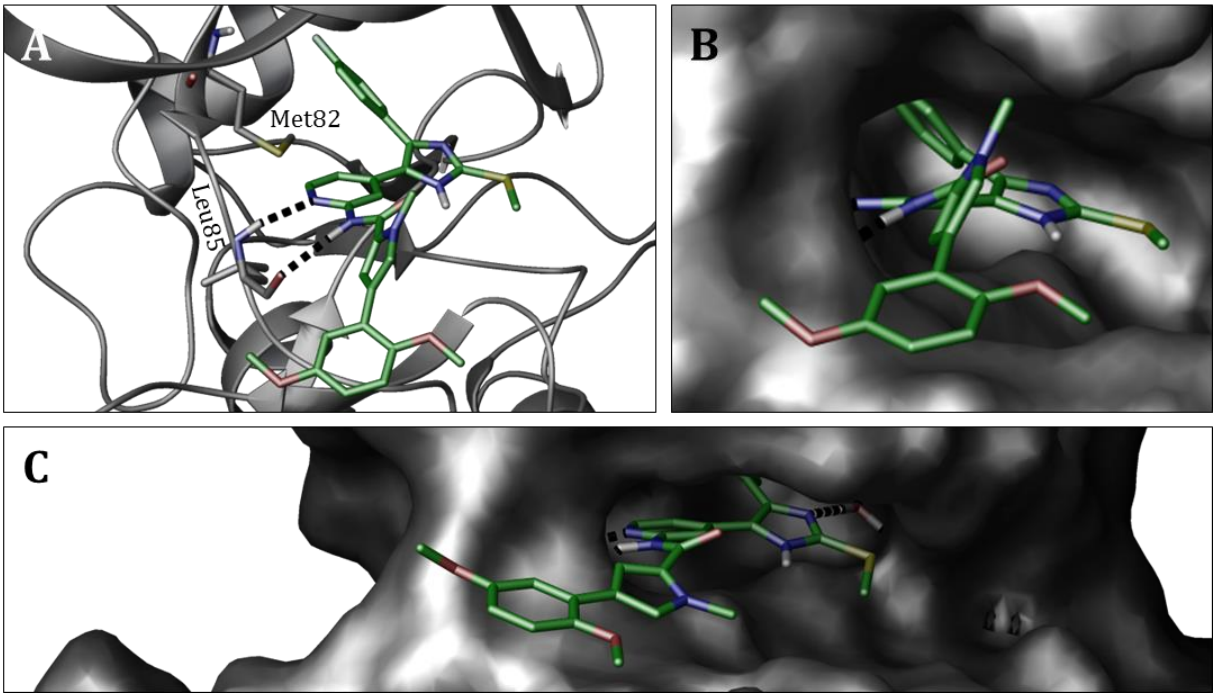

Figure 95 | Binding mode of 224 in CK1δ. The binding mode revealed by X-ray crystallography is presented as ribbon (A) and surface (B) diagram. The *in silico* predicted mode (C) shows different orientation of the pyrrole moiety. X-ray analysis has been performed by the group of PROF. DR. ULRICH BAUMANN.

Crystallographic analysis revealed the actual binding pose of **224** in CK1δ to be rather well predicted by the used *in silico* model, although the pyrrole moiety is rotated counterclockwise by approximately 90°. Consequently, the pyrrole and the dimethoxyphenyl ring are orientated vertically to each other rather than being situated in the same plane. Despite rotation of the pyrrole linker, however, positioning of the dimethoxyphenyl moiety has been predicted quite accurately. Furthermore, the geometry of the diaryl-imidazole pharmacophore has been calculated exactly including the bidentate hinge-binder and the penetration of the 4-fluorophenyl moiety into *HPI*. The buried water molecule, however, has not been resolved, thereby providing evidence that it might actually not be referred to as a structural water.

5.5 Characterization of Series 6

Kinase Assays

Porcn inhibitors **113** and **114** have recently been found to weakly inhibit CK1δ in kinase assays without affecting CK1ε (unpublished data by KUHL and KNIPPSCHILD). Therefore, hybrid inhibitors **266** and **267** were designed to resume this specificity to a certain degree. In addition, the bulky and non-flexible dihydro-thieno[3,2-*d*]pyrimidin-4-one moiety was expected to positively influence the overall selectivity regarding p38α[198]. Potency, however, was assumed comparable to series 2 and 4 derivatives (**191** Glide score = -13.6, **224** Glide score = -14.2) according to molecular modeling approaches that revealed Glide scores in an equivalent range (**266** Glide score = -13.5, **267** Glide score = -14.2). The cellular efficacy, on the contrary, might suffer from poor physicochemical properties regarding solubility and cell penetration, for instance. Nevertheless, the synthesis of hybrid inhibitors and their biological characterization were believed beneficial in order to evaluate the possibility of *HRII*-mediated selectivity for CK1δ in combination with the affinity-gaining teardrop scaffold **120**. Consequently, **266** and **267** have been examined in initial screens against CK1 isoforms δ and ε (**Figure 96**)[249].

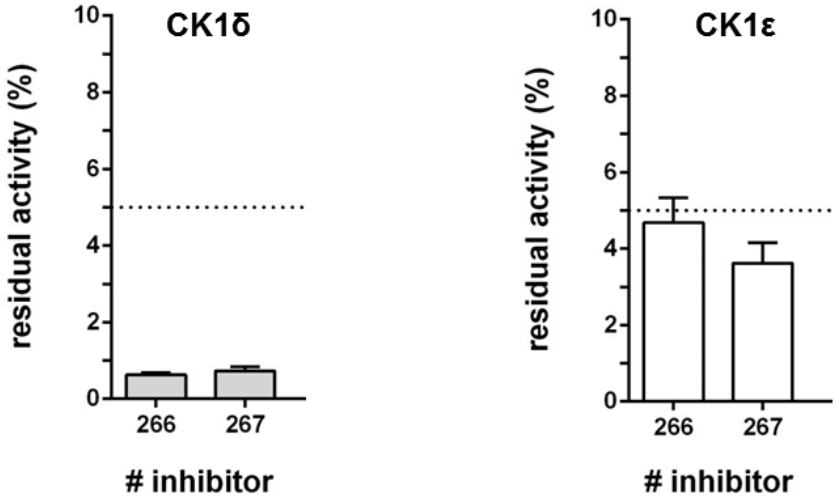

Figure 96 | Inhibition of CK1 isoform kinase activity by inhibitors of series 6 at a concentration of 10 μM. Compounds **266** and **267** have been biologically evaluated in kinase assays against CK1δ and CK1ε. α-Casein has been used as substrate. The inhibitors were screened in triplicate measurement in the presence of 10 μM ATP. Residual activities were normalized to DMSO. Error bars indicate the SEM[249].

The kinase assays confirmed the expected potent inhibition of CK1δ as both derivatives reduced the residual kinase activity below 1 % at a concentration of 10 μM. The obtained results

regarding isoform-specificity, though, were deflating because **266** and **267** effectively blocked CK1ε activity as well. Validation of these findings was maintained by IC_{50} determination for CK1 isoforms δ and ε (**Figure 97**)[249] as well as CK1δ and p38α (ProQinase GmbH, only **266**).

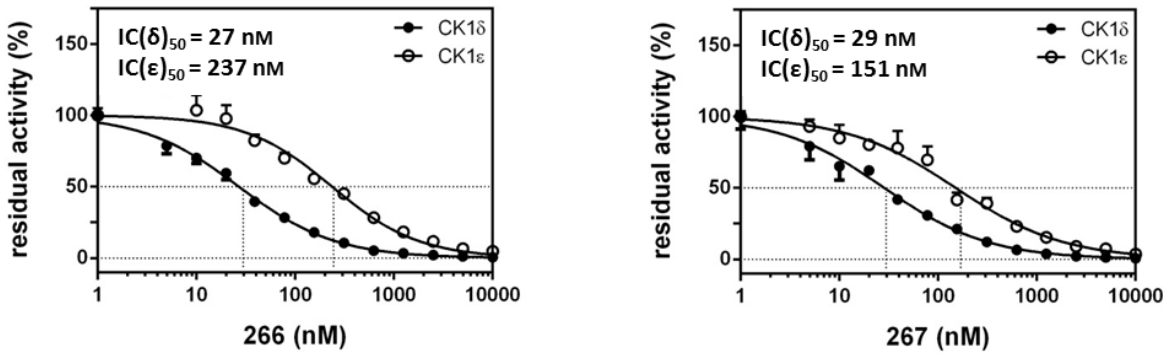

Figure 97 | IC_{50} determination of series 6 compounds 266 and 267. IC_{50} values have been determined using CK1δ or CK1ε and α-casein as substrate. Error bars indicate the SEM[249].

IC_{50} values in the low nanomolar range identified **266** and **267** as potent dual-specific inhibitors of CK1δ and p38α without selective discrimination of CK1 isoforms δ and ε (**Table 26**). **266** proved to be the more specific inhibitor favoring CK1δ by approximately nine-fold over CK1ε and up to 18-fold over p38α (ProQinase: CK1δ IC_{50} < 3 nM, corresponding to an interpolated IC_{50} = 2 nM, p38α IC_{50} = 36 nM).

Although the *in silico* prediction of affinity towards CK1δ has been confirmed, the expected effects regarding kinase- or even isoform-specificity were declined. Taken together, the practicability of conceptual substitution of building block **120** has to be reviewed, at least regarding selective inhibition of CK1δ.

Table 26 | IC_{50} values and Glide scores of series 4 compounds[249].

#	Structure	Glide Score (CK1δ)	IC_{50} (nM)
266	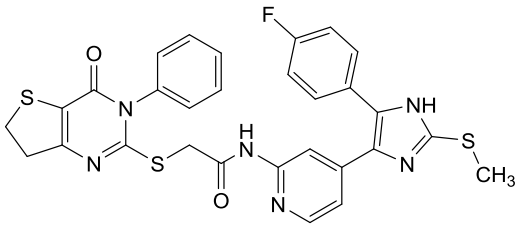	-13.5	27 (CK1δ) 237 (CK1ε) < 3 (CK1δ)[PQ] 36 (p38α)[PQ]
267	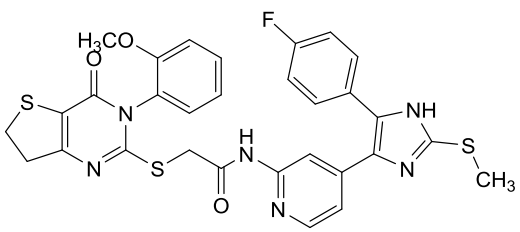	-14.2	29 (CK1δ) 151 (CK1ε) n.d. (p38α)

[PQ] IC_{50} value has been determined by ProQinase GmbH.

Cellular Assays

The cellular efficacy of **266** and **267** has subsequently been evaluated using the human pancreatic carcinoma cell lines Colo357, Panc-1, and MiaPaca-2[249]. As expected, both compounds are only slightly active in Panc-1 and MiaPaca-2 cells and did not significantly reduce cell viability of the Colo357 cell line which has been observed rather resistant in previous experiments. In Panc-1 and MiaPaca-2 cells, however, metabolic activity has been inhibited by approximately 20 % with compound **266** being slightly more effective than **267**. The high molecular weight of the inhibitors most likely accounted for unfavorable physicochemical properties which are suitable to explain the low efficacy on the cellular level regarding solubility and cell penetration.

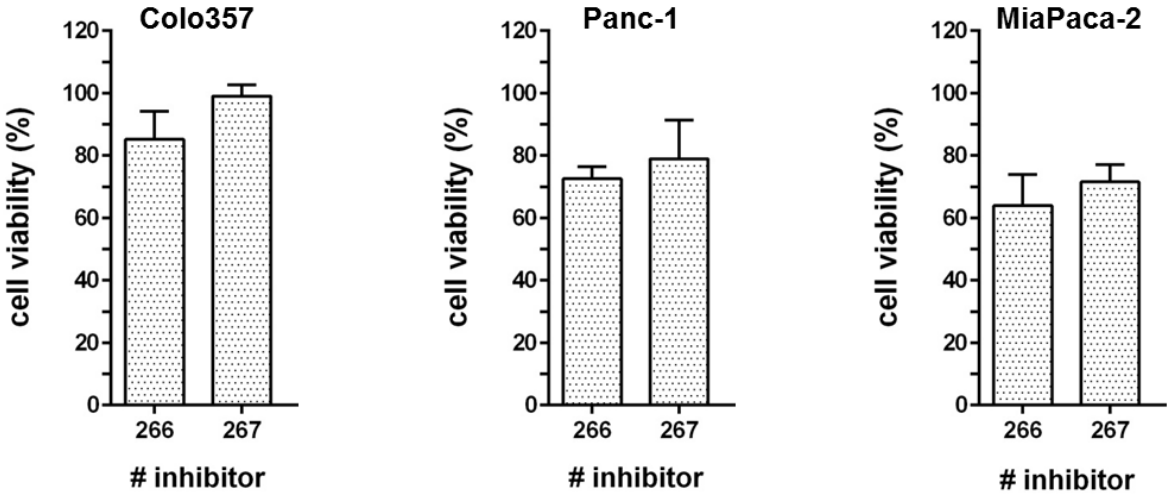

Figure 98 | Cell viability of Colo357, Panc-1, and MiaPaca-2 cells after treatment with series 6 compounds at a concentration of 15 µM. The inhibitors were screened in triplicate or quadruplicate measurement. Cell viability was normalized to mock. Error bars indicate the SEM[249].

X-ray Crystallography

Crystallization of CK1δ in complex with **266** was performed by the group of PROF. DR. ULRICH BAUMANN revealing two slightly different binding poses of the ligand in the kinase (**Figure 99**).

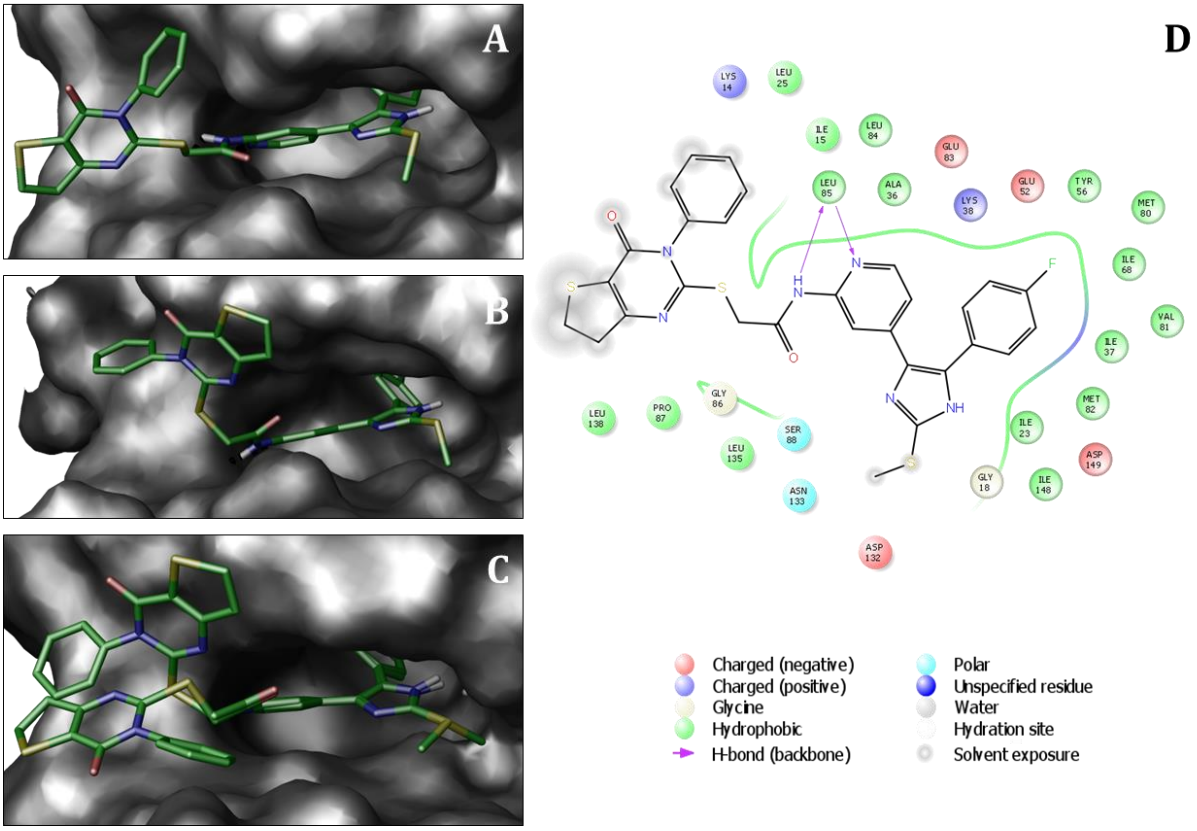

Figure 99 | Binding mode of 266 in CK1δ. X-ray crystallization revealed two poses for **266** in CK1δ *HRII* (A, B), opposed by the *in silico* predicted geometries (C). The 2D ligand interaction diagram refers to crystallization (D). X-ray analysis has been performed by the group of PROF. DR. ULRICH BAUMANN.

While the fitting of the diaryl-imidazole pharmacophore including the bidentate hinge-binder as well as the 4-fluorophenyl moiety within *HPI* is conserved in both crystals, two different conformations of **266** in *HRII* have been observed which are characterized by a 180° flip of the dihydrothieno[3,2-*d*]pyrimidin-4-one moiety. This flexibility is enabled by the 2-mercapto-acetamide linker and is most likely to be responsible for the unintended fitting into p38α despite the rigid and non-flexible thienopyrimidine. Interestingly, both binding poses have similarly been predicted *in silico*, thereby highlighting the quality of the established model. Another astonishing peculiarity that has not been observed previously is the presence of a different imidazole tautomer: both *in silico* studies and crystal structures indicate the imidazole NH group pointing towards the back of the ATP-pocket. Consequently, the water-mediated H-bond towards Lys38 and Asp149 is prohibited suggesting the bulky side chain to initiate a slightly

different positioning of the ligand in the ATP-binding cleft compared to previously discussed compounds. Considering the potent inhibition by **266**, however, an increased entropic contribution based on the large hydrophobic thienopyrimidine moiety can be assumed which partially overcompensated the loss of the discussed H-bond. The buried structural water molecule has repeatedly not been resolved.

6 Conclusions

6.1 Design and Synthesis of Potent and Selective CK1δ Inhibitors

In the framework of the current dissertation, CK1δ inhibitors have been designed, synthesized, and biologically evaluated. From a total of 38 tested compounds, 37 have not been reported in literature and therefore represent novel and optimized small molecule kinase inhibitors, originally deriving from lead structure **12** and its non-oxidized derivative **11**[176]. Compound **162**, however, has already been characterized as a moderate early-stage p38α teardrop-like inhibitor[197], although its effect on CK1 isoforms had not been examined.

The synthesized compounds exclusively depict ATP-competitive, presumably type I-like inhibitors of CK1δ, although a type I ½-similar mechanism has been proven for the interaction of **191** and p38α by crystallographic analysis as discussed in **chapter 5.2**. In this context it is noteworthy that equivalent DFG-in and DFG-out conformations have not been observed and are most likely non-relevant for CK1. The inhibitors have been classified in five distinct series based on structural and conceptual features.

Among them, several compounds exhibited excellent inhibition in the single-digit nanomolar range with **191** being the most effective ligand expressing an IC_{50} value of 4 nM in standardized kinase assays by our collaboration partner[248]. ProQinase GmbH even extrapolated the IC_{50} value of the compound to be approximately 1 nM. Followed by **224** and **232** with IC_{50} values of 8 nM (ProQinase: extrapolated IC_{50} = 1 nM) and 9 nM, respectively, these compounds are readily among the most potent CK1δ inhibitors reported to date. Actually, **191** might in fact represent the most effective agent regarding inhibition of CK1δ in kinase assay systems. **266** is another promising ligand whose IC_{50} value has been extrapolated by ProQinase GmbH to be 2 nM, although kinase assays in the hands of our collaboration partner[249] identified half maximal inhibition at a concentration of 27 nM, which is still highly active. Further nine compounds from the total set have been found to possess IC_{50} values in the low double-digit nanomolar range (< 50 nM). The complete set of tested compounds with their appropriate IC_{50} values is listed in **Supplementary Table 2**.

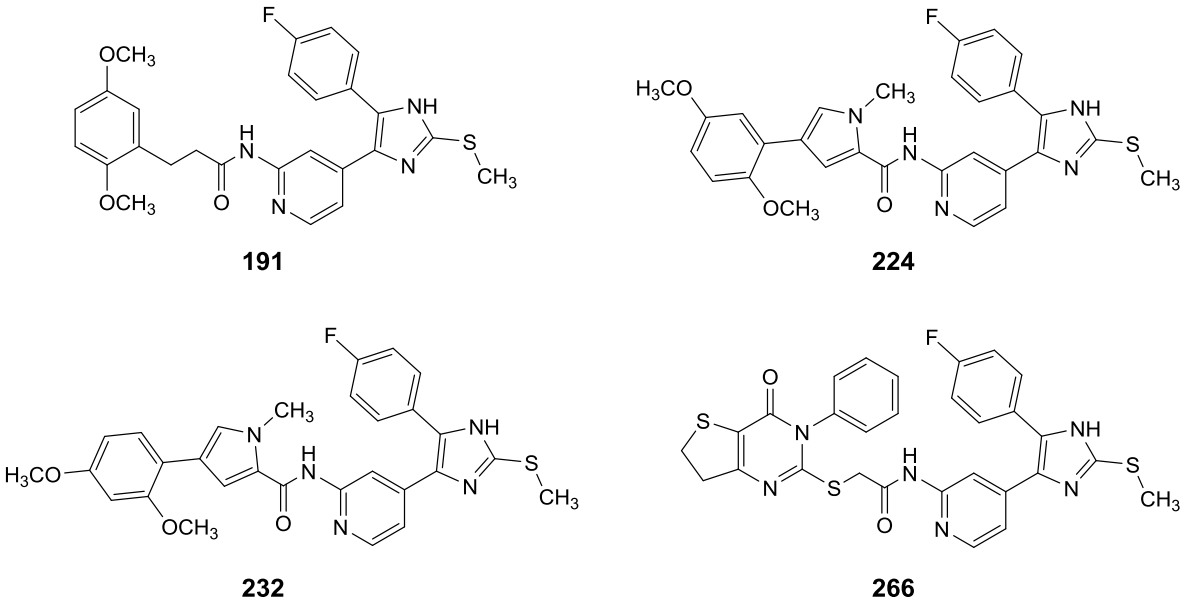

Figure 100 | Potent CK1δ inhibitors 191, 224, 232, and 266. The most potent compounds of the current work inhibit CK1δ with IC_{50} values in low nanomolar range.

Furthermore, **191** exhibited good selectivity hitting only five additional kinases (residual activity ≤ 50 %) apart from CK1 isoforms δ, ε, and α from a panel of 321 protein kinases as discussed in **chapter 5.2**. Mitogen-activated protein kinase p38α which is the defined main off-target of the current teardrop-like inhibitor class was effectively blocked ten-fold less potently compared to CK1δ with an IC_{50} value of 10 nM (ProQinase, in relation to CK1δ IC_{50} = 1 nM). Therefore, **191** has to be considered a potent dual-specific inhibitor of these kinases. Regarding isoform-specificity, however, profiling showed potent inhibition only of isoforms δ and ε, the latter approximately six-fold less effective with an IC_{50} value of 25 nM (in relation to CK1δ IC_{50} = 4 nM). CK1α residual activity was reduced to approximately 26 % while relevant inhibition of isoforms γ1-3 has not been observed in the same screening (ProQinase). Consequently, **191** should be referred to as a potent and specific inhibitor of CK1 isoforms δ and ε. In fact, none of the designed novel inhibitors achieved the intended isoform-selectivity of at least 100-fold, the most specific compound in this context being weakly potent **164** which favored CK1δ by approximately 17-fold. Among the set of potent inhibitors, **192** (CK1δ IC_{50} = 20 nM, CK1ε IC_{50} = 233 nM) and **204** (CK1δ IC_{50} = 19 nM, CK1ε IC_{50} = 227 nM) exhibited the most promising preference by twelve-fold, followed by ten-fold preference of **224** (CK1δ IC_{50} = 8 nM, CK1ε IC_{50} = 81 nM). Discrimination of p38α was most pronounced by **266** by approximately 18-fold, although it has to be noted that IC_{50} values regarding p38α have only been determined for four compounds.

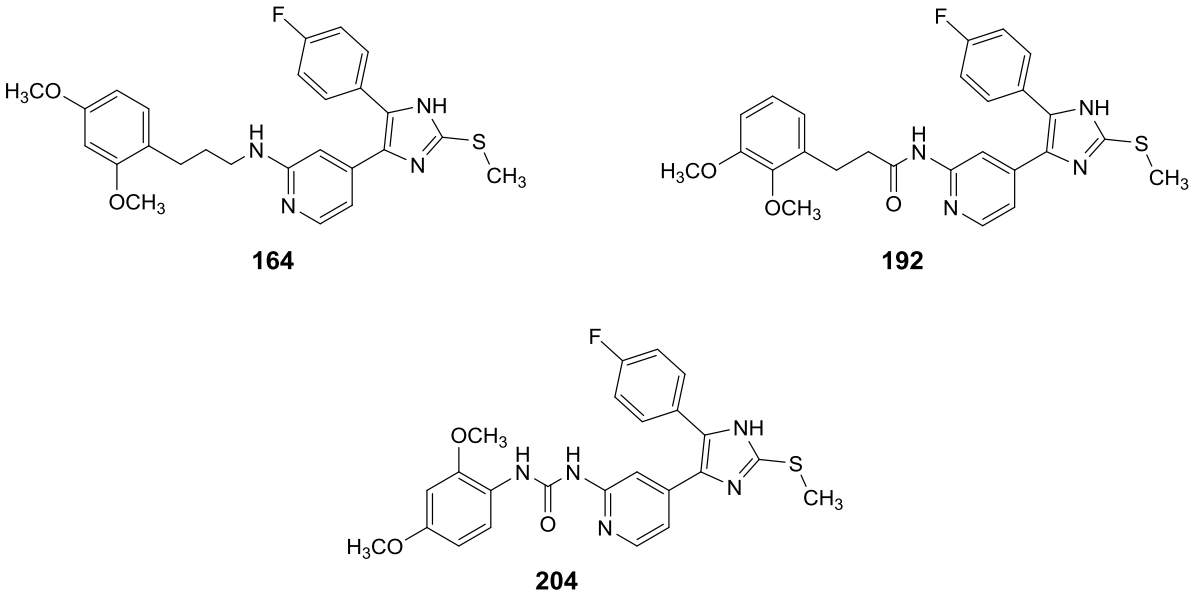

Figure 101 | CK1δ-preferring inhibitors 164, 192, and 204. The depicted compounds favor isoform δ over ε. **224** as well as p38α partially discriminating **266** are shown in **Figure 100**.

The potent inhibition observed in kinase assays, however, has not been necessarily translated into high efficacy on cellular level. In fact, the majority of tested inhibitors requires optimization of physicochemical properties. Amine-based compounds (series 1, **chapter 5.1**) were rather ineffective, even at elevated concentrations of 20 μM or 25 μM, although it is not known whether this due to poor cell penetration or metabolic instability[200]. **151** represented an exception being weakly active in HT-29 cells with an EC_{50} of 9.3 μM. In order to gain applicability in cell culture, propionic acid amides (series 2, **chapter 5.2**) exhibited a significant overall improvement identifying **191** to be the most active inhibitor with EC_{50} values in Colo357 and Panc89 cells of 3.5 μM and 1.5 μM, respectively. Carbamides (series 3, **chapter 5.3**) suffered from poor solubility leading to non-relevant efficacy in Colo357 and Panc89 cells in most cases. **104**, **204**, **205**, and **206**, however, revealed moderate effects on cell viability. Therefore, improvement of water-solubility of these compounds might prove extremely beneficial as this is likely to be their major limiting factor regarding cellular efficacy. **224**, **232**, **291** (series 4, **chapter 5.4**), **266**, and **267** (series 5, **chapter 5.5**) possess molecular weights > 500 $g \cdot mol^{-1}$, thereby violating LIPINSKI'S *rule of five*[251]. They can therefore be assumed unfavorable regarding solubility and absorption. Consequently, both series reduced metabolic activity of Colo357, Panc-1, and MiaPaca-2 cells rather weakly. Considering the number of possible H-bond donors and acceptors virtually all series are in accordance with LIPINSKI'S concept. The octanol-water distribution coefficients, however, have not been determined and should be assumed to represent another violation of the *rule of five* for most of the newly designed inhibitors.

Nevertheless, several compounds depict potent inhibitors of CK1δ in kinase assays. Especially **191** is a specific inhibitor for CK1 isoforms δ and ε with good selectivity regarding 321 protein

kinases that is among the most potent agents for CK1δ reported to date. Therefore we provide a suitable biological tool with promising properties which is also moderately active in cells and should further be optimized regarding its physicochemical properties.

6.2 Structure-Activity Relationship of CK1δ Inhibitors

Structurally, building block **120** represents the central pharmacophore of the newly designed and synthesized inhibitors as discussed in **chapter 3.1**. The 4-fluorophenyl moiety ideally fits into *HPI* of CK1 isoforms δ and ε as proven by X-ray crystallography (**Figure 102**), but also p38α and is mainly responsible for selectivity over most other kinases. Regarding the aspect of potency the bidentate hinge-binding 2-aminopyridine moiety has to be considered the major determinant. The imidazole ring which is predominantly situated in the adenine-binding region of the ATP-pocket bears an unsubstituted nitrogen atom that is another important H-bond acceptor[165,176,184,194–204]. Addressing the solvent-exposed *HRII* by the use of varying side chains is expected to enhance both potency and selectivity[176,195–197,200,201]. Especially bulky side chains have been considered as these are thought to reduce affinity for the highly similar p38α mitogen-activated protein kinase[198].

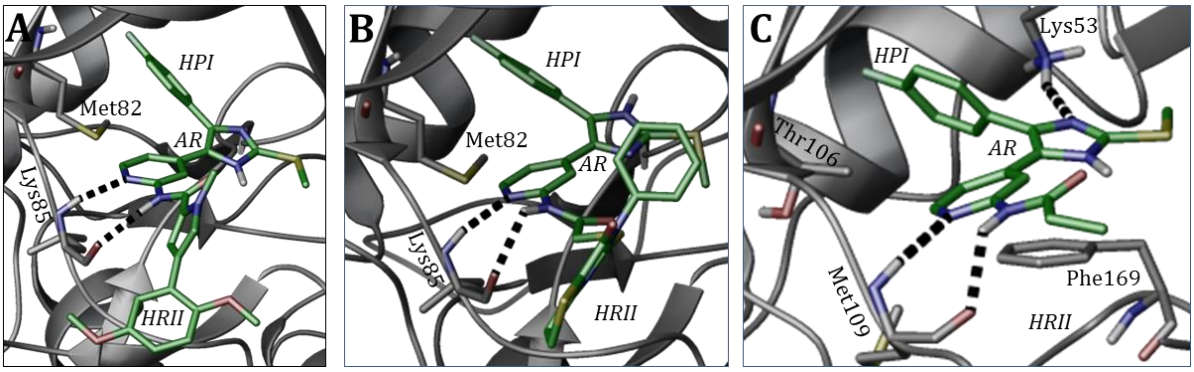

Figure 102 | Binding poses of 191, 224, and 266 in CK1δ or p38α. **224** (A) and **266** (B) have been co-crystallized with CK1δ while p38α has been crystallized in complex with **191**.

The current biological evaluation verified the use of sterically demanding and mainly lipophilic moieties to be highly beneficial in order to gain affinity for CK1 isoforms δ and ε. Large gains in binding free energy can be achieved by exploiting the hydrophobic effect whereupon lipophilic substituents enable replacement of the suboptimal hydration state of *HRII*. The release of water molecules from hydrophobic environments thereby increases entropy and thus directly depends on the size of the appropriate moiety[191,209].

In addition, sterically demanding side chains shield the hydrophobic surface and the deeper cavities of the catalytic cleft from surrounding water. Methoxyphenyl-substituted scaffolds

proved highly beneficial in this context. In fact, from a set of sixteen designed and tested inhibitors that possess IC_{50} values < 50 nM eleven include methoxyphenyl-substituted moieties situated in *HRII.* Therefore, different substitution pattern have been compared within the scope of series 2 revealing dimethoxyphenyl substitution to be slightly more effective than the appropriate trimethoxyphenyl-bearing **194** (IC_{50} = 27 nM). Furthermore, 2,5-dimethoxyphenyl derivative **191** (IC_{50} = 4 nM) showed enhanced potency in relation to the respective 2,3-, 2,4-, and 3,4-substituted compounds **192** (IC_{50} = 20 nM), **190** (IC_{50} = 20 nM), and **193** (IC_{50} = 14 nM, **Figure 103**). The 2,3-substitution, however, might be favorable regarding isoform-discrimination as this effect was slightly enhanced for **192**. The preference for the 2,5-dimethoxyphenyl substitution pattern was also reflected by **224** (IC_{50} = 8 nM) and **232** (IC_{50} = 9 nM, series 4), though the effect was rather weak in this case. Unfortunately, these *in vitro* results did not correlate with *in silico* predicted data assuming that the current model is not capable of an accurate prediction concerning the regio- and stereo-chemical impact of different methoxy substitution pattern.

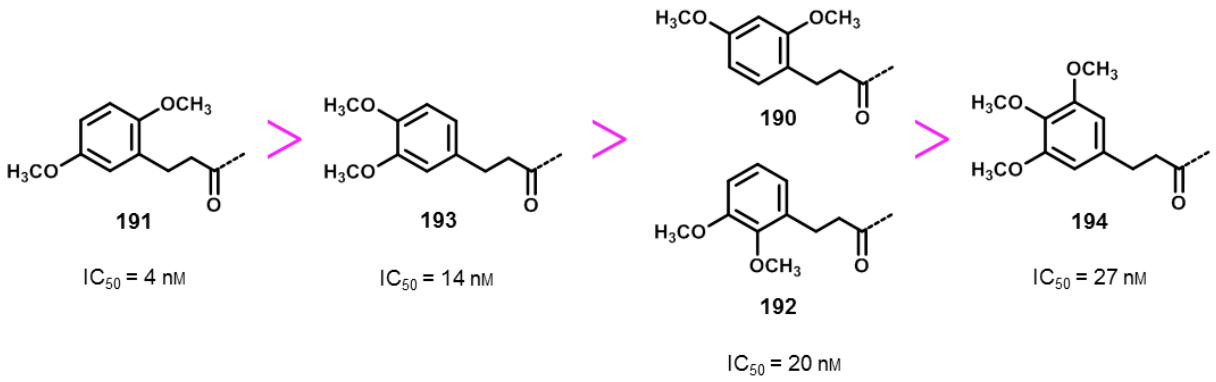

Figure 103 | Differently methoxy-substituted series 2 compounds 191, 192, 193, and 194. The di- and trimethoxy substitution pattern have been compared with regard to inhibition of CK1δ.

There is no doubt, though, that these observations can hardly be generalized as substitution has always to be considered in the context of the complete side chain: series 3 derivatives **204** (IC_{50} = 19 nM) and **205** (IC_{50} = 31 nM), for instance, exhibited inverted results. Regarding the relatively short and non-flexible side chain carbamide linker of these compounds to the longer equivalent structures of series 2 and 4 it might be suggested that the 2,5-substitution pattern is favored with an increasing linker length (**Figure 104**). Basically, the longer side chains of **191** and **224** proved superior compared to the shorter moiety of **205**.

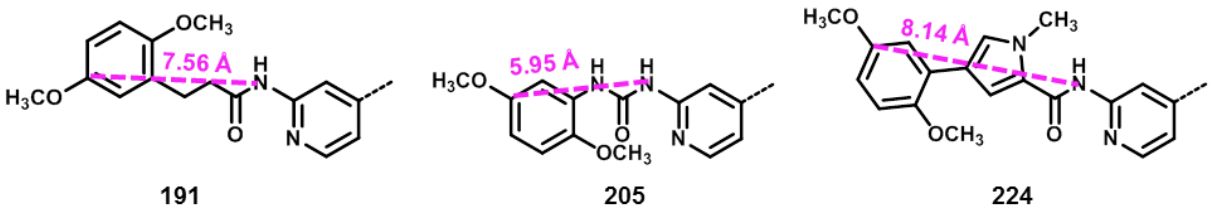

Figure 104 | Lengths of side chains might select for different dimethoxy substitution pattern. The measured distances refer to appropriate energetically minimized 3D structures.

Referring to kinase screening results of series 3 compounds the dimethoxyphenyl substitution of **205** seemed to outmatch the substitution pattern including a single methoxy group of **206**. As discussed in **chapter 3.1.5** mono-methoxy substitution was mainly left unconsidered as it has been reported to be most favorable for inhibition of p38α, whereas di- and trimethoxy substituents might forestall suitable fitting in this kinase[200].

Nevertheless, the hypothesis of bulky moieties prohibiting effective inhibition of p38α[198] could not be fully confirmed as even the steric highly demanding ligands **224** and **266** potently inhibited the mitogen-activated protein kinase with IC_{50} values of 10 nM and 36 nM (ProQinase) which is only up to maximal ten- and 18-fold less active than their respective efficacy against CK1δ. Previous modeling-based investigations further postulated an accommodation of inhibitor side chains within CK1δ *HRII* by residues of the L-78 loop that is not present in p38α[176]. However, this thesis has not been reassured by crystallization for the present ligands.

In general, structural comparison of series 1 to 4 reveals increasing planarity and size of the respective side chains. Starting from amine **164** (CK1δ IC_{50} = 386 nM, CK1ε IC_{50} = 6731 nM) introduction of the carbonyl function led to amide **190** (CK1δ IC_{50} = 20 nM, CK1ε IC_{50} = 129 nM) which was accompanied by a 19-fold increase of potency, although selectivity seemed to be significantly decreased. The weak inhibitory activity of **164** regarding inhibition of CK1ε in relation to CK1δ, however, is structurally not comprehensible as the sp^3 hybridization-based enhanced flexibility was predicted to improve adaptivity to *HRII* of both CK1δ and CK1ε. Based on these observations as well as the reported beneficial effects on metabolic stability[200] the carbonyl group has been accepted as mandatory for the following approaches. As discussed in **chapter 3.1.5** it was hypothesized that the negative inductive effect of the carbonyl group strengthens the adjacent H-bond donor while the planar conformation of the sp^2 hybridized amide function might be beneficial for positioning the N-H group in the correct angle. Structurally, substitution of the side chain α-methylene group by a nitrogen and shortening of the linker by deletion of the β-methylene led to planar carbamide derivative **204** (series 3, CK1δ IC_{50} = 19 nM, CK1ε IC_{50} = 227 nM) assuming less flexibility by an additional H-bond towards hinge residue Leu85. Biological analyzation of this effect, however, did not reveal significantly

increased potency providing an IC_{50} value of 19 nM for CK1δ which is nearly identical to **190**. Unfortunately, co-crystallization of CK1δ in complex with carbamide derivatives has not been achieved and it has therefore not been possible to evaluate, though, whether the discussed H-bond was existent. The discrepancy between the *in silico* predicted gain of binding free energy, reflected by Glide scores of -13.8 for **190** and -16.6 for **204**, and the *in vitro* data might consequently be due to energetic and steric prohibition of the tridentate hinge-binder or forestalled by low solubility of the carbamides. Isoform-selectivity, on the other hand, was increased for **204** by approximately two-fold compared to **190**. However, 2,5-dimethoxyphenyl-substituted carbamide **205** (CK1δ IC_{50} = 31 nM, CK1ε IC_{50} = 186 nM) did not improve isoform-specificity compared to appropriate propionic acid amide **191** (CK1δ IC_{50} = 4 nM, CK1ε IC_{50} = 28 nM) but exhibited in fact even significantly reduced potency. These results thereby further supported the thesis of an intrinsically tied interplay of substitution pattern and linker length as previously discussed. The expected effect regarding selectivity by enhanced rigidification of carbamide derivatives over p38α, however, has been disproved as **204** (CK1δ IC_{50} = 10 nM, p38α IC_{50} = 28 nM) is in fact even less specific than **191** (CK1δ IC_{50} = 1 nM, p38α IC_{50} = 10 nM), although the different substitution pattern is likely to contribute to these results. Subsequent substitution of the carbamide linker by the *N*-methylated pyrrolic acid scaffold of series 4 led to bulkier ligands with enhanced linker length which has already been discussed. While **232** and **224** exhibited an increase of potency for CK1δ with IC_{50} values of 9 nM (CK1ε IC_{50} = 45 nM) and 8 nM (CK1ε IC_{50} = 81 nM) they did not enhance isoform-specificity either. Considering selectivity over p38α which has been determined by ProQinase GmbH for **224** (CK1δ IC_{50} = 1 nM, p38α IC_{50} = 10 nM) revealed that CK1δ was preferred by about ten-fold. Thereby, properties of **224** proved comparable to **191** while the latter still showed highest efficacy and should be assumed favorable regarding activity in cell culture.

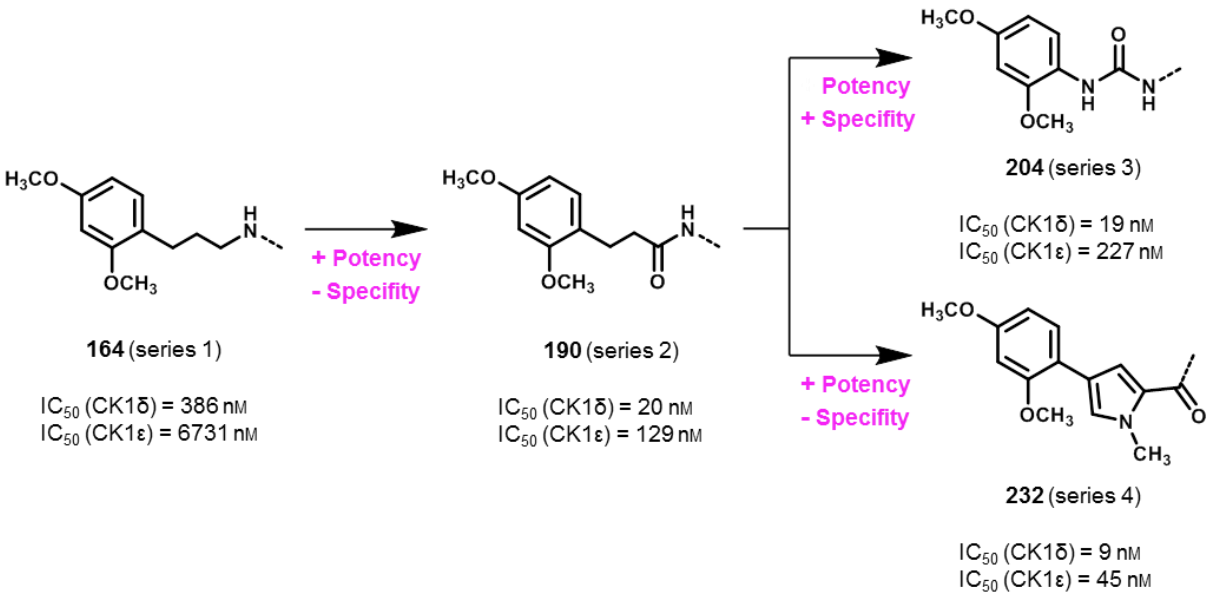

Figure 105 | Comparison of series 1 to 4 based on compounds 164, 190, 204, and 232. Potency and isoform-specificity were either increased (+), decreased (-), or unaffected.

Hybrid inhibitors **266** and **267** of series 6 were derived from known Porcn inhibitors and therefore structurally non-dependent on previous series. They exhibited good potency for CK1δ with IC_{50} values of 27 nM and 29 nM, though only moderate isoform-specificity favoring isoform δ by approximately nine-fold. Consequently, the approach to graft the astonishing selectivity of **113** and **114** onto pharmacophore **120** by hybrid synthesis failed in this context but proved beneficial otherwise: **266** showed the most effective discrimination of p38α by about 18-fold (ProQinase: CK1δ IC_{50} = 2 nM, p38α IC_{50} = 36 nM), although it was still a potent dual-specific inhibitor. Crystallographic analysis identified the flexible 2-mercaptoacetic acid linker to enable different binding poses and also has to be assumed responsible for fitting into off-target kinases such as p38α.

Taken together, the *in vitro* and crystallization results provide proof of concept for the established computational model of CK1δ which enabled prediction of binding poses rather correctly. Nevertheless, its limits were also identified as molecular modeling has neither been able to calculate the influence of different (methoxy) substitution pattern within highly flexible domain *HRII*, nor the impact of sulfoxidation.

Consequently, these results raise the question whether the current approach is suitable to achieve selectivity for CK1δ over highly similar CK1ε and other structurally related kinases as the most specific inhibitors were **164** (discriminating CK1ε by approx. 17-fold) and **266** (discriminating p38α by approx. 18-fold). In fact, pharmacophore **120** itself should be assumed rather effective regarding inhibition of CK1 isoforms δ and ε as well as p38α, considering the excellent fitting into their active sites which has been proven by X-ray crystallography. It seems

furthermore most likely that the highly flexible and solvent-exposed *HRII* is capable of adapting to various different side chains (induced fit). Crystallization also confirmed the respective domain of p38α to be significantly restricted in size and planarity compared to CK1δ and CK1ε. Therefore, decreased enthalpic gains can be suggested for p38α to arise from hydrophobic protein-ligand interaction within *HRII*: the discussed side chains are virtually "too large" to fully interfere with this region and consequently reach into the solvent space. Nevertheless, p38α was potently inhibited with IC_{50} values in the low nanomolar range, thereby indicating enthalpic compensation elsewhere which could be hypothesized to rely on the adenine-binding region: first, the H-bond which is accepted by the imidazole nitrogen is not mediated by water molecules in p38α and should therefore account for higher enthalpic gains; and second, the type I ½-like binding discussed in **chapter 5.2** enables the inhibitor to interact with p38α by additional π-π-stacking. Consequently, inhibitors that share teardrop-related scaffolds such as **120** consisting of a 4-fluorophenyl moiety penetrating into *HPI* and a 2-aminopyridine acting as a bidentate hinge-binder are unlikely to achieve selectivity as the addressed domains are highly conserved within the kinases in question and account for intrinsic efficacy. Nevertheless, the use of various side chains exhibited differently pronounced discrimination of CK1ε and p38α up to approximately 18-fold indicating *HRII* to be an important, if not the main determinant for selectivity in this context. It might therefore be beneficial for future approaches to focus on this domain while reducing or even relinquishing the teardrop-like pharmacophore, although an initial loss of potency has to be expected. Especially approaches that concentrate on thienopyrimidine-like (IWP-like) scaffolds (cp. **266**, **267**) might prove promising for further optimization, potentially amplified by methoxy substitution.

Finally, **191** has been identified as an extremely potent dual-specific inhibitor of CK1 isoforms δ and ε as well as p38α with good specificity regarding 321 protein kinases that is among the most effective CK1 inhibitors published to date. Although it is yet active in cellular systems with an EC_{50} value of at best 1.5 μM, optimization of its physicochemical properties will provide a bio-chemical tool that might be highly valuable in order to uncover further details regarding the physiological and pathophysiological characteristics of CK1δ.

7 Experimental

7.1 Molecular Modeling

7.1.1 Software and Computational Resources

Molecular modeling was performed on a DELL Precision T5500 eight core workstation utilizing Schrödinger software. Visualization was achieved by Maestro, version 10.6, Schrödinger, LLC, New York, NY, 2016, the interface of Schrödinger technologies. In general, molecular modeling calculations are energy[bb]-driven and therefore rely on force field-mediated local minimization of both protein and ligands. Energetic calculations of the present work were mainly obtained based on the Optimized Potentials for Liquid Simulations of 2005 force field (OPLS_2005)[252]. In 2015, the advanced OPLS3[253] has been presented which reportedly possesses a 30 % improvement in relation to the earlier variant. In fact, the main upgrade seems to refer to peptide modeling and validation of earlier results did not reveal significant differences.

7.1.2 Protein Preparation

Protein crystal structures were taken from the Research Collaboratory for Structural Bioinformatics (RCSB) protein data bank (PDB). CK1δ-based screenings were performed using a crystal structure (PDB code 3UZP) by LONG *et al.*[184] which was selected from a rather limited pool at that time. The enormous advantage of the chosen crystal structure referred to the co-crystallized ligand (PDB code 0CK) exhibiting structural similarity towards lead compound **12**. The most important determinants showed acceptable values, though occupancy has not been given: resolution = 1.94 Å, *R*-factor = 22.2 %, *B*-factor = 37 Å^2.

Prior to docking, crystal structures were prepared by the implemented Protein Preparation Wizard[205] synchronizing the following Schrödinger modules: Epik[254], version 3.6, 2016; Impact, version 7.1, 2016; Prime[255], version 4.4, 2016. In order to achieve high Enrichment-factors, the common refinement protocol by SASTRY *et al.*[205] has been adjusted: the process involved assignment of bond orders, addition of hydrogen atoms, identification of disulfide bonds, and the conversion of artificial selenomethionines to methionines (default settings). Missing side chains

[bb] binding free energy and solvation free energy

were filled in using Prime. Missing loops have not been detected. Water molecules beyond 5.0 Å from hetero atoms have been deleted automatically while water molecules within this range were reviewed manually: the previously discussed (**chapter 3.1.4**) structural water molecule was kept exclusively. H-bond optimization was performed in a standard sampling, the Root-mean-square deviation for atomic positions (RMSD) cutoff for heavy atoms in subsequent protein minimization was set to 0.3 Å. Manual inspection of the protein model and the RAMACHANDRAN plot (**Figure 106**) offered suitable quality: three residues were detected within RAMACHANDRAN outlier regions, though not in close proximity to the active site. The docking Grid was generated with Glide default settings picking the co-crystallized ligand to characterize the Grid box center (Glide, version 7.1, Schrödinger, LLC, New York, NY, 2016).

Analysis of the kinase active site regarding its druggability has been supported by the use of SiteMap, version 3.9, Schrödinger, LLC, New York, NY, 2016. SiteMap[256] has also proved beneficial for the identification of binding sites in kinase apo-structures.

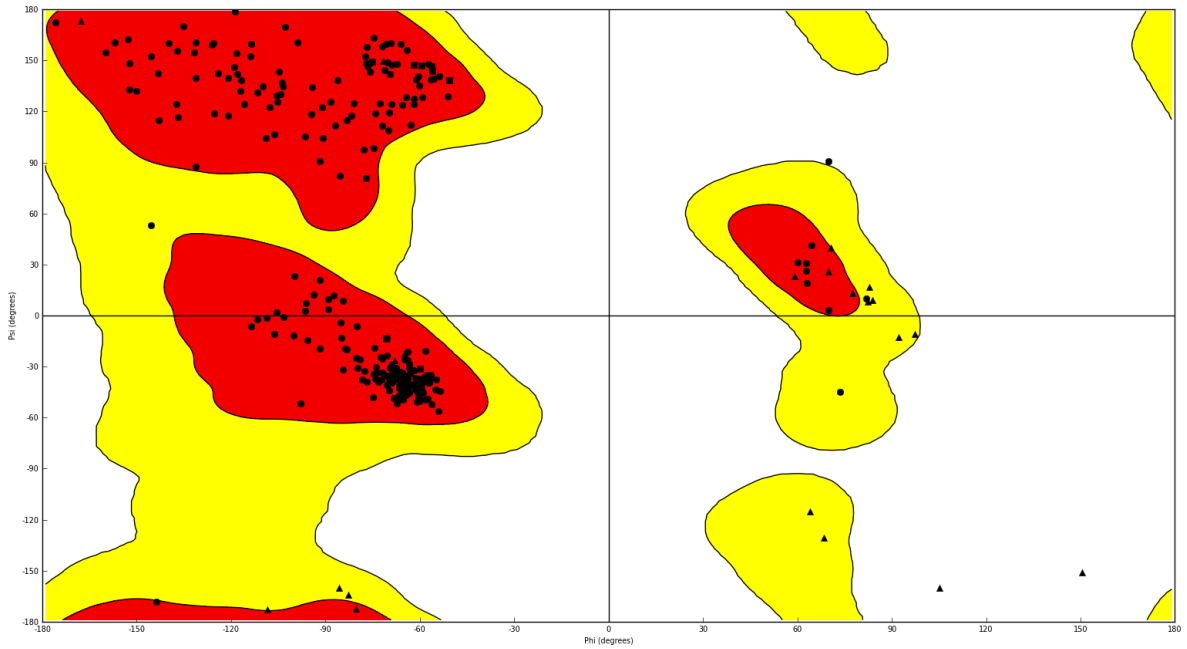

Figure 106 | RAMACHANDRAN plot of the protein model used for CK1δ screening. The colored squares refer to energetically favored (red), allowed (yellow), and disallowed (white) regions for amino acid residue dihedrals. Glycines are depicted as black triangles, prolines as black squares. All remaining amino acid residues are represented by black dots. The model refers to a crystal structure by LONG *et al.* (PDB code 3UZP)[184].

7.1.3 Ligand Preparation

Ligands were prepared to generate energetically minimized three-dimensional coordinates with an extended cutoff by MacroModel, version 11.2, Schrödinger, LLC, New York, NY, 2016. Ionization and tautomeric states were estimated at pH 7 ± 2 by LigPrep[205], version 3.8, Schrödinger, LLC, New York, NY, 2016, utilizing HAMMETT and TAFT methodology-based Epik[254]. Additionally, Epik state penalties (kcal · mol^{-1}) were calculated for each ligand to quantify the energetic cost for state transition in solution[205]. In order to indicate ligand flexibility, up to 50 bioactive conformers per ligand were identified and prioritized utilizing the conformational search module in the fast mode (ConfGen, version 3.6, Schrödinger, LLC, New York, NY, 2016)[257]. Core Hopping was performed with the homonymous module (Core Hopping, version 2.5, Schrödinger, LLC, New York, NY, 2016) by the use of the Glide fragment library (Schrödinger fragment collection).

7.1.4 Ligand Docking

Ligand docking was mainly performed with the extra precision (XP) Glide methodology[258]. The aim of this procedure is to semiquantitatively screen and rank ligand libraries to a specified and presumably rigid receptor conformation. Ligand affinity is thereby generally characterized by the Glide XP scoring module which is based on the following aspects: first, retainment of favorable VAN DER WAALS contacts in order to displace water from hydrophobic regions into the bulk leading to entropy-driven energetic gains; second, the ability of hydrogen-bonding and other strong electrostatic interactions with specific key structural motifs. H-bonds are therefore divided into three types referring to their long-range solvation (BORN) energy and electrostatic behavior as neutral-neutral, neutral-charged, and charged-charged; and third, the achievement of reasonable RMSD values in relation to the native complex. In contrast, desolvation effects and motional restriction of ligand and protein are considered to reduce binding affinity. These terms are implemented in the XP Glide score which is specified in detail by the following equations and ideally corresponds to the binding free energy ΔG (kcal · mol^{-1})[258]. A short description of these parameters is given in **Table 27**.

$$Glide\ score = E_{coul} + E_{vdW} + E_{bind} + E_{penalty}$$

$$E_{bind} = E_{hyd\_enclosure} + E_{hb\_nn\_motif} + E_{hb\_cc\_motif} + E_{PI} + E_{hb\_pair} + E_{phobic\_pair}$$

$$E_{penalty} = E_{desolv} + E_{ligand\_strain}$$

In addition, the sum of Glide score and the discussed Epik state penalty is referred to as the *docking score*[205]. Despite the advantages of this score it is reportedly error-prone leading to false positives and negatives[205]. Consequently, the Glide score has been favored over the docking score in the context of the present dissertation.

Table 27 | Energetic parameters for Glide score calculations[258,259].

Parameter	Description
E_{coul}	Coulomb energy
E_{vdW}	VAN DER WAALS energy
E_{bind}	Energetic terms that favor binding
E_{phobic_pair}	Hydrophobic atom-atom pair energy term including interatomic distances which heuristically represents the displacement of water by hydrophobic ligand atoms
$E_{hyd\_enclosure}$	Hydrophobic enclosure: advanced E_{phobic_pair} term discriminating between different environmental geometries
E_{hb_pair}	Hydrogen bond term calculated for all complementary possibilities of hydrogen bonds between ligand and protein atoms
$E_{hb\_nn\_motif}$	Special neutral-neutral hydrogen bond motif: advanced E_{hb_pair} term
$E_{hb\_cc\_motif}$	Special charged-charged hydrogen bond motif: advanced E_{hb_pair} term
E_{PI}	Minor term rewarding π-stacking and π-cation interaction, placement of halogen atoms in hydrophobic regions, and empirical correction favoring the binding of smaller ligands over larger ones
$E_{penalty}$	Energetic terms that hinder binding
E_{desolv}	Desolvation penalties
E_{ligand_strain}	Strain energy penalties

In cases when Glide Docking approaches failed, an Induced Fit Docking protocol has been performed[260]: the procedure repetitively combines rigid docking (Glide) and protein structure prediction (Prime) to account for both ligand and receptor flexibility. Default settings of the standard protocol were used, complemented by the side chain trimming function. Glide redocking was performed with the extra precision methodology. The final scoring is achieved by the equation:

$$IFD\ Score = Glide\ score + 0.05 \cdot Prime\ Energy$$

The less-dominant Prime Energy term is essential to separate predicted models from the random noise that is introduced by minor steric clashes[260].

7.2 Material and Methods

7.2.1 Reagents and Solvents

All reagents and solvents that have been applied in synthetic and analytic approaches were, if not specified otherwise, obtained from the commercial companies abcr GmbH (Karlsruhe, Germany), Sigma-Aldrich Chemie GmbH, Merck Group (Munich, Germany), Merck Millipore (Darmstadt, Germany), Acros Organics, Thermo Fisher Scientific (Geel, Belgium), and VWR International GmbH (Hannover, Germany). They were used without further purification.

7.2.2 Methods and Instruments

The following methods and instruments were used for synthesis, purification, and characterization of the specified (**chapter 7.2.3**) compounds:

High Pressure Reactor

Syntheses under high pressure were performed in a high*preactor*™ BR-25 (Berghof Products + Instruments GmbH, Eningen, Germany) at 180 °C and 20-30 bar. The reactor vessel consists of stainless steel with PTFE inserts and seals and a manometer. Consistent heating was achieved in a corresponding heating block on a Heidolph MR Hei-Standard laboratory heating plate (Heidolph Instruments GmbH & Co KG, Schwabach, Germany).

Microwave Synthesis

Syntheses were performed in a CEM Discover Microwave Synthesizer (CEM GmbH, Kamp-Lintfort, Germany) under air cooling and high stirring with a maximal power of 100 W. The reaction mixtures were scheduled in convenient thick-walled and snap-lid capped glass reaction vessels.

Photosynthesis

Irradiation was performed using light in the ultraviolet range of 365 nm with a LED-illuminant (12 · Nichia NCSU033B, Sahlmann Photochemical Solutions, Kiel, Germany).

TLC

Thin layer chromatography (TLC) was the main method of monitoring reaction progress and evaluating solvent gradients for column chromatography. Pre-coated silica gel polyester sheets (Polygram® SIL G/UV_{254}, 0.2 mm, Macherey-Nagel, Düren, Germany) and RP-18 modified silica gel aluminum plates (Silicagel 60 RP-18 F_{254S}, Merck Millipore, Darmstadt, Germany) were used.

HPLC

High-performance liquid chromatography (HPLC) was performed with a Hewlett Packard 1050 Series (Agilent Technologies, Waldbronn, Germany) and served for monitoring of reaction progress and purity control: all test compounds submitted to biological evaluation and X-ray structure analysis were proven to possess ≥ 95 % HPLC purity. All substances were dissolved in methanol for HPLC measurement.

The column was either a ZORBAX® Eclipse XDB-C8, 5 µm (150 · 4.6 mm, Agilent Technologies, Santa Clara, United States) or a Kinetex® C8, 5 µm (150 · 4.6 mm, Phenomenex, Aschaffenburg, Germany). For the mobile phase three different gradients of methanol and KH_2PO_4 buffer (10 mM, pH 2.3) were used (Methods 1, 2, 3, **Table 28**) with a fixed flow rate (1.5 ml · min^{-1}). UV detection was achieved at 254 nm.

Table 28 | HPLC gradient-dependent methods.

	Time (min)	Methanol (%)	KH_2PO_4 buffer (%)
Method 1	0	40	60
	8	85	15
	13	85	15
	14	40	60
	16	40	60
Method 2	0	20	80
	8	85	15
	13	85	15
	14	20	80
	15	20	80
Method 3	0	40	60
	8	85	15
	11	85	15
	12	40	60
	14	40	60

Flash Chromatography

Column chromatography was performed using a LaFlash system, VWR International GmbH (Hannover Germany). The crude product was loaded on silica gel 60 (63-200 µm, Macherey-Nagel, Düren, Germany) or RP-18 modified silica gel (PuriFlash IR-50 C18, 50 µm, Interchim, Montluçon, France) and packed in dry-load precolumns (PuriFlash-DLE/12G, Interchim). Pre-packed silica gel columns (PuriFlash-30SIHP, 30 µm, 40 g, Interchim) and RP-18 modified silica gel columns (PuriFlash-15C18HP, 15 µm, 55 g, Interchim) were used for separation. Composition and gradients of the mobile phases are given with the appropriate synthetic procedures (cp. **chapter 7.3**). Flow rates were usually adjusted to 30 ml · min^{-1} (PuriFlash-30SIHP) or 20.5 ml · min^{-1} (PuriFlash-15C18HP), respectively.

NMR

NMR spectra were recorded on a Bruker Avance III 300, tempered at 298 K: ^{1}H (300 MHz), ^{13}C (75 MHz), ^{19}F (282 MHz). Spectra were referenced to the respective deuterated solvents signals of DMSO-d_6 (δ ^{1}H NMR: 2.50 ppm, δ ^{13}C NMR: 39.52 ppm) and $CDCl_3$ (δ ^{1}H NMR: 7.26 ppm, δ ^{13}C NMR: 77.00 ppm) as an internal standard. H,H-COSY, HSQC, HMBC spectra were consulted in order to assign signals of complex structures if necessary.

The use of the relatively viscous DMSO-d_6 often led to different sets of signals with a maximal ratio of 1:3 which are most likely due to atropisomers and tautomers (imidazole). Although such sets have not been observed whenever $CDCl_3$ was used, DMSO-d_6 was the most frequented solvent regarding its favorable solubility-mediating properties. For reasons of clarity, only the dominant set of signals is given in the experimental section. The following abbreviations have been used to classify the appropriate signals: v (very), b (broad), s (singlet), d (doublet), t (triplet), q (quartet), quint (quintet), m (unresolved multiplet).

LC-MS

Liquid chromatographic (LC) separation was performed with an Agilent 1100 HPLC system (Agilent Technologies, Waldbronn, Germany) over an Agilent Eclipse XDB-C8 column (150 · 4.6 mm, 5 µm) using a 0.1 % acetic acid/acetonitrile gradient for mobile phase (flow rate = 1 ml · min^{-1}).

Mass spectra were recorded on a Bruker Esquire ~LC ion trap mass spectrometer (Bruker Daltonics, Bremen, Germany) with electron spray ionization (ESI) in the positive ion mode (dry gas 9 l · min^{-1}, nebulizer 35 psi, drying temperature 350 °C).

HRMS

High resolution mass spectra were recorded on an electron ionization (EI)/field desorption (FD) mass spectrometer JEOL AccuTOF™ GCv 4G (JEOL GmbH, Freising, Germany) at the Institute of Organic Chemistry, Christian-Albrechts University (Kiel, Germany).

IR spectrometry

IR spectra were recorded on a Shimadzu Fourier Transform Infrared Spectrometer IRAffinity-1S (Shimadzu Deutschland GmbH, Duisburg, Germany).

Melting Point

Melting points (uncorrected) were determined on a Stuart Scientific Melting Point Apparatus SMP3 (Bibby Scientific Limited, Staffordshire, United Kingdom).

X-ray Crystallography

X-ray ligand crystal structure analysis was performed by DR. DIETER SCHOLLMEYER at the Institute of Organic Chemistry, Johannes Gutenberg University (Mainz, Germany) on a Stoe IPDS 2T with Cu and Mo-X ray tubes and Oxford Cryostream.

7.3 Synthetic Procedures

7.3.1 Synthesis of Building Block 120

***tert*-Butyl (4-methylpyridin-2-yl)carbamate (132)**

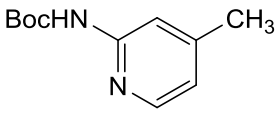

$C_{11}H_{16}N_2O_2$ (M_r 208.26)

2-Amino-4-methylpyridine (3.00 g, 27.7 mmol) and Boc_2O (6.70 g, 30.5 mmol) were stirred in 70 ml *tert*-butanol at rt for 12 h. The solvent was removed under reduced pressure and the crude product was purified by flash chromatography (SiO_2, 10-50 % ethyl acetate/petrol ether) and crystallized from 2-propanol to afford **132** as colorless crystals (100 % HPLC purity).

Yield: 5.35 g (25.7 mmol, 93 %) (Lit.[202]: 84 %).

m.p.: 125 °C.

^{1}H NMR (300 MHz, $CDCl_3$): δ = 1.53 (s, 9 H, ^{t}Bu), 2.35 (s, 3 H, CH_3), 6.79 (dq, ^3J = 5.3 Hz, ^4J = 0.6 Hz, 1 H, C^5H, Pyr), 7.88 (m, 1 H, C^3H, Pyr), 8.13 (dd, ^3J = 5.2 Hz, ^5J = 0.5 Hz, 1 H, C^6H, Pyr), 8.84 (bs, 1 H, NH) ppm.

^{13}C NMR (75 MHz, $CDCl_3$): δ = 21.6 (CH$_3$), 28.5 (C(CH$_3$)$_3$), 81.1 (C(CH$_3$)$_3$), 113.2 (C^3H, Pyr), 119.6 (C^5H, Pyr), 146.6 (C^6H, Pyr), 150.5 (CO), 152.3 (C^4, Pyr), 152.8 (C^2, Pyr) ppm.

IR (ATR): $\tilde{\nu}$ = 2990, 1717, 1616, 1576, 1526, 1474, 1418, 1389, 1364, 1292, 1273, 1250, 1229, 1148, 1115, 1055, 1036, 1007, 995, 889, 864, 804, 770, 743, 625 cm^{-1}.

HPLC (Method 1): t_R = 4.7 min.

LC-MS (ESI, 70 eV): m/z = 153 [MH$_2$-^{t}Bu]$^+$ (calc. m/z = 208).

1,3-Bis(4-methylpyridin-2-yl)carbamide (134)

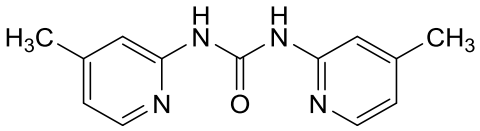

$C_{13}H_{14}N_4O$ (M_r 242.28)

2-Amino-4-methylpyridine (1.00 g, 9.25 mmol) and Boc_2O (2.42 g, 11.1 mmol) were stirred in 10 ml THF at rt for 12 h. The precipitate was filtered off and rinsed with THF to afford **134** as a colorless solid (100 % HPLC purity).

Yield: 1.11 g (4.58 mmol, quant.).

m.p.: 227 °C.

^{1}H NMR (300 MHz, $CDCl_3$): δ = 2.37 (s, 6 H, C*H*$_3$), 6.83 (dq, ^3J = 5.3 Hz, ^4J = 0.8 Hz, 2 H, C^5*H*, Pyr), 7.45 (bs, 2 H, C^3*H*, Pyr), 8.22 (d, ^3J = 5.3 Hz, 2 H, C^6*H*, Pyr) ppm.

^{13}C NMR (75 MHz, $CDCl_3$): δ = 21.5 (*C*H$_3$), 113.7 (*C*^{3}H, Pyr), 119.7 (*C*^{5}H, Pyr), 146.5 (*C*^{6}H, Pyr), 150.2 (*C*O), 152.4 (*C*^{4}, Pyr), 153.6 (*C*^{2}, Pyr) ppm.

IR (ATR): $\tilde{\nu}$ = 3090, 1690, 1616, 1566, 1551, 1512, 1476, 1454, 1412, 1383, 1312, 1289, 1256, 1231, 1179, 1165, 1122, 989, 954, 878, 866, 831, 810, 774, 721, 687, 561 cm^{-1}.

HPLC (Method 1): t_R = 4.0 min.

LC-MS (ESI, 70 eV): *m*/*z* = 243 $[MH]^+$, 135 $[M\text{-}C_6H_7N_2]^+$, 109 $[MH_2\text{-}C_7H_7N_2O]^+$ (calc. *m*/*z* = 242).

Di-*N*-*tert*-butoxycarbonyl-2-amino-4-methylpyridine (133)

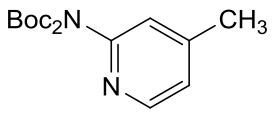

$C_{16}H_{24}N_2O_4$ (M_r 308.38)

4-DMAP (147 mg, 1.20 mmol) was added to a solution of **132** (500 mg, 2.40 mmol) and Boc_2O (790 mg, 3.60 mmol) in 4 ml THF and the mixture was stirred at rt for 24 h. The solvent was removed under reduced pressure, the residue was resuspended in ethyl acetate, washed with water and sat. aq. NaCl solution, and dried over anhyd. Na_2SO_4. The crude product was purified by flash chromatography (SiO_2, 10 % ethyl acetate/petrol ether) to afford **133** as colorless oil (96 % HPLC purity).

Yield: 300 mg (0.97 mmol, 41 %).

^{1}H NMR (300 MHz, DMSO-d_6): δ = 1.40 (s, 18 H, ^{t}Bu), 2.34 (s, 3 H, CH_3), 7.14-7.18 (m, 2 H, C$^{3/5}H$, Pyr), 8.28 (dd, ^3J = 5.0 Hz, ^5J = 0.5 Hz, 1 H, C^6H, Pyr) ppm.

^{13}C NMR (75 MHz, DMSO-d_6): δ = 20.3 (CH$_3$), 27.4 (C(CH$_3$)$_3$), 82.4 (C(CH$_3$)$_3$), 121.8 (C^3H, Pyr), 123.3 (C^5H, Pyr), 147.9 (C^6H, Pyr), 149.3 (C^2, Pyr), 151.0 (CO), 151.8 (C^3, Pyr) ppm.

HPLC (Method 3): t_R = 5.0 min.

LC-MS (ESI, 70 eV): m/z = 309 $[MH]^+$ (calc. m/z = 308).

1-(4-Fluorophenyl)-2-(2-fluoropyridin-4-yl)-ethan-1-one (123)

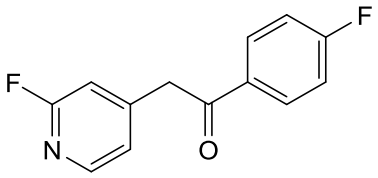

$C_{13}H_9F_2NO$ (M_r 233.22)

NaHMDS (66.7 ml 2 M solution in THF, 133 mmol) was slowly added dropwise to a stirred solution of 2-fluoro-4-methylpyridine (10.6 ml, 103 mmol) and ethyl 4-fluorobenzoate (18.1 ml, 123 mmol) in 40 ml anhyd. THF at 0 °C under a nitrogen atmosphere. After stirring at 0 °C for 2 h the reaction was allowed to reach rt and stirring continued for 1 h. The mixture was diluted with ethyl acetate and washed twice with 10 % aq. HCl. The organic layer was dried over anhyd. Na_2SO_4 and the solvent was removed under reduced pressure. The crude product was recrystallized from ethyl acetate to afford **123** as a colorless solid (100 % HPLC purity).

Yield: 23.9 g (103 mmol, quant.) (Lit.[203]: 86 %).

m.p.: 102 °C.

^{1}H NMR (300 MHz, DMSO-d_6): δ = 4.59 (s, 2 H, CH_2), 7.10 (s, 1 H, C^3*H*, Pyr), 7.25-7.27 (m, 1 H, C^5*H*, Pyr), 7.37-7.43 (m, 2 H, C$^{3/5}$*H*, F-Phe), 8.11-8.19 (m, 3 H, C$^{2/6}$*H*, F-Phe, C^6*H*, Pyr) ppm.

^{13}C NMR (75 MHz, DMSO-d_6): δ = 43.6 (d, $^4J_{CF}$ = 2.8 Hz, *C*H$_2$), 110.8 (d, $^2J_{CF}$ = 37.6 Hz, *C*^{3}H, Pyr), 115.8 (d, $^2J_{CF}$ = 22.0 Hz, *C*$^{3/5}$H, F-Phe), 123.8 (d, $^4J_{CF}$ = 3.8 Hz, *C*^{5}H, Pyr), 131.3 (d, $^3J_{CF}$ = 9.6 Hz, *C*$^{2/6}$H, F-Phe), 132.9 (d, $^4J_{CF}$ = 2.7 Hz, *C*^{1}, F-Phe), 147.0 (d, $^5J_{CF}$ = 15.5 Hz, *C*^{6}H, Pyr), 150.7 (d, $^3J_{CF}$ = 8.5 Hz, *C*^{1}, Pyr), 163.1 (d, $^1J_{CF}$ = 234.3 Hz, *C*^{2}F, Pyr), 165.2 (d, $^1J_{CF}$ = 252.0 Hz, *C*^{4}F, F-Phe), 194.6 (*C*O) ppm.

IR (ATR): ṽ = 3100, 2490, 1684, 1614, 1597, 1568, 1553, 1508, 1483, 1412, 1341, 1306, 1292, 1271, 1234, 1206, 1161, 118, 1115, 1103, 999, 964, 952, 921, 872, 853, 829, 812, 793, 760, 627, 582, 559 cm^{-1}.

HPLC (Method 1): t_R = 3.9 min.

LC-MS (ESI, 70 eV): *m*/*z* = 234 [MH]$^+$ (calc. *m*/*z* = 233).

2-(2-Bromopyridin-4-yl)-1-(4-fluorophenyl)ethan-1-one (128)

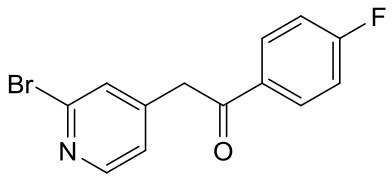

$C_{13}H_9FBrNO$ (M_r 294.12)

128 was synthesized according to the procedure for **123** from 2-bromo-4-methylpyridine (190 µl, 1.74 mmol), ethyl 4-fluorobenzoate (260 µl, 1.74 mmol) in 6 ml anhyd. THF and NaHMDS (1.74 ml 2 M solution in THF, 3.49 mmol). **128** was obtained as a brown solid (100 % HPLC purity).

Yield: 260 mg (884 µmol, 51 %) (Lit.[203]: 87 %).

^{1}H NMR (300 MHz, DMSO-d_6): δ = 4.54 (s, 2 H, CH_2), 7.35 (dd, ^3J = 5.0 Hz, ^4J = 1.4 Hz, 1 H, C^5H, Pyr), 7.37-7.43 (m, 2 H, C$^{3/5}H$, F-Phe), 7.59 (d, ^5J = 0.7 Hz, 1 H, C^3H, Pyr), 8.11-8.15 (m, 2 H, C$^{2/6}H$, F-Phe), 8.33 (dd, ^3J = 5.0 Hz, ^5J = 0.6 Hz, 1 H, C^6H, Pyr) ppm.

^{13}C NMR (75 MHz, DMSO-d_6): δ = 43.3 (CH$_2$), 115.9 (d, $^2J_{CF}$ = 22.0 Hz, $C^{3/5}$H, F-Phe), 125.3 (C^5H, Pyr), 129.5 (C^3H, Pyr), 131.3 (d, $^3J_{CF}$ = 9.6 Hz, $C^{2/6}$H, F-Phe), 132.9 (d, $^4J_{CF}$ = 2.9 Hz, C^1, F-Phe), 141.2 (CBr), 148.1 (C^4, Pyr), 150.0 (C^6H, Pyr), 165.2 (d, $^1J_{CF}$ = 252.3 Hz, CF), 194.6 (CO) ppm.

HPLC (Method 1): t_R = 4.6 min.

LC-MS (ESI, 70 eV): m/z = 294, 296 $[MH]^+$ (calc. m/z = 294).

***tert*-Butyl (4-(2-(4-fluorophenyl)-2-oxoethyl)pyridin-2-yl)carbamate (135)**

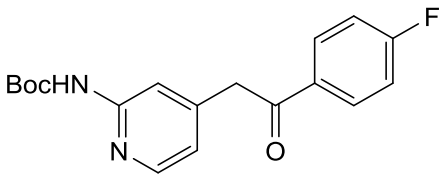

$C_{18}H_{19}FN_2O_3$ (M_r 330.36)

Method A. A solution of **132** (200 mg, 960 µmol) in 4 ml anhyd. THF under a nitrogen atmosphere was cooled down to -78 °C and NaHMDS (960 µl 2 M solution in THF, 1.92 mmol) was added dropwise. After stirring at 0 °C for 30 min the reaction was cooled to -78 °C before ethyl 4-fluorobenzoate (141 µl, 960 µmol) in 4 ml anhyd. THF was added very slowly over a syringe. The mixture was allowed to reach rt over 1 h and stirring continued at the same temp. for another 2 h. The suspension was diluted with ethyl acetate and washed twice with 10 % aq. HCl. The organic layer was dried over anhyd. Na_2SO_4 and the solvent was removed under reduced pressure. The crude product was purified by flash chromatography (SiO_2, 5-25 % ethyl acetate/petrol ether) to afford **135** as a colorless solid (100 % HPLC purity).

Yield: 35.5 mg (107 µmol, 11 %).

Method B. **135** was synthesized according to the procedure for **123** from **133** (300 mg, 973 µmol), ethyl 4-fluorobenzoate (143 µl, 973 µmol) in 1.2 ml anhyd. THF, and NaHMDS (973 µl 2 M solution in THF, 1.95 mmol), but required further purification by flash chromatography (SiO_2, 20-50 % ethyl acetate/petrol ether) to give **135** as a colorless solid (100 % HPLC purity).

Yield: 88.5 mg (268 µmol, 28 %).

^{1}H NMR (300 MHz, DMSO-d_6): δ = 1.46 (s, 9 H, ^{t}Bu), 4.46 (s, 2 H, CH_2), 6.93 (dd, ^3J = 5.1 Hz, ^4J = 1.5 Hz, 1 H, C^5H, Pyr), 7.35-7.41 (m, 2 H, C$^{3/5}H$, F-Phe), 7.73 (d, ^5J = 0.6 Hz, 1 H, C^3H, Pyr), 8.10-8.15 (m, 2 H, C$^{2/6}H$, F-Phe), 8.16 (dd, ^3J = 5.1 Hz, ^5J = 0.7 Hz, 1 H, C^6H, Pyr), 9.73 (bs, 1 H, NH) ppm.

^{13}C NMR (75 MHz, $CDCl_3$): δ = 28.0 (C(CH$_3$)$_3$), 44.3 (CH$_2$), 79.5 (C(CH$_3$)$_3$), 113.5 (C^3H, Pyr), 115.8 (d, $^2J_{CF}$ = 21.9 Hz, $C^{3/5}$H, F-Phe), 120.1 (C^5H, Pyr), 131.4 (d, $^3J_{CF}$ = 9.6 Hz, $C^{2/6}$H, F-Phe), 133.0 (d, $^4J_{CF}$ = 2.9 Hz, C^1, F-Phe), 145.9 (C^4, Pyr), 147.5 (C^6H, Pyr), 152.49 (COO^{t}Bu), 152.7 (C^1, Pyr), 165.2 (d, $^1J_{CF}$ = 252.2 Hz, CF), 195.31 (CO) ppm.

HPLC (Method 1): t_R = 5.8 min.

LC-MS (ESI, 70 eV): m/z = 331 [MH]$^+$, 275 [MH$_2$-^{t}Bu]$^+$ (calc. m/z = 330).

1-(4-Fluorophenyl)-2-(2-fluoropyridin-4-yl)-2-(hydroximino)ethan-1-one (124)

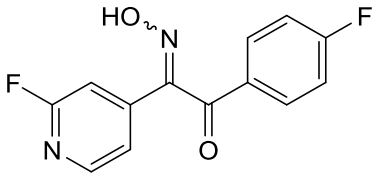

$C_{13}H_8F_2N_2O_2$ (M_r 262.22)

Sodium nitrite (2.06 g, 29.8 mmol) in 12 ml H_2O was added dropwise to a stirred solution of **1** (2.30 g, 9.86 mmol) in 17 ml glacial acetic acid at 10 °C over 10 min. After stirring at rt for 1 h, 30 ml H_2O were added and the resulting bright yellow suspension was stirred for another 3.5 h at the same temperature. The suspension was cooled to 8 °C, filtered, and the residue was washed with H_2O and dried under reduced pressure to afford **124** as a colorless solid (98 % HPLC purity).

Yield: 2.46 g (9.38 mmol, 95 %) (Lit.[203]: 84 %).

m.p.: 185 °C.

^{1}H NMR (300 MHz, DMSO-d_6): δ = 7.19 (bs, 1 H, C^3*H*, Pyr), 7.37-7.46 (m, 3 H, C^5*H*, Pyr and C$^{3/5}$*H*, F-Phe), 7.92-7.98 (m, 2 H, C$^{2/6}$*H*, F-Phe), 8.30 (d, ^3J = 5.3 Hz, 1 H, C^6*H*, Pyr), 12.67 (s, 1 H, O*H*) ppm.

^{13}C NMR (75 MHz, DMSO-d_6): δ = 105.4 (d, $^2J_{CF}$ = 38.9 Hz, *C*^{3}H, Pyr), 116.7 (d, $^2J_{CF}$ = 22.5 Hz, *C*$^{3/5}$H, F-Phe), 118.2 (d, $^4J_{CF}$ = 4.2 Hz, *C*^{5}H, Pyr), 130.8 (d, $^4J_{CF}$ = 2.7 Hz, *C*^{1}, F-Phe), 132.2 (d, $^3J_{CF}$ = 10.1 Hz, *C*$^{2/6}$H, F-Phe), 144.3 (d, $^3J_{CF}$ = 8.4 Hz, *C*^{4}, Pyr), 148.8 (d, $^5J_{CF}$ = 15.6 Hz, *C*^{6}H, Pyr), 151.9 (d, $^4J_{CF}$ = 4.0 Hz, *C*NOH), 163.5 (d, $^1J_{CF}$ = 235.6 Hz, *C*^{2}F, Pyr), 166.0 (d, $^1J_{CF}$ = 254.8 Hz, *C*^{4}F, F-Phe), 192.04 (*C*O) ppm.

IR (ATR): ṽ = 2860, 2373, 1667, 1593, 1543, 1504, 1417, 1289, 1262, 1233, 1192, 1153, 1074, 995, 945, 893, 868, 839, 752, 733, 694, 663, 637, 617, 588 cm^{-1}.

HPLC (Method 1): t_R = 4.4 min.

LC-MS (ESI, 70 eV): *m*/*z* = 263 [MH]$^+$ (calc. *m*/*z* = 262).

2-(2-Bromopyridin-4-yl)-1-(4-fluorophenyl)-2-hydroximino)ethan-1-one (129)

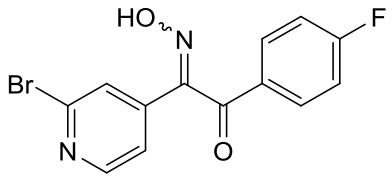

$C_{13}H_8BrFN_2O_2$ (M_r 323.12)

129 was synthesized according to the procedure for **124** from **128** (150 mg, 510 µmol) in 1 ml glacial acetic acid and sodium nitrite (106 mg, 1.54 mmol in 0.6 ml H_2O). **129** was obtained as a colorless solid (99 % HPLC purity).

Yield: 151 mg (466 µmol, 92 %) (Lit.[203]: 82 %).

^{1}H NMR (300 MHz, DMSO-d_6): δ = 7.40-7.46 (m, 3 H, C^5*H*, Pyr and C$^{3/5}$*H*, F-Phe), 7.63 (s, 1 H, C^3*H*, Pyr), 7.94-7.98 (m, 2 H, C$^{2/6}$*H*, F-Phe), 8.44 (d, ^3J = 5.0 Hz, 1 H, C^6*H*, Pyr), 12.70 (s, 1 H, NO*H*) ppm.

^{13}C NMR (75 MHz, DMSO-d_6): δ = 116.8 (d, $^2J_{CF}$ = 22.5 Hz, *C*$^{3/5}$H, F-Phe), 119.5 (*C*^{5}H, Pyr), 123.3 (*C*^{3}H, Pyr), 130.8 (d, $^4J_{CF}$ = 2.7 Hz, *C*^{1}, F-Phe), 132.3 (d, $^3J_{CF}$ = 10.1 Hz, *C*$^{2/6}$H, F-Phe), 141.7 (*C*^{4}, Pyr), 142.1 (*C*Br), 151.4 (*C*^{6}H, Pyr), 151.6 (*C*NOH), 166.1 (d, $^1J_{CF}$ = 254.9 Hz, *C*F), 192.0 (*C*O) ppm.

HPLC (Method 3): t_R = 5.3 min.

LC-MS (ESI, 70 eV): m/z = 323, 324, 325 $[MH]^+$ (calc. m/z = 323).

***tert*-Butyl (4-(2-(4-fluorophenyl)-1-(hydroxyimino)-2-oxoethyl)pyridin-2-yl)carbamate (136)**

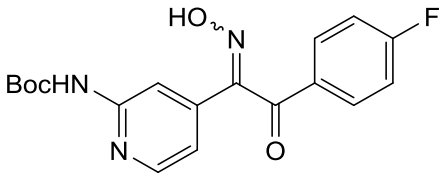

$C_{18}H_{18}FN_3O_4$ (M_r 359.36)

136 was synthesized according to the procedure for **124** from **135** (84.4 mg, 255 µmol) in 3 ml glacial acetic acid and sodium nitrite (53.3 mg, 772 µmol in 0.3 ml H_2O). **136** was obtained as a colorless solid (100 % HPLC purity).

Yield: 90.0 mg (250 µmol, 98 %).

^{1}H NMR (300 MHz, DMSO-d_6): δ = 1.43 (s, 9 H, ^{t}Bu), 7.04 (dd, ^3J = 5.2 Hz, ^4J = 1.5 Hz, 1 H, C^5*H*, Pyr), 7.40-7.46 (m, 2 H, C$^{3/5}$*H*, F-Phe), 7.91-7.96 (m, 2 H, C$^{2/6}$*H*, F-Phe), 7.98 (bs, 1 H, C^3*H*, Pyr), 8.27 (dd, ^3J = 5.2 Hz, ^5J = 0.5 Hz, 1 H, C^6*H*, Pyr), 9.93 (s, 1 H, N*H*), 12.36 (s, 1 H, NO*H*) ppm.

^{13}C NMR (75 MHz, DMSO-d_6): δ = 28.0 (C(*C*H$_3$)$_3$), 79.9 (*C*(CH$_3$)$_3$), 107.8 (*C*^{3}H, Pyr), 114.3 (*C*^{5}H, Pyr), 116.8 (d, $^2J_{CF}$ = 22.4 Hz, *C*$^{3/5}$H, F-Phe), 131.0 (d, $^4J_{CF}$ = 2.2 Hz, *C*^{1}, F-Phe), 132.1 (d, $^3J_{CF}$ = 10.0 Hz, *C*$^{2/6}$H, F-Phe), 140.3 (*C*^{4}, Pyr), 148.9 (*C*^{6}H, Pyr), 152.6 (*C*OO^{t}Bu), 153.0 (*C*NOH), 153.2 (*C*^{2}, Pyr), 165.9 (d, $^1J_{CF}$ = 254.9 Hz, *C*F), 192.7 (*C*O) ppm.

HPLC (Method 3): t_R = 5.6 min.

LC-MS (ESI, 70 eV): *m*/*z* = 304 [MH$_2$-^{t}Bu]$^+$ (calc. *m*/*z* = 359).

2-(4-Fluorophenyl)-1-(2-fluoropyridin-4-yl)-2-oxoethan-1-aminium chloride (125)

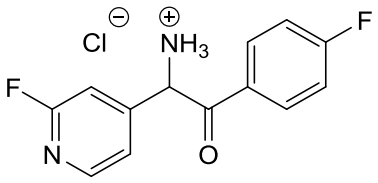

$C_{13}H_{11}ClF_2N_2O$ (M_r 284.69)

To an intensely stirred solution of **124** (1.60 g, 6.10 mmol) in 15 ml 2-propanol and 20 ml HCl-sat. 2-propanol, Pd/C 10 % (279 mg) was added in one portion under a nitrogen atmosphere and stirring continued for 12 h at rt. The crude product was obtained by filtration, the residue was resuspended in methanol, filtered again, and the solvent was removed under reduced pressure. Recrystallization from methanol/diethyl ether provided **125** as beige solid (98 % HPLC purity).

Yield: 1.43 g (5.03 mmol, 82 %) (Lit.[203]: quant.).

m.p.: 216 °C.

^{1}H NMR (300 MHz, DMSO-d_6): δ = 6.56 (s, 1 H, C*H*), 7.35-7.41 (m, 2 H, C$^{3/5}$*H*, F-Phe), 7.52-7.54 (m, 2 H, C$^{3/5}$*H*, Pyr), 8.21 (dd, ^3J = 8.4 Hz, ^4J = 5.6 Hz, 2 H, C$^{2/6}$*H*, F-Phe), 8.31 (d, ^3J = 5.4 Hz, 1 H, C^6*H*, Pyr), 9.36 (bs, 3 H, NH_3^+) ppm.

^{13}C NMR (75 MHz, DMSO-d_6): δ = 56.8 (*C*NH_3^+), 110.5 (d, $^2J_{CF}$ = 39.3 Hz, *C*^{3}H, Pyr), 116.9 (d, $^2J_{CF}$ = 22.1 Hz, *C*$^{3/5}$H, F-Phe), 122.3 (d, $^4J_{CF}$ = 4.2 Hz, *C*^{5}H, Pyr), 130.0 (d, $^4J_{CF}$ = 2.7 Hz, *C*^{1}, F-Phe), 132.9 (d, $^3J_{CF}$ = 9.8 Hz, *C*$^{2/6}$H, F-Phe), 147.4 (d, $^3J_{CF}$ = 8.0 Hz, *C*^{4}, Pyr), 149.4 (d, $^5J_{CF}$ = 15.0 Hz, *C*^{6}H, Pyr), 163.5 (d, $^1J_{CF}$ = 236.7 Hz, *C*^{2}F, Pyr), 166.3 (d, $^1J_{CF}$ = 255.1 Hz, *C*^{4}F, F-Phe), 191.4 (*C*O) ppm.

IR (ATR): ṽ = 2810, 2361, 1694, 1616, 1597, 1560, 1521, 1508, 1419, 1281, 1256, 1238, 1161, 1007, 974, 945, 849, 835, 792, 725, 681, 652, 606, 565, 554 cm^{-1}.

HPLC (Method 1): t_R = 2.3 min.

LC-MS (ESI, 70 eV): *m*/*z* 249 = [M-Cl]$^+$ (calc. *m*/*z* = 285).

1-(2-Bromopyridin-4-yl)-2-(4-fluorophenyl)-2-oxoethan-1-aminium chloride (130)

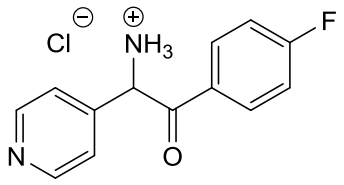

$C_{13}H_{12}ClFN_2O$ (M_r 266.70)

130 was synthesized according to the procedure for **125** from **129** (140 mg, 433 µmol) in 1 ml 2-propanol and 1.5 ml HCl-sat. 2-propanol, and Pd/C 10 % (24 mg). The crude product was obtained by filtration, the residue was resuspended in methanol, filtered again, and the solvent was removed under reduced pressure. **130** was obtained as a colorless solid (86 % HPLC purity).

Yield: 103 mg (298 µmol, 69 %) (Lit.[203]: quant.).

HPLC (Method 3): t_R = 1.7 min.

LC-MS (ESI, 70 eV): m/z = 231 $[M\text{-}Cl]^+$ (calc. m/z = 267).

1-(2-((*tert*-Butoxycarbonyl)amino)pyridin-4-yl)-2-(4-fluorophenyl)-2-oxoethan-1-aminium chloride and 4-(1-ammonio-2-(4-fluorophenyl)-2-oxoethyl)pyridin-2-aminium chloride (137)

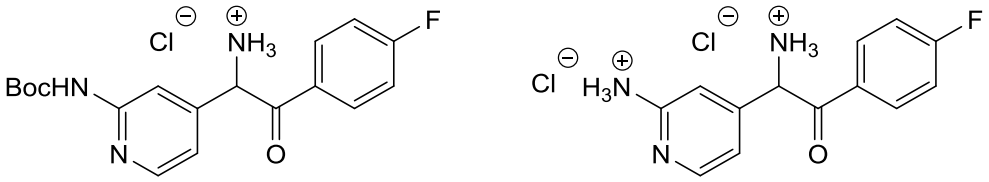

$C_{18}H_{21}ClFN_3O_3$ (M_r 381.83) and $C_{13}H_{14}Cl_2FN_3O$ (M_r 318.17)

137 was synthesized according to the procedure for **125** from **136** (80.0 mg, 223 µmol) in 0.5 ml 2-propanol and 1.0 ml HCl-sat. 2-propanol and Pd/C 10 % (14 mg) to afford **137** as a beige mixture of two solid derivatives (together 100 % HPLC purity).

Yield: 75.5 mg (approx. 205 µmol, 92 %).

HPLC (Method 3): t_{R1} = 3.4 min, t_{R2} = 1.4 min.

LC-MS (ESI, 70 eV): m/z = 346 $[MH\text{-}Cl]^+$, 290 $[MH\text{-}{}^t\text{Bu}, Cl]^+$ and m/z 246 $[M\text{-}H]^+$ (calc. m/z = 382, 318).

2-Fluoro-4-(5-(4-fluorophenyl)-2-(methylthio)-1*H*-imidazol-4-yl)pyridine (119)

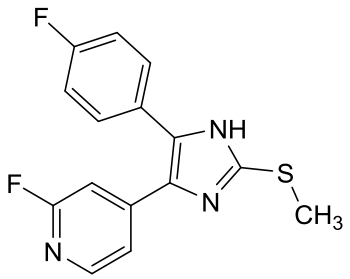

$C_{15}H_{11}F_2N_3S$ (M_r 303.33)

A mixture of **125** (4.41 g, 15.5 mmol) and methyl thiocyanate (3.18 ml, 46.5 mmol) was refluxed under a nitrogen atmosphere for 45 min in 140 ml anhyd. DMF and stirred 45 min at rt before ice-cold H_2O (400 ml) was added. The suspension was cooled to 8 °C, filtered, the residue was washed with H_2O, and dried under reduced pressure to afford **119** as fine yellow solid (100 % HPLC purity).

Yield: 3.59 g (11.8 mmol, 76 %) (Lit.[203]: 77 %).

m.p.: 205 °C.

^{1}H NMR (300 MHz, DMSO-d_6): δ = 2.63 (s, 3 H, SCH_3), 7.09 (bs, 1 H, C^3*H*, Pyr), 7.26-7.34 (m, 3 H, C^5*H*, Pyr and C$^{3/5}$*H*, F-Phe), 7.49-7.54 (m, 2 H, C$^{2/6}$*H*, F-Phe), 8.09 (d, ^3J = 5.3 Hz, 1 H, C^6*H*, Pyr), 12.84 (bs, 1 H, N*H*) ppm.

^{13}C NMR (75 MHz, DMSO-d_6): δ = 14.9 (S*C*H$_3$), 105.0 (d, $^2J_{CF}$ = 39.5 Hz, *C*^{3}H, Pyr), 115.9 (d, $^2J_{CF}$ = 21.6 Hz, *C*$^{3/5}$H, F-Phe), 118.5 (d, $^4J_{CF}$ = 2.5 Hz, *C*^{5}H, Pyr), 126.5 (*C*^{1}, F-Phe), 130.9 (*C*$^{2/6}$H, F-Phe), 132.9 (d, $^3J_{CF}$ = 8.6 Hz, *C*^{4}, Pyr), 143.0 (*C*^{2}, Imdz), 147.6 (d, $^3J_{CF}$ = 16.1 Hz, *C*^{6}H, Pyr), 162.1 (d, $^1J_{CF}$ = 246.4 Hz, *C*F, F-Phe), 163.7 (d, $^1J_{CF}$ = 233.3 Hz, *C*F, Pyr) ppm.

IR (ATR): $\tilde{\nu}$ = 2980, 1613, 1553, 1506, 1423, 1292, 1238, 1219, 1157, 1098, 1003, 982, 885, 868, 851, 829, 816, 702, 679, 635, 617, 586 cm^{-1}.

HPLC (Method 1): t_R = 4.8 min.

LC-MS (ESI, 70 eV): *m*/*z* = 304 [MH]$^+$ (calc. *m*/*z* = 303).

4-(5-(4-Fluorophenyl)-2-(methylthio)-1*H*-imidazol-4-yl)pyridin-2-amine (120)

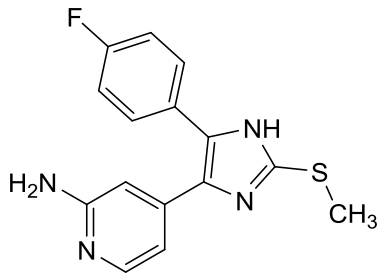

$C_{15}H_{13}FN_4S$ (M_r 300.36)

Method A. A solution of **119** (1.00 g, 3.30 mmol) in 15 ml 32 % aq. ammonia solution was heated in a high pressure reactor at 180 °C for 18 h. The reactor was allowed to reach rt and H_2O was added. The crude product was obtained by filtration, washed with H_2O and diisopropyl ether and purified by flash chromatography (SiO_2, 50-100 % ethyl acetate/petrol ether) to afford **120** as a beige solid (100 % HPLC purity).

Yield: 852 mg (2.84 mmol, 86 %) (Lit.[193]: 80 %).

Method B. **120** was synthesized according to the procedure for **119** from **137** (75.5 mg, approx. 205 µmol) and methyl thiocyanate (41.1 µl, 602 µmol) in 2 ml anhyd. DMF. The crude product was stirred in diluted aq. trifluoroacetic acid for 12 h, followed by neutralization with sat. aq. $NaHCO_3$ solution. The mixture was extracted with ethyl acetate, washed with H_2O and sat. aq. NaCl solution, and dried over anhyd. Na_2SO_4. The solvent was removed under reduced pressure to afford **120** as a beige solid (97 % HPLC purity).

Yield: 7.00 mg (233 µmol, 9 %).

^{1}H NMR (300 MHz, DMSO-d_6): δ = 2.60 (s, 1 H, SCH_3), 5.79-5.95 (m, 2 H, NH_2), 6.42-6.67 (m, 2 H, C$^{3/5}H$, Pyr), 7.17-7.27 (m, 2 H, C$^{3/5}H$, F-Phe), 7.48 (bs, 2 H, C$^{2/6}H$, F-Phe), 7.74-7.86 (m, 1 H, C^6H, Pyr), 12.58 (s, 1 H, NH) ppm.

^{13}C NMR (75 MHz, DMSO-d_6): δ = 15.1 (SCH$_3$), 105.1 (C^5H, Pyr), 110.0 (C^3H, Pyr), 115.7 (d, $^3J_{CF}$ = 21.1 Hz, $C^{3/5}$H, F-Phe), 127.0 (s, C^4/C^5, Imdz), 129.2 (s, C^1, F-Phe), 130.5 (d, $^4J_{CF}$ = 6.6 Hz, $C^{2/6}$-H, F-Phe), 147.5 (C^6H, Pyr), 160.1 (CF) ppm.

HPLC (Method 2): t_R = 4.4 min.

LC-MS (ESI, 70 eV): m/z = 301 $[MH]^+$ (calc. m/z = 300).

1-(4-Fluorophenyl)-2-(2-fluoropyridin-4-yl)ethane-1,2-dione (138)

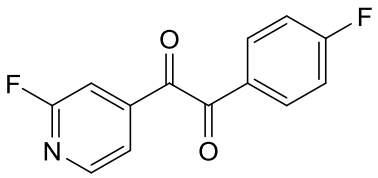

$C_{13}H_7F_2NO_2$ (M_r 247.20)

123 (1.00 g, 4.29 mmol) and selenium dioxide (523 mg, 4.72 mmol) were dissolved in 25 ml glacial acetic acid under intense stirring and heated to 95 °C for 1.5 h. After completion, the reaction was cooled to rt, extracted with ethyl acetate, washed with sat. aq. $NaHCO_3$ solution and sat. aq. NaCl solution, and dried over anhyd. Na_2SO_4. The solvent was removed under reduced pressure and the crude product was purified by flash chromatography (SiO_2, 40-60 % ethyl acetate/petrol ether) to afford **138** as a yellow solid (100 % HPLC purity).

Yield: 448 mg (1.81 mmol, 42 %) (Lit.[218]: 45 %).

^{1}H NMR (300 MHz, DMSO-d_6): δ = 7.43-7.51 (m, 2 H, C$^{3/5}$*H*, F-Phe), 7.67 (bs, 1 H, C^3*H*, Pyr), 7.81-7.83 (m, 1 H, C^5*H*, Pyr), 8.10-8.16 (m, 2 H, C$^{2/6}$*H*, F-Phe), 8.54 (d, ^3J = 5.1 Hz, 1 H, C^6*H*, Pyr) ppm.

^{13}C NMR (75 MHz, DMSO-d_6): δ = 109.5 (d, $^2J_{CF}$ = 39.5 Hz, *C*^{3}H, Pyr), 116.5 (d, $^2J_{CF}$ = 22.4 Hz, *C*$^{3/5}$H, F-Phe), 121.3 (d, $^4J_{CF}$ = 4.6 Hz, *C*^{5}H, Pyr), 128.7 (d, $^4J_{CF}$ = 2.7 Hz, *C*^{1}, F-Phe), 133.6 (d, $^3J_{CF}$ = 10.1 Hz, *C*$^{2/6}$H, F-Phe), 144.4 (d, $^3J_{CF}$ = 7.2 Hz, *C*^{4}, Pyr), 149.4 (d, $^3J_{CF}$ = 14.5 Hz, *C*^{6}H, Pyr), 163.5 (d, $^1J_{CF}$ = 237.7 Hz, *C*F, Pyr), 166.3 (d, $^1J_{CF}$ = 255.7 Hz, *C*F, F-Phe), 189.6 (Pyr-CO*C*O-Phe), 190.2 (d, $^4J_{CF}$ = 3.2 Hz, Pyr-*C*OCO-Phe) ppm.

HPLC (Method 2): t_R = 5.3 min.

LC-MS (ESI, 70 eV): *m*/*z* = 248 $[MH]^+$ (calc. *m*/*z* = 247).

2-Fluoro-4-(5-(4-fluorophenyl)-1*H*-imidazol-5-yl)pyridine (139)

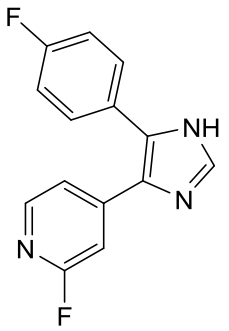

$C_{14}H_9F_2N_3$ (M_r 257.24)

A few drops (catalytic amount) of glacial acetic acid were added to **138** (105 mg, 425 µmol), methenamine (11.8 mg, 84.0 µmol), and ammonium acetate (276 mg, 3.58 mmol) in a microwave reaction vessel. The mixture was heated in a microwave oven (117 °C) for 4 min (100 W), poured into H_2O and 32 % aq. ammonia solution was added until pH 8 was reached. The precipitate was collected by filtration and purified by flash chromatography (SiO_2, 20-100 % ethyl acetate/petrol ether) to afford **139** as a voluminous colorless solid (100 % HPLC purity).

Yield: 60.1 mg (234 µmol, 55 %).

^{1}H NMR (300 MHz, DMSO-d_6): δ = 7.12-7.13 (m, 1 H, C^3*H*, Pyr), 7.30-7.36 (m, 3 H, C$^{3/5}$*H*, F-Phe and C^5*H*, Pyr), 7.50-7.55 (m, 2 H, C$^{2/6}$*H*, F-Phe), 7.92 (bs, 1 H, C^2*H*, Imdz), 8.10 (bs, 1 H, C^6*H*, Pyr), 12.84 (bs, 1 H, N*H*) ppm.

^{13}C NMR (75 MHz, DMSO-d_6): δ = 105.3 (*C*^{3}H, Pyr), 116.0 (d, $^2J_{CF}$ = 23.9 Hz, *C*$^{3/5}$H, F-Phe), 118.7 (d, $^4J_{CF}$ = 2.2 Hz, *C*^{5}H, Pyr), 122.0 (*C*^{1}, F-Phe), 127.1 (d, $^3J_{CF}$ = 10.5 Hz, *C*^{4}, Pyr), 129.3 (*C*^{5}, Imdz), 131.0 (*C*$^{2/6}$H, F-Phe), 132.1 (*C*^{4}, Imdz), 136.5 (*C*^{2}H, Imdz), 147.6 (d, $^3J_{CF}$ = 15.9 Hz, *C*^{6}H, Pyr), 162.2 (d, $^1J_{CF}$ = 253.8 Hz, *C*F, F-Phe), 163.7 (d, $^1J_{CF}$ = 233.2 Hz, *C*F, Pyr) ppm.

HPLC (Method 2): t_R = 4.9 min.

LC-MS (ESI, 70 eV): m/z = 258 $[MH]^+$ (calc. m/z = 257).

7.3.2 Syntheses of Series 1: Pyridine-2-amines and -piperazines

General procedure for preparation of 4-(5-fluorophenyl-2-(methylthio)-1*H*-imidazol-4-yl)pyridin-2-amines/piperazines (148-155)

119 (1.0 equiv) was suspended in the respective amine/piperazine (4.0 to 6.0 equiv) in a glass screw cap tube and the intensely stirred mixture was heated to 160 °C. Progress of the reaction was monitored by HPLC control. After complete conversion the mixture was diluted with ethyl acetate, washed with sat. aq. $NaHCO_3$ solution and H_2O, dried over anhyd. Na_2SO_4, and concentrated under reduced pressure. The crude product was purified by flash chromatography (stationary phase, eluent, and mixing ratio given for each compound, respectively) to afford the particular compound.

Syntheses were performed by LYDIA KUHL during her Bachelor thesis[220].

***N*-(2,4-Dimethoxyphenyl)-4-(5-(4-fluorophenyl)-2-(methylthio)-1*H*-imidazol-4-yl)-pyridin-2-amine (148)**

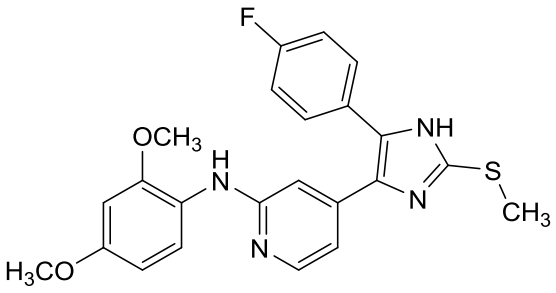

$C_{23}H_{21}FN_4O_2S$ (M_r 436.51)

148 was synthesized according to the general procedure from **119** (400 mg, 1.32 mmol) and 2,4-dimethoxyaniline (808 mg, 5.27 mmol). Purification was achieved by flash chromatography (SiO_2, 20-90 % ethyl acetate/petrol ether) to afford **148** as greyish crystals (97 % HPLC purity).

Yield: 312 mg (715 µmol, 54 %).

m.p.: 206 °C.

^{1}H NMR (300 MHz, DMSO-d_6): δ = 2.60 (s, 3 H, SC*H*$_3$), 3.75 (s, 6 H, 2 OC*H*$_3$), 6.39-6.44 (m, 1 H, C^5*H*, (OCH$_3$)$_2$-Phe), 6.56-6.58 (m, 1 H, C^3*H*, (OCH$_3$)$_2$-Phe), 6.63 (dd, ^3J = 5.3 Hz, ^4J = 1.2 Hz, 1 H, C^5*H*, Pyr), 6.82 (s, 1 H, C^3*H*, Pyr), 7.18-7.28 (m, 2 H, C$^{3/5}$*H*, F-Phe), 7.41-7.46 (m, 2 H, C$^{2/6}$*H*, F-Phe), 7.52 (d, ^3J = 8.7 Hz, 1 H, C^6*H*, (OCH$_3$)$_2$-Phe), 7.71 (s, 1 H, N*H*), 7.95 (d, ^3J = 5.3 Hz, 1 H, C^6*H*, Pyr), 12.60 (s, 1 H, N*H*, Imdz) ppm.

^{13}C NMR (75 MHz, DMSO-d_6): δ = 15.1 (S*C*H$_3$), 55.2 (O*C*H$_3$), 55.2 (O*C*H$_3$), 99.0 (*C*^{3}H, (OCH$_3$)$_2$-Phe), 104.0 (*C*^{5}H, (OCH$_3$)$_2$-Phe), 105.4 (*C*^{3}H, Pyr), 111.5 (*C*^{5}H, Pyr), 115.4 (dd, $^2J_{CF}$ = 21.8 Hz, *C*$^{3/5}$H, F-Phe), 122.5 (*C*, Imdz), 123.6 (*C*^{6}H, (OCH$_3$)$_2$-Phe), 126.8 (d, $^4J_{CF}$ = 3.1 Hz, *C*^{1}, F-Phe), 130.0 (d, $^3J_{CF}$ = 8.1 Hz, *C*$^{2/6}$H, F-Phe), 134.9 (*C*^{1}, (OCH$_3$)$_2$-Phe), 138.8 (*C*, Imdz), 141.7 (*C*^{2}OCH$_3$), 142.7 (*C*^{2}, Imdz), 147.6 (*C*^{6}H, Pyr), 152.2 (*C*^{4}OCH$_3$), 155.9 (*C*^{4}, Pyr), 157.4 (*C*^{2}, Pyr), 161.8 (d, $^1J_{CF}$ = 245.0 Hz, *C*F) ppm.

HPLC (Method 1): t_R = 3.4 min.

LC-MS (ESI, 70 eV): *m*/*z* = 437 [MH]$^+$, 219 [$C_{12}H_{15}N_2O_2$]$^+$ (calc. *m*/*z* = 436).

***N*-(2-Ethoxyphenyl)-4-(5-(4-fluorophenyl)-2-(methylthio)-1*H*-imidazol-4-yl)pyridin-2-amine (149)**

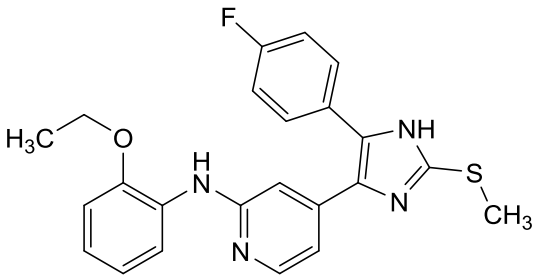

$C_{23}H_{21}FN_4OS$ (M_r 420.51)

149 was synthesized according to the general procedure from **119** (1.50 g, 4.95 mmol) and 2-ethoxyaniline (3.88 ml, 29.7 mmol). Purification was achieved by flash chromatography (SiO_2, 20-90 % ethyl acetate/petrol ether) to afford **149** as dark red crystals (100 % HPLC purity).

Yield: 1.10 g (2.62 mmol, 52 %).

m.p.: 179 °C.

^{1}H NMR (300 MHz, $CDCl_3$): δ = 1.39 (t, ^3J = 7.0 Hz, 3 H, CH_2CH_3), 2.63 (s, 3 H, SCH_3), 4.03 (q, ^3J = 7.0 Hz, 2 H, CH_2CH_3), 6.76 (t, ^3J = 7.7 Hz, 1 H, C^5*H*, EtO-Phe), 6.81-6.84 (m, 2 H, C^5*H*, Pyr and C^3*H*, EtO-Phe), 6.91 (t, ^3J = 7.7 Hz, 1 H, C^4*H*, EtO-Phe), 6.97 (bs, 1 H, C^3*H*, Pyr), 7.00-7.05 (t, ^3J = 8.7 Hz, 2 H, C$^{3/5}$*H*, F-Phe), 7.21 (bs, 1 H, N*H*), 7.37-7.41 (m, 2 H, C$^{2/6}$*H*, F-Phe), 7.49 (d, ^3J = 7.7 Hz, 1 H, C^6*H*, EtO-Phe), 8.00 (d, ^3J = 5.5 Hz, 1 H, C^6*H*, Pyr) ppm.

^{13}C NMR (75 MHz, $CDCl_3$): δ = 15.0 (CH_3CH_2), 16.6 (SCH_3), 64.3 (CH_2CH_3), 106.5 (*C*^{3}H, Pyr), 111.7 (*C*^{3}H, EtO-Phe), 112.9 (*C*^{5}H, Pyr), 116.0 (d, $^2J_{CF}$ = 21.7 Hz, *C*$^{3/5}$H, F-Phe), 120.0 (*C*^{6}H, EtO-Phe), 120.7 (*C*^{5}H, EtO-Phe), 122.6 (*C*^{4}H, EtO-Phe), 129.4 (*C*^{1}, EtO-Phe), 130.5 (d, $^3J_{CF}$ = 8.1 Hz, *C*$^{2/6}$H, F-Phe), 143.2 (*C*^{2}, Imdz), 146.8 (*C*^{6}H, Pyr), 148.7 (*C*OEt), 155.5 (*C*^{2}, Pyr), 162.5 (d, $^1J_{CF}$ = 249.0 Hz, *C*F) ppm.

HPLC (Method 1): t_R = 4.5 min.

LC-MS (ESI, 70 eV): *m*/*z* = 421 $[MH]^+$, 393 $[M\text{-}C_2H_5]^+$ (calc. *m*/*z* = 420).

***N*-(3,4-Dimethoxyphenethyl)-4-(5-(4-fluorophenyl)-2-(methylthio)-1*H*-imidazol-4-yl)-pyridin-2-amine (150)**

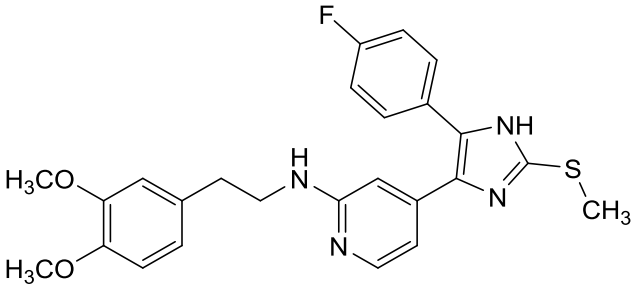

$C_{25}H_{25}FN_4O_2S$ (M_r 464.56)

150 was synthesized according to the general procedure from **119** (400 mg, 1.32 mmol) and 3,4-dimethoxyphenethylamine (900 µl, 5.31 mmol). Purification was achieved by flash chromatography (SiO_2, 20-90 % ethyl acetate/petrol ether) to afford **150** as yellow crystals (100 % HPLC purity).

Yield: 550 mg (1.18 mmol, 90 %).

m.p.: 87 °C.

^{1}H NMR (300 MHz, $CDCl_3$): δ = 2.55 (s, 3 H, SC*H*$_3$), 2.69 (t, ^3J = 6.9 Hz, 2 H, C*H*$_2$CH$_2$NH), 3.29 (m, 2 H, CH$_2$C*H*$_2$NH), 3.74 (s, 3 H, C^{3}OC*H*$_3$), 3.75 (s, 3 H, C^{4}OC*H*$_3$), 4.86 (bs, 1 H, CH$_2$CH$_2$N*H*), 6.51 (d, ^3J = 5.2 Hz, 1 H, C^5*H*, Pyr), 6.57 (d, ^4J = 2.0 Hz, 1 H, C^3*H*, Pyr), 6.57-6.70 (m, 3 H, C$^{2/5/6}$*H*, (OCH$_3$)$_2$-Phe), 6.91-6.96 (m, 2 H, C$^{3/5}$*H*, F-Phe), 7.32-7.36 (m, 2 H, C$^{2/6}$*H*, F-Phe), 7.74 (d, ^3J = 5.8 Hz, 1 H, C^6*H*, Pyr), 10.77 (bs, 1 H, N*H*) ppm.

^{13}C NMR (75 MHz, $CDCl_3$): δ = 16.4 (S*C*H$_3$), 35.1 (*C*H$_2$CH$_2$NH), 43.5 (CH$_2$*C*H$_2$NH), 55.9 (C^{3}O*C*H$_3$), 55.9 (C^{4}O*C*H$_3$), 104.1 (*C*^{3}H, Pyr), 111.0 (*C*^{5}H, Pyr), 111.4 (*C*^{5}H, (OCH$_3$)$_2$-Phe), 112.1 (*C*^{2}H, (OCH$_3$)$_2$-Phe), 115.7 (d, $^2J_{CF}$ = 21.7 Hz, *C*$^{3/5}$H, F-Phe), 120.7 (*C*^{6}H, (OCH$_3$)$_2$-Phe), 130.3 (d, $^3J_{CF}$ = 8.2 Hz, *C*$^{2/6}$H, F-Phe), 131.4 (*C*$^{4/5}$, Imdz), 142.9 (*C*^{4}, Pyr), 146.7 (*C*^{6}H, Pyr, 147.7 (*C*^{4}OCH$_3$), 149.0 (*C*^{3}OCH$_3$), 158.3 (*C*^{2}, Pyr), 162.6 (d, $^1J_{CF}$ = 248.5 Hz, *C*F) ppm.

HPLC (Method 1): t_R = 3.5 min.

LC-MS (ESI, 70 eV): *m*/*z* = 465 [MH]$^+$, 301 [MH-$C_{10}H_{13}O_2$]$^+$, 165 [$C_{10}H_{13}O_2$]$^+$ (calc. *m*/*z* = 464).

_N_-(2-(1_H_-Indol-3-yl)-ethyl)-4-(5-(4-fluorophenyl)-2-(methylthio)-1_H_-imidazol-4-yl)-pyridin-2-amine (151)

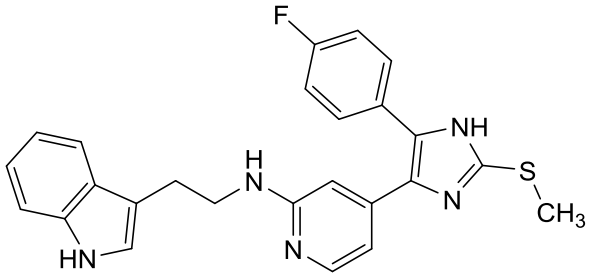

$C_{25}H_{22}FN_5S$ (M_r 443.54)

151 was synthesized according to the general procedure from **119** (400 mg, 1.32 mmol) and tryptamine (845 mg, 5.27 mmol). Purification was achieved by flash chromatography (SiO_2, 20-90 % ethyl acetate/petrol ether) to afford **151** as yellowish-brown crystals (100 % HPLC purity).

Yield: 427 mg (963 µmol, 73 %).

m.p.: 122 °C.

^{1}H NMR (300 MHz, $CDCl_3$): δ = 2.61 (s, 3 H, SCH_3), 2.95 (t, ^3J = 6.6 Hz, 2 H, CH_2CH$_2$NH), 3.39 (t, ^3J = 6.6 Hz, 2 H, CH$_2$CH_2NH), 6.52 (d, ^3J = 5.7 Hz, 1 H, C^5H, Pyr), 6.52 (bs, 1 H, C^2H, Indole), 6.87 (d, ^4J = 2.1 Hz, 1 H, C^3H, Pyr), 6.95-7.01 (m, 2 H, C$^{3/5}H$, F-Phe), 7.08 (t, ^3J = 7.8 Hz, 1 H, C^6H, Indole), 7.16 (t, ^3J = 7.9 Hz, 1 H, C^5H, Indole), 7.30 (d, ^3J = 7.9 Hz, 1 H, C^4H, Indole), 7.35-7.39 (m, 2 H, C$^{2/6}H$, F-Phe), 7.52 (d, ^3J = 7.7 Hz, 1 H, C^7H, Indole), 7.71 (d, ^3J = 5.7 Hz, 1 H, C^6H, Pyr), 8.38 (s, 1 H, NH, Indole) ppm.

^{13}C NMR (75 MHz, $CDCl_3$): δ = 16.4 (SCH$_3$), 25.1 (CH$_2$CH$_2$NH), 42.2 (CH$_2$$CH_2$NH), 104.0 ($C^3$H, Pyr), 110.6 ($C^5$H, Pyr), 111.3 ($C^4$H, Indole), 112.6 ($C^3$, Indole), 115.8 (d, $^2J_{CF}$ = 21.6 Hz, C$^{3/5}H$, F-Phe), 118.6 (C^7H, Indole), 119.4 (C^6H, Indole), 122.1 (C^5H, Indole), 122.5 (C^2H, Indole), 127.2 (C^{8a}, Indole), 130.3 ($^3J_{CF}$ = 8.3 Hz, $C^{2/6}$H, F-Phe), 136.4 (C^{3a}, Indole), 143.3 (C^2, Imdz), 145.1 (C^6H, Pyr), 158.0 (C^2, Pyr) ppm.

HPLC (Method 1): t_R = 3.9 min.

LC-MS (ESI, 70 eV): m/z = 444 $[MH]^+$, 301 $[MH\text{-}C_{10}H_9N]^+$, 144 $[C_{10}H_9N]^+$ (calc. m/z = 443).

***N*-(4-(5-(4-Fluorophenyl)-2-(methylthio)-1*H*-imidazol-4-yl)pyridin-2-yl)-*N'*,*N'*-dimethyl-propan-1,3-diamine (152)**

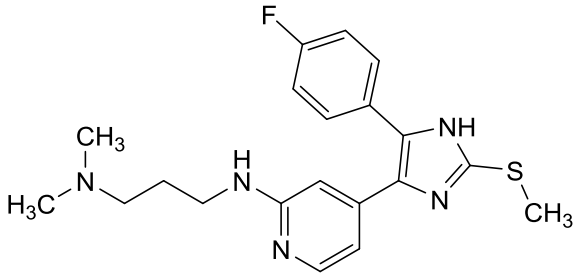

$C_{20}H_{24}FN_5S$ (M_r 385.51)

152 was synthesized according to the general procedure from **119** (400 mg, 1.32 mmol) and N^1,N^1-dimethylpropane-1,3-diamine (1.00 ml, 7.93 mmol). Purification was achieved by flash chromatography (SiO_2, 20-90 % ethyl acetate/petrol ether, then methanol) and subsequent filtration, to afford **152** as a yellow solid (100 % HPLC purity).

Yield: 175 mg (454 µmol, 35 %).

m.p.: 129 °C.

^{1}H NMR (300 MHz, $CDCl_3$): δ = 1.61 (t, ^3J = 6.8 Hz, 2 H, $CH_2CH_2CH_2$), 2.13 (s, 6 H, $N(CH_3)_2$), 2.29 (t, ^3J = 6.9 Hz, 2 H, $CH_2N(CH_3)_2$), 2.58 (s, 3 H, SCH_3), 3.11 (t, ^3J = 6.7 Hz, 2 H, CH_2NH), 5.22 (bs, 1 H, CH_2NH), 6.42-6.46 (m, 2 H, $C^{3/5}H$, Pyr), 6.95-7.01 (m, 2 H, $C^{3/5}H$, F-Phe), 7.35-7.39 (m, 2 H, $C^{2/6}H$, F-Phe), 7.78 (dd, ^3J = 5.4 Hz, ^5J = 0.6 Hz, 1 H, C^6H, Pyr) ppm.

^{13}C NMR (75 MHz, $CDCl_3$): δ = 16.5 (SCH_3), 26.7 ($CH_2CH_2CH_2$), 45.2 ($N(CH_3)_2$), 57.6 ($CH_2N(CH_3)_2$), 104.0 (C^3H, Pyr), 111.1 (C^5H, Pyr), 115.5 (d, $^2J_{CF}$ = 21.5 Hz, $C^{3/5}$H, F-Phe), 130.2 (d, $^3J_{CF}$ = 8.1 Hz, $C^{2/6}$H, F-Phe), 142.7 (C^2, Imdz), 147.9 (C^6H, Pyr), 159.2 (C^2, Pyr), 162.4 (d, $^1J_{CF}$ = 247.7 Hz, CF) ppm.

HPLC (Method 1): t_R = 1.9 min.

LC-MS (ESI, 70 eV): m/z = 386 $[MH]^+$, 301 $[MH\text{-}C_5H_{12}N]^+$ (calc. m/z = 385).

1-(4-(5-(4-Fluorophenyl)-2-(methylthio)-1*H*-imidazol-4-yl)pyridin-2-yl)-piperazine (153)

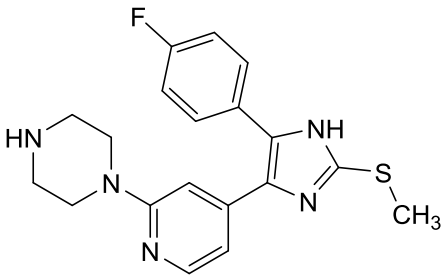

$C_{19}H_{20}FN_5S$ (M_r 369.46)

153 was synthesized according to the general procedure from **119** (300 mg, 989 µmol) and piperazine (341 mg, 3.96 mmol). Purification was achieved by flash chromatography (bas. Al_2O_3, 100 % methanol) to afford **153** as a yellow solid (100 % HPLC purity).

Yield: 63.0 mg (171 µmol, 17 %).

m.p.: 146 °C.

^{1}H NMR (300 MHz, DMSO-d_6): δ = 2.60 (bs, 3 H, SCH_3), 2.73 (t, ^3J = 4.5 Hz, 4 H, C$^{2/6}H_2$, Piperazine), 3.31 (t, ^3J = 4.6 Hz, 4 H, C$^{3/5}H_2$, Piperazine), 6.56 (d, ^3J = 5.1 Hz, 1 H, C^5H, Pyr), 6.80 (bs, 1 H, C^3H, Pyr), 7.20-7.26 (m, 2 H, C$^{3/5}H$, F-Phe), 7.47-7.51 (m, 2 H, C$^{2/6}H$, F-Phe), 7.97 (d, ^3J = 5.1 Hz, 1 H, C^6H, Pyr) ppm.

^{13}C NMR (75 MHz, DMSO-d_6): δ = 15.1 (SCH$_3$), 45.3 ($C^{2/6}$H$_2$, Piperazine), 45.8 ($C^{3/5}$H$_2$, Piperazine), 103.8 (C^3H, Pyr), 110.6 (C^5H, Pyr), 115.4 (d, $^2J_{CF}$ = 21.6 Hz, $C^{3/5}$H, F-Phe), 130.3 (d, $^3J_{CF}$ = 7.6 Hz, $C^{2/6}$H, F-Phe), 142.3 (C^2, Imdz), 147.6 (C^6H, Pyr), 159.6 (C^2, Pyr), 161.6 (d, $^1J_{CF}$ = 245.1 Hz, CF) ppm.

HPLC (Method 1): t_R = 2.9 min.

LC-MS (ESI, 70 eV): m/z = 370 [MH]$^+$, 327 [$C_{17}H_{16}FN_4S$]$^+$, 164 [$C_9H_{14}N_3$]$^+$ (calc. m/z = 369).

1-(4-(5-(4-Fluorophenyl)-2-(methylthio)-1*H*-imidazol-4-yl)pyridin-2-yl)-4-methyl-piperazine (154)

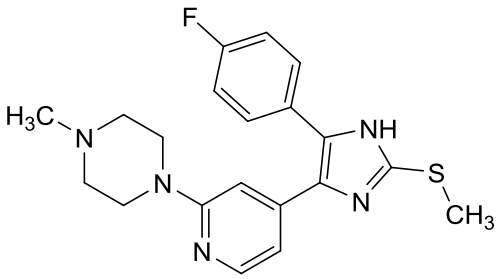

$C_{20}H_{22}FN_5S$ (M_r 383.49)

154 was synthesized according to the general procedure from **119** (400 mg, 1.32 mmol) and *N*-methylpiperazine (600 µl, 5.39 mmol). Purification was achieved by flash chromatography (RP-18, 20-90 % methanol/H_2O) to afford **154** as a pale yellow solid (95 % HPLC purity).

Yield: 115 mg (300 µmol, 23 %).

m.p.: 111 °C.

^{1}H NMR (300 MHz, $CDCl_3$): δ = 2.28 (s, 3 H, CH_3), 2.45 (t, ^3J = 4.8 Hz, 4 H, C$^{3/5}H_2$, Piperazine), 2.57 (s, 3 H, SCH_3), 3.40 (t, ^3J = 4.8 Hz, 4 H, C$^{2/6}H_2$, Piperazine), 6.54 (dd, ^3J = 5.3 Hz, ^4J = 1.1 Hz, 1 H, C^5H, Pyr), 6.73 (bs, 1 H, C^3H, Pyr), 6.91-6.97 (m, 2 H, C$^{3/5}H$, F-Phe), 7.32-7.37 (m, 2 H, C$^{2/6}H$, F-Phe), 7.94 (d, ^3J = 5.3 Hz, 1 H, C^6H, Pyr) ppm.

^{13}C NMR (75 MHz, $CDCl_3$): δ = 16.5 (SCH$_3$), 44.7 ($C^{2/6}H_2$, Piperazine), 45.6 (CH$_3$), 54.4 ($C^{3/5}H_2$, Piperazine), 104.9 (C^3H, Pyr), 111.9 (C^5H, Pyr), 115.7 (d, $^2J_{CF}$ = 21.6 Hz, $C^{3/5}$H, F-Phe), 128.2 (d, $^4J_{CF}$ = 4.1 Hz, C^1, F-Phe), 130.2 (d, $^3J_{CF}$ = 8.1 Hz, $C^{2/6}$H, F-Phe), 142.8 (C^2, Imdz), 147.9 (C^6H, Pyr), 159.6 (C^2, Pyr), 162.5 (d, $^1J_{CF}$ = 248.3 Hz, CF) ppm.

HPLC (Method 1): t_R = 2.8 min.

LC-MS (ESI, 70 eV): m/z = 384 $[MH]^+$, 327 $[C_{17}H_{16}FN_4S]^+$, 192 $[C_{10}H_8FNS]^+$, 177 $[C_{10}H_{15}N_3]^+$ (calc. m/z = 383).

1-(4-(5-(4-Fluorophenyl)-2-(methylthio)-1*H*-imidazol-4-yl)pyridin-2-yl)-4-phenyl-piperazine (155)

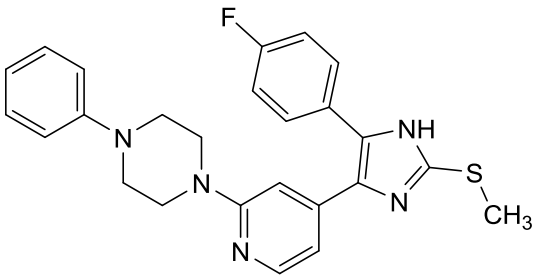

$C_{20}H_{22}FN_5S$ (M_r 445.56)

155 was synthesized according to the general procedure from **119** (400 mg, 1.32 mmol) and *N*-phenylpiperazine (800 µl, 5.23 mmol). The combined organic phases were extracted with 2 M aq. HCl solution, the aq. layer was neutralized with 2 M aq. KOH solution, and the pale yellow precipitate was collected by filtration, and purified by flash chromatography (SiO_2, 20-90 % ethyl acetate/petrol ether) to afford **155** as yellow crystals (100 % HPLC purity).

Yield: 291 mg (653 µmol, 50 %).

m.p.: 101 °C.

^{1}H NMR (300 MHz, $CDCl_3$): δ = 2.64 (s, 3 H, SC*H*$_3$), 3.19 (t, ^3J = 5.1 Hz, 4 H, C$^{2/6}$*H*$_2$, Piperazine), 3.58 (t, ^3J = 5.1 Hz, 4 H, C$^{3/5}$*H*$_2$, Piperazine), 6.64 (dd, ^3J = 5.4 Hz, ^4J = 1.2 Hz, 1 H, C^5*H*, Pyr), 6.93-6.85 (m, 4 H, C^3*H*, Pyr and C$^{2/4/6}$*H*, Phe), 6.99-7.05 (m, 2 H, C$^{3/5}$*H*, F-Phe), 7.26 (t, ^3J = 8.0 Hz, 2 H, C$^{3/5}$*H*, Phe), 7.39-7.44 (m, 2 H, C$^{2/6}$*H*, F-Phe), 8.00 (d, ^3J = 5.5 Hz, 1 H, C^6*H*, Pyr) ppm.

^{13}C NMR (75 MHz, $CDCl_3$): δ = 16.5 (S*C*H$_3$), 45.4 (*C*$^{2/6}$H$_2$, Piperazine), 49.0 (*C*$^{3/5}$H$_2$, Piperazine), 105.1 (*C*^{3}H, Pyr), 111.6 (*C*^{5}H, Pyr), 115.8 (d, $^2J_{CF}$ = 21.7 Hz, *C*$^{3/5}$H, F-Phe), 116.3 (*C*$^{2/6}$H, Phe), 120.2 (*C*^{4}H, Phe), 129.2 (*C*$^{3/5}$H, Phe), 130.3 (d, $^3J_{CF}$ = 8.1 Hz, *C*$^{2/6}$H, F-Phe), 143.0 (*C*^{2}, Imdz), 146.9 (*C*^{6}H, Pyr), 151.1 (*C*^{1}, Phe), 159.0 (*C*^{2}, Pyr), 162.6 (d, $^1J_{CF}$ = 248.5 Hz, *C*F) ppm.

HPLC (Method 1): t_R = 6.2 min.

LC-MS (ESI, 70 eV): *m*/*z* = 446 $[MH]^+$ (calc. *m*/*z* = 445).

3-(2,4-Dimethoxyphenyl)propionic acid (158)

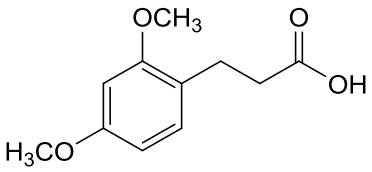

$C_{11}H_{14}FO_4$ (M_r 210.23)

2,4-Dimethoxycinnamic acid (100 mg, 471 µmol), one spatula of Pd/C 10 % and cyclohexene (0.2 ml) were dissolved in 5 ml methanol and the mixture was heated for 3 min to 95 °C in a microwave oven (100 W). After cooling to rt, the solids were filtered off and the solvent was removed under reduced pressure to afford **158** as a colorless solid (100 % HPLC purity).

Yield: 96.0 mg (457 µmol, 95 %) (Lit.[221]: n.d.).

^{1}H NMR (300 MHz, $CDCl_3$): δ = 2.60-2.65 (m, 2 H, CH_2CH_2COOH), 2.85-2.90 (m, 2 H, CH_2CH_2COOH), 3.79 (s, 3 H, C^4OCH_3), 3.80 (s, 3 H, C^2OCH_3), 6.41 (dd, ^3J = 8.1 Hz, ^4J = 2.4 Hz, 1 H, C^5H, $(OCH_3)_2$-Phe), 6.44 (d, ^4J = 2.4 Hz, 1 H, C^3H, $(OCH_3)_2$-Phe), 7.05 (dd, ^3J = 8.1 Hz, ^5J = 0.3 Hz, 1 H, C^6H, $(OCH_3)_2$-Phe), 10.30 (vbs, 1 H, COOH) ppm.

^{13}C NMR (75 MHz, $CDCl_3$): δ = 24.4 (CH_2CH_2COOH), 33.3 (CH_2CH_2COOH), 54.3 (C^4OCH_3), 54.5 (C^2OCH_3), 97.6 (C^3H, $(OCH_3)_2$-Phe), 103.0 (C^5H, $(OCH_3)_2$-Phe), 120.1 (C^1, $(OCH_3)_2$-Phe), 129.3 (C^6H, $(OCH_3)_2$-Phe), 157.5 (C^2OCH_3), 158.8 (C^4OCH_3), 178.7 (COOH) ppm.

HPLC (Method 2): t_R = 5.1 min.

3-(2,4-Dimethoxyphenyl)propan-1-ol (159)

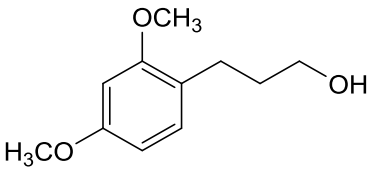

$C_{11}H_{16}O_3$ (M_r 196.25)

Under a nitrogen atmosphere a solution of lithium aluminum hydride (120 mg, 3.16 mmol) in 3 ml anhyd. THF was added dropwise to **158** (508 mg, 2.42 mmol) in 6 ml anhyd. THF at rt with intense stirring that continued for 1 h at the same temp. After completion, the reaction was cooled down in an ice-bath and quenched by successive addition of H_2O (120 µl), 15 % aq. NaOH solution (120 µl), and H_2O (360 µl). The precipitate was filtered off, washed with THF, and the filtrate was concentrated under reduced pressure. The crude product was purified by flash chromatography (SiO_2, 20-30 % ethyl acetate/petrol ether) to afford **159** as colorless oil (97 % HPLC purity).

Yield: 457 mg (2.33 mmol, 96 %) (Lit.[221]: n.d.).

^{1}H NMR (300 MHz, $CDCl_3$): δ = 1.78-1.83 (m, 2 H, $CH_2CH_2CH_2OH$), 2.65 (t, ^3J = 7.3 Hz, 2 H, $CH_2CH_2CH_2OH$), 3.59 (t, ^3J = 6.3 Hz, 1 H, $CH_2CH_2CH_2OH$), 3.78 (s, 1 H, O*H*), 3.79 (s, 3 H, C^4OCH_3), 3.81 (s, 3 H, C^2OCH_3), 6.42-6.46 (m, 2 H, $C^{3/5}H$, $(OCH_3)_2$-Phe), 7.03 (dd, ^3J = 7.7 Hz, ^5J = 0.6 Hz, 1 H, C^6H, $(OCH_3)_2$-Phe) ppm.

^{13}C NMR (75 MHz, $CDCl_3$): δ = 25.4 ($CH_2CH_2CH_2OH$), 33.2 ($CH_2CH_2CH_2OH$), 55.5 ($C^{2/4}OCH_3$), 62.1 ($CH_2CH_2CH_2OH$), 98.6 (C^3H, $(OCH_3)_2$-Phe), 104.3 (C^5H, $(OCH_3)_2$-Phe), 122.4 (C^1, $(OCH_3)_2$-Phe), 130.4 (C^6H, $(OCH_3)_2$-Phe), 158.3 (C^2OCH_3), 159.3 (C^4OCH_3) ppm.

HPLC (Method 2): t_R = 5.0 min.

1-(3-Bromopropyl)-2,4-dimethoxybenzene (156)

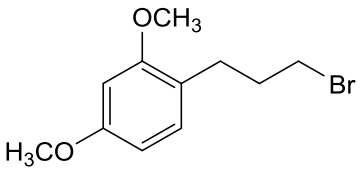

$C_{11}H_{15}BrO$ (M_r 259.14)

To an ice-cold solution of **159** (260 mg, 1.33 mmol) in 4 ml anhyd. DCM, triphenylphosphine (412 mg, 1.57 mmol) and *N*-bromosuccinimide (263 mg, 1.48 mmol) were added under a nitrogen atmosphere and the reaction was stirred for 2 h at the same temp. The mixture was washed with H_2O and sat. aq. NaCl solution, dried over anhyd. Na_2SO_4, and the solvent was removed under reduced pressure. Diethyl ether was added, the precipitate filtered off, and the filtrate was concentrated and purified by flash chromatography (SiO_2, 2-10 % ethyl acetate/petrol ether) to afford **156** as colorless oil (95 % HPLC purity).

Yield: 205 mg (791 µmol, 60 %) (Lit.[222]: 76 %).

^{1}H NMR (300 MHz, $CDCl_3$): δ = 2.11 (quint, ^3J = 5.6 Hz, 2 H, $CH_2CH_2CH_2Br$), 2.70 (t, ^3J = 7.2 Hz, 2 H, $CH_2CH_2CH_2Br$), 3.39 (t, ^3J = 6.8 Hz, 2 H, $CH_2CH_2CH_2Br$), 3.80 (s, 6 H, $C^{2/4}OCH_3$), 6.42 (dd, ^3J = 8.0 Hz, ^4J = 2.5 Hz, 1 H, C^5H, $(OCH_3)_2$-Phe), 6.45 (d, ^4J = 2.3 Hz, 1 H, C^3H, $(OCH_3)_2$-Phe), 7.05 (dd, ^3J = 8.0 Hz, ^5J = 0.5 Hz, 1 H, C^6H, $(OCH_3)_2$-Phe) ppm.

^{13}C NMR (75 MHz, $CDCl_3$): δ = 28.4 ($CH_2CH_2CH_2Br$), 33.0 ($CH_2CH_2CH_2Br$), 33.9 ($CH_2CH_2CH_2Br$), 55.3 (C^4OCH_3), 55.5 (C^2OCH_3), 98.7 (C^3H, $(OCH_3)_2$-Phe), 103.9 (C^5H, $(OCH_3)_2$-Phe), 121.4 (C^1, $(OCH_3)_2$-Phe), 130.5 (C^6H, $(OCH_3)_2$-Phe), 158.5 (C^2OCH_3), 159.6 (C^4OCH_3) ppm.

HPLC (Method 2): t_R = 6.5 min.

***tert*-Butyl benzyl(4-methylpyridin-2-yl)carbamate (161)**

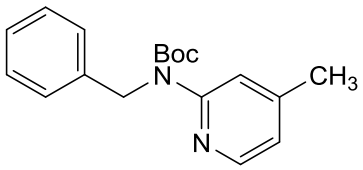

$C_{18}H_{22}N_2O_2$ (M_r 298.39)

A suspension of sodium hydride (1.30 g 60 % dispersion in mineral oil, 31.3 mmol) in 50 ml anhyd. DMF was added dropwise to a stirred solution of **132** (5.20 g, 25.0 mmol) in 57 ml anhyd. DMF at 0 °C under a nitrogen atmosphere, whereupon the temp. had to stay below 5 °C. The mixture was stirred for 20 min at 0 °C before benzyl bromide (3.40 ml, 28.8 mmol) was slowly added dropwise and stirring continued at the same temp. for 30 min. The mixture was allowed to reach rt over 1 h and stirring continued for another 1 h. The reaction was quenched by addition of H_2O and extracted with ethyl acetate. The organic phase was washed with sat. aq. $NaHCO_3$ solution and sat. aq. NaCl solution, dried over anhyd. Na_2SO_4, and the solvent was removed under reduced pressure. The crude product was purified by flash chromatography (SiO_2, 10-25 % ethyl acetate/petrol ether) to afford **161** as a colorless solid (100 % HPLC purity).

Yield: 6.62 g (22.2 mmol, 87 %).

^{1}H NMR (300 MHz, $CDCl_3$): δ = 1.43 (s, 9 H, ^{t}Bu), 2.37 (s, 3 H, CH_3), 5.23 (s, 2 H, CH_2, Bn), 6.89 (dd, ^3J = 5.1 Hz, ^4J = 0.7 Hz, 1 H, C^5*H*, Pyr), 7.21-7.29 (m, 5 H, ^{ar}C*H*, Bn), 7.54 (bs, 1 H, C^3*H*, Pyr), 8.23 (d, ^3J = 5.2 Hz, 1 H, C^6*H*, Pyr) ppm.

^{13}C NMR (75 MHz, $CDCl_3$): δ = 21.4 (*C*H_3), 28.3 (C(*C*H_3)$_3$), 50.3 (*C*H_2, Bn), 81.5 (*C*(CH$_3$)$_3$), 120.5 (*C*^{3}H, Pyr), 121.1 (s, *C*^{5}H, Pyr), 126.9 (s, ^{ar}*C*^{4}H, Bn), 127.3 (^{ar}*C*$^{2/6}$H, Bn), 128.3 (^{ar}*C*$^{3/5}$H, Bn), 139.5 (^{ar}*C*^{1}, Bn), 146.9 (*C*^{6}H, Pyr), 149.0 (*C*^{4}, Pyr), 154.3 (*C*O) ppm.

IR (ATR): $\tilde{\nu}$ = 2990, 1701, 1595, 1559, 1495, 1451, 1377, 1366, 1289, 1269, 1240, 1153, 1138, 1105, 1074, 1063, 990, 955, 893, 883, 858, 822, 795, 774, 748, 733, 708 cm^{-1}.

HPLC (Method 1): t_R = 6.9 min.

LC-MS (ESI, 70 eV): m/z = 299 [MH]$^+$, 243 [MH$_2$-^{t}Bu]$^+$ (calc. m/z = 298).

3-(2,4-Dimethoxyphenyl)-*N*-(4-methylpyridin-2-yl)propanamide (171)

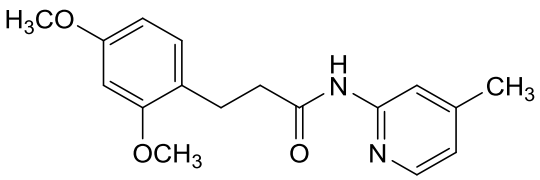

$C_{17}H_{20}N_2O_3$ (M_r 300.36)

3-(2,4-Dimethoxyphenyl)propionic acid (600 mg, 2.85 mmol), PyBOP (1.78 g, 3.42 mmol), and DIPEA (1.49 ml, 8.53 mmol) were stirred in 10 ml anhyd. DMF at rt under a nitrogen atmosphere before 2-amino-4-methylpyridine (430 mg, 3.98 mmol) was added in one portion. The reaction was stirred for 12 h at 110 °C, quenched by addition of H_2O, cooled to rt, and extracted with ethyl acetate. The combined organic phases were washed with H_2O and sat. aq. NaCl solution, dried over anhyd. Na_2SO_4, and the solvent was removed under reduced pressure. The crude product was purified by flash chromatography (SiO_2, 20-40 % ethyl acetate/petrol ether and RP-18, 50-100 % methanol/H_2O) to afford **171** as a colorless solid (100 % HPLC purity).

Yield: 248 mg (826 µmol, 29 %).

m.p.: 87 °C.

^{1}H NMR (300 MHz, $CDCl_3$): δ = 2.36 (s, 3 H, CH_3), 2.63 (t, ^3J = 7.6 Hz, 2 H, CH_2CH_2CONH), 2.96 (t, ^3J = 7.7 Hz, 2 H, CH_2CH_2CONH), 3.77 (s, 3 H, C^{4}OCH_3), 3.78 (s, 3 H, C^{2}OCH_3), 6.39 (dd, ^3J = 8.1 Hz, ^4J = 2.5 Hz, 1 H, C^5H, $(OCH_3)_2$-Phe), 6.43 (d, ^4J = 2.4 Hz, 1 H, C^3H, $(OCH_3)_2$-Phe), 6.83 (dq, ^3J = 5.1 Hz, ^4J = 0.7 Hz, 1 H, C^5H, Pyr), 7.06 (d, ^3J = 8.1 Hz, 1 H, C^6H, $(OCH_3)_2$-Phe), 8.07 (dd, ^3J = 5.3 Hz, ^5J = 0.4 Hz, 1 H, C^6H, Pyr), 8.09 (bs, 1 H, C^3H, Pyr), 8.46 (vbs, 1 H, NH) ppm.

^{13}C NMR (75 MHz, $CDCl_3$): δ = 21.5 (CH$_3$), 26.0 (CH$_2$CH$_2$CONH), 38.2 (CH$_2C$H$_2$CONH), 55.3 (COCH$_3$), 55.5 (COCH$_3$), 98.6 (C^3H, $(OCH_3)_2$-Phe), 104.1 (C^5H, $(OCH_3)_2$-Phe), 114.7 (C^3H, Pyr), 120.9 (C^5H, Pyr), 121.2 (C^1, $(OCH_3)_2$-Phe), 130.4 (C^6H, $(OCH_3)_2$-Phe), 147.1 (C^6H, Pyr), 150.2 (C^4, Pyr), 151.6 (C^2, Pyr), 158.4 (C^2OCH$_3$), 159.7 (C^4OCH$_3$), 171.7 (CO) ppm.

HPLC (Method 2): t_R = 4.8 min.

LC-MS (ESI, 70 eV): m/z = 301 $[MH]^+$ (calc. m/z = 300).

***N*-(3-(2,4-Dimethoxyphenyl)propyl)-4-methylpyridin-2-amine (172)**

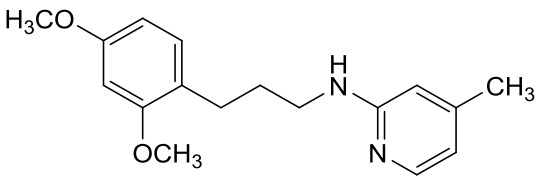

$C_{17}H_{22}N_2O_2$ (M_r 286.38)

172 was synthesized according to the procedure for **159** from **171** (500 mg, 1.67 mmol) in 5 ml anhyd. THF and lithium aluminum hydride solution (78.0 mg, 2.06 mmol in 2 ml anhyd. THF). The crude product was purified by flash chromatography (SiO_2, 20-40 % ethyl acetate/petrol ether and RP-18, 50-100 % methanol/H_2O) to afford **172** as a colorless crystalline solid (100 % purity, HPLC).

Yield: 133 mg (464 µmol, 28 %).

m.p.: 88 °C.

^{1}H NMR (300 MHz, $CDCl_3$): δ = 1.87 (quint, ^3J = 7.2 Hz, 2 H, $CH_2CH_2CH_2NH$), 2.22 (s, 3 H, CH_3), 2.65 (t, ^3J = 7.5 Hz, 2 H, $CH_2CH_2CH_2NH$), 3.23 (q, ^3J = 6.5 Hz, 2 H, $CH_2CH_2CH_2NH$), 3.79 (s, 6 H, 2 OCH_3), 4.59 (m, 1 H, NH), 6.15-6.16 (m, 1 H, C^3H, Pyr), 6.38-6.41 (m, 1 H, C^5H, Pyr), 6.42 (dd, ^3J = 8.1 Hz, ^4J = 2.5 Hz, 1 H, C^5H, $(OCH_3)_2$-Phe), 6.45 (d, ^4J = 2.3 Hz, 1 H, C^3H, $(OCH_3)_2$-Phe), 7.03 (d, ^3J = 8.0 Hz, 1 H, C^6H, $(OCH_3)_2$-Phe), 7.93 (d, ^3J = 5.2 Hz, 1 H, C^6H, Pyr) ppm.

^{13}C NMR (75 MHz, $CDCl_3$): δ = 21.4 (CH_3), 27.1 ($CH_2CH_2CH_2NH$), 29.9 ($CH_2CH_2CH_2NH$), 41.9 ($CH_2CH_2CH_2NH$), 55.4 (OCH_3), 55.5 (OCH_3), 98.6 (C^3H, $(OCH_3)_2$-Phe), 104.0 (C^5H, $(OCH_3)_2$-Phe), 106.7 (C^3H, Pyr), 114.3 (C^5H, Pyr), 122.5 (C^1, $(OCH_3)_2$-Phe), 130.2 (C^6H, $(OCH_3)_2$-Phe), 147.8 (C^6H, Pyr), 148.6 (C^4, Pyr), 158.4 (C^2OCH_3), 159.3 (C^2, Pyr), 159.4 (C^4OCH_3) ppm.

HPLC (Method 2): t_R = 4.2 min.

LC-MS (ESI, 70 eV): m/z = 287 $[MH]^+$ (calc. m/z = 286).

***tert*-Butyl (3-(2,4-dimethoxyphenyl)propyl)(4-methylpyridin-2-yl)carbamate (167)**

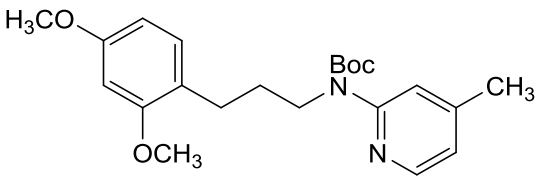

$C_{22}H_{30}N_2O_4$ (M_r 386.49)

Method A. **132** (138 mg, 663 µmol) was dissolved in 1.5 ml anhyd. DMF at 0 °C under a nitrogen atmosphere before sodium hydride (39.0 mg 60 % dispersion in mineral oil, 975 µmol) in 2 ml anhyd. DMF was slowly added whereas the temp. was kept below 5 °C. The mixture was stirred at the same temp. for 20 min, **156** (144 mg, 556 µmol) in 3 ml anhyd. DMF was added, and stirring continued for another 30 min at 0 °C. The reaction was allowed to reach rt over 1 h, stirred for another 1 h, and quenched with H_2O. The mixture was extracted with ethyl acetate, washed with 0.1 M aq. HCl, sat. aq. $NaHCO_3$ solution, and sat. aq. NaCl solution, dried over anhyd. Na_2SO_4, and the solvent was removed under reduced pressure to afford **167** as pale yellowish oil (100 % HPLC purity).

Yield: 202 mg (523 µmol, 94 %).

Method B. A solution of **172** (120 mg, 419 µmol), Boc_2O (134 mg, 614 µmol) and 4-DMAP (30.0 mg, 246 µmol) in anhyd. THF was stirred for 24 h at rt. The solvent was removed under reduced pressure, the residue was resuspended in ethyl acetate, washed with H_2O and sat. aq. NaCl solution, and dried over anhyd. Na_2SO_4. The solvent was removed under reduced pressure and the crude product was purified by flash chromatography (SiO_2, 10-40 % ethyl acetate/petrol ether) to afford **167** as colorless oil (100 % HPLC purity)

Yield: 109 mg (282 µmol, 67 %).

^{1}H NMR (300 MHz, $CDCl_3$): δ = 1.48 (s, 9 H, ^{t}Bu), 1.79-1.90 (m, 2 H, $CH_2CH_2CH_2NR_2$), 2.33 (s, 3 H, CH_3), 2.54 (t, ^3J = 7.8 Hz, 2 H, $CH_2CH_2CH_2NR_2$), 3.75 (s, 3 H, C^2OCH_3), 3.77 (s, 3 H, C^4OCH_3), 3.95 (t, ^3J = 7.4 Hz, 2 H, $CH_2CH_2CH_2NR_2$), 6.38 (dd, ^3J = 8.0 Hz, ^4J = 2.5 Hz, 1 H, C^5H, $(OCH_3)_2$-Phe), 6.41 (d, ^4J = 2.3 Hz, 1 H, C^3H, $(OCH_3)_2$-Phe), 6.83 (dq, ^3J = 5.1 Hz, ^4J = 0.7 Hz, 1 H, C^5H, Pyr), 6.99 (dd, ^3J = 8.0 Hz, ^5J = 0.3 Hz, 1 H, C^6H, $(OCH_3)_2$-Phe), 7.39 (m, 1 H, C^3H, Pyr), 8.23 (dd, ^3J = 5.1 Hz, ^5J = 0.5 Hz, 1 H, C^6H, Pyr) ppm.

^{13}C NMR (75 MHz, $CDCl_3$): δ = 21.2 ($\mathit{C}H_3$), 27.1 ($\mathit{C}H_2CH_2CH_2NR_2$), 28.4 ($C(\mathit{C}H_3)_3$), 29.2 ($CH_2\mathit{C}H_2CH_2NR_2$), 47.0 ($CH_2CH_2\mathit{C}H_2NR_2$), 55.3 ($C^2O\mathit{C}H_3$), 55.5 ($C^4O\mathit{C}H_3$), 80.7 ($\mathit{C}(CH_3)_3$), 98.5 ($\mathit{C}^3$H, $(OCH_3)_2$-Phe), 103.8 (C^5H, $(OCH_3)_2$-Phe), 121.0 (C^5H, Pyr), 121.0 (C^3H, Pyr), 122.9 (C^1, $(OCH_3)_2$-Phe), 129.9 (C^6H, $(OCH_3)_2$-Phe), 147.4 (C^6H, Pyr), 148.1 (C^4, Pyr), 154.5 ($\mathit{C}O$), 154.9 (C^2, Pyr), 158.4 (C^2OCH_3), 159.2 (C^4OCH_3) ppm.

HPLC (Method 2): t_R = 6.6 min.

LC-MS (ESI, 70 eV): m/z = 387 $[MH]^+$, 331$[MH_2$-^{t}Bu$]^+$, 287 $[MH_2$-Boc$]^+$ (calc. m/z = 386).

tert-Butyl benzyl(4-(2-(4-fluorophenyl)-2-oxoethyl)pyridin-2-yl)carbamate (163)

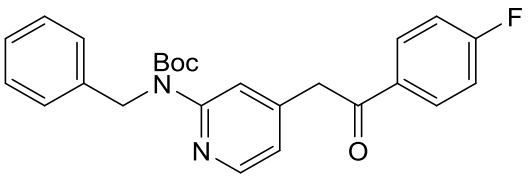

$C_{25}H_{25}FN_2O_3$ (M_r 420.48)

163 was synthesized according to the procedure for **123** from **161** (6.38 g, 21.4 mmol), ethyl 4-fluorobenzoate (6.28 ml, 42.8 mmol) in 26 ml anhyd. THF, and NaHMDS (21.4 ml 2 M solution in THF, 42.8 mmol), but required further purification by flash chromatography (SiO_2, 5-20 % ethyl acetate/petrol ether). **163** was obtained as a colorless solid (98 % HPLC purity).

Yield: 8.40 g (20.0 mmol, 93 %).

^{1}H NMR (300 MHz, $CDCl_3$): δ = 1.30 (s, 9 H, ^{t}Bu), 4.16 (s, 2 H, CH_2), 5.11 (s, 2 H, CH_2, Bn), 6.83 (dd, ^3J = 5.1 Hz, ^4J = 1.5 Hz, 2 H, C^5H, Pyr), 7.02-7.19 (m, 7 H, ^{ar}CH, Bn and C$^{3/5}H$, F-Phe), 7.60 (d, ^5J = 0.6 Hz, 1 H, C^3H, Pyr), 7.90-7.95 (m, 2 H, C$^{2/6}H$, F-Phe), 8.23 (dd, ^3J = 5.1 Hz, ^5J = 0.6 Hz, 1 H, C^6H, Pyr) ppm.

^{13}C NMR (75 MHz, $CDCl_3$): δ = 28.2 (C(CH$_3$)$_3$), 44.9 (CH$_2$), 50.2 (CH$_2$, Bn), 81.5 (C(CH$_3$)$_3$), 116.0 (d, $^2J_{CF}$ = 22.0 Hz, $C^{3/5}$H, F-Phe), 120.2 (C^3H, Pyr), 120.7 (C^5H, Pyr), 126.8 ($^{ar}C^4$H, Bn), 127.3 ($^{ar}C^{2/6}$H, Bn), 128.2 ($^{ar}C^{3/5}$H, Bn), 131.3 (d, $^3J_{CF}$ = 9.4 Hz, $C^{2/6}$H, F-Phe), 132.8 (d, $^4J_{CF}$ = 3.0 Hz, C^1, F-Phe), 139.6 ($^{ar}C^1$, Bn), 144.5 (C^4, Pyr), 147.7 (C^6H, Pyr), 154.3 (C^2, Pyr), 154.9 (COO^{t}Bu), 166.0 (d, $^1J_{CF}$ = 255.5 Hz, CF), 194.5 (CO) ppm.

HPLC (Method 1): t_R = 7.2 min.

LC-MS (ESI, 70 eV): m/z = 421 [MH]$^+$, 365 [MH$_2$-^{t}Bu]$^+$ (calc. m/z = 420).

***tert*-Butyl (3-(2,4-dimethoxyphenyl)propyl)(4-(2-(4-fluorophenyl)-2-oxoethyl)pyridin-2-yl)carbamate (168)**

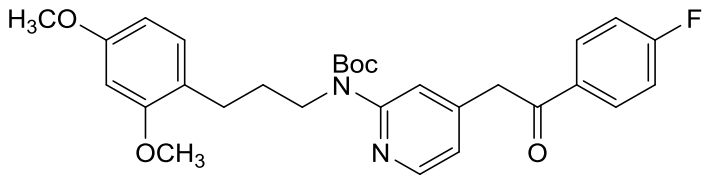

$C_{29}H_{33}FN_2O_5$ (M_r 508.59)

168 was synthesized according to the procedure for **123** from **167** (202 mg, 517 µmol), ethyl 4-fluorobenzoate (200 µl, 1.36 mmol) in 3 ml anhyd. THF, and NaHMDS (500 µl 2 M solution in THF, 1.00 mmol), but required further purification by flash chromatography (SiO_2, 5-35 % ethyl acetate/petrol ether). **168** was obtained as yellow oil (100 % HPLC purity).

Yield: 126 mg (249 µmol, 48 %).

^{1}H NMR (300 MHz, $CDCl_3$): δ = 1.47 (s, 9 H, ^{t}Bu), 1.85-1.90 (m, 2 H, $CH_2CH_2CH_2NR_2$), 2.55 (t, ^3J = 7.7 Hz, 2 H, $CH_2CH_2CH_2NR_2$), 3.75 (s, 3 H, C^2OCH_3), 3.77 (s, 3 H, C^4OCH_3), 3.97 (t, ^3J = 7.5 Hz, 2 H, $CH_2CH_2CH_2NR_2$), 4.24 (s, 2 H, CH_2), 6.38 (dd, ^3J = 8.0 Hz, ^4J = 2.5 Hz, 1 H, C^5H, $(OCH_3)_2$-Phe), 6.41 (d, ^4J = 2.3 Hz, 1 H, C^3H, $(OCH_3)_2$-Phe), 6.90 (dd, ^3J = 5.1 Hz, ^4J = 1.5 Hz, 1 H, C^5H, Pyr), 6.99 (d, ^3J = 8.1 Hz, 1 H, C^6H, $(OCH_3)_2$-Phe), 7.10-7.16 (m, 2 H, $C^{3/5}H$, F-Phe), 7.57 (bs, 1 H, C^6H, Pyr), 7.99-8.04 (m, 2 H, $C^{2/6}H$, F-Phe), 8.32 (dd, ^3J = 5.1 Hz, ^5J = 0.6 Hz, 1 H, C^6H, Pyr) ppm.

^{13}C NMR (75 MHz, $CDCl_3$): δ = 27.1 ($CH_2CH_2CH_2NR_2$), 28.4 ($C(CH_3)_3$), 29.2 ($CH_2CH_2CH_2NR_2$), 44.9 (CH_2), 47.0 ($CH_2CH_2CH_2NR_2$), 55.3 (C^2OCH_3), 55.5 (C^4OCH_3), 81.0 ($C(CH_3)_3$), 98.5 (C^3H, $(OCH_3)_2$-Phe), 103.8 (C^5H, $(OCH_3)_2$-Phe), 116.1 (d, $^2J_{CF}$ = 22.0 Hz, $C^{3/5}H$, F-Phe), 120.6 (C^5H, Pyr), 120.8 (C^6H, Pyr), 122.8 (C^1, $(OCH_3)_2$-Phe), 129.9 (C^6H, $(OCH_3)_2$-Phe), 131.3 (d, $^3J_{CF}$ = 9.4 Hz, $C^{2/6}H$, F-Phe), 132.8 (d, $^4J_{CF}$ = 2.9 Hz, C^1, F-Phe), 144.3 (C^4, Pyr), 147.6 (C^3H, Pyr), 154.3 (COO^tBu), 155.1 (C^2, Pyr), 158.4 (C^2OCH_3), 159.2 (C^4OCH_3), 166.1 (d, $^1J_{CF}$ = 255.7 Hz, CF), 194.5 (CO) ppm.

HPLC (Method 2): t_R = 6.8 min.

LC-MS (ESI, 70 eV): m/z = 509 $[MH]^+$, 453 $[MH_2\text{-}^t Bu]^+$ (calc. m/z = 508).

tert-Butyl benzyl(4-(2-(4-fluorophenyl)-1-(hydroxyimino)-2-oxoethyl)pyridin-2-yl)-carbamate (165)

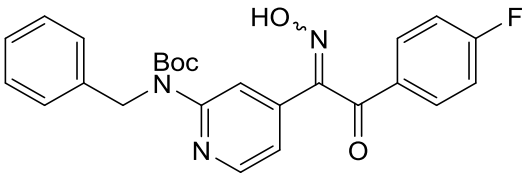

$C_{25}H_{24}FN_3O_4$ (M_r 449.48)

165 was synthesized according to the procedure for **124** from **163** (8.40 g, 20.0 mmol) in 95 ml glacial acetic acid, and sodium nitrite (4.17 g, 60.4 mmol in 23 ml H_2O). **165** was obtained as a pale beige solid (97 % HLC purity).

Yield: 8.61 g (19.2 mmol, 96 %).

^{1}H NMR (300 MHz, $CDCl_3$): δ = 1.35 (s, 9 H, ^{t}Bu), 5.17 (s, 2 H, CH_2, Bn), 7.09 (dd, ^3J = 5.3 Hz, ^4J = 1.5 Hz, 1 H, C^5*H*, Pyr), 7.12-7.24 (m, 7 H, ^{ar}C*H*, Bn and C$^{3/5}$*H*, F-Phe), 7.87 (bs, 1 H, C^3*H*, Pyr), 7.91-7.95 (m, 2 H, C$^{2/6}$*H*, F-Phe), 8.35 (dd, ^3J = 5.3 Hz, ^5J = 0.7 Hz, 1 H, C^6*H*, Pyr), 9.09 (bs, 1 H, NO*H*) ppm.

^{13}C NMR (75 MHz, $CDCl_3$): δ = 28.2 (C(*C*H$_3$)$_3$), 50.4 (*C*H$_2$, Bn), 82.5 (*C*(CH$_3$)$_3$), 116.2 (*C*^{3}H, Pyr), 116.4 (*C*^{5}H, Pyr), 116.6 (d, $^2J_{CF}$ = 22.3 Hz, *C*$^{3/5}$H, F-Phe), 127.1 (^{ar}*C*^{4}H, Bn), 127.3 (^{ar}*C*$^{2/6}$H, Bn), 128.4 (^{ar}*C*$^{3/5}$H, Bn), 131.1 (d, $^4J_{CF}$ = 3.1 Hz, *C*^{1}, F-Phe), 132.4 (d, $^3J_{CF}$ = 9.7 Hz, *C*$^{2/6}$H, F-Phe), 138.8 (^{ar}*C*^{1}, Bn), 140.6 (*C*^{4}, Pyr), 147.7 (*C*^{6}H, Pyr), 154.0 (*C*NOH), 154.4 (*C*^{2}, Pyr), 154.8 (*C*OO^{t}Bu), 167.0 (d, $^1J_{CF}$ = 258.0 Hz, *C*F), 191.8 (*C*O) ppm.

HPLC (Method 1): t_R = 7.1 min.

LC-MS (ESI, 70 eV): m/z = 450 [MH]$^+$, 394 [MH-^{t}Bu]$^+$ (calc. m/z = 449).

***tert*-Butyl (3-(2,4-dimethoxyphenyl)propyl)(4-(2-(4-fluorophenyl)-1-(hydroxyimino)-2-oxoethyl)pyridin-2-yl)carbamate (169)**

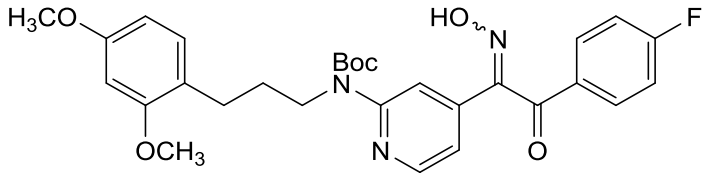

$C_{29}H_{32}FN_3O_6$ (M_r 537.59)

169 was synthesized according to the procedure for **124** from **168** (110 mg, 216 µmol) in 3 ml glacial acetic acid, and sodium nitrite (45.0 mg, 652 µmol in 0.5 ml H_2O). **169** was obtained as brownish oil (98 % HPLC purity).

Yield: 114 mg (212 µmol, quant.).

^{1}H NMR (300 MHz, $CDCl_3$): δ = 1.41 (s, 9 H, ^{t}Bu), 1.81-1.86 (m, 2 H, $CH_2CH_2CH_2CH_2NR_2$), 2.52 (t, ^3J = 7.7 Hz, 2 H, $CH_2CH_2CH_2NR_2$), 3.73 (s, 3 H, C^2OCH_3), 3.77 (s, 3 H, C^4OCH_3), 3.94 (t, ^3J = 7.4 Hz, 2 H, $CH_2CH_2CH_2NR_2$), 6.37 (dd, ^3J = 8.1 Hz, ^4J = 2.5 Hz, 1 H, C^5H, $(OCH_3)_2$-Phe), 6.40 (d, ^4J = 2.3 Hz, 1 H, C^3H, $(OCH_3)_2$-Phe), 6.96 (d, ^3J = 8.1 Hz, 1 H, C^6H, $(OCH_3)_2$-Phe), 7.09 (dd, ^3J = 5.3 Hz, ^4J = 1.5 Hz, 1 H, C^5H, Pyr), 7.12-7.18 (m, 2 H, $C^{3/5}H$, F-Phe), 7.77 (bs, 1 H, C^3H, Pyr), 7.93-7.98 (m, 2 H, $C^{2/6}H$, F-Phe), 8.35 (dd, ^3J = 5.3 Hz, ^5J = 0.8 Hz, 1 H, C^6H, Pyr), 9.01 (vbs, 1 H, CNO*H*) ppm.

^{13}C NMR (75 MHz, $CDCl_3$): δ = 27.0 ($CH_2CH_2CH_2NR_2$), 28.3 ($C(CH_3)_3$), 29.1 ($CH_2CH_2CH_2NR_2$), 47.2 ($CH_2CH_2CH_2NR_2$), 55.3 (C^2OCH_3), 55.5 (C^4OCH_3), 81.5 ($C(CH_3)_3$), 98.6 (C^3H, $(OCH_3)_2$-Phe), 103.9 (C^5H, $(OCH_3)_2$-Phe), 116.2 (C^5H, Pyr), 116.6 (d, $^2J_{CF}$ = 22.4 Hz, $C^{3/5}$H, F-Phe), 116.8 (C^3H, Pyr), 122.7 (C^1, $(OCH_3)_2$-Phe), 129.9 (C^6H, $(OCH_3)_2$-Phe), 131.2 (d, $^4J_{CF}$ = 2.9 Hz, C^1, F-Phe), 132.4 (d, $^3J_{CF}$ = 9. 8 Hz, $C^{2/6}$H, F-Phe), 139.8 (C^4, Pyr), 148.3 (C^6H, Pyr), 154.1 (COO^tBu), 154.8 (*C*NOH), 155.5 (C^2, Pyr), 158.4 (C^2OCH_3), 159.2 (C^4OCH_3), 166.9 (d, $^1J_{CF}$ = 258.0 Hz, *C*F), 191.8 (*C*O) ppm.

HPLC (Method 2): t_R = 6.8 min.

LC-MS (ESI, 70 eV): m/z = 538 $[MH]^+$, 482 $[MH_2\text{-}^t Bu]^+$ (calc. m/z = 537).

1-(2-(Benzyl(*tert*-butoxycarbonyl)amino)pyridin-4-yl)-2-(4-fluorophenyl)-2-oxoethan-1-aminium chloride (166)

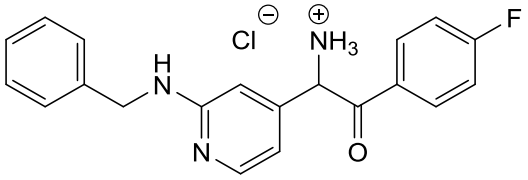

$C_{20}H_{19}ClFN_3O$ (M_r 371.84)

166 was synthesized according to the procedure for **125** from **165** (8.18 g, 18.2 mmol) in 34 ml 2-propanol and 66 ml HCl-sat. 2-propanol, and Pd/C 10 % (1.4 g). Recrystallization from diethyl ether afforded **166** as a beige solid (100 % HPLC purity).

Yield: 6.49 g (17.5 mmol, 96 %).

^{1}H NMR (300 MHz, DMSO-d_6): δ = 4.65 (s, 2 H, CH_2, Bn), 6.52 (s, 1 H, C*H*), 6.98 (dd, ^3J = 6.5 Hz, ^4J = 1.4 Hz, 1 H, C^5*H*, Pyr), 7.28-7.41 (m, 9 H, ^{ar}C*H*, Bn and N*H* and C^3*H*, Pyr and C$^{3/5}$*H*, F-Phe), 8.02 (d, ^3J = 6.5 Hz, 1 H, C^6*H*, Pyr), 8.14-8.19 (m, 2 H, C$^{2/6}$*H*, F-Phe), 9.36 (bs, 3 H, NH_3^+) ppm.

^{13}C NMR (75 MHz, DMSO-d_6): δ = 45.2 (*C*H_2, Bn), 56.6 (*C*NH_3^+), 111.3 (*C*^{5}H, Pyr), 113.2 (*C*^{3}H, Pyr), 116.4 (d, $^2J_{CF}$ = 22.3 Hz, *C*$^{3/5}$H, F-Phe), 127.6 (^{ar}*C*^{4}H, Bn), 127.8 (^{ar}*C*$^{2/6}$H, Bn), 128.5 (^{ar}*C*$^{3/5}$H, Bn), 129.6 (d, $^4J_{CF}$ = 2.7 Hz, *C*^{1}, F-Phe), 132.4 (d, $^3J_{CF}$ = 9.7 Hz, *C*$^{2/6}$H, F-Phe), 136.7 (^{ar}*C*^{1}, Bn), 138.6 (*C*^{6}H, Pyr), 146.9 (*C*^{4}, Pyr), 153.0 (*C*^{2}, Pyr), 165.8 (d, $^1J_{CF}$ = 255.0 Hz, *C*F), 190.7 (*C*O) ppm.

HPLC (Method 1): t_R = 3.4 min.

LC-MS (ESI, 70 eV): m/z = 336 [M-Cl]$^+$ (calc. m/z = 371).

1-(2-((3-(2,4-Dimethoxyphenyl)propyl)amino)pyridin-4-yl)-2-(4-fluorophenyl)-2-oxoethan-1-aminium chloride (170)

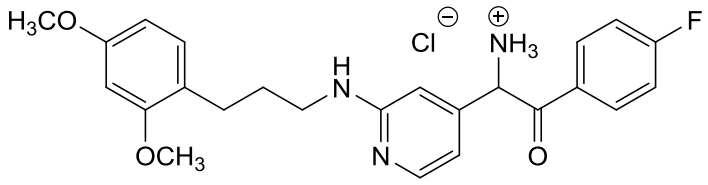

$C_{24}H_{27}ClFN_3O_3$ (M_r 459.95)

170 was synthesized according to the procedure for **125** from **169** (110 mg, 205 µmol) in 1 ml 2-propanol and 1.5 ml HCl-sat. 2-propanol, and Pd/C 10 % (20 mg). The crude product was obtained by filtration, the residue was rinsed with methanol. The filtrate was concentrated under reduced pressure. **170** was obtained by crystallization from diethyl ether as a colorless solid (97 % HPLC purity).

Yield: 94.0 mg (204 µmol, 99 %).

HPLC (Method 2): t_R = 3.7 min.

LC-MS (ESI, 70 eV): m/z = 424 $[M\text{-}Cl]^+$ (calc. m/z = 459).

***tert*-Butyl (4-(5-(4-fluorophenyl)-2-(methylthio)-1*H*-imidazol-4-yl)pyridin-2-yl)-carbamate (160)**

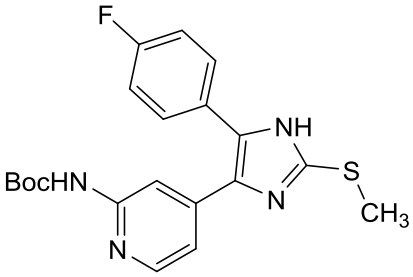

$C_{20}H_{21}FN_4O_2S$ (M_r 400.47)

160 was synthesized according to the procedure described for **132** from **120** (200 mg, 666 µmol) and Boc_2O (189 mg, 866 µmol) in 2 ml *tert*-butanol. After completion, the mixture was diluted with ethyl acetate, washed with sat. aq. $NaHCO_3$ solution, H_2O, and sat. aq. NaCl solution, and dried over anhyd. Na_2SO_4. The solvent was removed under reduced pressure to afford **160** as a colorless solid (97 % HPLC purity).

Yield: 134 mg (335 mmol, 50 %).

m.p.: 177 °C.

^{1}H NMR (300 MHz, $CDCl_3$): δ = 1.43 (s, 9 H, ^{t}Bu), 2.62 (s, 3 H, SC*H*$_3$), 6.93-6.97 (m, 1 H, C^5*H*, Pyr), 7.13-7.31 (m, 2 H, C$^{3/5}$*H*, F-Phe), 7.44-7.52 (m, 2 H, C$^{2/6}$*H*, F-Phe), 7.85-8.01 (m, 1 H, C^3*H*, Pyr), 8.05-8.18 (m, 1 H, C^6*H*, Pyr), 9.59-9.78 (m, 1 H, N*H*), 12.70-12.76 (m, 1 H, N*H*, Imdz) ppm.

^{13}C NMR (75 MHz, $CDCl_3$): δ = 15.2 (S*C*H$_3$), 28.0 (C(*C*H$_3$)$_3$), 79.4 (*C*(CH$_3$)$_3$), 109.4 (*C*^{3}H, Pyr), 115.0 (*C*^{5}H, Pyr), 115.8 (d, $^2J_{CF}$ = 21.7 Hz, *C*$^{3/5}$H, F-Phe), 126.7 (*C*^{2}, Imdz), 130.8 (d, $^3J_{CF}$ = 8.5 Hz, *C*$^{2/6}$H, F-Phe), 134.5 (*C*^{4}, Pyr), 138.7, 139.5 (*C*$^{4/5}$, Imdz), 143.6 (*C*^{2}, Pyr), 147.5 (*C*^{6}H, Pyr), 152.9 (*C*O), 162.0 (d, $^1J_{CF}$ = 244.8 Hz, *C*F) ppm.

IR (ATR): $\tilde{\nu}$ = 2990, 2400, 1730, 1607, 1559, 1505, 1418, 1368, 1292, 1271, 1231, 1155, 1117, 1053, 995, 837, 814, 766, 740, 698 cm^{-1}.

HPLC (Method 1): t_R = 5.1 min.

LC-MS (ESI, 70 eV): *m*/*z* = 401 [MH]$^+$, 345 [MH$_2$-^{t}Bu]$^+$, 301 [MH$_2$-C$_5$H$_9$O$_2$]$^+$ (calc. *m*/*z* = 400).

HRMS (EI, 70 eV): *m*/*z* = 400.1369 [M]$^+$ (calc. *m*/*z* = 400.1369).

***N*-Benzyl-4-(4-(4-fluorophenyl)-2-(methylthio)-1*H*-imidazol-5-yl)pyridin-2-amine (162)**

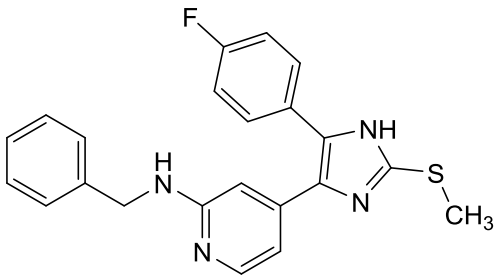

$C_{22}H_{19}FN_4S$ (M_r 390.48)

Method A. **162** was synthesized according to the procedure for **161** from **120** (107 mg, 356 µmol), sodium hydride (14.4 mg 60 % dispersion in mineral oil, 360 µmol), and benzyl bromide (50.0 ml, 418 µmol) in 2 ml anhyd. DMF. The crude product was purified by flash chromatography (SiO_2, 10-60 % ethyl acetate/petrol ether) to afford **162** as a yellow solid (95 % HPLC purity).

Yield: 23.0 mg (58.9 µmol, 17 %).

Method B. **162** was synthesized according to the procedure for **161** from **160** (117 mg, 292 µmol), sodium hydride (12.0 mg 60 % dispersion in mineral oil, 300 µmol), and benzyl bromide (50.0 ml, 418 µmol) in 2 ml anhyd. DMF. The crude product was stirred in diluted aq. trifluoroacetic acid at rt for 12 h. The mixture was neutralized, concentrated, and purified by flash chromatography (SiO_2, 10-60 % ethyl acetate/petrol ether) to afford **162** as a yellow solid (95 % HPLC purity).

Yield: 42.0 mg (108 µmol, 32 %).

Method C. **162** was synthesized according to the procedure for **119** from **166** (156 mg, 420 µmol) in 4 ml anhyd. DMF, and methyl thiocyanate (100 µl, 1.45 mmol), but required further purification by flash chromatography (SiO_2, 10-60 % ethyl acetate/petrol ether). **162** was obtained as a yellow solid (95 % HPLC purity).

Yield: 99.0 mg (254 µmol, 60 %).

m.p.: 175 °C.

^{1}H NMR (300 MHz, DMSO-d_6): δ = 2.60 (s, 3 H, SCH_3), 4.42 (d, ^4J = 6.0 Hz, 2 H, CH_2, Bn), 6.48 (dd, ^3J = 5.3 Hz, ^4J = 0.7 Hz, 1 H, C^5*H*, Pyr), 6.73 (bs, 1 H, C^3*H*, Pyr), 7.10-7.29 (m, 8 H, C$^{3/5}$*H*, F-Phe and ^{ar}C*H*, Bn and N*H*), 7.46 (m, 2 H, C$^{2/6}$*H*, F-Phe), 7.81-7.90 (m, 1 H, C^6*H*, Pyr), 12.60 (bs, 1 H, N*H*, Imdz) ppm.

^{13}C NMR (75 MHz, DMSO-d_6): δ = 15.1 (S*C*H$_3$), 44.2 (*C*H$_2$, Bn), 105.2 (*C*^{3}H, Pyr), 110.1 (*C*^{5}H, Pyr), 115.5 (*C*$^{3/5}$H, F-Phe), 126.5 (^{ar}*C*^{4}H, Bn), 127.1 (^{ar}*C*$^{2/6}$H, Bn), 128.1 (^{ar}*C*$^{3/5}$H, Bn), 129.4 (*C*$^{4/5}$, Imdz), 130.6 (*C*$^{2/6}$H, F-Phe), 134.9 (*C*^{4}, Pyr), 140.5 (^{ar}*C*^{1}, Bn), 142.0 (*C*^{2}, Imdz), 146.7 (*C*^{6}H, Pyr), 158.8 (*C*^{1}, Pyr) ppm.

HPLC (Method 1): t_R = 4.3 min.

LC-MS (ESI, 70 eV): m/z = 391 [MH]$^+$, 301 [MH$_2$-Bn]$^+$, 286 [MH$_2$-NHBn]$^+$, 91 [Bn]$^+$ (calc. m/z = 390).

HRMS (EI, 70 eV): m/z = 390.1314 [M]$^+$ (calc. m/z = 390.1314).

_N_-(3-(2,4-Dimethoxyphenyl)propyl)-4-(5-(4-fluorophenyl)-2-(methylthio)-1_H_-imidazol-4-yl)pyridin-2-amine (164)

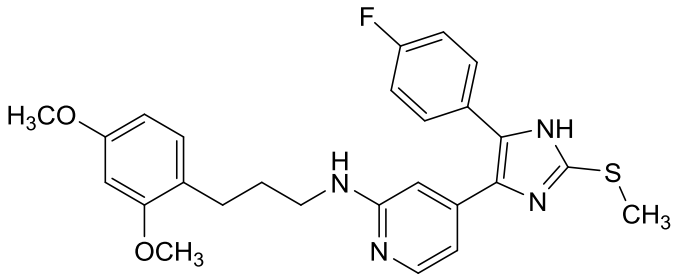

$C_{26}H_{27}FN_4O_2S$ (M_r 478.59)

164 was synthesized according to the procedure for **119** from **170** (90.0 mg, 196 µmol) in 3 ml anhyd. DMF, and methyl thiocyanate (50.0 µl, 725 µmol), but required further purification by flash chromatography (SiO_2, 20-100 % ethyl acetate/petrol ether and RP-18, 50-100 % methanol/H_2O). **164** was obtained as a yellow solid (100 % HPLC purity).

Yield: 36.0 mg (75.2 µmol, 38 %).

^{1}H NMR (300 MHz, DMSO-d_6): δ = 1.67-1.72 (m, 2 H, $CH_2CH_2CH_2NH$), 2.48-2.52 (m, 2 H, $CH_2CH_2CH_2NH$), 2.60 (s, 3 H, SCH_3), 3.13-3.17 (m, 2 H, $CH_2CH_2CH_2NH$), 3.72 (s, 3 H, C^4OCH_3), 3.74 (s, 3 H, C^2OCH_3), 6.41-6.50 (m, 5 H, $C^{3/5}H$, Pyr and $C^{3/5}H$, $(OCH_3)_2$-Phe and $CH_2CH_2CH_2NH$), 7.01 (d, ^3J = 8.2 Hz, 1 H, C^6H, $(OCH_3)_2$-Phe), 7.22 (m, 2 H, $C^{3/5}H$, F-Phe), 7.48 (m, 2 H, $C^{2/6}H$, F-Phe), 7.85 (bs, C^6H, Pyr), 12.58 (bs, 1H, N*H*) ppm.

^{13}C NMR (75 MHz, DMSO-d_6): δ = 15.1 (SCH_3), 26.6 ($CH_2CH_2CH_2NH$), 29.3 ($CH_2CH_2CH_2NH$), 40.7 ($CH_2CH_2CH_2NH$), 55.1 (C^4OCH_3), 55.2 (C^2OCH_3), 98.3 (C^3H, $(OCH_3)_2$-Phe), 104.3 (C^5H, $(OCH_3)_2$-Phe), 104.9 (C^3H, Pyr), 109.7 (C^5H, Pyr), 115.4 ($C^{3/5}$H, F-Phe), 121.8 (C^1, $(OCH_3)_2$-Phe), 126.5 (C^4, Imdz), 127.0 (C^5, Imdz), 129.7 (C^1, F-Phe), 129.7 (C^6H, $(OCH_3)_2$-Phe), 130.1 ($C^{2/6}$H, F-Phe), 142.1 (C^2, Imdz), 147.5 (C^6H, Pyr), 157.9 (C^2OCH_3), 158.8 (C^4OCH_3), 159.3 (C^2, Pyr) ppm.

HPLC (Method 2): t_R = 5.4 min.

LC-MS (ESI, 70 eV): m/z = 479 $[MH]^+$ (calc. m/z = 478).

HRMS (EI, 70 eV): m/z = 478.1839 $[M]^+$ (calc. m/z = 478.1839).

7.3.3 Syntheses of Series 2: Amide Coupling

3-(2,5-Dimethoxyphenyl)-*N*-(4-methylpyridin-2-yl)propanamide (174)

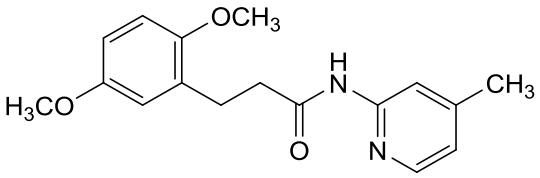

$C_{17}H_{20}N_2O_3$ (M_r 300.36)

Method A. 3-(2,5-Dimethoxyphenyl)propionic acid (203 mg, 966 µmol) and CDI (190 mg, 1.17 mmol) were stirred in 5 ml anhyd. DMF at rt until no further formation of CO_2 was observed. Excess CDI was eliminated by heating to 50 °C for 2 h. The mixture was cooled to rt and added dropwise to a solution of 2-amino-4-methylpyridine (146 mg, 1.35 mmol) and DIPEA (500 µl, 2.86 mmol) in 3 ml anhyd. DMF under a nitrogen atmosphere. The reaction was stirred at 110 °C for 12 h, quenched by addition of H_2O, cooled to rt, and extracted with ethyl acetate. The combined organic phases were washed with H_2O and sat. aq. NaCl solution, dried over anhyd. Na_2SO_4, and the solvent was removed under reduced pressure. The crude product was purified by flash chromatography (SiO_2, 20-40 % ethyl acetate/petrol ether) to afford **174** as a colorless solid (100 % HPLC purity).

Yield: 209 mg (696 µmol, 72 %).

Method B. 3-(2,5-Dimethoxyphenyl)propionic acid (210 mg, 994 µmol), PyBOP (602 mg, 1.16 mmol), and DIPEA (500 µl, 2.86 mmol) were stirred in 5 ml anhyd. DMF at rt under a nitrogen atmosphere before 2-amino-4-methylpyridine (146 mg, 1.35 mmol) was added in one portion. The reaction was stirred for 12 h at 110 °C, quenched by addition of H_2O, and cooled to rt. Purification was achieved as described above (Method A) to afford **174** as a colorless solid (100 % HPLC purity).

Yield: 234 mg (778 µmol, 78 %).

Method C. 3-(2,5-Dimethoxyphenyl)propionic acid (212 mg, 1.01 mmol), HATU (453 mg, 1.19 mmol), and DIPEA (500 µl, 2.86 mmol) were stirred in 5 ml anhyd. DMF at rt under a nitrogen atmosphere before 2-amino-4-methylpyridine (148 mg, 1.37 mmol) was added in one portion. The reaction was stirred for 12 h at 110 °C, quenched by addition of H_2O, and cooled to

rt. Purification was achieved as described above (Method A) to afford **174** as a colorless solid (100 % HPLC purity).

Yield: 226 mg (753 µmol, 75 %).

Method D. 3-(2,5-Dimethoxyphenyl)propionic acid (202 mg, 961 µmol), 2-amino-4-methyl-pyridine (140 mg, 1.30 mmol), and HOBt (157 mg, 1.16 mmol) were dissolved in 5 ml anhyd. DMF at rt under a nitrogen atmosphere. EDCI (240 mg, 1.25 mmol) and DIPEA (500 µl, 2.86 mmol) were added and the reaction was stirred for 12 h at 110 °C, quenched by addition of H_2O, and cooled to rt. Purification was achieved as described above (Method A) to afford **174** as a colorless solid (100 % HPLC purity).

Yield: 159 mg (528 µmol, 55 %).

Method E. 3-(2,5-Dimethoxyphenyl)propionic acid (203 mg, 966 µmol), 2-amino-4-methyl-pyridine (146 mg, 1.35 mmol), 4-DMAP (10.0 mg, 82.0 µmol), and HOBt (155 mg, 1.15 mmol) were dissolved in 5 ml anhyd. DMF at rt under a nitrogen atmosphere. DCC (254 mg, 1.23 mmol) and DIPEA (500 µl, 2.86 mmol) were added and the reaction was stirred for 12 h at 110 °C, quenched by addition of H_2O, and cooled to rt. Purification was achieved as described above (Method A) to afford **174** as a colorless solid (100 % HPLC purity).

Yield: n.d.

m.p.: 111 °C.

^{1}H NMR (300 MHz, $CDCl_3$): δ = 2.37 (s, 3 H, CH_3), 2.68 (t, ^3J = 7.7 Hz, 2 H, CH_2CH_2CONH), 3.00 (t, ^3J = 7.7 Hz, 2 H, CH_2CH_2CONH), 3.72 (s, 3 H, C^5OCH_3), 3.77 (s, 3 H, C^2OCH_3), 6.70 (dd, ^3J = 8.9 Hz, ^4J = 2.8 Hz, 1 H, C^4H, $(OCH_3)_2$-Phe), 6.74-6.77 (m, 2 H, $C^{3/6}H$, $(OCH_3)_2$-Phe), 6.86 (dq, ^3J = 5.2 Hz, ^5J = 0.8 Hz, 1 H, C^5H, Pyr), 8.06 (dd, ^3J = 5.3 Hz, ^5J = 0.5 Hz, 1 H, C^6H, Pyr), 8.12 (bs, 1 H, C^3H, Pyr), 8.86 (bs, 1 H, NH) ppm.

^{13}C NMR (75 MHz, $CDCl_3$): δ = 21.7 (CH$_3$), 26.7 (CH$_2$CH$_2$CONH), 37.9 (CH$_2C$H$_2$CONH), 55.8 (C^5OCH_3), 55.9 (C^2OCH_3), 111.2 (C^6H, $(OCH_3)_2$-Phe), 111.9 (C^4H, $(OCH_3)_2$-Phe), 115.0 (C^3H, Pyr), 116.5 (C^3H, $(OCH_3)_2$-Phe), 120.9 (C^5H, Pyr), 129.9 (C^1, $(OCH_3)_2$-Phe), 146.1 (C^6H, Pyr), 151.0 (C^4, Pyr), 151.4 (C^2, Pyr), 151.7 (C^2OCH_3), 153.6 (C^5OCH_3), 171.7 (CO) ppm.

IR (ATR): $\tilde{\nu}$ = 3000, 1688, 1611, 1578, 1537, 1503, 1418, 1279, 1221, 1177, 1126, 1055, 1034, 868, 799, 754, 708 cm^{-1}.

HPLC (Method 2): t_R = 4.8 min.

LC-MS (ESI, 70 eV): m/z = 301 $[MH]^+$ (calc. m/z = 300).

3-(2,4-Dimethoxyphenyl)-*N*-(4-(5-(4-fluorophenyl)-2-(methylthio)-1*H*-imidazol-4-yl)-pyridin-2-yl)propanamide (190)

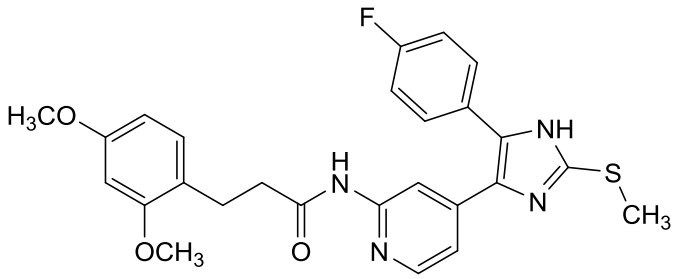

$C_{26}H_{25}FN_4O_3S$ (M_r 492.57)

158 (560 mg, 2.66 mmol) and CDI (475 mg, 2.93 mmol) were stirred in 3 ml anhyd. DMF until formation of CO_2 was undetectable. **120** (400 mg, 1.33 mmol) was added to the reaction and the mixture was heated at 110 °C under a nitrogen atmosphere for 12 h. The reaction was cooled to rt and ethyl acetate was added. The resulting mixture was washed with H_2O and sat. aq. NaCl solution, dried over anhyd. Na_2SO_4, and the solvent was removed under reduced pressure. The crude product was purified by flash chromatography (SiO_2, 30-50 % ethyl acetate/petrol ether and RP-18, 30-80 % methanol/H_2O) to afford **190** as a beige solid (98 % HPLC purity).

Yield: 177 mg (359 µmol, 27 %).

m.p.: 90 °C.

^{1}H NMR (300 MHz, DMSO-d_6): δ = 2.57 (t, ^3J = 7.4 Hz, 2 H, COCH_2CH$_2$), 2.62 (s, 3 H, SCH_3), 2.75 (t, ^3J = 7.5 Hz, 2 H, COCH$_2$CH_2), 3.72 (s, 3 H, C^{2}OH_3), 3.77 (s, 3 H, C^{4}OCH_3), 6.42 (dd, ^3J = 8.3 Hz, ^4J = 2.4 Hz, 1 H, C^5H, (OCH$_3$)$_2$-Phe), 6.51 (d, ^4J = 2.4 Hz, 1 H, C^3H, (OCH$_3$)$_2$-Phe), 6.99 (dd, ^3J = 5.3 Hz, 1 H, C^5H, Pyr), 7.03 (d, ^3J = 8.3 Hz, 1 H, C^6H, (OCH$_3$)$_2$-Phe), 7.28 (bs, 2 H, C$^{3/5}H$, F-Phe), 7.46-7.51 (m, 2 H, C$^{2/6}H$, F-Phe), 8.12 (bs, 1 H, C^6H, Pyr), 8.32 (bs, 1 H, C^3H, Pyr), 10.29 (bs, 1 H, CON*H*), 12.72 (bs, 1 H, N*H*) ppm.

^{13}C NMR (75 MHz, DMSO-d_6): δ = 15.1 (SCH$_3$), 24.7 (COCH$_2$CH$_2$), 36.3 (COCH$_2$CH$_2$), 55.1 (C^{2}OCH$_3$), 55.3 (C^{4}OCH$_3$), 98.3 (C^{3}H, (OCH$_3$)$_2$-Phe), 104.3 (C^{5}H, (OCH$_3$)$_2$-Phe), 110.6 (C^{3}H, Pyr), 115.8 (d, $^2J_{CF}$ = 24.1 Hz, C$^{3/5}$H, F-Phe), 116.4 (C^{5}H, Pyr), 120.9 (C^1, (OCH$_3$)$_2$-Phe), 126.7 (C^1, F-Phe), 129.8 (C^{6}H, (OCH$_3$)$_2$-Phe), 130.7 (C^5, Imdz and C$^{2/6}$H, F-Phe), 134.5 (C^4, Imdz), 143.7 (C^2, Imdz), 147.6 (C^{6}H, Pyr), 148.0 (C^4, Pyr), 152.5 (C^2, Pyr), 157.9 (C^4, (OCH$_3$)$_2$-Phe), 159.0 (C^2, (OCH$_3$)$_2$-Phe), 161.9 (d, $^1J_{CF}$ = 246.7 Hz, CF), 171.4 (CO) ppm.

IR (ATR): $\tilde{\nu}$ = 2935, 1670, 1609, 1547, 1505, 1414, 1289, 1262, 1221, 1207, 1153, 1121, 1036, 835 cm^{-1}.

HPLC (Method 1): t_R = 5.3 min.

LC-MS (ESI, 70 eV): m/z = 493 $[MH]^+$ (calc. m/z = 492).

HRMS (EI, 70 eV): m/z = 492.1631 $[M]^+$ (calc. m/z = 492.1631).

3-(2,5-Dimethoxyphenyl)-*N*-(4-(5-(4-fluorophenyl)-2-(methylthio)-1*H*-imidazol-4-yl)-pyridin-2-yl)propanamide (191)

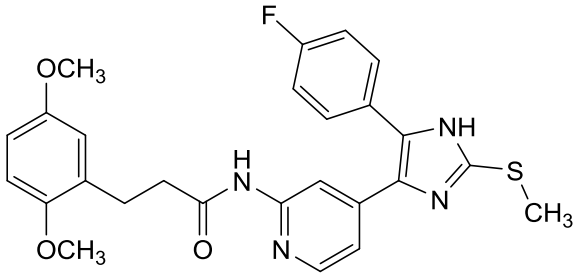

$C_{26}H_{25}FN_4O_3S$ (M_r 492.57)

191 was synthesized according to the procedure for **190** from 3-(2,5-dimethoxy-phenyl)propionic acid (560 mg, 2.66 mmol), CDI (475 mg, 2.93 mmol), and **120** (400 mg, 1.33 mmol) in 3 ml of anhyd. DMF. The crude product was purified by flash chromatography (SiO_2, 20-100 % ethyl acetate/petrol ether and RP-18, 20-100 % methanol/H_2O) to afford **191** as a colorless solid (100 % HPLC purity).

Yield: 255 mg (518 µmol, 39 %).

m.p.: 91 °C.

^{1}H NMR (300 MHz, DMSO-d_6): δ = 2.59-2.64 (m, 5 H, SCH_3 and COCH_2CH$_2$), 2.80 (t, ^3J = 7.5 Hz, 2 H, COCH$_2$CH_2), 3.66 (s, 3 H, C^{5}OCH_3), 3.73 (s, 3 H, C^{2}OCH_3), 6.72 (dd, ^3J = 8.8 Hz, ^4J = 3.1 Hz, 1 H, C^4H, (OCH$_3$)$_2$-Phe), 6.78 (d, ^4J = 3.0 Hz, 1 H, C^6H, (OCH$_3$)$_2$-Phe), 6.86 (d, ^3J = 8.8 Hz, 1 H, C^3H, (OCH$_3$)$_2$-Phe), 6.99 (dd, ^3J = 5.2 Hz, ^4J = 1.6 Hz, 1 H, C^5H, Pyr), 7.26 (bs, 2 H, C$^{3/5}H$, F-Phe), 7.46-7.51 (m, 2 H, C$^{2/6}H$, F-Phe), 8.13 (bs, 1 H, C^6H, Pyr), 8.32 (bs, 1 H, C^3H, Pyr), 10.34 (bs, 1 H, CON*H*), 12.72 (bs, 1 H, N*H*) ppm.

^{13}C NMR (75 MHz, DMSO-d_6): δ = 15.1 (S*C*H$_3$), 25.3 (COCH$_2$*C*H$_2$), 36.0 (CO*C*H$_2$CH$_2$), 55.2 (C^{5}O*C*H$_3$), 55.8 (C^{2}O*C*H$_3$), 110.6 (*C*^{3}H, Pyr), 111.2 (*C*^{4}H, (OCH$_3$)$_2$-Phe), 111.5 (*C*^{3}H, (OCH$_3$)$_2$-Phe), 115.6 (*C*$^{3/5}$H, F-Phe), 115.9 (*C*^{6}H, (OCH$_3$)$_2$-Phe), 116.5 (*C*^{5}H, Pyr), 126.7 (*C*^{1}, F-Phe), 130.0 (*C*^{1}, (OCH$_3$)$_2$-Phe), 130.6 (*C*^{5}, Imdz and *C*$^{2/6}$H, F-Phe), 134.5 (*C*^{4}, Imdz), 142.3 (*C*^{2}, Imdz), 147.7 (*C*^{4} and *C*^{6}H, Pyr), 151.2 (*C*^{2}, (OCH$_3$)$_2$-Phe), 152.5 (*C*^{2}, Pyr), 153.0 (*C*^{5}, (OCH$_3$)$_2$-Phe), 161.9 (d, $^1J_{CF}$ = 247.3, *C*F), 171.3 (*C*O) ppm.

IR (ATR): $\tilde{\nu}$ = 2925, 2400, 1668, 1607, 1551, 1499, 1416, 1221, 1157, 1045, 837, 814, 708 cm^{-1}.

HPLC (Method 2): t_R = 4.1 min.

LC-MS (ESI, 70 eV): m/z = 494 $[MH]^+$ (calc. m/z = 492).

HRMS (EI, 70 eV): m/z = 492.1631 $[M]^+$ (calc. m/z = 492.1631).

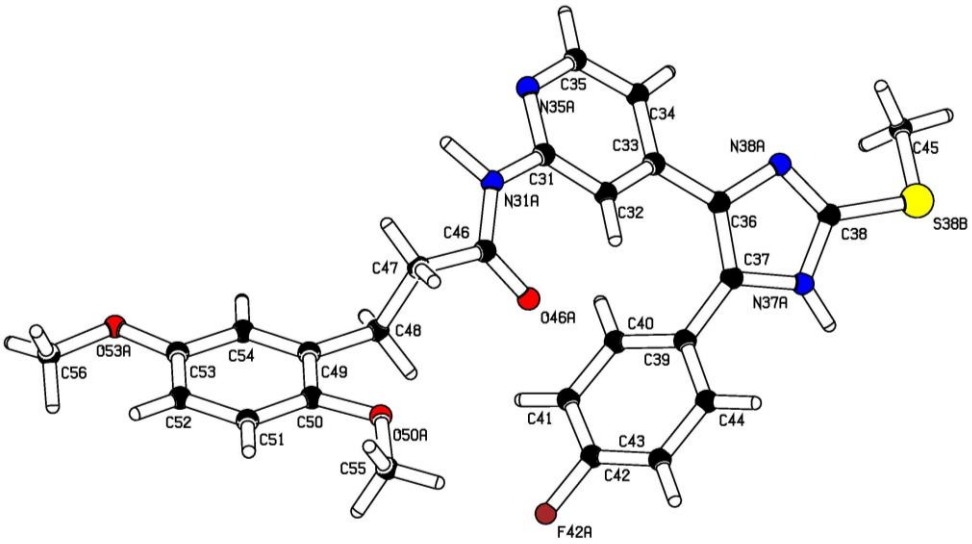

Figure 107 | Molecular structure of 191. Determined by X-ray crystallography by Dr. Dieter Schollmeyer.

3-(2,3-Dimethoxyphenyl)-*N*-(4-(5-(4-fluorophenyl)-2-(methylthio)-1*H*-imidazol-4-yl)-pyridin-2-yl)propanamide (192)

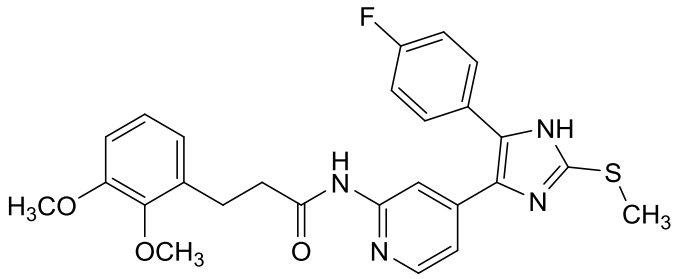

$C_{26}H_{25}FN_4O_3S$ (M_r 492.57)

192 was synthesized according to the procedure for **190** from 3-(2,3-dimethoxy-phenyl)propionic acid (700 mg, 3.33 mmol), CDI (594 mg, 3.66 mmol), and **120** (500 mg, 1.67 mmol) in 4 ml of anhyd. DMF. The crude product was purified by flash chromatography (SiO_2, 30-100 % ethyl acetate/petrol ether and RP-18, 50-100 % methanol/H_2O) to afford **192** as a colorless solid (100 % HPLC purity).

Yield: 515 mg (1.05 mmol, 63 %).

^{1}H NMR (300 MHz, DMSO-d_6): δ = 2.62 (s, 3 H, SCH_3), 2.59-2.66 (m, 2 H, COCH_2CH$_2$), 2.84 (t, ^3J = 7.7 Hz, 2 H, COCH$_2$CH_2), 3.73 (s, 3 H, C^{2}OCH_3), 3.78 (s, 3 H, C^{3}OCH_3), 6.79 (dd, ^3J = 7.5 Hz, ^4J = 1.6 Hz, 1 H, C^6H, (OCH$_3$)$_2$-Phe), 6.88 (dd, ^3J = 8.1 Hz, ^4J = 1.2 Hz, 1 H, C^4H, (OCH$_3$)$_2$-Phe), 6.97 (t, ^3J = 7.8 Hz, 1 H, C^5H, (OCH$_3$)$_2$-Phe), 7.01 (dd, ^3J = 5.3 Hz, ^4J = 1.5 Hz, 1 H, C^5H, Pyr), 7.26-7.32 (m, 2 H, C$^{3/5}H$, F-Phe), 7.45-7.51 (m, 2 H, C$^{2/6}H$, F-Phe), 8.11 (d, ^3J = 5.3 Hz, 1 H, C^6H, Pyr), 8.34 (bs, 1 H, C^3H, Pyr), 10.35 (s, 1 H, CONH), 12.70 (s, 1 H, NH) ppm.

^{13}C NMR (75 MHz, DMSO-d_6): δ = 15.1 (SCH_3), 24.8 (COCH$_2$CH_2), 36.8 (COCH_2CH$_2$), 55.3 (C^{3}OCH_3), 60.0 (C^{2}OCH_3), 110.6 (C^{3}H, Pyr), 110.9 (C^{4}H, (OCH$_3$)$_2$-Phe), 115.8 (d, $^2J_{CF}$ = 21.8 Hz, C$^{3/5}$H, F-Phe), 116.4 (C^{5}H, Pyr), 121.4 (C^{6}H, (OCH$_3$)$_2$-Phe), 123.7 (C^{5}H, (OCH$_3$)$_2$-Phe), 126.6 (d, $^4J_{CF}$ = 3.1 Hz, C^1, F-Phe), 130.1 (C^5, Imdz), 130.7 (d, $^3J_{CF}$ = 8.4 Hz, C$^{2/6}$H, F-Phe), 134.4 (C^1, (OCH$_3$)$_2$-Phe), 134.5 (C^4, Imdz), 142.2 (C^2, Imdz), 143.8 (C^4, Pyr), 146.6 (C^{2}OCH$_3$), 147.6 (C^{6}H, Pyr), 152.4 (C^{3}OCH$_3$), 152.5 (C^2, Pyr), 162.0 (d, $^1J_{CF}$ = 244.7 Hz, CF), 171.1 (CO) ppm.

HPLC (Method 2): t_R = 5.7 min.

LC-MS (ESI, 70 eV): m/z = 493 $[MH]^+$ (calc. m/z = 492).

3-(3,4-Dimethoxyphenyl)-*N*-(4-(5-(4-fluorophenyl)-2-(methylthio)-1*H*-imidazol-4-yl)-pyridin-2-yl)propanamide (193)

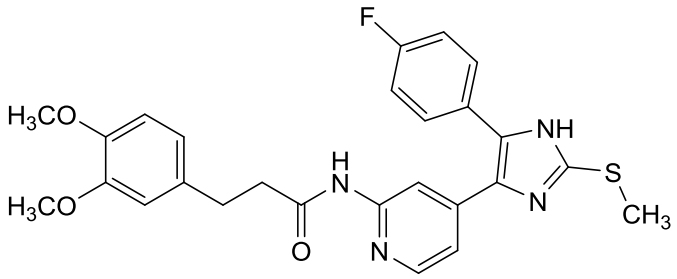

$C_{26}H_{25}FN_4O_3S$ (M_r 492.57)

193 was synthesized according to the procedure for **190** from 3-(3,4-dimethoxyphenyl)propionic acid (700 mg, 3.33 mmol), CDI (594 mg, 3.66 mmol), and **120** (500 mg, 1.67 mmol) in 4 ml of anhyd. DMF. The crude product was purified by flash chromatography (SiO_2, 30-100 % ethyl acetate/petrol ether and RP-18, 50-100 % methanol/H_2O) to afford **193** as a colorless solid (97 % HPLC purity).

Yield: 468 mg (950 µmol, 57 %).

^{1}H NMR (300 MHz, DMSO-d_6): δ = 2.62 (s, 3 H, SCH_3), 2.62-2.67 (m, 2 H, COCH_2CH$_2$), 2.81 (t, ^3J = 7.4 Hz, 2 H, COCH$_2$CH_2), 3.70 (s, 3 H, C^{4}OCH_3), 3.72 (s, 3 H, C^{3}OCH_3), 6.73 (dd, ^3J = 8.2 Hz, ^4J = 1.9 Hz, 1 H, C^6H, (OCH$_3$)$_2$-Phe), 6.84 (d, ^3J = 8.3 Hz, 1 H, C^5H, (OCH$_3$)$_2$-Phe), 6.85 (bs, 1 H, C^2H, (OCH$_3$)$_2$-Phe), 7.00 (dd, ^3J = 5.2 Hz, ^4J = 1.5 Hz, 1 H, C^5H, Pyr), 7.26-7.31 (m, 2 H, C$^{3/5}H$, F-Phe), 7.46-7.50 (m, 2 H, C$^{2/6}H$, F-Phe), 8.10-8.34 (m, 2 H, C$^{3/6}H$ Pyr), 10.33 (s, 1 H, CONH), 12.71 (s, 1 H, NH) ppm.

^{13}C NMR (75 MHz, DMSO-d_6): δ = 15.1 (SCH$_3$), 30.4 (COCH$_2$$CH_2$), 38.0 (CO$CH_2CH_2$), 55.4 (C^{4}O$CH_3$), 55.5 (C^{3}O$CH_3$), 110.6 ($C^3$H, Pyr), 111.9 ($C^5$H, (OCH$_3$)$_2$-Phe), 112.3 ($C^2$H, (OCH$_3$)$_2$-Phe), 115.8 (d, $^2J_{CF}$ = 22.5 Hz, $C^{3/5}$H, F-Phe), 116.4 (C^5H, Pyr), 120.0 (C^6H, (OCH$_3$)$_2$-Phe), 130.6 ($C^{2/6}$H, F-Phe), 133.5 (C^1, (OCH$_3$)$_2$-Phe), 147.1 (C^4OCH$_3$), 147.6 (C^6H, Pyr), 148.6 (C^3OCH$_3$), 152.5 (C^2, Pyr), 165.8 (d, $^1J_{CF}$ = 242.6 Hz, CF), 171.2 (CO) ppm.

HPLC (Method 2): t_R = 5.5 min.

LC-MS (ESI, 70 eV): m/z = 493 [MH]$^+$ (calc. m/z = 492).

3-(3,4,5-Trimethoxyphenyl)-*N*-(4-(5-(4-fluorophenyl)-2-(methylthio)-1*H*-imidazol-4-yl)-pyridin-2-yl)propanamide (194)

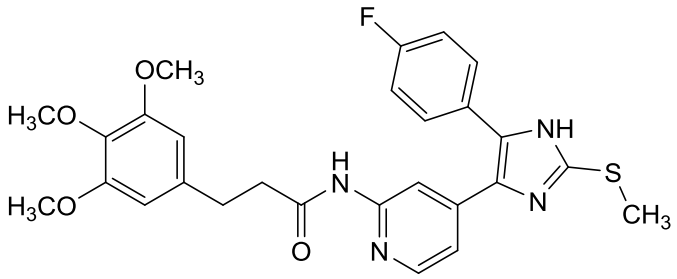

$C_{27}H_{27}FN_4O_4S$ (M_r 522.60)

194 was synthesized according to the procedure for **190** from 3-(3,4,5-trimethoxy-phenyl)propionic acid (800 mg, 3.33 mmol), CDI (594 mg, 3.66 mmol), and **120** (500 mg, 1.67 mmol) in 4 ml of anhyd. DMF. The crude product was purified by flash chromatography (SiO_2, 20-100 % ethyl acetate/petrol ether and RP-18, 50-100 % methanol/H_2O) to afford **194** as a pale yellowish solid (99 % HPLC purity).

Yield: 422 mg (807 µmol, 49 %).

^{1}H NMR (300 MHz, DMSO-d_6): δ = 2.62 (s, 3 H, SCH_3), 2.62-2.69 (m, 2 H, COCH_2CH$_2$), 2.80-2.85 (m, 2 H, COCH$_2$CH_2), 3.61 (s, 3 H, C^{4}OCH_3), 3.74 (bs, 6 H, C$^{3/5}$OCH_3), 6.56 (s, 2 H, C$^{2/6}$*H*, (OCH$_3$)$_3$-Phe), 7.01 (dd, ^3J = 5.3 Hz, ^4J = 1.6 Hz, 1 H, C^5*H*, Pyr), 7.26-7.32 (m, 2 H, C$^{3/5}$*H*, F-Phe), 7.46-7.51 (m, 2 H, C$^{2/6}$*H*, F-Phe), 8.11 (dd, ^3J = 5.3 Hz, ^5J = 0.5 Hz, 1 H, C^6*H*, Pyr), 8.36 (bs, 1 H, C^3*H*, Pyr), 10.36 (s, 1 H, CON*H*), 12.70 (s, 1 H, N*H*) ppm.

^{13}C NMR (75 MHz, DMSO-d_6): δ = 15.1 (S*C*H$_3$), 31.3 (COCH$_2$*C*H$_2$), 37.9 (CO*C*H$_2$CH$_2$), 55.7 (C$^{3/5}$O*C*H$_3$), 59.9 (C^{4}O*C*H$_3$), 105.5 (*C*$^{2/6}$H, (OCH$_3$)$_3$-Phe), 110.6 (*C*^{3}H, Pyr), 115.8 (d, $^2J_{CF}$ = 21.7 Hz, *C*$^{3/5}$H, F-Phe), 116.4 (*C*^{5}H, Pyr), 126.6 (d, $^4J_{CF}$ = 3.3 Hz, *C*^{1}, F-Phe), 130.1 (*C*^{5}, Imdz), 130.7 (d, $^3J_{CF}$ = 8.4 Hz, *C*$^{2/6}$H, F-Phe), 134.5 (*C*^{4}, Imdz), 135.7 (*C*^{4}OCH$_3$), 136.8 (*C*^{1}, (OCH$_3$)$_3$-Phe), 142.2 (*C*^{2}, Imdz), 143.8 (*C*^{4}, Pyr), 147.6 (*C*^{6}H, Pyr), 152.5 (*C*^{2}, Pyr), 152.7 (*C*$^{3/5}$OCH$_3$), 162.0 (d, $^1J_{CF}$ = 245.4 Hz, *C*F), 171.2 (*C*O) ppm.

HPLC (Method 2): t_R = 5.5 min.

LC-MS (ESI, 70 eV): m/z = 523 [MH]$^+$ (calc. m/z = 522).

7.3.4 Syntheses of Series 3: Carbamide Derivatives

General procedure for the preparation of carbamide derivatives (204-212)

Compound **120** (1.0 equiv) and the respective isocyanate (1.1 equiv) were dissolved in 5 ml anhyd. DMF under a nitrogen atmosphere. DIPEA (1.2 equiv) was added and stirring continued at rt for 12 h. The solvent was removed under reduced pressure, the residue resuspended in ethyl acetate, and washed with 0.1 M aq. HCl, sat. aq. $NaHCO_3$ solution, and sat. aq. NaCl solution, dried over anhyd. Na_2SO_4, and concentrated under reduced pressure. The crude product was purified by flash chromatography (SiO_2 and RP-18, eluent and mixing ratio given for each compound, respectively) to afford the particular compound.

1-(2,4-Dimethoxyphenyl)-3-(4-(5-(4-fluorophenyl)-2-(methylthio)-1*H*-imidazol-4-yl)-pyridin-2-yl)carbamide (204)

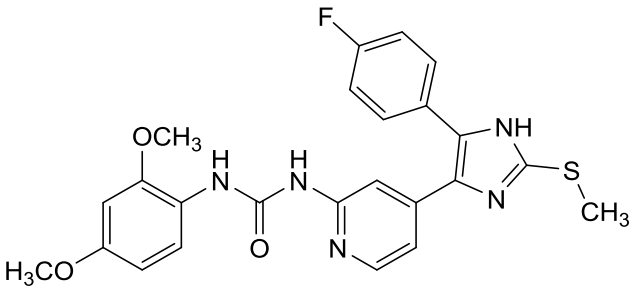

$C_{24}H_{22}FN_5O_3S$ (M_r 479.53)

204 was synthesized according to the general procedure from **120** (400 mg, 1.33 mmol), 2,4-dimethoxyphenyl isocyanate (262 mg, 1.47 mmol), and DIPEA (300 µl, 1.60 mmol). Purification was achieved by flash chromatography (SiO_2, 0-10 % methanol/dichloromethane and RP-18, 50-100 % methanol/H_2O) to afford **204** as a colorless solid (100 % HPLC purity).

Yield: 135 mg (280 µmol, 21 %).

m.p.: 214 °C.

^{1}H NMR (300 MHz, DMSO-d_6): δ = 2.63 (s, 3 H, SCH_3), 3.74 (s, 3 H, C^{4}OCH_3), 3.88 (s, 3 H, C^{2}OCH_3), 6.48 (dd, ^3J = 8.9 Hz, ^4J = 2.7 Hz, 1 H, C^5H, $(OCH_3)_2$-Phe), 6.62 (d, ^4J = 2.7 Hz, 1 H, C^3H, $(OCH_3)_2$-Phe), 6.92 (dd, ^3J = 5.4 Hz, ^4J = 1.5 Hz, 1 H, C^5H, Pyr), 7.30-7.51 (m, 5 H, C$^{3/5}H$, F-Phe and C^3H, Pyr and C$^{2/6}H$, F-Phe), 8.03 (d, ^3J = 8.9 Hz, 1 H, C^6H, $(OCH_3)_2$-Phe), 8.12 (bs, 1 H, C^6H, Pyr), 9.64 (bs, 1 H, N*H*), 10.89-11.26 (m, 1 H, N*H*), 12.74 (bs, 1 H, N*H*, Imdz) ppm.

^{13}C NMR (75 MHz, DMSO-d_6): δ = 15.1 (S*C*H$_3$), 55.3 (C^{4}O*C*H$_3$), 56.0 (C^{2}O*C*H$_3$), 98.8 (*C*^{3}H, $(OCH_3)_2$-Phe), 104.1 (*C*^{5}H, $(OCH_3)_2$-Phe), 108.6 (*C*^{3}H, Pyr), 114.6 (*C*^{5}H, Pyr), 115.7 (*C*$^{2/6}$H, F-Phe), 119.7 (*C*^{6}H, $(OCH_3)_2$-Phe), 121.9 (*C*^{1}, $(OCH_3)_2$-Phe), 130.7 (*C*$^{3/5}$H, F-Phe), 134.2 (*C*^{4}, Pyr), 142.3 (*C*^{2}, Imdz), 146.1 (*C*^{6}H, Pyr), 149.4 (*C*^{2}, $(OCH_3)_2$-Phe), 152.2 (*C*O), 153.6 (*C*^{2}, Pyr), 155.2 (*C*^{4}, $(OCH_3)_2$-Phe), 161.8 (d, $^1J_{CF}$ = 241.6 Hz, *C*F) ppm.

IR (ATR): $\tilde{\nu}$ = 3220, 1663, 1614, 1582, 1572, 1541, 1520, 1456, 1366, 1279, 1207, 1155, 1051, 1036, 837, 824, 787, 763, 669, 613 cm^{-1}.

HPLC (Method 3): t_R = 5.4 min.

LC-MS (ESI, 70 eV): *m*/*z* = 480 $[MH]^+$ (calc. *m*/*z* = 479).

1,3-Bis(2,4-dimethoxyphenyl)carbamide (215)

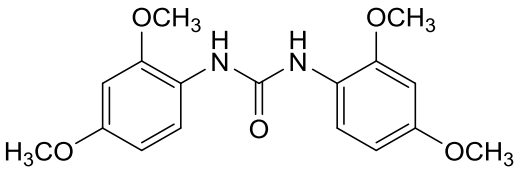

$C_{17}H_{20}N_2O_5$ (M_r 332.36)

215 was isolated as a by-product from the synthesis of **204**. The crude product was purified by flash chromatography (SiO_2, 0-10 % methanol/dichloromethane and RP-18, 50-100 % methanol/H_2O) to afford **215** as a colorless solid (100 % HPLC purity).

m.p.: 200 °C.

^{1}H NMR (300 MHz, DMSO-d_6): δ = 3.72 (s, 6 H, C^4OCH_3), 3.84 (s, 6 H, C^2OCH_3), 6.45 (dd, ^3J = 8.9 Hz, ^4J = 2.7 Hz, 2 H, C^5H, $(OCH_3)_2$-Phe), 6.59 (d, ^4J = 2.6 Hz, 2 H, C^3H, $(OCH_3)_2$-Phe), 7.87 (d, ^3J = 8.9 Hz, 2 H, C^6H, $(OCH_3)_2$-Phe), 8.47 (s, 2 H, NH) ppm.

^{13}C NMR (75 MHz, DMSO-d_6): δ = 55.2 (C^4OCH_3), 55.7 (C^2OCH_3), 98.7 (C^3H, $(OCH_3)_2$-Phe), 104.0 (C^5H, $(OCH_3)_2$-Phe), 120.4 (C^6H), 122.1 (C^1, $(OCH_3)_2$-Phe), 149.5 (C^2OCH_3), 153.0 (CO), 154.8 (C^4OCH_3) ppm.

IR (ATR): $\tilde{\nu}$ = 3296, 1645, 1613, 1557, 1497, 1464, 1414, 1277, 1159, 1134, 1057, 1036, 1028, 922, 829, 808, 795, 654 cm^{-1}.

HPLC (Method 3): t_R = 3.8 min.

LC-MS (ESI, 70 eV): m/z = 333 $[MH]^+$ (calc. m/z = 332).

1-(2,5-Dimethoxyphenyl)-3-(4-(5-(4-fluorophenyl)-2-(methylthio)-1*H*-imidazol-4-yl)-pyridin-2-yl)carbamide (205)

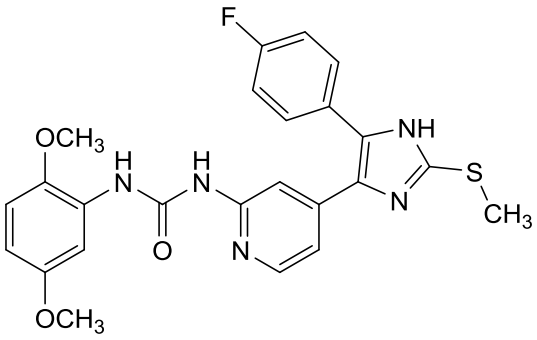

$C_{24}H_{22}FN_5O_3S$ (M_r 479.53)

205 was synthesized according to the general procedure from **120** (323 mg, 1.08 mmol), 2,5-dimethoxyphenyl isocyanate (300 mg, 1.67 mmol), and DIPEA (300 µl, 1.72 mmol). Purification was achieved by flash chromatography (SiO_2, 20-100 % ethyl acetate/petrol ether) to afford **205** as a pale yellowish solid (100 % HPLC purity).

Yield: 79.9 mg (167 µmol, 15 %).

m.p.: 184 °C.

^{1}H NMR (300 MHz, DMSO-d_6): δ = 2.63 (s, 3 H, SCH_3), 3.70 (s, 3 H, C^{5}OCH_3), 3.84 (s, 3 H, C^{2}OCH_3), 6.52 (dd, ^3J = 8.8 Hz, ^4J = 2.9 Hz, 1 H, C^4H, $(OCH_3)_2$-Phe), 6.91-6.96 (m, 1 H, C^3H, $(OCH_3)_2$-Phe), 6.95 (dd, ^3J = 5.5 Hz, ^4J = 1.4 Hz, 1 H, C^5H, Pyr), 7.28-7.38 (m, 2 H, C$^{3/5}H$, F-Phe), 7.47-7.51 (m, 3 H, C$^{2/6}H$, F-Phe and C^3H, Pyr), 7.92 (d, ^4J = 2.9 Hz, 1 H, C^6H, $(OCH_3)_2$-Phe), 8.13 (d, ^3J = 5.4 Hz, 1 H, C^6H, Pyr), 9.76 (bs, 1 H, NH), 11.52 (vbs, 1 H, NH), 12.74 (bs, 1 H, NH, Imdz) ppm.

^{13}C NMR (75 MHz, DMSO-d_6): δ = 15.1 (SCH$_3$), 55.3 (C^{5}OCH$_3$), 55.6 (C^{2}OCH$_3$), 105.6 (C^6H, $(OCH_3)_2$-Phe), 105.8 (C^4H, $(OCH_3)_2$-Phe), 108.5 (C^3H, Pyr), 111.7 (C^3H, $(OCH_3)_2$-Phe), 114.7 (C^5H, Pyr), 115.9 (d, $^2J_{CF}$ = 22.0 Hz, $C^{3/5}$H, F-Phe), 126.5 (d, $^4J_{CF}$ = 3.3 Hz, C^1, F-Phe), 129.6 (C^1, $(OCH_3)_2$-Phe), 130.4 (C^5, Imdz), 130.8 (d, $^3J_{CF}$ = 8.4 Hz, $C^{2/6}$H, F-Phe), 134.1 (C^4, Imdz), 142.3 (C^2, Imdz), 142.4 (C^2OCH$_3$), 144.2 (C^4, Pyr), 146.1 (C^6H, Pyr), 152.2 (CO), 153.4 (C^5OCH$_3$), 153.4 (C^2, Pyr), 162.1 (d, $^1J_{CF}$ = 245.9 Hz, CF) ppm.

IR (ATR): $\tilde{\nu}$ = 3098, 2960, 2832, 1672, 1599, 1574, 1539, 1506, 1489, 1462, 1368, 1304, 1279, 1244, 1221, 1198, 1165, 1140, 1047, 1026, 976, 868, 845, 814, 743, 712 cm^{-1}.

HPLC (Method 2): t_R = 5.6 min.

LC-MS (ESI, 70 eV): m/z = 480 $[MH]^+$ (calc. m/z = 479).

1-(4-(5-(4-Fluorophenyl)-2-(methylthio)-1*H*-imidazol-4-yl)pyridin-2-yl)-3-(4-methoxyphenyl)carbamide (206)

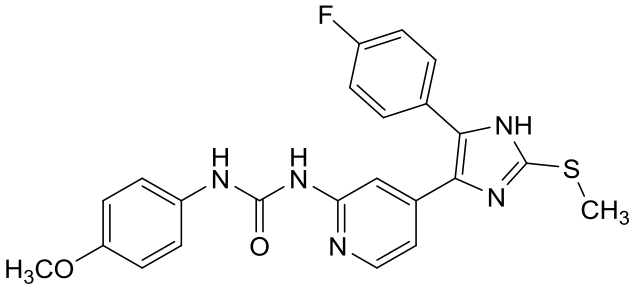

$C_{23}H_{20}FN_5O_2S$ (M_r 449.50)

206 was synthesized according to the general procedure from **120** (347 mg, 1.16 mmol), 4-methoxyphenyl isocyanate (165 µl, 1.27 mmol), and DIPEA (200 µl, 1.39 mmol). Purification was achieved by flash chromatography (SiO_2, 50-100 % ethyl acetate/petrol ether and RP-18, 60-100 % methanol/H_2O) to afford **206** as a pale yellow solid (99 % HPLC purity).

Yield: 137 mg (305 µmol, 26 %).

m.p.: 201 °C.

^{1}H NMR (300 MHz, DMSO-d_6): δ = 2.62 (s, 3 H, SCH_3), 3.72 (s, 3 H, OCH_3), 6.86-6.90 (m, 2 H, C$^{3/5}H$, H_3CO-Phe), 6.92 (dd, ^3J = 5.4 Hz, ^4J = 1.5 Hz, 1 H, C^5H, Pyr), 7.30 (bs, 2 H, C$^{3/5}H$, F-Phe), 7.39-7.44 (m, 2 H, C$^{2/6}H$, H_3CO-Phe), 7.47-7.51 (m, 2 H, C$^{2/6}H$, F-Phe), 7.58 (bs, 1 H, C^3H, Pyr), 8.11 (bs, 1 H, C^6H, Pyr), 9.40 (bs, 1 H, N*H*), 10.35-10.71 (m, 1 H, N*H*), 12.74 (s, 1 H, N*H*, Imdz) ppm.

^{13}C NMR (75 MHz, DMSO-d_6): δ = 15.1 (S*C*H_3), 55.2 (O*C*H_3), 105.3 (*C*^{4}, Pyr), 108.7 (*C*^{3}H, Pyr), 114.0 (*C*$^{3/5}$H, H_3CO-Phe), 114.6 (*C*^{5}H, Pyr), 115.8 (d, $^2J_{CF}$ = 22.0 Hz, *C*$^{3/5}$H, F-Phe), 120.6 (*C*$^{2/6}$H, H_3CO-Phe), 130.6-130.8 (*C*$^{2/6}$H, F-Phe), 132.0 (*C*^{1}, H_3CO-Phe), 142.3 (*C*^{2}, Imdz), 146.4 (*C*^{6}H, Pyr), 152.3 (*C*O), 153.5 (*C*^{2}, Pyr), 154.9 (*C*^{4}, H_3CO-Phe), 162.1 (d, $^1J_{CF}$ = 252.6 Hz, *C*F) ppm.

IR (ATR): ṽ = 3400, 1668, 1607, 1574, 1541, 1510, 1466, 1418, 1370, 1296, 1244, 1223, 1030, 843, 822, 750 cm^{-1}.

HPLC (Method 3): t_R = 5.1 min.

LC-MS (ESI, 70 eV): m/z = 450 $[MH]^+$ (calc. m/z = 449).

1-(4-(5-(4-Fluorophenyl)-2-(methylthio)-1*H*-imidazol-4-yl)pyridin-2-yl)-3-(*m*-tolyl)-carbamide (208)

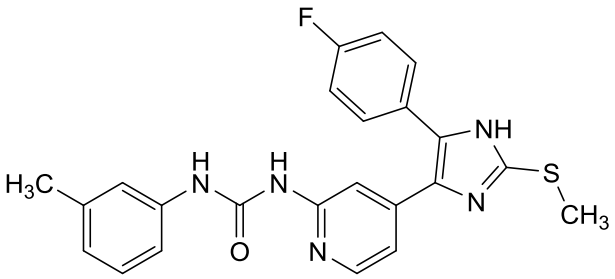

$C_{23}H_{20}FN_5OS$ (M_r 433.51)

208 was synthesized according to the general procedure from **120** (600 mg, 2.00 mmol), 3-methylphenyl isocyanate (284 µl, 2.20 mmol), and DIPEA (420 µl, 2.40 mmol). Purification was achieved by flash chromatography (SiO_2, 30-100 % ethyl acetate/petrol ether and RP-18, 60-80 % methanol/H_2O) to afford **208** as a pale colorless solid (100 % HPLC purity).

Yield: 241 mg (557 µmol, 28 %).

m.p.: 211 °C.

^{1}H NMR (300 MHz, DMSO-d_6): δ = 2.29 (s, 3 H, CH_3), 2.63 (s, 3 H, SCH_3), 6.83 (d, ^3J = 7.4 Hz, 1 H, C^4H, Tol), 6.95 (dd, ^3J = 5.4 Hz, ^4J = 1.5 Hz, 1 H, C^5H, Pyr), 7.15-7.35 (m, 2 H, C$^{3/5}H$, F-Phe), 7.17 (t, ^3J = 7.6 Hz, 1 H, C^5H, Tol), 7.31 (d, ^3J = 8.0 Hz, 1 H, C^6H, Tol), 7.35 (s, 1 H, C^2H, Tol), 7.47-7.52 (m, 2 H, C$^{2/6}H$, F-Phe), 7.61 (bs, 1 H, C^3H, Pyr), 8.13 (bs, 1 H, C^6H, Pyr), 9.44 (s, 1 H, NH), 10.42-10.78 (m, 1 H, NH), 12.74 (bs, 1 H, NH, Imdz) ppm.

^{13}C NMR (75 MHz, DMSO-d_6): δ = 15.1 (SCH$_3$), 21.2 (CH$_3$), 108.7 (C^3H, Pyr), 114.8 (C^5H, Pyr), 115.8 (d, $^2J_{CF}$ = 22.3 Hz, $C^{3/5}$H, F-Phe), 116.0 (C^6H, Tol), 119.3 (C^2H, Tol), 123.2 (C^4H, Tol), 126.6 (d, $^4J_{CF}$ = 2.6 Hz, C^1, F-Phe), 128.7 (C^5H, Tol), 129.7 (C^5, Imdz), 130.8 ($C^{2/6}$H, F-Phe), 134.2 (C^4, Imdz), 138.1 (C^3, Tol), 139.0 (C^1, Tol), 142.4 (C^2, Imdz), 144.3 (C^4, Pyr), 146.4 (C^6H, Pyr), 152.1 (CO), 153.4 (C^2, Pyr), 162.0 (d, $^1J_{CF}$ = 243.0 Hz, CF) ppm.

IR (ATR): $\tilde{\nu}$ = 3358, 3200, 2980, 1674, 1607, 1581, 1549, 1518, 1476, 1462, 1366, 1294, 1219, 1207, 1157, 1094, 843, 810, 770, 737, 725, 679, 611 cm^{-1}.

HPLC (Method 3): t_R = 6.8 min.

LC-MS (ESI, 70 eV): m/z = 434 $[MH]^+$ (calc. m/z = 433).

1-(3-Chloro-4-methylphenyl)-3-(4-(5-(4-fluorophenyl)-2-(methylthio)-1*H*-imidazol-4-yl)-pyridin-2-yl)carbamide (209)

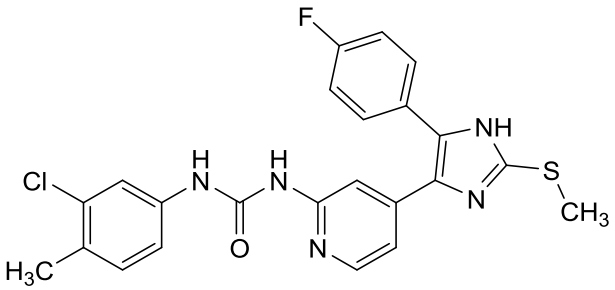

$C_{23}H_{19}ClFN_5OS$ (M_r 467.95)

209 was synthesized according to the general procedure from **120** (400 mg, 1.33 mmol), 3-chloro-4-methylyphenyl isocyanate (205 µl, 1.47 mmol), and DIPEA (279 µl, 1.60 mmol). Purification was achieved by flash chromatography (SiO_2, 0-10 % methanol/dichloromethane and RP-18, 70-100 % methanol/H_2O and SiO_2, 20-100 % ethyl acetate/petrol ether) to afford **209** as a colorless solid (98 % HPLC purity).

Yield: 210 mg (450 µmol, 34 %).

m.p.: 210 °C.

^{1}H NMR (300 MHz, DMSO-d_6): δ = 2.27 (s, 3 H, CH_3), 2.63 (s, 3 H, SCH_3), 6.96 (dd, ^3J = 5.5 Hz, ^4J = 1.4 Hz, 1 H, C^5*H*, Pyr), 7.26 (m, 2 H, C$^{5/6}$*H*, Cl-Tol), 7.28-7.34 (m, 2 H, C$^{3/5}$*H*, F-Phe), 7.46-7.50 (m, 2 H, C$^{2/6}$*H*, F-Phe), 7.59 (bs, 1 H, C^3*H*, Pyr), 7.77 (s, 1 H, C^2*H*, Cl-Tol), 8.12 (d, ^3J = 5.4 Hz, 1 H, C^6*H*, Pyr), 9.51 (s, 1 H, N*H*), 10.99 (s, 1 H, N*H*), 12.73 (s, 1 H, N*H*, Imdz) ppm.

^{13}C NMR (75 MHz, DMSO-d_6): δ = 15.1 (S*C*H$_3$), 18.8 (*C*H$_3$), 108.7 (*C*^{3}H, Pyr), 114.8 (*C*^{5}H, Pyr), 115.9 (d, $^2J_{CF}$ = 21.7 Hz, *C*$^{3/5}$H, F-Phe), 117.6 (*C*^{6}H, Cl-Tol), 118.7 (*C*^{2}H, Cl-Tol), 126.5 (d, $^4J_{CF}$ = 3.1 Hz, *C*^{1}, F-Phe), 128.9 (*C*^{4}, Cl-Tol), 130.4 (*C*^{5}, Imdz), 130.8 (d, $^3J_{CF}$ = 8.3 Hz, *C*$^{2/6}$H, F-Phe), 131.2 (*C*^{5}H, Cl-Tol), 133.2 (*C*^{3}, Cl-Tol), 134.1 (*C*^{4}, Imdz), 138.2 (*C*^{1}, Cl-Tol), 142.3 (*C*^{2}, Imdz), 144.3 (*C*^{4}, Pyr), 146.4 (*C*^{6}H, Pyr), 152.2 (*C*O), 153.2 (*C*^{2}, Pyr), 162.1 (d, $^1J_{CF}$ = 245.5 Hz, *C*F) ppm.

IR (ATR): $\tilde{\nu}$ = 3400, 2920, 1672, 1605, 1543, 1520, 1499, 1464, 1364, 1368, 1302, 1265, 1272, 1159, 880, 860, 839, 816, 754 cm^{-1}.

HPLC (Method 3): t_R = 6.9 min.

LC-MS (ESI, 70 eV): *m*/*z* = 468 [MH]$^+$ (calc. *m*/*z* = 467).

1-(4-(5-(4-Fluorophenyl)-2-(methylthio)-1*H*-imidazol-4-yl)pyridin-2-yl)-3-(3-(trifluoromethyl)phenyl)carbamide (210)

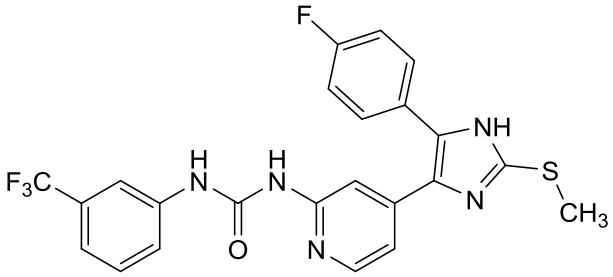

$C_{23}H_{17}FN_5OS$ (M_r 487.48)

210 was synthesized according to the general procedure from **120** (600 mg, 2.00 mmol), 3-(trifluoromethyl)phenyl isocyanate (300 µl, 2.20 mmol), and DIPEA (420 µl, 2.40 mmol). Purification was achieved by flash chromatography (SiO_2, 40 % methanol/dichloromethane) and subsequent filtration to afford **210** as a colorless solid (98 % HPLC purity).

Yield: 255 mg (523 µmol, 26 %).

m.p.: 234 °C.

^{1}H NMR (300 MHz, DMSO-d_6): δ = 2.63 (s, 3 H, SCH_3), 6.99 (dd, ^3J = 5.6 Hz, ^4J = 1.2 Hz, 1 H, C^5*H*, Pyr), 7.28-7.37 (m, 3 H, C$^{3/5}$*H*, F-Phe and C^4*H*, F_3C-Phe), 7.46-7.66 (m, 5 H, C^3*H*, Pyr and C$^{2/6}$*H*, F-Phe and C$^{5/6}$*H*, F_3C-Phe), 8.08 (bs, 1 H, C^2*H*, F_3C-Phe), 8.14 (d, ^3J = 5.5 Hz, 1 H, C^6*H*, Pyr), 9.56 (s, 1 H, N*H*), 11.12 (s, 1 H, N*H*), 12.74 (s, 1 H, N*H*, Imdz) ppm.

^{13}C NMR (75 MHz, DMSO-d_6): δ = 15.1 (S*C*H$_3$), 108.7 (*C*^{3}H, Pyr), 114.7 (*C*^{2}H, F_3C-Phe), 115.0 (*C*^{5}H, Pyr), 115.9 (d, $^2J_{CF}$ = 21.8 Hz, *C*$^{3/5}$H, F-Phe), 118.7 (*C*^{4}H, F_3C-Phe), 122.5 (*C*^{6}H, F_3C-Phe), 124.2 (q, $^1J_{CF}$ = 272.1 Hz, *C*F$_3$, F_3C-Phe), 126.5 (d, $^4J_{CF}$ = 2.9 Hz, *C*^{1}, F-Phe), 129.6 (q, $^2J_{CF}$ = 31.3 Hz, *C*^{3}, F_3C-Phe), 130.0 (*C*^{5}H, F_3C-Phe), 130.5 (*C*^{5}, Imdz), 130.8 (d, $^3J_{CF}$ = 8.3 Hz, *C*$^{2/6}$H, F-Phe), 134.0 (*C*^{4}, Imdz), 139.9 (*C*^{1}, F_3C-Phe), 142.3 (*C*^{2}, Imdz), 144.3 (*C*^{4}, Pyr), 146.6 (*C*^{6}H, Pyr), 152.2 (*C*O), 153.0 (*C*^{2}, Pyr), 162.0 (d, $^1J_{CF}$ = 245.2 Hz, *C*F) ppm.

IR (ATR): $\tilde{\nu}$ = 3300, 2900, 1670, 1609, 1581, 1541, 1520, 1497, 1464, 1381, 1370, 1331, 1312, 1294, 1256, 1217, 1207, 1180, 1157, 1134, 1099, 1072, 986, 923, 889, 871, 839, 814, 791, 754, 694 cm^{-1}.

HPLC (Method 3): t_R = 7.3 min.

LC-MS (ESI, 70 eV): m/z = 488 $[MH]^+$ (calc. m/z = 487).

HRMS (EI, 70 eV): m/z = 487.1090 $[M]^+$ (calc. m/z = 487.1090)

1-(4-(5-(4-Fluorophenyl)-2-(methylthio)-1*H*-imidazol-4-yl)pyridin-2-yl)-3-(naphthalen-1-yl)carbamide (212)

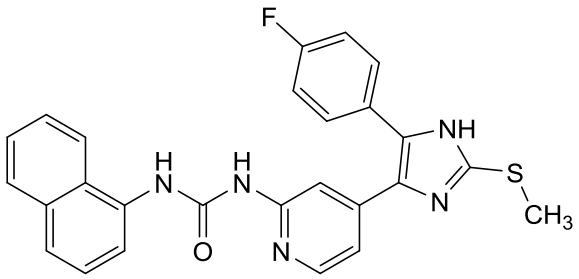

$C_{26}H_{20}FN_5OS$ (M_r 469.54)

212 was synthesized according to the general procedure from **120** (400 mg, 1.33 mmol), naphthyl isocyanate (211 µl, 1.47 mmol), and DIPEA (280 µl, 1.60 mmol). Purification was achieved by flash chromatography (SiO_2, 0-10 % methanol/dichloromethane and SiO_2, 30-100 % ethyl acetate/petrol ether and RP-18, 50-100 % methanol/H_2O) to afford **212** as a pale yellow solid (100 % HPLC purity).

Yield: 257 mg (546 µmol, 41 %).

m.p.: 249 °C.

^{1}H NMR (300 MHz, DMSO-d_6): δ = 2.64 (s, 3 H, SCH_3), 7.01 (dd, ^3J = 5.5 Hz, ^4J = 1.4 Hz, 1 H, C^5*H*, Pyr), 7.30-7.36 (m, 2 H, C$^{3/5}$*H*, F-Phe), 7.42-7.59 (m, 5 H, C^3*H*, Pyr and C$^{2/6}$*H*, F-Phe and C$^{3/6}$*H*, Naph), 7.63-7.68 (m, 2 H, C$^{4/7}$*H*, Naph), 7.95 (d, ^3J = 8.1 Hz, 1 H, C^5*H*, Naph), 8.16-8.22 (m, 2 H, C$^{2/8}$*H*, Naph), 8.27 (d, ^3J = 5.5 Hz, 1 H, C^6*H*, Pyr), 9.87 (s, 1 H, N*H*), 11.86 (bs, 1 H, N*H*), 12.77 (s, 1 H, N*H*, Imdz) ppm.

^{13}C NMR (75 MHz, DMSO-d_6): δ = 15.1 (S*C*H$_3$), 108.7 (*C*^{3}H, Pyr), 114.7 (*C*^{5}H, Pyr), 115.9 (d, $^2J_{CF}$ = 21.7 Hz, *C*$^{3/5}$H, F-Phe), 116.7 (*C*^{2}H, Naph), 120.9 (*C*^{8}H, Naph), 123.0 (*C*^{4}H, Naph), 125.4 (*C*^{1}, Naph), 126.0 (*C*$^{3/6}$H, Naph), 126.3 (*C*^{7}H, Naph), 126.5 (d, $^4J_{CF}$ = 3.2 Hz, *C*^{1}, F-Phe), 128.6 (*C*^{5}H, Naph), 130.6 (*C*^{5}, Imdz), 130.8 (d, $^3J_{CF}$ = 8.3 Hz, *C*$^{2/6}$H, F-Phe), 133.7 (*C*^{4a}, Naph), 134.0 (*C*^{8a}, Naph), 134.2 (*C*^{4}, Imdz), 142.4 (*C*^{2}, Imdz), 144.5 (*C*^{4}, Pyr), 146.1 (*C*^{6}H, Pyr), 152.6 (*C*O), 153.5 (*C*^{2}, Pyr), 162.1 (d, $^1J_{CF}$ = 246.2 Hz, *C*F) ppm.

IR (ATR): $\tilde{\nu}$ = 3040, 1686, 1614, 1601, 1571, 1497, 1481, 1362, 1346, 1304, 1225, 976, 837, 791, 770, 739, 716, 683 cm^{-1}.

HPLC (Method 3): t_R = 7.6 min.

LC-MS (ESI, 70 eV): m/z = 471 [MH]$^+$ (calc. m/z = 469).

7.3.5 Syntheses of Series 4: Five-membered Heterocycles

1-(*tert*-Butyl) 2-ethyl 4-bromo-1*H*-pyrrole-1,2-dicarboxylate (218)

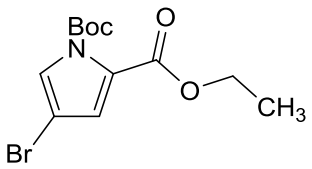

$C_{12}H_{16}BrNO_4$ (M_r 318.17)

4-DMAP (137 mg, 1.12 mmol) and Boc_2O (3.18 g, 14.6 mmol) were added to a solution of ethyl 4-bromo-1*H*-pyrrole-2-carboxylate (2.37 g, 10.9 mmol) in 18 ml anhyd. acetonitrile under a nitrogen atmosphere and the resulting mixture was stirred at rt for 1 h. Ethyl acetate was added and the mixture was washed with sat. aq. $NaHSO_4$ solution, H_2O, and sat. aq. NaCl solution. The organic phase was dried over anhyd. Na_2SO_4 and the solvent was removed under reduced pressure. The crude product was purified by flash chromatography (SiO_2, 2-10 % ethyl acetate/petrol ether) to afford **218** as clear yellowish oil (98 % HPLC purity).

Yield: 3.39 g (10.7 mmol, 98 %) (Lit.[230]: 93 %).

^{1}H NMR (300 MHz, DMSO-d_6): δ = 1.26 (t, ^3J = 7.1 Hz, 3 H, $COOCH_2CH_3$), 1.52 (s, 9 H, ^{t}Bu), 4.23 (q, ^3J = 7.1 Hz, 2 H, $COOCH_2CH_3$), 6.93 (d, ^4J = 1.8 Hz, 1 H, C^3*H*, Pyrrole), 7.62 (d, ^4J = 1.8 Hz, 1 H, C^5*H*, Pyrrole) ppm.

^{13}C NMR (75 MHz, DMSO-d_6): δ = 13.9 (CH_3), 27.0 ($C(CH_3)_3$), 61.0 (CH_2), 85.7 ($C(CH_3)_3$), 98.1 (*C*Br), 120.9 (*C*^{3}H, Pyrrole), 125.5 (*C*^{5}H, Pyrrole), 125.5 (*C*^{2}, Pyrrole), 146.8 (*C*O), 159.3 ($COOCH_2CH_3$) ppm.

IR (ATR): $\tilde{\nu}$ = 2982, 1755, 1726, 1456, 1397, 1370, 1348, 1296, 1267, 1258, 1217, 1150, 1067, 922, 845, 771 cm^{-1}.

HPLC (Method 2): t_R = 7.6 min.

LC-MS (ESI, 70 eV): m/z = 340, 342 $[NaM]^+$, 262, 263, 264, 265 $[MH_2$-^{t}Bu$]^+$, 216, 217, 218 $[MH_2$-$C_5H_{10}O_2]^+$ (calc. m/z = 317).

Ethyl 4-bromo-1-methyl-1*H*-pyrrole-2-carboxylate (226)

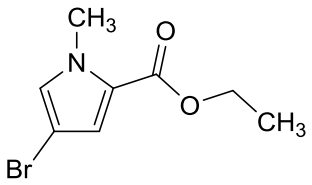

$C_8H_{10}BrNO_2$ (M_r 232.08)

Sodium hydride (240 mg 60 % dispersion in mineral oil, 6.05 mmol) was added in one portion to a solution of 4-bromo-1*H*-pyrrole-2-carboxylate (1.17 g, 5.34 mmol) in 15 ml anhyd. DMF at 0 °C under a nitrogen atmosphere. The suspension was stirred for 20 min at the same temp. before methyl iodide (400 µl, 6.43 mmol) was carefully added dropwise and stirring continued at 0 °C for 15 min and another 2.5 h at rt. The reaction was quenched with H_2O and extracted with ethyl acetate. The combined organic phases were washed with H_2O and sat. aq. NaCl solution, dried over anhyd. Na_2SO_4, and the solvent was removed under reduced pressure. Purification was achieved by flash chromatography (SiO_2, 2-10 % ethyl acetate/petrol ether) to afford **226** as clear colorless oil that crystallized on standing as colorless needles (100 % HPLC purity).

Yield: 1.22 g (5.25 mmol, 98 %).

m.p.: 43 °C.

^{1}H NMR (300 MHz, DMSO-d_6): δ = 1.26 (t, ^3J = 7.1 Hz, 3 H, $COOCH_2CH_3$), 3.83 (d, J = 0.2 Hz, 3 H, CH_3), 4.21 (q, ^3J = 7.1 Hz, 2 H, $COOCH_2CH_3$), 6.84 (d, ^4J = 2.0 Hz, 1 H, C^3H, Pyrrole), 7.28 (d, ^4J = 1.7 Hz, 1 H, C^5H, Pyrrole) ppm.

^{13}C NMR (75 MHz, DMSO-d_6): δ = 14.2 ($COOCH_2CH_3$), 36.6 (CH_3), 59.8 ($COOCH_2CH_3$), 93.8 (CBr), 118.1 (C^3H, Pyrrole), 122.7 (C^2, Pyrrole), 129.5 (C^5H, Pyrrole), 159.5 ($COOCH_2CH_3$) ppm.

IR (ATR): $\tilde{\nu}$ = 3129, 2984, 1703, 1688, 1468, 1414, 1400, 1389, 1331, 1242, 1186, 1111, 1078, 1057, 1022, 926, 818, 785, 750 cm^{-1}.

HPLC (Method 2): t_R = 6.1 min.

Ethyl 4-(2,4-dimethoxyphenyl)-1*H*-pyrrole-2-carboxylate (219)

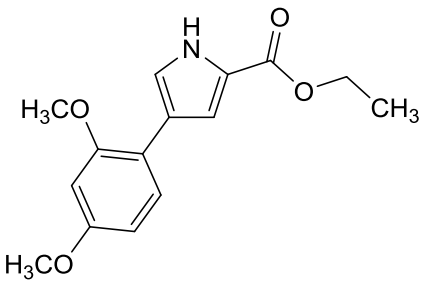

$C_{15}H_{17}NO_4$ (M_r 275.30)

To a stirred solution of **218** (1.40 g, 4.40 mmol), 2,4-dimethoxyphenyl boronic acid (2.41 g, 13.3 mmol), and $Pd(PPh_3)_4$ (259 mg, 224 µmol) in 50 ml DMF, 22 ml 2 M aq. Na_2CO_3 solution were added. The mixture was stirred under reflux for 4 h and another 12 h at rt. After addition of H_2O the mixture was extracted with ethyl acetate and the combined organic phases were washed with H_2O and sat. aq. NaCl solution, dried over anhyd. Na_2SO_4, and the solvent was removed under reduced pressure. The crude product was purified by flash chromatography (SiO_2, 5-10 % ethyl acetate/petrol ether) to afford **219** as a colorless solid (100 % HPLC purity).

Yield: 1.15 g (4.19 mmol, 95 %).

m.p.: 121 °C.

^{1}H NMR (300 MHz, DMSO-d_6): δ = 1.29 (t, ^3J = 7.1 Hz, 3 H, $COOCH_2CH_3$), 3.77 (s, 3 H, C^2OCH_3), 3.84 (s, 3 H, C^4OCH_3), 4.25 (q, ^3J = 7.1 Hz, 2 H, $COOCH_2CH_3$), 6.52 (dd, ^3J = 8.5 Hz, ^4J = 2.5 Hz, 1 H, C^5H, $(OCH_3)_2$-Phe), 6.60 (d, ^4J = 2.4 Hz, 1 H, C^3H, $(OCH_3)_2$-Phe), 7.12 (dd, ^4J = 2.6 Hz, ^5J = 1.7 Hz, 1 H, C^5H, Pyrrole), 7.36 (dd, ^4J = 3.1 Hz, ^5J = 1.7 Hz, 1 H, C^3H, Pyrrole), 7.48 (d, ^3J = 8.5 Hz, 1 H, C^6H, $(OCH_3)_2$-Phe), 11.85 (bs, 1 H, N*H*) ppm.

^{13}C NMR (75 MHz, DMSO-d_6): δ = 14.5 ($COOCH_2CH_3$), 55.2 (C^2OCH_3), 55.4 (C^4OCH_3), 59.5 ($COOCH_2CH_3$), 98.8 (C^3H, $(OCH_3)_2$-Phe), 105.2 (C^5H, $(OCH_3)_2$-Phe), 113.4 (C^5, Pyrrole), 115.8 (C^1, $(OCH_3)_2$-Phe), 121.2 (C^4, Pyrrole), 121.6 (C^2, Pyrrole), 122.6 (C^3H, Pyrrole), 127.9 (C^6H, $(OCH_3)_2$-Phe), 156.7 (C^4OCH_3), 158.7 (C^2OCH_3), 160.5 (*C*O) ppm.

IR (ATR): $\tilde{\nu}$ = 3304, 2950, 1676, 1614, 1579, 1518, 1462, 1435, 1402, 1379, 1358, 1304, 1292, 1244, 1207, 1165, 1148, 1130, 1051, 1030, 972, 936, 835, 804, 795, 770, 731, 604 cm^{-1}.

HPLC (Method 2): t_R = 5.6 min.

LC-MS (ESI, 70 eV): m/z = 276 $[MH]^+$ (calc. m/z = 275).

Ethyl 4-(2,4-dimethoxyphenyl)-1-methyl-1*H*-pyrrole-2-carboxylate (227)

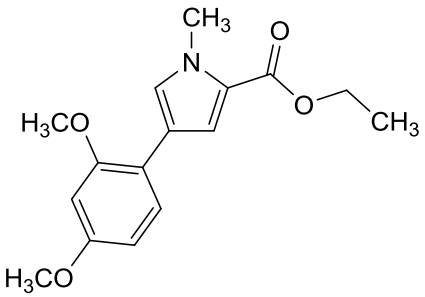

$C_{16}H_{19}NO_4$ (M_r 289.33)

Method A. **227** was synthesized according to the procedure described for **219** from **226** (1.22 g, 5.26 mmol), 2,4-dimethoxyphenyl boronic acid (2.89 g, 15.9 mmol), $Pd(PPh_3)_4$ (306 mg, 265 µmol) in 80 ml DMF, and 27 ml 2 M aq. Na_2CO_3 solution. Purification was achieved by flash chromatography (SiO_2, 5-10 % ethyl acetate/petrol ether and RP-18, 50-70 % methanol/H_2O) to afford **227** as a colorless solid (100 % HPLC purity).

Yield: 1.02 g (3.52 mmol, 67 %).

Method B. **227** was synthesized according to the procedure for **226** from 2**19** (800 mg, 2.91 mmol), sodium hydride (164 mg 60 % dispersion in mineral oil, 4.10 mmol), and methyl iodide (270 µl, 4.34 mmol) in 10 ml anhyd. DMF. **227** was obtained as a colorless solid (100 % HPLC purity).

Yield: 720 mg (2.49 mmol, 86 %).

^{1}H NMR (300 MHz, DMSO-d_6): δ = 1.29 (t, ^3J = 7.1 Hz, 3 H, $COOCH_2CH_3$), 3.77 (s, 3 H, C^4OCH_3), 3.84 (s, 3 H, C^2OCH_3), 3.87 (s, 3 H, CH_3), 4.23 (q, ^3J = 7.1 Hz, 2 H, $COOCH_2CH_3$), 6.53 (dd, ^3J = 8.5 Hz, ^4J = 2.5 Hz, 1 H, C^5H, $(OCH_3)_2$-Phe), 6.60 (d, ^4J = 2.5 Hz, 1 H, C^3H, $(OCH_3)_2$-Phe), 7.17 (d, ^4J = 2.0 Hz, 1 H, C^3H, Pyrrole), 7.44 (d, ^3J = 8.5 Hz, 1 H, C^6H, $(OCH_3)_2$-Phe), 7.46 (dd, ^4J = 2.0 Hz, ^5J = 0.4 Hz, 1 H, C^5H, Pyrrole) ppm.

^{13}C NMR (75 MHz, DMSO-d_6): δ = 14.4 ($COOCH_2\mathit{C}H_3$), 36.4 ($\mathit{C}H_3$), 55.2 ($C^4O\mathit{C}H_3$), 55.4 ($C^2O\mathit{C}H_3$), 59.4 ($\mathit{C}H_2$), 98.8 (C^3H, $(OCH_3)_2$-Phe), 105.2 (C^5H, $(OCH_3)_2$-Phe), 115.4 (C^3H, Pyrrole), 115.5 (C^1, $(OCH_3)_2$-Phe), 119.0 (C^4, Pyrrole), 121.3 (C^2, Pyrrole), 127.7 (C^6H, $(OCH_3)_2$-Phe), 129.0 (C^5H, Pyrrole), 156.7 (C^4OCH_3), 158.74 (C^2OCH_3), 160.5 ($\mathit{C}OOCH_2CH_3$) ppm.

IR (ATR): $\tilde{\nu}$ = 1676, 1613, 1559, 1495, 1466, 1435, 1412, 1360, 1287, 1204, 1180, 1128, 1109, 1051, 1032, 947, 828, 756 cm^{-1}.

HPLC (Method 2): t_R = 6.7 min.

LC-MS (ESI, 70 eV): m/z = 290 $[MH]^+$ (calc. m/z = 289).

Ethyl 1-benzyl-4-(2,4-dimethoxyphenyl)-1*H*-pyrrole-2-carboxylate (228)

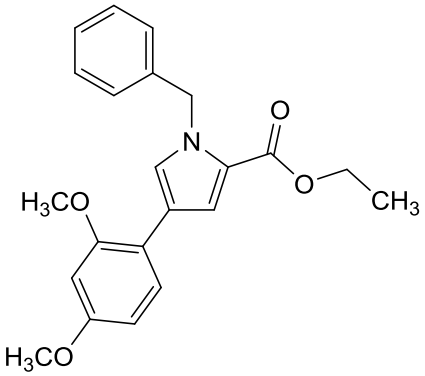

$C_{22}H_{23}NO_4$ (M_r 365.43)

228 was synthesized according to the procedure for **226** from **219** (216 mg, 783 µmol), sodium hydride (45.0 mg 60 % dispersion in mineral oil, 1.13 mmol), and benzyl bromide (180 µl, 1.51 mmol) in 6 ml anhyd. DMF. The crude product was purified by flash chromatography (SiO_2, 2-10 % ethyl acetate/petrol ether) to afford **228** as a colorless solid (98 % HPLC purity).

Yield: 186 mg (508 µmol, 65 %).

^{1}H NMR (300 MHz, DMSO-d_6): δ = 1.22 (t, ^3J = 7.1 Hz, 3 H, CH_3), 3.77 (s, 3 H, OCH_3), 3.83 (s, 3 H, OCH_3), 4.17 (q, ^3J = 7.1 Hz, 2 H, CH_2), 5.57 (s, 2 H, CH_2 Bn), 6.54 (dd, ^3J = 8.5 Hz, ^4J = 2.5 Hz, 1 H, C^5H, $(OCH_3)_2$-Phe), 6.61 (d, ^4J = 2.4 Hz, 1 H, C^6H, $(OCH_3)_2$-Phe), 7.10-7.13 (m, 2 H, ^{ar}CH, Bn), 7.23-7.34 (m, 3 H, ^{ar}CH, Bn), 7.27 (d, ^4J = 2.0 Hz, 1 H, C^3H, Pyrrole), 7.49 (d, ^3J = 8.5 Hz, 1 H, C^6H, $(OCH_3)_2$-Phe), 7.66 (d, ^4J = 2.0 Hz, 1 H, C^5H, Pyrrole) ppm.

HPLC (Method 3): t_R = 8.0 min.

LC-MS (ESI, 70 eV): m/z = 366 $[MH]^+$ (calc. m/z = 365).

Ethyl 4-(2,5-dimethoxyphenyl)-1-methyl-1*H*-pyrrole-2-carboxylate (229)

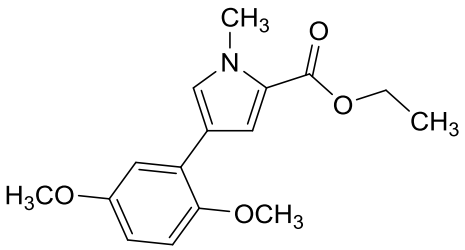

$C_{16}H_{19}NO_4$ (M_r 289.33)

229 was synthesized according to the general procedure for **219** from **217** (1.11 g, 4.78 mmol), 2,4-dimethoxyphenyl boronic acid (2.65 g, 14.6 mmol), $Pd(PPh_3)_4$ (289 mg, 250 µmol) in 80 ml DMF, and 25 ml 2 M aq. Na_2CO_3 solution. Purification was achieved by flash chromatography (SiO_2, 2-10 % ethyl acetate/petrol ether and RP-18, 65 % methanol/H_2O) to afford **229** as a colorless solid (100 % HPLC purity).

Yield: 984 mg (3.40 mmol, 71 %).

m.p.: > 360 °C.

^{1}H NMR (300 MHz, DMSO-d_6): δ = 1.30 (t, ^3J = 7.1 Hz, 3 H, $COOCH_2CH_3$), 3.74 (s, 3 H, C^5OCH_3), 3.79 (s, 3 H, C^2OCH_3), 3.89 (s, 3 H, CH_3), 4.24 (q, ^3J = 7.1 Hz, 2 H, $COOCH_2CH_3$), 6.74 (dd, ^3J = 8.9 Hz, ^4J = 3.1 Hz, 1 H, C^4H, $(OCH_3)_2$-Phe), 6.96 (d, ^3J = 8.9 Hz, 1 H, C^3H, $(OCH_3)_2$-Phe), 7.09 (d, ^4J = 3.1 Hz, 1 H, C^6H, $(OCH_3)_2$-Phe), 7.28 (d, ^4J = 2.0 Hz, 1 H, C^3H, Pyrrole), 7.60 (dd, ^4J = 2.0 Hz, ^5J = 0.4 Hz, 1 H, C^5H, Pyrrole) ppm.

^{13}C NMR (75 MHz, DMSO-d_6): δ = 14.3 ($COOCH_2CH_3$), 36.5 (CH_3), 55.4 (C^5OCH_3), 55.9 (C^2OCH_3), 59.4 ($COOCH_2CH_3$), 111.7 (C^4H, $(OCH_3)_2$-Phe), 112.5 (C^6H, $(OCH_3)_2$-Phe), 112.9 (C^3H, $(OCH_3)_2$-Phe), 116.1 (C^3H, Pyrrole), 118.9 (C^4, Pyrrole), 121.6 (C^1, Pyrrole), 123.4 (C^1, $(OCH_3)_2$-Phe), 130.0 (C^5H, Pyrrole), 150.0 (C^2OCH_3), 153.4 (C^5OCH_3), 160.5 ($COOCH_2CH_3$) ppm.

HPLC (Method 2): t_R = 6.2 min.

LC-MS (ESI, 70 eV): m/z = 290 $[MH]^+$, 244 $[MH\text{-}CH_3CH_2O]^+$ (calc. m/z = 289).

4-(2,4-Dimethoxyphenyl)-1*H*-pyrrole-2-carboxylic acid (216)

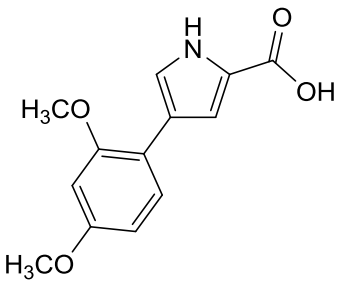

$C_{13}H_{13}NO_4$ (M_r 247.25)

23 ml 4 M aq. NaOH were added to a solution of **219** (3.08 g, 11.2 mmol) in 60 ml THF and 30 ml methanol and the mixture was stirred at 50 °C for 5 h and then 12 h at rt. H_2O was added to the reaction, the pH was adjusted to 3 using 1 M aq. HCl, and the mixture was extracted with ethyl acetate. The combined organic phases were washed with H_2O and sat. aq. NaCl solution, the organic phase was dried over anhyd. Na_2SO_4, and the solvent was removed under reduced pressure to afford **216** as a beige solid (100 % purity, HPLC).

Yield: 2.78 g (11.2 mmol, quant.).

m.p.: 170 °C.

^{1}H NMR (300 MHz, DMSO-d_6): δ = 3.76 (s, 3 H, C^{2}OCH_3), 3.83 (s, 3 H, C^{4}OCH_3), 6.52 (dd, ^3J = 8.5 Hz, ^4J = 2.5 Hz, 1 H, C^5H, $(OCH_3)_2$-Phe), 6.59 (d, ^4J = 2.4 Hz, 1 H, C^3H, $(OCH_3)_2$-Phe), 7.08 (dd, ^4J = 2.6 Hz, ^5J = 1.7 Hz, 1 H, C^3H, Pyrrole), 7.32 (dd, ^4J = 3.0 Hz, ^5J = 1.7 Hz, 1 H, C^5H, Pyrrole), 7.46 (d, ^3J = 8.5 Hz, 1 H, C^6H, $(OCH_3)_2$-Phe), 11.71 (bs, 1 H, N*H*), 12.22 (bs, 1 H, COO*H*) ppm.

^{13}C NMR (75 MHz, DMSO-d_6): δ = 55.2 (C^{2}O*C*H$_3$), 55.4 (C^{4}O*C*H$_3$), 98.8 (*C*^{3}H, $(OCH_3)_2$-Phe), 105.2 (*C*^{5}H, $(OCH_3)_2$-Phe), 113.3 (*C*^{3}H, Pyrrole), 116.1 (*C*^{1}, $(OCH_3)_2$-Phe), 121.0 (*C*^{4}, Pyrrole), 122.1 (*C*^{5}H, Pyrrole), 122.4 (*C*^{2}, Pyrrole), 127.8 (*C*^{6}H, $(OCH_3)_2$-Phe), 156.7 (*C*^{4}OCH$_3$), 158.6 (*C*^{2}OCH$_3$), 162.0 (*C*OOH) ppm.

IR (ATR): $\tilde{\nu}$ = 3356, 2910, 1667, 1614, 1580, 1520, 1437, 1362, 1306, 1287, 1248, 1206, 1140, 1130, 1051, 1032, 972, 934, 829, 789, 764, 623 cm^{-1}.

HPLC (Method 2): t_R = 3.8 min.

LC-MS (ESI, 70 eV): m/z = 248 $[MH]^+$ (calc. m/z = 247).

4-(2,4-Dimethoxyphenyl)-1-methyl-1*H*-pyrrole-2-carboxylic acid (225)

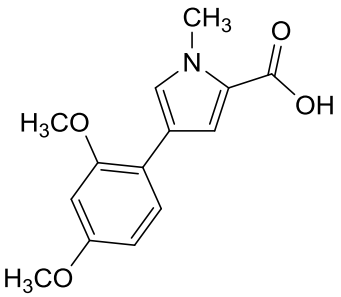

$C_{14}H_{15}NO_4$ (M_r 261.28)

Method A. **225** was synthesized according to the general procedure for **216** from **227** (990 mg, 3.42 mmol) in 18 ml THF and 9 ml methanol, and 7 ml 4 M aq. NaOH to afford **225** as a brown solid (99 % HPLC purity).

Yield: 894 mg (3.42 mmol, quant.).

Method B. To a solution of **216** (130 mg, 526 µmol) in 5 ml anhyd. DMF under a nitrogen atmosphere at 0 °C, sodium hydride (32.0 mg 60 % dispersion in mineral oil, 800 µmol) was added in one portion. The suspension was stirred at the same temp. for 20 min before methyl iodide (46.0 µl, 739 µmol) was added dropwise. After stirring for another 15 min at 0 °C and 2.5 h at rt, the reaction was quenched with H_2O, and extracted with ethyl acetate. The combined organic phases were washed with H_2O and sat. aq. NaCl solution, dried over anhyd. Na_2SO_4, and the solvent was removed under reduced pressure. The crude product was purified by flash chromatography (SiO_2, 2-30 % ethyl acetate/petrol ether) to afford **225** as a light pink solid (93 % HPLC purity).

Yield: 70.9 mg (271 µmol, 52 %).

m.p.: 164 °C.

^{1}H NMR (300 MHz, DMSO-d_6): δ = 3.76 (s, 3 H, C^{4}OCH_3), 3.83 (s, 3 H, C^{2}OCH_3), 3.86 (s, 3 H, CH_3), 6.53 (dd, ^3J = 8.5 Hz, ^4J = 2.4 Hz, 1 H, C^5H, $(OCH_3)_2$-Phe), 6.59 (d, ^4J = 2.4 Hz, 1 H, C^3H, $(OCH_3)_2$-Phe), 7.14 (d, ^4J = 2.0 Hz, 1 H, C^3H, Pyrrole), 7.41 (d, ^4J = 2.0 Hz, 1 H, C^5H, Pyrrole), 7.42 (d, ^3J = 8.4 Hz, 1 H, C^6H, $(OCH_3)_2$-Phe), 12.17 (bs, 1 H, COO*H*) ppm.

^{13}C NMR (75 MHz, DMSO-d_6): δ = 36.3 (*C*H_3), 55.2 (C^{4}O*C*H_3), 55.4 (C^{2}O*C*H_3), 98.8 (*C*^{3}H, $(OCH_3)_2$-Phe), 105.2 (*C*^{5}H, $(OCH_3)_2$-Phe), 115.7 (*C*^{3}H, Pyrrole), 115.7 (*C*^{1}, $(OCH_3)_2$-Phe), 118.8 (*C*^{4}, Pyrrole), 122.0 (*C*^{2}, Pyrrole), 127.6 (*C*^{6}H, $(OCH_3)_2$-Phe), 128.6 (*C*^{5}H, Pyrrole), 156.7 (*C*^{2}OCH_3), 158.7 (*C*^{4}OCH_3), 162.1 (*C*OOH) ppm.

IR (ATR): $\tilde{\nu}$ = 3316, 1678, 1611, 1578, 1516, 1449, 1379, 1290, 1242, 1206, 1161, 1144, 1051, 1032, 993, 936, 822, 797, 768, 725 cm^{-1}.

HPLC (Method 2): t_R = 5.5 min.

LC-MS (ESI, 70 eV): m/z = 262 $[MH]^+$ (calc. m/z = 261).

1-Benzyl-4-(2,4-dimethoxyphenyl)-1*H*-pyrrole-2-carboxylic acid (230)

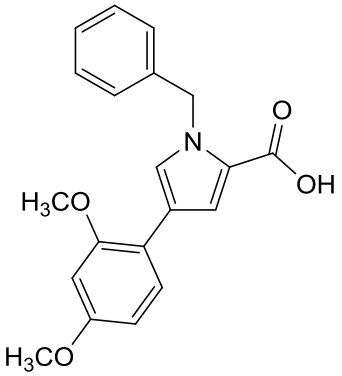

$C_{20}H_{19}NO_4$ (M_r 337.38)

230 was synthesized according to the general procedure for **216** from **219** (186 mg, 508 µmol) in 3 ml THF and 1.5 ml methanol, and 2 ml 4 M aq. NaOH to afford **230** as a pale orange solid (100 % HPLC purity).

Yield: 107 mg (318 µmol, 63 %).

^{1}H NMR (300 MHz, DMSO-d_6): δ = 3.77 (s, 3 H, C^4OCH_3), 3.83 (s, 3 H, C^2OCH_3), 5.58 (s, 2 H, CH_2, Bn), 6.54 (dd, ^3J = 8.5 Hz, ^4J = 2.5 Hz, 1 H, C^5H, $(OCH_3)_2$-Phe), 6.60 (d, ^4J = 2.4 Hz, 1 H, C^3H, $(OCH_3)_2$-Phe), 7.11-7.14 (m, 2 H, $^{ar}C^{2/6}H$, Bn), 7.21-7.34 (m, 3 H, $^{ar}C^{3-5}H$, Bn), 7.24 (d, ^4J = 2.0 Hz, 1 H, C^3H, Pyrrole), 7.47 (d, ^3J = 8.5 Hz, 1 H, C^6H, $(OCH_3)_2$-Phe), 7.60 (d, ^4J = 2.0 Hz, 1 H, C^5H, Pyrrole), 12.20 (s, 1 H, COO*H*) ppm.

^{13}C NMR (75 MHZ, DMSO-d_6): δ = 50.9 (CH_2, Bn), 55.2 (C^4OCH_3), 55.4 (C^2OCH_3), 98.8 (C^3H, $(OCH_3)_2$-Phe), 105.2 (C^5H, $(OCH_3)_2$-Phe), 115.4 (C^1, $(OCH_3)_2$-Phe), 116.3 (C^3H, Pyrrole), 119.4 (C^4, Pyrrole), 121.6 (C^2, Pyrrole), 126.6 ($^{ar}C^{2/6}$H, Bn), 127.1 ($^{ar}C^4$H, Bn), 127.7 (C^6H, $(OCH_3)_2$-Phe), 128.1 (C^5H, Pyrrole), 128.4 ($^{ar}C^{3/5}$H, Bn), 139.2 ($^{ar}C^1$, Bn), 156.7 (C^2OCH_3), 158.8 (C^4OCH_3), 161.9 (*C*OOH) ppm.

IR (ATR): $\tilde{\nu}$ = 2924, 1661, 1611, 1576, 1508, 1451, 1433, 1375, 1296, 1254, 1206, 1182, 1150, 1109, 1055, 1030, 937, 912, 837, 826, 785, 748, 727 cm^{-1}.

HPLC (Method 3): t_R = 6.5 min.

LC-MS (ESI, 70 eV): m/z = 338 $[MH]^+$ (calc. m/z = 337).

4-(2,5-Dimethoxyphenyl)-1-methyl-1*H*-pyrrole-2-carboxylic acid (222)

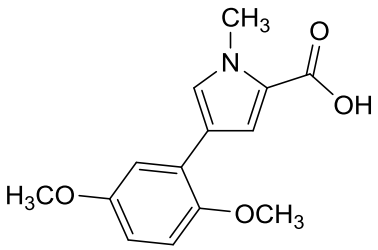

$C_{14}H_{15}NO_4$ (M_r 261.28)

222 was synthesized according to the procedure for **216** from **229** (980 mg, 3.39 mmol) in 19 ml THF and 10 ml methanol, and 7 ml 4 M aq. NaOH to afford **222** as a brown solid (100 % HPLC purity).

Yield: 885 mg (3.39 mmol, quant.).

m.p.: 149 °C.

^{1}H NMR (300 MHz, DMSO-d_6): δ = 3.74 (s, 3 H, C^{2}OCH_3), 3.79 (s, 3 H, C^{5}OCH_3), 3.88 (CH_3), 6.72 (dd, ^3J = 8.9 Hz, ^4J = 3.1 Hz, 1 H, C^4H, $(OCH_3)_2$-Phe), 6.95 (d, ^3J = 8.9 Hz, 1 H, C^3H, $(OCH_3)_2$-Phe), 7.08 (d, ^4J = 3.1 Hz, 1 H, C^6H, $(OCH_3)_2$-Phe), 7.25 (d, ^4J = 2.0 Hz, 1 H, C^3H, Pyrrole), 7.55 (d, ^4J = 2.0 Hz, 1 H, C^5H, Pyrrole), 12.15 (bs, 1 H, COOH) ppm.

^{13}C NMR (75 MHz, DMSO-d_6): δ = 36.4 (CH$_3$), 55.4 (C^{2}OCH$_3$), 55.9 (C^{5}OCH$_3$), 111.5 (C^4H, $(OCH_3)_2$-Phe), 112.5 (C^6H, $(OCH_3)_2$-Phe), 112.9 (C^3H, $(OCH_3)_2$-Phe), 116.2 (C^3H, Pyrrole), 118.7 (C^4, Pyrrole), 122.4 (C^2, Pyrrole), 123.6 (C^1, $(OCH_3)_2$-Phe), 129.6 (C^5H, Pyrrole), 150.1 (C^5OCH$_3$), 153.4 (C^2OCH$_3$), 162.1 (COOH) ppm.

IR (ATR): ṽ = 2940, 2832, 1667, 1603, 1553, 1505, 1462, 1437, 1410, 1352, 1300, 1273, 1258, 1219, 1202, 1172, 1130, 1113, 1071, 1045, 1024, 889, 856, 842, 822, 806, 737, 708. 663 cm^{-1}.

HPLC (Method 2): t_R = 5.6 min.

LC-MS (ESI, 70 eV): m/z = 262 $[MH]^+$, 218 $[M\text{-}CO_2]^+$ (calc. m/z = 261).

1*H*-Benzo[*d*][1,2,3]triazol-1-yl 4-(2,4-dimethoxyphenyl)-1-methyl-1*H*-pyrrole-2-carboxylate (224)

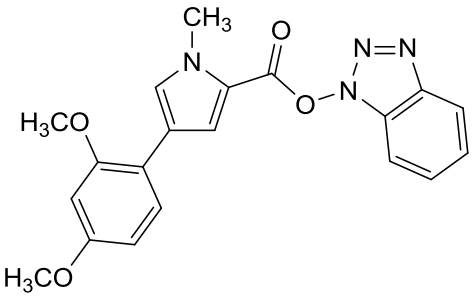

$C_{20}H_{18}N_4O_4$ (M_r 378.39)

225 (101 mg, 387 µmol) was dissolved in 5 ml anhyd. DMF and PyBOP (244 mg, 469 µmol) and DIPEA (210 µl, 1.20 mmol) were added. The mixture was stirred at rt for 1.5 h, quenched with H_2O, and extracted with ethyl acetate. The combined organic phases were washed with H_2O and sat. aq. NaCl solution, and dried over anhyd. Na_2SO_4. The solvent was removed under reduced pressure and the crude product was purified by flash chromatography (SiO_2, 2-30 % ethyl acetate/petrol ether) to afford **224** as a voluminous bright yellow solid (99 % HPLC purity).

Yield: 119 mg (314 µmol, 82 %).

^{1}H NMR (300 MHz, DMSO-d_6): δ = 3.80 (s, 3 H, C^{4}OCH_3), 3.89 (s, 3 H, C^{2}OCH_3), 3.93 (s, 3 H, CH_3), 6.59 (dd, ^3J = 8.5 Hz, ^4J = 2.5 Hz, 1 H, C^5H, $(OCH_3)_2$-Phe), 6.66 (d, ^4J = 2.4 Hz, 1 H, C^3H, $(OCH_3)_2$-Phe), 7.51-7.56 (m, 1 H, C^5H, Bt), 7.60 (d, ^3J = 8.5 Hz, 1 H, C^6H, $(OCH_3)_2$-Phe), 7.65-7.70 (m, 1 H, C^6H, Bt), 7.83 (d, ^4J = 1.9 Hz, 1 H, C^3H,Pyrrole), 7.86 (dt, ^3J = 8.2 Hz, ^4J = 0.8 Hz, 1 H, C^7H, Bt), 7.91 (d, ^4J = 1.9 Hz, 1 H, C^5H, Pyrrole), 8.17 (dt, ^3J = 8.4 Hz, ^4J = 0.9 Hz, 1 H, C^4H, Bt) ppm.

^{13}C NMR (75 MHz, DMSO-d_6): δ = 36.5 (*C*H_3), 55.2 (C^{4}O*C*H_3), 55.5 (C^{2}O*C*H_3), 98.9 (*C*^{3}H, $(OCH_3)_2$-Phe), 105.4 (*C*^{5}H, $(OCH_3)_2$-Phe), 109.3 (*C*^{7}H, Bt), 114.4 (*C*^{1}, $(OCH_3)_2$-Phe), 114.8 (*C*^{2}, Pyrrole), 119.1 (*C*^{3}H, Pyrrole), 119.8 (*C*^{4}H, Bt), 121.0 (*C*^{4}, Pyrrole), 125.2 (*C*^{5}H, Bt), 128.1 (*C*^{6}H, $(OCH_3)_2$-Phe), 128.7 (*C*^{7a}, Bt), 129.1 (*C*^{6}H, Bt), 133.5 (*C*^{5}H, Pyrrole), 142.8 (*C*^{3a}, Bt), 156.3 (*C*O), 156.9 (*C*^{2}OCH_3), 159.3 (*C*^{4}OCH_3) ppm.

HPLC (Method 3): t_R = 7.1 min.

LC-MS (ESI, 70 eV): m/z = 379 $[MH]^+$ (calc. m/z = 378).

_N_-(4-Methylpyridin-2-yl)-1_H_-pyrrole-2-carboxamide (221)

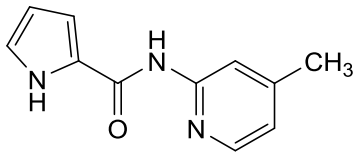

$C_{11}H_{11}N_3O$ (M_r 201.23)

A solution of 1*H*-pyrrole-2-carboxylic acid (201 mg, 1.81 mmol), PyBOP (1.13 g, 2.17 mmol), and DIPEA (950 µl, 5.44 mmol) in 5 ml anhyd. DMF was stirred under a nitrogen atmosphere for 30 min at rt before 2-amino4-methylpyridine (270 mg, 2.50 mmol) was added in one portion. The reaction was stirred for 12 h at 110 °C, quenched with H_2O, and extracted with ethyl acetate. The combined organic phases were washed with H_2O and sat. aq. NaCl solution, dried over anhyd. Na_2SO_4, and the solvent was removed under reduced pressure. The crude product was purified by flash chromatography (SiO_2, 20-100 % ethyl acetate/petrol ether) to afford **221** as a beige solid (99 % HLC purity).

Yield: 99.7 mg (495 mmol, 27 %).

^{1}H NMR (300 MHz, DMSO-d_6): δ = 2.33 (s, 3 H, CH_3), 6.14-6.17 (m, 1 H, C^4H, Pyrrole), 6.94 (dq, ^3J = 5.1 Hz, ^4J = 0.7 Hz, 1 H, C^5H, Pyr), 6.98-7.00 (m, 1 H, C^3H, Pyrrole), 7.23-7.26 (m, 1 H, C^5H, Pyrrole), 8.04 (m, 1 H, C^3H, Pyr), 8.19 (dd, ^3J = 5.0 Hz, ^5J = 0.5 Hz, 1 H, C^6H, Pyr), 10.21 (bs, 1 H, CONH), 11.67 (bs, 1 H, NH) ppm.

^{13}C NMR (75 MHz, DMSO-d_6): δ = 20.7 (CH$_3$), 108.9 (C^4H, Pyrrole), 112.4 (C^5H, Pyrrole), 114.2 (C^3H, Pyr), 119.8 (C^5H, Pyr), 122.8 (C^3H, Pyrrole), 125.3 (C^1, Pyrrole), 147.1 (C^6H, Pyr), 148.3 (C^4, Pyr), 152.2 (C^2, Pyr), 158.9 (CONH) ppm.

IR (ATR): ṽ = 3321, 3163, 3111, 2965, 2864, 1643, 1614, 1568, 1555, 1528, 1468, 1420, 1400, 1323, 1298, 1269, 1179, 1138, 1113, 1068, 1042, 999, 959, 891, 880, 847, 810, 745, 677 cm^{-1}.

HPLC (Method 2): t_R = 2.5 min.

LC-MS (ESI, 70 eV): m/z = 425 $[NaM_2]^+$, 202 $[MH]^+$ (calc. m/z = 201).

4-(2,4-Dimethoxyphenyl)-*N*-(4-(5-(4-fluorophenyl)-2-(methylthio)-1*H*-imidazol-4-yl)-pyridin-2-yl)-1*H*-pyrrole-2-carboxamide (220)

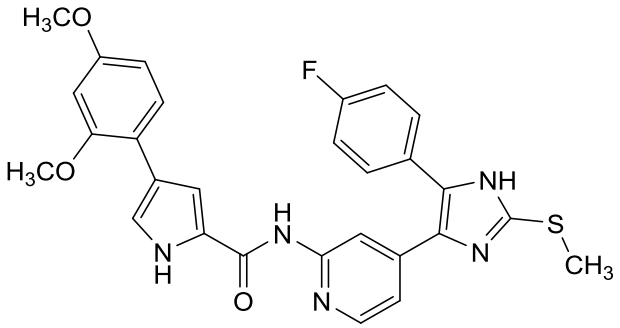

$C_{28}H_{24}FN_5O_3S$ (M_r 529.59)

A solution of **216** (1.01 g, 4.07 mmol), PyBOP (2.54 g, 4.88 mmol), and DIPEA (2.15 ml, 12.3 mmol) was stirred in 14 ml anhyd. DMF under a nitrogen atmosphere for 30 min at rt. **120** (1.60 g, 5.31 mmol) was added in one portion and the mixture was stirred for 12 h at 110 °C. The reaction was quenched with H_2O and extracted with ethyl acetate. The combined organic phases were washed with H_2O and sat. aq. NaCl solution, dried over anhyd. Na_2SO_4, and the solvent was removed under reduced pressure. The crude product was purified by flash chromatography (SiO_2, 30-100 % ethyl acetate/petrol ether and RP-18, 50-100 % methanol/H_2O) to afford **220** as a beige solid (95 % HPLC purity).

Yield: 285 mg (538 µmol, 13 %).

^{1}H NMR (300 MHz, DMSO-d_6): δ = 2.64 (s, 3 H, SCH_3), 3.78 (s, 3 H, C^{2}OCH_3), 3.85 (s, 3 H, C^{4}OCH_3), 6.57 (dd, ^3J = 8.5 Hz, ^4J = 2.4 Hz, 1 H, C^5H, $(OCH_3)_2$-Phe), 6.61 (d, ^4J = 2.3 Hz, 1 H, C^3H, $(OCH_3)_2$-Phe), 7.07 (dd, ^3J = 5.1 Hz, ^4J = 1.0 Hz, 1 H, C^5H, Pyr), 7.27-7.33 (m, 2 H, C$^{3/5}H$, F-Phe), 7.36 (bs, 1 H, C^3H, Pyrrole), 7.4 (d, ^3J = 8.4 Hz, 1 H, C^6H, $(OCH_3)_2$-Phe), 7.49-7.58 (m, 2 H, C$^{2/6}H$, F-Phe), 7.64 (bs, 1 H, C^5H, Pyrrole), 8.19 (d, ^3J = 5.2 Hz, 1 H, C^6H, Pyr), 8.31 (bs, 1 H, C^3H, Pyr), 10.20 (bs, 1 H, CONH), 11.69 (bs, 1 H, NH, Pyrrole), 12.71 (bs, 1 H, NH) ppm.

^{13}C NMR (75 MHz, DMSO-d_6): δ = 15.0 (SCH$_3$), 55.2 (C^{2}OCH$_3$), 55.4 (C^{4}OCH$_3$), 98.9 (C^3H, $(OCH_3)_2$-Phe), 105.2 (C^5H, $(OCH_3)_2$-Phe), 111.3 (C^3H, Pyr), 111.3 (C^5H, Pyrrole), 115.9 (d, $^2J_{CF}$ = 21.7 Hz, $C^{3/5}$H, F-Phe), 116.3 (C^5H, Pyr), 122.0 (C^2, Pyrrole), 125.1 (C^1,F-Phe), 127.6 (C^6H, $(OCH_3)_2$-Phe), 130.6 (d, $^3J_{CF}$ = 8.4 Hz, $C^{2/6}$H, F-Phe), 134.5 (C^5, Imdz), 142.3 (C^2, Imdz), 143.8 (C^4, Imdz), 147.6 (C^6H, Pyr), 152.8 (C^2, Pyr), 156.7 (C^4OCH_3), 158.5 (C^2OCH_3), 159.1 (CONH), 160.8 (d, $^1J_{CF}$ = 241.0 Hz, CF) ppm.

HPLC (Method 2): t_R = 5.7 min.

LC-MS (ESI, 70 eV): m/z = 530 $[MH]^+$, 546 $[MOH]^+$ (calc. m/z = 529).

4-(2,4-Dimethoxyphenyl)-*N*-(4-(5-(4-fluorphenyl)-2-(methylthio)-1*H*-imidazol-4-yl)-pyridin-2-yl)-1-methyl-1*H*-pyrrole-2-carboxamide (231)

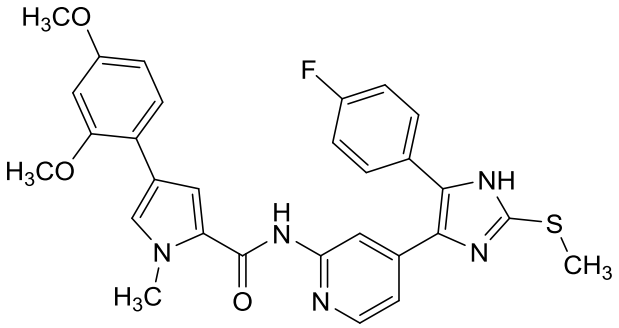

$C_{29}H_{26}FN_5O_3S$ (M_r 543.62)

231 was synthesized according to the procedure for **220** from **225** (604 mg, 2.31 mmol), PyBOP (1.44 g, 2.77 mmol), DIPEA (1.20 ml, 6.87 mmol), and **120** (904 mg, 2.99 mmol) in 12 ml anhyd. DMF. The crude product was purified by flash chromatography (SiO_2, 30-100 % ethyl acetate/petrol ether and RP-18, 50-100 % methanol/H_2O) to afford **231** as a beige solid (99 % HPLC purity).

Yield: 303 mg (558 µmol, 24 %).

m.p.: 236 °C.

^{1}H NMR (300 MHz, DMSO-d_6): δ = 2.64 (s, 3 H, SCH_3), 3.78 (s, 3 H, C^{2}OCH_3), 3.86 (s, 3 H, C^{4}OCH_3), 3.90 (s, 3 H, CH_3), 6.57 (dd, ^3J = 8.5 Hz, ^4J = 2.3 Hz, 1 H, C^5H, $(OCH_3)_2$-Phe), 6.61 (d, ^4J = 2.3 Hz, 1 H, C^3H, $(OCH_3)_2$-Phe), 7.06 (dd, ^3J = 5.3 Hz, ^4J = 1.2 Hz, 1 H, C^5H, Pyr), 7.28-7.34 (m, 2 H, C$^{3/5}H$, F-Phe), 7.41 (d, ^4J = 1.3 Hz, 1 H, C^3H, Pyrrole), 7.46 (d, ^3J = 8.4 Hz, 1 H, C^6H, $(OCH_3)_2$-Phe), 7.49-7.54 (m, 2 H, C$^{2/6}H$, F-Phe), 7.66 (d, ^4J = 1.4 Hz, 1 H, C^5H, Pyrrole), 8.18 (d, ^3J = 5.2 Hz, 1 H, C^6H, Pyr), 8.38 (bs, 1 H, C^3H, Pyr), 10.10 (bs, 1 H, CONH), 12.73 (bs, 1 H, NH) ppm.

^{13}C NMR (75 MHz, DMSO-d_6): δ = 15.3 (SCH$_3$), 36.5 (CH$_3$), 55.2 (C^{2}OCH$_3$), 55.5 (C^{4}OCH$_3$), 98.8 (C^3H, $(OCH_3)_2$-Phe), 105.2 (C^5H, $(OCH_3)_2$-Phe), 111.3 (C^3H, Pyr), 113.2 (C^5H, Pyrrole), 115.9 (d, $^2J_{CF}$ = 21.9 Hz, $C^{3/5}$H, F-Phe), 115.9 (C^1, $(OCH_3)_2$-Phe), 116.3 (C^5H, Pyr), 118.5 (C^4, Pyrrole), 124.1 (C^2, Pyrrole), 126.7 (d, $^4J_{CF}$ = 3.5 Hz, C^1, F-Phe), 127.5 (C^6H, $(OCH_3)_2$-Phe), 128.5 (C^3H, Pyrrole), 130.8 (d, $^3J_{CF}$ = 8.4 Hz, $C^{2/6}$H, F-Phe), 134.5 (C^5, Imdz), 142.1 (C^2, Imdz), 143.6 (C^4, Imdz), 147.6 (C^6H, Pyr), 152.7 (C^2, Pyr), 156.7 (C^4OCH$_3$), 158.6 (C^2OCH$_3$), 159.8 (CONH), 162.0 (d, $^1J_{CF}$ = 245.6 Hz, CF) ppm.

IR (ATR): $\tilde{\nu}$ = 3380, 2950, 1641, 1611, 1547, 1518, 1505, 1464, 1408, 1393, 1304, 1285, 1256, 1217, 1204, 1155, 1038, 843, 829, 797, 737, 692 cm^{-1}.

HPLC (Method 2): t_R = 6.0 min.

LC-MS (ESI, 70 eV): m/z = 544 $[MH]^+$ (calc. m/z = 543).

HRMS (EI, 70 eV): m/z = 543.1740 $[M]^+$ (calc. m/z = 543.1740).

4-(2,5-Dimethoxyphenyl)-*N*-(4-(5-(4-fluorphenyl)-2-(methylthio)-1*H*-imidazol-4-yl)-pyridin-2-yl)-1-methyl-1*H*-pyrrole-2-carboxamide (223)

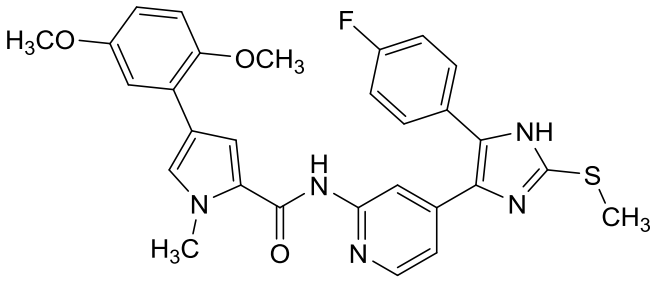

$C_{29}H_{26}FN_5O_3S$ (M_r 543.62)

224 was synthesized according to the procedure for **220** from **222** (604 mg, 2.31 mmol), PyBOP (1.45 g, 2.79 mmol), DIPEA (1.20 ml, 6.87 mmol), and **120** (904 mg, 3.01 mmol) in 12 ml anhyd. DMF. The crude product was purified by flash chromatography (SiO_2, 30-100 % ethyl acetate/petrol ether and RP-18, 50-100 % methanol/H_2O) to afford **223** as a pale yellowish solid (100 % HPLC purity).

Yield: 255 mg (469 µmol, 20 %).

m.p.: 127 °C.

^{1}H NMR (300 MHz, DMSO-d_6): δ = 2.64 (s, 3 H, SCH_3), 3.76 (s, 3 H, C^{5}OCH_3), 3.81 (s, 3 H, C^{2}OCH_3), 3.92 (s, 3 H, CH_3), 6.73 (dd, ^3J = 8.9 Hz, ^4J = 3.1 Hz, 1 H, C^4H, $(OCH_3)_2$-Phe), 6.96 (d, ^3J = 9.0 Hz, 1 H, C^3H, $(OCH_3)_2$-Phe), 7.06 (dd, ^3J = 5.3 Hz, ^4J = 1.6 Hz, 1 H, C^5H, Pyr), 7.17 (d, ^4J = 3.1 Hz, 1 H, C^6H, $(OCH_3)_2$-Phe), 7.24-7.30 (m, 2 H, C$^{3/5}H$, F-Phe), 7.50-7.55 (m, 2 H, C$^{2/6}H$, F-Phe), 7.56 (d, ^4J = 1.7 Hz, 1 H, C^5H, Pyrrole), 7.80 (d, ^4J = 1.8 Hz, 1 H, C^3H, Pyrrole), 8.22 (d, ^3J = 5.2 Hz, 1 H, C^6H, Pyr), 8.35 (bs, 1 H, C^3H, Pyr), 10.15 (bs, 1 H, CONH), 12.77 (vbs, 1 H, NH) ppm.

^{13}C NMR (75 MHz, DMSO-d_6): δ = 15.2 (SCH$_3$), 36.7 (CH$_3$), 55.4 (C^{5}OCH$_3$), 55.9 (C^{2}OCH$_3$), 111.3 (C^4H, $(OCH_3)_2$-Phe and C^3H, Pyr), 112.5 (C^6H, $(OCH_3)_2$-Phe), 112.8 (C^3H, $(OCH_3)_2$-Phe), 113.6 (C^3H, Pyrrole), 115.7 (d, $^2J_{CF}$ = 21.5 Hz, $C^{3/5}$H, F-Phe), 116.5 (C^5H, Pyr), 118.3 (C^4, Pyrrole), 123.8 (C^1, $(OCH_3)_2$-Phe), 124.3 (C^2, Pyrrole), 129.7 (C^5H, Pyrrole), 130.42 ($C^{2/6}$H, F-Phe), 142.5 (C^2, Imdz and C^4, Pyr), 147.7 (C^6H, Pyr), 150.1 (C^2OCH$_3$), 152.7 (C^1, Pyr), 153.4 (C^5OCH$_3$), 159.8 (CONH), 161.9 (d, $^1J_{CF}$ = 247.7 Hz, CF) ppm.

IR (ATR): $\tilde{\nu}$ = 2935, 2832, 1667, 1607, 1547, 1505, 1412, 1393, 1362, 1285, 1219, 1169, 1045, 1024, 837, 814, 739, 721, 654 cm^{-1}.

HPLC (Method 2): t_R = 6.1 min.

LC-MS (ESI, 70 eV): m/z = 544 $[MH]^+$ (calc. m/z = 543).

HRMS (EI, 70 eV): m/z = 543.170 $[M]^+$ (calc. m/z = 543.1740).

2-Bromo-1-phenylethan-1-one (141)

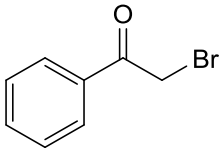

C_8H_7BrO (M_r 199.05)

Acetophenone (2.70 ml, 22.9 mmol) was dissolved in 8 ml glacial acetic acid and few droplets of hydrogen bromide in glacial acetic acid were added before dropwise addition of bromine (1.40 ml, 27.2 mmol) whereupon the temp. should not exceed 20 °C. The reaction was stirred for 90 min at rt, poured into ice-cold H_2O, filtered, and the residue was washed with 50 % (v/v) ethanol. The crude product was purified by flash chromatography (SiO_2, 10 % ethyl acetate/petrol ether) to afford **241** as light green crystals (96 % HPLC purity).

Yield: 2.63 g (13.2 mmol, 58 %) (Lit.[231]: 60 %).

m.p.: 48 °C.

^{1}H NMR (300 MHz, $CDCl_3$): δ = 4.46 (s, 2 H, CH_2), 7.47-7.52 (m, 2 H, C$^{3/5}H$, Phe), 7.59-7.64 (m, 1 H, C^4H, Phe), 7.97-8.01 (m, 2 H, C$^{2/6}H$, Phe) ppm.

^{13}C NMR (75 MHz, $CDCl_3$): δ = 30.0 (CH$_2$), 128.0 ($C^{3/5}$H, Phe), 128.1 ($C^{2/6}$H, Phe), 133.1 (C^4, Phe), 133.1 (C^1, Phe), 190.4 (CO) ppm.

HPLC (Method 2): t_R = 5.0 min.

2-Bromo-1-(5-bromo-2,4-dimethoxyphenyl)ethan-1-one (242)

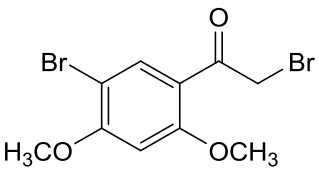

$C_{10}H_{10}Br_2O_3$ (M_r 338.00)

Method A. **242** was synthesized according to the procedure for **241** from 2,4-dimethoxy-acetophenone (1.01 g, 5.61 mmol) and bromine (340 µl, 6.62 mmol) in 10 ml glacial acetic acid. The crude product was crystallized from methanol to afford **242** as a pale pink solid (88 % HPLC purity).

Yield: 979 mg (2.90 mmol, 52 %).

Method B. Bromine (340 µl, 6.62 mmol) in 12 ml anhyd. chloroform was carefully added dropwise to a solution of 2,4-dimethoxyacetophenone (1.01 g, 5.61 mmol) in 10 ml anhyd. chloroform under a nitrogen atmosphere. The mixture was stirred for 30 min at rt and then heated to reflux for 2 h. The solvent was removed under reduced pressure and the crude product was purified by flash chromatography (SiO_2, 15-40 % ethyl acetate/petrol ether) to afford **242** as a pale beige solid (79 % HPLC purity).

Yield: 1.00 g (2.96 mmol, 53 %).

^{1}H NMR (300 MHz, $CDCl_3$): δ = 3.97 (s, 3 H, OCH_3), 3.98 (s, 3 H, OCH_3), 4.52 (s, 2 H, CH_2), 6.45 (s, 1 H, C^3H, $(OCH_3)_2$-Phe), 8.09 (s, 1 H, C^6H, $(OCH_3)_2$-Phe) ppm.

^{13}C NMR (75 MHz, $CDCl_3$): δ = 37.5 (CH_2), 56.3 (OCH_3), 56.7 (OCH_3), 95.8 (C^3H, $(OCH_3)_2$-Phe), 103.6 (C^5Br), 118.3 (C^1, $(OCH_3)_2$-Phe), 136.1 (C^6H, $(OCH_3)_2$-Phe), 160.4 ($COCH_3$), 161.1 ($COCH_3$), 189.3 (CO) ppm.

HPLC (Method 2): t_R = 5.9 min.

2-Bromo-1-(2,4-dimethoxyphenyl)ethan-1-one (237)

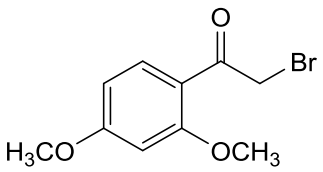

$C_{10}H_{11}BrO_3$ (M_r 259.10)

Copper(II)bromide (1.26 g, 5.64 mmol) was added in one portion to 2,4-dimethoxy-acetophenone (505 mg, 2.80 mmol) in 11 ml ethyl acetate and the mixture was heated to reflux for 90 min. After completion of the reaction the mixture was allowed to cool to rt, the solids were filtered off and washed with ethyl acetate. The filtrate was concentrated under reduced pressure and the crude product was purified by flash chromatography (SiO_2, 10 % ethyl acetate/petrol ether) to afford **237** as pale beige solid (100 % HPLC purity).

Yield: 701 mg (2.70 mmol, 97 %).

m.p.: 103 °C.

^{1}H NMR (300 MHz, $CDCl_3$): δ = 3.87 (s, 3 H, C^5OCH_3), 3.92 (s, 3 H, C^2OCH_3), 4.57 (s, 2 H, CH_2), 6.46 (d, ^4J = 2.3 Hz, 1 H, C^3H, $(OCH_3)_2$-Phe), 6.56 (dd, ^3J = 8.8 Hz, ^4J = 2.3 Hz, 1 H, C^5H, $(OCH_3)_2$-Phe), 7.91 (d, ^3J = 8.8 Hz, 1 H, C^6H, $(OCH_3)_2$-Phe) ppm.

^{13}C NMR (75 MHz, $CDCl_3$): δ = 38.1 (CH_2), 55.8 (C^5OCH_3), 55.9 (C^2OCH_3), 98.4 (C^3H, $(OCH_3)_2$-Phe), 106.0 (C^5H, $(OCH_3)_2$-Phe), 118.0 (C^1, $(OCH_3)_2$-Phe), 134.0 (C^6H, $(OCH_3)_2$-Phe), 161.0 (C^2OCH_3), 165.5 (C^5OCH_3), 190.3 (CO) ppm.

HPLC (Method 2): t_R = 5.5 min.

2-Chloro-1-(2,4-dimethoxyphenyl)ethan-1-one (238)

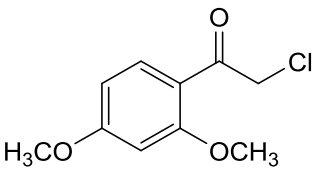

$C_{10}H_{11}ClO_3$ (M_r 214.65)

1,3-Dimethoxybenzene (557 mg, 4.03 mmol) was carefully added to a solution of aluminum chloride (1.20 g, 9.00 mmol) in 10 ml chloroacetyl chloride at 0 °C under a nitrogen atmosphere and the mixture was stirred for 3 h at the same temp. The reaction was quenched with H_2O, extracted with ethyl acetate, and the combined organic phases were washed with sat. aq. $NaHCO_3$ solution, dried over anhyd. Na_2SO_4, and concentrated under reduced pressure. The crude product was purified by flash chromatography (SiO_2, 10 % ethyl acetate/petrol ether) to afford **238** as a voluminous white solid (98 % HPLC purity).

Yield: 664 mg (3.10 mmol, 77 %).

m.p.: 113.

^{1}H NMR (300 MHz, $CDCl_3$): δ = 3.86 (s, 3 H, C^4OCH_3), 3.91 (s, 3 H, C^2OCH_3), 4.74 (s, 2 H, CH_2), 6.45 (d, ^4J = 2.3 Hz, 1 H, C^3H, $(OCH_3)_2$-Phe), 6.56 (dd, ^3J = 8.8 Hz, ^4J = 2.3 Hz, 1 H, C^5H, $(OCH_3)_2$-Phe), 7.94 (d, ^3J = 8.8 Hz, 1 H, C^6H, $(OCH_3)_2$-Phe) ppm.

^{13}C NMR (75 MHz, $CDCl_3$): δ = 51.4 (CH_2), 55.8 ($C^{2/4}OCH_3$), 98.3 (C^3H, $(OCH_3)_2$-Phe), 106.1 (C^5H, $(OCH_3)_2$-Phe), 118.2 (C^1, $(OCH_3)_2$-Phe), 133.7 (C^6H, $(OCH_3)_2$-Phe), 161.1 (C^2OCH_3), 165.5 (C^4OCH_3), 190.2 (CO) ppm.

HPLC (Method 2): t_R = 5.3 min.

Ethyl 4-(2,4-dimethoxyphenyl)-thiazole-2-carboxylate (239)

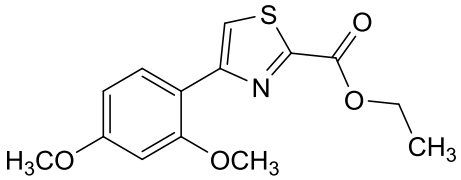

$C_{14}H_{15}NO_4S$ (M_r 293.34)

Method A. **237** (410 mg, 1.58 mmol) and ethyl 2-amino-2-thioxoacetate (330 mg, 2.45 mmol) in 5 ml ethanol were implemented in a microwave reaction for 10 min at 80 °C (100 W). The solvent was removed under reduced pressure and the crude product was purified by flash chromatography (SiO_2, 5-10 % ethyl acetate/petrol ether) to afford **239** as a colorless solid (96 % HPLC purity).

Yield: 349 mg (1.19 mmol, 76 %).

Method B. **239** was synthesized according to the procedure described above (Method A) from **238** (300 mg, 1.40 mmol) and ethyl 2-amino-2-thioxoacetate (287 mg, 2.16 mmol) in 5 ml ethanol to afford **239** as a colorless solid (95 % HPLC purity).

Yield: 236 mg (805 µmol, 58 %).

m.p.: 98 °C.

^{1}H NMR (300 MHz, DMSO-d_6): δ = 1.35 (t, ^3J = 7.1 Hz, 3 H, $COOCH_2CH_3$), 3.83 (s, 3 H, C^2OCH_3), 3.93 (s, 3 H, C^4OCH_3), 4.40 (q, ^3J = 7.0 Hz, 2 H, $COOCH_2CH_3$), 6.65-6.71 (m, 2 H, $C^{3/5}H$, $(OCH_3)_2$-Phe), 8.06 (d, ^3J = 8.6 Hz, 1 H, C^6H, $(OCH_3)_2$-Phe), 8.28 (s, 1 H, C^5H, Thiazole) ppm.

^{13}C NMR (75 MHz, DMSO-d_6): δ = 14.1 ($COOCH_2CH_3$), 55.4 (C^4OCH_3), 55.7 (C^2OCH_3), 62.1 ($COOCH_2CH_3$), 98.7 (C^3H, $(OCH_3)_2$-Phe), 105.6 (C^5H, $(OCH_3)_2$-Phe), 114.8 (C^1, $(OCH_3)_2$-Phe), 122.0 (C^5H, Thiazole), 130.3 (C^6H, $(OCH_3)_2$-Phe), 152.5 (C^4, Thiazole), 155.5 (C^2, Thiazole), 157.9 (C^2OCH_3), 159.5 ($COOCH_2CH_3$), 160.8 (C^4OCH_3) ppm.

IR (ATR): ṽ = 1724, 1614, 1578, 1522, 1491, 1435, 1414, 1319, 1283, 1256, 1240, 1211, 1169, 1126, 1088, 1059, 1026, 1011, 928, 855, 831, 810, 793 cm^{-1}.

HPLC (Method 2): t_R = 5.9 min.

LC-MS (ESI, 70 eV): m/z = 294 $[MH]^+$ (calc. m/z = 293).

4-(2,4-Dimethoxyphenyl)thiazole (245)

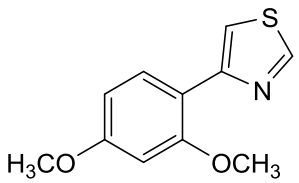

$C_{11}H_{11}NO_2S$ (M_r 221.27)

0.5 ml of 4 M aq. NaOH were added to a solution of **239** (60.0 mg, 205 µmol) in 1.3 ml THF and 0.6 ml methanol and the mixture was stirred 48 h at rt. H_2O was added to the reaction, the pH was adjusted to 3 using 1 M aq. HCl, and the mixture was extracted with ethyl acetate. The combined organic phases were washed with H_2O and sat. aq. NaCl solution, the organic phase was dried over anhyd. Na_2SO_4, and the solvent was removed under reduced pressure to afford **245** as a light brown solid (99 % HPLC purity).

Yield: 45.4 mg (205 µmol, quant.).

m.p.: 62 °C.

^{1}H NMR (300 MHz, $CDCl_3$): δ = 3.86 (s, 3 H, C^4OCH_3), 3.94 (s, 3 H, C^2OCH_3), 6.57 (d, ^4J = 2.4 Hz, 1 H, C^3H, $(OCH_3)_2$-Phe), 6.62 (dd, ^3J = 8.6 Hz, ^4J = 2.4 Hz, 1 H, C^5H, $(OCH_3)_2$-Phe), 7.86 (d, ^4J = 2.1 Hz, 1 H, C^5H, Thiazole), 8.19 (d, ^3J = 8.6 Hz, 1 H, C^6H, $(OCH_3)_2$-Phe), 8.93 (d, ^4J = 2.1 Hz, 1 H, C^2H, Thiazole) ppm.

^{13}C NMR (75 MHz, $CDCl_3$): δ = 55.6 (C^4OCH_3), 55.7 (C^2OCH_3), 99.0 (C^3H, $(OCH_3)_2$-Phe), 105.0 (C^5H, $(OCH_3)_2$-Phe), 115.0 (C^5H, Thiazole), 115.6 (C^1, $(OCH_3)_2$-Phe), 131.0 (C^6H, $(OCH_3)_2$-Phe), 151.3 (C^4, Thiazole), 151.4 (C^2H, Thiazole), 158.0 (C^2OCH_3), 161.0 (C^4OCH_3) ppm.

IR (ATR): ṽ = 3152, 3082, 3001, 2972, 2938, 2837, 1605, 1576, 1516, 1483, 1462, 1435, 1410, 1310, 1289, 1279, 1210, 1157, 1126, 1047, 1030, 924, 887, 828, 814, 748, 725 cm^{-1}.

HPLC (Method 2): t_R = 5.7 min.

LC-MS (ESI, 70 eV): m/z = 222 $[MH]^+$ (calc. m/z = 221).

Methyl 5-(2,4-dimethoxyphenyl)oxazole-4-carboxylate (250)

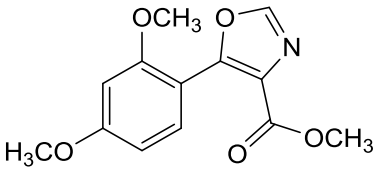

$C_{13}H_{13}NO_5$ (M_r 263.25)

2,4-Dimethoxybenzoic acid (500 mg, 2.75 mmol) and CDI (542 mg, 3.34 mmol) were stirred in 5 ml anhyd. THF at rt until formation of CO_2 was undetectable. The reaction was heated to 50 °C for 2 h, cooled to rt, and added dropwise to a solution of methyl isocyanoacetate (280 µl, 3.08 mmol) and NaHMDS (500 ml 2 M solution in THF, 1.00 mmol) in 5 ml anhyd. THF. The resulting mixture was stirred for 12 h at rt. The solvent was removed under reduced pressure, the residue dissolved in ethyl acetate, washed with H_2O and sat. aq. NaCl solution, dried over anhyd. Na_2SO_4, and the solvent was removed under reduced pressure. The crude product was purified by flash chromatography (SiO_2, 5-40 % ethyl acetate/petrol ether) to afford **250** as a beige solid (100 % HPLC purity).

Yield: 404 mg (1.54 mmol, 56 %).

m.p.: 122 °C.

^{1}H NMR (300 MHz, DMSO-d_6): δ = 3.70 (s, 3 H, COOCH_3), 3.76 (s, 3 H, C^{2}OCH_3), 3.84 (s, 3 H, C^{4}OCH_3), 6.65 (dd, ^3J = 8.5 Hz, ^4J = 2.3 Hz, 1 H, C^5H, $(OCH_3)_2$-Phe), 6.69 (d, ^4J = 2.3 Hz, 1 H, C^3H, $(OCH_3)_2$-Phe), 7.40 (d, ^3J = 8.5 Hz, 1 H, C^6H, $(OCH_3)_2$-Phe), 8.49 (s, 1 H, C^2H, Oxazole) ppm.

^{13}C NMR (75 MHz, DMSO-d_6): δ = 51.6 (COOCH$_3$), 55.5 (C^{4}OCH$_3$), 55.7 (C^{2}OCH$_3$), 98.5 (C^3H, $(OCH_3)_2$-Phe), 105.3 (C^5H, $(OCH_3)_2$-Phe), 108.2 (C^1, $(OCH_3)_2$-Phe), 127.2 (C^4, Oxazole), 131.8 (C^6H, $(OCH_3)_2$-Phe), 151.0 (C^2H, Oxazole), 151.8 (C^5, Oxazole), 158.3 (C^2OCH_3), 161.94 (COOCH$_3$), 162.54 (C^4OCH_3) ppm.

IR (ATR): ṽ = 3131, 2950, 1713, 1614, 1591, 1505, 1479, 1433, 1416, 1362, 1323, 1298, 1289, 1277, 1236, 1217, 1194, 1180, 1117, 1090, 1067, 1030, 1001, 943, 934, 868, 821, 808, 793, 654, 644 cm^{-1}.

HPLC (Method 2): t_R = 4.9 min.

LC-MS (ESI, 70 eV): m/z = 549 $[NaM_2\text{-}H]^+$, 527 $[M_2]^+$, 286 $[NaM\text{-}H]^+$, 264 $[MH]^+$, 232 $[M\text{-}CH_3OH]^+$ (calc. m/z = 263).

2-(2,4-Dimethoxyphenyl)-2-oxoethan-1-aminium chloride (247)

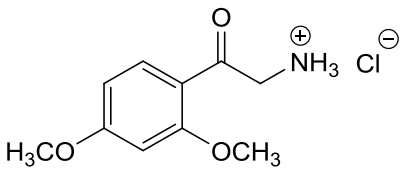

$C_{10}H_{14}ClNO_3$ (M_r 231.68)

Method A. A solution of **250** (78.0 mg, 296 µmol) in 4 ml methanol and 4 ml conc. aq. HCl was stirred under reflux for 4 h. The solvent was removed under reduced pressure, the residue was suspended in acetone, filtered, and the precipitate was washed with cold diethyl ether to afford **247** as a pale yellowish solid (100 % HPLC purity).

Yield: 65.0 mg (281 µmol, 95 %).

Method B. Methenamine (110 mg, 786 µmol) was added in one portion to a stirred solution of **237** (200 mg, 772 µmol) in 2 ml chloroform at rt and stirring continued at the same temp. for 4 h. The precipitate was filtered off and refluxed in 3 ml methanol and 0.2 ml conc. aq. HCl for 3 h. The precipitate was collected by filtration, rinsed with methanol, and the filtrate concentrated under reduced pressure to afford **247** as a brown solid (100 % HPLC purity).

Yield: 178 mg (768 µmol, quant.).

m.p.: 172 °C.

^{1}H NMR (300 MHz, DMSO-d_6): δ = 3.88 (s, 3 H, C^{4}OCH_3), 3.95 (s, 3 H, C^{2}OCH_3), 4.20 (bs, 2 H, CH_2), 6.68-6.72 (m, 2 H, *H*-3, C$^{3/5}$*H*, $(OCH_3)_2$-Phe), 7.86 (d, ^3J = 8.6 Hz, 1 H, C^6*H*, $(OCH_3)_2$-Phe), 8.37 (bs, 3 H, NH_3) ppm.

^{13}C NMR (75 MHz, DMSO-d_6): δ = 48.2 (*C*H$_2$), 55.9 (C^{4}O*C*H$_3$), 56.2 (C^{2}O*C*H$_3$), 98.4 (*C*^{3}H, $(OCH_3)_2$-Phe), 107.1 (*C*^{5}H), 116.3 (*C*^{1}, $(OCH_3)_2$-Phe), 132.2 (*C*^{6}H, $(OCH_3)_2$-Phe), 162.0 (*C*^{2}OCH$_3$), 165.8 (*C*^{4}OCH$_3$), 190.1 (*C*O) ppm.

IR (ATR): ṽ = 2950, 2900, 2698, 2612, 1667, 1597, 1568, 1493, 1458, 1430, 1298, 1252, 1231, 1207, 1165, 1140, 1119, 1061, 1032, 1022, 970, 916, 843, 812, 802 cm^{-1}.

HPLC (Method 2): t_R = 2.6 min.

LC-MS (ESI, 70 eV): *m*/*z* = 391 $[M_2$-HCl, Cl$]^+$, 196 [M-Cl]$^+$, 179 [M-NH_4Cl]$^+$ (calc. *m*/*z* = 231).

Ethyl 4-(2,4-dimethoxyphenyl)-1*H*-imidazole-2-carboxylate (246)

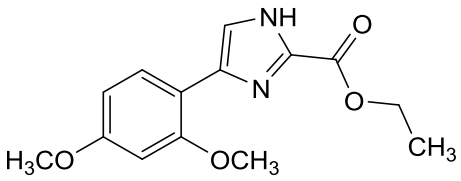

$C_{14}H_{16}N_2O_4$ (M_r 276.29)

Method A. A solution of **247** (180 mg, 777 µmol), ethyl 2-amino-2-thioxoacetate (129 mg, 971 µmol), and sodium acetate (156 mg, 1.90 mmol) in 1 ml glacial acetic acid was heated to reflux for 3 h. After cooling to rt, the mixture was neutralized with Na_2CO_3 and extracted with ethyl acetate. The combined organic phases were washed with sat. aq. NaCl solution and dried over anhyd. Na_2SO_4. Flash chromatography (SiO_2, 20-55 % ethyl acetate/petrol ether) afforded **246** as a yellow solid (100 % HPLC purity).

Yield: 74.5 mg (270 µmol, 35 %).

Method B. Trimethyloxonium tetrafluoroborate (60.0 mg, 406 µmol) was added in three portions over 1 h to an intensely stirred solution of ethyl 2-amino-2-thioxoacetate (45.0 mg, 338 µmol) in 2 ml DCM at rt and stirring continued for another 30 min. The solvent was removed under reduced pressure and sodium acetate (47.0 mg, 570 µmol), **247** (64.0 mg, 275 µmol), and 1 ml glacial acetic acid were added. The resulting mixture was heated to 100 °C for 3 h. Afterwards, the reaction was cooled to rt, diluted with H_2O, and extracted with ethyl acetate. The combined organic phases were washed with H_2O and sat. aq. NaCl solution, dried over anhyd. Na_2SO_4, and the solvent was removed under reduced pressure. The crude product was purified by flash chromatography (SiO_2, 20-55 % ethyl acetate/petrol ether) to afford **246** as a yellow solid (100 % HPLC purity).

Yield: 59.4 mg (215 µmol, 78 %).

m.p.: 87 °C.

^{1}H NMR (300 MHz, DMSO-d_6): δ = 1.33 (t, ^3J = 7.1 Hz, 3 H, $COOCH_2CH_3$), 3.79 (s, 3 H, C^2OCH_3), 3.89 (s, 3 H, C^4OCH_3), 4.34 (q, ^3J = 7.1 Hz, 2 H, $COOCH_2CH_3$), 6.06 (dd, ^3J = 8.5 Hz, ^4J = 2.4 Hz, 1 H, C^5H, $(OCH_3)_2$-Phe), 6.63 (d, ^4J = 2.2 Hz, 1 H, C^3H, $(OCH_3)_2$-Phe), 7.56 (s, 1 H, C^4H, Imdz), 7.95 (d, ^3J = 8.1 Hz, 1 H, C^6H, $(OCH_3)_2$-Phe), 13.28 (bs, 1 H, N*H*) ppm.

^{13}C NMR (75 MHz, DMSO-d_6): δ = 14.3 ($COOCH_2\mathit{C}H_3$), 55.2 ($C^2O\mathit{C}H_3$), 55.4 ($CO\mathit{C}H_3$), 60.7 ($COO\mathit{C}H_2CH_3$), 98.5 (C^3H, $(OCH_3)_2$-Phe), 105.2 (C^5H, $(OCH_3)_2$-Phe), 113.6 (C^1, $(OCH_3)_2$-Phe), 119.1 (C^5H, Imdz), 127.9 (C^6H, $(OCH_3)_2$-Phe), 136.0 (C^2, Imdz), 137.8 (C^5H, Imdz), 157.0 (C^4OCH_3), 158.5 ($\mathit{C}OOCH_2CH_3$), 159.7 (C^2OCH_3) ppm.

IR (ATR): $\tilde{\nu}$ = 3302, 2930, 1713, 1694, 1622, 1582, 1560, 1522, 1481, 1456, 1439, 1383, 1354, 1312, 1285, 1256, 1211, 1192, 1161, 1153, 1138, 1115, 1078, 1069, 949, 824, 789, 731, 652 cm^{-1}.

HPLC (Method 2): t_R = 5.0 min.

LC-MS (ESI, 70 eV): m/z = 277 $[MH]^+$, 249 $[MH\text{-}C_2H_5]^+$, 553 $[M_2H]^+$, 575 $[NaM_2]^+$ (calc. m/z = 276).

2,4-Dimethoxybenzohydrazide (256)

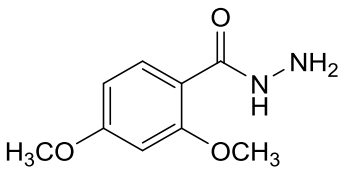

$C_9H_{12}N_2O_3$ (M_r 196.21)

2,4-Dimethoxybenzoic acid (1.00 g, 5.50 mmol) in 6 ml anhyd. methanol and 0.1 ml sulfuric acid was stirred under reflux for 4 h. The solution was cooled to rt before hydrazine hydrate (2.20 ml, 44.6 mmol) was added and the mixture was heated to reflux for another 30 min. The solvent was removed under reduced pressure, the residue heated to reflux in ethanol, filtered at that temp., and crystallized to afford **256** as a colorless solid (100 % HPLC purity).

Yield: 1.07 g (5.47 mmol, quant.).

m.p.: 109 °C.

^{1}H NMR (300 MHz, DMSO-d_6): δ = 3.81 (s, 3 H, C^{4}OCH_3), 3.88 (s, 3 H, C^{2}OCH_3), 4.48 (bs, 2 H, NH_2), 6.59-6.23 (m, 2 H, C$^{3/5}H$, $(OCH_3)_2$-Phe), 7.76 (d, ^3J = 8.9 Hz, 1 H, C^6H, $(OCH_3)_2$-Phe), 9.00 (bs, 1 H, NH) ppm.

^{13}C NMR (75 MHz, DMSO-d_6): δ = 55.5 (C^{4}OCH$_3$), 55.9 (C^{2}OCH$_3$), 98.4 (C^3H, $(OCH_3)_2$-Phe), 105.5 (C^5H, $(OCH_3)_2$-Phe), 114.1 (C^1, $(OCH_3)_2$-Phe), 131.1 (C^6H, $(OCH_3)_2$-Phe), 158.4 (C^2OCH$_3$), 162.6 (C^4OCH$_3$), 164.4 (CO) ppm.

IR (ATR): $\tilde{\nu}$ = 3348, 3296, 1622, 1599, 1481, 1451, 1445, 1327, 1265, 1215, 1182, 1163, 1098, 1024, 957, 839, 829, 716, 652, 629, 602 cm^{-1}.

HPLC (Method 2): t_R = 3.2 min.

LC-MS (ESI, 70 eV): m/z = 415 $[NaM_2]^+$, 197 $[MH]^+$ (calc. m/z = 196).

7.3.6 Syntheses of Series 5: Propiolic Acid

1-(2,2-Dibromovinyl)-2,4-dimethoxybenzene (260)

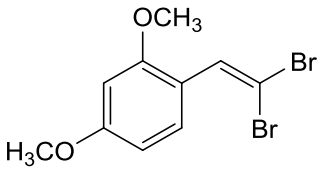

$C_{10}H_{10}Br_2O_2$ (M_r 322.00)

2,4-Dimethoxybenzaldehyde (500 mg, 3.01 mmol) and triphenylphosphine (1.58 g, 6.02 mmol) were stirred in 7 ml anhyd. DCM at rt under a nitrogen atmosphere. The mixture was cooled to 0 °C before tetrabromomethane (1.17 g, 3.54 mmol) in 1 ml anhyd. DCM was carefully added dropwise whereupon the temp. was kept below 5 °C. The reaction was stirred for 30 min at the same temp., filtered, and the filtrate concentrated under reduced pressure. The crude product was purified by flash chromatography (SiO_2, 10 % ethyl acetate/petrol ether) to afford **260** as a colorless solid (99 % HPLC purity).

Yield: 397 mg (1.23 mmol, 41 %).

m.p.: 57 °C.

^{1}H NMR (300 MHz, DMSO-d_6): δ = 3.79 (s, 3 H, C^4OCH_3), 3.80 (s, 3 H, C^2OCH_3), 6.56-6.60 (m, 2 H, $C^{3/5}H$, $(OCH_3)_2$-Phe), 7.51 (s, 1 H, $CHCBr_2$), 7.56 (dd, ^3J = 8.9 Hz, ^4J = 0.6 Hz, 1 H, C^6H, $(OCH_3)_2$-Phe) ppm.

^{13}C NMR (75 MHz, DMSO-d_6): δ = 55.4 (C^4OCH_3), 55.7 (C^2OCH_3), 87.9 ($CHCBr_2$), 98.2 (C^3H, $(OCH_3)_2$-Phe), 105.0 (C^5H, $(OCH_3)_2$-Phe), 116.1 (C^1, $(OCH_3)_2$-Phe), 129.3 (C^6H, $(OCH_3)_2$-Phe), 132.4 ($CHCBr_2$), 157.6 (C^2OCH_3), 161.1 (C^4OCH_3) ppm.

IR (ATR): $\tilde{\nu}$ = 2920, 1608, 1576, 1497, 1470, 1454, 1435, 1416, 1323, 1289, 1263, 1207, 1184, 1161, 1121, 1030, 922, 868, 843, 828, 781, 766 cm^{-1}.

HPLC (Method 1): t_R = 7.6 min.

LC-MS (ESI, 70 eV): m/z = 321, 323, 325 $[MH]^+$, 242, 244 $[C_{10}H_{12}BrO_2]^+$ (calc. m/z = 320).

Methyl 3-(2,4-dimethoxyphenyl)propiolate (258)

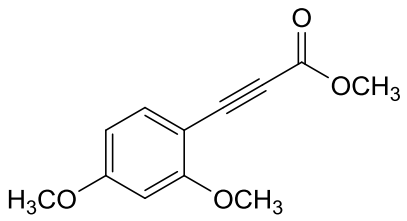

$C_{12}H_{12}O_4$ (M_r 220.22)

n-Butyllithium (2.70 ml 1.6 M solution in hexanes, 4.32 mmol) was slowly added dropwise to a stirred solution of **260** (640 mg, 1.99 mmol) in 8 ml anhyd. THF at -78 °C under a nitrogen atmosphere. Stirring continued for 15 min at the same temp. and 1 h at rt before methyl chloroformate (190 µl, 2.46 mmol) was added dropwise at -78 °C. The mixture was stirred another 3 h at rt, quenched with sat. aq. NH_4Cl solution, and extracted with ethyl acetate. The combined organic phases were dried over anhyd. Na_2SO_4 and the crude product was purified by flash chromatography (SiO_2, 2-10 % ethyl acetate/petrol ether) to afford **258** as a colorless solid (100 % HPLC purity).

Yield: 382 mg (1.73 mmol, 87 %).

m.p.: 88 °C.

^{1}H NMR (300 MHz, DMSO-d_6): δ = 3.74 (s, 3 H, COOCH_3), 3.83 (s, 3 H, C^{2}OCH_3), 3.86 (s, 3 H, C^{4}OCH_3), 6.60 (dd, ^3J = 8.6 Hz, ^4J = 2.3 Hz, 1 H, C^5H, $(OCH_3)_2$-Phe), 6.66 (d, ^4J = 2.3 Hz, 1 H, C^3H, $(OCH_3)_2$-Phe), 7.50 (d, ^3J = 8.6 Hz, 1 H, C^6H, $(OCH_3)_2$-Phe) ppm.

^{13}C NMR (75 MHz, DMSO-d_6): δ = 52.7 (COOCH$_3$), 55.7 (C^{2}OCH$_3$), 56.0 (C^{4}OCH$_3$), 83.5 (CCCOOCH$_3$), 84.6 (CCCOOCH$_3$), 98.5 (C^3H, $(OCH_3)_2$-Phe), 99.4 (C^1, $(OCH_3)_2$-Phe), 106.5 (C^5H, $(OCH_3)_2$-Phe), 136.0 (C^6H, $(OCH_3)_2$-Phe), 154.0 (COOCH$_3$), 163.1 (C^4OCH$_3$), 163.5 (C^2OCH$_3$) ppm.

IR (ATR): $\tilde{\nu}$ = 2212, 1750, 1611, 1568, 1508, 1456, 1436, 1416, 1310, 1292, 1256, 1215, 1196, 1167, 1128, 1038, 1026, 990, 929, 874, 820, 791, 743 cm^{-1}.

HPLC (Method 1): t_R = 5.1 min.

LC-MS (ESI, 70 eV): m/z = 221 $[MH]^+$ (calc. m/z = 220).

3-(2,4-Dimethoxyphenyl)propiolic acid (257)

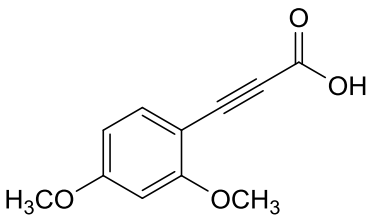

$C_{11}H_{10}O_4$ (M_r 206.20)

Lithium hydroxide monohydrate (95 mg, 2.26 mmol) was added to a stirred solution of **258** (350 mg, 1.59 mmol) in 6 ml THF, 1.5 ml water, and 1.5 ml methanol and stirring continued for 12 h at rt. The mixture was extracted with ethyl acetate, the combined organic phases were washed with H_2O and sat. aq. NaCl solution, and dried over anhyd. Na_2SO_4 to afford **257** as a beige solid (99 % HPLC purity).

Yield: 297 mg (1.44 mmol, 91 %).

m.p.: 137 °C.

^{1}H NMR (300 MHz, DMSO-d_6): δ = 3.82 (s, 3 H, C^{2}OCH_3), 3.85 (s, 3 H, C^{4}OCH_3), 6.59 (dd, ^3J = 8.6 Hz, ^4J = 2.3 Hz, 1 H, C^5H, $(OCH_3)_2$-Phe), 6.65 (d, ^4J = 2.3 Hz, 1 H, C^3H, $(OCH_3)_2$-Phe), 7.46 (d, ^3J = 8.5 Hz, 1 H, C^6H, $(OCH_3)_2$-Phe), 13.42 (bs, 1 H, COOH) ppm.

^{13}C NMR (75 MHz, DMSO-d_6): δ = 55.7 (C^{2}OCH$_3$), 55.9 (C^{4}OCH$_3$), 82.9 (CCCOOH), 84.8 (CCCOOH), 98.5 (C^3H, $(OCH_3)_2$-Phe), 100.0 (C^1, $(OCH_3)_2$-Phe), 106.3 (C^5H, $(OCH_3)_2$-Phe), 135.8 (C^6H, $(OCH_3)_2$-Phe), 154.7 (COOH), 162.8 (C^4OCH_3), 163.1 (C^2OCH_3) ppm.

IR (ATR): $\tilde{\nu}$ = 2900, 2195, 1667, 1601, 1566, 1508, 1456, 1435, 1414, 1294, 1260, 1227, 1204, 1157, 1136, 1036, 1024, 883, 829, 810, 739 cm^{-1}.

HPLC (Method 2): t_R = 5.1 min.

LC-MS (ESI, 70 eV): m/z = 207 $[MH]^+$, 163 $[MH\text{-}CO_2]^+$ (calc. m/z = 206).

7.3.7 Syntheses of Series 6: Hybrid Inhibitors

Methyl 3-amino-4,5-dihydrothiophene-2-carboxylate (271)

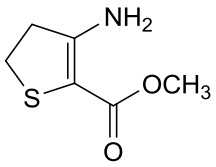

$C_6H_9NO_2S$ (M_r 159.20)

Acrylonitrile (1.30 ml, 19.6 mmol) and thioglycolic acid methyl ester (1.70 ml, 18.9 mmol) were added to a stirred solution of DBU (6.30 ml, 41.8 mmol) in 11 ml anhyd. methanol at 0 °C under a nitrogen atmosphere and stirring continued at the same temp. for 5 h and then 12 h at 80 °C. Afterwards, the reaction was cooled to rt, the solvent was removed under reduced pressure, sat. aq. NH_4Cl solution was added, and the resulting suspension was extracted with ethyl acetate. The combined organic phases were dried over anhyd. Na_2SO_4 and the crude product was purified by flash chromatography (SiO_2, 20-22 % ethyl acetate/petrol ether) to afford **271** as a bright yellow solid (100 % HPLC purity).

Yield: 1.35 g (8.49 mmol, 45 %) (Lit.[245]: 70 %).

m.p.: 103 °C.

^{1}H NMR (300 MHz, $CDCl_3$): δ = 2.89 (t, ^3J = 7.9 Hz, 2 H, C$^4H_2$), 3.07 (t, ^3J = 7.9 Hz, 2 H, C$^5H_2$), 3.72 (s, 3 H, COOCH_3), 5.82 (vbs, 2 H, NH_2) ppm.

^{13}C NMR (75 MHz, $CDCl_3$): δ = 27.8 (C^5H_2), 39.3 (C^4H_2), 51.2 (COOCH$_3$), 90.4 (C^2), 156.8 (C^3), 166.3 (COOCH$_3$) ppm.

IR (ATR): $\tilde{\nu}$ = 3410, 3300, 3212, 3142, 2986, 2943, 1651, 1620, 1537, 1447, 1425, 1924, 1279, 1265, 1188, 1134, 1076, 1036, 993, 986, 964, 912, 828, 766, 683 cm^{-1}.

HPLC (Method 2): t_R = 3.7 min.

LC-MS (ESI, 70 eV): m/z = 160 $[MH]^+$ (calc. m/z = 159).

3-Phenyl-2-thioxo-2,3,6,7-tetrahydrothieno[3,2-*d*]pyrimidin-4(1*H*)-one (272)

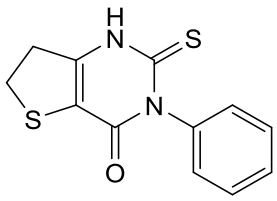

$C_{12}H_{10}N_2OS_2$ (M_r 262.35)

271 (303 mg, 1.90 mmol) and phenyl isothiocyanate (300 µl, 2.51 mmol) were stirred in 6 ml anhyd. pyridine for 12 h at 100 °C under a nitrogen atmosphere. The solvent was removed under reduced pressure and the residue was purified by flash chromatography (SiO_2, 30 % ethyl acetate/petrol ether, then acetone) and crystallized from methanol to afford **272** as a beige solid (96 % HPLC purity).

Yield: 140 mg (534 µmol, 28 %) (Lit.[210]: 42 %).

m.p.: 262 °C.

^{1}H NMR (300 MHz, DMSO-d_6): δ = 3.25 (t, ^3J = 7.9 Hz, 2 H, C^5H_2), 3.38 (t, ^3J = 7.9 Hz, 2 H, C^4H_2), 7.16-7.19 (m, 2 H, $C^{2/6}H$, Phe), 7.38-7.48 (m, 3 H, $C^{3\text{-}5}H$, Phe), 13.23 (bs, 1 H, N*H*) ppm.

^{13}C NMR (75 MHz, DMSO-d_6): δ = 29.0 (C^4H_2), 34.6 (C^5H_2), 114.4 (C^5, Pyrimidine), 128.2 (C^4H, Phe), 128.6 ($C^{2/6}$H, Phe), 129.0 ($C^{3/5}$H, Phe), 139.1 (C^1, Phe), 149.5 (C^6, Pyrimidine), 156.9 (*C*O), 175.3 (*C*S) ppm.

IR (ATR): $\tilde{\nu}$ = 1653, 1622, 1595, 1508, 1454, 1418, 1350, 1223, 793, 750, 694, 660, 602 cm^{-1}.

HPLC (Method 2): t_R = 4.2 min.

LC-MS (ESI, 70 eV): *m*/*z* = 525 $[M_2H]^+$, 263 $[MH]^+$ (calc. *m*/*z* = 262).

3-(2-Methoxyphenyl)-2-thioxo-2,3,6,7-tetrahydrothieno[3,2-*d*]pyrimidin-4(1*H*)-one (273)

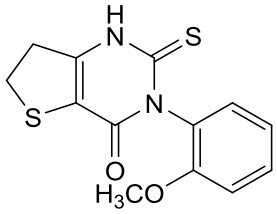

$C_{13}H_{12}N_2O_2S_2$ (M_r 292.37)

273 was synthesized according to the procedure for **272** from **271** (1.24 g, 7.79 mmol) and 2-methoxyphenyl isothiocyanate (1.30 ml, 9.36 mmol) in 24 ml anhyd. pyridine. The crude product was purified by flash chromatography (SiO_2, 30 % ethyl acetate/petrol ether, then acetone) to afford **273** as a brown solid (79 % HPLC purity) that was used without further purification in the next step.

Yield: 315 mg (1.08 mmol, 14 %).

^{1}H NMR (300 MHz, DMSO-d_6): δ = 3.24-3.29 (m, 2 H, C^5H_2), 3.36-3.39 (m, 2 H, C^4H_2), 3.72 (s, 3 H, COCH_3), 7.00 (dt, ^3J = 7.5 Hz, ^4J = 1.2 Hz, 1 H, C^5*H*, H_3CO-Phe), 7.11 (dd, ^3J = 7.7 Hz, ^4J = 1.8 Hz, 1 H, C^3*H*, H_3CO-Phe), 7.13 (dd, ^3J = 8.4 Hz, ^4J = 1.1 Hz, 1 H, C^6*H*, H_3CO-Phe), 7.35-7.40 (m, 1 H, C^4*H*, H_3CO-Phe), 13.19 (bs, 1 H, N*H*) ppm.

^{13}C NMR (75 MHz, DMSO-d_6): δ = 29.0 (*C*^{4}H_2), 34.6 (*C*^{5}H_2), 55.7 (CO*C*H_3), 112.4 (*C*^{6}H, H_3CO-Phe), 114.0 (*C*^{5}, Pyrimidine), 120.7 (*C*^{5}H, H_3CO-Phe), 127.4 (*C*^{1}, H_3CO-Phe), 129.7 (*C*^{3}H, H_3CO-Phe), 129.9 (*C*^{4}H, H_3CO-Phe), 149.6 (*C*^{6}, Pyrimidine), 154.2 (*C*OCH_3), 156.4 (*C*O), 175.2 (*C*S) ppm.

HPLC (Method 2): t_R = 4.2 min.

LC-MS (ESI, 70 eV): *m*/*z* = 585 $[M_2H]^+$, 293 $[MH]^+$ (calc. *m*/*z* = 292).

2-Chloro-*N*-(4-methylpyridin-2-yl)acetamide (276)

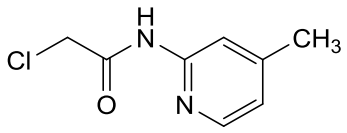

$C_8H_9ClN_2O$ (M_r 184.62)

A solution of 2-amino-4-methylpyridine (675 mg, 6.24 mmol) and Et_3N (970 µl, 6.90 mmol) in 10 ml anhyd. DCM was carefully added dropwise to chloroacetyl chloride (540 µl, 6.79 mmol) in 3 ml anhyd. DCM over a period of 30 min under a nitrogen atmosphere. The resulting mixture was stirred at rt for 12 h. Afterwards, the solvent was removed under reduced pressure and the crude product was purified by flash chromatography (SiO_2, 5-40 % ethyl acetate/petrol ether) to afford **276** as pink crystals (99 % HPLC purity).

Yield: 781 mg (4.23 mmol, 68 %).

m.p.: 73 °C.

^{1}H NMR (300 MHz, $CDCl_3$): δ = 2.40 (t, ^4J = 0.5 Hz, 3 H, CH_3), 4.20 (s, 2 H, CH_2), 6.96 (dq, ^3J = 5.3 Hz, ^4J = 0.7 Hz, 1 H, C^5H, Pyr), 8.08 (bs, 1 H, C^3H, Pyr), 8.15 (dd, ^3J = 5.2 Hz, ^5J = 0.5 Hz, 1 H, C^6H, Pyr), 9.33 (vbs, 1 H, CONH) ppm.

^{13}C NMR (75 MHz, $CDCl_3$): δ = 21.7 (CH$_3$), 43.0 (CH$_2$), 115.0 (C^3H, Pyr), 121.9 (C^5H, Pyr), 146.3 (C^6H, Pyr), 150.2 (C^2, Pyr), 151.6 (C^4, Pyr), 164.9 (CO) ppm.

IR (ATR): ṽ = 3250, 3100, 3017, 2957, 1667, 1572, 1560, 1425, 1416, 1379, 1304, 1275, 1246, 1200, 1167, 1146, 972, 883, 818, 785, 718, 623 cm^{-1}.

HPLC (Method 2): t_R = 3.3 min.

LC-MS (ESI, 70 eV): m/z = 185 $[MH]^+$ (calc. m/z = 184).

2-Chloro-*N*-(4-(5-(4-fluorophenyl)-2-(methylthio)-1*H*-imidazol-4-yl)pyridin-2-yl)-acetamide (279)

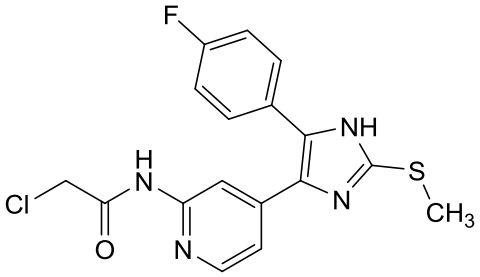

$C_{17}H_{14}ClFN_4OS$ (M_r 376.83)

A solution of **120** (470 mg, 1.57 mmol) and Et_3N (300 µl, 2.14 mmol) in 8 ml anhyd. DCM and 2 ml anhyd. DMF was carefully added dropwise to chloroacetyl chloride (150 µl, 1.89 mmol) in 2 ml anhyd. DCM over a period of 30 min under a nitrogen atmosphere. The resulting mixture was stirred at rt for 12 h. Afterwards, the solvent was removed under reduced pressure, the residue was dissolved in ethyl acetate, washed with H_2O and sat. aq. NaCl solution, dried over anhyd. Na_2SO_4, and concentrated under reduced pressure. The crude product was purified by flash chromatography (SiO_2, 5-50 % ethyl acetate/petrol ether) to afford **279** as a yellow solid (96 % HPLC purity).

Yield: 284 mg (754 µmol, 48 %).

^{1}H NMR (300 MHz, DMSO-d_6): δ = 2.62 (s, 3 H, SCH_3), 4.31 (s, 2 H, CH_2), 7.08 (dd, ^3J = 5.3 Hz, ^4J = 1.6 Hz, 1 H, C^5*H*, Pyr), 7.23-7.29 (m, 2 H, C$^{3/5}$*H*, F-Phe), 7.46-7.51 (m, 2 H, C$^{2/6}$*H*, F-Phe), 8.19 (d, ^3J = 5.0 Hz, 1 H, C^6*H*, Pyr), 8.23 (bs, 1 H, C^3*H*, Pyr), 10.72 (bs, 1 H, CON*H*), 12.75 (vbs, 1 H, N*H*) ppm.

^{13}C NMR (75 MHz, DMSO-d_6): δ = 15.0 (S*C*H$_3$), 43.4 (*C*H$_2$), 110.5 (*C*^{3}H, Pyr), 115.7 (d, $^2J_{CF}$ = 22.4 Hz, *C*$^{3/5}$H, F-Phe), 117.1 (*C*^{5}H, Pyr), 130.5 (*C*$^{2/6}$H, F-Phe), 142.7 (*C*^{2}, Imdz), 148.0 (*C*^{6}H, Pyr), 151.8 (*C*^{2}, Pyr), 161.9 (d, $^1J_{CF}$ = 245.0 Hz, *C*F), 165.2 (*C*O) ppm.

HPLC (Method 2): t_R = 5.2 min.

LC-MS (ESI, 70 eV): *m*/*z* = 377 $[MH]^+$ (calc. *m*/*z* = 376).

_N_-(4-methylpyridin-2-yl)-2-(phenylamino)acetamide (277)

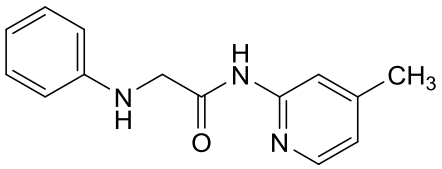

$C_{14}H_{15}N_3O$ (M_r 241.29)

Aniline (150 µl, 1.64 mmol), **276** (203 mg, 1.10 mmol), and Et_3N (510 µl, 3.25 mmol) in 10 ml anhyd. DMF were stirred under a nitrogen atmosphere for 2 h at 80 °C. The reaction was quenched with H_2O, extracted with ethyl acetate, and the combined organic phases were washed with H_2O and sat. aq. NaCl solution, and dried over anhyd. Na_2SO_4. The solvent was removed under reduced pressure and the crude product was purified by flash chromatography (SiO_2, 5-50 % ethyl acetate/petrol ether) to afford **277** as a pale yellowish solid (100 % HPLC purity).

Yield: 55.2 mg (229 mmol, 21 %).

^{1}H NMR (300 MHz, DMSO-d_6): δ = 2.29 (s, 3 H, CH_3), 3.91 (d, ^3J = 6.3 Hz, 2 H, CH_2), 6.07 (t, ^3J = 6.3 Hz, 1 H, NH), 6.56-6.62 (m, 3 H, C$^{2/4/6}H$, Phe), 6.93 (dq, ^3J = 5.1 Hz, ^4J = 0.7 Hz, 1 H, C^5H, Pyr), 7-07-7.12 (m, 2 H, C$^{3/5}H$, Phe), 7.94 (bs, 1 H, C^3H, Pyr), 8.14 (dd, ^3J = 5.1 Hz, ^5J = 0.5 Hz, 1 H, C^6H, Pyr), 10.13 (s, 1 H, CONH) ppm.

^{13}C NMR (75 MHz, DMSO-d_6): δ = 47.2 (CH$_2$), 112.3 ($C^{2/6}$H, Phe), 113.6 (C^3H, Pyr), 116.6 (C^4H, Phe), 120.5 (C^5H, Pyr), 129.0 ($C^{3/5}$H, Phe), 147.6 (C^6H, Pyr), 148.1 (C^1, Phe), 149.0 (C^4, Pyr), 151.6 (C^1, Pyr), 170.1 (CONH) ppm.

HPLC (Method 2): t_R = 5.1 min.

LC-MS (ESI, 70 eV): m/z = 242 $[MH]^+$ (calc. m/z = 241).

***N*-(4-Methylpyridin-2-yl)-2-((4-oxo-3-phenyl-3,4,6,7-tetrahydrothieno[3,2-*d*]pyrimidin-2-yl)thio)acetamide (278)**

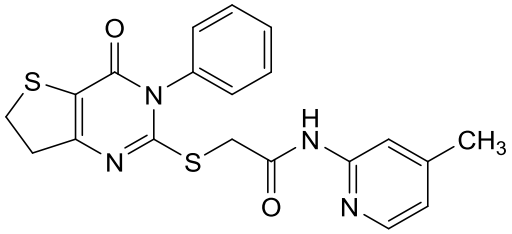

$C_{20}H_{18}N_4O_4S_2$ (M_r 410.51)

278 was synthesized according to the procedure for **277** from **276** (66.0 mg, 357 µmol), **272** (80.0 mg, 305 µmol), and Et_3N (150 µl, 956 µmol) in 4 ml anhyd. DMF. The crude product was purified by flash chromatography (SiO_2, 10-80 % ethyl acetate/petrol ether) to afford **278** as a colorless solid (100 % HPLC purity).

Yield: 17.6 mg (42.9 µmol, 14 %).

m.p.: 243 °C.

^{1}H NMR (300 MHz, $CDCl_3$): δ = 2.44 (s, 3 H, CH_3), 3.39-3.42 (m, 4 H, C$^{4/5}H_2$), 3.88 (s, 2 H, CH_2CO), 6.99 (d, ^3J = 5.5 Hz, 1 H, C^5H, Pyr), 7.28-7.31 (m, 2 H, C$^{2/6}H$, Phe), 7.51-7.54 (m, 3 H, C$^{3\text{-}5}H$, Phe), 8.09 (d, ^3J = 5.4 Hz, 1 H, C^6H, Pyr), 8.17 (bs, 1 H, C^3H, Pyr), 10.85 (vbs, 1 H, CONH) ppm.

^{13}C NMR (75 MHz, $CDCl_3$): δ = 22.1 (CH$_3$), 29.4 (C^5H$_2$), 37.4 (CH$_2$CO), 37.7 (C^4H$_2$), 115.5 (C^3H, Pyr), 121.2 (C^5H, Pyr), 122.2 (C^5, Pyrimidine), 128.8 ($C^{2/6}$H, Phe), 130.1 ($C^{3/5}$H, Phe), 130.6 (C^4H, Phe), 135.1 (C^1, Phe), 143.3 (C^6H, Pyr), 150.2 (C^2, Pyr), 154.1 (C^4, Pyr), 157.6 (C^2, Pyrimidine), 160.5 (CO), 167.5 (CONH) ppm.

IR (ATR): ṽ = 3212, 3050, 2928, 2855, 1695, 1674, 1611, 1570, 1560, 1541, 1468, 1451, 1410, 1371, 1306, 1236, 1192, 1175, 1159, 1146, 1053, 1042, 1023, 995, 858, 818, 775, 758, 750, 691, 664 cm^{-1}.

HPLC (Method 2): t_R = 5.1 min.

LC-MS (ESI, 70 eV): m/z = 411 $[MH]^+$, 303 $[M\text{-}C_6H_7N_2]^+$ (calc. m/z = 410).

***N*-(4-(5-(4-Fluorophenyl)-2-(methylthio)-1*H*-imidazol-4-yl)pyridin-2-yl)-2-((3-phenyl-4-oxo-3,4,6,7-tetrahydrothieno[3,2-*d*]pyrimidin-2-yl)thio)acetamide (266)**

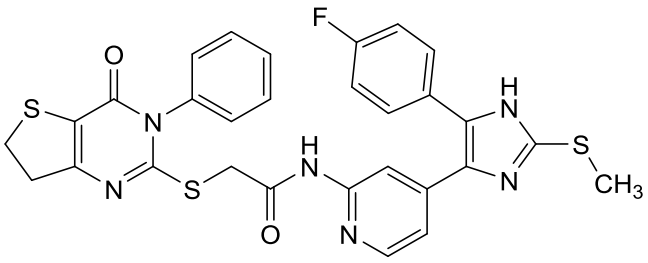

$C_{29}H_{23}FN_6O_2S_3$ (M_r 602.72)

A solution of **272** (80.0 mg, 305 µmol), **279** (80.0 mg, 433 µmol), and Et_3N (200 µl, 1.28 mmol) in 5 ml anhyd. DMF was stirred under a nitrogen atmosphere for 2 h at 80 °C. The reaction was quenched with H_2O, extracted with ethyl acetate, and the combined organic phases were washed with H_2O and sat. aq. NaCl solution, and dried over anhyd. Na_2SO_4. The solvent was removed under reduced pressure and the crude product was purified by flash chromatography (SiO_2, 10-80 % ethyl acetate/petrol ether) to afford **266** as a beige solid (100 % HPLC purity).

Yield: 108 mg (179 µmol, 59 %).

m.p.: 254 °C.

^{1}H NMR (300 MHz, DMSO-d_6): δ = 2.61 (s, 3 H, SCH_3), 3.17 (t, ^3J = 8.6 Hz, 2 H, C$^4H_2$), 3.34 (t, ^3J = 8.6 Hz, 2 H, C$^5H_2$), 4.02 (s, 2 H, CH_2CO), 7.02 (dd, ^3J = 5.3 Hz, ^4J = 1.4 Hz, 1 H, C^5H, Pyr), 7.22-7.31 (m, 2 H, C$^{3/5}H$, F-Phe), 7.39-7.42 (m, 2 H, C$^{2/6}H$, Phe), 7.45-7.49 (m, 2 H, C$^{2/6}H$, F-Phe), 7.57-7.61 (m, 3 H, C$^{3\text{-}5}H$, Phe), 8.14 (bs, 1 H, C^6H, Pyr), 8.23 (bs, 1 H, C^3H, Pyr), 10.59 (bs, 1 H, CON*H*), 12.71 (bs, 1 H, N*H*) ppm.

^{13}C NMR (75 MHz, DMSO-d_6): δ = 15.1 (S*C*H$_3$), 28.5 (*C*^{5}H$_2$), 37.0 (*C*H$_2$CO), 37.2 (*C*^{4}H$_2$), 110.5 (*C*^{3}H, Pyr), 115.8 (d, $^2J_{CF}$ = 21.0 Hz, *C*$^{3/5}$H, F-Phe), 166.6 (*C*^{5}H, Pyr), 119.7 (*C*^{5}, Pyrimidine), 122.0 (d, $^4J_{CF}$ = 3.6 Hz, *C*^{1}, F-Phe), 127.1 (*C*^{5}, Imdz), 128.8 (*C*$^{2/6}$H, Phe), 129.7 (*C*$^{3/5}$H, Phe), 130.0 (*C*^{4}, Imdz), 130.1 (*C*^{4}H, Phe), 130.7 (*C*$^{2/6}$H, F-Phe), 134.3 (*C*^{4}, Pyr), 135.5 (*C*^{1}, Phe), 143.8 (*C*^{2}, Imdz), 147.8 (*C*^{6}H, Pyr), 152.1 (*C*^{2}, Pyr), 157.0 (*C*^{6}, Pyrimidine), 159.0 (*C*^{2}, Pyrimidine), 161.7 (d, $^1J_{CF}$ = 253.4 Hz, *C*F), 160.7 (*C*O), 166.1 (*C*ONH) ppm.

IR (ATR): $\tilde{\nu}$ = 3200, 2928, 1697, 1661, 1611, 1559, 1500, 1466, 1422, 1304, 1238, 1221, 1163, 1057, 977, 959, 839, 762, 752, 705, 692, 665 cm^{-1}.

HPLC (Method 2): t_R = 5.6 min.

LC-MS (ESI, 70 eV): m/z = 603 $[MH]^+$ (calc. m/z = 602).

***N*-(4-(5-(4-Fluorophenyl)-2-(methylthio)-1*H*-imidazol-4-yl)pyridin-2-yl)-2-((3-(2-methoxyphenyl)-4-oxo-3,4,6,7-tetrahydrothieno[3,2-*d*]pyrimidin-2-yl)thio)acetamide (267)**

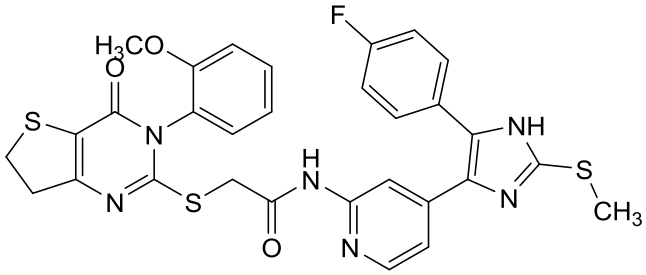

$C_{30}H_{25}FN_6O_3S_3$ (M_r 632.75)

267 was synthesized according to the procedure for **266** from **273** (210 mg, 718 µmol), **279** (318 mg, 844 µmol), and Et_3N (440 ml, 2.81 mmol) in 10 ml anhyd. DMF. The crude product was purified by flash chromatography (SiO_2, 20-75 % ethyl acetate/petrol ether) to afford **267** as a light brown crystalline solid (100 % HPLC purity).

Yield: 346 mg (547 µmol, 76 %).

m.p.: 139 °C.

^{1}H NMR (300 MHz, DMSO-d_6): δ = 2.61 (s, 3 H, SCH_3), 3.12-3.22 (m, 2 H, C$^4H_2$), 3.32-3.39 (m, 2 H, C$^5H_2$), 3.79 (s, 3 H, OCH_3), 4.02 (s, 1 H, CH_2CO), 7.03 (dd, ^3J = 5.2 Hz, ^4J = 1.6 Hz, 1 H, C^5H, Pyr), 7.12 (dt, ^3J = 7.6 Hz, ^4J = 1.0 Hz, 1 H, C^5H, H_3CO-Phe), 7.24-7.31 (m, 2 H, C$^{3/5}H$, F-Phe), 7.26 (dd, ^3J = 8.3 Hz, ^4J = 0.8 Hz, 1 H, C^6H, H_3CO-Phe), 7.34 (dd, ^3J = 7.7 Hz, ^4J = 1.7 Hz, 1 H, C^3H, H_3CO-Phe), 7.44-7.50 (m, 2 H, C$^{2/6}H$, F-Phe), 7.52-7.58 (m, 1 H, C^5H, H_3CO-Phe), 8.13 (dd, ^3J = 5.3 Hz, ^5J = 0.6 Hz, 1 H, C^6H, Pyr), 8.24 (bs, 1 H, C^3H, Pyr), 10.56 (bs, 1 H, CONH), 12.71 (bs, 1 H, NH) ppm.

^{13}C NMR (75 MHz, DMSO-d_6): δ = 15.1 (SCH$_3$), 28.5 (C^5H$_2$), 36.8 (CH$_2$CO), 37.3 (C^4H$_2$), 56.0 (OCH$_3$), 110.5 (C^3H, Pyr), 112.9 (C^6H, H_3CO-Phe), 115.8 (d, $^2J_{CF}$ = 21.6 Hz, $C^{3/5}$H, F-Phe), 116.6 (C^5H, Pyr), 119.4 (C^5, Pyrimidine), 121.1 (C^5H, H_3CO-Phe), 123.5 (d, $^4J_{CF}$ = 2.6 Hz, C^1, F-Phe), 125.6 (C^5, Imdz), 126.6 (C^1, H_3CO-Phe), 130.1 (C^3H, H_3CO-Phe), 130.7 (d, $^3J_{CF}$ = 8.4 Hz, $C^{2/6}$H, F-Phe), 132.0 (C^4H, H_3CO-Phe), 134.3 (C^4, Pyr), 138.8 (C^4, Imdz), 142.3 (C^2, Imdz), 147.8 (C^6H, Pyr), 152.1 (C^2, Pyr), 154.7 (C^2OCH$_3$), 156.5 (C^6, Pyrimidine), 159.6 (C^2, Pyrimidine), 160.8 (CO), 162.0 (d, $^1J_{CF}$ = 246.1 Hz, CF), 166.1 (CONH) ppm.

IR (ATR): $\tilde{\nu}$ = 2930, 1680, 1661, 1603, 1549, 1499, 1474, 1416, 1371, 1283, 1263, 1221, 1159, 1121, 1049, 1020, 837, 814, 752, 664 cm^{-1}.

HPLC (Method 2): t_R = 5.6 min.

LC-MS (ESI, 70 eV): m/z = 633 $[MH]^+$ (calc. m/z = 632).

HRMS (EI, 70 eV): m/z = 632.1134 $[M]^+$ (calc. m/z = 632.1134).

4-((4-Methylpiperazin-1-yl)methyl)benzoic acid (281)

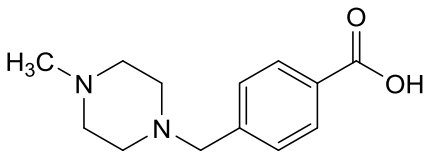

$C_{13}H_{18}N_2O_2$ (M_r 234.30)

N-Methylpiperazine (3.10 ml, 27.9 mmol) was added in one portion to a solution of 4-bromomethylbenzoic acid (2.01 g, 9.33 mmol) in 125 ml *tert*-butanol and the resulting mixture was stirred at rt for 6 h. The solvent was removed under reduced pressure and the crude product was crystallized from 2-propanol to afford **281** as a colorless solid (100 % HPLC purity).

Yield: 1.09 g (4.64 mmol, 50 %).

^{1}H NMR (300 MHz, DMSO-d_6): δ = 2.51 (s, 3 H, CH_3), 2.58 (bs, 4 H, C$^{3/5}H_2$, Piperazine), 2.88 (bs, 4 H, C$^{2/6}H_2$, Piperazine), 3.59 (s, 2 H, CH_2), 7.43 (d, ^3J = 8.3 Hz, 2 H, C$^{3/5}H$, Phe), 7.90 (d, ^3J = 8.3 Hz, 2 H, C$^{2/6}H$, Phe) ppm.

^{13}C NMR (75 MHz, DMSO-d_6): δ = 43.2 (CH$_3$), 50.2 ($C^{3/5}$H$_2$, Piperazine), 53.1 ($C^{2/6}$H$_2$, Piperazine), 60.8 (CH$_2$), 128.9 ($C^{3/5}$H, Phe), 129.3 ($C^{2/6}$H, Phe), 129.8 (C^1, Phe), 142.8 (C^4, Phe) ,167.2 (CO) ppm.

HPLC (Method 3): t_R = 1.3 min.

LC-MS (ESI, 70 eV): m/z = 235 $[MH]^+$ (calc. m/z = 234).

1,4-Bis(4-carboxybenzyl)-1-methylpiperazin-1-ium (283)

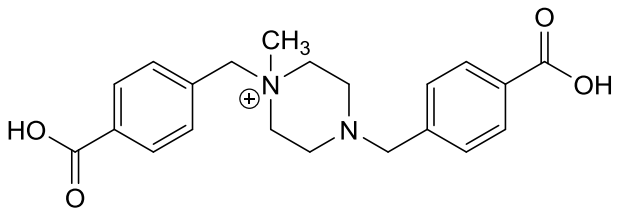

$C_{21}H_{25}N_2O_4^+$ (M_r 369.44)

N-Methylpiperazine (466 µl, 4.19 mmol) was slowly added to a solution of 4-bromomethylbenzoic acid (600 mg, 2.79 mmol) in 23 ml *tert*-butanol and the resulting mixture was stirred at rt for 6 h. The solvent was removed under reduced pressure and the crude product was crystallized from 2-propanol to afford **283** as a colorless solid (100 % HPLC purity).

Yield: 194 mg (525 µmol, 38 %).

^{1}H NMR (300 MHz, DMSO-d_6): δ = 2.69-2.91 (m, 4 H, C$^{3/5}$*H*, Piperazine), 3.00 (s, 3 H, CH_3), 3.45-3.55 (m, 4 H, C$^{2/6}$*H*, Piperazine), 3.72 (s, 2 H, CH_2N), 4.76 (s, 2 H, CH_2N$^+$), 7.44 (d, ^3J = 8.2 Hz, 2 H, C$^{3/5}$*H*, BnN), 7.70 (d, ^3J = 8.3 Hz, 2 H, C$^{3/5}$*H*, BnN$^+$), 7.93 (d, ^3J = 8.2 Hz, 2 H, C$^{2/6}$*H*, BnN$^+$), 8.04 (d, ^3J = 8.2 Hz, 2 H, C$^{2/6}$*H*, BnN), 12.34 (bs, 1 H, COO*H*) ppm.

HPLC (Method 3): t_R = 1.4 min.

LC-MS (ESI, 70 eV): m/z = 369 $[M]^+$ (calc. m/z = 369).

7.3.8 Sulfoxidation of Compounds: 4,5-Diaryl-2-(methylsulfinyl)-1*H*-imidazoles

General procedure for sulfoxidation of compounds (82, 84, 85, 102-104, 285-291)

The respective sulfide (1.0 equiv) was dissolved in THF and H_2O was added (approx. 3:1). The mixture was stirred at 0 °C for 10 min before an ice-cold aq. solution of potassium peroxomonosulfate (Oxone®, 0.6 equiv.) was added and stirring continued for 0.5-2 h at the same temp. After completion of the reaction sat. aq. $NaHCO_3$ solution, H_2O, and ethyl acetate were added and the phases were separated. The organic layer was washed with H_2O and sat. aq. NaCl solution, dried over anhyd. Na_2SO_4, and the solvent was removed under reduced pressure. Purification of the crude products was achieved by crystallization from ethyl acetate or flash chromatography (SiO_2 and RP-18, eluent and mixing ratio given for each compound) to afford the appropriate compound.

Syntheses of **84** and **85** have been performed by LYDIA KUHL during her Bachelor thesis[220].

***tert*-Butyl (4-(5-(4-fluorophenyl)-2-(methylsulfinyl)-1*H*-imidazol-4-yl)pyridin-2-yl)-carbamate (285)**

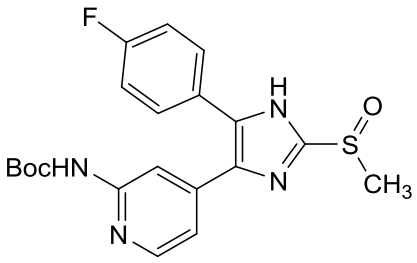

$C_{20}H_{21}FN_4O_3S$ (M_r 416.47)

Synthesis was performed according to the general procedure for sulfoxidation from **160** (50.0 mg, 125 µmol) and Oxone® (42.2 mg, 68.7 µmol in 0.7 ml H_2O) in 1 ml THF and 0.3 ml H_2O. Flash chromatography (SiO_2, 40-50 % ethyl acetate/petrol ether) afforded **285** as a colorless solid (100 % HPLC purity).

Yield: 38.8 mg (93.2 µmol, 75 %).

m.p.: 203 °C.

^{1}H NMR (300 MHz, DMSO-d_6): δ = 1.44 (s, 9 H, ^{t}Bu), 3.09 (s, 3 H, SCH_3), 6.97 (dd, ^3J = 5.2 Hz, ^4J = 1.3 Hz, 1 H, C^5H, Pyr), 7.30 (bs, 2 H, C$^{3/5}H$, F-Phe), 7.50-7.55 (m, 2 H, C$^{2/6}H$, F-Phe), 8.03 (s, 1 H, C^3H, Pyr), 8.13 (bs, 1 H, C^6H, Pyr), 9.69 (bs, 1 H, NH), 13.88 (bs, 1 H, NH, Imdz) ppm.

^{13}C NMR (300 MHz, DMSO-d_6): δ = 27.9 (C(CH$_3$)$_3$), 39.1 (SCH$_3$), 79.5 (C(CH$_3$)$_3$), 109.9 (C^3H, Pyr), 115.7 (C^5H, Pyr), 116.0 ($C^{3/5}$H, F-Phe), 131.1 ($C^{2/6}$H, F-Phe), 135.1 (C^4, Pyr), 147.8 (C^6H, Pyr), 149.1 (C^2, Imdz), 152.5 (CO), 152.9 (C^2, Pyr), 160.2 (C^1, F-Phe), 163.6 (CF) ppm.

IR (ATR): $\tilde{\nu}$ = 2950, 1724, 1607, 1559, 1501, 1456, 1418, 1366, 1290, 1269, 1231, 1159, 1117, 1057, 1017, 995, 835, 814, 766, 702 cm^{-1}.

HPLC (Method 1): t_R = 4.6 min.

LC-MS (ESI, 70 eV): m/z = 417 [MH]$^+$, 361 [MH$_2$-^{t}Bu]$^+$ (calc. m/z = 416).

_N_-Benzyl-4-(5-(4-fluorophenyl)-2-(methylsulfinyl)-1_H_-imidazol-4-yl)pyridin-2-amine (82)

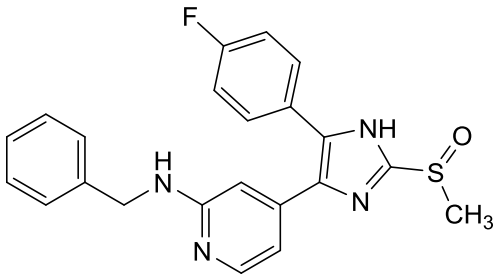

$C_{22}H_{19}FN_4OS$ (M_r 406.48)

Synthesis was performed according to the general procedure for sulfoxidation from **162** (400 mg, 1.02 mmol) and Oxone® (331 mg, 538 µmol in 6 ml H_2O) in 8 ml THF and 2 ml H_2O. Flash chromatography (SiO_2, 50-100 % ethyl acetate/cyclohexane) afforded **82** as a yellowish solid (100 % HPLC purity).

Yield: 197 mg (485 µmol, 47 %).

m.p.: 180 °C.

^{1}H NMR (300 MHz, DMSO-d_6): δ = 3.07 (s, 3 H, SCH_3), 4.43 (d, ^4J = 6.0 Hz, 2 H, CH_2, Bn), 6.50 (dd, ^3J = 5.3 Hz, ^4J = 1.3 Hz, 1 H, C^{5}H, Pyr), 6.65 (bs, 1 H, C^{3}H, Pyr), 7.13-7.32 (m, 8 H, C$^{3/5}$H, F-Phe and ^{ar}CH, Bn and CH_2NH), 7.49-7.54 (m, 2 H, C$^{2/6}$H, F-Phe), 7.90 (bs, 1 H, C^{6}H, Pyr), 13.76 (bs, 1 H, NH) ppm.

^{13}C NMR (75 MHz, DMSO-d_6): δ = 39.2 (SCH$_3$), 44.2 (CH$_2$, Bn), 105.7 (C^3H, Pyr), 110.4 (C^5H, Pyr), 115.6 (d, $^2J_{CF}$ = 21.9 Hz, $C^{3/5}$H, F-Phe), 126.5 ($^{ar}C^4$H, Bn), 127.1 ($^{ar}C^{2/6}$H, Bn), 128.2 ($^{ar}C^{3/5}$H, Bn), 130.6 ($C^{2/6}$H, F-Phe), 104.6 ($^{ar}C^1$, Bn), 147.9 (C^4, Pyr), 148.3 (C^6H, Pyr), 159.0 (C^2, Pyr) ppm.

IR (ATR): $\tilde{\nu}$ = 3350, 3020, 1607, 1559, 1495, 1460, 1360, 1200, 1155, 1047, 981, 864, 837, 814, 741, 696, 682 cm^{-1}.

HPLC (Method 1): t_R = 2.6 min.

LC-MS (ESI, 70 eV): m/z = 407 $[MH]^+$ (calc. m/z = 406).

HRMS (EI, 70 eV): m/z = 406.1264 $[M]^+$ (calc. m/z = 406.1264).

_N_-(2-Ethoxyphenyl)-4-(5-(4-fluorophenyl)-2-(methylsulfinyl)-1_H_-imidazol-4-yl)pyridin-2-amine (84)

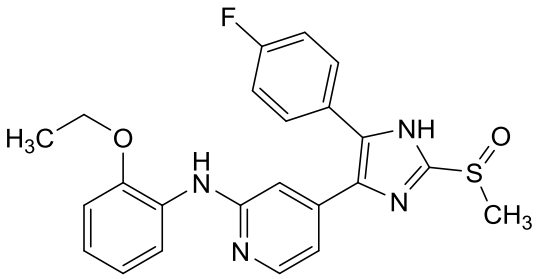

$C_{23}H_{21}FN_4O_2S$ (M_r 436.51)

Synthesis was performed according to the general procedure for sulfoxidation from **149** (300 mg, 713 µmol) and Oxone® (219 mg, 356 µmol in 4 ml H_2O) in 5 ml THF and 2 ml H_2O. Flash chromatography (RP-18, 20-90 % methanol/H_2O) afforded **84** as a voluminous yellow solid (100 % HPLC purity).

Yield: 255 mg (584 µmol, 82 %).

m.p.: 152 °C.

^{1}H NMR (300 MHz, $CDCl_3$): δ = 1.42 (t, ^3J = 7.0 Hz, 3 H, CH_3), 3.03 (s, 3 H, SCH_3), 4.07 (q, ^3J = 7.0 Hz, 2 H, CH_2), 6.94-6.78 (m, 4 H, C$^{4\text{-}6}H$, EtO-Phe and C^5H, Pyr), 7.03 (dd, ^4J = 1.4 Hz, ^5J = 0.7 Hz, 1 H, C^3H, Pyr), 7.07-7.13 (m, 3 H, C$^{3/5}H$, F-Phe and NH), 7.46-7.50 (m, 2 H, C$^{2/6}H$, F-Phe), 7.62 (dd, ^3J = 7.8 Hz, ^4J = 1.5 Hz, 1 H, C^3H, EtO-Phe), 8.14 (dd, ^3J = 5.3 Hz, ^5J = 0.7 Hz, 1 H, C^6H, Pyr) ppm.

^{13}C NMR (75 MHz, $CDCl_3$): δ = 14.9 (CH$_3$), 40.8 (SCH$_3$), 64.1 (CH$_2$), 106.9 (C^3H, Pyr), 111.5 (C^3H, EtO-Phe), 113.3 (C^5H, Pyr), 116.0 (d, $^2J_{CF}$ = 21.7 Hz, $C^{3/5}$H, F-Phe), 118.2 (C^6H, EtO-Phe), 120.6 (C^5H, EtO-Phe), 121.9 (C^4H, EtO-Phe), 129.9 (C^1, EtO-Phe), 130.6 (d, $^3J_{CF}$ = 8.2 Hz, $C^{2/6}$H, F-Phe), 146.7 (C^2, Imdz), 148.2 (C^2, EtO-Phe), 148.5 (C^6H, Pyr), 156.0 (C^2, Pyr), 162.9 (d, $^1J_{CF}$ = 248.8 Hz, CF) ppm.

HPLC (Method 1): t_R = 3.7 min.

LC-MS (ESI, 70 eV): m/z = 437 $[MH]^+$ (calc. m/z = 436).

_N_-(3,4-Dimethoxyphenethyl)-4-(5-(4-fluorophenyl)-2-(methylsulfinyl)-1_H_-imidazol-4-yl)-pyridin-2-amine (85)

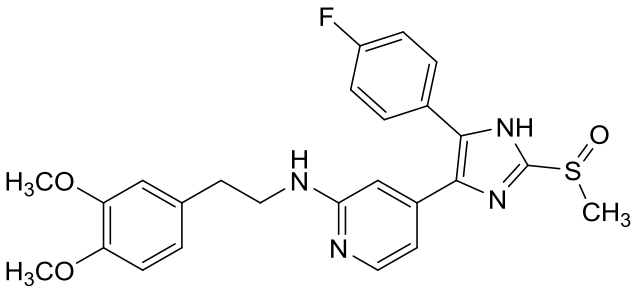

$C_{25}H_{25}FN_4O_3S$ (M_r 480.56)

Synthesis was performed according to the general procedure for sulfoxidation from **150** (500 mg, 1.08 mmol) and Oxone® (330 mg, 537 µmol in 5 ml H_2O) in 9 ml THF and 3 ml H_2O. Flash chromatography (RP-18, 20-90 % methanol/H_2O) afforded **85** as a pale yellow solid (92 % HPLC purity).

Yield: 208 mg (433 µmol, 39 %).

m.p.: 183 °C.

^{1}H NMR (300 MHz, $CDCl_3$): δ = 2.74 (t, ^3J = 6.8 Hz, 1 H, CH_2CH$_2$NH), 2.97 (s, 3 H, SCH_3), 3.36 (m, 2 H, CH$_2$CH_2NH), 3.76 (s, 6 H, 2 OCH_3), 5.00 (bs, 1 H, CH$_2$CH$_2$NH), 6.49 (bs, 1 H, C^3H, Pyr), 6.52 (dd, ^3J = 5.4 Hz, ^4J = 1.3 Hz, 1 H, C^5H, Pyr), 6.60-6.63 (m, 2 H, C$^{2/6}H$, $(OCH_3)_2$-Phe), 6.71 (d, ^3J = 8.7 Hz, 1 H, C^5H, $(OCH_3)_2$-Phe), 6.96-7.02 (m, 2 H, C$^{3/5}H$, F-Phe), 7.36-7.41 (m, 2 H, C$^{2/6}H$, F-Phe), 7.80 (d, ^3J = 5.5 Hz, 1 H, C^6H, Pyr) ppm.

^{13}C NMR (75 MHz, $CDCl_3$): δ = 35.1 (CH$_2$CH$_2$NH), 40.7 (SCH$_3$), 43.3 (CH$_2$$CH_2$NH), 55.9 (C^{3}O$CH_3$), 55.9 (C^{4}O$CH_3$), 104.6 ($C^3$H, Pyr), 111.2 ($C^5$H, Pyr), 111.4 ($C^5$H, $(OCH_3)_2$-Phe), 112.1 (C^2H, $(OCH_3)_2$-Phe), 115.9 (d, $^2J_{CF}$ = 21.7 Hz, $C^{3/5}$H, F-Phe), 120.7 (C^6H, $(OCH_3)_2$-Phe), 127.2 (C^1, F-Phe), 130.5 (d, $^3J_{CF}$ = 8.2 Hz, $C^{2/6}$H, F-Phe), 131.5 (C^1, $(OCH_3)_2$-Phe), 135.3 ($C^{4/5}$, Imdz), 141.6 (C^4, Pyr), 146.8 (C^2, Imdz), 147.4 (C^6H, Pyr), 147.7 (C^4OCH_3), 149.0 (C^3OCH_3), 158.6 (C^2, Pyr), 162.9 (d, $^1J_{CF}$ = 249.2 Hz, CF) ppm.

HPLC (Method 1): t_R = 2.6 min.

LC-MS (ESI, 70 eV): m/z = 481 $[MH]^+$ (calc. m/z = 480).

3-(2,4-Dimethoxyphenyl)-*N*-(4-(5-(4-fluorphenyl)-2-(methylsulfinyl)-1*H*-imidazol-4-yl)-pyridin-2-yl)propanamide (102)

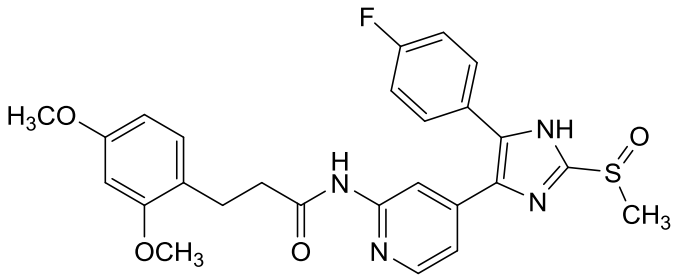

$C_{26}H_{25}FN_4O_4S$ (M_r 508.57)

Synthesis was performed according to the general procedure for sulfoxidation from **190** (100 mg, 203 µmol) and Oxone® (64.9 mg, 106 µmol in 1 ml H_2O) in 2 ml THF and 0.6 ml H_2O. Flash chromatography (SiO_2, 40-100 % ethyl acetate/petrol ether) afforded **102** as a colorless solid (99 % HPLC purity).

Yield: 96.1 mg (189 µmol, 93 %).

m.p.: 209 °C.

^{1}H NMR (300 MHz, DMSO-d_6): δ = 2.58 (t, ^3J = 7.5 Hz, 2 H, CH_2CH_2CO), 2.75 (t, ^3J = 7.4 Hz, 2 H, CH_2CH_2CO), 3.08 (s, 3 H, SCH_3), 3.72 (s, 3 H, C^2OCH_3), 3.77 (s, 3 H, C^4OCH_3), 6.42 (dd, ^3J = 8.3 Hz, ^4J = 2.4 Hz, 1 H, C^5H, $(OCH_3)_2$-Phe), 6.51 (d, ^4J = 2.4 Hz, 1 H, C^3H, $(OCH_3)_2$-Phe), 7.01-7.05 (m, 2 H, C^5H, Pyr and C^6H, $(OCH_3)_2$-Phe), 7.26-7.32 (m, 2 H, $C^{3/5}H$, F-Phe), 7.51-7.55 (m, 2 H, $C^{2/6}H$, F-Phe), 8.19 (d, ^3J = 5.2 Hz, 1 H, C^6H, Pyr), 8.34 (bs, 1 H, C^3H, Pyr), 10.40 (s, 1 H, CON*H*), 13.89 (bs, N*H*) ppm.

^{13}C NMR (75 MHz, DMSO-d_6): δ = 24.7 (CH_2CH_2CO), 36.3 (CH_2CH_2CO), 39.1 (SCH_3), 55.1 (C^2OCH_3), 55.3 (C^4OCH_3), 98.3 (C^3H, $(OCH_3)_2$-Phe), 104.3 (C^5H, $(OCH_3)_2$-Phe), 111.1 (C^3H, Pyr), 115.8 (d, $^2J_{CF}$ = 21.7 Hz, $C^{3/5}H$, F-Phe), 117.0 (C^5H, Pyr), 120.9 (C^1, $(OCH_3)_2$-Phe), 127.3 (C^1, F-Phe), 129.8 (C^6H, $(OCH_3)_2$-Phe), 130.8 (d, $^3J_{CF}$ = 8.2 Hz, $C^{2/6}H$, F-Phe), 133.4 (C^4, Imdz), 133.9 (C^5, Imdz), 142.2 (C^4, Pyr), 147.9 (C^6H, Pyr), 148.9 (C^2, Imdz), 152.6 (C^2, Pyr), 157.9 (C^4OCH_3), 159.0 (C^2OCH_3), 162.1 (d, $^1J_{CF}$ = 245.5 Hz, *C*F), 171.54 (*C*O) ppm.

IR (ATR): $\tilde{\nu}$ = 2955, 1701, 1609, 1573, 1545, 1528, 1506, 1412, 1287, 1221, 1209, 1153, 1121, 1034, 986, 831, 706 cm^{-1}.

HPLC (Method 1): t_R = 5.0 min.

LC-MS (ESI, 70 eV): m/z = 509 $[MH]^+$ (calc. m/z = 508).

HRMS (EI, 70 eV): m/z = 508.1581 $[M]^+$ (calc. m/z = 508.1581).

3-(2,5-Dimethoxyphenyl)-*N*-(4-(5-(4-fluorophenyl)-2-(methylsulfinyl)-1*H*-imidazol-4-yl)-pyridin-2-yl)propanamide (103)

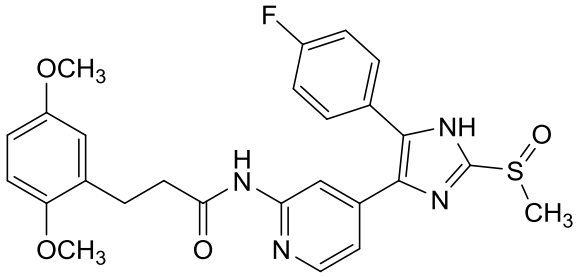

$C_{26}H_{25}FN_4O_4S$ (M_r 508.57)

Synthesis was performed according to the general procedure for sulfoxidation from **191** (100 mg, 203 µmol) and Oxone® (68.6 mg, 112 µmol in 1 ml H_2O) in 2 ml THF and 0.6 ml H_2O. Crystallization from ethyl acetate afforded **103** as a colorless solid (100 % HPLC purity).

Yield: 26.6 mg (52.3 mmol, 26 %).

m.p.: 204 °C.

^{1}H NMR (300 MHz, DMSO-d_6): δ = 2.62 (t, ^3J = 7.7 Hz, 2 H, CH_2CH_2CO), 2.80 (t, ^3J = 7.5 Hz, 2 H, CH_2CH_2CO), 3.09 (s, 3 H, SCH_3), 3.66 (s, 3 H, C^5OCH_3), 3.72 (s, 3 H, C^2OCH_3), 6.72 (dd, ^3J = 8.8 Hz, ^4J = 3.1 Hz, 1 H, C^4H, $(OCH_3)_2$-Phe), 6.77 (d, ^4J = 3.0 Hz, 1 H, C^6H, $(OCH_3)_2$-Phe), 6.86 (d, ^3J = 8.8 Hz, 1 H, C^3H, $(OCH_3)_2$-Phe), 7.02 (dd, ^3J = 5.2 Hz, ^4J = 1.5 Hz, 1 H, C^5H, Pyr), 7.25-7.31 (m, 2 H, $C^{3/5}H$, F-Phe), 7.51-7.55 (m, 2 H, $C^{2/6}H$, F-Phe), 8.19 (d, ^3J = 5.0 Hz, 1 H, C^6H, Pyr), 8.33 (s, 1 H, C^3H, Pyr), 10.45 (s, 1 H, CON*H*), 14.00 (bs, 1 H, N*H*) ppm.

^{13}C NMR (75 MHz, DMSO-d_6): δ = 25.3 (CH_2CH_2CO), 36.0 (CH_2CH_2CO), 39.0 (SCH_3), 55.2 (C^5OCH_3), 55.8 (C^2OCH_3), 111.2 (C^4H, $(OCH_3)_2$-Phe), 111.3 (C^3H, Pyr), 111.5 (C^3H, $(OCH_3)_2$-Phe), 115.8 (d, $^2J_{CF}$ = 21.3 Hz, $C^{3/5}$H, F-Phe), 115.9 (C^6H, $(OCH_3)_2$-Phe), 126.5 (C^1, F-Phe), 130.8 (d, $^3J_{CF}$ = 8.3 Hz, $C^{2/6}$H, F-Phe), 142.1 (C^4, Pyr), 148.0 (C^6H, Pyr), 148.8 (C^2, Imdz), 151.2 (C^2OCH_3), 152.58 (C^2, Pyr), 153.0 (C^5OCH_3), 162.1 (d, $^1J_{CF}$ = 245.6 Hz, *C*F), 171.42 (*C*O) ppm.

IR (ATR): $\tilde{\nu}$ = 2960, 1705, 1609, 1557, 1497, 1454, 1437, 1416, 1296, 1283, 1236, 1219, 1184, 1168, 1138, 1113, 1047, 1026, 876, 843, 816, 706 cm^{-1}.

HPLC (Method 3): t_R = 5.1 min.

LC-MS (ESI, 70 eV): *m/z* = 509 $[MH]^+$ (calc. *m/z* = 508).

1-(2,4-Dimethoxyphenyl)-3-(4-(5-(4-fluorophenyl)-2-(methylsulfinyl)-1*H*-imidazol-4-yl)-pyridin-2-yl)carbamide (104)

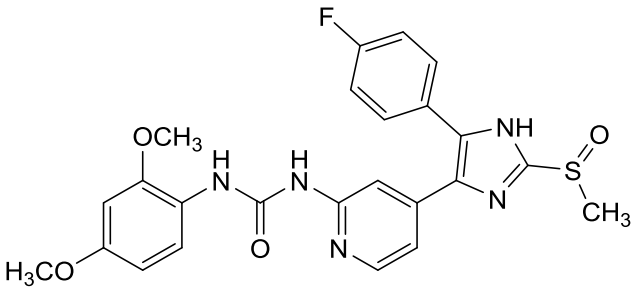

$C_{24}H_{22}FN_5O_4S$ (M_r 495.53)

Synthesis was performed according to the general procedure for sulfoxidation from **204** (85.0 mg, 177 µmol) and Oxone® (59.9 mg, 97.5 µmol in 1 ml H_2O) in 3.4 ml THF and 1 ml H_2O. Flash chromatography (SiO_2, 35-100 % ethyl acetate/petrol ether and RP-18, 55-100 % methanol/H_2O) afforded **104** as a colorless solid (100 % HPLC purity).

Yield: 18.9 mg (38.1 µmol, 22 %).

m.p.: 227 °C.

^{1}H NMR (300 MHz, DMSO-d_6): δ = 3.08 (s, 3 H, SCH_3), 3.74 (s, 3 H, C^{4}OCH_3), 3.88 (s, 3 H, C^{2}OCH_3), 6.48 (dd, ^3J = 8.9 Hz, ^4J = 2.7 Hz, 1 H, C^5H, $(OCH_3)_2$-Phe), 6.62 (d, ^4J = 2.7 Hz, 1 H, C^3H, $(OCH_3)_2$-Phe), 6.95 (dd, ^3J = 5.4 Hz, ^4J = 1.5 Hz, 1 H, C^5H, Pyr), 7.27-7.33 (m, 2 H, C$^{3/5}H$, F-Phe), 7.46 (bs, 1 H, C^3H, Pyr), 7.51-7.56 (m, 2 H, C$^{2/6}H$, F-Phe), 8.02 (d, ^3J = 8.9 Hz, 1 H, C^6H, $(OCH_3)_2$-Phe), 8.19 (d, ^3J = 5.3 Hz, 1 H, C^6H, Pyr), 9.70 (s, 1 H, NH), 11.07 (bs, 1 H, NH), 13.87 (bs, 1 H, NH, Imdz) ppm.

^{13}C NMR (75 MHz, DMSO-d_6): δ = 39.1 (SCH$_3$), 55.3 (C^{2}OCH$_3$), 56.0 (C^{4}OCH$_3$), 98.8 (C^3H, $(OCH_3)_2$-Phe), 104.1 (C^5H, $(OCH_3)_2$-Phe), 109.2 (C^3H, Pyr), 115.1 (C^5H, Pyr), 115.8 (d, $^2J_{CF}$ = 21.7 Hz, $C^{3/5}$H, F-Phe), 119.8 (C^6H, $(OCH_3)_2$-Phe), 121.8 (C^1, $(OCH_3)_2$-Phe), 127.2 (C^1, F-Phe), 130.8 (d, $^3J_{CF}$ = 8.4 Hz, $C^{2/6}$H, F-Phe), 132.7 (C^4, Imdz), 134.1 (C^5, Imdz), 142.8 (C^4, Pyr), 146.5 (C^6H, Pyr), 149.1 (C^2, Imdz), 149.4 (C^2OCH$_3$), 152.2 (CO), 153.6 (C^2, Pyr), 155.2 (C^4OCH$_3$), 162.14 (d, $^1J_{CF}$ = 244.6 Hz, CF) ppm.

IR (ATR): $\tilde{\nu}$ = 2950, 1657, 1603, 1564, 1547, 1508, 1454, 1360, 1298, 1281, 1215, 1179, 1155, 1132, 1051, 1032, 978, 837, 824, 750 cm^{-1}.

HPLC (Method 3): t_R = 4.8 min.

LC-MS (ESI, 70 eV): m/z = 496 $[MH]^+$ (calc. m/z = 495).

1-(4-(5-(4-Fluorophenyl)-2-(methylsulfinyl)-1*H*-imidazol-4-yl)pyridin-2-yl)-3-(4-methoxyphenyl)carbamide (286)

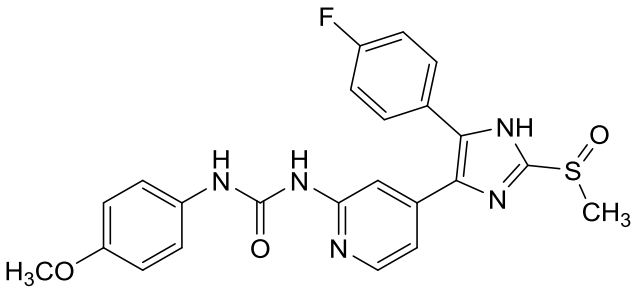

$C_{23}H_{20}FN_5O_3S$ (M_r 465.50)

Synthesis was performed according to the general procedure for sulfoxidation from **206** (100 mg, 225 µmol) and Oxone® (75.2 mg, 122 µmol in 1 ml H_2O) in 2 ml THF and 0.6 ml H_2O. Flash chromatography (RP-18, 50-70 % methanol/H_2O) afforded **286** as a colorless solid (99 % HPLC purity).

Yield: 62.6 mg (135 µmol, 61 %).

m.p.: 233 °C.

^{1}H NMR (300 MHz, DMSO-d_6): δ = 3.09 (s, 3 H, SCH_3), 3.73 (s, 3 H, C^{4}OCH_3), 6.89 (d, ^3J = 9.1 Hz, 2 H, C$^{3/5}H$, H_3CO-Phe), 6.95 (dd, ^3J = 5.4 Hz, ^4J = 1.5 Hz, 1 H, C^5H, Pyr), 7.28-7.34 (m, 2 H, C$^{3/5}H$, F-Phe), 7.41 (d, ^3J = 9.1 Hz, 2 H, C$^{2/6}H$, H_3CO-Phe), 7.51-7.56 (m, 2 H, C$^{2/6}H$, F-Phe), 7.65 (bs, 1 H, C^3H, Pyr), 8.18 (d, ^3J = 5.4 Hz, 1 H, C^6H, Pyr), 9.43 (s, 1 H, N*H*), 10.47 (bs, 1 H, N*H*), 13.92 (bs, 1 H, N*H*, Imdz) ppm.

^{13}C NMR (75 MHz, DMSO-d_6): δ = 39.1 (S*C*H_3), 55.2 (C^{4}O*C*H_3), 109.4 (*C*^{3}H, Pyr), 114.0 (*C*$^{3/5}$H, H_3CO-Phe), 115.2 (*C*^{5}H, Pyr), 115.9 (d, $^2J_{CF}$ = 21.7 Hz, *C*$^{3/5}$H, F-Phe), 120.6 (*C*$^{2/6}$H, H_3CO-Phe), 127.5 (*C*^{1}, F-Phe), 130.9 (d, $^3J_{CF}$ = 8.7 Hz, *C*$^{2/6}$H, F-Phe), 132.0 (*C*^{1}, H_3CO-Phe), 146.9 (*C*^{6}H, Pyr), 148.8 (*C*^{2}, Imdz), 152.2 (*C*O), 153.5 (*C*^{2}, Pyr), 154.9 (*C*^{4}OCH_3), 162.2 (d, $^1J_{CF}$ = 246.7 Hz, *C*F) ppm.

IR (ATR): $\tilde{\nu}$ = 2950, 1661, 1603, 1568, 1557, 1508, 1471, 1298, 1238, 1209, 1180, 1161, 1058, 976, 876, 835, 818, 789, 737, 718, 681 cm^{-1}.

HPLC (Method 3): t_R = 4.7 min.

LC-MS (ESI, 70 eV): m/z = 466 [MH]$^+$ (calc. m/z = 465).

1-(4-(5-(4-Fluorophenyl)-2-(methylsulfinyl)-1*H*-imidazol-4-yl)pyridin-2-yl)-3-(*m*-tolyl)-carbamide (287)

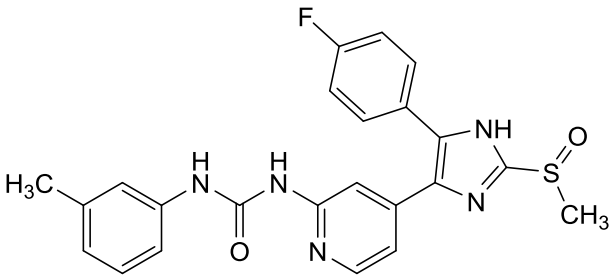

$C_{23}H_{20}FN_5O_2S$ (M_r 449.50)

Synthesis was performed according to the general procedure for sulfoxidation from **208** (100 mg, 231 µmol) and Oxone® (73.7 mg, 120 µmol in 1 ml H_2O) in 2 ml THF and 0.6 ml H_2O. Flash chromatography (SiO_2, 20-100 % ethyl acetate/petrol ether) afforded **287** as a colorless solid (99 % HPLC purity).

Yield: 74.8 mg (166 µmol, 72 %).

m.p.: 235 °C.

^{1}H NMR (300 MHz, DMSO-d_6): δ = 2.29 (s, 3 H, CH_3), 3.09 (s, 3 H, SCH_3), 6.83 (d, ^3J = 7.4 Hz, 1 H, C^4H, Tol), 6.97 (dd, ^3J = 5.4 Hz, ^4J = 1.4 Hz, 1 H, C^5H, Pyr), 7.18 (t, ^3J = 7.7 Hz, 1 H, C^5H, Tol), 7.29-7.35 (m, 4 H, C$^{3/5}H$, F-Phe and C$^{2/6}H$, Tol), 7.52-7.57 (m, 2 H, C$^{2/6}H$, F-Phe), 7.69 (s, 1 H, C^3H, Pyr), 8.19 (d, ^3J = 5.1 Hz, 1 H, C^6H, Pyr), 9.48 (s, 1 H, NH), 10.54 (bs, 1 H, NH), 13.92 (bs, 1 H, NH, Imdz) ppm.

^{13}C NMR (75 MHz, DMSO-d_6): δ = 21.2 (*C*H$_3$), 39.1 (S*C*H$_3$), 109.3 (*C*^{3}H, Pyr), 115.3 (*C*^{5}H, Pyr), 115.9 (d, $^2J_{CF}$ = 21.5 Hz, *C*$^{3/5}$H, F-Phe), 116.0 (*C*^{6}H, Tol), 119.3 (*C*^{2}H, Tol), 123.2 (*C*^{4}H, Tol), 128.7 (*C*^{5}H, Tol), 130.9 (*C*$^{2/6}$H, F-Phe), 138.1 (*C*^{3}, Tol), 138.9 (*C*^{1}, Tol), 143.1 (*C*^{4}, Pyr), 147.0 (*C*^{6}H, Pyr), 148.7 (*C*^{2}, Imdz), 152.1 (*C*O), 153.4 (*C*^{2}, Pyr), 162.2 (d, $^1J_{CF}$ = 244.0 Hz, *C*F) ppm.

IR (ATR): $\tilde{\nu}$ = 2950, 1667, 1605, 1562, 1514, 1476, 1393, 1362, 1314, 1300, 1244, 1221, 1167, 1044, 976, 883, 842, 827, 810, 770, 745, 716, 689 cm^{-1}.

HPLC (Method 3): t_R = 6.4 min.

LC-MS (ESI, 70 eV): *m*/*z* = 450 [MH]$^+$ (calc. *m*/*z* = 449).

1-(3-Chloro-4-methylphenyl)-3-(4-(5-(4-fluorophenyl)-2-(methylsulfinyl)-1*H*-imidazol-4-yl)pyridin-2-yl)carbamide (288)

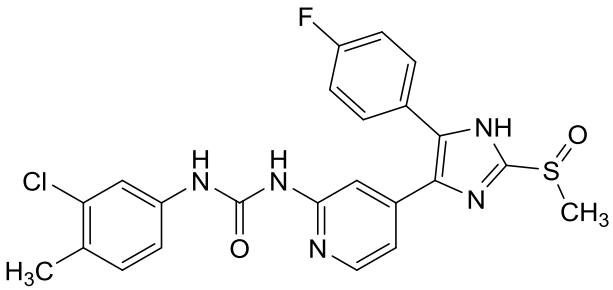

$C_{23}H_{19}ClFN_5O_2S$ (M_r 483.95)

Synthesis was performed according to the general procedure for sulfoxidation from **209** (100 mg, 214 µmol) and Oxone® (72.3 mg, 118 µmol in 1 ml water) in 4 ml THF and 1 ml H_2O. Flash chromatography (SiO_2, 20-100 % ethyl acetate/petrol ether and RP-18, 50-100 % methanol/H_2O) afforded **288** as a beige solid (98 % HPLC purity).

Yield: 78.0 mg (161 µmol, 75 %).

^{1}H NMR (300 MHz, DMSO-d_6): δ = 2.27 (s, 3 H, CH_3), 3.09 (s, 3 H, SCH_3), 6.99 (dd, ^3J = 5.4 Hz, ^4J = 1.3 Hz, 1 H, C^5*H*, Pyr), 7.26 (s, 1 H, C^5*H*, Cl-Tol), 7.26 (s, 1 H, C^6*H*, Cl-Tol), 7.29-7.35 (m, 2 H, C$^{3/5}$*H*, F-Phe), 7.52-7.56 (m, 2 H, C$^{2/6}$*H*, F-Phe), 7.65 (bs, 1 H, C^3*H*, Pyr), 7.76 (bs, 1 H, C^2*H*, Cl-Tol), 9.55 (s, 1 H, N*H*), 10.77 (bs, 1 H, N*H*), 13.93 (bs, 1 H, N*H*, Imdz) ppm.

^{13}C NMR (75 MHz, DMSO-d_6): δ = 18.8 (*C*H$_3$), 39.1 (S*C*H$_3$), 109.2 (*C*^{3}H, Pyr), 115.4 (*C*^{5}H, Pyr), 115.9 (d, $^2J_{CF}$ = 21.5 Hz, *C*$^{3/5}$H, F-Phe), 117.5 (*C*^{6}H, Cl-Tol), 118.7 (*C*^{2}H, Cl-Tol), 129.0 (*C*^{4}, Cl-Tol), 131.1 (*C*$^{2/6}$H, F-Phe), 131.2 (*C*^{5}, Imdz and *C*^{5}H, Cl-Tol), 133.2 (*C*^{3}, Cl-Tol), 134.6 (*C*^{4}, Imdz), 138.2 (*C*^{1}, Cl-Tol), 147.0 (*C*^{6}H, Pyr), 148.7 (*C*^{2}, Imdz), 152.1 (*C*O), 153.2 (*C*^{2}, Pyr), 162.3 (d, $^1J_{CF}$ = 249.9 Hz, *C*F) ppm.

IR (ATR): ṽ = 3000, 1668, 1597, 1551, 1520, 1497, 1476, 1398, 1366, 1312, 1217, 1049, 835, 808, 745 cm^{-1}.

HPLC (Method 3): t_R = 7.4 min.

LC-MS (ESI, 70 eV): m/z = 484 [MH]$^+$ (calc. m/z = 483).

1-(4-(5-(4-Fluorophenyl)-2-(methylsulfinyl)-1*H*-imidazol-4-yl)pyridin-2-yl)-3-(3-(trifluormethyl)phenyl)carbamide (289)

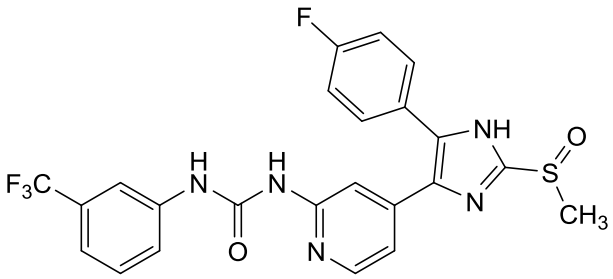

$C_{23}H_{17}F_4N_5O_2S$ (M_r 503.48)

Synthesis was performed according to the general procedure for sulfoxidation from **210** (20.0 mg, 41.0 µmol) and Oxone® (13.9 mg, 22.6 µmol in 0.2 ml H_2O) in 0.4 ml THF and 0.1 ml water. Flash chromatography (SiO_2, 40-100 % ethyl acetate/petrol ether) afforded **289** as a colorless solid (96 % HPLC purity).

Yield: 15.1 mg (30.0 µmol, 73 %).

m.p.: 235 °C.

^{1}H NMR (300 MHz, DMSO-d_6): δ = 3.10 (s, 3 H, SCH_3), 7.02 (dd, ^3J = 5.4 Hz, ^4J = 1.4 Hz, 1 H, C^5H, Pyr), 7.30-7.37 (m, 2 H, C$^{3/5}H$, F-Phe), 7.36 (d, ^3J = 7.7 Hz, 1 H, C^4H, F_3C-Phe), 7.51-7.57 (m, 3 H, C$^{2/6}H$, F-Phe and C^5H, F_3C-Phe), 7.65 (d, ^3J = 8.3 Hz, 1 H, C^6H, F_3C-Phe), 7.71 (s, 1 H, C^2H, F_3C-Phe), 8.08 (bs, 1 H, C^3H, Pyr), 8.22 (bs, 1 H, C^6H, Pyr), 9.59 (s, 1 H, N*H*), 10.90 (bs, 1 H, N*H*), 13.93 (bs, 1 H, N*H*, Imdz) ppm.

^{13}C NMR (75 MHz, DMSO-d_6): δ = 39.1 (S*C*H$_3$), 109.3 (*C*^{2}H, F_3C-Phe), 114.7 (q, $^3J_{CF}$ = 2.5 Hz, *C*^{3}H, Pyr), 115.5 (*C*^{5}H, Pyr), 115.9 (d, $^3J_{CF}$ = 21.9 Hz, *C*$^{3/5}$H, F-Phe), 118.7 (q, $^3J_{CF}$ = 2.1 Hz, *C*^{4}H, F_3C-Phe), 122.5 (*C*^{6}H, F_3C-Phe), 124.2 (q, $^1J_{CF}$ = 272.2 Hz, *C*F$_3$), 125.9 (d, $^4J_{CF}$ = 3.2 Hz, *C*^{1}, F-Phe), 129.6 (q, $^2J_{CF}$ = 31.4 Hz, *C*^{3}, F_3C-Phe), 130.0 (*C*^{5}H, F_3C-Phe), 130.8 (*C*^{5}, Imdz), 131.1 (d, $^4J_{CF}$ = 11.4 Hz, *C*$^{2/6}$H, F-Phe), 134.5 (*C*^{4}, Imdz), 139.9 (*C*^{1}, F_3C-Phe), 143.4 (*C*^{4}, Pyr), 147.1 (*C*^{6}H, Pyr), 148.7 (*C*^{2}, Imdz), 152.2 (*C*O), 162.4 (d, $^1J_{CF}$ = 242.12 Hz, *C*F) ppm.

IR (ATR): ṽ = 2900, 1680, 1607, 1576, 1516, 1495, 1476, 1265, 1240, 1229, 1163, 1121, 1099, 1049, 997, 977, 922, 876, 835, 785, 745, 716, 694 cm^{-1}.

HPLC (Method 3): t_R = 6.8 min.

LC-MS (ESI, 70 eV): *m*/*z* = 504 [MH]$^+$ (calc. *m*/*z* = 503).

1-(4-(5-(4-Fluorophenyl)-2-(methylthio)-1*H*-imidazol-4-yl)pyridin-2-yl)-3-(naphthalen-1-yl)carbamide (290)

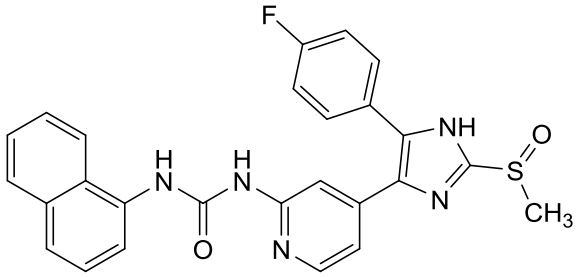

$C_{26}H_{20}FN_5O_2S$ (M_r 485.54)

Synthesis was performed according to the general procedure for sulfoxidation from **212** (51.0 mg, 109 µmol) and Oxone® (36.7 mg, 59.7 µmol in 1 ml H_2O) in 5 ml THF and 1.5 ml H_2O. Flash chromatography (SiO_2, 20-100 % ethyl acetate/petrol ether) afforded **290** as a colorless solid (100 % HPLC purity).

Yield: 37.0 mg (76.2 µmol, 70 %).

m.p.: 244 °C.

^{1}H NMR (300 MHz, DMSO-d_6): δ = 3.10 (s, 3 H, SCH_3), 7.04 (dd, ^3J = 5.4 Hz, ^4J = 1.4 Hz, 1 H, C^5H, Pyr), 7.31-7.36 (m, 2 H, C$^{3/5}H$, F-Phe), 7.49 (t, ^3J = 7.9 Hz, 1 H, C^3H, Naph), 7.54-7.59 (m, 4 H, C^3H, Pyr and C$^{2/6}H$, F-Phe and C^6H, Naph), 7.63-7.68 (m, 2 H, C$^{4/7}H$, Naph), 7.96 (dd, ^3J = 8.1 Hz, ^4J = 0.8 Hz, 1 H, C^5H, Naph), 8.16-8.20 (m, 2 H, C$^{2/8}H$, Naph), 8.34 (d, ^3J = 5.4 Hz, 1 H, C^6H, Pyr), 8.93 (s, 1 H, NH), 11.58 (bs, 1 H, NH), 13.95 (bs, 1 H, NH, Imdz) ppm.

^{13}C NMR (75 MHz, DMSO-d_6): δ = 39.1 (SCH$_3$), 109.4 (C^3H, Pyr), 115.3 (C^5H, Pyr), 115.9 (d, $^2J_{CF}$ = 21.8 Hz, $C^{3/5}$H, F-Phe), 116.9 (C^2H, Naph), 120.9 (C^8H, Naph), 123.1 (C^4H, Naph), 125.5 (C^1, Naph), 126.0 (C^6H, Naph), 126.0 (C^3H, Naph), 126.3 (C^7H, Naph), 128.6 (C^5H, Naph), 130.7 (C^5, Imdz), 130.9 ($C^{2/6}$H, F-Phe), 133.7 (C^{4a}, Naph), 134.1 (C^{8a}, Naph), 143.5 (C^4, Pyr), 146.7 (C^6H, Pyr), 148.9 (C^2, Imdz), 152.6 (CO), 153.6 (C^2, Pyr), 162.3 (d, $^1J_{CF}$ = 246.9 Hz, CF) ppm.

IR (ATR): $\tilde{\nu}$ = 2920, 1668, 1601, 1574, 1552, 1472, 1407, 1362, 1346, 1304, 1267, 1240, 1213, 1157, 1053, 974, 873, 842, 792, 770, 754 cm^{-1}.

HPLC (Method 3): t_R = 7.1 min.

LC-MS (ESI, 70 eV): m/z = 486 $[MH]^+$ (calc. m/z = 485).

4-(2,4-Dimethoxyphenyl)-*N*-(4-(5-(4-fluorophenyl)-2-(methylsulfinyl)-1*H*-imidazol-4-yl)-pyridin-2-yl)-1-methyl-1*H*-pyrrol-2-carboxamide (291)

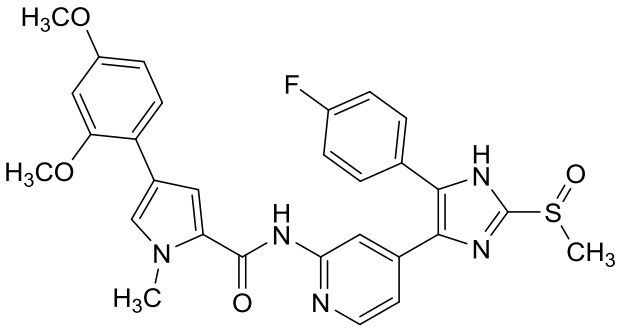

$C_{29}H_{26}FN_5O_4S$ (M_r 559.62)

Synthesis was performed according to the general procedure for sulfoxidation from **231** (196 mg, 368 µmol) and Oxone® (133 mg, 216 µmol in 2 ml H_2O) in 4 ml THF and 1 ml H_2O. Flash chromatography (SiO_2, 40-100 % ethyl acetate/petrol ether) afforded **291** as a yellow solid (95 % HLC purity).

Yield: 182 mg (325 µmol, 88 %).

m.p.: 136 °C.

^{1}H NMR (300 MHz, DMSO-d_6): δ = 3.11 (s, 3 H, SCH_3), 3.78 (s, 3 H, C^{2}OCH_3), 3.86 (s, 3 H, C^{4}OCH_3), 3.90 (s, 3 H, CH_3), 6.57 (dd, ^3J = 8.5 Hz, ^4J = 2.4 Hz, 1 H, C^5H, $(OCH_3)_2$-Phe), 6.61 (d, ^4J = 2.3 Hz, 1 H, C^3H, $(OCH_3)_2$-Phe), 7.07 (d, ^3J = 4.8 Hz, 1 H, C^5H, Pyr), 7.23-7.38 (m, 2 H, C$^{3/5}H$, F-Phe), 7.42 (bs, 1 H, C^3H, Pyrrole), 7.46 (d, ^3J = 8.4 Hz, 1 H, C^6H, $(OCH_3)_2$-Phe), 7.54-7.59 (m, 2 H, C$^{2/6}H$, F-Phe), 7.68 (bs, 1 H, C^5H, Pyrrole), 8.22 (d, ^3J = 4.5 Hz, 1 H, C^6H, Pyr), 8.42 (s, 1 H, C^3H, Pyr), 10.17 (s, 1 H, CON*H*), 13.89 (s, 1 H, N*H*) ppm.

^{13}C NMR (75 MHz, DMSO-d_6): δ = 36.6 (*C*H_3), 39.2 (S*C*H_3), 55.2 (C^{2}O*C*H_3), 55.4 (C^{4}O*C*H_3), 98.8 (*C*^{3}H, $(OCH_3)_2$-Phe), 105.2 (*C*^{5}H, $(OCH_3)_2$-Phe), 111.8 (*C*^{3}H, Pyr), 113.3 (*C*^{5}H, Pyrrole), 115.9 (*C*^{1}, $(OCH_3)_2$-Phe), 116.0 (d, $^2J_{CF}$ = 22.4 Hz, *C*$^{3/5}$H, F-Phe), 116.1 (*C*^{5}H, Pyr), 118.5 (*C*^{4}, Pyrrole), 124.0 (*C*^{2}, Pyrrole), 125.8 (d, $^4J_{CF}$ = 3.3 Hz, *C*^{1}, F-Phe), 127.5 (*C*^{6}H, $(OCH_3)_2$-Phe), 128.6 (*C*^{3}H, Pyrrole), 131.3 (d, $^3J_{CF}$ = 8.3 Hz, *C*$^{2/6}$H. F-Phe), 131.9 (*C*^{4}, Imdz), 135.1 (*C*^{5}, Imdz), 143.0 (*C*^{4}, Pyr), 147.8 (*C*^{6}H, Pyr), 148.5 (*C*^{2}, Imdz), 152.9 (*C*^{2}, Pyr), 156.7 (*C*^{4}OCH$_3$), 158.6 (*C*^{2}OCH$_3$), 159.9 (*C*O), 162.4 (d, $^1J_{CF}$ = 244.3 Hz, *C*F) ppm.

IR (ATR): $\tilde{\nu}$ = 2960, 1685, 1609, 1520, 1506, 1480, 1412, 1395, 1300, 1285, 1254, 1230, 1206, 1157, 1092, 1057, 1030, 941, 862, 835, 791, 702, 627 cm^{-1}.

HPLC (Method 2): t_R = 5.9 min.

LC-MS (ESI, 70 eV): m/z = 560 $[MH]^+$ (calc. m/z = 559).

7.3.9 Irradiation of *N*-Benzyl-4-(5-(4-fluorophenyl)-2-(methylthio)-1*H*-imidazol-4-yl)pyridin-2-amine

_N_-Benzyl-9-fluoro-2-(methylthio)-1_H_-benzo[_h_]imidazo[4,5-_f_]isoquinolin-5-amine (292)

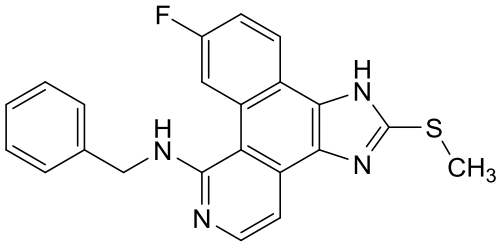

$C_{22}H_{17}FN_4S$ (M_r 388.46)

162 (100 mg, 256 µmol) was dissolved in 40 ml THF. 2 ml of the solution were transferred into a pointed flask and irradiated for 2 min with UV light of 365 nm and 5.4 W power. The procedure was repeated 20 times. All reactive approaches were combined and the solvent was removed under reduced pressure. The crude product was purified by flash chromatography (SiO_2, 30-100 % ethyl acetate/petrol ether) to give **292** as a yellow solid (100 % HPLC purity).

Yield: 24.1 mg (62.1 µmol, 24 %).

^{1}H NMR (300 MHz, DMSO-d_6): δ = 2.81 (s, 3 H, SCH_3), 4.76 (d, ^4J = 4.8 Hz, 2 H, CH_2, Bn), 7.20-7.25 (m, 1 H, ^{ar}C^4H, Bn), 7.31-7.36 (m, 2 H, ^{ar}C$^{3/5}H$, Bn), 7.40 (d, ^3J = 5.2 Hz, 1 H, CH, Pyr), 7.46-7.49 (m, 2 H, ^{ar}C$^{2/6}H$, Bn), 7.54-7.66 (m, 2 H, CH, F-Phe and NH), 8.12 (d, $^3J_{CF}$ = 5.3 Hz, 1 H, CH, Pyr), 8.36-8.54 (m, 1 H, CH, F-Phe), 8.98-9.06 (m, 1 H, CH, F-Phe), 13.40-13.49 (m, 1 H, NH, Imdz) ppm.

^{13}C NMR (75 MHz, DMSO-d_6): δ = 14.5 (SCH$_3$), 45.2 (CH$_2$, Bn), 105.2 (CH, Pyr), 111.3 (CH, F-Phe), 114.5 (d, $^2J_{CF}$ = 22.3 Hz, CH, F-Phe), 123.7 (CH, F-Phe), 126.3 ($^{ar}C^4$H, Bn), 127.3 ($^{ar}C^{2/6}$H, Bn), 128.1 ($^{ar}C^{3/5}$H, Bn), 140.8 ($^{ar}C^1$, Bn), 143.5 (CH, Pyr), 149.5 (C^2, Imdz), 156.3 (C^2, Pyr), 161.0 (CF) ppm.

HPLC (Method 2): t_R = 5.3 min.

LC-MS (ESI, 70 eV): m/z = 389 $[MH]^+$ (calc. m/z = 388).

7.4 Biological Evaluation

7.4.1 Kinase Assays (IC_{50} determination)

In vitro kinase reactions were used to determine the capacity of substrate phosphorylation by distinct kinases. Consequently, the decrease of enzyme activity in the presence of small molecule kinase inhibitors was used as a surrogate parameter for the inhibitory potency which is indicated by the half maximal inhibitory concentration (IC_{50}).

The appropriate reaction-mix contained 2 µl 10 mM inhibitor dilution in DMSO (or pure DMSO), 3 µl kinase diluted in kinase buffer (1x) without ATP, 1.5 µl kinase buffer (10x) with ATP, 0.2 µl γ-^{32}P-ATP (2 µCi per reaction), 5.3 µl H_2O, and 3 µl substrate accounting for a total volume of 15 µl 1.5 ml Eppendorf® Safe-Lock microcentrifuge tubes. After 30 min incubation at 30 °C the reaction was terminated by the addition of 3 µl stopping buffer and subsequent protein denaturation at 99 °C for 5 min. Buffers are given in detail in **Table 29**. Protein separation (SDS-PAGE) and protein staining via anionic Coommassie dye were followed by de-staining in de-staining solution and drying of the polyacrylamide gels on a vacuum gel-dryer. The amount of radioactive ^{32}P was then quantified by Cherenkov counting of the excised bands of phosphorylated protein (Cherenkov counter LSC000IC, Beckman).

Table 29 | Kinase assay buffers.

Buffer	Contents
Kinase buffer (1x) without ATP	25 mM Tris-HCl (pH 7.5), 10 mM $MgCl_2$, 0.1 mM EDTA
Kinase buffer (10x) with ATP	1 mM ATP, 250 mM Tris-HCl (pH 7.5), 100 mM $MgCl_2$, 1 mM EDTA
Stopping buffer	250 mM Tris-HCl (pH 6.8), 25 % (v/v) β-mercaptoethanol, 50 % (v/v) glycerol, 10 % (w/v) SDS, 0.5 % (w/v) bromophenol blue

The applied kinase activities were either recombinant human GST-CK1δ TV1 (approx. 10 ng · reaction^{-1}), recombinant rat CK1δ (FP449, approximately 15 ng · reaction^{-1})[261], or commercially available kinase domain of CK1δ (50 ng · reaction^{-1}, New England Biolabs, Ipswich, USA), and CK1ε (15 ng · reaction^{-1}, Carlsbad, USA), as well as bovine GST-CK1α, human

GST-CK1γ3 TV X6 and commercially available p38α (SignalChem, BIOZOL, Eching, Germany). α-Casein, GST-p53 fragment (aa 1-64), and GST-CK1δ fragment (aa 305-375) have been used as substrates. Residual kinase activity (% in relation to DMSO negative control) has been determined at an inhibitor concentration of 10 µM. The most promising candidates have serially been diluted for IC_{50} determination with concentrations ranging from 10 µM to 5 nM. GraphPad Prism 6 software (GraphPad, San Diego, USA) has been utilized for statistical analysis[262].

These kinase assays have been performed by MARC KRÜGER[248] and CHIARA IANES (current work)[249] in the group of PROF. DR. UWE KNIPPSCHILD at the Department of General and Visceral Surgery, Ulm University Hospital, Germany. The following compounds have been tested:

Table 30 | Test compounds (kinase assays). Sulfoxides are implemented in the appropriate series.

	Kinase	Series	Compounds
10 µM screening	CK1δ, CK1ε	1	**82**, **84**, **85**, **148-155**, **162**, **164**
		2	**102**, **103**, **190-194**
		3	**104**, **204-206**, **208-210**, **212**, **286-290**
		4	**224**, **232**, **291**
		6	**266**, **267**
	CK1α	1	**84**, **85**, **148-155**
		2	**103**, **190**, **191**
		3	**104**, **204**, **206**, **209**, **210**, **212**, **286**
	CK1γ3	1	**84**, **85**, **148-155**
	p38α	1	**84**, **85**, **148-155**
IC_{50} determination	CK1δ, CK1ε	1	**150**, **151**, **164**
		2	**102**, **103**, **190-194**
		3	**104**, **204**, **205**, **208-210**, **287-290**
		4	**224**, **232**, **291**
		6	**266**, **267**

In addition, CK1δ and p38α IC_{50} values have been determined for compounds **191** (series 2), **204** (series 3), **223** (series 4), and **266** (series 6) using a radiometric ^{33}PanQinase® assay[263] by ProQinase GmbH, Freiburg, Germany. The appropriate IC_{50} profiles were received by testing ten concentrations per compound in semi-log steps and triplicate measurement with the highest concentration being $1 \cdot 10^{-4}$ M. Serial dilution of the compounds has been fulfilled from a 10 mM stock solution in DMSO. The final DMSO concentration was 1 % in each reaction-mix.

7.4.2 Kinase Profiling

Kinase profiling has been performed for compound **191** (series 2) against 320 wild-type protein kinases plus $BRAF^{V600E}$ by ProQinase, Freiburg, Germany. Residual kinase activity has been determined at 100 nM in singlicate using an activity-based radiometric ^{33}PanQinase® assay[263]. The final DMSO concentration was 1 % in each reaction-mix.

7.4.3 MTT Viability Assays

Cytotoxic activity of compounds was analyzed using conventional MTT assays: approximately $5 \cdot 10^4$ cells were seeded in 96-well plates and cultivated for 24 h. The cell lines were treated with 10 µM, 15 µM, 20 µM, or 25 µM inhibitor and incubated for 48 h whereupon the procedure included untreated and DMSO-treated cells serving as control. Subsequently, 10 µl MTT solution (5 mg · ml^{-1} MTT in PBS, Sigma Aldrich, Schnelldorf, Germany) were added. After incubation for another 4 h the medium was removed and the plates were shaken on an orbital shaker for 30 min with 100 µl acidic isopropanol (0.04 M HCl in 2-propanol) per well. Dissolved formazan crystals were analyzed spectrophotometrically at 570 nm with control well mean optical density defined as 100 %. Half maximal effective concentration (EC_{50}) values have been determined for **151** and **191** utilizing GraphPad 6 Prism software (GraphPad, San Diego, USA). Cell culture experiments have been performed in triplicate. The used human CK1-dependent cancer cell lines are given in **Table 31**.

MTT assays have been performed by MARC KRÜGER[248] and CHIARA IANES (current work)[249] in the group of PROF. DR. UWE KNIPPSCHILD at the Department of General and Visceral Surgery, Ulm University Hospital, Germany.

Table 31 | Human CK1-dependent cancer cell lines used in MTT assays with their respective origin. The compounds tested on the cell lines are given with their respective series.

Cell line	Origin	Series	Compounds
Colo357	Human lymph node metastasis pancreatic adeno-carcinoma cell line[264]	2	**102**, **103**, **190-194**
		3	**104**, **204-206**, **208-210**, **212**, **286-290**
		4	**224**, **232**, **291**
		6	**266**, **267**
HT-29	Human colorectal adenocarcinoma epithelial cell line[265]	1	**82**, **84**, **85**, **148-155**, **162**, **164**
MiaPaca-2	Human pancreatic carcinoma epithelial cell line[266]	2	**190**
		4	**224**, **232**, **291**
		6	**266**, **267**
Panc-1	Human pancreatic epithelioid carcinoma cell line[267]	2	**190**
		4	**224**, **232**, **291**
		6	**266**, **267**
Panc89	Human pancreatic adenocarcinoma cell line[268]	2	**102**, **103**, **190-194**
		3	**104**, **204-206**, **208-210**, **212**, **286-290**

7.5 X-ray Crystallography

Co-crystallization of **191** with inactive, non-phosphorylated wild-type p38α MAPK was performed by the group of PROF. DR. DANIEL RAUH (Institute of Chemical Biology, Dortmund University of Technology, Germany) following established protocols for protein expression and purification[269], and an adapted procedure for crystallization[270]. The protein-ligand mixture consisting of 20 µl 10 mg · ml^{-1} wild-type p38α and 0.2 µl 50 mM inhibitor stock solution in DMSO were incubated on ice for 60 min and centrifuged at 13,000 rpm for 10 min in order to remove excess ligand. Crystals were cultivated using the hanging drop vapor diffusion method in 24-well EasyXtal Tools (QIAGEN, Hilden, Germany) and by adding 0.5 µl reservoir solution (100 mM MES buffer pH 5.6-6.2, 20-30 % PEG4000, and 50 mM BOG) to 1.5 µl protein-ligand mixture. PEG400-protected crystals were flash frozen in liquid nitrogen. Diffraction data of protein-ligand complexes were determined at the PX II beamline of the Swiss Light Source (Paul Scherrer Institute, Villingen, Switzerland) using wavelengths close to 1 Å. The obtained datasets were integrated and scaled using XDS and XSCALE[271], complex structures were interpreted by molecular replacement based on published p38α templates (PDB code 4LDI) utilizing PHASER[272], and molecules in the asymmetric unit were modified manually with COOT[273]. Structures were refined by the use of REFMAC[274] and validated performing RAMACHANDRAN plot analysis using RAMPAGE[275]. Ligand topology files were generated utilizing the Dundee PRODRG server[276]. Data collection, structure refinement statistics, and RAMACHANDRAN plot results for the obtained crystal structure of wild-type p38α MAPK in complex with **191** are given in **Table 32**.

Co-crystallization of **224** and **266** with CK1δ were performed by the group of PROF. DR. ULRICH BAUMANN (Department for Chemistry, University of Cologne, Germany) following similar procedures as described above, though by utilizing the sitting drop methodology instead (unpublished data). The protein-ligand mixture consisted of 30 µl 10 mg · ml^{-1} CK1δ and 1 µl 10 µM inhibitor stock solution in DMSO. Precipitant solutions contained 0.1 M HEPES buffer pH 7.0 M, 0.7 M sodium dihydrogen phosphate, and 0.7 M potassium dihydrogen phosphate for **224** and 20 % PEG1000, 200 mM lithium sulfate, and 100 mM phosphate citrate buffer pH 4.2 in the case of **266**. Cryoprotection was achieved using saturated sucrose solution (**224**) or PEG1000 (**266**). Diffraction data of protein-ligand complexes including **224** were determined at the ID23-1 beamline of the European Synchrotron Radiation Facility (Grenoble, France) while measurement of crystals containing **266** was performed at Xo6DA (PXIII) beamline of the Swiss Light Source (Paul Scherrer Institute, Villingen, Switzerland). However, the structures represent preliminary results and require further refinement. Crystallization data is given in **Table 33**.

Table 32 | Crystallographic statistics of wild-type p38α in complex with 191. X-ray crystallography has been performed by the group of PROF. DR. DANIEL RAUH. Values in parenthesis refer to the highest resolution shell.

		191/p38α
Wavelength (Å)		1.0000
Temperature (K)		90
Data collection		
Space group		$P2_12_12_1$
Unit cell	a, b, c (Å)	66.50, 69.39, 74.14
	α, β, γ (°)	90, 90, 90
Resolution (Å)		50.0-1.90 (1.95-1.90)
R_{meas} (%)		9.0 (82.0)
$\langle I/\sigma(I) \rangle$		22.69 (3.38)
Completeness (%)		100 (100)
Redundancy		0.98 (1.05)
Refinement		
Resolution (Å)		48.01-1.90 (1.949-1.900)
No. reflections		26280 (1891)
R_{work}/R_{free}		0.19/0.24
No. atoms	Total	2865
	Protein	2667
	Ligand/Ion	95
B-factors	Protein	27.26
	Ligand/Ion	29.04
	Water	26.74
RMSD	Bond length (Å)	0.019
	Bond angles (°)	1.966
RAMACHANDRAN plot		
Res. in favored regions		315
Res. in allowed regions		6
Res. in outlier regions		0

Table 33 | Crystallographic statistics of CK1δ in complex with 224 and 266. X-ray crystallography has been performed by the group of PROF. DR. ULRICH BAUMANN. Values in parenthesis refer to the highest resolution shell.

		224/CK1δ	266/CK1δ
Wavelength (Å)		0.972420	0.999990
Space group		C 1 2 1	P 61
Unit cell	a, b, c (Å)	195.485, 126.653, 152.281	176.282, 176.282, 111.25
	α, β, γ (°)	90, 113.272, 90	90, 90, 120
Reflections	Total	192836 (30989)	1316615 (193931)
	Unique	55965 (5445)	64064 (6304)
Resolution (Å)		54.12-3.201 (3.315-3.201)	47.04-2.549 (2.64-2.549)
R_{merge} (%)		9.9 (70.6)	-
R_{meas} (%)		11.7 (77.2)	20.7 (158.7)
$\langle I/\sigma(I) \rangle$		11.92 (1.81)	17.4 (2.29)
Completeness (%)		99 (95)	100 (100)
Redundancy		3.44 (3.4)	20.2 (30.7)
$CC_{1/2}$ (%)		99.7 (76.6)	99.8 (74)
Reflections used in refinement		55952 (5445)	64048 (6304)
Reflections used for R_{free}		1995 (194)	1501 (142)
R_{work}/R_{free}		0.2092 (0.3193)/0.2463 (0.3458)	0.2118 (0.2892)/0.2273 (0.2690)
No. atoms	Non-hydrogen	13878	9379
	Macromolecules	13653	9180
	Ligands	225	199
	Protein Residues	1703	1133
B-factors	Average	95.52	55.84
	Macromolecules	95.51	55.63
	Ligands	96.15	65.64
	Wilson	85.21	45.00
RMSD	Bond length (Å)	0.004	0.002
	Bond angles (°)	0.66	0.55
Clashscore		12.59	1.57
No. of TLS groups		6	4
RAMACHANDRAN favored (%)		92	96
RAMACHANDRAN allowed (%)		6.5	3.9
RAMACHANDRAN outlier (%)		1.5	0.27
Rotamer outliers (%)		1.3	0.82

8 References

1. Adams, J. A. Kinetic and Catalytic Mechanisms of Protein Kinases. *Chem. Rev.* **101,** 2271–2290 (2001).
2. Fang, Z., Grütter, C. & Rauh, D. Strategies for the Selective Regulation of Kinases with Allosteric Modulators: Exploiting Exclusive Structural Features. *ACS Chem. Biol.* **8,** 58–70 (2013).
3. Schwartz, P. A. & Murray, B. W. Protein kinase biochemistry and drug discovery. *Bioorg. Chem.* **39,** 192–210 (2011).
4. Cheng, H.-C., Qi, R. Z., Paudel, H. & Zhu, H.-J. Regulation and Function of Protein Kinases and Phosphatases. *Enzyme Res.* **2011,** 1–3 (2011).
5. Manning, G., Whyte, D. B., Martinez, R., Hunter, T. & Sudarsanam, S. The Protein Kinase Complement of the Human Genome. *Science* **298,** 1912–1934 (2002).
6. Rask-Andersen, M., Zhang, J., Fabbro, D. & Schiöth, H. B. Advances in kinase targeting: current clinical use and clinical trials. *Trends Pharmacol. Sci.* **35,** 604–620 (2014).
7. Wu, P., Nielsen, T. E. & Clausen, M. H. FDA-approved small-molecule kinase inhibitors. *Trends Pharmacol. Sci.* **36,** 422–439 (2015).
8. Venerando, A., Ruzzene, M. & Pinna, L. A. Casein kinase: the triple meaning of a misnomer. *Biochem. J.* **460,** 141–156 (2014).
9. Knippschild, U. *et al.* The CK1 Family: Contribution to Cellular Stress Response and Its Role in Carcinogenesis. *Front. Oncol.* **4**: 96 (2014).
10. Zhai, L. *et al.* Casein Kinase Iγ Subfamily. *J. Biol. Chem.* **21,** 12717–12724 (1995).
11. Gross, S. D. & Anderson, R. A. Casein Kinase I: Spatial Organization and Positioning of a Multifunctional Protein Kinase Family. *Cell. Signal.* **10,** 699–711 (1998).
12. Knippschild, U. *et al.* The Role of the Casein Kinase 1 (CK1) Family in Different Signaling Pathways Linked to Cancer Development. *Onkologie* **28,** 508–514 (2005).
13. Knippschild, U. *et al.* The casein kinase 1 family: participation in multiple cellular processes in eukaryotes. *Cell. Signal.* **17,** 675–689 (2005).
14. Kusuda, J., Hidari, N., Hirai, M. & Hashimoto, K. Sequence Analysis of the cDNA for the Human Casein Kinase I δ (CSNK1D) Gene and Its Chromosomal Localization. *Genomics* **32,** 140–143 (1996).
15. Cheong, J. K. & Virshup, D. M. Casein kinase 1: Complexity in the family. *Int. J. Biochem. Cell Biol.* **43,** 465–469 (2011).

16. Sievers, F. *et al.* Fast, scalable generation of high-quality protein multiple sequence alignments using Clustal Omega. *Mol. Syst. Biol.* **7**: 539 (2011).

17. Longenecker, K. L., Roach, P. J. & Hurley, T. D. Three-dimensional Structure of Mammalian Casein Kinase I: Molecular Basis for Phosphate Recognition. *J. Mol. Biol.* **257,** 618–631 (1996).

18. Xu, R. M., Carmel, G., Sweet, R. M., Kuret, J. & Cheng, X. Crystal structure of casein kinase-1, a phosphate-directed protein kinase. *EMBO J.* **14,** 1015–1023 (1995).

19. Graves, P. R., Haas, D. W., Hagedorn, C. H., DePaoli-Roach, A. A. & Roach, P. J. Molecular Cloning, Expression, and Characterization of a 49-Kilodalton Casein Kinase I Isoform from Rat Testis. *J. Biol. Chem.* **268,** 6394–6401 (1993).

20. Roof, D. M., Meluh, P. B. & Rose, M. D. Kinesin-related Proteins Required for Assembly of the Mitotic Spindle. *J. Cell. Biol.* **118,** 95–108 (1992).

21. Longenecker, K. L., Roach, P. J. & Hurley, T. D. Crystallographic studies of casein kinase I δ: toward a structural understanding of auto-inhibition. *Acta Cryst.* **D54,** 473–475 (1998).

22. Huang, H. *et al.* Structure-Based Design of Potent and Selective CK1γ Inhibitors. *ACS Med. Chem. Lett.* **3,** 1059–1064 (2012).

23. Traxler, P. & Furet, P. Strategies toward the Design of Novel and Selective Protein Tyrosine Kinase Inhibitors. *Pharmacol. Ther.* **82,** 195–206 (1999).

24. Agostinis, P. *et al.* A synthetic peptide substrate specific for casein kinase-1. *FEBS Lett.* **259,** 75–78 (1989).

25. Flotow, H. *et al.* Phosphate Groups as Substrate Determinants for Casein Kinase I Action. *J. Biol. Chem.* **265,** 14264–14269 (1990).

26. Flotow, H. & Roach, P. J. Role of Acidic Residues as Substrate Determinants for Casein Kinase I. *J. Biol. Chem.* **266,** 3724–3727 (1991).

27. Meggio, F., Perich, J. W., Reynolds, E. C. & Pinna, L. A. A synthetic β-casein phosphopeptide and analogues as model substrates for casein kinase-1, a ubiquitous, phosphate directed protein kinase. *FEBS Lett.* **283,** 303–306 (1991).

28. Marin, O. *et al.* A noncanonical sequence phosphorylated by casein kinase 1 in β-catenin may play a role in casein kinase 1 targeting of important signaling proteins. *Proc. Natl. Acad. Sci. USA* **100,** 10193–10200 (2011).

29. Kawakami, F., Suzuki, K. & Ohtsuki, K. A Novel Consensus Phosphorylation Motif in Sulfatide- and Cholesterol-3-sulfate-Binding Protein Substrates for CK1 in Vitro. *Biol. Pharm. Bull.* **31,** 193–200 (2008).

30. Pulgar, V. *et al.* Optimal sequences for non-phosphate-directed phoshorylation by protein kinase CK1 (casein kinase-1) - a re-evaluation. *Eur. J. Biochem.* **260,** 520–526 (1999).

31. Wolff, S. *et al.* Interaction of casein kinase 1 delta (CK1δ) with the light chain LC2 of microtubule associated protein 1A (MAP1A). *Biochim. Biophys. Acta.* **1745,** 196–206 (2005).

32. Okamura, H. *et al.* A Conserved Docking Motif for CK1 Binding Controls the Nuclear Localization of NFAT1. *Mol. Cell. Biol.* **24,** 4184–4195 (2004).

33. Zyss, D., Ebrahimi, H. & Gergely, F. Casein kinase I delta controls centrosome positioning during T cell activation. *J. Cell Biol.* **195,** 781–797 (2011).

34. Bustos, V. H. *et al.* The first armadillo repeat is involved in the recognition and regulation of β-catenin phosphorylation by protein kinase CK1. *Proc. Natl. Acad. Sci. USA* **103,** 19725–19730 (2006).

35. Dahlberg, C. L., Nguyen, E. Z., Goodlett, D., Kimelman, D. & Xu, W. Interactions between Casein Kinase Iε (CKIε) and Two Substrates from Disparate Signaling Pathways Reveal Mechanisms for Substrate-Kinase Specificity. *PLoS ONE* **4,** e4766 (2009).

36. Venerando, A. *et al.* Isoform specific phosphorylation of p53 by protein kinase CK1. *Cell. Mol. Life Sci.* **67,** 1105–1118 (2010).

37. Knippschild, U. *et al.* p53 is phosphorylated in vitro and in vivo by the delta and epsilon isoforms of casein kinase 1 and enhances the level of casein kinase 1 delta in response to topoisomerase-directed drugs. *Oncogene* **15,** 1727–1736 (1997).

38. Winter, M. *et al.* Protein Kinase CK1δ Phosphorylates Key Sites in the Acidic Domain of Murine Double-Minute Clone 2 Protein (MDM2) That Regulate p53 Turnover. *Biochemistry* **43,** 16356–16364 (2004).

39. Kalousi, A. *et al.* Casein kinase 1 regulates human hypoxia-inducible factor HIF-1. *J. Cell Sci.* **123,** 2976–2986 (2010).

40. Grozav, A. G. *et al.* Casein kinase I δ/ε phosphorylates topoisomerase II at serine-1106 and modulates DNA cleavage activity. *Nucleic Acids Res.* **37,** 382–392 (2008).

41. Sugiyama, Y. *et al.* The DNA-binding activity of mouse DNA methyltransferase 1 is regulated by phosphorylation with casein kinase 1δ/ε. *Biochem. J.* **427,** 489–497 (2010).

42. Chen, H. *et al.* DNA Damage Regulates UHRF1 Stability via the SCF β-TrCP E3 Ligase. *Mol. Cell. Biol.* **33,** 1139–1148 (2013).

43. Gao, Z.-H., Metherall, J. & Virshup, D. M. Identification of Casein Kinase I Substrates by in Vitro Expression Cloning Screening. *Biochem. Biophys. Res. Com.* **268,** 562–566 (2000).

44. Regad, T., Roth, M., Bredenkamp, N., Illing, N. & Papalopulu, N. The neural progenitor-specifying activity of FoxG1 is antagonistically regulated by CKI and FGF. *Nat. Cell Biol.* **9,** 531–540 (2007).

45. Brookheart, R. T., Lee, C. Y. S. & Espenshade, P. J. Casein Kinase 1 Regulates Sterol Regulatory Element-binding Protein (SREBP) to Control Sterol Homeostasis. *J. Biol. Chem.* **289,** 2725–2735 (2014).

46. Ho, Y., Mason, S., Kobayashi, R., Hoekstra, M. & Andrews, B. Role of the casein kinase I isoform, Hrr25, and the cell cycle-regulatory transcription factor, SBF, in the transcriptional response to DNA damage in Saccharomyces cerevisiae. *Proc. Natl. Acad. Sci. USA* **94,** 581–586 (1997).

47. Zemp, I. *et al.* CK1δ and CK1ε are components of human 40S subunit precursors required for cytoplasmic 40S maturation. *J. Cell Sci.* **127,** 1242–1253 (2014).

48. Ghalei, H. *et al.* Hrr25/CK1δ-directed release of Ltv1 from pre-40S ribosomes is necessary for ribosome assembly and cell growth. *J. Cell Biol.* **208,** 745–759 (2015).

49. Biswas, A. *et al.* Opposing Action of Casein Kinase 1 and Calcineurin in Nucleo-cytoplasmic Shuttling of Mammalian Translation Initiation Factor eIF6. *J. Biol. Chem.* **286,** 3129–3138 (2011).

50. Penas, C. *et al.* Casein Kinase 1δ-dependent Wee1 Protein Degradation. *J. Biol. Chem.* **289,** 18893–18903 (2014).

51. Ishiguro, T., Tanaka, K., Sakuno, T. & Watanabe, Y. Shugoshin–PP2A counteracts casein-kinase-1-dependent cleavage of Rec8 by separase. *Nat. Cell Biol.* **12,** 500–506 (2010).

52. Isoda, M. *et al.* Dynamic Regulation of Emi2 by Emi2-Bound Cdk1/Plk1/CK1 and PP2A-B56 in Meiotic Arrest of Xenopus Eggs. *Dev. Cell* **21,** 506–519 (2011).

53. Behrend, L. *et al.* Interaction of casein kinase 1 delta (CK1δ) with post-Golgi structures, microtubules and the spindle apparatus. *Eur. J. Cell Biol.* **79,** 240–251 (2000).

54. Behrend, L. *et al.* IC261, a specific inhibitor of the protein kinases casein kinases 1-delta and -epsilon, triggers the mitotic checkpoint and induces p53-dependent postmitotic effects. *Oncogene* **19,** 5303–5313 (2000).

55. Li, G., Yin, H. & Kuret, J. Casein Kinase 1 Delta Phosphorylates Tau and Disrupts Its Binding to Microtubules. *J. Biol. Chem.* **279,** 15938–15945 (2004).

56. Wolff, S., García-Reyes, B., Henne-Bruns, D., Bischof, J. & Knippschild, U. Protein kinase CK1 interacts with and phosphorylates RanBPM in vitro. *J. Mol. Biochem.* **4,** 11–19 (2015).

57. Tillement, V. *et al.* Phosphorylation of RhoB by CK1 impedes actin stress fiber organization and epidermal growth factor receptor stabilization. *Exp. Cell Res.* **314,** 2811–2821 (2008).

58. Cooper, C. D. Casein Kinase 1 Regulates Connexin-43 Gap Junction Assembly. *J. Biol. Chem.* **277,** 44962–44968 (2002).

59. Johnson, A. E., Chen, J.-S. & Gould, K. L. CK1 is required for a mitotic checkpoint that delays cytokinesis. *Curr. Biol.* **23,** 1920–1926 (2013).

60. Zemlickova, E., Johannes, F.-J., Aitken, A. & Dubois, T. Association of CPI-17 with protein kinase C and casein kinase I. *Biochem. Biophys. Res. Commun.* **316,** 39–47 (2004).

61. Wolff, S. *et al.* Casein kinase 1 delta (CK1δ) interacts with the SNARE associated protein snapin. *FEBS Lett.* **580,** 6477–6484 (2006).

62. Von Blume, J. *et al.* Phosphorylation at Ser244 by CK1 determines nuclear localization and substrate targeting of PKD2. *EMBO J.* **26,** 4619–4633 (2007).

63. Yu, S. & Roth, M. G. Casein Kinase I Regulates Membrane Binding by ARF GAP1. *Mol. Biol. Cell* **13,** 2559–2570 (2002).

64. Walter, J. *et al.* Phosphorylation Regulates Intracellular Trafficking of β-Secretase. *J. Biol. Chem.* **276,** 14634–14641 (2001).

65. Walter, J., Grünberg, J., Schindzielorz, A. & Haass, C. Proteolytic Fragments of the Alzheimer's Disease Associated Presenilins-1 and -2 Are Phosphorylated in Vivo by Distinct Cellular Mechanisms. *Biochem. J.* **37,** 5961–5967 (1998).

66. Sharma, P., Sharma, M., Amin, N. D., Albers, R. W. & Pant, H. C. Regulation of cyclin-dependent kinase 5 catalytic activity by phosphorylation. *Proc. Natl. Acad. Sci. USA* **96,** 1156–1160 (1999).

67. Okochi, M. *et al.* Constitutive Phosphorylation of the Parkinson's Disease Associated α-Synuclein. *J. Biol. Chem.* **275,** 390–397 (2000).

68. Yamamoto, A. *et al.* Parkin Phosphorylation and Modulation of Its E3 Ubiquitin Ligase Activity. *J. Biol. Chem.* **280,** 3390–3399 (2005).

69. Shanware, N. P., Trinh, A. T., Williams, L. M. & Tibbetts, R. S. Coregulated Ataxia Telangiectasia-mutated and Casein Kinase Sites Modulate cAMP-response Element-binding Protein-Coactivator Interactions in Response to DNA Damage. *J. Biol. Chem.* **282,** 6283–6291 (2006).

70. Nonaka, T. *et al.* Phosphorylation of TAR DNA-binding Protein of 43 kDa (TDP-43) by Truncated Casein Kinase 1δ Triggers Mislocalization and Accumulation of TDP-43. *J. Biol. Chem.* **291,** 5473–5483 (2016).

71. Shanware, N. P. *et al.* Casein Kinase 1-dependent Phosphorylation of Familial Advanced Sleep Phase Syndrome-associated Residues Controls PERIOD 2 Stability. *J. Biol. Chem.* **286,** 12766–12774 (2011).

72. Miyazaki, K. *et al.* Phosphorylation of clock protein PER1 regulates its circadian degradation in normal human fibroblasts. *Biochem. J.* **380,** 95–103 (2004).

73. Vielhaber, E. L., Eide, E. J., Rivers, A., Gao, Z.-H. & Virshup, D. M. Nuclear Entry of the Circadian Regulator mPER1 Is Controlled by Mammalian Casein Kinase I ε. *Mol. Cell. Biol.* **20,** 4888–4899 (2000).

74. Etchegaray, J.-P. *et al.* Casein Kinase 1 Delta Regulates the Pace of the Mammalian Circadian Clock. *Mol. Cell. Biol.* **29,** 3853–3866 (2009).

75. Eide, E. J., Vielhaber, E. L., Hinz, W. A. & Virshup, D. M. The Circadian Regulatory Proteins BMAL1 and Cryptochromes Are Substrates of Casein Kinase Iε. *J. Biol. Chem.* **277,** 17248–17254 (2002).

76. Li, S., Chen, X.-W., Yu, L., Saltiel, A. R. & Lin, J. D. Circadian Metabolic Regulation through Crosstalk between Casein Kinase 1δ and Transcriptional Coactivator PGC-1α. *Mol. Endocrinol.* **25,** 2084–2093 (2011).

77. He, Q., Cha, J., Lee, H.-C., Yang, Y. & Liu, Y. CKI and CKII mediate the FREQUENCY-dependent phosphorylation of the WHITE COLLAR complex to close the Neurospora circadian negative feedback loop. *Genes Dev.* **20,** 2552–2565 (2006).

78. Huang, G. *et al.* Protein kinase A and casein kinases mediate sequential phosphorylation events in the circadian negative feedback loop. *Genes Dev.* **21,** 3283–3295 (2007).

79. Desagher, S. *et al.* Phosphorylation of Bid by Casein Kinases I and II Regulates Its Cleavage by Caspase 8. *Mol. Cell.* **8,** 601–611 (2001).

80. Amit, S. *et al.* Axin-mediated CKI phosphorylation of β-catenin at Ser 45: a molecular switch for the Wnt pathway. *Genes Dev.* **16,** 1066–1076 (2002).

81. Gao, Z.-H., Seeling, J. M., Hill, V., Yochum, A. & Virshup, D. M. Casein kinase I phosphorylates and destabilizes the β-catenin degradation complex. *Proc. Natl. Acad. Sci. USA* **99,** 1182–1187 (2002).

82. Teran, E., Branscomb, A. D. & Seeling, J. M. Dpr Acts as a Molecular Switch, Inhibiting Wnt Signaling when Unphosphorylated, but Promoting Wnt Signaling when Phosphorylated by Casein Kinase Iδ/ε. *PLoS ONE* **4,** e5522 (2009).

83. Price, M. A. & Kalderon, D. Proteolysis of the Hedgehog Signaling Effector Cubitus interruptus Requires Phosphorylation by Glycogen Synthase Kinase 3 and Casein Kinase 1. *Cell* **108,** 823–835 (2002).

84. Zhao, B., Li, L., Tumaneng, K., Wang, C.-Y. & Guan, K.-L. A coordinated phosphorylation by Lats and CK1 regulates YAP stability through SCFβ-TRCP. *Genes Dev.* **24,** 72–85 (2010).

85. Yim, D. G. R., Ghosh, S., Guy, G. R. & Virshup, D. M. Casein kinase 1 regulates Sprouty2 in FGF–ERK signaling. *Oncogene* **34,** 474–484 (2014).

86. Sopko, R. *et al.* Phosphorylation of the tumor suppressor Fat is regulated by its ligand Dachsous, and the kinase, Discs Overgrown. *Curr. Biol.* **19,** 1112–1117 (2009).

87. Liu, J. *et al.* SCF β-TRCP-mediated degradation of NEDD4 inhibits tumorigenesis through modulating the PTEN/Akt signaling pathway. *Oncotarget* **5,** 1026–1037 (2014).

88. Zhong, J. *et al.* SCFβ-TRCP targets MTSS1 for ubiquitination-mediated destruction to regulate cancer cell proliferation and migration. *Oncotarget* **4,** 2339–2353 (2013).

89. Garzia, L. *et al.* Phosphorylation of nm23-H1 by CKI induces its complex formation with h-prune and promotes cell motility. *Oncogene* **27,** 1853–1864 (2007).

90. Smal, C. *et al.* Casein kinase 1δ activates human recombinant deoxycytidine kinase by Ser-74 phosphorylation, but is not involved in the in vivo regulation of its activity. *Arch. Biochem. Biophys.* **502,** 44–52 (2010).

91. Hirner, H. *et al.* Impaired CK1 Delta Activity Attenuates SV40-Induced Cellular Transformation In Vitro and Mouse Mammary Carcinogenesis In Vivo. *PLoS ONE* **7,** e29709 (2012).

92. Chaurushiya, M. S. *et al.* Viral E3 ubiquitin ligase-mediated degradation of a cellular E3: viral mimicry of a cellular phosphorylation mark targets the RNF8 FHA domain. *Mol. Cell.* **46,** 79–90 (2012).

93. Alvisi, G. *et al.* Multiple phosphorylation sites at the C-terminus regulate nuclear import of HCMV DNA polymerase processivity factor ppUL44. *Virology* **417,** 259–267 (2011).

94. Giamas, G. *et al.* CK1 modulates the transcriptional activity of ERα via AIB1 in an estrogen-dependent manner and regulates ERα-AIB1 interactions. *Nucleic Acids Res.* **37,** 3110–3123 (2009).

95. Xu, P. *et al.* Gene expression levels of Casein kinase 1 (CK1) isoforms are correlated to adiponectin levels in adipose tissue of morbid obese patients and site-specific phosphorylation mediated by CK1 influences multimerization of adiponectin. *Mol. Cell. Endocrinol.* **406,** 87–101 (2015).

96. Watts, A. D. *et al.* A casein kinase I motif present in the cytoplasmic domain of members of the tumour necrosis factor ligand family is implicated in 'reverse signalling'. *EMBO J.* **18,** 2119–2126 (1999).

97. Zhou, M. *et al.* Forebrain overexpression of CK1δ leads to down-regulation of dopamine receptors and altered locomotor activity reminiscent of ADHD. *Proc. Natl. Acad. Sci. USA* **107,** 4401–4406 (2010).

98. Greengard, P. The Neurobiology of Slow Synaptic Transmission. *Science* **294,** 1024–1030 (2001).

99. Tuazon P. T. & Traugh J. A. Casein kinase I and II--multipotential serine protein kinases: structure, function, and regulation. *Adv. Second Messenger Phosphoprotein Res.* **23,** 123–164 (1991).

100. Löhler, J. *et al.* Immunohistochemical Characterisation of Cell-Type Specific Expression of CK1δ in Various Tissues of Young Adult BALB/c Mice. *PLoS ONE* **4,** e4174 (2009).

101. Elias, L., Li, A. P. & Longmire, J. Cyclic Adenosine 3':5'-Monophosphate-dependent and -independent Protein Kinase in Acute Myeloblastic Leukemia. *Cancer Res.* **41,** 2182–2188 (1981).

102. Cobb, M. H. & Rosen, O. M. Description of a Protein Kinase Derived from Insulin-treated 3T3-L1 Cells That Catalyzes the Phosphorylation of Ribosomal Protein S6 and Casein. *J. Biol. Chem.* **258,** 12472–12481 (1983).

103. Milne, D. M., Looby, P. & Meek, D. W. Catalytic Activity of Protein Kinase CK1δ (Casein Kinase 1δ) Is Essential for Its Normal Subcellular Localization. *Exp. Cell Res.* **263,** 43–54 (2001).

104. Good, M. C., Zalatan, J. G. & Lim, W. A. Scaffold Proteins: Hubs for Controlling the Flow of Cellular Information. *Science* **332,** 680–686 (2011).

105. Sillibourne, J. E., Milne, D. M., Takahashi, M., Ono, Y. & Meek, D. W. Centrosomal Anchoring of the Protein Kinase CK1δ Mediated by Attachment to the Large, Coiled-coil Scaffolding Protein CG-NAP/AKAP450. *J. Mol. Biol.* **322,** 785–797 (2002).

106. Greer, Y. E. & Rubin, J. S. Casein kinase 1 delta functions at the centrosome to mediate Wnt-3a–dependent neurite outgrowth. *J. Cell. Biol.* **192,** 993–1004 (2011).

107. Cruciat, C.-M. *et al.* RNA Helicase DDX3 Is a Regulatory Subunit of Casein Kinase 1 in Wnt-β-Catenin Signaling. *Science* **339,** 1436–1441 (2013).

108. Yin, H., Laguna, K. A., Li, G. & Kuret, J. Dysbindin Structural Homologue CK1BP Is an Isoform-Selective Binding Partner of Human Casein Kinase-1. *Biochemistry* **45,** 5297–5308 (2006).

109. Graves, P. R. & Roach, P. J. Role of COOH-terminal Phosphorylation in the Regulation of Casein Kinase Iδ. *J. Biol. Chem.* **270,** 21689–21694 (1995).

110. Giamas, G. *et al.* Phosphorylation of CK1δ: Identification of Ser 370 as the major phosphorylation site targeted by PKA in vitro and in vivo. *Biochem. J.* **406,** 389–398 (2007).

111. Meng, Z. *et al.* CK1δ kinase activity is modulated by protein kinase C α (PKCα)-mediated site-specific phosphorylation. *Amino Acids* **48,** 1185–1197 (2016).

112. Bischof, J. *et al.* CK1δ Kinase Activity Is Modulated by Chk1-Mediated Phosphorylation. *PLoS ONE* **8,** e68803 (2013).

113. Ianes, C. *et al.* CK1δ activity is modulated by CDK2/E- and CDK5/p35-mediated phosphorylation. *Amino Acids* **48,** 579–592 (2016).

114. Nygren, P. J. & Scott, J. D. Therapeutic strategies for anchored kinases and phosphatases: Exploiting short linear motifs and intrinsic disorder. *Front. Pharmacol.* **6**: 158 (2015).

115. Marin, O., Meggio, F., Sarno, S., Andretta, M. & Pinna, L. A. Phosphorylation of synthetic fragments of inhibitor-2 of protein phosphatase-1 by casein kinase-1 and -2. Evidence that phoshorylated residues are not strictly required for efficient targeting by casein kinase-1. *Eur. J. Biochem.* **223,** 647–653 (1994).

116. Cegielska, A., Fish Gietzen, K., Rivers, A. & Virshup, D. M. Autoinhibition of Casein Kinase I ε (CKIε) Is Relieved by Protein Phosphatases and Limited Proteolysis. *J. Biol. Chem.* **273,** 1357–1364 (1998).

117. Penas, C. *et al.* Casein Kinase 1δ Is an APC/CCdh1 Substrate that Regulates Cerebellar Granule Cell Neurogenesis. *Cell Rep.* **11,** 249–260 (2015).

118. Huart, A.-S., MacLaine, N. J., Meek, D. W. & Hupp, T. R. CK1α Plays a Central Role in Mediating MDM2 Control of p53 and E2F-1 Protein Stability. *J. Biol. Chem.* **284,** 32384–32394 (2009).

119. Salado, I. G. *et al.* Protein Kinase CK-1 Inhibitors As New Potential Drugs for Amyotrophic Lateral Sclerosis. *J. Med. Chem.* **57,** 2755–2772 (2014).

120. Stöter, M. *et al.* Inhibition of casein kinase I delta alters mitotic spindle formation and induces apoptosis in trophoblast cells. *Oncogene* **24,** 7964–7975 (2005).

121. Murakami, A., Kimura, K. & Nakano, A. The Inactive Form of a Yeast Casein Kinase I Suppresses the Secretory Defect of the sec12 Mutant. Implcation of Negative Regulation by the

Hrr25 Kinase in the Vesicle Budding from the endoplasmic Reticulum. *J. Biol. Chem.* **274,** 3804–3810 (1999).

122. Greer, Y. E. *et al.* Casein kinase 1δ functions at the centrosome and Golgi to promote ciliogenesis. *Mol. Biol. Cell* **25,** 1629–1640 (2014).

123. Lee, K. H. *et al.* Identification of a novel Wnt5a-CK1ε-Dvl2-Plk1-mediated primary cilia disassembly pathway. *EMBO J.* **31,** 3104–3117 (2012).

124. Schrøder, J. M. *et al.* EB1 and EB3 promote cilia biogenesis by several centrosome-related mechanisms. *J. Cell Sci.* **124,** 2539–2551 (2011).

125. Ghoshal, N. *et al.* A New Molecular Link between the Fibrillar and Granulovacuolar Lesions of Alzheimer's Disease. *Am. J. Pathol.* **155,** 1163–1172 (1999).

126. Yasojima, K., Kuret, J., DeMaggio, A. J., McGeer, E. & McGeer, P. L. Casein kinase 1 delta mRNA is upregulated in Alzheimer disease brain. *Brain Res.* **865,** 116–120 (2000).

127. Flajolet, M. *et al.* Regulation of Alzheimer's disease amyloid-β formation by casein kinase I. *Proc. Natl. Acad. Sci. USA* **104,** 4159–4164 (2007).

128. Chauhan, A., Chauhan, V. P. S., Murakami, N., Brockerhoff, H. & Wisniewski, H. M. Amyloid β-protein stimulates casein kinase I and casein kinase II activities. *Brain Res.* **629,** 47–52 (1993).

129. Kelleher, F. C., Rao, A. & Maguire, A. Circadian molecular clocks and cancer. *Cancer Lett.* **342,** 9–18 (2014).

130. Yu, W., Nomura, M. & Ikeda, M. Interactivating Feedback Loops within the Mammalian Clock: BMAL1 Is Negatively Autoregulated and Upregulated by CRY1, CRY2, and PER2. *Biochem. Biophys. Res. Commun.* **290,** 933–941 (2002).

131. Liu, C., Li, S., Liu, T., Borjigin, J. & Lin, J. D. Transcriptional coactivator PGC-1α integrates the mammalian clock and energy metabolism. *Nature* **447,** 477–481 (2007).

132. Gery, S. *et al.* The Circadian Gene Per1 Plays an Important Role in Cell Growth and DNA Damage Control in Human Cancer Cells. *Mol. Cell* **22,** 375–382 (2006).

133. Mullenders, J., Fabius, A. W. M., Madiredjo, M., Bernards, R. & Beijersbergen, R. L. A Large Scale shRNA Barcode Screen Identifies the Circadian Clock Component ARNTL as Putative Regulator of the p53 Tumor Suppressor Pathway. *PLoS ONE* **4,** e4798 (2009).

134. Fu, L., Pelicano, H., Liu, J., Huang, P. & Lee, C. C. The Circadian Gene Period2 Plays an Important Role in Tumor Suppression and DNA-Damage Response In Vivo. *Cell* **111,** 41–50 (2002).

135. Fu, L. & Lee, C. C. The Circadian Clock: Pacemaker and Tumour Suppressor. *Nat. Rev. Cancer* **3,** 350–361 (2003).

136. Lee, H.-m. *et al.* The period of the circadian oscillator is primarily determined by the balance between casein kinase 1 and protein phosphatase 1. *Proc. Natl. Acad. Sci. USA* **108,** 16451–16456 (2011).

137. Smadja Storz, S. *et al.* Casein Kinase 1δ Activity: A Key Element in the Zebrafish Circadian Timing System. *PLoS ONE* **8,** e54189 (2013).

138. Kategaya, L. S. *et al.* Casein Kinase 1 Proteomics Reveal Prohibitin 2 Function in Molecular Clock. *PLoS ONE* **7,** e31987 (2012).

139. Lee, C., Weaver, D. R. & Reppert, S. M. Direct Association between Mouse PERIOD and CKIε Is Critical for a Functioning Circadian Clock. *Mol. Cell. Biol.* **24,** 584–594 (2004).

140. Xu, Y. *et al.* Functional consequences of a CKIδ mutation causing familial advanced sleep phase syndrome. *Nature* **434,** 640–644 (2005).

141. Arey, R. & McClung, C. A. An inhibitor of casein kinase 1 ε/δ partially normalizes the manic-like behaviors of the ClockΔ19 mouse. *Behav. Pharmacol.* **23,** 392–396 (2012).

142. Tsai, I.-C. *et al.* Disease-associated casein kinase I δ mutation may promote adenomatous polyps formation via a Wnt/β-catenin independent mechanism. *Int. J. Cancer* **120,** 1005–1012 (2007).

143. Richter, J. *et al.* Effects of altered expression and activity levels of CK1δ and ε on tumor growth and survival of colorectal cancer patients. *Int. J. Cancer* **136,** 2799–2810 (2015).

144. Kumar, A., Rajendran, V., Sethumadhavan, R. & Purohit, R. Relationship between a point mutation S97C in CK1δ protein and its affect on ATP-binding affinity. *J. Biomol. Struct. Dyn.* **32,** 394–405 (2013).

145. Schittek, B. & Sinnberg, T. Biological functions of casein kinase 1 isoforms and putative roles in tumorigenesis. *Mol. Cancer* **13**: 231 (2014).

146. Richter, J. *et al.* Decreased CK1δ expression predicts prolonged survival in colorectal cancer patients. *Tumor Biol.,* epub ahead of print (2016).

147. Brockschmidt, C. *et al.* Anti-apoptotic and growth-stimulatory functions of CK1 delta and epsilon in ductal adenocarcinoma of the pancreas are inhibited by IC261 in vitro and in vivo. *Gut* **57,** 799–806 (2008).

148. Winkler, B. S. *et al.* CK1δ in lymphoma: gene expression and mutation analyses and validation of CK1δ kinase activity for therapeutic application. *Front. Cell Dev. Biol.* **3**: 9 (2015).

149. Rosenberg, L. H. *et al.* Therapeutic targeting of casein kinase 1δ in breast cancer. *Sci. Transl. Med.* **7,** 318ra202 (2015).

150. Polakis, P. Wnt Signaling in Cancer. *Cold Spring Harb. Perspect. Biol.* **4,** a008052 (2012).

151. Cruciat, C.-M. Casein kinase 1 and Wnt/β-catenin signaling. *Curr. Opin. Chem. Biol.* **31,** 46–55 (2014).

152. Wu, P., Nielsen, T. E. & Clausen, M. H. Small-molecule kinase inhibitors: an analysis of FDA-approved drugs. *Drug Discovery Today* **21,** 5–10 (2016).

153. Cohen, P. Protein kinases — the major drug targets of the twenty-first century? *Nat. Rev. Drug Discov.* **1,** 309–315 (2002).

154. Dar, A. C. & Shokat, K. M. The Evolution of Protein Kinase Inhibitors from Antagonists to Agonists of Cellular Signaling. *Annu. Rev. Biochem.* **80,** 769–795 (2011).

155. Fabbro, D. 25 Years of Small Molecular Weight Kinase Inhibitors: Potentials and Limitations. *Mol. Pharmacol.* **87,** 766–775 (2015).

156. Zhang, J., Yang, P. L. & Gray, N. S. Targeting cancer with small molecule kinase inhibitors. *Nat. Rev. Cancer* **9,** 28–39 (2009).

157. Okamoto, K. *et al.* Distinct Binding Mode of Multikinase Inhibitor Lenvatinib Revealed by Biochemical Characterization. *ACS Med. Chem. Lett.* **6,** 89–94 (2015).

158. Zhao, Z. *et al.* Exploration of Type II Binding Mode: A Privileged Approach for Kinase Inhibitor Focused Drug Discovery? *ACS Chem. Biol.* **9,** 1230–1241 (2014).

159. Freitag, A. & Laufer, S. ProteinkinaseInhibitoren: selektiv und wirksam. *Nachrichten aus der Chemie* **63,** 420–425 (2015).

160. Meharena, H. S. *et al.* Deciphering the Structural Basis of Eukaryotic Protein Kinase Regulation. *PLoS Biol.* **11,** e1001680 (2013).

161. Fischer, S. *et al.* Dibenzosuberones as p38 Mitogen-Activated Protein Kinase Inhibitors with Low ATP Competitiveness and Outstanding Whole Blood Activity. *J. Med. Chem.* **56,** 241–253 (2013).

162. Giamas, G., Stebbing, J., Vorgias, C. E. & Knippschild, U. Protein kinases as targets for cancer treatment. *Pharmacogenomics* **8,** 1005–1016 (2007).

163. Imai, K. & Takaoka, A. Comparing antibody and small-molecule therapies for cancer. *Nat. Rev. Cancer.* **6,** 714–727 (2006).

164. Zhang, X., Crespo, A. & Fernández, A. Turning promiscuous kinase inhibitors into safer drugs. *Trends Biotechnol.* **26,** 295–301 (2008).

165. Mente, S. *et al.* Ligand–Protein Interactions of Selective Casein Kinase 1δ Inhibitors. *J. Med. Chem.* **56,** 6819–6828 (2013).

166. Cozza, G. & Pinna, L. A. Casein kinases as potential therapeutic targets. *Expert Opin. Ther. Targets* **20,** 319–340 (2015).

167. Chijiwa, T., Hagiwara, M. & Hidaka, H. A Newly Synthesized Selective Casein Kinase I Inhibitor, N-(2-Aminoethyl)-5-chloroisoquinoline-8-sulfonamide, and Affinity Purification of Casein Kinase I from Bovine Testis. *J. Biol. Chem.* **264,** 4924–4927 (1989).

168. Xu, R.-M., Carmel, G., Kuret, J. & Cheng, X. Structural basis for selectivity of the isoquinoline sulfonamide family of protein kinase inhibitors. *Proc. Natl. Acad. Sci. USA* **93,** 6308–6313 (1996).

169. Mashhoon, N. *et al.* Crystal Structure of a Conformation-selective Casein Kinase-1 Inhibitor. *J. Biol. Chem.* **275,** 20052–20060 (2000).

170. Cheong, J. K. *et al.* IC261 induces cell cycle arrest and apoptosis of human cancer cells via CK1δ/ε and Wnt/β-catenin independent inhibition of mitotic spindle formation. *Oncogene* **30,** 2558–2569 (2011).

171. Yokoyama, T., Okano, M., Noshita, T., Funayama, S. & Ohtsuki, K. Characterization of (-)-Matairesinol as a Potent Inhibitor of Casein Kinase I in Vitro. *Biol. Pharm. Bull.* **26,** 371–374 (2003).

172. Baunbæk, D. *et al.* Anticancer Alkaloid Lamellarins Inhibit Protein Kinases. *Mar. Drugs* **6,** 514–527 (2008).

173. Rena, G., Bain, J., Elliott, M. & Cohen, P. D4476, a cell-permeant inhibitor of CK1, suppresses the site-specific phosphorylation and nuclear exclusion of FOXO1a. *EMBO Rep.* **5,** 60–65 (2004).

174. Shanware, N. P., Williams, L. M., Bowler, M. J. & Tibbets, R. S. Non-specific in vivo inhibition of CK1 by the pyridinyl imidazole p38 inhibitors SB 203580 and SB 202190. *BMP Rep.* **42,** 142–147 (2009).

175. Walton, K. M. *et al.* Selective Inhibition of Casein Kinase 1ε Minimally Alters Circadian Clock Period. *J. Pharmacol. Exp. Ther.* **330,** 430–439 (2009).

176. Peifer, C. *et al.* 3,4-Diaryl-isoxazoles and -imidazoles as Potent Dual Inhibitors of p38α Mitogen Activated Protein Kinase and Casein Kinase 1δ. *J. Med. Chem.* **52,** 7618–7630 (2009).

177. Meggio, F., Shugar, D. & Pinna, L. A. Ribofuranosyl-benzimidazole derivatives as inhibitors of casein kinase-2 and casein kinase-1. *Eur. J. Biochem.* **187,** 89–94 (1990).

178. Andrzejewska, M., Pagano, M. A., Meggio, F., Brunati, A. M. & Kazimierczuk, Z. Polyhalogenobenzimidazoles: Synthesis and Their Inhibitory Activity against Casein Kinases. *Bioorg. Med. Chem.* **11,** 3997–4002 (2003).

179. Muraki, M. *et al.* Manipulation of Alternative Splicing by a Newly Developed Inhibitor of Clks. *J. Biol. Chem.* **279,** 24246–24254 (2004).

180. Isojima, Y. *et al.* CKIε/δ-dependent phosphorylation is a temperature-insensitive, period-determining process in the mammalian circadian clock. *Proc. Natl. Acad. Sci. USA* **106,** 15744–15749 (2009).

181. Bischof, J. *et al.* 2-Benzamido-N-(1H-benzo[d]imidazol-2-yl)thiazole-4-carboxamide derivatives as potent inhibitors of CK1δ/ε. *Amino Acids* **43,** 1577–1591 (2012).

182. Richter, J. *et al.* Difluoro-dioxolo-benzoimidazol-benzamides As Potent Inhibitors of CK1δ and ε with Nanomolar Inhibitory Activity on Cancer Cell Proliferation. *J. Med. Chem.* **57,** 7933–7946 (2014).

183. Hua, Z. *et al.* 2-Phenylamino-6-cyano-1H-benzimidazole-based isoform selective casein kinase 1 gamma (CK1γ) inhibitors. *Bioorg. Med. Chem. Lett.* **22,** 5392–5395 (2012).

184. Long, A., Zhao, H. & Huang, X. Structural Basis for the Interaction between Casein Kinase 1 Delta and a Potent and Selective Inhibitor. *J. Med. Chem.* **55,** 956–960 (2011).

185. Oumata, N. *et al.* Roscovitine-Derived, Dual-Specificity Inhibitors of Cyclin-Dependent Kinases and Casein Kinases 1. *J. Med. Chem.* **51,** 5229–5242 (2008).

186. Bibian, M. *et al.* Development of highly selective casein kinase 1δ/1ε (CK1δ/ε) inhibitors with potent antiproliferative properties. *Bioorg. Med. Chem. Lett.* **23,** 4374–4380 (2013).

187. Yang, L.-L. *et al.* Discovery of N6-phenyl-1H-pyrazolo[3,4-d]pyrimidine-3,6-diamine derivatives as novel CK1 inhibitors using common-feature pharmacophore model based virtual screening and hit-to-lead optimization. *Eur. J. Med. Chem.* **56,** 30–38 (2012).

188. Huart, A.-S. *et al.* A Casein kinase 1/Checkpoint kinase 1 pyrazolo-pyridine protein kinase inhibitor as novel activator of the p53 pathway. *Bioorg. Med. Chem. Lett.* **23,** 5578–5585 (2013).

189. Cozza, G. *et al.* Identification of novel protein kinase CK1 delta (CK1δ) inhibitors through structure-based virtual screening. *Bioorg. Med. Chem. Lett.* **18,** 5672–5675 (2008).

190. Ferreira, L., Dos Santos, R., Oliva, G. & Andricopulo, A. Molecular Docking and Structure-Based Drug Design Strategies. *Molecules* **20,** 13384–13421 (2015).

191. Bissantz, C., Kuhn, B. & Stahl, M. A Medicinal Chemist's Guide to Molecular Interactions. *J. Med. Chem.* **53,** 5061–5084 (2010).

192. Dubinina, G. G. *et al.* In Silico Design of Protein Kinase Inhibitors: Successes and Failures. *Anticancer Agents Med. Chem.* **7,** 171–188 (2007).

193. Bühler, S., Goettert, M., Schollmeyer, D., Albrecht, W. & Laufer, S. A. Chiral Sulfoxides as Metabolites of 2-Thioimidazole-Based p38α Mitogen-Activated Protein Kinase Inhibitors: Enantioselective Synthesis and Biological Evaluation. *J. Med. Chem.* **54,** 3283–3297 (2011).

194. Wager, T. T. *et al.* Casein Kinase 1δ/ε Inhibitor PF-5006739 Attenuates Opioid Drug-Seeking Behavior. *ACS Chem. Neurosci.* **5,** 1253–1265 (2014).

195. Wang, Z. *et al.* Structural basis of inhibitor selectivity in MAP kinases. *Structure* **6,** 1117–1128 (1998).

196. Golebiowski, A. *et al.* The development of monocyclic pyrazolone based cytokine synthesis inhibitors. *Bioorg. Med. Chem. Lett.* **15,** 2285–2289 (2005).

197. Laufer, S. A., Hauser, D. R. J., Domeyer, D. M., Kinkel, K. & Liedtke, A. J. Design, Synthesis, and Biological Evaluation of Novel Tri- and Tetrasubstituted Imidazoles as Highly Potent and Specific ATP-Mimetic Inhibitors of p38 MAP Kinase: Focus on Optimized Interactions with the Enzyme's Surface-Exposed Front Region. *J. Med. Chem.* **51,** 4122–4149 (2008).

198. Laufer, S. *et al.* Tri- and tetrasubstituted imidazoles as p38α mitogen-activated protein kinase inhibitors. *Bioorg. Med. Chem. Lett.* **20,** 6671–6675 (2010).

199. Peifer, C. *et al.* Implications for selectivity of 3,4-diarylquinolinones as p38αMAP kinase inhibitors. *Bioorg. Med. Chem. Lett.* **18,** 1431–1435 (2008).

200. Ziegler, K., Hauser, D. R. J., Unger, A., Albrecht, W. & Laufer, S. A. 2-Acylaminopyridin-4-ylimidazoles as p38 MAP Kinase Inhibitors: Design, Synthesis, and Biological and Metabolic Evaluations. *ChemMedChem* **4,** 1939–1948 (2009).

201. Selig, R. *et al.* Conformational effects on potency of thioimidazoles and dihydrothiazolines. *Med. Chem. Commun.* **2,** 261–269 (2011).

202. Laufer, S. & Koch, P. Towards the improvement of the synthesis of novel 4(5)-aryl-5(4)-heteroaryl-2-thio-substituted imidazoles and their p38 MAP kinase inhibitory activity. *Org. Biomol. Chem.* **6,** 437–439 (2008).

203. Laufer, S. A. & Liedtke, A. J. A concise and optimized four-step approach toward 2-(aryl-)alkylsulfanyl-, 4(5)-aryl-, 5(4)-heteroaryl-substituted imidazoles using alkyl- or arylalkyl thiocyanates. *Tetrahedron Lett.* **47,** 7199–7203 (2006).

204. Seerden, J.-P. G. *et al.* Synthesis and structure–activity relationships of 4-fluorophenyl-imidazole p38α MAPK, CK1δ and JAK2 kinase inhibitors. *Bioorg. Med. Chem. Lett.* **24,** 3412–3418 (2014).

205. Sastry, G. M., Adzhigirey, M., Day, T., Annabhimoju, R. & Sherman, W. Protein and ligand preparation: parameters, protocols, and influence on virtual screening enrichments. *J. Comput. Aided Mol. Des.* **27,** 221–234 (2013).

206. Liverton, N. J. *et al.* Design and Synthesis of Potent, Selective, and Orally Bioavailable Tetrasubstituted Imidazole Inhibitors of p38 Mitogen-Activated Protein Kinase. *J. Med. Chem.* **42,** 2180–2190 (1999).

207. Craig, P. N. Interdependence between Physical Parameters and Selection of Substituent Groups for Correlation Studies. *J. Med. Chem.* **14,** 680–684 (1971).

208. Schmidt, D. Master Thesis. Christian-Albrechts-Universität, 2015.

209. G. Klebe (ed.). *Wirkstoffdesign. Entwurf und Wirkung von Arzneistoffen* (Spektrum Akademischer Verlag, Heidelberg, 2009).

210. Wang, X. *et al.* The Development of Highly Potent Inhibitors for Porcupine. *J. Med. Chem.* **56,** 2700–2704 (2013).

211. Deininger, M., Buchdunger, E. & Druker, B. J. The development of imatinib as a therapeutic agent for chronic myeloid leukemia. *Blood* **105,** 2640–2653 (2005).

212. Thompson, J. E. *et al.* Photochemical Preparation of a Pyridone Containing Tetracycle: A Jak Protein Kinase Inhibitor. *Bioorg. Med. Chem. Lett.* **12,** 1219–1223 (2002).

213. Laufer, S. A., Wagner, G. K., Kotschenreuther, D. A. & Albrecht, W. Novel Substituted Pyridinyl Imidazoles as Potent Anticytokine Agents with Low Activity against Hepatic Cytochrome P450 Enzymes. *J. Med. Chem.* **46,** 3230–3244 (2003).

214. Asinger, F., Fabian, K., Vossen, H. & Hentschel, K. Reaktionen von α-Mercaptoketonen. Über die gemeinsame Einwirkung von elementarem Schwefel und gasförmigem Ammoniak auf Ketone, LXXXVII. *Liebigs Ann. Chem.,* 410–414 (1974).

215. Schehr, M. Master Thesis. Christian-Albrechts-Universität, 2014.

216. Xue, F. *et al.* Improved Synthesis of Chiral Pyrrolidine Inhibitors and Their Binding Properties to Neuronal Nitric Oxide Synthase. *J. Med. Chem.* **54,** 6399–6403 (2011).

217. Thaher, B. A., Koch, P., Schattel, V. & Laufer, S. Role of the Hydrogen Bonding Heteroatom-Lys53 Interaction between the p38alpha Mitogen-Activated Protein (MAP) Kinase and Pyridinyl-Substituted 5-Membered Heterocyclic Ring Inhibitors. *J. Med. Chem.* **52,** 2613–2617 (2009).

218. Koch, P., Jahns, H., Schattel, V., Goettert, M. & Laufer, S. Pyridinylquinoxalines and Pyridinylpyridopyrazines as Lead Compounds for Novel p38α Mitogen-Activated Protein Kinase Inhibitors. *J. Med. Chem.* **53,** 1128–1137 (2010).

219. Bratulescu, G. Synthesis of 4,5-Substituted Imidazoles by a Fast Condensation of 1,2-Diketones and Urotropine in Heterogeneous Medium. *Synthesis,* 2319–2320 (2009).

220. Kuhl, L. Bachelor Thesis. Christian-Albrechts-Universität, 2013.

221. Lal, K. Ghosh, S. Salomon, R.G. Hydroxyl-Directed Regioselective Monodemethylation of Polymethoxyarenes. *J. Org. Chem.* **52,** 1072–1078 (1987).

222. Kiuchi, M., Marukawa, K., Hamada, M. & Sugahara, K. *Preparation of 2-amino-2-(2-phenylethyl)propane-1,3-diol derivatives for the treatment and/or prevention of autoimmune diseases or allergic diseases*. PCT Int. Appl., 2008153159, 18 Dec. 2008

223. El-Faham, A. & Albericio, F. Peptide Coupling Reagents, More than a Letter Soup. *Chem. Rev.* **111,** 6557–6602 (2011).

224. Valeur, E. & Bradley, M. Amide bond formation: beyond the myth of coupling reagents. *Chem. Soc. Rev.* **38,** 606–631 (2009).

225. Frérot, E., Coste, J., Pantaloni, A., Dufour, M.-N. & Jousn, P. PyBOP® and PyBroP: Two reagents for the difficult coupling of the α,α-dialkyl amino acid, Aib. *Tetrahedron* **47,** 259–270 (1991).

226. Qian, D. & Zhang, J. Catalytic oxidation/C-H functionalization of N-arylpropiolamides by means of gold carbenoids: concise route to 3-acyloxindoles. *Chem. Commun.* **48,** 7082–7084 (2012).

227. Engen, W. *et al.* Synthesis of Aryl-Heteroaryl Ureas (AHUs) Based on 4-Aminoquinoline and Their Evaluation Against the Insulin-Like Growth Factor Receptor (IGF-1R). *Bioorg. Med. Chem.* **18,** 5995–6005 (2010).

228. R. Brückner (ed.). *Reaktionsmechanismen. Organische Reaktionen, Stereochemie, moderne Synthesemethoden* (Elsevier, Spektrum, Akad. Verl., München, Heidelberg, 2004).

229. Johannes, E. Dissertation. Christian-Albrechts-Universität zu Kiel, 2015.

230. Handy, S. T., Zhang, Y. & Bregman, H. A Modular Synthesis of the Lamellarins: Total Synthesis of Lamellarin G Trimethyl Ether. *J. Org. Chem.* **69,** 2362–2366 (2004).

231. H. G. O. Becker & R. Beckert (eds.). *Organikum. Organisch-chemisches Grundpraktikum* (Wiley-VCH, Weinheim, [Great Britain], 2009).

232. King, L. C. & Ostrum, G. Selective Bromination with Copper(II) Bromide. *J. Org. Chem.* **29,** 3459–3461 (1964).

233. Kosower, E. M. & Wu, G.-S. Halogenation with Copper(II). II. Unsaturated Ketones. *J. Org. Chem.* **28,** 633–638 (1963).

234. Gaikwad, S. A., Patil, A. A. & Deshmukh, M. B. An Efficient, Uncatalyzed, and Rapid Synthesis of Thiazoles and Aminothiazoles Under Microwave Irradiation and Investigation of Their Biological Activity. *Phosphorus Sulfur Silicon Relat. Elem.* **185,** 103–109 (2010).

235. J. Clayden, N. Greeves & S. G. Warren (eds.). *Organische Chemie* (Springer, Berlin, 2013).

236. Suzuki, M., Iwasaki, T., Matsumoto, K. & Okumura, K. Convenient Syntheses of Aroylamino Acids and α-amino ketones. *Synth. Commun.* **2,** 237–242 (1972).

237. Kauffman, J. M. & Moyna, G. Diarylamino Groups as Photostable Auxofluors in 2-Benzoxazolylfluorene, 2,5-Diphenyloxazoles, 1,3,5-Hexatrienes, 1,4-Distyrylbenzenes, and 2,7-Distyrylfluorenes. *J. Org. Chem.* **34,** 839–853 (2003).

238. Jimonet, P. *et al.* Bioisosteres of 9-Carboxymethyl-4-oxo-imidazo[1,2-a]indeno-[1,2-e]pyrazin-2-carboxylic Acid Derivatives. Progress Towards Selective, Potent In Vivo AMPA Antagonists with Longer Durations of Action. *Bioorg. Med. Chem.* **11,** 127–132 (2001).

239. Oliver, J. E. & Sonnet, P. E. Improved routes to methyl 4-methylimidazole-2-carboxylate and methyl 5-methyl-1,2,4-triazole-3-carboxylate. *J. Org. Chem.* **38,** 1437–1438 (1973).

240. Palace-Berl, F. *et al.* 5-Nitro-2-furfuriliden derivatives as potential anti-Trypanosoma cruzi agents: design, synthesis, bioactivity evaluation, cytotoxicity and exploratory data analysis. *Bioorg. Med. Chem.* **21,** 5395–5406 (2013).

241. Vaněk, T., Veloková, V. & Gut, J. Preparation of 3- and 3,5-substituted 1,2,4-Triazoles. *Collect. Czech. Chem. Comm.* **49,** 2492–2495 (1984).

242. Pallela, V. R. *et al.* Hydrothiolation of benzyl mercaptan to arylacetylene: application to the synthesis of (E) and (Z)-isomers of ON 01910.Na (Rigosertib(R)), a phase III clinical stage anti-cancer agent. *Org. Biomol. Chem.* **11,** 1964–1977 (2013).

243. Dayal, B. *et al.* Lithium hydroxide/aqueous methanol: mild reagent for the hydrolysis of bile acid methyl esters. *Steroids* **55,** 233–237 (1990).

244. MacDonald, P. & Rossetto, P. *Process for the Preparation of Imatinib*. U.S. Pat. Appl. Publ., 20080103305, 01 May 2008.

245. Baraldi, P. G. *et al.* Unusual Ring-Opening Reaction of 6,7-Dihydrothieno[3,2-d]pyrimidine-2,4-dione Derivatives Leading to 5-(Alkylthio)-6-vinyluracils. *J. Org. Chem.* **60,** 1461–1463 (1995).

246. Yu, B. *et al.* Catalyst-free approach for solvent-dependent selective oxidation of organic sulfides with oxone. *Green Chem.* **14,** 957–962 (2012).

247. Mahajan, N. S., Jadhav, R. L., Mali, K. K., Pimpodkar, N. V. & Manikrao, A. M. Facile and Efficient Oxidation of Sulfides to Sulfoxides Using Oxone® and its Biological Evaluation. *Asian J. Research Chem.* **2,** 407–410 (2009).

248. Krüger, M. Dissertation. University Hospital Ulm, 2016.

249. Ianes, C. Dissertation. University Hospital Ulm, current work.

250. Gill, A. L. *et al.* Identification of Novel p38alpha MAP Kinase Inhibitors Using Fragment-Based Lead Generation. *J. Med. Chem.* **48,** 414–426 (2005).

251. Lipinski, C. A., Lombardo, F., Dominy, B. W. & Feeney, P. J. Experimental and computational approaches to estimate solubility and permeability in drug discovery and development settings. *Adv. Drug Deliv. Rev.* **46,** 3–26 (2001).

252. Shivakumar, D. *et al.* Prediction of Absolute Solvation Free Energies using Molecular Dynamics Free Energy Perturbation and the OPLS Force Field. *J. Chem. Theory Comput.* **6,** 1509–1519 (2010).

253. Harder, E. *et al.* OPLS3: A Force Field Providing Broad Coverage of Drug-like Small Molecules and Proteins. *J. Chem. Theory Comput.* **12,** 281–296 (2016).

254. Greenwood, J. R., Calkins, D., Sullivan, A. P. & Shelley, J. C. Towards the comprehensive, rapid, and accurate prediction of the favorable tautomeric states of drug-like molecules in aqueous solution. *J. Comput. Aided Mol. Des.* **24,** 591–604 (2010).

255. Jacobson, M. P. *et al.* A Hierarchical Approach to All-Atom Protein Loop Prediction. *Proteins* **55,** 351–367 (2004).

256. Halgren, T. A. Identifying and Characterizing Binding Sites and Assessing Druggability. *J. Chem. Inf. Model.* **49,** 377–389 (2009).

257. Watts, K. S. *et al.* ConfGen: A Conformational Search Method for Efficient Generation of Bioactive Conformers. *J. Chem. Inf. Model.* **50,** 534–546 (2010).

258. Friesner, R. A. *et al.* Extra Precision Glide: Docking and Scoring Incorporating a Model of Hydrophobic Enclosure for Protein-Ligand Complexes. *J. Med. Chem.* **49,** 6177–6196 (2006).

259. Eldridge, M. D., Murray, C. W., Auton, T. R., Paolini, G. V. & Mee, R. P. Empirical scoring functions: I. The development of a fast empirical scoring function to estimate the binding affinity of ligands in receptor complexes. *J. Comput. Aided Mol. Des.* **11,** 425–445 (1997).

260. Sherman, W., Day, T., Jacobson, M. P., Friesner, R. A. & Farid, R. Novel Procedure for Modeling Ligand/Receptor Induced Fit Effects. *J. Med. Chem.* **49,** 534–553 (2006).

261. Knippschild, U., Milne, D., Campbell, L. & Meek, D. p53 N-terminus-targeted protein kinase activity is stimulated in response to wild type p53 and DNA damage. *Oncogene* **13,** 1387–1393 (1996).

262. Neubig, R. R., Spedding, M., Kenakin, T. & Christopoulos, A. International Union of Pharmacology Committee on Receptor Nomenclature and Drug Classification. XXXVIII. Update on Terms and Symbols in Quantitative Pharmacology. *Pharmacol. Rev.* **55,** 597–606 (2003).

263. ProQinase GmbH. 33PanQinase® assay. Available at http://www.proqinase.com.

264. Morgan, R. T. *et al.* Human cell line (COLO 357) of metastatic pancreatic adenocarcinoma. *Int. J. Cancer* **25,** 591–598 (1980).

265. J. Fogh (ed.). *Human tumor cells in vitro* (Springer Science+Business Media, New York, 1975).

266. Yunis, A. A., Arimura, G. K. & Russin, D. J. Human pancreatic carcinoma (MIA PaCa-2) in continuous culture: sensitivity to asparaginase. *Int. J. Cancer* **19,** 128–135 (1977).

267. Lieber, M., Mazzetta, J., Nelson-Rees, W., Kaplan, M. & Todaro, G. Establishment of a continuous tumor-cell line (panc-1) from a human carcinoma of the exocrine pancreas. *Int. J. Cancer* **15,** 741–747 (1975).

268. Ungefroren, H. *et al.* Human pancreatic adenocarcinomas express Fas and Fas ligand yet are resistant to Fas-mediated apoptosis. *Cancer Res.* **58,** 1741–1749 (1998).

269. Simard, J. R. *et al.* Development of a fluorescent-tagged kinase assay system for the detection and characterization of allosteric kinase inhibitors. *J. Am. Chem. Soc.* **131,** 13286–13296 (2009).

270. Bukhtiyarova, M. *et al.* Improved expression, purification, and crystallization of p38alpha MAP kinase. *Prot. Expr. Purif.* **37,** 154–161 (2004).

271. Kabsch, W. Automatic processing of rotation diffraction data from crystals of initially unknown symmetry and cell constants. *J. Appl. Crystallogr.* **26,** 795–800 (1993).

272. Read, R. J. Pushing the boundaries of molecular replacement with maximum likelihood. *Acta Cryst.* **57,** 1373–1382 (2001).

273. Emsley, P. & Cowtan, K. Coot: model-building tools for molecular graphics. *Acta Cryst.* **D60,** 2126–2132 (2004).

274. Murshudov, G. N., Vagin, A. A. & Dodson, E. J. Refinement of Macromolecular Structures by the Maximum-Likelihood Method. *Acta Cryst.* **D53,** 240–255 (1997).

275. Lovell, S. C. *et al.* Structure Validation by Cα Geometry: ϕ, ψ and Cβ Deviation. *Protein Struct. Funct. Genet.* **50,** 437–450 (2003).

276. Schüttelkopf, A. W. & van Aalten, D. M. F. PRODRG: a tool for high-throughput crystallography of protein-ligand complexes. *Acta crysta.* **60,** 1355–1363 (2004).

9 Appendix

Supplementary Table 1 | Selectivity profiling of compound 191. The inhibitor has been screened at a concentration of 100 nM over a panel of 320 wild-type protein kinases and B-Raf V600E by ProQinase GmbH. Classification of protein kinase families refers to MANNING *et al*[5]: AGC = containing PKA, PKG, PKC families; CAMK = calcium/calmodulin-dependent protein kinase; CK1 = formerly known as casein kinase 1; CMGC = containing Cdk, MAPK, GSK3, CLK families; STE = homologs of yeast sterile 7, sterile 11, sterile 20 kinases; TK = tyrosine kinase; TKL = tyrosine kinase-like.

#	Kinase name	Kinase family	Residual activity (%)
1	ABL1	TK	100
2	ABL2	TK	91
3	ACK1	TK	96
4	ACV-R1	TKL	95
5	ACV-R1B	TKL	101
6	ACV-R2A	TKL	98
7	ACV-R2B	TKL	97
8	ACV-RL1	TKL	99
9	AKT1 aa106-480	AGC	90
10	AKT2 aa107-481	AGC	97
11	AKT3 aa106-479	AGC	83
12	ALK (GST-HIS-tag)	TK	114
13	AMPK-alpha1 aa1-550	CAMK	96
14	ARK5	CAMK	88
15	ASK1	STE	93
16	Aurora-A	OTHER	93
17	Aurora-B	OTHER	92
18	Aurora-C	OTHER	93
19	AXL	TK	104
20	BLK	TK	77
21	BMPR1A	TKL	102
22	BMX	TK	98
23	B-RAF V600E	TKL	102
24	B-RAF	TKL	91
25	BRK	TK	98
26	BRSK1	CAMK	89
27	BRSK2	CAMK	105
28	BTK	TK	105
29	BUB1B	OTHER	102
30	CAMK1D	CAMK	78
31	CAMK2A	CAMK	95
32	CAMK2B	CAMK	103
33	CAMK2D	CAMK	96
34	CAMK2G	CAMK	105
35	CAMK4	CAMK	95
36	CAMKK1	OTHER	99
37	CAMKK2	OTHER	96
38	CDC42BPA	AGC	104
39	CDC42BPB	AGC	88

40	CDC7/ASK	OTHER	97
41	CDK1/CycA2	CMGC	91
42	CDK1/CycB1	CMGC	95
43	CDK1/CycE1	CMGC	97
44	CDK19/CycC	CMGC	86
45	CDK2/CycA2	CMGC	87
46	CDK2/CycE1	CMGC	99
47	CDK3/CycC	CMGC	95
48	CDK3/CycE1	CMGC	98
49	CDK4/CycD1	CMGC	98
50	CDK4/CycD3	CMGC	88
51	CDK5/p25NCK	CMGC	117
52	CDK5/p35NCK	CMGC	85
53	CDK6/CycD1	CMGC	105
54	CDK6/CycD3		97
55	CDK7/CycH/MAT1	CMGC	102
56	CDK8/CycC	CMGC	90
57	CDK9/CycK	CMGC	103
58	CDK9/CycT1	CMGC	93
59	CHK1	CAMK	92
60	CHK2	CAMK	98
61	CK1-alpha1	CK1	26
62	CK1-delta	CK1	3
63	CK1-epsilon	CK1	7
64	CK1-gamma1	CK1	100
65	CK1-gamma2	CK1	91
66	CK1-gamma3	CK1	73
67	CK2-alpha1	OTHER	97
68	CK2-alpha2	OTHER	90
69	CLK1	CMGC	105
70	CLK2	CMGC	101
71	CLK3	CMGC	98
72	CLK4	CMGC	95
73	COT	STE	111
74	CSF1-R	TK	104
75	CSK	TK	101
76	DAPK1	CAMK	96
77	DAPK2	CAMK	95
78	DAPK3	CAMK	85
79	DCAMKL2	CAMK	94
80	DDR2	TK	101
81	DMPK	AGC	103
82	DNA-PK	ATYP	95
83	DYRK1A	CMGC	96
84	DYRK1B	CMGC	101
85	DYRK2	CMGC	99
86	DYRK3	CMGC	97
87	DYRK4	CMGC	100
88	EEF2K	ATYPICAL	84
89	EGF-R	TK	113
90	EIF2AK2	OTHER	91
91	EIF2AK3	OTHER	91
92	EPHA1	TK	104

93	EPHA2	TK	95
94	EPHA3	TK	97
95	EPHA4	TK	96
96	EPHA5	TK	97
97	EPHA6	TK	100
98	EPHA7	TK	99
99	EPHA8	TK	115
100	EPHB1	TK	96
101	EPHB2	TK	55
102	EPHB3	TK	92
103	EPHB4	TK	97
104	ERBB2	TK	97
105	ERBB4	TK	98
106	ERK1	CMGC	94
107	ERK2	CMGC	103
108	ERK5	CMGC	95
109	ERK7	CMGC	93
110	FAK aa2-1052	TK	105
111	FER	TK	93
112	FES	TK	91
113	FGF-R1	TK	113
114	FGF-R2	TK	101
115	FGF-R3	TK	99
116	FGF-R4	TK	86
117	FGR	TK	103
118	FLT3	TK	109
119	FRK	TK	93
120	FYN	TK	119
121	GRK2	AGC	113
122	GRK3	AGC	91
123	GRK4	AGC	86
124	GRK5	AGC	97
125	GRK6	AGC	100
126	GRK7	AGC	83
127	GSG2	OTHER	121
128	GSK3-alpha	CMGC	107
129	GSK3-beta	CMGC	89
130	HCK	TK	58
131	HIPK1	CMGC	102
132	HIPK2	CMGC	92
133	HIPK3	CMGC	94
134	HIPK4	CMGC	94
135	HRI	OTHER	97
136	IGF1-R	TK	114
137	IKK-alpha	OTHER	98
138	IKK-beta	OTHER	92
139	IKK-epsilon	OTHER	102
140	INS-R	TK	101
141	INSR-R	TK	92
142	IRAK1	TKL	99
143	IRAK4 (untagged)	TKL	98
144	ITK	TK	66
145	JAK1 aa850-1154	TK	107

146	JAK2	TK	93
147	JAK3	TK	88
148	JNK1	CMGC	103
149	JNK2	CMGC	21
150	JNK3	CMGC	37
151	KIT	TK	103
152	LCK	TK	26
153	LIMK1	TKL	96
154	LIMK2	TKL	100
155	LRRK2	TKL	94
156	LTK	TK	101
157	LYN	TK	105
158	MAP3K1	STE	99
159	MAP3K10	STE	63
160	MAP3K11	STE	87
161	MAP3K7/MAP3K7IP1	STE	60
162	MAP3K9	STE	97
163	MAP4K2	STE	96
164	MAP4K4	STE	97
165	MAP4K5	STE	94
166	MAPKAPK2	CAMK	90
167	MAPKAPK3	CAMK	108
168	MAPKAPK5	CAMK	112
169	MARK1	CAMK	106
170	MARK2	CAMK	94
171	MARK3	CAMK	94
172	MARK4	CAMK	97
173	MATK	TK	101
174	MEK1	STE	92
175	MEK2	STE	100
176	MEK5	STE	93
177	MEKK2	STE	97
178	MEKK3	STE	101
179	MELK	CAMK	97
180	MERTK	TK	85
181	MET	TK	105
182	MINK1	STE	89
183	MKK4	STE	103
184	MKK6 S207D/T211D**	STE	89
185	MKK7	STE	96
186	MKNK1	CAMK	99
187	MKNK2	CAMK	101
188	MLK4	TKL	94
189	MST1	STE	124
190	MST2	STE	107
191	MST3	STE	92
192	MST4	STE	101
193	mTOR	ATYPICAL	96
194	MUSK	TK	102
195	MYLK	CAMK	97
196	MYLK2	CAMK	100
197	MYLK3	CAMK	98
198	NEK1	OTHER	101

199	NEK11	OTHER	77
200	NEK2	OTHER	103
201	NEK3	OTHER	93
202	NEK4	OTHER	89
203	NEK6	OTHER	99
204	NEK7	OTHER	113
205	NEK9	OTHER	98
206	NIK	STE	88
207	NLK	CMGC	78
208	p38-alpha	CMGC	22
209	p38-beta	CMGC	52
210	p38-delta	CMGC	99
211	p38-gamma	CMGC	99
212	PAK1	STE	93
213	PAK2	STE	121
214	PAK3	STE	100
215	PAK4	STE	101
216	PAK6	STE	103
217	PAK7	STE	129
218	PASK	CAMK	98
219	PBK	OTHER	121
220	PCTAIRE1/CycY	CMGC	148
221	PDGFR-alpha	TK	102
222	PDGFR-beta	TK	99
223	PDK1	AGC	106
224	PHKG1	CAMK	91
225	PHKG2	CAMK	99
226	PIM1	CAMK	95
227	PIM2	CAMK	99
228	PIM3	CAMK	102
229	PKA	AGC	100
230	PKC-alpha	AGC	99
231	PKC-beta1	AGC	99
232	PKC-beta2	AGC	106
233	PKC-delta	AGC	88
234	PKC-epsilon	AGC	98
235	PKC-eta	AGC	80
236	PKC-gamma	AGC	93
237	PKC-iota	AGC	98
238	PKC-mu	AGC	117
239	PKC-nu	AGC	72
240	PKC-theta	AGC	87
241	PKC-zeta	AGC	95
242	PKMYT1	OTHER	112
243	PLK1	OTHER	106
244	PLK3	OTHER	97
245	PRK1	AGC	108
246	PRK2	AGC	78
247	PRKD2	CAMK	104
248	PRKG1	AGC	94
249	PRKG2	AGC	87
250	PRKX	AGC	100
251	PYK2	TK	101

252	RAF1 Y340D/Y341D (untagged)**	TKL	84
253	RET	TK	113
254	RIPK2	TKL	45
255	RIPK5	TKL	97
256	ROCK1	AGC	92
257	ROCK2	AGC	99
258	RON	TK	110
259	ROS	TK	97
260	RPS6KA1	AGC	102
261	RPS6KA2	AGC	95
262	RPS6KA3	AGC	94
263	RPS6KA4	AGC	110
264	RPS6KA5	AGC	96
265	RPS6KA6	AGC	141
266	S6K	AGC	111
267	S6K-beta	AGC	98
268	SAK	OTHER	103
269	SGK1	AGC	111
270	SGK2	AGC	99
271	SGK3	AGC	90
272	SIK1	CAMK	101
273	SIK2	CAMK	117
274	SIK3	CAMK	96
275	SLK	STE	98
276	SNARK	CAMK	92
277	SNK	OTHER	94
278	SRC (GST-HIS-tag)	TK	100
279	SRMS	TK	117
280	SRPK1	CMGC	104
281	SRPK2	CMGC	105
282	STK17A	CAMK	98
283	STK23	CAMK	104
284	STK25	STE	96
285	STK33	CAMK	90
286	STK39	STE	109
287	SYK aa1-635	TK	108
288	TAOK2	STE	86
289	TAOK3	STE	89
290	TBK1	OTHER	96
291	TEC	TK	100
292	TGFB-R1	TKL	100
293	TGFB-R2	TKL	99
294	TIE2	TK	71
295	TLK1	AGC	107
296	TLK2	AGC	122
297	TNK1	TK	99
298	TRK-A	TK	101
299	TRK-B	TK	117
300	TRK-C	TK	116
301	TSF1	OTHER	99
302	TSK2	CAMK	93
303	TSSK1	CAMK	97
304	TTBK1	CK1	96

305	TTBK2	CK1	98
306	TTK	OTHER	94
307	TXK	TK	95
308	TYK2	TK	84
309	TYRO3	TK	94
310	VEGF-R1	TK	98
311	VEGF-R2	TK	90
312	VEGF-R3	TK	96
313	VRK1	CK1	100
314	VRK2	CK1	104
315	WEE1	OTHER	94
316	WNK1	OTHER	96
317	WNK2	OTHER	101
318	WNK3	OTHER	101
319	YES	TK	100
320	ZAK	TKL	96
321	ZAP70	TK	81

** Constitutively active kinase.

Supplementary Table 2 | Register of test compounds from the current work[248,249].

#	Structure	IC_{50} (CK1δ)	IC_{50} (CK1ε)	IC_{50} (p38α)
82	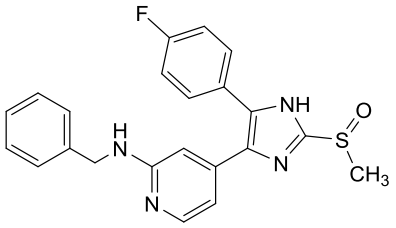	n.d.	n.d.	139 nM[197]
84	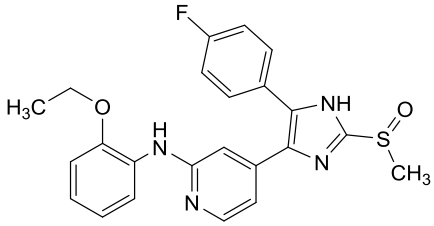	n.d.	n.d.	n.d.
85	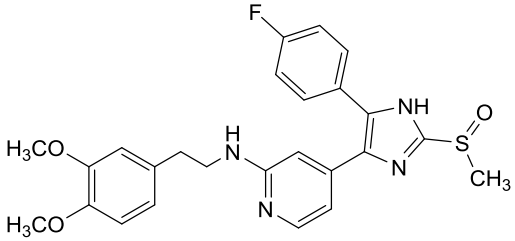	n.d.	n.d.	n.d.
102	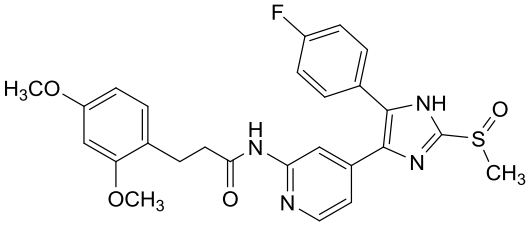	93 nM	499 nM	n.d.
103	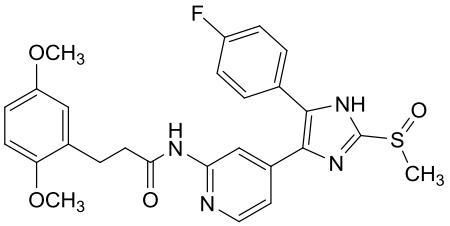	87 nM	573 nM	n.d.
104	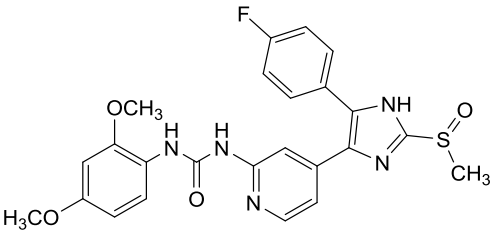	153 nM	910 nM	n.d.
148	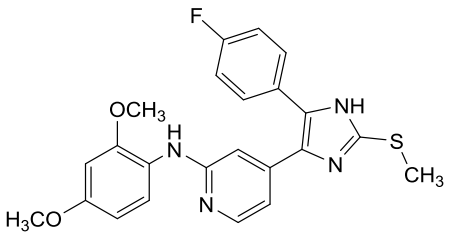	n.d.	n.d.	n.d.

149	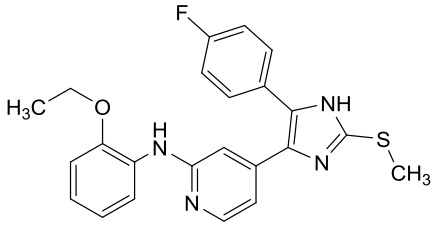	n.d.	n.d.	n.d.
150	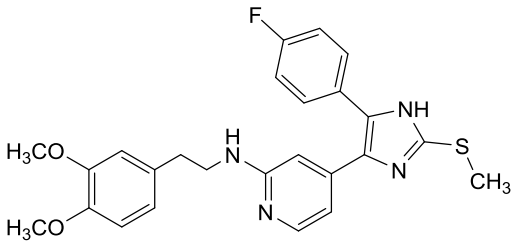	644 nM	3323 nM	n.d.
151	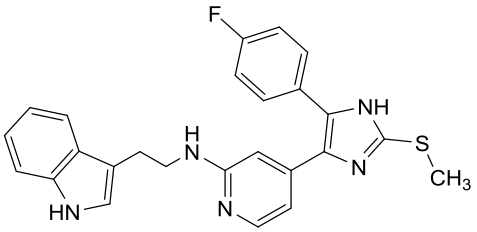	344 nM	1753 nM	n.d.
152	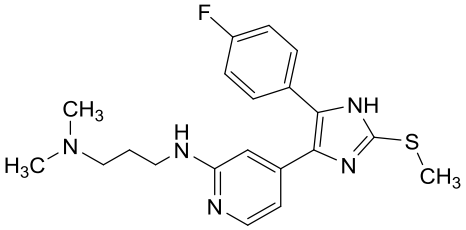	n.d.	n.d.	n.d.
153	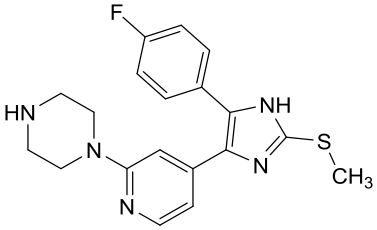	n.d.	n.d.	n.d.
154	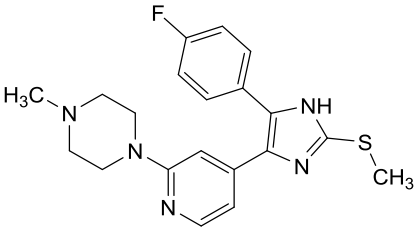	n.d.	n.d.	n.d.
155	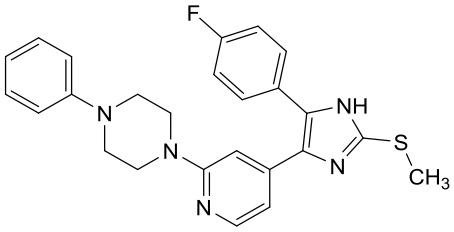	n.d.	n.d.	n.d.

162	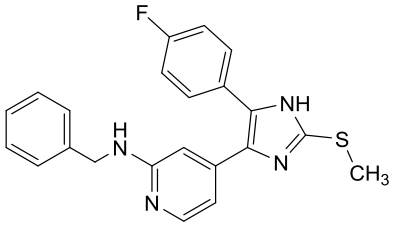	n.d.	n.d.	n.d.
164	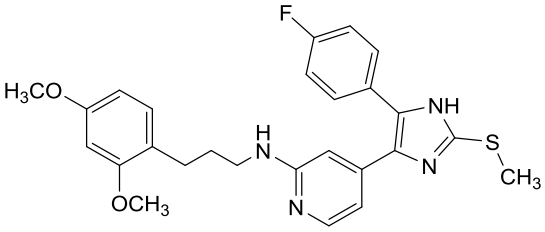	386 nM	6731 nM	n.d.
190	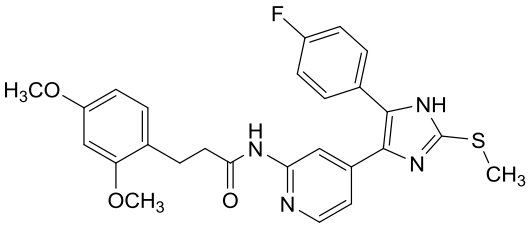	20 nM	129 nM	n.d.
191	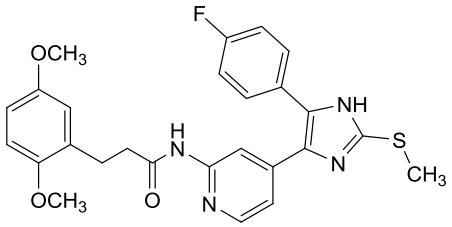	4 nM < 3 nM[PQ]	25 nM	10 nM[PQ]
192	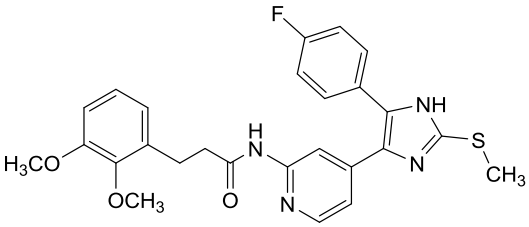	20 nM	233 nM	n.d.
193	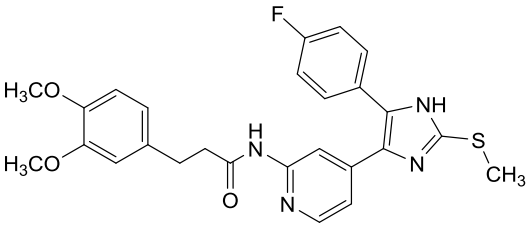	14 nM	91 nM	n.d.
194	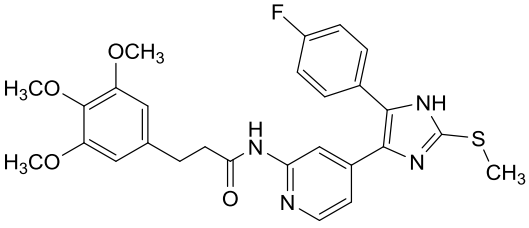	27 nM	204 nM	n.d.

204	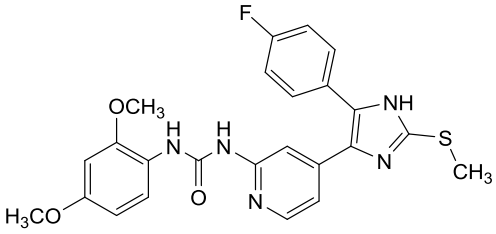	19 nM 10 nM[PQ]	227 nM	28 nM[PQ]
205	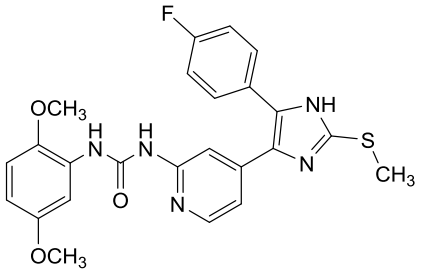	31 nM	186 nM	n.d.
206	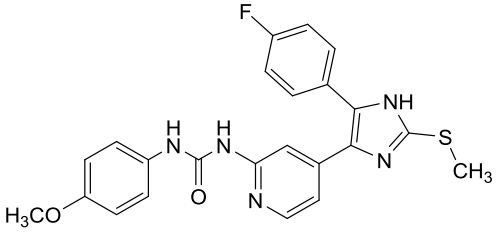	n.d.	n.d.	n.d.
208	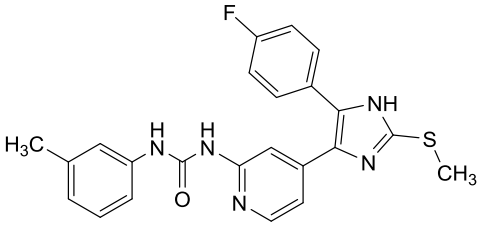	47 nM	272 nM	n.d.
209	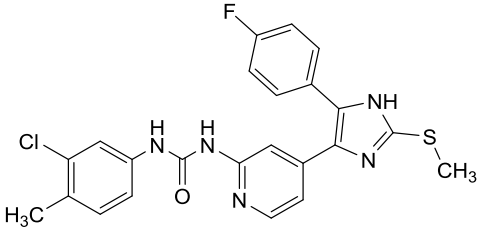	35 nM	203 nM	n.d.
210	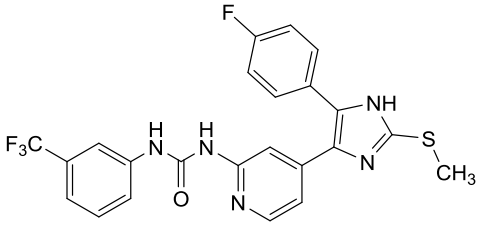	169 nM	498 nM	n.d.
212	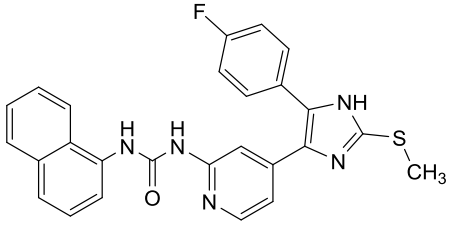	n.d.	n.d.	n.d.

224	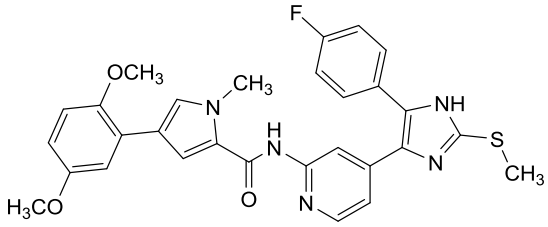	8 nM < 3 nM[PQ]	81 nM	10 nM[PQ]
232	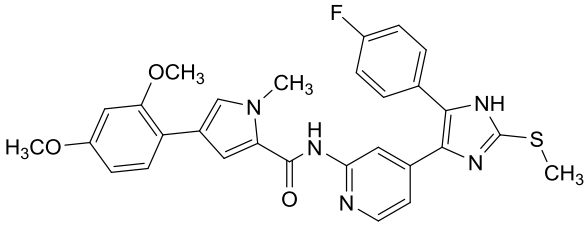	9 nM	45 nM	n.d.
266	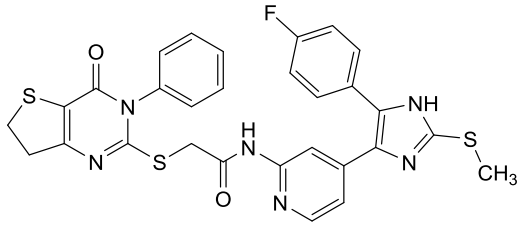	27 nM < 3 nM[PQ]	237 nM	36 nM[PQ]
267	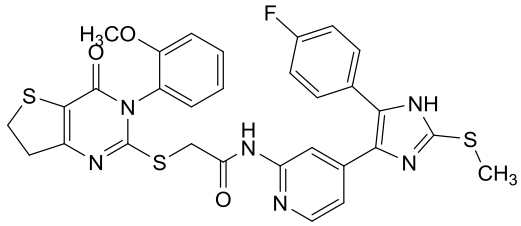	29 nM	151 nM	n.d.
286	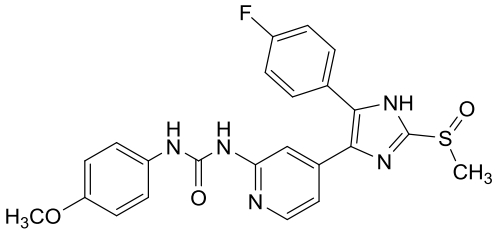	n.d.	n.d.	n.d.
287	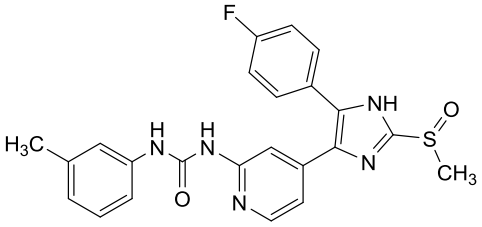	160 nM	804 nM	n.d.
288	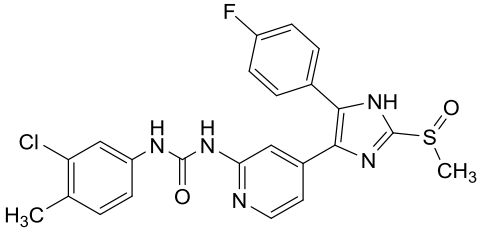	115 nM	764 nM	n.d.

289	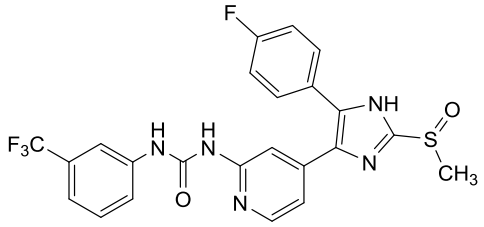	88 nM	623 nM	n.d.
290	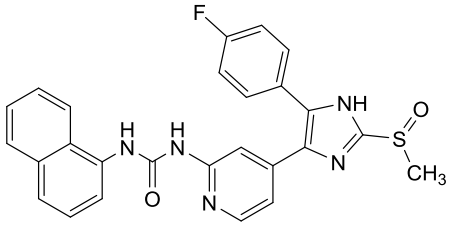	48 nM	182 nM	n.d.
291	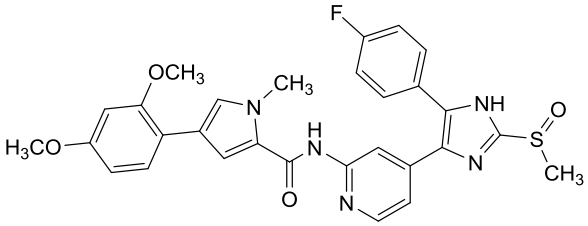	32 nM	181 nM	n.d.

[PQ] IC_{50} value has been determined by ProQinase GmbH.

List of Abbreviations

#	number (of compound)
°	degrees
°C	degrees Celsius
2D	two-dimensional
3D	three-dimensional
βAPP	amyloid-β precursor protein
δ (NMR)	chemical shift
µCi	microcurie
µl	microliter(s)
µM	micromolar
µmol	micromole(s)
$\tilde{\nu}$	wavenumber
A	alanine
Å	Ångström
aa	amino acid(s)
AB	adenine-binding region
ACN	acetonitrile
AD	Alzheimer's disease
ADP	adenosine diphosphate
AGC	containing PKA, PKG, PKC families
AIB1	amplified in breast cancer 1
AKAP450	A-kinase anchoring protein 450
Akt	protein kinase B
Ala	alanine
ALS	amyotrophic lateral sclerosis
AMP	adenosine monophosphate
anhyd.	anhydrous
APC/C	anaphase-promoting complex/cyclosome
approx.	approximately
aq.	aqueous
^{ar}C (NMR)	aromatic carbon atom (only denoted if ambiguous)
ARF GAP1	ADP-ribosylation factor GTPase-activating protein
Arg	arginine
Asn	asparagine
Asp	aspartic acid
ATP	adenosine triphosphate
ATR	attenuated total reflection
B-factor	Debye-Waller-/Temperature-factor
BACE1	β-secretase
Bcr-Abl	breakpoint cluster region-Abelson tyrosine kinase
bind.	binding
BMAL1	brain and muscle ARNT-like protein
Bn	benzyl
BnBr	benzyl bromide
Boc_2O	di-*tert*-butyl dicarbonate
BOG	*β*-octyl glucoside
B-Raf	rapidly accelerated fibrosarcoma B
bs (NMR)	broad singlet
Bt	benzotriazole
BYSL	bystin
cat	catalytic
CAMK	calcium/calmodulin-dependent protein kinase
CCK2R	cholecystokinin 2 receptor
Cdh1	cadherin 1
Cdk2/E	cyclin-dependent kinase 2/cyclin E
Cdk5/p35	cyclin-dependent kinase 5/p35
Chk1	checkpoint kinase 1
Ci-155	full-length cubitus interruptus
CK1	protein kinase CK1
CK1BP	CK1-binding protein
CK2	protein kinase CK2
CLK1-4	CDC-like kinases 1-4
CLS	centrosomal localization signal
cm	centimeter(s)
CMGC	containing Cdk, MAPK, GSK3, CLK families
CML	chronic myelogenous leukemia
CNS	central nervous system
conc.	concentrated
COSY	correlation spectroscopy
cp.	compare
CPI-17	protein kinase C-potentiated myosin phosphatase inhibitor of 17 kDa
CREB	cyclic AMP response element-binding protein
CRY 1/2	cryptochrome 1/2
Cx43	connexin-43
Cys	cysteine
d (NMR)	doublet

D	asparagine
DARPP-32	dopamine- and cAMP-regulated neuronal phosphoprotein
DBU	1,8-diazabicyclo[5.4.0]undec-7-ene
DCC	*N*,*N*'-Dicyclohexylcarbodiimide
dCK	deoxycytidine kinase
DCM	dichloromethane
dd (NMR)	doublet of doublets
DDX3	DEAD-box RNA-helicase 3
dq (NMR)	doublet of quartets
DEPT	distortionless enhancement by polarization transfer
4-DMAP	4-dimethylaminopyridine
DMSO	dimethyl sulfoxide
DNA	deoxyribonucleic acid
Dnmt1	DNA methyltransferase 1
Dpr1a	dapper 1a
dt (NMR)	doublet of triplets
Dvl	dishevelled
DYRK1A/1B	dual specificity tyrosine-phosphorylation-regulated kinases 1A and 1B
E	glutamic acid
E-box	enhancer box
e.g.	exempli gratia (for example)
EB1	microtubule plus-end-binding protein 1
EC_{50}	half maximal effective concentration
EDCI	1-ethyl-3-(3-dimethylaminoproyl)-carbodiimid
EDTA	ethylenediaminetetraacetic acid
EGFR	epidermal growth factor receptor
EI	electron ionization
eIF6	eukaryotic initiation factor 6
Emi2	endogenous meiotic inhibitor 2
equiv	equivalents
ER	endoplasmic reticulum
ERα	estrogen receptor α
ESI	electron spray ionization
Et_3N	triethylamine
eV	electronvolt
F	phenylalanine
Fam20C	family with sequence similarity 20C
FASPS	familial advanced sleep phase syndrome
Fat	*Drosophila melanogaster* homolog of human FAT
FD	field desorption
FDA	Food and Drug administration
FLT1-3	Fms-like tyrosine kinases 1-3
FoxG1	forkhead box G1
FRQ	frequency
g	gram(s)
G-CK	Golgi casein kinase
Gln	glutamine
Glu	glutamic acid
Gly	glycine
GSK-3	glycogen synthase kinase 3
h	hour(s)
H-bond	hydrogen bond
HATU	1-[bis(dimethylamino)methylene]-1*H*-1,2,3-triazolo[4,5-b]pyridinium-3-oxid hexafluorophosphate
HEPES	2-(4-(2-hydroxyethyl)piperazin-1-yl)ethanesulfonic acid
Her2	human epidermal growth factor receptor 2
Hh	Hedgehog
HHV	human herpes virus
HIF-1α	hypoxia-inducible factor 1α
His	histidine
HMBC	heteronuclear multiple bond coherence
hnRNP A1	heterogeneous nuclear ribonucleoprotein A1
HOBt	hydroxybenzotriazole
HPI	hydrophobic pocket I
HPLC	high performance liquid chroma-tography
HRII	hydrophobic region II
HRMS	high resolution mass spectrometry
HSAB	hard soft acids and bases
HSQC	heteronuclear single quantum coherence spectroscopy
Hz	Hertz
I	isoleucine
I/σ(I)	signal-to-noise ratio
IC_{50}	half maximal inhibitory concentration

ICP0	HHV E3 ubiquitin ligase
i.e.	id est
Ile	isoleucine
Imdz	imidazole
IR	infrared spectroscopy
J (NMR)	coupling constant
JAK	Janus kinase
JNK2/3	c-Jun N-terminal kinase 2/3
K	Kelvin
kDa	Kilodalton
KHD	kinesin homology domain
L	leucine
LATS	large tumor suppressor kinase
LC	liquid chromatography
LCK	lymphocyte-specific protein tyrosine kinase
Leu	leucine
Lit.	literature
LRP5/6	low-density lipoprotein receptor-related proteins 5 or 6
Lys	lysine
m (NMR)	unresolved multiplet
M	molar
M_r	relative molecular mass
m.p.	melting point
m/z	mass-to-charge ratio
MAP1A	microtubule-associated protein 1A
MAP4	microtubule-associated protein 4
MAPK	mitogen-activated protein kinase
MBP	myelin basic protein
MCLK3	myosin light chain kinase 3
MDM2	mouse double minute 2 homolog
MES	2-(*N*-morpholino)ethanesulfonic acid
Met	methionine
mg	milligram(s)
MHz	Megahertz
min	minute(s)
ml	milliliter(s)
mM	millimolar
mmol	millimole(s)
mol	mole(s)
mRNA	messenger RNA
MS	mass spectrometry
mTNFα	transmembrane tumor necrosis factor α
mTOR	mammalian target of rapamycin
MTSS1	metastasis suppressor 1
MTT	3-(4,5-dimethyl-thiazol-2-yl)-2,5-diphenyltetrazolium bromide
N	asparagine
n.d.	not determined
NaHMDS	sodium bis(trimethylsilyl)amide
Naph	naphthyl
^{n}BuLi	*n*-butyllithium
NEDD4	neural precursor cell expressed developmentally down-regulated protein 4
NFAT1	nuclear factor of activated T-cells 1
NLS	nuclear localization signal
nM	nanomolar
nm23-H1	nucleoside diphosphate kinase A
NMP	*N*-methyl-2-pyrrolidone
NMR	nuclear magnetic resonance spectrometry
No.	number
Nop56	nucleolar protein 56
NPAS2	neuronal PAS domain protein 2
q (NMR)	quartet
quant.	quantitative
quint (NMR)	quintet
P	proline
PB	phosphate-binding region
PBS	phosphate-buffered saline
Pd-C 10 %	palladium on carbon, loading 10 % w/w
PDB	Research Collaboratory for Structural Bioinformatics (RCSB) protein data bank
PDGFR	platelet-derived growth factor receptor
PDK1	phosphoinositide-dependent kinase 1
$Pd(PPh_3)_4$	tetrakis(triphenylphosphine)-palladium(0)
PEG	polyethylene glycol
PER 1-3	Period 1-3
PGC-1α	peroxisome proliferator-activated receptor γ coactivator 1α
pH	potentia hydrogenii

PHB2	prohibitin 2
Phe (NMR)	phenyl
Phe	phenylalanine
PIP5K2C	phosphatidylinositol 5-phosphate 4-kinase type-2γ
PK	protein kinases
PKA	cAMP-dependent protein kinase
PKCα	protein kinase C α
PKD2	protein kinase D2
PKI	heat stable protein kinase inhibitor
Porcn	Porcupine
Pro	proline
$PP1_C$	catalytic subunit of protein phosphatase 1
PPh_3	triphenylphosphine
ppm	parts per million
ppUL44	human cytomegalovirus phosphoprotein
PS-2	presenilin-2
PTFE	polytetrafluoroethylene
PyBOP	(Benzotriazol-1-yloxy)tripyrrolidinophosphonium hexafluorophosphate
Pyr	pyridine
R-factor	reliability factor
R_{free}	free R-factor
R_{meas}	corrected R-factor
R_{merge}	internal agreement factor
R_{work}	R-factor
RanBPM	Ran-binding protein microtubule-organization center
Rec8	Rec8 meiotic recombination protein
RhoA/B	Ras homolog family member A/B
RIPK2	Receptor-interacting Ser/Thr-protein kinase 2
RMSD	root-mean-square deviation (for atomic positions)
RNA	ribonucleic acid
RORα	retinoid acid receptor-related orphan receptor α
RP	reversed phase
RPL4, 8, 13	ribosomal protein L4, 8, 13
rpm	revolutions per minute
rt	room temperature
s	second(s)
s (NMR)	singlet
S	serine
sat.	saturated
SCS	sulfatide and cholesterol-3-sulfate
SEM	standard error of the mean
Ser	serine
siRNA	small interfering RNA
SLS	Swiss Light Source
smKI	small molecule kinase inhibitors
SNARE	soluble *N*-ethylmaleimide-sensitive fusion protein attachment protein receptor
SP	sugar pocket
SPRY2	sprouty 2
Sre1N	yeast sterol regulatory element-binding protein homolog
start.	starting material
STE	homologs of yeast sterile 7, sterile 11, sterile 20 kinases
SV40 T-Ag	simian virus 40 large T-antigen
Swi6	chromatin-associated protein swi6
t (NMR)	triplet
T3P	1-propylphosphonic acid cyclic anhydride
TDP-43	TAR DNA-binding protein of 43 kDa
^{t}Bu	*tert*-butyl
^{t}BuLi	*tert*-butyllithium
TAR	trans-activation response element
TCF/LEF	T-cell factor/lymphoid enhancer factor
TDP-43	TAR DNA-binding protein of 43 kDa
temp.	temperature
tert	tertiary
TGN	trans Golgi network
Thr	threonine
TK	tyrosine kinase
TKL	tyrosine kinase-like
TLC	thin layer chromatography
Tol	tolyl
TOP2A	topoisomerase Iiα
t_R	retention time
Tris	2-Amino-2-hydroxymethyl-propane-1,3-diol
Trp	tryptophane

TTBK1/2	tau tubulin kinases 1 and 2
TV	transcription variant
Tyr	tyrosine
UV	ultraviolet
UHRF1	ubiquitin-like, with PHD and RING finger domains
v/v	volume/volume
vbs (NMR)	very broad singlet
VEGF	vascular endothelial growth factor
VEGFR	VEGF receptor
VRK1-3	vaccinia-related kinases 1-3
W	Watt(s)
WC-1	white collar-1
Wnt	Wingless/Int-1
X	any amino acid
Y	any amino acid except Ser/Thr
YAP	Yes-associated protein

List of Figures

Figure 1 | The human kinome. Human kinases are subdivided into seven distinct groups: AGC = containing PKA, PKG, PKC families; CAMK = calcium/calmodulin-dependent protein kinase; CK1 = formerly known as casein kinase 1; CMGC = containing Cdk, MAPK, GSK3, CLK families; STE = homologs of yeast sterile 7, sterile 11, sterile 20 kinases; TK = tyrosine kinases; TKL = tyrosine kinase-like. Obviously, CK1 and CK2 (black arrow) family members are non-related. The phylogenetic tree is taken from MANNING *et al.*[5]. The dendrogram (right) is made in accordance to the same publication. 2

Figure 2 | Sequence alignment of human CK1δ transcription variants and CK1ε. The conserved N-terminal domain consists of amino acids 1-8, followed by the kinase domain (286 amino acids). Identical residues within the kinase domain are highlighted in green, different residues in yellow. The non-conserved C-terminal domains of CK1δ TV1/TV2 and CK1ε exhibit highly variable sequences. The alignment was generated by Clustal Omega[16] using transcript sequences for CK1δ TV1 (Gene Bank AAH03558.1), CK1δ TV2 (Gene Bank ABM64211.1), and CK1ε (Gene Bank ABM64212.1). For abbreviations DFG, KHD, SIN, NLS cp. **chapter 1.2**..... 4

Figure 3 | Structural presentation of the CK1δ kinase domain. The N- (red) and C-terminal lobe (blue) are connected by the hinge region (yellow). The nucleotide binding site (not occupied) lies within the cleft between the domains. Indicated by arrows are the kinesin homology domain (KHD) and the nuclear localization signal (NLS). The significance of the DFG (Asp, Phe, Gly) motif for CK1δ has not been determined yet. The nomenclature is adapted from XU *et al.*[18] and LONGENECKER *et al.*[17]. The figure refers to CK1δ crystallization by HUANG *et al.* (PDB code 4HGT)[22]..... 6

Figure 4 | ATP-binding mode in CK1δ. The representation is in accordance with crystallization results of CKi1 and magnesium-ATP complex (PDB code 1CSN) and the pharmacophore model by TRAXLER and FURET. For clarity, water molecules are left out[17,18,23]..... 7

Figure 5 | Detailed ATP-binding mode in CKi1. Direct and water-mediated contacts between CKi1 and ATP adenine (A), ribose (B), and magnesium-phosphate moiety (C). Interactions were modeled according to XU *et al.* (PDP code 1CSN)[18]. 8

Figure 6 | Postulated substrate-binding mode at CK1δ phosphate-binding moiety W1. An *in silico* peptide (yellow) consisting of Ser(P)-Ala-Ala-Ser is coordinated by Arg178 (T-loop, green in A), Gly215 (L-EF, red in A) and Lys224 (αF, blue in A). The phosphorylatable Ser hydroxyl group is placed in H-bonding range towards ATP (maroon) γ-phosphate. A surface model (B) visualizes the close fitting of Mg^{2+}-ATP and substrate to the catalytic cleft of CK1δ. Modeling was performed based on MARIN *et al.*[28] (PDB code 1CSN[18], 4HGT[22]) utilizing Schrödinger software (**chapter 7.1**). 10

Figure 7 | Scaffold protein-mediated subcellular spatial organization. AKAP450 anchors CK1δ/ε to membranes and organelles, DDX3 binds CK1δ/ε and promotes Dvl phosphorylation, CRY-PER-CK1δ/ε complexes translocate to the nucleus, CK1BP binds and inhibits CK1δ. Phosphorylation is represented by yellow stars. The figure is adapted from GOOD *et al*.[104]. 14

Figure 8 | Homodimerization of CK1δ. Monomers 1 (purple) and 2 (green) form dimers via interaction of their dimerization domains (A). The dimerization domain (yellow) includes various amino acid residues of strands β1, β2, β3, and β7 as well as loops L-12 and L-78, helix αB, and the hinge region (B, PDB code 4HGT[22]). 15

Figure 9 | Post-translational regulation of CK1δ. Mechanisms of post-translational regulation (A): inactivation by C-terminal autophosphorylation (1) or phosphorylation by other kinases (4) and subsequent activation by phosphatases (1, 4 *vice versa*), C-term truncation (2, 5) or interaction with activator molecules (3). Truncation is also imaginable without previous phosphorylation (6). CK1δ is marked for degradation by ubiquitination (7). Brackets indicate insufficient evidence. Phosphorylation sites within the CK1δ TV1 C-terminal domain (B, adapted from KNIPPSCHILD *et al*.[9]). Colocalization of CK1δ, PKA, and $PP1_C$ is mediated by AKAPs (C)[109–117]. 17

Figure 10 | Interruption of the hydrophobic spine by type I ½ inhibitors on the example of dibenzosuberone derivative 1 in p38α mitogen-activated protein kinase. Binding of the inhibitor (green) interrupts the hydrophobic spine (red). H-bonds (black dashed lines) are formed towards hinge and αC-helix. Hydrophobic interaction (yellow dashed line) accommodates DFG Phe169. Dibenzosuberone derivative **1** refers to (*S*)-*N*-(5-((7-(2,3-dihydroxypropoxy)-5-oxo-10,11-dihydro-5*H*-dibenzo[*a*,*d*][7]annulen-2-yl)amino)-2-fluorophenyl)benzamide (**1**) by FISCHER *et al*. The figure was modeled in accordance to the same publication (PDB code 3UVQ)[161]. 27

Figure 11 | Binding mode of irreversible type V inhibitor afatinib. Afatinib (**2**) displays a type I binding mode: the quinazoline core occupies the adenine-binding region and forms an H-bond towards a hinge residue. The halogen-substituted phenyl moiety extends into *HPI*. But unlike type I inhibition, the enone moiety reacts with a nucleophilic cysteine residue in a MICHAEL addition and covalently attaches the ligand to the active site of epidermal growth factor receptor (EGFR)[7]. 28

Figure 12 | Crystal structures of inhibitors 9 and 16 in CK1δ. Comparison of teardropbinder **9** (A, PDB code 3UZP)[184] and linearbinder **16** (B, PDB code 4TWC)[181] in CK1δ. 34

Figure 13 | Postulated binding mode of lead structure 12 in CK1δ. The 2D interaction diagram (B) was generated in accordance to the modeling results (A, PDB code 3UZP). 41

Figure 14 | Central pharmacophore for *in silico* lead structure optimization. The central pharmacophore has been defined with X and Y being carbon, nitrogen, oxygen, or sulfur (n = 0-3). 45

Figure 15 | Positioning of the 4-fluorophenyl moiety of 12 within the selectivity pocket of CK1δ. The halogenated aryl moiety penetrates deeply into the pocket forming hydrophobic interactions (violet) with Met80 and Met82. Met82 is rotated towards Pro66 (PDB code 3UZP)[184]. 47

Figure 16 | Postulated binding mode of 51 in CK1δ. Hydroxyl moieties of the iminosaccharide (yellow) form H-bonds with residues Ser17 and Asp132. Interactions between other parts of the ligand and the kinase are not shown (PDB code 3UZP)..... 51

Figure 17 | *In vitro* biological evaluation of diaryl-oxazoles by SCHMIDT. Iminosaccharide-substituted compounds **64**, **65**, **66** derived from unsubstituted compound **63** (left). Residual activity of CK1δ at 10 μM inhibitor is shown in relation to control (DMSO). Each bar shows the mean value of n = 3 experiments ± standard deviation (right, modified from SCHMIDT[208])..... 52

Figure 18 | Postulated binding modes of 12, 73, and 74 in CK1δ. Smaller aromatic systems dictate increased angles leading to less optimal fitting of the azete scaffold **74** (violet) compared to imidazole **12** (green) and pyridine **73** (black) scaffolds. The indicated distances refer to the 3D structure and thus the angle of torsion. All data refer to energetically minimized structures. 55

Figure 19 | Replacement of a conserved water molecule in CK1δ. One conserved water molecule in the CK1δ active site interacts with Lys38, Asp149, and the ligand **12** (A). It might be replaceable by a hydroxymethyl group in 2-position of the 4-fluorophenyl moiety in **75** (B) and a hydroxyethyl group in **76** (C) or a chiral hydroxycyclopropyl group in **77** (D) at the imidazole nitrogen. The (*E*)-3-(2,4-dimethoxyphenyl)acrylamide side chains (cp. lead structure **12**) in 2-position of the pyridine are not displayed. Glide scores are given beyond the structures. 57

Figure 20 | Positioning of 12 in the hydrophobic region II of CK1δ, CK1ε, and p38α. The lipophilic groove (yellow) is restricted by acid and hydrophilic residues at the rim of the region (red). Modeling refers to PDB codes 3UZP, 4HNI, and 1BMK..... 58

Figure 21 | Protein structure alignment of CK1δ, CK1ε, and p38α. The hinge of p38α (red) is displaced in relation to CK1δ (green) and CK1ε (yellow, left). Different conformation of ligands (**12**) taken from the protein structure alignment (right), though the (*E*)-conformation (grey box) is preserved. Modeling refers to PDB codes 3UZP, 4HNI, and 1BMK. 59

Figure 22 | Schematic representation of series 1 to 6 deriving from 78. Residues (R) are defined in the following chapters..... 60

Figure 23 | Postulated binding modes of 79 in CK1δ. Alignment of several possible binding modes illustrates the high flexibility of the *N*-3-(2,4-dimethoxyphenyl)propyl side chain within the hydrophobic region II (left). In contrast, the diaryl-imidazole scaffold is highly conserved in all binding modes (right). Modeling refers to PDB code 3UZP. 61

Figure 24 | *In silico* binding mode of 80 and 81 addressing Asp91. Positively charged dimethylamino side chains linked to the 2-aminopyridine through aliphatic (A) or cyclic (B)

linkers (cp. **Table 15**). Asp91 is positioned at the rim of CK1δ hydrophobic region II (PDB code 3UZP)..... 62

Figure 25 | Postulated binding mode of carbamide derivative 104 in CK1δ. The 2D interaction diagram (B) was formulated in accordance to the modeling results (A, PDB code 3UZP)..... 66

Figure 26 | Postulated binding modes of 105 and 106 in CK1δ. Three H-bonds are formed between compound **105** (series 4) and hinge Leu85 (arrow) while compound **106** (series 5) represents a bidentate hinge-binder. *HRII* residues are indicated with their VAN DER WAALS radii by yellow spheres (PDB code 3UZP)..... 67

Figure 27 | Hybrid inhibitors 115 and 116 deriving from Porcn inhibitors 113 and 114. The postulated binding mode of **115** in CK1δ is depicted (right) (PDB code 3UZP). 69

Figure 28 | Hybrid inhibitor 118 deriving from imatinib. The postulated binding mode in CK1δ is depicted (right) (PDB code 3UZP)..... 70

Figure 29 | Synthetic route towards inhibitors of series 1-6. Syntheses are given as an overview and will be discussed in detail in the following chapters (**4.1** to **4.8**)..... 71

Figure 30 | Synthesis of ethanone derivatives 123 and 128. **121**, **123**: R = F; **127**, **128**: R = Br. **a**) NaHMDS, anhyd. THF, 2 h 0 °C then 1 h rt. Yield: quant. (**123**), 51 % (**128**). 72

Figure 31 | Synthesis of α-oximinoketones 124 and 129. **123**, **124**: R = F; **128**, **129**: R = Br. **a**) Glacial acetic acid, $NaNO_2$, 1h 0 °C then 3.5 h rt. Yield: 95 % (**124**), 92 % (**129**). 73

Figure 32 | Reduction of hydroximes 124, 128 towards α-aminoketones 125, 130. **124**, **125**: $R^1 = R^2 = F$; **129**, **130**: R^1 = Br, R^2 = H. **a**) H_2, Pd/C, 1 atm, HCl-saturated 2-propanol, 12 h rt. Yield: 82 % (**125**), 69 % (**130**)..... 73

Figure 33 | Ring closure of α-ketoamine 125 towards key intermediate 119. **a**) Methyl thiocyanate, DMF, 45 min reflux then 45 min rt. 74

Figure 34 | Synthesis of building block 120 by S_NAr. **a**) Conc. aq. NH_3, 20-30 bar, 18 h 180 °C. 74

Figure 35 | Alternative potential procedure for the preparation of 120 from 119 via tetrazolo derivative 131. **a**) NaN_3, DMSO, 3 h 140 °C. 75

Figure 36 | Synthetic procedure B towards building block 120. **137**: R = $NH_3^+Cl^-$, NHBoc. **a**) Boc_2O, *tert*-butanol, 12 h rt. **b**) Boc_2O, 4-DMAP, THF, 24 h rt. **c**) **122**, NaHMDS, THF, 2 h 0 °C then 1 h rt. **d**) NaHMDS, **122**, 1 h -78 °C to rt then 2 h rt. **e**) Glacial acetic acid, $NaNO_2$, 1h 0 °C then 3.5 h rt. **f**) H_2, Pd/C, 1 atm, HCl-saturated 2-propanol, 12 h rt. **g**) Methyl thiocyanate, DMF, 45 min reflux then 45 min rt. 76

Figure 37 | Synthesis of 2-unsubstituted 4,5-diary-imidazole 139. **a**) SeO_2, glacial acetic acid, 1.5 h 95 °C. **b**) CH_3COONH_4, methenamine, glacial acetic acid (cat.), 4 min 117 °C (microwave). 77

Figure 38 | Synthesis of pyridin-2-amine derivatives. Moieties (R) are given in **Table 18**..... 78

Figure 39 | Reduction of 2,4-dimethoxycinnamic acid (157). **a**) Pd/C, cyclohexene, methanol, 3 min (microwave). **b**) $LiAlH_4$, THF, 1 h rt. 80
Figure 40 | Conversion of primary alcohol 159 into alkyl bromide 156 by APPEL reaction. **a**) NBS, PPh_3, dichloromethane (DCM), 2 h rt. 80
Figure 41 | *De-novo* synthesis of *N*-alkylated 4,5-diaryl-imidazoles. **161**-**163**, **165**, **166**: R = benzyl; **164**, **167**-**170**: R = 3-(2,4-dimethoxyphenyl)propyl. **a**) NaH, benzyl bromide or **156**, DMF, 20 min 0 °C then 2 h 0 °C to rt. Yield: 87 % (**161**), 94 % (**167**). **b**) **122**, NaHMDS, THF, 2 h 0 °C then 1 h rt. Yield: 93 % (**163**), 48 % (**168**). **c**) Glacial acetic acid, $NaNO_2$, 1h 0 °C then 3.5 h rt. Yield: 96 % (**165**), quant. (**169**). **d**) H_2, Pd/C, 1 atm, HCl-saturated 2-propanol, 12 h rt. Yield: 96 % (**166**), 99 % (**170**). **e**) Methyl thiocyanate, DMF, 45 min reflux then 45 min rt. Yield: 60 % (**162**), 38 % (**164**). 81
Figure 42 | Mechanism of CDI-mediated amide coupling. R = 3-(2,5-dimethoxyphenyl)propyl. 83
Figure 43 | Coupling reagents HATU (178) and PyBOP (180). At least for HATU, *O*- and *N*-isomers have been reported. 83
Figure 44 | Mechanism of HATU- and PyBOP-mediated amide coupling. R = 3-(2,5-dimethoxy-phenyl)propyl; NR'_2 = pyrrolidin-1-yl. **179**: Z = N; **181** Z = C. 84
Figure 45 | Mechanism of DCC-mediated amide coupling. R = 3-(2,5-dimethoxyphenyl)propyl. 85
Figure 46 | Amide coupling of 3-(di-/tri-methoxyphenyl)propionic acids and 120. **158**, **190**: 2,4-dimethoxyphenyl; **173**, **191**: 2,5-dimethoxyphenyl; **187**, **192**: 2,3-dimethoxyphenyl; **188**, **193**: 3,4-dimethoxyphenyl; **189**, **194**: 3,4,5-trimethoxyphenyl. **a**) CDI, 120 °C, DMF, rt then 12 h 110 °C. Yield: 27 % (**190**), 39 % (**191**), 63 % (**192**), 57 % (**193**), 49 % (**194**). 85
Figure 47 | Mechanism of carbamide derivative synthesis. For isocyanate R^1 cp. **Table 20**. 86
Figure 48 | Formation of dimer carbamide by-product 215 from isocyanate 195 in the presence of water. R = 2,4-dimethoxyphenyl. 86
Figure 49 | Schematic representation of acid side chains of series 4. A, B, D refer to carbon, nitrogen, or sulfur. 88
Figure 50 | Synthesis of carboxamides 220, 223, 231 of Series 4. **220**: R = H, 2,4 dimethoxyphenyl; **227**, **225**, **231**: R = CH_3, 2,4-dimethoxyphenyl; **228**, **230**: R = Bn, 2,4 dimethoxyphenyl; **223**, **224**, **230**: R = CH_3, 2,5-dimethoxyphenyl. **a**) Boc_2O, 4-DMAP, ACN, 1 h rt. **b**) 2,4-dimethoxyphenyl boronic acid, $Pd(PPh_3)_4$, aq. Na_2CO_3, DMF, 4 h reflux then 12 h rt. Yield: 67 % (**227**), 71 % (**229**). **c**) aq. NaOH, THF/methanol, 5 h 50 °C then 12 h rt. Yield: 63 % (**230**), quant. (**222**), quant. (**225**) **d**) PyBOP, DIPEA, DMF, 30 min rt, then **120**, 12 h 110 °C. Yield: 13 % (**220**), 20 % (**223**), 24 % (**231**). **e**) NaH, DMF, 20 min 0 °C, then CH_3I, 15 min 0 °C then 2.5 h rt. Yield: 52 % (**225**). **f**) NaH, DMF, 20 min 0 °C, then CH_3I or BnBr, 15 min 0 °C then 2.5 h rt. Yield: 65 % (**228**), 86 % (**227**). 89

Figure 51 | Reaction of building block 120 and active ester 224 in the presence of base. **a**) NaH, DMF, 30 min rt, then **224**, 72 h rt. 90
Figure 52 | Aimed reaction procedure towards 231 via intermediate protection of the imidazole nitrogen. R = 4-(2,4-dimethoxyphenyl)-1-methyl-1*H*-pyrrole-2-yl. **a**) ^{n}BuLi, THF, 35 min -78 °C, then CO_2, 1.5 h -40 °C. **b**) ^{t}BuLi, 30 min -78 °C, then **224**, -78 °C to rt over 12 h, 12 h rt. 90
Figure 53 | Acid-catalyzed ω-bromination of acetophenones with bromine. **235**: R = H; **237**: R = Br. 91
Figure 54 | Selective radical ω-bromination of 2,4-dimethoxyacetophenone with Copper(II) bromide. R = 2,4-dimethoxyphenyl. 92
Figure 55 | FRIEDEL-CRAFTS acylation of 1,3-dimethoxybenzene. **a**) $AlCl_3$, 3 h 0 °C. 92
Figure 56 | Cyclization mechanism of phenacyl halides and thioamide 244 by HANTZSCH synthesis. R^1 = ethyl carboxylate; R^2 = 2,4-dimethoxyphenyl; X = Br, Cl. 93
Figure 57 | Ester hydrolysis and subsequent decarboxylation of ethyl thiazole-2-carboxylate 239. R = 2,4-dimethoxyphenyl. **a**) Aq. NaOH, THF/methanol, 48 h rt. 93
Figure 58 | Synthesis of α-ketoamine 247 in two steps via an oxazole intermediate. **a**) CDI, methyl isocyanate, NaHMDS, THF, 12 h rt. **b**) Conc. HCl/methanol (1:1), 4 h reflux. 94
Figure 59 | DELÉPINE synthesis of α-ketoamine 247. **a**) Methenamine, chloroform, 4 h rt. **b**) Conc. HCl/methanol, 3 h reflux. 95
Figure 60 | Cyclization mechanism of α-ketoamine 247 with thioamide 244. R^1 = ethyl carboxylate; R^2 = 2,4-dimethoxyphenyl. 95
Figure 61 | Ester hydrolysis and subsequent decarboxylation of ethyl imidazole-2-carboxylate 246. R = 2,4-dimethoxyphenyl. **a**) Aq. NaOH, THF/methanol, 48 h rt. 96
Figure 62 | Synthesis of 2,4-dimethoxybenzohydrzide 256. **a**) Conc. H_2SO_4, methanol, 4 h reflux, then N_2H_4, 30 min rt to reflux. **b**) **244**, optional $[(CH_3)_2O]BF_4$, optional DMF or NMP, h 180 °C. 96
Figure 63 | Reaction mechanism of the COREY-FUCHS synthesis of methyl propiolate 258. R = 2,4-dimethoxyphenyl 98
Figure 64 | Ester hydrolysis of methyl propiolate 258. **a**) $LiOH \cdot H_2O$, THF/methanol/water (4:1:1), 12 h rt. 98
Figure 65 | Coupling of propiolic acid 257 and building block 120 failed in different approaches. At least purification could not be performed successfully. 99
Figure 66 | Retrosynthetic contemplation of propiolic carboxamide 264. 99
Figure 67 | Reaction mechanism of consecutive MICHAEL-like addition and THORPE-ZIEGLER-like cyclization to afford 271. 100
Figure 68 | Cyclization mechanism of 271 and phenyl isothiocyanates towards thienopyrimidines. **274**, **272**: R = H; **275**, **273**: R = OCH_3. 101

Figure 69 | Synthesis of hybrid inhibitors 266, 267. **266**: R = H; **267**: R = OCH_3. **a**) Chloroacetyl chloride, Et_3N, DCM, 12 h rt. **b**) Aniline, Et_3N, DMF, 2 h 80 °C. **c**) **272** or **273**, Et_3N, DMF, 2 h 80 °C. Yield: 59 % (**266**), 76 % (**267**). 102
Figure 70 | Ampholytic character of 281 in pH neutral solution. 103
Figure 71 | Synthesis of hybrid inhibitor 280. **a**) *N*-Methylpiperazine, *n*-butanol, 2 h rt. **283** has been isolated as a by-product. **b**) **120**, HATU, DIPEA, NMP, 30 min rt then 30 min 90 °C (100 W). **280** has not been isolated purely..... 103
Figure 72 | Postulated reaction mechanism of sulfide oxidation using Oxone®. 104
Figure 73 | Photochemical $_{\pi}6_a$-electrocyclization of 162. **a**) THF, 2 min 365 nm (5.4 W). ... 107
Figure 74 | WOODWARD-HOFFMANN-based photochemical $_{\pi}6_a$-electrocyclization mechanism of 162..... 107
Figure 75 | Reaction mechanism of $_{\pi}6_a$-electrocyclization towards 292. Dihydro-intermediate **293** is initially oxidized in the presence of atmospheric oxygen. 108
Figure 76 | Inhibition of CK1 isoform and p38α kinase activity by inhibitors of series 1 at a concentration of 10 µM. Compounds **148-155**, **84**, **85** have been biologically evaluated in kinase assays against CK1δ, CK1ε, CK1α, CK1γ3, and p38α. Compounds **162**, **82**, **164** have only been tested against CK1δ and CK1ε. GST-p53 fragment (aa 1-64) (CK1δ, ε, α), α-casein (CK1γ3), or GST-CK1δ fragment (aa 305-375) (p38α) have been used as substrate. The inhibitors were screened in triplicate measurement in the presence of 100 µM ATP. Residual activities were normalized to DMSO. Error bars indicate the standard error of the mean (SEM)[248,249]..... 110
Figure 77 | IC_{50} determination of series 1 compounds 150, 151, and 164. IC_{50} values have been determined using CK1δ or CK1ε and α-casein as substrate. Error bars indicate the SEM[248,249]..... 111
Figure 78 | Cell viability of HT-29 cells after treatment with series 1 compounds at concentrations of 10 µM, 20 µM, or 25 µM. The inhibitors were screened in triplicate measurement. Cell viability was normalized to mock. Error bars indicate the SEM[248,249]. 113
Figure 79 | EC_{50} determination of compound 151 in HT-29 cells. Error bars indicate the SEM[248]. 114
Figure 80 | Inhibition of CK1 isoform kinase activity by inhibitors of series 2 at a concentration of 10 µM. Compounds **190-194**, **102**, **103** have been biologically evaluated in kinase assays against CK1δ and CK1ε. Compounds **190**, **191**, **103** have additionally been tested against CK1α. α-Casein has been used as substrate. The inhibitors were screened in triplicate measurement in the presence of 10 µM ATP. Residual activities were normalized to DMSO. Error bars indicate SEM[248,249]..... 116
Figure 81 | IC_{50} determination of series 2 compounds 190-194, 102, and 103. IC_{50} values have been determined using CK1δ or CK1ε and α-casein as substrate. Error bars indicate the SEM[248,249]..... 117

Figure 82 | Schematic representation of the selectivity profile of 191 at a concentration of 100 nM. The inhibitor has been screened over a panel of 320 wild-type protein kinases and B-Raf V600E by ProQinase GmbH. The phylogenetic tree is taken from MANNING *et al*.[5] 120
Figure 83 | Cell viability of Colo357 and Panc89 cells after treatment with series 2 compounds at a concentration of 10 µM. The inhibitors were screened in triplicate measurement. Cell viability was normalized to mock. Error bars indicate the SEM[248,249]. 121
Figure 84 | Cell viability of Colo357, Panc-1, and MiaPaca-2 cells after treatment with 190 at a concentration of 15 µM. The inhibitor was screened in quadruplicate measurement. Cell viability was normalized to mock. Error bars indicate the SEM[248,249] 121
Figure 85 | EC_{50} determination of compound 191 in Colo357 and Panc89 cells. Error bars indicate the SEM[248]. 122
Figure 86 | Binding mode of 191 in p38α MAPK. Binding mode revealed by X-ray crystallography (A) in comparison to the *in silico* model (B). The DFG Phe169 occupies different conformations: DFG-out (A), DFG-in (B). The propionic acid side chain has not been completely resolved by X-ray analysis (A). Modeling (B) refers to PDB code 1BMK[195]. π-π-stacking is indicated by a violet dashed line. X-ray analysis has been performed by the group of PROF. DR. DANIEL RAUH. 123
Figure 87 | Protein alignment of the obtained crystal structure of 191 in p38α with published DFG-in and DFG-out conformations of the kinase. Rotation of Phe169 from the active DFG-in (turquoise, PDB code 1BMK)[195] towards the DFG-out conformation (yellow, PDB code 1WBT)[250] permits access to the deep pocket. The obtained crystal structure (violet) exhibits a conformation halfway between DFG-in and DFG-out. Fitting of **191** (green) into the DFG-out state of the kinase might be forestalled by steric clashes (bad contacts, red dashed lines). 124
Figure 88 | Inhibition of CK1 isoform kinase activity by inhibitors of series 3 at a concentration of 10 µM. Compounds **204**-**206**, **208**-**210**, **212**, **104**, and **286**-**290** have been biologically evaluated in kinase assays against CK1δ and CK1ε. Compounds **204**, **104**, **206**, **286**, **209**, **210**, and **212** have additionally been tested against CK1α. α-Casein has been used as substrate. The inhibitors were screened in triplicate measurement in the presence of 10 µM ATP. Residual activities were normalized to DMSO. Error bars indicate the SEM[248,249]. 126
Figure 89 | IC_{50} determination of series 3 compounds 204, 205, 208-210, 104, and 287-290. IC_{50} values have been determined using CK1δ or CK1ε and α-casein as substrate. Error bars indicate the SEM[248,249]. 127
Figure 90 | Cell viability of Colo357 and Panc89 cells after treatment with series 3 compounds at a concentration of 10 µM. The inhibitors were screened in triplicate or quadruplicate measurement. Cell viability was normalized to mock. Error bars indicate the SEM[248,249] 130

Figure 91 | Postulated binding modes of 105 (A) and 291 (B) in CK1δ. (PDB code 3UZP). 131
Figure 92 | Inhibition of CK1 isoform kinase activity by inhibitors of series 4 at a concentration of 10 μM. Compounds **232, 291,** and **224** have been biologically evaluated in kinase assays against CK1δ and CK1ε. α-Casein has been used as substrate. The inhibitors were screened in triplicate measurement in the presence of 10 μM ATP. Residual activities were normalized to DMSO. Error bars indicate the SEM[249]. 132
Figure 93 | IC_{50} determination of series 4 compounds 232, 291, and 224. IC_{50} values have been determined using CK1δ or CK1ε and α-casein as substrate. Error bars indicate the SEM[249]. 132
Figure 94 | Cell viability of Colo357, Panc-1, and MiaPaca-2 cells after treatment with series 4 compounds at a concentration of 15 μM. The inhibitors were screened in triplicate or quadruplicate measurement. Cell viability was normalized to mock. Error bars indicate the SEM[249]. 134
Figure 95 | Binding mode of 224 in CK1δ. The binding mode revealed by X-ray crystallography is presented as ribbon (A) and surface (B) diagram. The *in silico* predicted mode (C) shows different orientation of the pyrrole moiety. X-ray analysis has been performed by the group of PROF. DR. ULRICH BAUMANN. 135
Figure 96 | Inhibition of CK1 isoform kinase activity by inhibitors of series 6 at a concentration of 10 μM. Compounds **266** and **267** have been biologically evaluated in kinase assays against CK1δ and CK1ε. α-Casein has been used as substrate. The inhibitors were screened in triplicate measurement in the presence of 10 μM ATP. Residual activities were normalized to DMSO. Error bars indicate the SEM[249]. 136
Figure 97 | IC_{50} determination of series 6 compounds 266 and 267. IC_{50} values have been determined using CK1δ or CK1ε and α-casein as substrate. Error bars indicate the SEM[249]. 137
Figure 98 | Cell viability of Colo357, Panc-1, and MiaPaca-2 cells after treatment with series 6 compounds at a concentration of 15 μM. The inhibitors were screened in triplicate or quadruplicate measurement. Cell viability was normalized to mock. Error bars indicate the SEM[249]. 138
Figure 99 | Binding mode of 266 in CK1δ. X-ray crystallization revealed two poses for **266** in CK1δ *HRII* (A, B), opposed by the *in silico* predicted geometries (C). The 2D ligand interaction diagram refers to crystallization (D). X-ray analysis has been performed by the group of PROF. DR. ULRICH BAUMANN. 139
Figure 100 | Potent CK1δ inhibitors 191, 224, 232, and 266. The most potent compounds of the current work inhibit CK1δ with IC_{50} values in low nanomolar range. 142
Figure 101 | CK1δ-preferring inhibitors 164, 192, and 204. The depicted compounds favor isoform δ over ε. **224** as well as p38α partially discriminating **266** are shown in **Figure 100**. 143

Figure 102 | Binding poses of 191, 224, and 266 in CK1δ or p38α. **224** (A) and **266** (B) have been co-crystallized with CK1δ while p38α has been crystallized in complex with **191**..... 144
Figure 103 | Differently methoxy-substituted series 2 compounds 191, 192, 193, and 194. The di- and trimethoxy substitution pattern have been compared with regard to inhibition of CK1δ..... 145
Figure 104 | Lengths of side chains might select for different dimethoxy substitution pattern. The measured distances refer to appropriate energetically minimized 3D structures. 146
Figure 105 | Comparison of series 1 to 4 based on compounds 164, 190, 204, and 232. Potency and isoform-specificity were either increased (+), decreased (-), or unaffected. 148
Figure 106 | RAMACHANDRAN plot of the protein model used for CK1δ screening. The colored squares refer to energetically favored (red), allowed (yellow), and disallowed (white) regions for amino acid residue dihedrals. Glycines are depicted as black triangles, prolines as black squares. All remaining amino acid residues are represented by black dots. The model refers to a crystal structure by LONG *et al*. (PDB code 3UZP)[184]. 151
Figure 107 | Molecular structure of 191. Determined by X-ray crystallography by DR. DIETER SCHOLLMEYER..... 207

List of Tables

Table 1 | Specified *in vitro* and *in vivo* CK1δ substrates of different species. The list is admittedly incomplete due to the fact that many CK1 substrates have not been assigned to distinct isoforms. The classification of substrates in this table is based on their major function and in association with **chapter 1.2.4**. Several substrates could appear in more than the assigned group. 11

Table 2 | CK1δ mutants in different tumor entities. The structural domain comprising the point mutation(s) is given in parentheses. P66T, R69K refers to a double mutant. 22

Table 3 | CK1δ misregulation in different tumor entities. Increase and/or decrease primarily refer to *CK1δ* mRNA, although this is predominantly in accordance with up-/downregulation on protein level. In cases of *altered expression* the reference did not specify levels compared to healthy tissue. *Reduced immunostaining* has not been specified as well. 22

Table 4 | FDA-approved small molecule kinase inhibitors as of January 2016. FDA-approval refers only to the first date of authorization. More than three targets for a single inhibitor are referred to as *multiple*. Ser/Thr kinase (1), tyrosine kinase (2), lipid kinase (3) smKI, rapalogs (4)[6,7,152,155–158]. For explanation of types I to V cp. **chapter 1.3.1**. Abbreviations: INN, international nonproprietary name; ALL, acute lymphoblastic leukemia; AMD, age-related macula degeneration; B-Raf^{V600}, B-Raf V600 mutant; CLL, chronic lymphocytic leukemia; CML, chronic myelogenous leukemia; CRC, colorectal cancer; FL, follicular lymphoma; GIST, gastrointestinal stromal tumors; HCC, hepatocellular cancer; IPF, idiopathic pulmonary fibrosis; MCL, mantle cell lymphoma; MTC, medullary thyroid cancer; NSCL, non-small cell lung carcinoma; PC, pancreatic cancer; RCC, renal cell carcinoma; SEGA, subependymal giant cell astrocytoma; SLL, small lymphocytic leukemia; STS, soft-tissue sarcoma; TC, thyroid carcinoma; TP, transplantation. 25

Table 5 | First generation CK1δ inhibitors[167–169,171–173] 31

Table 6 | Pyridinyl-imidazole and -isoxazole CK1δ inhibitors[173–176]. 32

Table 7 | Benzimidazole and benzothiazole CK1δ inhibitors[22,119,177–183]. Abbreviation: n.d., not defined. 35

Table 8 | Purine and pyrazolo-pyrimidine or –pyridine CK1δ inhibitors[185–188] 37

Table 9 | Amino-anthraquinone CK1δ inhibitor 26[189]. 38

Table 10 | Schematic binding modes of related diaryl-heterocyclic inhibitors crystallized with CK1δ or p38α. H-bonds formed between inhibitor and hinge residues are indicated by arrows[165,194–196]. 41

Table 11 | *In silico* influence of different substituents for R^1 and R^2 in CK1δ. Lead structure **12** is deposited in grey 48

Table 12 | *In silico* screening top hits with different hydrophilic moieties for R^3 in CK1δ. 50

Table 13 | *In silico* core hopping results for the imidazole of lead 12 in CK1δ. H-bond acceptors are indicated by arrows. 54

Table 14 | Screening hits for the replacement of the structural water. Glide scores are given beyond **75**, **76**, **77**, and lead **12**. R = (*E*)-4-(2-(3-(2,4-dimethoxyphenyl)acrylamido)pyridin-4-yl. 56

Table 15 | *In silico* screened compounds of series 1 that have been selected for syntheses. Series 1 refers to primary and secondary amine substituents. As these compounds exhibit considerable losses in ΔG anyway, they are sorted by structure instead of Glide score. 63

Table 16 | *In silico* screened compounds of series 2. Series 2 refers to di- and trimethoxy-substituted 3-phenylpropionic acid side chains at the 2-aminopyridine. 65

Table 17 | *In silico* screened compounds of series 4 and 5. These series refer to acyl side chains that were designed to mimic the (*E*)-configured π-bond of the lead structure bearing either five-membered heterocycles (series 4) or an alkyne moiety (series 5). R = 2,4-dimethoxyphenyl. 68

Table 18 | Amines applied for S_NAr reaction towards pyrdin-2-amines. (Series 1). 79

Table 19 | Determination of different amide coupling reagents. 82

Table 20 | Isocyanates applied for synthesis of carbamide derivatives. (Series 3). 87

Table 21 | Sulfoxidation of selected compounds. R = 4-fluorophenyl. Products are assigned to the appropriate series 1, 2, 3, and 4. Test compound **160** does not belong to any series. Start. = starting material. 105

Table 22 | IC_{50} values and Glide scores of compounds 150, 151, and 164[248,249]. 112

Table 23 | IC_{50} values and Glide scores of series 2 compounds[248,249]**.** 118

Table 24 | IC_{50} values and Glide scores of series 3 compounds[248,249]. 128

Table 25 | IC_{50} values and Glide scores of series 4 compounds[249]. 133

Table 26 | IC_{50} values and Glide scores of series 4 compounds[249]. 137

Table 27 | Energetic parameters for Glide score calculations[258,259] 153

Table 28 | HPLC gradient-dependent methods. 156

Table 29 | Kinase assay buffers. 287

Table 30 | Test compounds (kinase assays). Sulfoxides are implemented in the appropriate series. 288

Table 31 | Human CK1-dependent cancer cell lines used in MTT assays with their respective origin. The compounds tested on the cell lines are given with their respective series. 290

Table 32 | Crystallographic statistics of wild-type p38α in complex with 191. X-ray crystallography has been performed by the group of PROF. DR. DANIEL RAUH. Values in parenthesis refer to the highest resolution shell. 292

Table 33 | Crystallographic statistics of CK1δ in complex with 224 and 266. X-ray crystallography has been performed by the group of PROF. DR. ULRICH BAUMANN. Values in parenthesis refer to the highest resolution shell. 293

Erklärung zu § 8 Abs. 1 der Promotionsordnung

Die vorliegende Arbeit wurde unter Anleitung von Herrn Prof. Dr. Christian Peifer im Fachbereich Pharmazeutische und Medizinische Chemie des Pharmazeutischen Institutes der Christian-Albrechts-Universität zu Kiel im Zeitraum von Oktober 2012 bis Juli 2016 angefertigt.

Inhalt und Form dieser Abhandlung wurden, abgesehen von der Beratung durch meinen Betreuer, selbstständig von mir erarbeitet. Es wurden keine weiteren Quellen als angegeben herangezogen. Die Arbeit hat an keiner Stelle im Rahmen eines Prüfungsverfahrens vorgelegen und ist unter Einhaltung der Regeln guter wissenschaftlicher Praxis der Deutschen Forschungsgemeinschaft entstanden.

Kiel, Juli 2016

_____

Jakob Zacharias Halekotte

Teilergebnisse dieser Arbeit wurden in folgenden Beiträgen bereits veröffentlicht:

Fachzeitschriften

Knippschild, U., Krüger, M., Richter, J., Xu, P., García-Reyes, B., Peifer, C., Halekotte, J., Bakulev, V., Bischof, J. The CK1 Family: Contribution to Cellular Stress Response and Ist Role in Carcinogenesis. *Front. Oncol.* **4**: 96 (2014).

Richter, J., Ullah, K., Xu, P., Alscher, V., Blatz, A., Peifer, C., Halekotte, J., Leban, J., Vitt, D., Holzmann, K., Bakulev, V., Pinna, L. A., Henne-Bruns, D., Hillenbrand, A., Kornmann, M., Leithäuser, F., Bischof, J., Knippschild, U. Effects of altered expression and activity levels of CK1δ and ε on tumor growth and survival of colorectal cancer patients. *Int. J. Cancer* **136**, 2799-2810 (**2015**).

Dolde, C., Grüter, S., Bischof, J., Montada, A., Halekotte, J., Peifer, C., Kalbacher, H., Baumann, U., Knippschild, U., Suter, B. DDX3X is an activator of CK1ε, turning promiscuous and uncontrolled by medulloblastoma mutations. Submitted.

Posterbeiträge

Halekotte, J., Luxenburger, A., Bischof, J., Knippschild, U., Peifer, C. 3,4-Diaryl-isoxazole and -imidazole Derivatives as Potent and Selective Inhibitors of Casein Kinase 1δ. *7th Polish-German Symposium on Pharmaceutical Sciences*, **2013**, Gdańsk, Poland.

Halekotte, J., Bischof, J., Knippschild, U., Peifer, C. 3,4-Diaryl-isoxazole and -imidazole Derivatives as Potent and Selective Inhibitors of Casein Kinase 1δ. *DPhG Jahrestagung*, **2013**, Freiburg, Deutschland.

Halekotte, J., Kuhl, L., Bischof, J., Knippschild, U., Peifer, C. 3,4-Diaryl-isoxazole and -imidazole Derivatives as Potent and Selective Inhibitors of Casein Kinase 1δ. *Life Sciences Studierendentagung*, **2013**, Kiel, Deutschland.

Danksagung

An erster Stelle gilt mein Dank Herrn Prof. Dr. Christian Peifer für das Vertrauen und die Förderung sowie die Freiheit in der Forschung die ich fortwährend genießen durfte. Hervorheben möchte ich besonders deine menschliche Art und deine ständige Diskussionsbereitschaft. Danke, dass ich dafür nicht Angeln lernen musste.

Herrn Prof. Dr. Bernd Clement danke ich nicht zuletzt für die Übernahme des Zweitgutachtens, besonders aber für den maßgeblichen Anteil an meiner pharmazeutisch chemischen Ausbildung sowie meinem Interesse für die medizinische Chemie. Letzteres gilt ebenfalls für die Profes. Dres. Eric Beitz, Dieter Heber, Thomas Kunze und Holger Gohlke.

Herzlicher Dank geht an Lydia Kuhl, die im Rahmen ihrer Bachelorarbeit zu meinem Projekt beigetragen hat. Danke für die entspannte und produktive gemeinsame Arbeit in Labor und Büro, für Achterbahnen und Füchse.

Herrn Dr. Ulrich Girreser und seinem Team danke ich für die Aufnahme der NMR- und Massenspektren sowie die Beratung in analytischen Fragestellungen. Sven Wichmann, Karl Willi Bock und Dirk Böhme danke ich außerdem für Wartung und Reparatur diverser Geräte sowie für Rollbretter, Bolzenschneider und andere Werkzeuge.

Dem Arbeitskreis um Prof. Dr. Uwe Knippschild danke ich herzlich für die biologische Testung und die gute fachliche Zusammenarbeit. Namentlich danken möchte ich in diesem Zusammenhang Dr. Marc Krüger und Chiara Ianes. Den Arbeitskreisen um Prof. Dr. Ulrich Baumann und Prof. Dr. Daniel Rauh danke ich für die Kristallisation ausgewählter Verbindungen und Kinasen.

Danke all denen die die Arbeit so schön machen. Danke meinem gesamten Arbeitskreis für die hervorragende Atmosphäre in und außerhalb des Institutes. Danke für viele Kuchen.

Eugen Bethke von dem ich zwar nicht alles gelernt habe was ich kann, aber einiges. Bring mir Suppe, Dr. Johannes. Im selben Atemzuge, aber charmanter, Rebecca Horbert alias Dr. Robert Hornung. Danke euch beiden für spannende Filme, . . . Musik und die gemeinsame Zeit. Danke Alexander Döbbe(le)r für ganz neue sportliche Aspekte im Büro.

Danke Miriam Schehr für ihre wunderbare Art triviale Dringe neu zu erfinden. Immer wieder. Danke Miri für deinen chemischen Input, aber ich glaube du musst noch backen. Danke Boris Pinchuk für so einiges, aber nicht für Schafe. Herzlicher Dank gilt außerdem Martin Schütt, der unermüdlichen guten schwarzen Seele des Arbeitskreises. Danke Dorian Schmidt, für eine unbestreitbare Seelenverwandtschaft was die Organisation von Arbeitsplätzen anbelangt.

Danke Lydia, Alex, Boris, Dorian, Miri und Eugen für das Korrekturlesen dieser Arbeit. Für selbiges ganz besonderer Dank an Frau Marlies Nüsperling.

Dr. Andreas Luxenburger danke ich für so manche chemische Hilfestellung. Ebenso danke ich Dr. Dieter Schollmeyer für die Aufnahme der Kristallstruktur einer Verbindung.

Bei allen nicht namentlich erwähnten Kolleginnen und Kollegen bedanke ich mich für die gute Atmosphäre bei der Arbeit, der Praktikumsbetreuung und dem gesamten Institutsalltag.

Dank an Hannes, Gregor, Sebastian und Matthias, dass ihr so überhaupt gar nichts mit Pharmazie zu tun habt, außer vielleicht einmal Kopfschmerzen. Dank an Erk, Matthias, Christoph, Arda, Michel, Till und Linda für das Gegenteil. Dank an Jörn für das dazwischen. Hammer auf Amboss.

Danke Elke und Arno, dass ich mich bei euch willkommen fühle, wo auch immer das sein mag.

Das Beste kommt zu Schluss. Mein allergrößter Dank gilt meiner Familie und meiner wunderbaren Freundin Annika. Meinen Eltern, meinen langen Brüdern und meiner kleinen Schwester. Danke euch allen für das grenzenlose Verständnis, auch wenn ich manchmal nicht zu verstehen bin. Danke für das, was den Rahmen jeder Danksagung sprengen würde.

Curriculum Vitae

Persönliche Daten

Name	Jakob Zacharias Halekotte
Geburtsdatum	08. März 1986
Geburtsort	Soest
Staatsangehörigkeit	deutsch

Ausbildung

1992 bis 1996	Walburgisgrundschule Werl
1996 bis 2003	Ursulinengymnasium Werl
2003 bis 2005	Mariengymnasium zu Werl
Juni 2005	allgemeine Hochschulreife
Sept. 2005 bis Mai 2006	Zivildienst, Hedwig-Dransfeld-Schule Werl
Okt. 2006 bis Febr. 2007	Studium der Biologie, Ruprecht-Karls-Universität Heidelberg
April 2007 bis Juni 2011	Studium der Pharmazie, Christian-Albrechts-Universität zu Kiel
März 2009	Erster Abschnitt der Pharmazeutischen Prüfung
Juni 2011	Zweiter Abschnitt der Pharmazeutischen Prüfung
Juni 2011 bis Nov. 2011	Pharmaziepraktikum, Anfertigung einer Diplomarbeit im Fachbereich Pharmazie unter Leitung von Prof. Dr. Dr. Ingolf Cascorbi am Institut für Experimentelle und Klinische Pharmakologie des Universitätsklinikums Schleswig-Holsteins
Dez. 2011 bis Mai 2012	Pharmaziepraktikum, DocMorris Apotheke im famila Markt, Kiel
August 2012	Dritter Abschnitt der Pharmazeutischen Prüfung und Erhalt der Approbation als Apotheker

Beruflicher Werdegang, Promotion und Weiterbildung

Aug. 2012 bis Aug. 2015	Apotheker in der DocMorris Apotheke im famila Markt (kielgesund Apotheke in der Wik), Kiel
seit Oktober 2012	wissenschaftlicher Mitarbeiter und Promotion unter Leitung von Prof. Dr. Christian Peifer am Pharmazeutischen Institut der Christian-Albrechts-Universität zu Kiel
seit November 2012	Weiterbildung zum Fachapotheker für pharmazeutische Analytik
Mai 2013	Best Poster Award beim 7th Polish-German Symposium on Pharmaceutical Sciences in Gdańsk, Polen
Sept. 2015 bis Mai 2016	Apotheker in der Kronen-Apotheke, Kiel